SEDIMENTOLOGY AND SUBAERIAL EXPOSURE SURFACES OF THE MIDDLE DEVONIAN SNIPE LAKE REEF COMPLEX, SWAN HILLS FORMATION, WEST-CENTRAL ALBERTA

By

Beverly Jane Mack

A Thesis
Submitted to the Faculty of Graduate Studies
in Partial Fulfillment of the Requirements
for the Degree of

MASTER OF SCIENCE

Department of Geological Sciences
University of Manitoba
Winnipeg, Manitoba

© Beverly Jane Mack, June 5th, 2006

Library and Archives Canada
Bibliothèque et Archives Canada

Published Heritage Branch
Direction du Patrimoine de l'édition

395 Wellington Street
Ottawa ON K1A 0N4
Canada

395, rue Wellington
Ottawa ON K1A 0N4
Canada

978-0-494-22557-8

Your file Votre référence
ISBN:
Our file Notre reference
ISBN:

NOTICE:
The author has granted a non-exclusive license allowing Library and Archives Canada to reproduce, publish, archive, preserve, conserve, communicate to the public by telecommunication or on the Internet, loan, distribute and sell theses worldwide, for commercial or non-commercial purposes, in microform, paper, electronic and/or any other formats.

The author retains copyright ownership and moral rights in this thesis. Neither the thesis nor substantial extracts from it may be printed or otherwise reproduced without the author's permission.

AVIS:
L'auteur a accordé une licence non exclusive permettant à la Bibliothèque et Archives Canada de reproduire, publier, archiver, sauvegarder, conserver, transmettre au public par télécommunication ou par l'Internet, prêter, distribuer et vendre des thèses partout dans le monde, à des fins commerciales ou autres, sur support microforme, papier, électronique et/ou autres formats.

L'auteur conserve la propriété du droit d'auteur et des droits moraux qui protège cette thèse. Ni la thèse ni des extraits substantiels de celle-ci ne doivent être imprimés ou autrement reproduits sans son autorisation.

In compliance with the Canadian Privacy Act some supporting forms may have been removed from this thesis.

While these forms may be included in the document page count, their removal does not represent any loss of content from the thesis.

Conformément à la loi canadienne sur la protection de la vie privée, quelques formulaires secondaires ont été enlevés de cette thèse.

Bien que ces formulaires aient inclus dans la pagination, il n'y aura aucun contenu manquant.

Canada

THE UNIVERSITY OF MANITOBA

FACULTY OF GRADUATE STUDIES

*****

COPYRIGHT PERMISSION

SEDIMENTOLOGY AND SUBAERIAL EXPOSURE SURFACES OF THE MIDDLE DEVONIAN SNIPE LAKE REEF COMPLEX, SWAN HILLS FORMATION, WEST-CENTRAL ALBERTA

BY

Beverly Jane Mack

A Thesis/Practicum submitted to the Faculty of Graduate Studies of The University of Manitoba in partial fulfillment of the requirement of the degree

OF

MASTER OF SCIENCE

Beverly Jane Mack © 2006

Permission has been granted to the Library of the University of Manitoba to lend or sell copies of this thesis/practicum, to the National Library of Canada to microfilm this thesis and to lend or sell copies of the film, and to University Microfilms Inc. to publish an abstract of this thesis/practicum.

This reproduction or copy of this thesis has been made available by authority of the copyright owner solely for the purpose of private study and research, and may only be reproduced and copied as permitted by copyright laws or with express written authorization from the copyright owner.

ABSTRACT

The Snipe Lake reef complex in the Swan Hills Formation (earliest Frasnian) is a well-preserved, hydrocarbon-bearing reef buildup in west-central Alberta. It consists of five platform megacycles and five reef megacycles which are arranged in an overall backstepping pattern. This study uses an integrated approach that combines core examination, detailed petrography and geochemistry to evaluate the depositional and diagenetic history of the reef complex. This study focuses on the P4 and P5 platform successions and the R0.5 reefal succession and, in particular, the subaerial exposure features in these successions.

Nine lithofacies have been recognized in the P4 to R0.5 successions that range from tidal flat lithofacies in the platform-reef interior to reef foreslope lithofacies at the reef margin. Lithofacies can be grouped into lagoonal lithofacies associations and reef margin lithofacies associations. Cyclical deposition in the Snipe Lake reef complex was recorded by the stacking patterns of third-order reefal cycles and fourth-order lagoonal cycles. The P4 and P5 platform successions are composed of a series of backstepping shallowing-upward lagoonal cycles, whereas the R0.5 reefal succession is composed of a progradational reefal cycle at the reef margin and a series of lagoonal cycles in the reef interior.

Subaerial exposure surfaces have been recognized at the P4 and R0.5 cycle contacts. Detailed petrographic and isotope geochemistry analysis has identified several phases of diagenesis below these emergent surfaces, including early marine diagenesis, meteoric diagenesis during subaerial exposure, a subsequent phase of marine diagenesis as

relative sea level rose and a final phase of burial diagenesis as sediments were progressively buried.

A variety of pedogenic diagenetic features are observed below the P4 and R0.5 subaerial exposure surfaces which include, from top to bottom, green shale horizons, rhizoliths, fitted-fabric lithoclasts, glaebules, peds, laminar calcretes, green shale in cracks and vugs, marine pendant cements developed in vugs and meteoric pendant cements. Four types of paleosol profiles (A, B, C and D) have been recognized that characterize these features below the subaerial exposure surfaces. The P4 paleosol ranges from 0.75 to 2.1 m thick and is composed predominantly of the type A paleosol and rarely the type B paleosols. The R0.5 paleosol ranges from 0.12 to 1.3 m thick and is composed of types B, C and D paleosols. These subaerial exposure surfaces are interpreted to be the result of relative sea level falls which are estimated to be a minimum of 2.1 m and 1.3 m at the top of the P4 and R0.5 successions, respectively. The main factors that influenced the development of paleosols include climate, topography, vegetation and organisms, and length of exposure. In addition, erosion during the ensuing transgression significantly affected the preservation of paleosol profiles.

ACKNOWLEDGEMENTS

First and foremost, I like to express my deepest appreciation and respect to my supervisor, Dr. Nancy Chow for her continued support and guidance throughout this thesis. I am grateful for the many conversations we shared that challenged me both technically and creatively. I also thank her for her patience with the long distance correspondence during the last phase of my writing. I would like to also extend my thanks to Dr. Jack Wendte from the Geological Survey of Canada in Calgary who shared with me his immense knowledge in the subject and supported me logistically during the first phase of my research. I am also grateful to Dr. Iain Muir (Suncor Engery) and Dr. Frank Stoakes (Stoakes Consulting Group) for sharing with me the work they have done in the study area. I am grateful to the other members of my committee, Dr. Bob Elias and Dr. Tee Boon Goh for examining my thesis and for their insightful criticism. I also thank the University of Calgary Gallagher Library for providing me copies of several relevant M.Sc. and Ph.D. theses.

This project would not have been possible without the funding NSERC and the University of Manitoba provided my supervisor. I would also like to thank Devon Canada Corporation, Suncor Energy and the AEUB Core Research Centre for the additional funding and logistical assistance that they provided by supporting the core and petrographic analysis components of this project.

Thanks to all the staff and students in the Department Geological Sciences at the University of Manitoba for welcoming me into your and my second home. A special

thanks to the technical staff including Sergio Mejia and Neil Ball for helping me use the equipment.

Above all, I would like to gratefully acknowledge all my family and friends for their unconditional love and support throughout this whole process. Thank for you welcoming me back each time I came home and for understanding when I left again. I would like to especially thank my other half. I am grateful for your love, patience and support all these years and providing me with support even when I didn't know I needed it.

TABLE OF CONTENTS

page

ABSTRACT i

ACKNOWLEDGEMENTS iii

LIST OF APPENDICES x

LIST OF FIGURES xi

LIST OF COPYRIGHTED MATERIAL xiv

LIST OF TABLES xv

LIST OF OVERSIZED ENCLOSURES xv

1. INTRODUCTION 1
- 1.1 Prologue 1
- 1.2 Previous Work 2
- 1.3 Geological Setting 3
  - 1.3.1 Global Setting 3
  - 1.3.2 Regional Setting 5
  - 1.3.3 Snipe Lake Reef Complex 8
- 1.4 Snipe Lake Oil Field History 10
- 1. 5 This Study 10
  - 1.5.1 Study Location 10
  - 1.5.2 Objectives of Study 12

2. METHODOLOGY 13
- 2.1 Introduction 13
- 2.2 Selection of Wells 13
- 2.3 Cross-section Construction 14
  - 2.3.1 Datum 14
- 2.4 Core Examination 16
  - 2.4.1 Classification Schemes 17
- 2.5 Carbonate Petrography 22
- 2.6 Cathodoluminescence Microscopy 25
- 2.7 Epi-fluorescence Microscopy 25
- 2.8 Scanning Electron Microscopy 26
- 2.9 Electron Microprobe Analyses 27
- 2.10 Stable Isotope Analyses 28
- 2.11 X-ray Diffraction Analyses 29

3. STRATIGRAPHY 31
3.1 Introduction 31
3.2 Platform and Reef Stacking Patterns 31
3.3 Beaverhill Lake Group 34
3.4 Swan Hills Formation 36
3.5 Waterways Formation 38
3.6 Swan Hills Formation at the Snipe Lake Reef Complex 41
3.6.1 Previous Stratigraphic Studies 41
3.6.2 Stratigraphic Approach Used in This Study 48

4. LITHOFACIES ANALYSIS 50
4.1 Introduction 50
4.2 Lithofacies A: Peloid Packstones 54
4.2.1 Description 54
4.2.3 Interpretation 58
4.3 Lithofacies B: Robust Branching Cylindrical Stromatoporoid Rudstones 59
4.3.1 Description 59
4.3.2 Interpretation 59
4.4 Lithofacies C: Branching Cylindrical Stromatoporoid Floatstones 61
4.4.1 Description 61
4.4.2 Interpretation 63
4.5 Lithofacies D: Light Tan *Amphipora* Floatstones 64
4.5.1 Description 64
4.5.2 Interpretation 64
4.6 Lithofacies E: Dark Brown *Amphipora* Rudstones 66
4.6.1 Description 66
4.6.2 Interpretation 68
4.7 Lithofacies F: Stromatoporoid Floatstones to Rudstones 69
4.7.1 Description 69
4.7.2 Interpretation 71
4.8 Lithofacies G: Tabular Stromatoporoid Rudstones 72
4.8.1 Description 72
4.8.2 Interpretation 74
4.9 Lithofacies H: Thin Tabular Stromatoporoid Floatstones 74
4.9.1 Description 74
4.9.2 Interpretation 76
4.10 Lithofacies I: Skeletal Grainstones 77
4.10.1 Description 77
4.10.2 Interpretation 78
4.11 Lithofacies Associations 79
4.11.1 Reef Margin Associations 80
4.11.2 Lagoonal Associations 82

5. PLATFORM-REEF CYCLICITY 86

5.1 Introduction 86
5.2 Depositional Cycles 86
5.3 Third-order Reefal Cycles 87
5.4 Fourth-order Lagoonal Cycles 90
5.4.1 Correlation of Lagoonal Cycles 93
5.5 Platform and Reef Evolution (P4 to R0.5) 96
5.5.1 Megacycle P4 96
5.5.2 Megacycle P5 98
5.5.3 Megacycle R0.5 102

6. CEMENT PETROLOGY 105
6.1 Introduction 105
6.2 Diagenetic Environments 105
6.2.1 Marine Diagenetic Environment 107
6.2.2 Meteoric Diagenetic Environment 109
6.2.3 Burial Diagenetic Environment 111
6.3 Cement Petrography 112
6.3.1 Micrite 113
6.3.2 Isopachous Fibrous Calcite 113
6.3.3 Pendant Radiaxial Fibrous Calcite 117
6.3.4 Crystal Silt 120
6.3.5 Pendant Prismatic Calcite 120
6.3.6 Meniscus Blocky Calcite 124
6.3.7 Syntaxial Calcite Overgrowths 124
6.3.8 Isopachous Prismatic Calcite 126
6.3.9 Blocky-prismatic Calcite 126
6.3.10 Blocky Calcite Mosaics 126
6.3.11 Dolomite Rhombs 129
6.3.12 Saddle Dolomite 131
6.4 Paragenetic Sequence 131
6.4.1 Marine Cements in Primary Pores 131
6.4.2 Meteoric Cements 134
6.4.3 Marine Cements in Secondary Pores 137
6.4.4 Burial Cements 137
6.5 Stable Isotope Analysis 139
6.5.1 Stable Isotope Results 143
6.5.2 Stable Isotope Interpretations 144
6.6 Summary 150

7. SUBAERIAL EXPOSURE FEATURES 152
7.1 Introduction 152
7.2 Rhizoliths 152
7.2.1 Description 152
7.2.2 Interpretation 155
7.3 Pendant Cements 156
7.4 Green Shales 157
7.4.1 Description 157

7.4.2 Mineralogy 162
7.4.3 Interpretation 162
7.5 Laminar Calcretes 166
7.5.1 Description 166
7.5.2 Interpretation 168
7.6 Fitted-fabric Lithoclasts 169
7.6.1 Description 169
7.6.2 Interpretation 171
7.7 Glaebules 172
7.7.1 Description 172
7.7.2 Interpretation 174
7.8 Peds 175
7.8.1 Description 175
7.8.2 Interpretation 175
7.9 Stable Isotope Analysis 179
7.9.1 Results 180
7.9.2 Interpretations 180
7.10 Summary 184

8. PALEOSOLS 186
8.1 Introduction 186
8.2 Paleosols 186
8.3 P4 Subaerial Exposure Surface 191
8.4 R0.5 Subaerial Exposure Surface 191
8.5 Localized Exposure Surfaces 196
8.6 P5 Megacycle Contact 196
8.7 Types of Paleosol Profiles 196
8.7.1 Type A 197
8.7.2 Type B 197
8.7.3 Type C 199
8.7.4 Type D 200
8.8 Trends in Pedogenic Features 200
8.8.1 Distribution within Paleosols 200
8.8.2 Areal Distribution 201

9. DISCUSSION 207
9.1 Introduction 207
9.2 Autocyclic verus Allocyclic Controls on the P4 and R0.5 Subaerial Exposure Surfaces 207
9.3 Implications for Magnitude of Relative Sea Level Fall 209
9.4 Other Controlling Factors on the P4 and R0.5 Subaerial Exposure Surfaces 210
9.4.1 Climate 211
9.4.2 Topography 211
9.4.3 Vegetation and Organisms 212
9.4.4 Time 213
9.4.5 Substrate 214

9.4.6 Erosion 216
9.5 Local Subaerial Exposure Surfaces 217
9.6 Source of Siliciclastic Sediment 218
9.7 Effect on Reservoir Quality 219
9.8 P4 to R0.5 Evolution 221
9.9 Future Work 223

10. CONCLUSIONS 225
10.1 Lithofacies Analysis 225
10.2 Platform-Reef Cyclicity 228
10.3 Platform and Reef Megacycles (P4 to R0.5) 229
10.4 Paragenetic Sequence 231
10.5 Subaerial Exposure Features 233
10.6 Paleosols 235
10.7 Controls on the P4 and R0.5 Subaerial Exposure Surfaces 237
10.8 Localized Subaerial Exposure Surfaces 239
10.9 Effect on Reservoir Quality 239
10.10 Sea Level History (P4 to R0.5) 240

REFERENCES 241

LIST OF APPENDICES

APPENDIX A	**FORMATION AND MEGACYCLE TOPS USED IN THIS STUDY**	A1
APPENDIX B	**CORE DESCRIPTIONS**	B1
APPENDIX C	**DETAILED SUBAERIAL EXPOSURE PROFILE DESCRIPTIONS**	C1
APPENDIX D	**PETROGRAPHIC TECHNIQUES**	D1
	D.1 Staining Techniques for Carbonates	D1
	D.2 Diffused Plane-Polarized Light Method	D2
APPENDIX E	**THIN SECTION DESCRIPTIONS**	E1
APPENDIX F	**X-RAY POWDER DIFFRACTION METHODS AND RESULTS**	F1
	F.1 Bulk Mineralogy	F1
	F.2 Clay Mineralogy	F1
	F.3 Bulk and Clay Mineralogy Data	F6
APPENDIX G	**MEGACYCLE TOPS USED IN ISOPACH MAPS**	G1

LIST OF FIGURES

		page
Figure 1.1	Paleogeography of North America during the Devonian	4
Figure 1.2	Beaverhill Lake regional paleogeography	6
Figure 1.3	Stratigraphic correlation chart of the Beaverhill Lake Group	7
Figure 1.4	Paleogeography of the Swan Hills Complex	9
Figure 1.5	Location map of the Snipe Lake reef complex	11
Figure 2.1	Classification of limestones	18
Figure 2.2	Classification of porosity	19
Figure 2.3	Classification of stromatoporoids	21
Figure 2.4	Stromatoporoid paleoenvironments	21
Figure 2.5	Classification of cement morphologies	24
Figure 3.1	Cross-section of Devonian strata in the Alberta Basin	31
Figure 3.2	Reef and platform stacking styles in Devonian strata	32
Figure 3.3	Beaverhill Lake Group stratigraphic nomenclature	35
Figure 3.4	Beaverhill Lake depositional model by Wendte and Uyeno (2005)	40
Figure 3.5	Isopach map of the Swan Hills Formation, Snipe Lake reef complex	42
Figure 3.6	Snipe Lake reef complex depositional model by Fischbuch (1968)	43
Figure 3.7	Snipe Lake reef complex depositional model by Wendte and Muir (1995)	45
Figure 3.8	Snipe Lake reef complex depositional model used in this study	49
Figure 4.1	Paleobathymetric profile of the Snipe Lake platform succession	55

Figure 4.2 Paleobathymetric profile of the Snipe Lake reef successions 56

Figure 4.3 Lithofacies A: peloid packstones 57

Figure 4.4 Lithofacies B: robust branching cylindrical stromatoporoid rudstones 60

Figure 4.5 Lithofacies C: branching cylindrical stromatoporoid floatstones . 62

Figure 4.6 Lithofacies D: light tan *Amphipora* floatstones 65

Figure 4.7 Lithofacies E: dark brown *Amphipora* rudstones 67

Figure 4.8 Lithofacies F: stromatoporoid floatstones to rudstones 70

Figure 4.9 Lithofacies G: tabular stromatoporoid rudstones 73

Figure 4.10 Lithofacies H: thin tabular stromatoporoid floatstones 75

Figure 4.11 Lithofacies I: skeletal grainstones 78

Figure 5.1 Reefal cycle 88

Figure 5.2 Lagoonal cycle 91

Figure 5.3 Lagoonal cycle contacts 92

Figure 5.4 Lagoonal cycle correlations 94

Figure 5.5 P4 and P5 megacycle contacts 97

Figure 5.6 Depositional cycles in the platform-reef margin 99

Figure 5.7 Depositional cycles in the platform-reef interior 100

Figure 5.8 R0.5 megacycle contact 103

Figure 6.1 Diagenetic environments 106

Figure 6.2 Micrite cements 115

Figure 6.3 Isopachous fibrous calcite cements 116

Figure 6.4 Pendant radiaxial fibrous calcite cements 118

Figure 6.5 Crystal silt 121

Figure 6.6 Pendant prismatic calcite cements 122

Figure 6.7 Meniscus blocky calcite cements 125

Figure 6.8 Isopachous prismatic calcite cements 127

Figure 6.9 Blocky-prismatic calcite cements 128

Figure 6.10 Blocky calcite mosaics, dolomite rhombs and saddle dolomite cements 130

Figure 6.11 Paragenetic sequence 132

Figure 6.12 $\delta^{18}O$ and $\delta^{13}C$ plot for calcite and dolomite cements 141

Figure 6.13 $\delta^{18}O$ and $\delta^{13}C$ plot for saddle dolomite cements 142

Figure 7.1 Rhizoliths (core photographs) 153

Figure 7.2 Rhizoliths (photomicrographs) 154

Figure 7.3 Green shales (core photographs) 158

Figure 7.4 Green shales (photomicrographs) 159

Figure 7.5 Green shales in cracks and vugs 161

Figure 7.6 Green shale mineralogy at the P4 and R0.5 subaerial exposure surfaces in the Snipe Lake reef complex 163

Figure 7.7 Green shale mineralogy at the R0.5 subaerial exposure surface in the Judy Creek reef complex 164

Figure 7.8 Laminar calcretes 167

Figure 7.9 Fitted-fabric lithoclasts 170

Figure 7.10 Glaebules 173

Figure 7.11 Peds 176

Figure 7.12 $\delta^{18}O$ and $\delta^{13}C$ plot for subaerial exposure features 179

Figure 8.1 Location map and legend for cross-sections (D-D', E-E' and F-F') 187

Figure 8.2 Paleosol cross-section D-D' 188

Figure 8.3 Paleosol cross-section E-E' 189

Figure 8.4 Paleosol cross-section F-F' 190

Figure 8.5 P4 subaerial exposure surface 192

Figure 8.6 R0.5 subaerial exposure surface 194

Figure 8.7 Type paleosol profiles 198

Figure 8.8 Distribution map of pedogenic features below the P4 subaerial exposure surface 202

Figure 8.9 Distribution map of pedogenic features below the R0.5 subaerial exposure surface 203

Figure 8.10 P4 isopach map 205

Figure 8.11 R0.5 isopach map 206

Figure 9.1 Platform and reef evolution (P4 to R0.5) 222

LIST OF COPYRIGHTED MATERIAL

"Composite schematic cross-section across the Alberta Basin illustrating the cyclicity of Devonian successions and the distribution of their major facies." American Association of Petroleum Geologists, 1995, Memoir 63 – Unconformities and Porosity in Carbonate Strata. Page 32 in text.

"Stratigraphic cross-section of Beaverhill Lake strata from well 4-1-66-8W5 southwest through well 16-7-64-10W5, along the northeastern periphery of the isolated Judy Creek reef, into the center of the reef complex (well 4-35-63-11W5)." Bulletin of Canadian Petroleum Geology, 2005, v. 53. Page 40 in text.

"Megacycle-facies cross section across the windward side of the Snipe Lake reef platform and complex." American Association of Petroleum Geologists, 1995, Memoir 63 – Unconformities and Porosity in Carbonate Strata. Page 45 in text.

LIST OF TABLES

		page
Table 2.1	List of core examined in this study	16
Table 2.2	Size scale for crystalline sedimentary rocks	23
Table 4.1	Summary of lithofacies	51
Table 6.1	Summary of cement types	114
Table 6.2	$\delta^{18}O$ and $\delta^{13}C$ data for calcite and dolomite cements	140
Table 7.1	$\delta^{18}O$ and $\delta^{13}C$ data for subaerial exposure features	178
Table 8.1	Summary of subaerial exposure features below the P4 subaerial exposure surface	193
Table 8.2	Summary of diagenetic features below the R0.5 subaerial exposure surface	195

LIST OF OVERSIZED ENCLOSURES

Enclosure 1	Cross-section A-A'	Back pocket
Enclosure 2	Cross-section B-B'	Back pocket
Enclosure 3	Cross-section C-C'	Back pocket

CHAPTER 1 – INTRODUCTION

1.1 Prologue

Devonian strata of the Western Canada Sedimentary Basin (WCSB) are best known for the occurrence and preservation of reefs (Wendte, 1992a). These reef complexes are among the best-preserved examples of ancient reef systems in the world and are of prime economic importance. Devonian strata are host to an estimated 55% of recoverable conventional crude oil reserves and 27% of recoverable gas reserves in Western Canada (Podruski et al., 1988; Reinson et al., 1993).

Growth of Devonian reef complexes was strongly influenced by transgressions and regressions resulting in the formation of sedimentary cycles and intermittent subaerial exposure of platforms (e.g. Fischbuch, 1968; Wendte and Uyeno, 2005). Recognition of subaerial exposure surfaces in these reef complexes is important for investigations of facies patterns, sequence stratigraphy, paleoenvironmental reconstruction, diagenesis and reservoir potential (e.g. Wright, 1988; Vail et al., 1991; Moore, 2001). Karst and pedogenic processes associated with subaerial exposure surfaces can extensively modify the rock fabric, affecting both reservoir quality and pathway of fluid migration (e.g. Beach, 1995; Hurley et al., 1995; Wagner et al., 1995; Wendte and Muir, 1995; Moore, 2001). Previous studies have documented a number of subaerial exposure surfaces in reef complexes in the Upper Devonian Swan Hills Formation (e.g. Havard, 1974; Wong, 1978; Wendte and Muir, 1995, Chow and Wendte, 2004). However, in spite of their scientific and potential economic significance, such surfaces have not received adequate attention.

Characterization of the physical and chemical attributes of subaerial exposure surfaces will aid in the detection of more subtle exposure features in other reef complexes in the WCSB. Interpretation of subaerial exposure surfaces in the context of cycle-stacking patterns can be used to help evaluate and modify established sequence-stratigraphic models and reef paleogeography. This study uses an integrated approach combining stratigraphic, sedimentological and geochemical data obtained from detailed core and thin section analysis to understand the origin and implications of subaerial exposure surfaces within the Snipe Lake reef complex.

1.2 Previous Work

Devonian strata of the WCSB are host to many hydrocarbon pools and as a result the lithostratigraphic framework has been extensively documented (e.g. Burrowes and Krause, 1987; Moore, 1988; Moore, 1989; Campbell, 1992; Wendte, 1992a; Meijer Drees, 1994; Oldale and Munday, 1994; Potma et al., 2001, Wendte and Uyeno, 2005). The stratigraphy and sedimentology of the Beaverhill Lake Group and Swan Hills Formation have been well established by many authors through early studies of many of the isolated reef complexes (e.g. Fong, 1960; Murray, 1966; Fischbuch, 1968; Jenik and Lerbekmo, 1968; Leavitt and Fischbuch, 1968; Hemphill, 1975; Wendte and Stoakes, 1982; Wendte, 1992c). This work provided the framework for later studies which investigated the diagenetic history of Swan Hills Formation deposits using detailed petrographic and geochemical analyses (e.g. Wong, 1978; Viau, 1986; Kaufman et al., 1990; Walls and Burrowes, 1990; Duggan et al., 2001; Saller et al., 2001; Duggan, 2004). The majority of these studies was primarily concerned with the timing and mechanism of

dolomitization and its effects on reservoir quality. Subaerial exposure surfaces at the Snipe Lake reef complex were noted only in a few studies (e.g. Havard, 1974; Wendte and Muir, 1995), but the development of pedogenic features was not documented in detail. Few studies have provided detailed descriptions of paleosols in Swan Hills reef build-ups and addressed their implications for sea level history and platform-reef evolution (e.g. Chow and Wendte, 2004). Nonetheless, meteoric diagenesis and its associated pedogenic and karst features have been described extensively in other studies (e.g. Esteban and Klappa, 1983; Retallack, 1988, 2001; Blodgett, 1988; Ettensohn et al., 1988; Goldstein, 1991; Goldstein et al., 1991; Pelechaty and James, 1991; Milnes, 1992; Webb, 1994; Wright, 1994; Williams and Krause, 1998, 2000; Mora and Driese, 1999; Alonso-Zarza, 2003; Fu et al., 2004a, b).

1.3 Geologic Setting

1.3.1 Global Setting

The WCSB was situated along the western margin of the old Laurussia Continent during the Devonian Period (Heckel and Witzke, 1979; Witzke and Heckel, 1988). Paleolatitude reconstructions, integrating paleomagnetic, paleoclimatic, paleobiogeographic and tectonic data, position the WCSB in the Southern Hemisphere during most of the Devonian (Figure 1.1) (Heckel and Witzke, 1979; Witzke and Heckel, 1988). The reconstructions show Laurussia moving progressively north throughout Devonian time. This places the WCSB in the arid to semiarid, easterly trade wind belt during mid to late Devonian time. Devonian lithofacies summarized by Heckel and Witzke (1979) are consistent with extensive Elk Point evaporite deposits during the Middle Devonian and

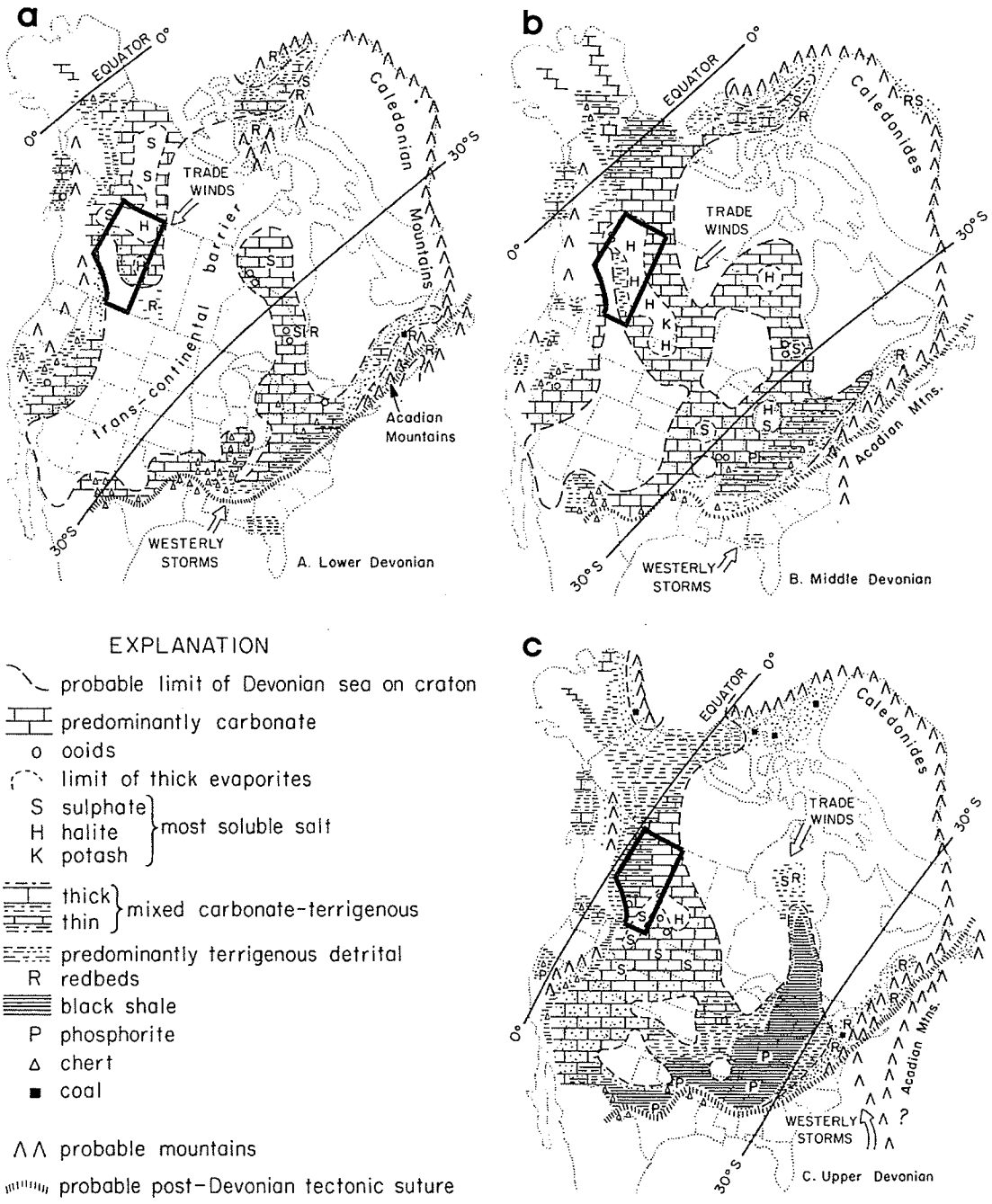


Figure 1.1 Interpreted paleogeography and generalized lithofacies of North America during the Devonian. Location of Alberta is outlined in red (modified from Heckel and Witzke, 1979). a) Lower Devonian (Gedinnian-Emsian) paleogeography map. b) Middle Devonian (Emsian-Givetian) paleogeography map shows extensive Elk Point evaporite deposits in the central Alberta Basin. c) Upper Devonian (Frasnian-Famennian) paleogeography map shows the return of the seas and inundation of the Alberta Basin with evaporite and open marine carbonate deposits. Figures a to c show progressive northward movement of Laurussia relative to the paleoequator during the Devonian.

restricted to open marine Beaverhill Lake carbonate deposits during the Late Devonian. Additional evidence for northeast to southwest water circulation that supports easterly trade winds in an arid tropical climatic belt is cited by Wendte (1992a).

1.3.2 Regional Setting

During Beaverhill Lake time the WCSB was covered by a broad epicontinental sea. Beaverhill Lake deposition was characterized by a transgressive reefal phase and a regressive basin-fill phase (e.g. Fischbuch, 1968; Oldale and Munday, 1994). Campbell (1992) and Oldale and Munday (1994) recognized six paleogeographic areas during Beaverhill Lake deposition; from north to south, they are the Horn River Basin, the Hay River Bank, the Peace River Arch Fringing Reef Complex, the Swan Hills Complex, the Waterways Basin and the Souris River Shelf (Figure 1.2). The Peace River Arch and West Alberta Ridge were paleotopographic high features that influenced Beaverhill Lake deposition. Stratigraphy of the Beaverhill Lake Group is summarized in Figure 1.3.

The following depositional history of the Swan Hills Complex is summarized from Murray (1966), Fishbuch (1968), Campbell (1992) and Oldale and Munday (1994). The Swan Hills Complex is located on the western margin of the Alberta Basin (Figures 1.2 and 1.3). It is flanked by the Western Alberta Ridge on the west and grades laterally into the Waterways Basin towards the north and east. The transgressive phase was initiated by a relative sea level rise during post-Elk Point time which resulted in marine inundation of the intracratonic Elk Point Basin. Initial relative sea level rise resulted in a brief period of restricted-marine, meso- to hypersaline conditions where argillaceous

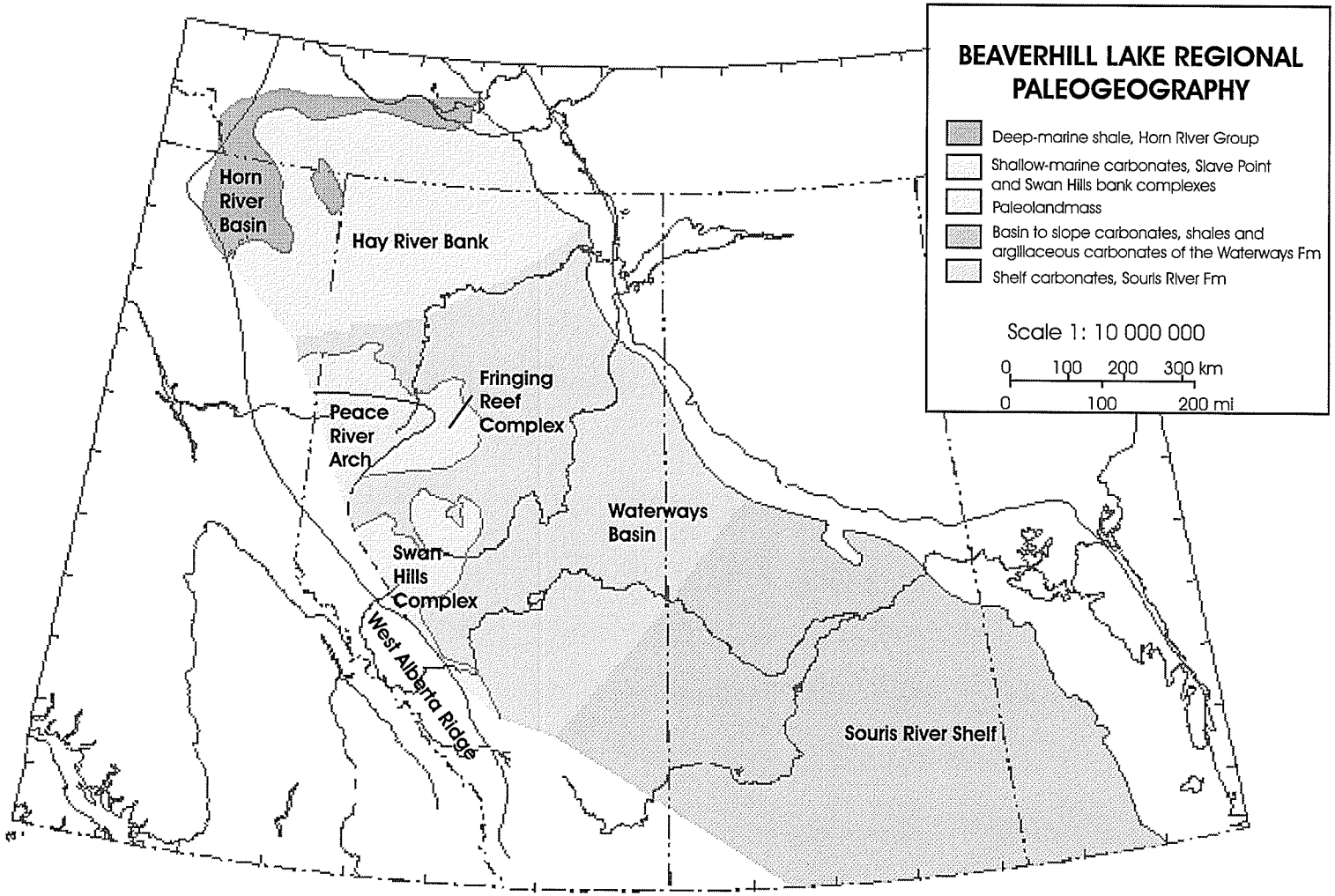


Figure 1.2 Beaverhill Lake regional paleogeography illustrating the six main paleogeographic areas (modified from Oldale and Munday, 1994).

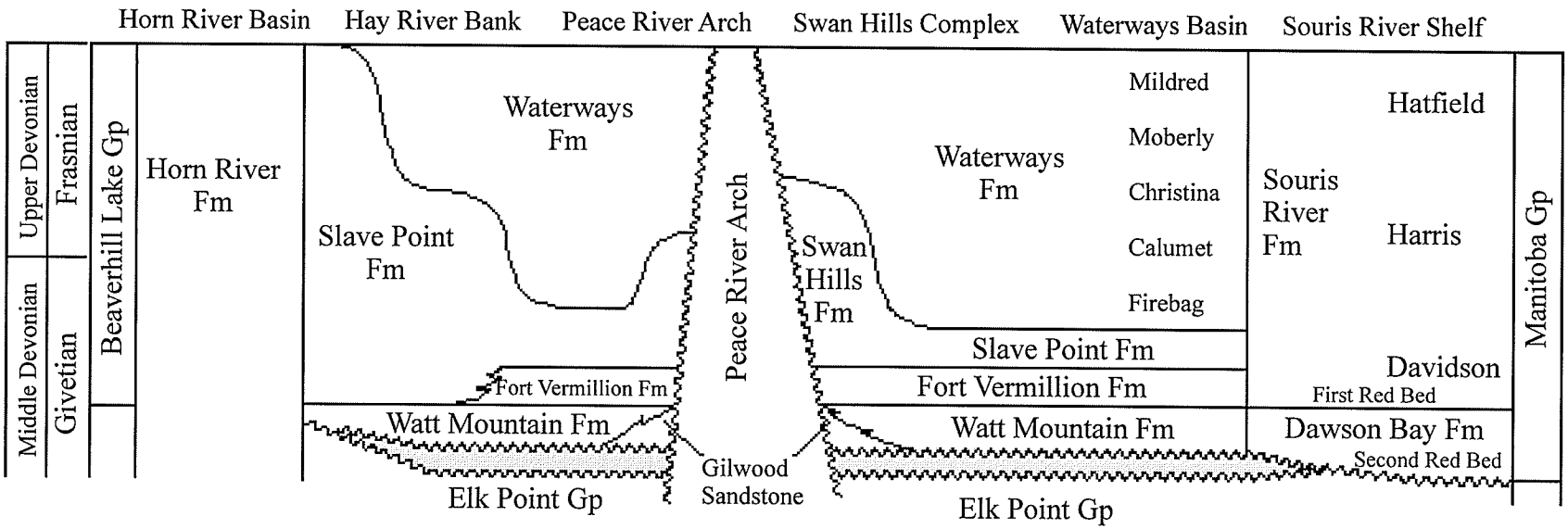


Figure 1.3 Correlation chart for the Middle and Upper Devonian strata of the Beaverhill Lake Group in the six paleogeographic areas in the WCSB (modified from Oldale and Munday, 1994).

carbonate rocks and evaporites of the Fort Vermillion Formation were deposited. Continued relative sea level rise created open marine conditions favorable for stromatoporoid growth and allowed for the first phase of reef-building activity in the Swan Hills Complex. An extensive carbonate platform developed in the Swan Hills area and in the basin (Slave Point Formation) with subsequent isolated reef buildups nucleating on backstepped platform highs. The Snipe Lake reef complex is one among many reefs in the Swan Hills Complex (Figure 1.4). The platform and isolated reef complexes are composed of a series of shallowing upward megacycles (discussed in Chapters 3 and 5). The regressive phase occurred during relative sea level fall or decreased rates in relative sea level rise. It is characterized by shales and argillaceous carbonate rocks of the Waterways Formation in basinal and interbank areas.

1.3.3 Snipe Lake Reef Complex

The Snipe Lake reef complex in the Swan Hills Formation in central Alberta is located 260 km northwest of Edmonton and covers an area approximately 22 km by 34 km (Figure 1.4; Havard and Oldershaw, 1976). It developed on the northwestern portion of an aerially extensive carbonate platform with the northeast side of the reef facing the prevailing northeasterly winds (Leavitt, 1966). The Swan Hills platform extends approximately 13 000 km^2 along the southwest margin of the Alberta Basin (I. Muir and others, unpublished data, 1988). Atoll-reef complexes, including the Snipe Lake reef complex, nucleated on paleotopographic highs of the underlying platform (e.g. Murray, 1966; Wendte and Stoakes, 1982; Wendte 1992c; Wendte and Muir, 1995).

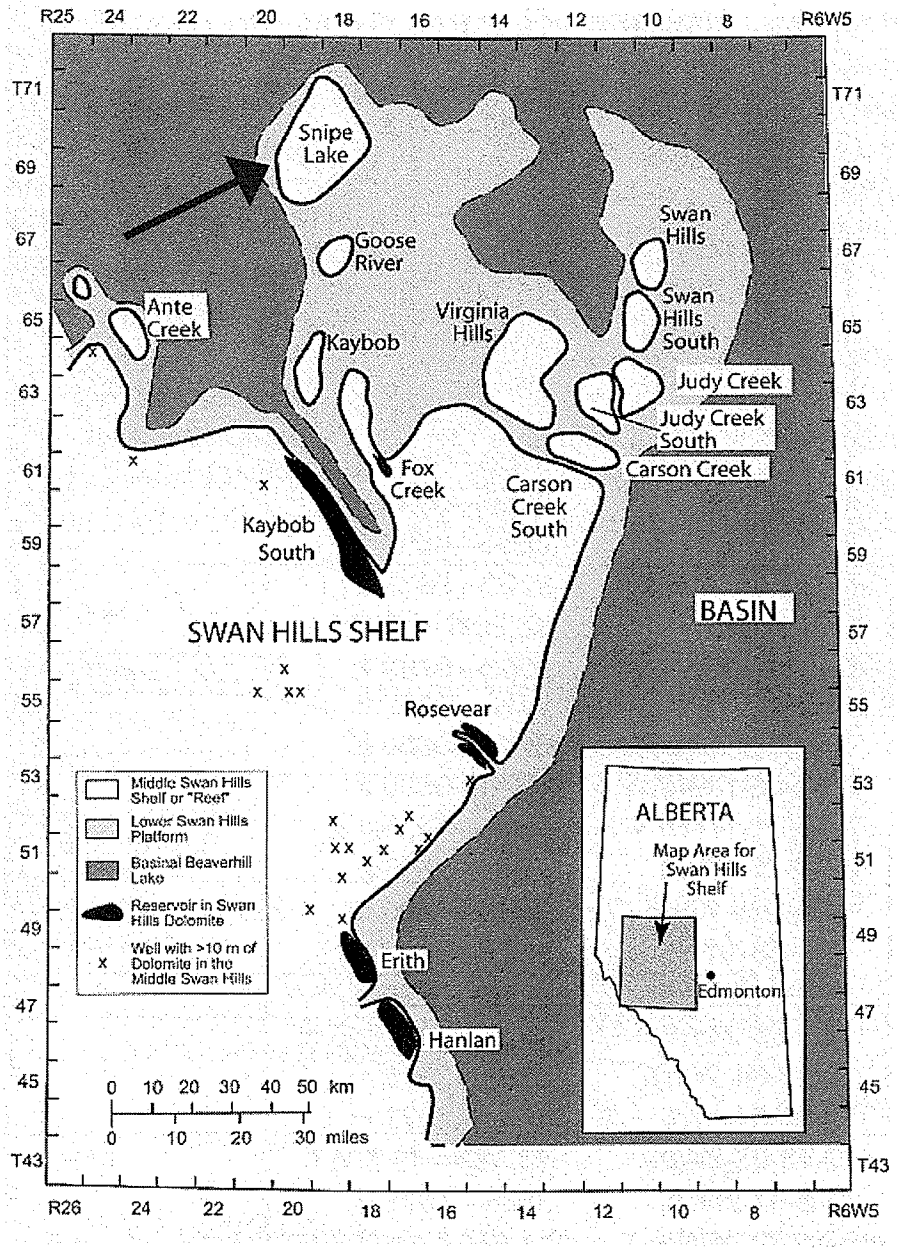


Figure 1.4 General paleogeography of the Swan Hills Complex in west-central Alberta (modified from Saller et al., 2001). Swan Hills isolated carbonate buildups developed on an underlying extensive carbonate platform. The Snipe Lake reef complex is located on the northwestern margin of the Swan Hills platform (arrow).

1.4 Snipe Lake Oil Field History

Production of the Snipe Lake BHL-A pool began in 1962 with the ACL SNIPELK 10-21-70-18W5 discovery well (Springate et al., 1992). Only the updip, eastern margin of the reef complex is oil prone covering an area of approximately 70 km^2. Production increased steadily from its initial discovery and peaked in the 1970's (I. Muir and others, unpublished data, 1988). Production rates started to decline by 1978 until 1985 when five infill wells were drilled. Water production was initially non-existent in the early stages of production but started to increase by 1975 and subsequently decreased in 1985 due to production from the infill wells. The gas-oil ratio increased steadily and peaked by the early 1980's but was reduced by water injection wells. The Snipe Lake BHL-A pool has an estimated oil-in-place volume of approximately 31.1 x 10^6 m^3 (Springate et al., 1992). Production as of April 2004 included 1.0 x 10^7 m^3 of oil, 6.1 x 10^8 m^3 of gas and 9.3 x 10^6 m^3 of water (IHS Accumap, accessed in April 2004).

1.5 This Study

1.5.1 Study Location

The study area in the Snipe Lake reef complex ranges approximately from Township 69 to 71 and Ranges 17 to 19W5 (Figure 1.5). The reef complex has a regional structural dip of 9 m per km towards the southwest and currently lies at a burial depth of approximately 2620 m (Springate et al., 1992). Fourteen wells were examined in this study (see Chapter 2); thirteen wells are located along the northeastern reef margin and one well is located in the reef interior. This study examines the strata from the P4 and P5 platform successions and the R0.5 reefal succession (see Chapter 3 for more details).

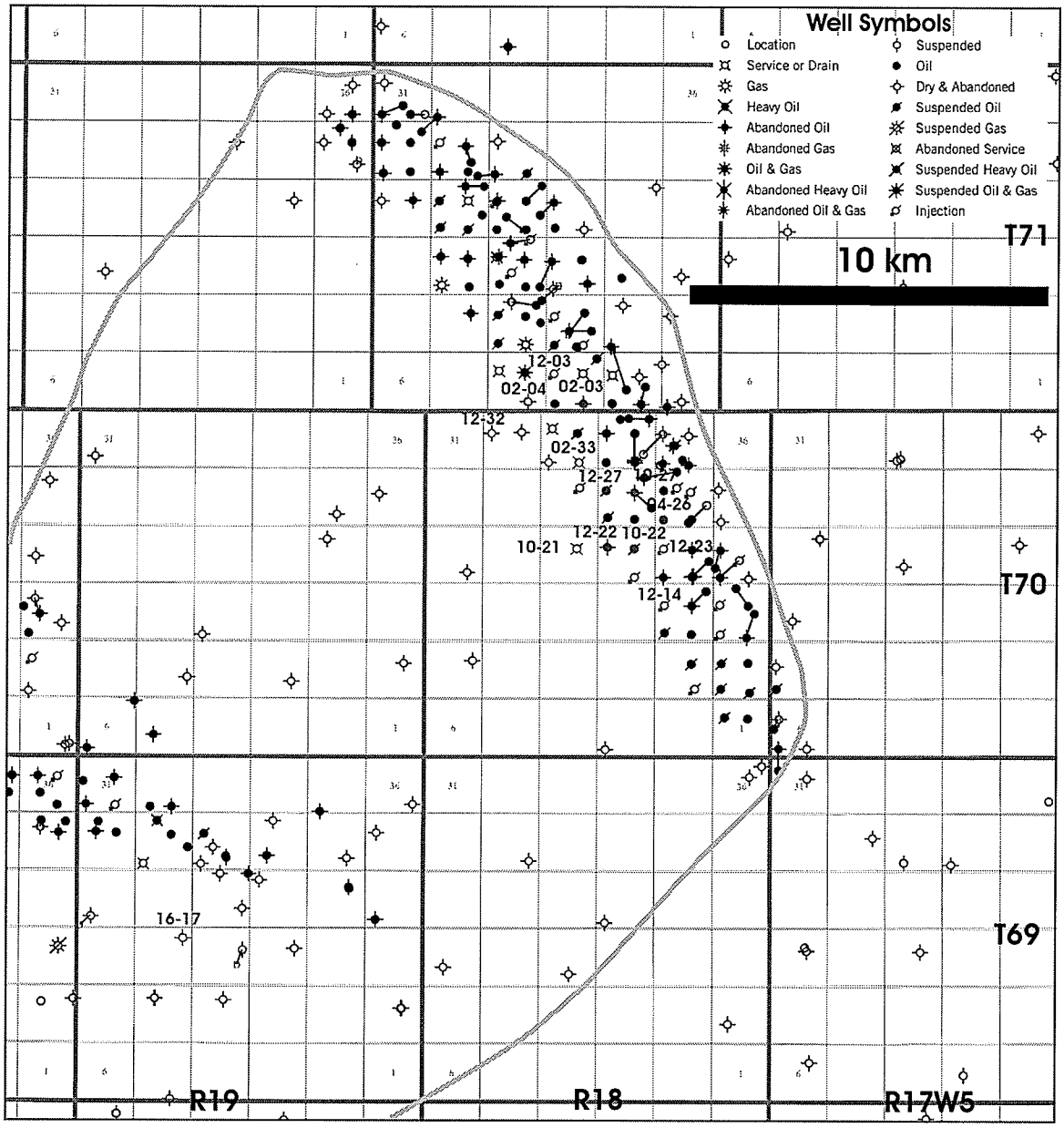


Figure 1.5 Location map of the study area showing the Snipe Lake reef complex and the location of wells (black and red) and approximate reef margin shown by the blue line (Havard, 1974). Wells examined in this study are highlighted in red and identified by their short UWI (unique well identifier) names.

1.5.2 Objectives of Study

The P4 to R0.5 successions of the Swan Hills Formation at the Snipe Lake reef complex were examined using an integrated approach that combines stratigraphy, lithofacies analysis, detailed petrography and geochemistry to accomplish the following objectives:

(1) To provide a stratigraphic and sedimentological analysis of the P4 to R0.5 successions in the Snipe Lake reef complex and in particular, to refine the stratigraphic correlations of third-order platform and reefal cycles and to develop a better understanding of smaller scale, fourth-order cyclicity within each succession.

(2) To provide adequate criteria for the recognition of subaerial exposure surfaces and paleosols in the Snipe Lake reef complex.

(3) To understand the controls and processes related to meteoric diagenesis and pedogenesis below subaerial exposure surfaces.

(4) To identify the role (if any) of meteoric diagenesis and paleosol development on reef reservoirs.

(5) To discuss the implications of subaerial exposure surfaces for sea level history and platform-reef evolution.

CHAPTER 2 - METHODOLOGY

2.1 Introduction

Data collection and analysis were completed in several phases: (1) detailed core examination and description; (2) conventional thin section petrography; (3) advanced thin section petrography and (4) geochemical and mineralogical analyses. Techniques used in this study are summarized in the following sections.

2.2 Selection of Wells

The Snipe Lake reef complex has excellent well control, in particular along the eastern margin of the reef complex (Figure 1.5). Fourteen wells were examined in this study and were selected based on several criteria. The first criterion was the penetration of petrophysical well log data and availability of core down to the P4 and R0.5 intervals. The second criterion was the presence of green shales at or near the P4 or R0.5 megacycle contacts because they were noted by some workers (e.g. J. Wendte, pers. comm., 2004) as potential indicators of subaerial exposure. The presence of green shales was inferred from well log responses; high clay content in green shales produces a notably higher gamma ray log response in comparison to limestones in the Swan Hills Formation. The third criterion was the occurrence of other interesting diagenetic features noted in previous studies by I. Muir and others (unpublished data, 1988) and J. Wendte (pers. comm., 2004). The last criterion was to include wells from the reef interior to the reef margin. Only one well (16-17-69-19W5) in the reef interior met the other requirements listed above and was selected.

2.3 Cross-section Construction

One cross-section, A-A' (Enclosure 1), was constructed using petrophysical well logs (gamma ray, spontaneous potential, sonic and resistivity) to illustrate reef geometry and reef cyclicity (megacycles) in the Swan Hills Formation in the Snipe Lake reef complex. Two additional cross-sections, B-B' (Enclosure 2) and C-C' (Enclosure 3), were constructed in greater detail showing only the interval between the P4 and R0.5 megacycle contacts. Lagoonal cycles (see section 5.4) and lithofacies contacts within each megacycle were correlated to illustrate the evolution of the reef complex at a more detailed scale within the reef interior and reef margin.

Megacycle contacts were correlated using petrophysical well log signatures (gamma ray, spontaneous potential, sonic and resistivity) and core examination based primarily on stratigraphic work completed by I. Muir and others (unpublished data, 1988) and later revisions by J. Wendte (pers. comm., 2004) (Appendix A). Lagoonal cycles and lithofacies correlations were based on detailed core examination and carbonate petrography completed in this study. Petrophysical well log signatures within each megacycle were not found to be particularly effective in correlating these smaller scale changes.

2.3.1 Datum

Two stratigraphic datums were used in this study: 1) the top of the Fort Vermillion Formation, and 2) the base of the Duvernay Formation. The Fort Vermillion Formation is characterized by restricted-marine conditions with widespread deposition of evaporites

and argillaceous dolostones and is interpreted to be indicative of deposition close to sea level (e.g. Oldale and Munday, 1994). Regional structure maps of the top of the Fort Vermillion Formation reveal no apparent anomalies (I. Muir and others, unpublished data, 1988). The upper contact is interpreted to be depositionally flat and a time-synchronous boundary. Therefore the top of the Fort Vermillion Formation is used as a stratigraphic datum where well penetration is deep enough (cross-section A-A', Enclosure 1). Similarly, Wendte and Muir (1995) used the top of the Fort Vermillion Formation as a datum in the Snipe Lake reef complex.

The Duvernay Formation, which overlies the Beaverhill Lake Group, is characterized by extensive basinal deposits of dark brown bituminous shales and limestones deposited throughout the WCSB (e.g. Switzer et al., 1994). The base of the Duvernay Formation marks an event of accelerated sea level rise which represents a time synchronous boundary. However, the base of the Duvernay Formation is not parallel to the inferred sea level and differential compaction can be problematic for regional correlations, but this effect is considered to be minimal within smaller scale studies (I. Muir and others, unpublished data, 1988). Therefore, it is used as a stratigraphic datum in this study where petrophysical well log data are not available down to the top of the Fort Vermillion Formation (cross-sections B-B' and C-C'). Wendte (1992c) and Wendte and Muir (1995) also used the base of the Duvernay Formation as a datum in the Judy Creek reef complex.

2.4 Core Examination

Fourteen wells and approximately 273 meters of core from the Snipe Lake reef complex were examined in this study (Table 2.1). The work was completed from May to August,

Table 2.1 Well locations and core intervals examined in this study at the Snipe Lake reef complex. Well status abbreviations, OIL = oil, WATER INJ = water injection, ABND = abandoned, SUSP = suspended, PUMP = pumping, ABNDWHP = abandoned and whipstocked.

WELL ID	WELL NAME	STATUS	LOGGED CORE INTERVAL			
			Bottom (ft)	Top (ft)	Total Feet	Total Meters
00/16-17-069-19W5/0	TEXCAN SUNSET 16-17-69-19W5	ABND	9004	8928	76.0	23.2
00/12-14-070-18W5/0	ACL SNIPELK 12-14-70-18W5	WATER INJ	8724	8628	96.0	29.3
00/10-21-070-18W5/0	ACL SNIPELK 10-21-70-18W5	WATER SUSP INJ	8800	8695	105.0	32.0
00/10-22-070-18W5/0	ACL SNIPELK 10-22-70-18W5	OIL PUMP	8735	8689	12.0	3.7
00/12-22-070-18W5/0	ACL SNIPELK 12-22-70-18W5	OIL SUSP	8761	8670	91.0	27.7
00/12-23-070-18W5/0	ACL SNIPELK 12-23-70-18W5	WATER INJ	8657	8576	81.0	24.7
00/04-26-070-18W5/0	ACL SNIPELK 4-26-70-18W5	OIL PUMP	8673	8581	92.0	28.0
00/10-27-070-18W5/0	ACL SNIPELK 10-27-70-18W5	OIL ABDWHP	8681	8672	31.0	9.4
00/12-27-070-18W5/0	ACL SNIPELK 12-27-70-18W5	OIL SUSP	8699	8630	69.0	21.0
00/12-32-070-18W5/0	MARATHON SNIPE LAKE 12-32-70-18W5	ABND	8603	8542	61.0	18.6
00/02-33-070-18W5/0	ACL SNIPELK 2-33-70-18W5	WATER SUSP INJ	8691	8630	61.0	18.6
00/02-03-071-18W5/0	ACL SNIPELK 2-3-71-18W5	OIL ABND	8651	8564	87.0	26.5
00/12-03-071-18W5/0	ACL SNIPELK 12-3-71-18W5	WATER INJ	8615	8611	20.5	6.2
00/02-04-071-18W5/0	POCO SNIPE IN 2-4-71-18W5	ABND	8545	8521	13.0	4.0
			TOTAL		**895.5**	**272.9**

2004 at the Core Research Centre at the Alberta Energy and Utilities Board in Calgary, Alberta. Petrophysical well logs were used to locate the interval of interest (P4 to R0.5) on the drill core and to correct core depth to log depth.

Slabbed drill cores of 8.9 cm (3½ inch) diameter were examined using a hand lens and a binocular microscope. Core pieces were etched with 20% hydrochloric acid and sprayed wet to enhance depositional and diagenetic textures. Core examination included descriptions of lithology, sedimentary structures, fauna, diagenetic fabrics and any other recognizable constituents (Appendix B). Detailed descriptions of exposure profiles were recorded at a finer scale (1:2.4) below the P4, R0.5 and occasionally below the P5 and R1 megacycle contacts (Appendix C). Drill core intervals were photographed and representative samples were taken from core for preparation into polished slabs, thin sections and for mineralogical and geochemical analysis.

2.4.1 Classification Schemes

Dunham's (1962) textural classification scheme as modified by Embry and Klovan (1971) was used to describe carbonate rocks in this study (Figure 2.1). Choquette and Pray's (1970) porosity classification scheme was used to describe porosity type and distribution (Figure 2.2).

Stromatoporoids are volumetrically the most abundant skeletal component in the Swan Hills Formation and in this study are classified according to their growth forms (e.g. Murray, 1966; Fischbuch, 1968). With the exception of *Amphipora* no attempt was made

<table>
<tr><td colspan="6">Allochthonous Limestone
Original components not organically bound during deposition</td><td colspan="3">Autochthonous Limestone
Original components organically bound during deposition</td></tr>
<tr><td colspan="4">Less than 10% >2 mm components</td><td colspan="2">Greater than 10% >2 mm components</td><td rowspan="2">By organisms that build a rigid framework</td><td rowspan="2">By organisms that encrust and bind</td><td rowspan="2">By organisms that act as baffles</td></tr>
<tr><td colspan="3">Contains lime mud (<0.03 mm)</td><td>No lime mud</td><td rowspan="3">Matrix-supported</td><td rowspan="3">Supported by grain components coarser than 2 mm</td></tr>
<tr><td colspan="2">Mud-supported</td><td colspan="2" rowspan="2">Grain-supported</td><td colspan="3">Boundstone</td></tr>
<tr><td>Less than 10% grains (>0.03 mm <2 mm)</td><td>Greater than 10% grains</td><td>Mudstone</td><td>Wackestone</td><td>Packstone</td><td>Grainstone</td><td>Floatstone</td><td>Rudstone</td><td>Framestone</td><td>Bindstone</td><td>Baffiestone</td></tr>
</table>

Figure 2.1 Dunham's (1962) classification scheme for limestones as modified by Embry and Klovan (1972).

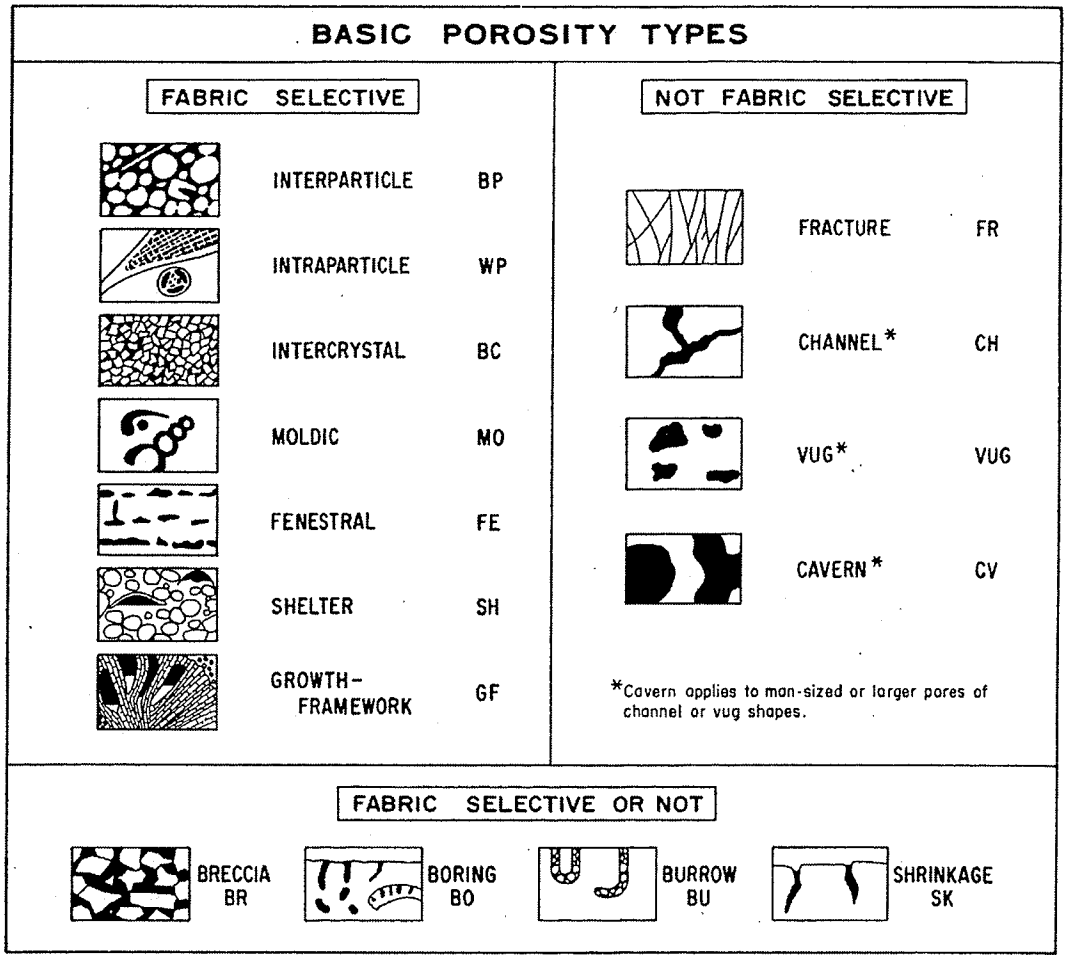


Figure 2.2 Geological classification of pores types and pore systems in carbonate rocks (modified from Choquette and Pray, 1970).

in this study to classify their genus or species. Morphological variations in stromatoporoid growth forms are interpreted to be at least partially environmentally controlled and therefore are useful in interpreting depositional environments of lithofacies (Figures 2.3 and 2.4) (e.g. Klovan, 1964; Murray, 1966; Fischbuch, 1968; Jenik and Lerbekmo, 1968; Abbott, 1973; Kobluk, 1975; James and Bourque, 1992; Kershaw, 1998). The stomatoporoid classification used in this study is as follows. Hemispherical or domical stromatoporoids have a flat base and convex upper surface that have arcuate laminae (Murray, 1966). They have a vertical to basal ratio (V/B) of 0.1-1.0 (Kershaw, 1998). Bulbous stromatoporoids include spherical and oblate, "golf-ball-like" forms that have a V/B ratio close to 1.0 and range from 2 to 8 cm in diameter (Murray, 1966; Kershaw, 1998). Nodular stromatoporoids are similar in shape to the bulbous forms but are <2 cm in diameter (J. Wendte, pers. comm., 2004). Tabular stromatoporoids are flat to slightly undulating, plate-like forms that have a V/B ratio of less than 0.1 and range from 2 to 4 cm thick (Murray, 1966; Jenik and Lerbekmo, 1968; Kershaw, 1998). Thin tabular stromatoporoids are also flat, plate-like forms that are 0.5-2.0 cm thick (J. Wendte, pers. comm., 2004). Branching cylindrical or dendroid stromatoporoids are irregularly branching forms that range from 4 mm to 2.0 cm in diameter (Murray, 1966; Jenik and Lerbekmo, 1968; Kershaw, 1998). *Amphipora* are small delicate stick-like forms that are 1 to 4 mm in diameter with an irregular pattern of canals or astrorhizae (Murray, 1966; Jenik and Lerbekmo, 1968; J. Wendte, pers. comm., 2004).

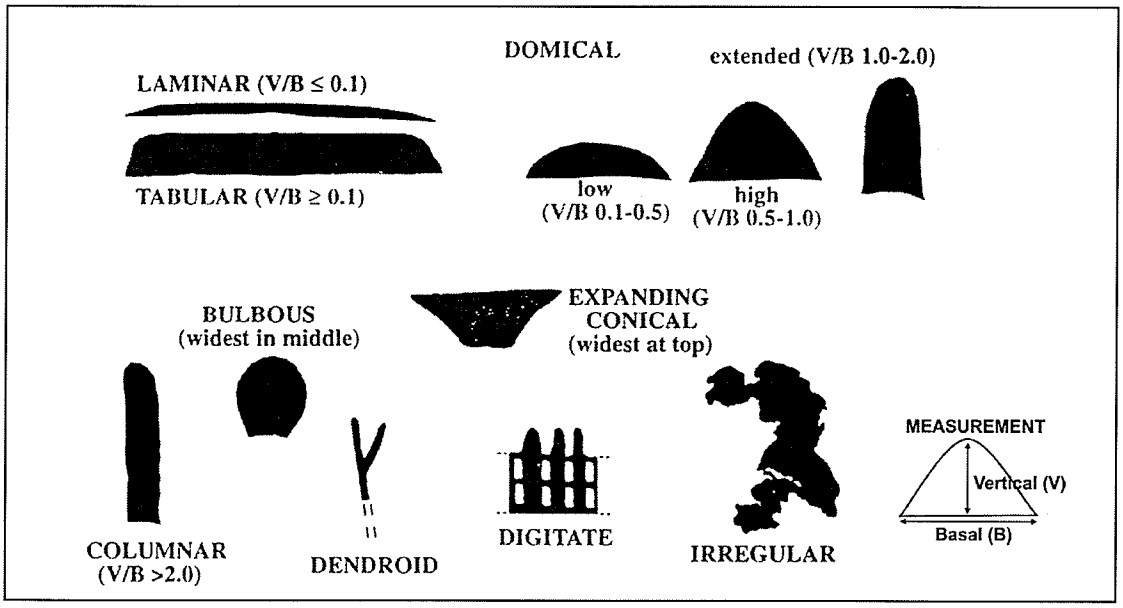


Figure 2.3 Classification of different morphologies of stromatoporoids according to their vertical to base (V/B) ratios (modified from Kershaw, 1998).

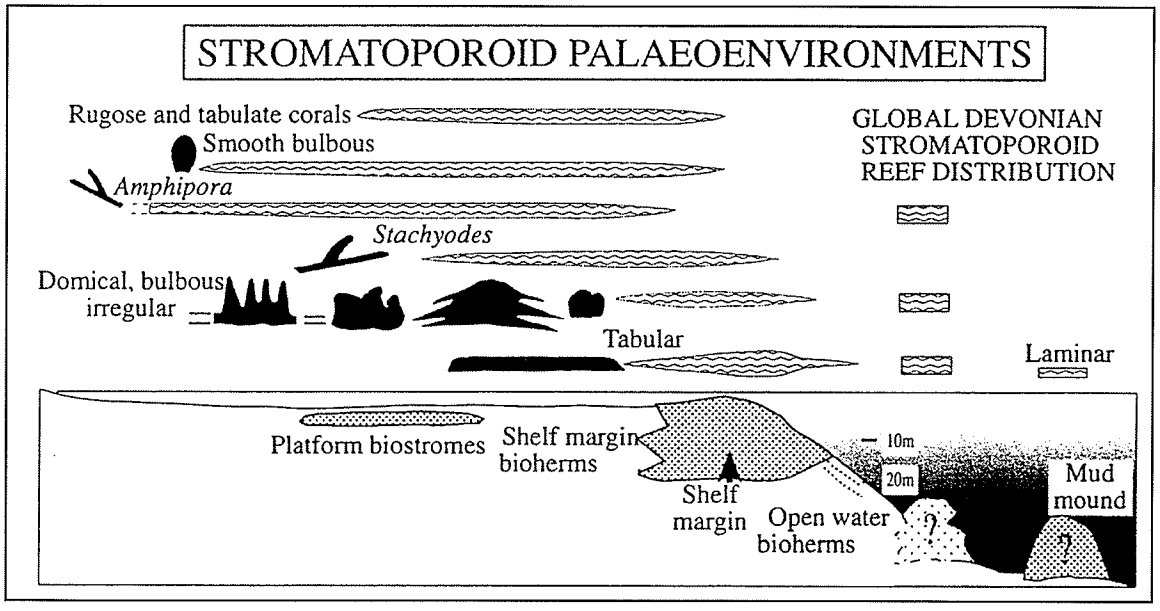


Figure 2.4 Distribution and paleoenvironments of stromatoporoid morphologies in Devonian reefs (modified from Kershaw, 1998).

2.5 Carbonate Petrography

Representative samples were taken from core and prepared into 5 cm x 7.5 cm thin-sections. Ninety-three thin-sections were prepared in total. Thin-sections were stained according to Dickson (1966), but using a solution of two parts Alizarin Red-S to three parts potassium ferricyanide (Appendix D.1). Alizarin Red-S was used to differentiate calcite from dolomite. Potassium ferricyanide was used to identify ferroan and non-ferroan carbonates. Samples were coated with Buehler Metcoat Specimen Protective Lacquer for better viewing under the microscope. Thin-sections were examined using a conventional Nikon OPTIPHOT-POL petrographic microscope under transmitted light, cross-polarized light and diffused plane-polarized light (Delgado, 1977; Dravis, 1991; Appendix D.2). Samples were also viewed under transmitted light using a binocular microscope. Photomicrographs were taken using a Nikon COOLPIX 4500 digital camera. Thin-sections were described in detail including the abundance and types of allochems, matrix, sedimentary structures, diagenetic fabrics and pedogenic features (Appendix E). Modal abundances (% volume) were visually estimated using comparison charts (Terry and Chilingar, 1955; Compton, 1985). Crystal sizes were described according to Folk (1962) (Table 2.2); crystal habits and cement morphologies were described according to terminology used by Choquette and James (1990) and James and Choquette (1990a; 1990b) (Figure 2.5).

Table 2.2 Crystal size scale for crystalline sedimentary rocks (after Folk, 1962).

Extremely coarsely crystalline	4 mm
Very coarsely crystalline	1 mm
Coarsely crystalline	0.25 mm
Medium crystalline	0.062 mm
Finely crystalline	0.016 mm
Very finely crystalline	0.004 mm
Aphanocrystalline	

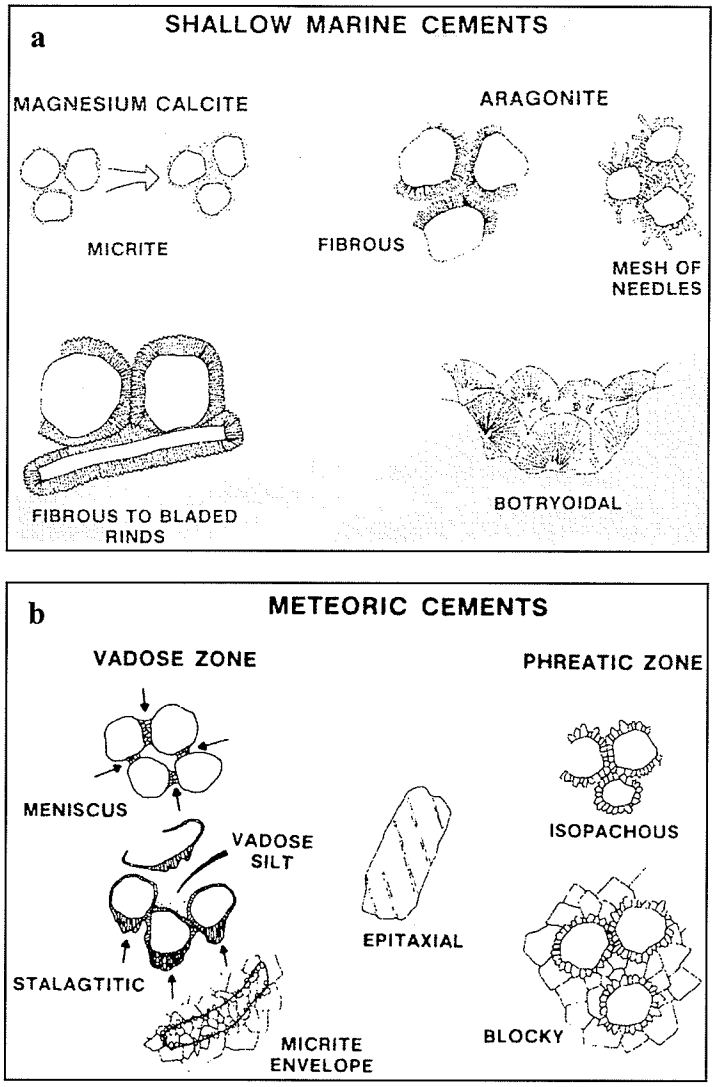


Figure 2.5 Types of cement morphologies. a) Modern sea-floor carbonate cements (modified from James and Choquette, 1990a). b) Cements precipitated in the meteoric diagenetic environment, vadose (left) and phreatic (right). Epitaxial cements can be precipitated in both zones (modified from James and Choquette, 1990b). c) Cements precipitated in the burial diagenetic environment, shown in plane light (left) and cathodoluminescence (right) (modified from Choquette and James, 1990).

2.6 Cathodoluminescence Microscopy

Seventeen selected thin-sections were viewed using cold cathodoluminescence microscopy to delineate zoning and for qualitative determination of minor and trace elements. Samples were viewed uncovered, unstained and polished for the best results (e.g. Pierson, 1981; Miller, 1988). Thin-sections were polished using cerium oxide 0.3 μm powder to remove the spray coating and staining (see section 2.5).

Cathodoluminescence was achieved using a Technosyn Cold Cathodoluminescence Model 8200 MkII operating with an accelerating voltage of 15-20 kV and a gun current ranging from 200-500 μA. The relative intensity of luminescence was estimated using visual comparisons between different types of cements viewed in this study (no standard reference specimen was used). Photomicrographs were taken using a Kodak MD290 digital camera.

2.7 Epi-fluorescence Microscopy

Epi-fluorescence microscopy was done on sixteen thin-sections to try to recognize depositional textures, delineate diagenetic fabrics, porosity and their relative timing that may not be visible using standard petrographic techniques. This technique requires no special sample preparation and thin-sections were viewed uncovered, unpolished, stained and unstained (Dravis and Yurewicz, 1985). To enhance the appearance of relict grains or fabrics, samples were exposed to fluorescence light for several minutes and often viewed using the modified white-card technique (Dravis, 1991; Appendix D.2).

Epi-fluorescence microscopy was achieved using a standard petrographic microscope (Nikon OPTIPHOT-POL) with a fluorescence attachment (Nikon OPTIPHOT LABOPHOT EPISCOPIC-FLUORESCENCE ATTACHMENT EF-D) and a mercury light source. Samples were viewed under violet and blue light excitor filters. The violet light filter (V-2A model) has an excitation wavelength of 380-425 nm and a barrier wavelength of 450 nm. The blue light filter (B-2A model) has an excitation wavelength of 450-490 nm and a barrier wavelength of 520 nm. Photomicrographs were taken using a Nikon COOLPIX 4500 digital camera.

2.8 Scanning Electron Microscopy

The scanning electron microscope (SEM) was used for semi-quantitative elemental analysis of different phases. Eight selected samples were examined using the SEM. Thin-sections were polished, as described in section 2.6, and were later carbon coated.

Scanning electron microscopy was done using a Cambridge Stereoscan 120 with the electron beam operating at an accelerating voltage of 20 kV. A backscattered electron (BSE) detector was used to obtain images to recognize different mineral phases present as represented by different levels of grey (Robinson and Nickel, 1979; Dilks and Graham, 1985; Trewin, 1988). An energy dispersive x-ray analysis system (EDAX Genesis Program) was used to collect emissions from a spot, a specific line or the whole screen area. EDAX was used to identify elemental composition in spot analysis with a spot size of 2 μm. EDAX line analysis was collected using 64-300 points/per line and dwell times ranging from 200-1000 milliseconds.

Backscattered electron and EDAX analysis did not detect any compositional differences or presence of minor and trace elements such as Mn, Sr and Na in any of the samples possibly because their concentrations were below the detection limit of backscattered electron analysis of approximately 1.0 wt ‰ (S. Mejia, pers. comm., 2005). Samples viewed under the SEM did not reveal any features that were not already visible under plane polarized light.

2.9 Electron Microprobe Analyses

One sample showing zoned luminescence (12-27-70-18W5 8651') was analyzed by electron microprobe for Ca, Mg, Mn, Fe and Sr. The thin-section was prepared by trimming it to 2.5 x 4.5 cm using a diamond saw, removing the spray coating and staining (see section 2.6), and was later carbon coated.

Microprobe analysis was conducted on a CAMECA SX 100 with an accelerating voltage of 15kV and an electron beam of 1 μm diameter. Backscattered electron (BSE) images of atomic number contrast images were used to navigate the electron beam to the desired locations. EDAX data were obtained using PGT Excalibur 4.03.10 software to collect semi-quantitative data at several locations. Minor and trace elements were determined from the presence of peaks on the EDAX spectrum (Fairchild et al., 1988).

Similar to the backscattered electron analysis, no compositional differences in minor or trace elements (Mg, Mn, Fe, Sr) were detected in the sample. This is interpreted to be attributed to concentrations below the detection limit of 250 to 300 ppm (S. Mejia, pers.

comm., 2005).

2.10 Stable Isotope Analyses

Thirty-six samples were collected and analyzed for stable carbon ($\delta^{13}C$) and oxygen ($\delta^{18}O$) isotopes. Microsampling of polished slabs of thin-section offcuts (Prezbindowski, 1980) was used to collect different types of cements, in particular early cements and other possible pedogenic features. The polished slabs were viewed under a binocular microscope for increased accuracy and powdered samples (sample weights 0.40-5.2 mg) were collected manually using a hand drill (5 HP ¼ carbide drill bit).

Collection of samples was completed at the University of Manitoba and sent to the Stable Isotope Laboratory in the Department of Earth Sciences at the University of Windsor for analyses. $\delta^{13}C$ and $\delta^{18}O$ values were obtained using acid reactions for samples containing pure calcite or dolomite phases and selective acid extraction was used for samples containing more than one carbonate phase (McCrea, 1950; Al-Aasm et al., 1990); details are provided below. Isotopic compositions of calcite and dolomite samples were collected with a ThermoFinnigan Delta Plus IRMS using multiports (M. Price, pers. comm., 2005). Isotopic values are reported with respect to SMOW (oxygen) and VPDB (oxygen and carbon) and are precise to 0.01-0.03‰.

Samples were reacted with 100% phosphoric acid and CO_2 was extracted for analysis following procedures described by Al-Aasm et al. (1990). CO_2 was collected for pure calcite samples after a 2-hour reaction at 25°C. CO_2 was collected for pure dolomite

samples after a 4-hour reaction at 50°C. Isotope analysis was completed on mixed carbonate (calcite and dolomite) samples using selective extraction. Samples were reacted at 25°C, and after 2 hours CO_2 was collected and analyzed for calcite. The calcite reaction was allowed to continue to completion for 24 hours and the CO_2 was discarded. The sample was then reacted at 50°C for 4 hours and CO_2 was analyzed for dolomite. When only small sample sizes were available (<15 μmol) a coldfinger device was used to trap and freeze CO_2 gas before it was released to the mass spectrometer (M. Price, pers. comm., 2005). Freezing causes the CO_2 gas to expand which allows for higher pressure and more accurate measurements.

2.11 X-ray Diffraction Analyses

Green shale samples were analyzed for bulk and clay mineralogy using X-ray powder diffraction (XRD). Eight green shales occurring at the P4 and R0.5 megacycle contacts at Snipe Lake were collected from core for mineralogical analyses and six samples of P4 and R0.5 basinal shale equivalents (J. Wendte, pers. comm., 2005) were also collected for comparison. Fourteen unoriented smear mounts were prepared for whole rock or bulk mineralogy analysis and fourteen oriented smear mounts were prepared for clay mineralogy analysis (Drever, 1973; Last, 2001; see Appendix F for detailed procedures).

X-ray diffraction analysis was achieved using a Philips PW1710 Powder Diffractometer using copper-α radiation and a Phillips PW3840 generator with operating conditions of 40 kV and 40 mA. Data were collected using MDI DataScan 3.2 software. Unoriented smear mounts were analyzed and bulk mineralogy was determined using a search/match

program MDI Jade 6.2 XRD Pattern Processing Software (Appendix F.1). Oriented smear mounts were analyzed three times: the first XRD scan was done on an untreated smear mount, a second XRD scan after the slide was glycolated, and a third XRD scan after the slide was heated (Appendix F.2.2). Qualitative identification of clay minerals was achieved by comparing diffraction patterns of the samples to a set of standard patterns (Carroll, 1970; Last, 2001; Appendix F.2.3). Semi-quantitative calculations of the relative abundances of the major clay mineral groups (expandable clay minerals, kaolinite, chlorite and illite) were determined by using a weighted peak area method (Johns et al., 1954; Last, 2001; Appendix F.2.4).

CHAPTER 3 – BEAVERHILL LAKE GROUP STRATIGRAPHY

3.1 Introduction

Devonian strata in the Alberta Basin can be divided into six major first-order cycles: Lower Elk Point, Upper Elk Point, Beaverhill Lake, Woodbend, Winterburn and Wabamun successions (Wendte, 1992b, Figure 3.1). These cycles generally coincide with group or subgroup-level stratigraphy summarized by Meijer Drees (1994), Oldale and Munday (1994) and Switzer et al. (1994). Each succession shows major shifts in facies belts that represent large-scale transgressive-regressive sequences (Wendte, 1992b). The transgressive portion of these cycles is expressed by a landward shift of shallow water facies, whereas the regressive portion of these cycles is expressed by a basinward shift of shallow water facies. First-order cycles are controlled by allocyclic (external) processes such as eustatic sea level rise and basin uplift/subsidence.

3.2 Platform and Reef Stacking Patterns

Four major stacking styles in platform and reef complexes are recognized in Devonian strata (Wendte, 1992b): backstepping, retreating, upstepping and forestepping (Figure 3.2). Backstepping and retreating stacking styles involve the movement and reestablishment of facies towards the platform interior. They are a result of the rate of relative sea level rise outpacing the rate of sedimentation or carbonate production (e.g. James and Bourque, 1992; Jones and Desrochers, 1992). Backstepping involves a lateral separation of platform-margin facies between cycles, whereas retreating does not. An upstepping reef or platform involves the vertical stacking of platform-margin facies

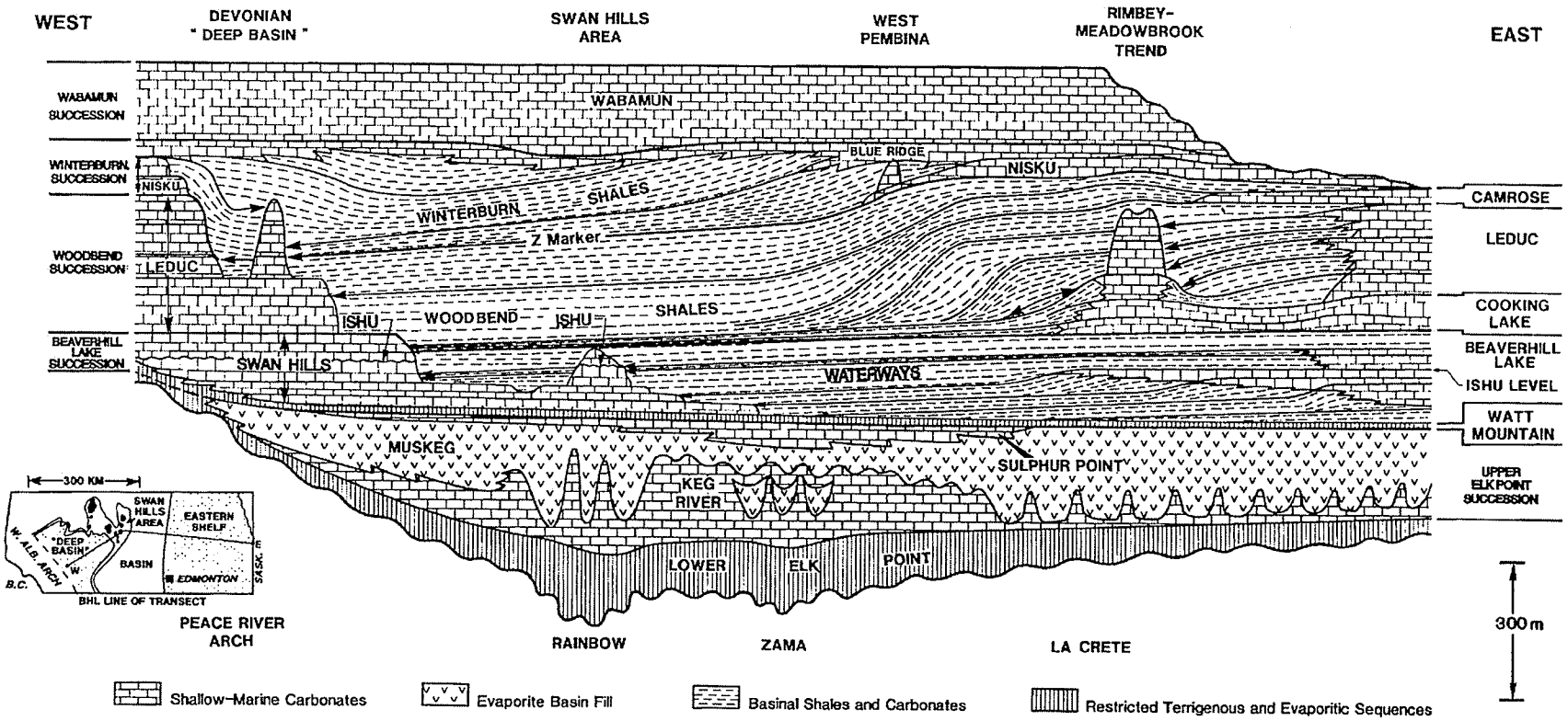


Figure 3.1 Cross-section of Devonian strata across the Alberta Basin illustrating six major first-order cycles (from Wendte and Muir, 1995, reprinted by permission of the AAPG whose permission is required for further use). ISHU = Intraformational Swan Hills Unconformity; now referred to in this study as R4 megacycle contact.

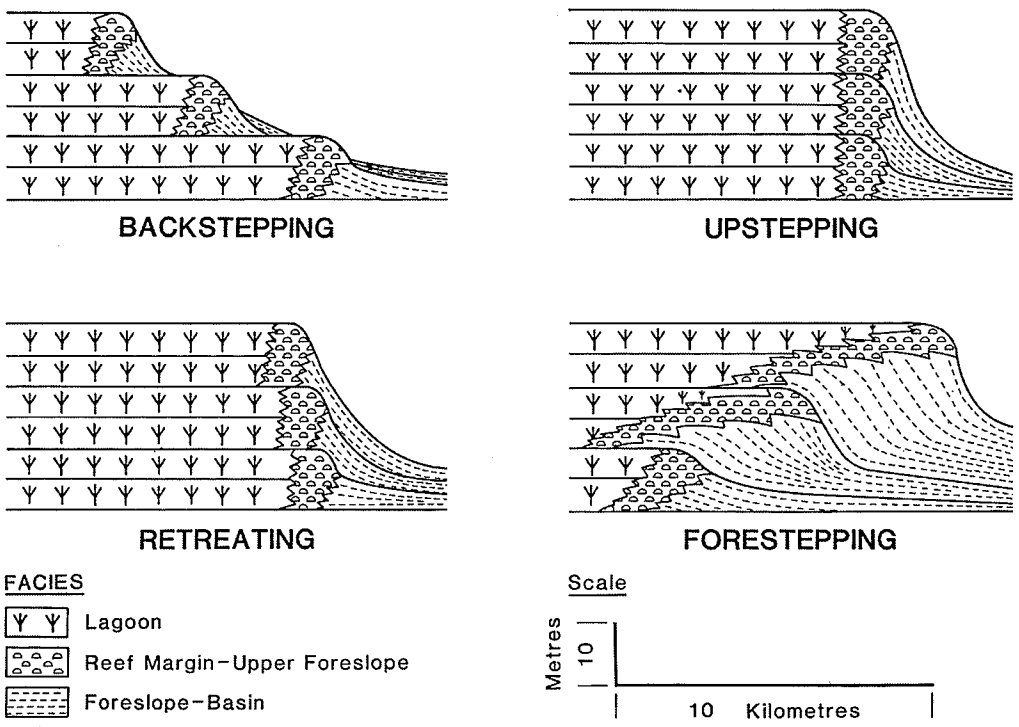


Figure 3.2 Four major reef and platform stacking styles recognized in Devonian strata in the Alberta Basin (from Wendte, 1992b).

and is a result of sedimentation or carbonate production that just barely matched the rate of relative sea level rise (e.g. James and Bourque, 1992; Jones and Desrochers, 1992). A forestepping reef or platform style involves a basinal shift in facies belts where there is often a lateral separation of platform-margin facies between growth cycles. This growth style occurred when sedimentation or carbonate production exceeded the rates of relative sea level rise (e.g. James and Bourque, 1992; Jones and Desrochers, 1992).

3.3 Beaverhill Lake Group

Middle to Upper Devonian strata were first defined as the Beaverhill Lake Group in the Alberta Basin by Leavitt and Fischbuch (1968). They redefined the Beaverhill Lake Formation, as defined by Fong (1959, 1960), to include the underlying Fort Vermillion Formation and raised it to group status (Figure 3.3). Similarly, the Swan Hills Member, as defined by Fong (1959, 1960) and Murray (1966), was raised to formation status. The lower boundary of the Beaverhill Lake Group is variably defined throughout the literature. Murray (1966), Fischbuch (1968), Leavitt and Fischbuch (1968) and Wendte and Uyeno (2005) have placed the division at the base of the Fort Vermillion Formation. In contrast, Campbell (1992) and Oldale and Munday (1994) have included the Watt Mountain Formation and the Fort Vermillion Formation in the Beaverhill Lake Group (Figure 3.3). For the purpose of this study, the latter scheme has been adopted.

In the Swan Hills area the Beaverhill Lake Group (Upper Givetian to Lower Frasnian) is composed of, in ascending order, the Watt Mountain Formation, the Fort Vermillion Formation, the Swan Hills Formation and the Waterways Formation (Figure 3.3)

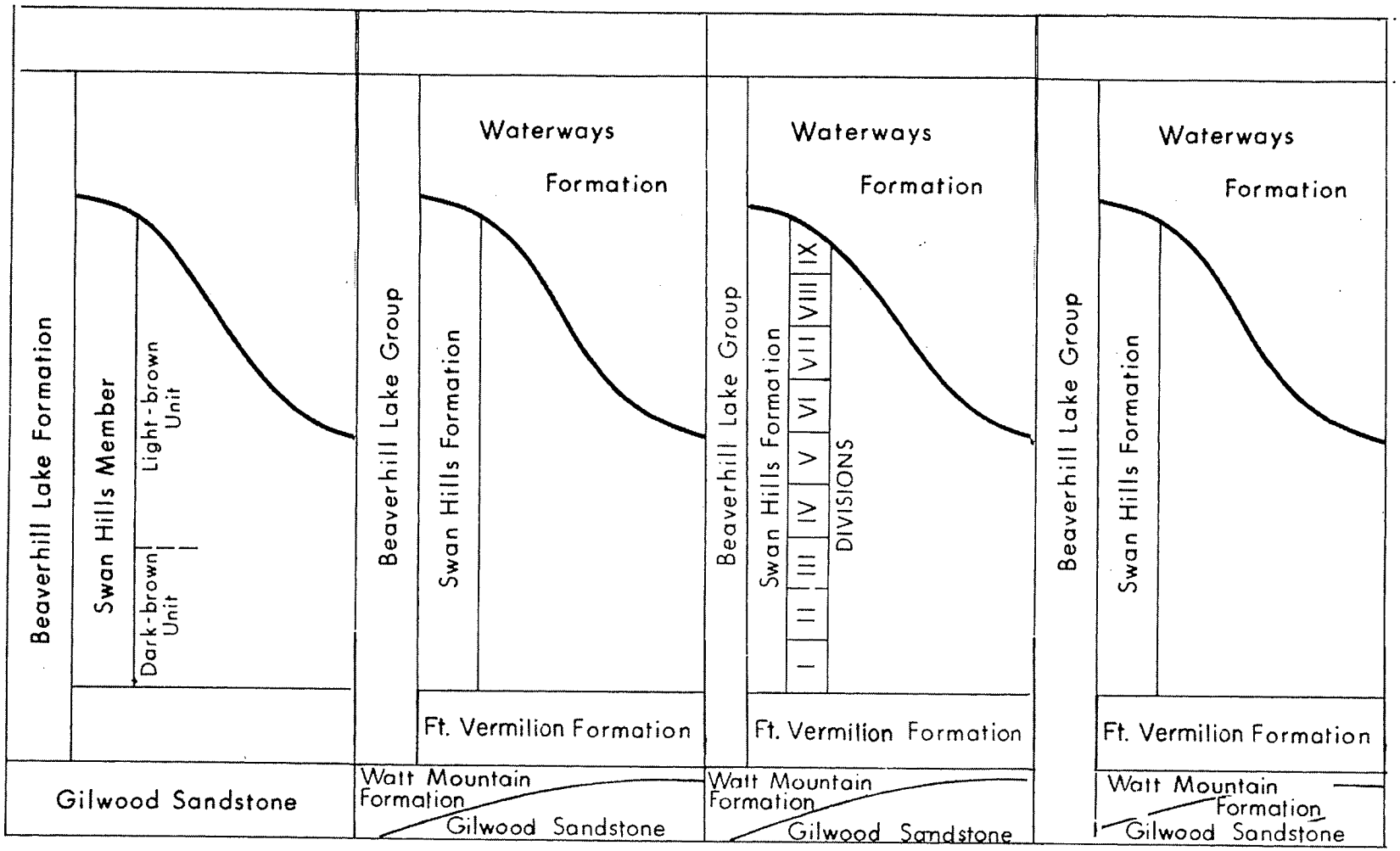


Figure 3.3 Stratigraphic nomenclature of the Beaverhill Lake Group in the Swan Hills Area (modified from Fischbuch, 1968; Campbell, 1992)

(Campbell, 1992; Oldale and Munday, 1994). Together these units were interpreted to represent a complete first-order transgressive-regressive cycle (Campbell, 1992). The post-Elk Point unconformity marks the lower boundary of the Beaverhill Lake Group (Figure 1.3), and the Woodbend Group conformably to disconformably overlies the Beaverhill Lake Group (Figure 3.1; Oldale and Munday, 1994).

A sequence stratigraphic study by Wendte and Uyeno (2005) re-defined the order of transgressive-regressive cycles in Beaverhill Lake strata. The first-order cycle extends from the base of the sub-Watt Mountain subaerial unconformity to the lower part of the Cooking Lake or Leduc formations (Figure 3.1). Two second-order cycles were defined within this interval; the lower second-order cycle extends from the base of the Watt Mountain Formation to the R4 or Upper C subaerial unconformity in the Swan Hills Formation (see section 3.6), and the upper second-order cycle extends from this subaerial unconformity to the top of the lower Cooking Lake or Leduc formations. Third-order cycles were also recognized but are discussed later in sections 3.4 and 3.6.1.

3.4 Swan Hills Formation

The Swan Hills Formation is the uppermost unit of the transgressive, shallow open-marine phase of the Beaverhill Lake Group (Figure 3.3). It conformably overlies an interbedded succession approximately 3 to 12 m thick of anhydrites and calcareous shales of the Fort Vermillion Formation (Fischbuch, 1968; Leavitt and Fischbuch, 1968; Fischbuch and Havard, 1977). The basal portion of the Swan Hills Formation, known as the Swan Hills carbonate platform, is correlative with the Slave Point Formation platform

in the Waterways Basin (Figure 1.3). The Swan Hills Formation in the northwestern portion of the Swan Hills Complex is correlative with the fringing reef complex of the Slave Point Formation which terminates against and onlaps the Peace River Arch (Leavitt and Fischbuch, 1968; Hemphill et al., 1975; Oldale and Munday, 1994). Further north in the Swan Hills Complex, the Swan Hills Formation is correlative with the extensive bank complex (Slave Point Formation) developed in the Hay River Bank.

The Swan Hills Formation is characterized by open marine carbonates, mostly limestones with locally dolomitized areas (e.g. Leavitt and Fischbuch, 1968). The succession in the Swan Hills area is composed of lithologies ranging from high energy, reef margin facies in which stromatoporoids are the dominant organic frame builders to low energy, muddy reef interior or lagoonal facies (e.g. Murray, 1966; Fishbuch, 1968; Wendte and Stoakes, 1982; Wendte, 1992c; Wendte and Muir, 1995). Swan Hills carbonate deposits extend throughout the Alberta Basin covering over 18, 000 km^2 (7000 mi^2; Figure 1.4) and range up to a maximum thickness of 152 m thick in the Virginia Hills reef (e.g. Fong, 1960; Fischbuch, 1968; Leavitt and Fischbuch, 1968; Fischbuch and Havard, 1977). Platform successions are generally thicker towards the east, away from the subsiding western edge of the Alberta Basin (e.g. Wendte and Muir, 1995). Within each reef complex, the formation is thickest near the center and towards the southwest side of the buildup (e.g. Fishbuch, 1968).

The Swan Hills Formation was initially subdivided into two members: a lower Dark

Brown member and an upper Light Brown Member (Figure 3.3; e.g. Fong, 1959, 1960; Jenik and Lerbekmo, 1968; Hemphill et al., 1975). Leavitt and Fischbuch (1968) noted that the subdivisions could not be separated throughout the whole Swan Hills area and therefore did not recognize them as formal subdivisions of the Swan Hills Formation. Murray (1966) recognized nine informal stratigraphic units in the Swan Hills Formation at the Judy Creek reef complex that corresponded to major rock types and depositional environments. Similarly, Fischbuch (1968) recognized nine separate stages of growth in Swan Hill reef complexes and they were designated, from bottom to top, Divisions I to IX (Figure 3.3). Each division represents a separate stage of reef growth and is composed of several distinct facies that were terminated by a relative sea level fall. Studies by Wendte and Stoakes (1982), Springate et al. (1992), Wendte (1992a) and Wendte and Muir (1995) have recognized second-order depositional sequences (each 10-30 m thick) in the Swan Hills Formation that can be correlated throughout the Judy Creek and Snipe Lake reef complexes. These sequences are recognized based on the natural cyclicity of the reef complexes and differ from growth stages defined by Fischbuch (1968). The depositional sequences recognized by Wendte and Muir (1995) were later re-defined by Wendte and Uyeno (2005) as third-order transgressive-regressive cycles.

3.5 Waterways Formation

The Waterways Formation is composed of calcareous shales and argillaceous lime mudstones that were deposited in a basin to slope environment (e.g. Sheasby, 1971; Hemphill et al., 1975; Oldale and Munday, 1994; Wendte and Uyeno, 2005). It is characterized by a series of shallowing-upward cycles and is approximately 225 m thick

at its type section in the Bear Biltmore 7-11-87-17W4M well (Hemphill et al., 1975). In the northern and eastern portion of the Swan Hills Complex, the Swan Hills Formation intertongues with and is overlain by the Waterways Formation (e.g. Wendte and Stoakes, 1982; Wendte, 1992c; Wendte and Muir, 1995). Correlation of the open marine carbonate platform and reef deposits of the Swan Hills Formation with the Waterways Formation has been debated throughout the literature. Some workers observed an onlap/downlap relationship between the Swan Hills and Waterways formations, and therefore they did not consider the formations to be contemporaneous deposits (e.g. Sheasby, 1971; Wendte and Stoakes, 1982; Oldale and Munday, 1994). Other authors have observed that Swan Hill Formation limestones "intertongue" with basinal shales and the two units have similar fauna. Therefore, the Waterways Formation is at least in part correlative with the Swan Hill Formation, but correlations have proven to be difficult (e.g. Fischbuch, 1968; Leavitt and Fischbuch, 1968; Hemphill, 1975; Springate et al., 1992; Wendte 1992c; Wendte and Muir, 1995). Some authors have interpreted the argillaceous outer ramp and ramp interior carbonate deposits of the Waterways Formation to be time-equivalent to the Swan Hills reef complexes (e.g. Potma et al., 2001). The most recent work by Wendte and Uyeno (2005) identified 14 third-order sequences and used conodont biostratigraphy to correlate calcareous shales and argillaceous limestones of the Waterways Formation to reef-equivalent strata or related events (Figure 3.4). They determined that basinal successions have bank or reef-equivalent strata during intervals of rising base level, whereas basinal successions are interpreted to be correlative to subaerial unconformities on the banks and reefs during periods of falling base level.

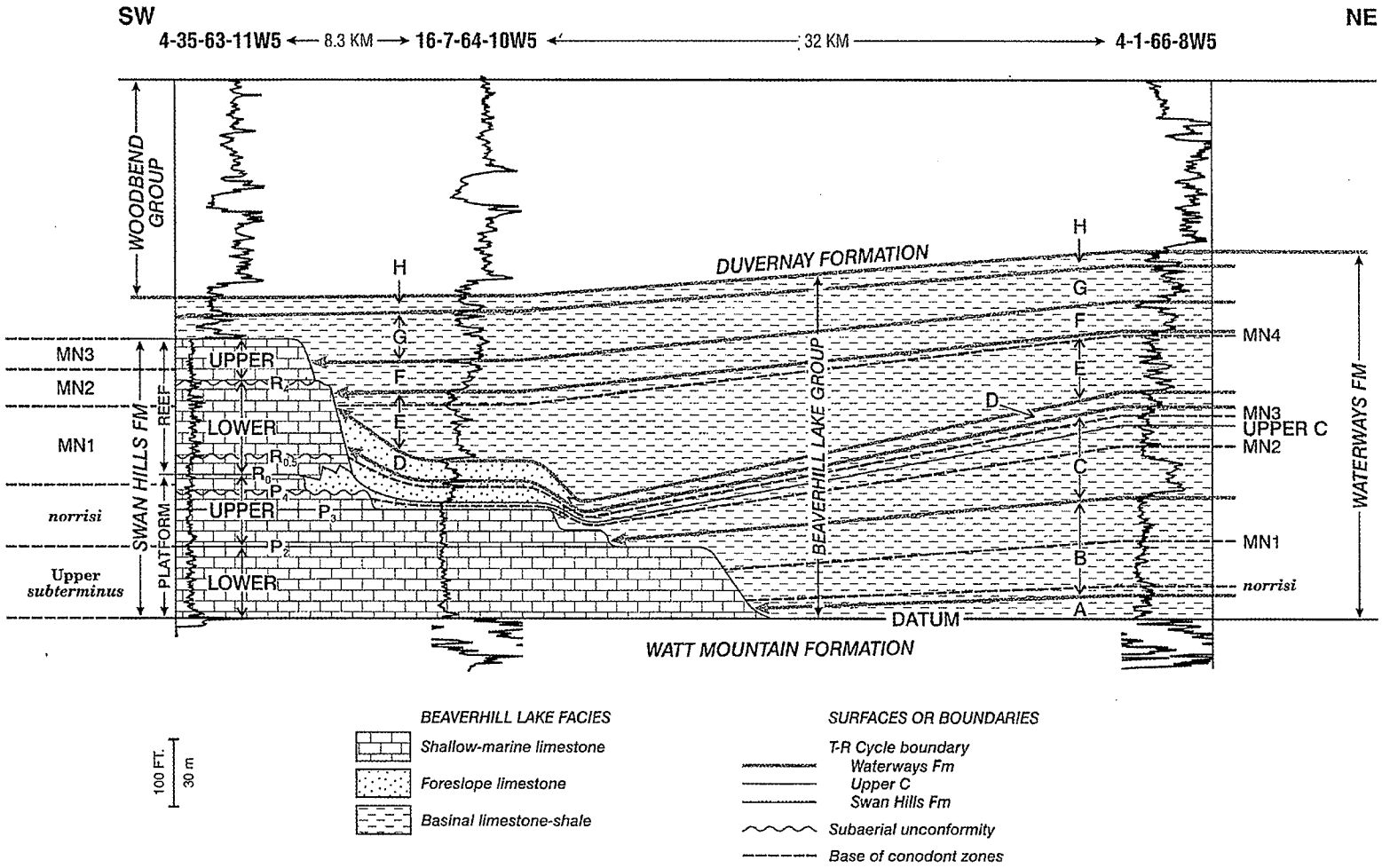


Figure 3.4 Cross-section through Beaverhill Lake strata from the northeastern edge of the Judy Creek reef complex (Swan Hills Formation) to the Waterways Formation (from Wendte and Uyeno, 2005). Third-order sequences (P2 to R4 and A to H) and their correspondence to conodont zones (*norrisi* to MN4) are illustrated in the diagram. Major subaerial unconformities (P4, R0.5 and R4) are also shown.

3.6 Swan Hills Formation at the Snipe Lake Reef Complex

The Swan Hills Formation is up to 110 m thick in the Snipe Lake reef complex and measures an area of approximately 22 km by 34 km (Figure 3.5). The carbonate platform reaches a maximum thickness of 52 m in the center of the reef (Havard and Oldershaw, 1976; Wendte and Muir, 1995).

3.6.1 Previous Stratigraphic Studies

Stratigraphic divisions of the Swan Hills Formation in the Snipe Lake reef complex have been proposed by various authors, notably Fischbuch (1968), Springate et al. (1992) and Wendte and Muir (1995).

Fischbuch (1968) documented eight stages of reef growth in the Snipe Lake reef complex (Figure 3.6). Divisions I to III progressively decrease in areal extent and Divisions IV and V show a pronounced decrease in areal extent. Fischbuch (1968) attributed the considerably thicker lagoonal deposits relative to fore-reef deposits to post-depositional erosion. Division V is limited to the northeastern portion of the reef complex and was interpreted to have been restricted depositionally and undergone post-depositional erosion. Green shale beds are present in Divisions IV and V and are easily traced through the reef complex at the top of Division V. Division VI extends beyond the limits of Divisions IV and V and rests on Division III. Division VI and VII appear to have been modified by subaerial erosion and thin green shales are present in the upper portion of each division. Division VIII is the final growth stage and the step-like geometry was interpreted to be erosional terraces. Fischbuch (1968) postulated a retreat

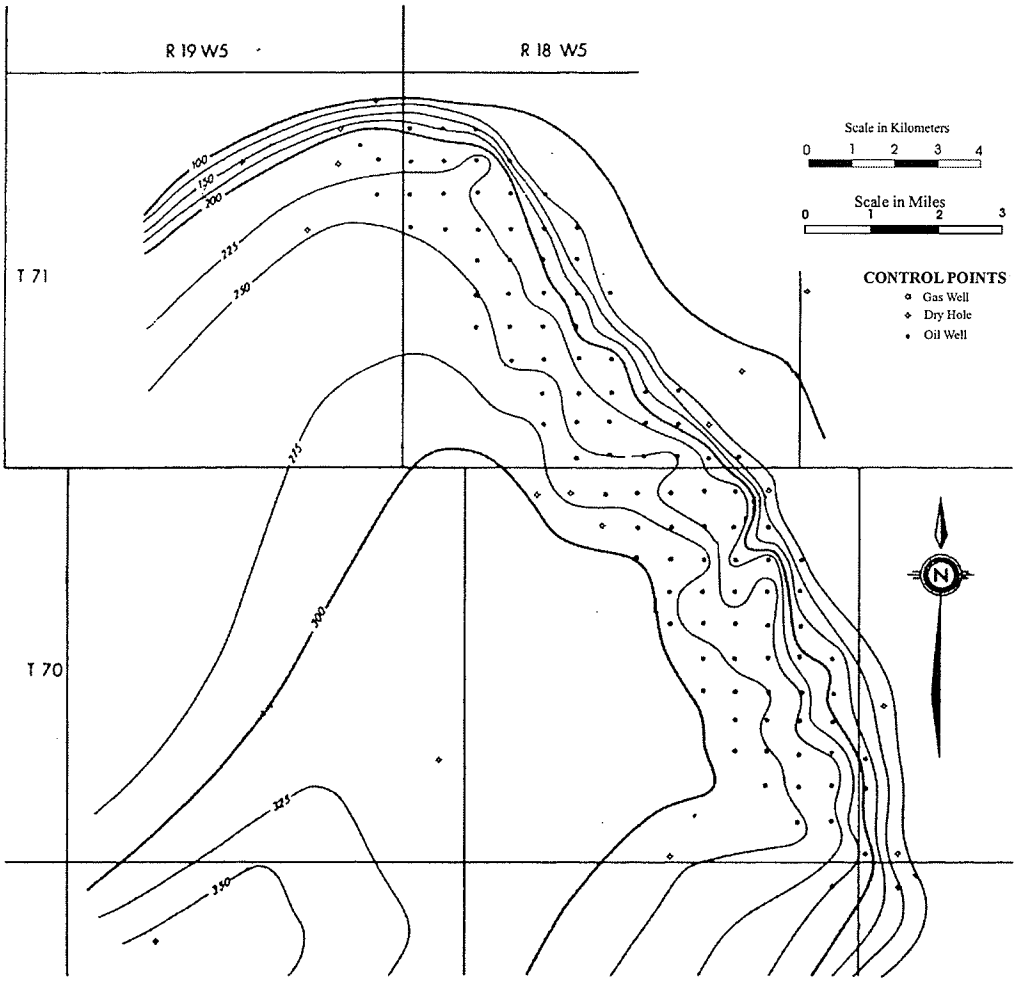


Figure 3.5 Swan Hills Formation isopach map at the Snipe Lake reef complex. Isopach lines are given in feet (modified from Fischbuch, 1968).

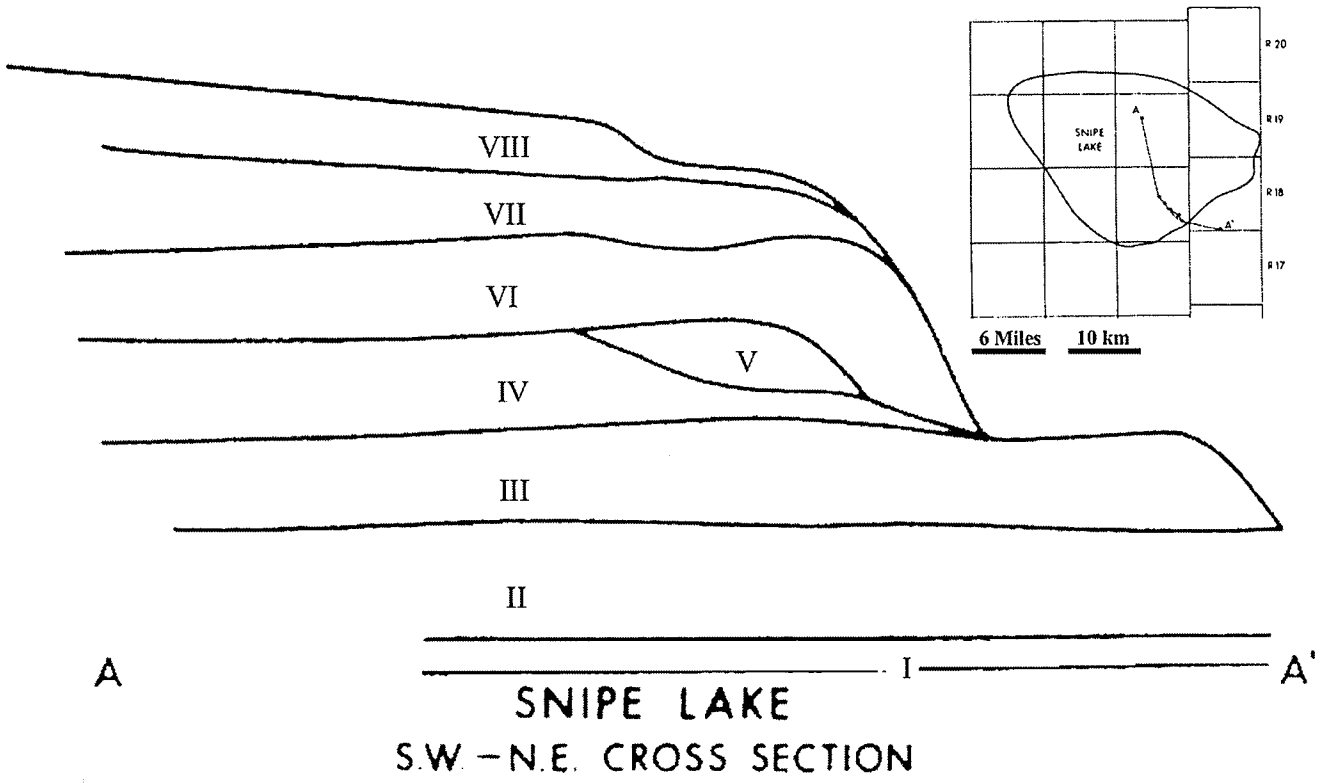


Figure 3.6 Depositional cycles in the Snipe Lake reef complex showing eight separate stages (I to VIII) of reef growth (modified from Fischbuch, 1968). No vertical scale is implied.

deposition of Division V beds and accompanying subaerial erosion.

Return of the late Devonian sea re-initiated reef growth in Divisions VI-VIII with final termination of reef growth at the end of Division VIII after considerable shallowing of the sea.

The stratigraphic approach proposed by Springate et al. (1992) and Wendte and Muir (1995) recognized ten second-order depositional sequences or megacycles that were correlated through the Snipe Lake reef complex (Figure 3.7). In the lower platform succession, five major megacycles are defined whose upper surfaces are defined as P1, P2, P3, P4 and P5 (Wendte and Muir, 1995). In the upper reef succession, five major megacycles are recognized whose upper surfaces are defined as R1, R2, R3, R4 and the top of the Swan Hills Formation.

The recognition of megacycles was determined by the presence of one or more of the following features (Wendte and Muir, 1995): (1) an abrupt change in lithofacies from shallow water lithofacies to relatively deeper water lithofacies across megacycle contacts; (2) sharp megacycle contacts or hardgrounds in the reef margin, showing truncated grains, *Trypanites* borings and/or encrustation by thin tabular stromatoporoids; (3) progressively shallowing-upward lagoonal cycles in the platform-reef interior; (4) the presence of stenohaline faunal communities (e.g., crinoids, brachiopods, branching corals) which help to interpret water circulation at reef margins and relative sea level rises; and (5) evidence for subaerial exposure (e.g., continuously lithified contacts, green shale, meteoric leaching).

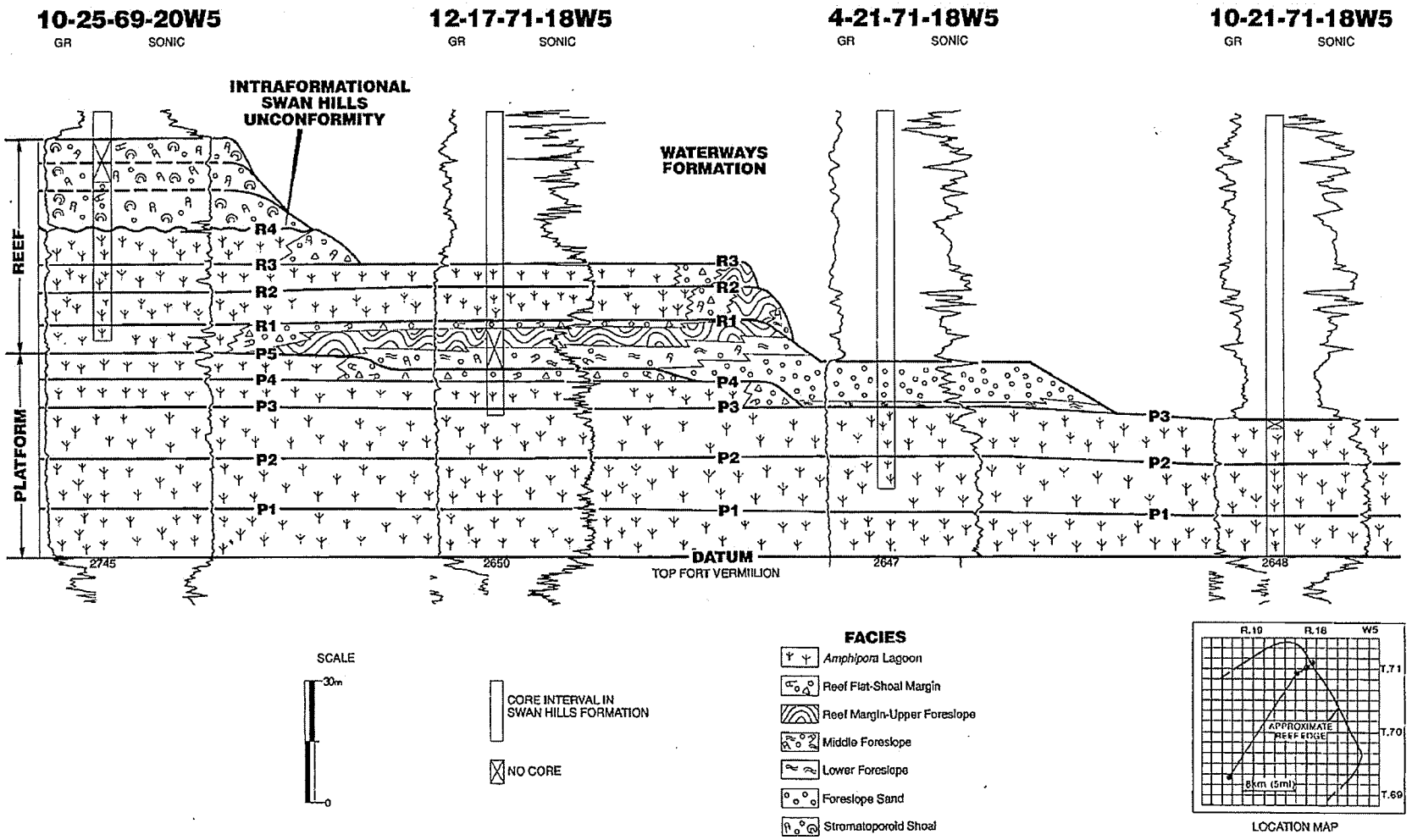


Figure 3.7 Cross-section across the Snipe Lake reef complex illustrating ten third-order sequences or megacycles (taken from Wendte and Muir, 1995, reprinted by permission of the AAPG whose permission is required for further use). The platform succession is composed of five megacycles, P1, P2, P3, P4 and P5. The reef succession is composed of four rimmed-reef megacycles, R1, R2, R3, R4 and a ramp-bounded shoal succession.

Based on the criteria described above, the evolution and stacking pattern of megacycles in the Snipe Lake reef complex, as interpreted by I. Muir and others (unpublished data, 1988), Wendte and Muir (1995) and Wendte and Uyeno (2005), are summarized below:

(1) Following deposition of the Fort Vermillion Formation, relative sea level rise and incursion of open marine waters initiated Swan Hills Formation deposition. Initially, the rate of sediment production and accumulation exceeded the rate of relative sea level rise and resulted in the deposition of progradational platform successions P1 and P2. Rise in relative sea level terminated deposition of the P2 cycle and initiated deposition of the P3 cycle. The P3 cycle showed a gradual upbuilding or aggradational growth style. Another subsequent pulse of accelerated relative sea level rise terminated P3 deposition and initiated deposition of the P4 cycle.

(2) The platform significantly decreased in areal extent during P4 and P5 deposition. The P4 platform margin backstepped approximately 1000 to 1600 m from the underlying drowned P3 platform margin and the P5 platform margin backstepped approximately another 700-1000 m from the P4 platform margin. P4 and P5 deposition were terminated by pulses of increased rates in relative sea level rise.

(3) Subsequent to drowning of the P5 platform, a rise in relative sea level initiated the first stage of reef growth (R1) at the Snipe Lake reef complex. The reef complex preferentially initiated on the highest point on the underlying platform as indicated by the growth of the reef complex on the thickest portions of the platform.

(4) Lower rates of relative sea level rise resulted in sedimentation rates that kept up with relative sea level rise and produced aggradational to slightly backstepped R1, R2 and R3 reef margins. R1 backstepped approximately 300-600 m from the underlying R0.5 reef margin and R2 retreated another 200-400 m from the R1 margin. Similarly, the R3 megacycle showed a gradual retreat from the drowned R2 reef margin. The top of the R1, R2 and R3 successions were interpreted to have been drowned as a result of increased rates of relative sea level rise.

(5) The R4 megacycle reef margin significantly backstepped towards the southwest. The R4 megacycle contact has been referred to as the Intraformational Swan Hills Unconformity (ISHU) and is interpreted to be a result of a relative sea level fall due to gradually decreasing rates of relative sea level rise and decreased accommodation space. Four criteria were used to interpret a relative drop in sea level at the ISHU: (1) a continuously lithified surface across the reef; (2) shallow tidal flat deposits overlie deeper subtidal deposits; (3) evidence of meteoric dissolution in underlying deposits, and (4) oxidation of sediments below the ISHU.

(6) After emergence at the R4 subaerial exposure surface, a gradual rise in relative sea level deposited shallow tidal flat sediments over the ISHU and the ramp-bounded shoal megacycle. Increasing relative sea level rise resulted in a gradually retreating to backstepping margin until the final drowning and termination of the Snipe Lake reef complex.

The most recent study by Wendte and Uyeno (2005) used the same stratigraphic approach as Springate et al. (1992) and Wendte and Muir (1995) for the Swan Hills Formation, but with two important changes: (1) an additional depositional cycle was recognized (R0.5), with a total of eleven megacyclces in the Swan Hills Formation and (2) these depositional cycles were re-defined to be third-order transgressive-regressive cycles (Figure 3.4).

3.6.2 Stratigraphic Approach Used in This Study

This study adopts the stratigraphic approach used for the Snipe Lake reef complex by Springate et al. (1992) and Wendte and Muir (1995), as modified by Wendte and Uyeno (2005). However, evidence presented in this study suggests that termination of the P4 megacycle was a result of a relative sea level fall (instead of increase in the rate of relative sea level rise). As well, an additional depositional cycle and subaerial exposure surface have been recognized between the P5 and R1 megacycle contacts; the top of the cycle is appropriately denoted as R0.5 (discussed in Chapter 5). A schematic diagram of the modified stratigraphy at the Snipe Lake reef complex is illustrated in Figure 3.8 and megacycle correlations are illustrated in cross-section A-A' (Enclosure 1). The evolution of the P4 to R0.5 successions and smaller scale fourth-order lagoonal cycles will also be described in greater detail in Chapter 5.

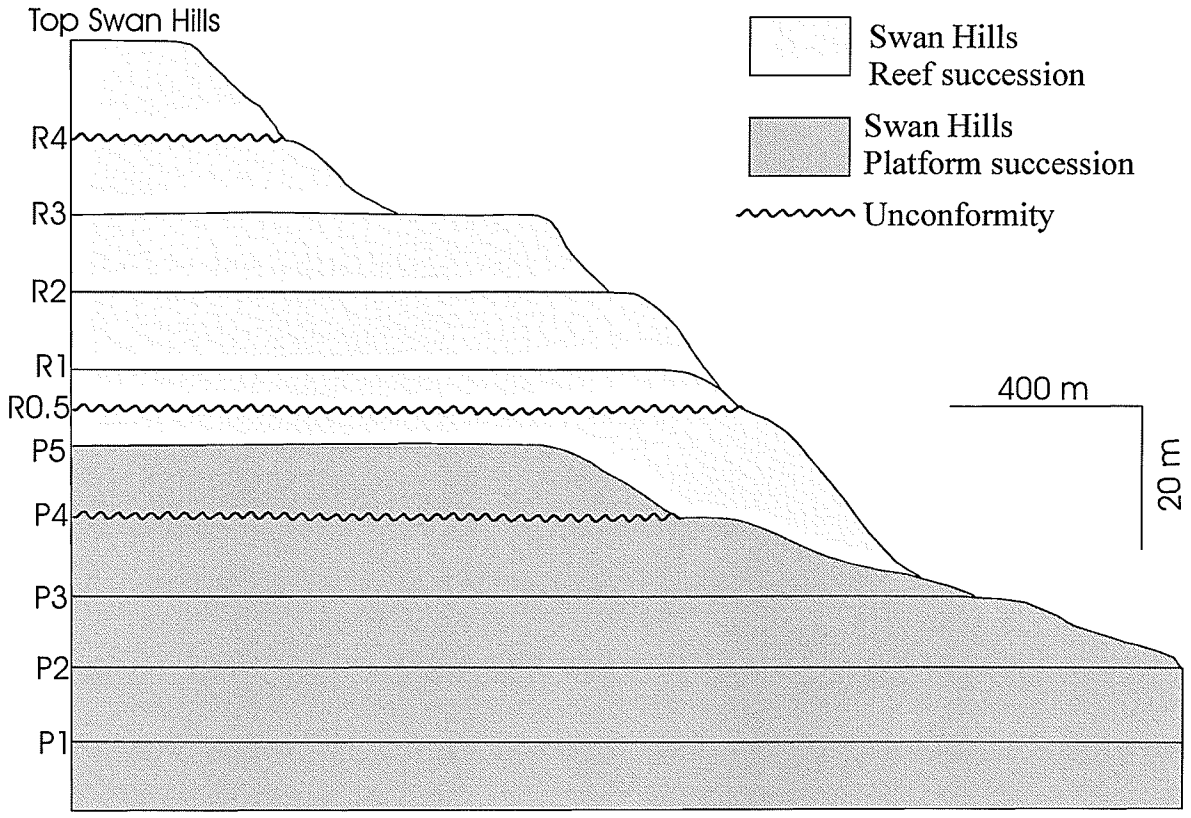


Figure 3.8 Schematic diagram of cycle stacking patterns in the Snipe Lake reef complex (based on Springate et al., 1992). The tops of platform megacycles are labelled P1, P2, P3, P4 and P5. The tops of the reef megacycles are labelled R0.5, R1, R2, R3, R4 and top of Swan Hills Formation.

CHAPTER 4: LITHOFACIES ANALYSIS

4.1 Introduction

Nine lithofacies have been recognized in the P4 to R0.5 successions in the Snipe Lake reef complex based on detailed core and thin section examination (Appendices B and E). Lithofacies were defined by lithologic characteristics, the type and occurrence of fauna, sedimentary structures, and other recognizable constituents (Table 4.1). The distribution and occurrence of lithofacies across the Snipe Lake reef complex are illustrated in cross-sections B to B' and C to C' (Enclosures 2 and 3). The lithofacies recognized in this study are similar to lithofacies described by Havard (1974), Wendte and Stoakes (1982), Springate et al. (1992), Wendte (1992) and Wendte and Muir (1995). This chapter will describe primary depositional features of each lithofacies and, with the exception of porosity, all diagenetic features including cements and subaerial exposure features will be discussed in Chapters 6 and 7.

The upper P4 and the P5 platform successions examined in this study are composed of five lithofacies: A) peloid packstones, B) robust branching cylindrical stromatoporoid rudstones, C) branching cylindrical stromatoporoid floatstones, D) light tan *Amphipora* floatstones, and E) dark brown *Amphipora* rudstones. The R0.5 reefal succession is composed of all nine lithofacies, which in addition to the five lithofacies listed above include lithofacies F) stromatoporoid floatstones to rudstones, G) tabular stromatoporoid rudstones, H) dark brown thin tabular stromatoporoid floatstones, and I) skeletal grainstones. The interpreted lateral relationship of these nine lithofacies is illustrated in

Table 4.1 Summary of the main characteristics of lithofacies in the P4 to R0.5 successions in the Snipe Lake reef complex.

	LITHOFACIES NAME	COLOR	LITHOLOGY	THICKNESS (m)	SEDIMENTARY STRUCTURES	ALLOCHEMS (% VOLUME)	MAJOR CONSTITUENTS (%)	MINOR CONSTITUENTS (%)	POROSITY	DEPOSITIONAL ENVIRONMENT	LITHOFACIES ASSOCIATION
A	Peloid packstones	tan, light brown	lime mudstone to peloid/peloid-skeletal packstones, local *Amphipora* floatstones with peloid wackestone to packstone matrix	0.2 - 1.6 m	crinkly to parallel laminated, irregular and laminar fenestrae	5 - 85%	peloids (0.04-3.0 mm, 2-72%), brachiopods (<3.6 mm, <10%), and ostracods (0.1-1.2 mm, <10%)	*Amphipora* (1-5 mm, rarely locally up to 60%), branching cylindrical stromatoporoids (0.35-1.0 cm, <7%, rarely locally up to 40-60%), calcispheres (0.06-0.3 mm, <5%), echinoderms (0.4-1.0 mm, <1%), gastropods (0.4-2.0 mm, 1-5%), rare oncoids (2.0-4.4 mm, locally <15%) and rare encrusting stromatoporoids (<0.5 mm, <1%)	0-10% dominantly interparticle, minor intraparticle, fenestral, vuggy and moldic	low energy, tidal flat along shorelines in the platform interior or back-reef	Lagoonal
B	Robust branching cylindrical stromatoporoid rudstones	medium brown, grey	robust branching cylindrical stromatoporoid rudstones with minor peloid packstone to grainstone matrix, local floatstones	0.2 - 1.5 m	massive	30 - 75%	robust branching cylindrical stromatoporoids (5 mm-2 cm, up to 75%)	*Amphipora* (1-3 mm, up to 30%), peloids (0.1-0.4 mm, up to 30%), bulbous and stromatoporoid fragments (1-9 mm) and rare gastropods (<2 mm)	3-15% shelter	high energy shorelines (intertidal to supratidal) in the platform interior or back-reef, beach deposits	Lagoonal
C	Branching cylindrical stromatoporoid floatstones	tan, light to medium brown	branching cylindrical stromatoporoid floatstones to rudstones, peloid to peloid-skeletal packstone to grainstone matrix (minor peloid wackestone)	0.2 - 2.0 m, rarely up to 3.7 m	overall massive, occasional medium grey to black mottling	50 - 85%	branching cylindrical stromatoporoids (4 mm-1.5 cm, up to 45%), *Amphipora* (1-4 mm, 2-45%)	local bulbous stromatoporoids (7-10 cm, locally 25-60%), rare hemispherical stromatoporoid clasts, rare oncoids, peloids (0.2-0.8 mm, 2-30%), skeletal fragments (3-20%) including brachiopods (<1.2 mm), ostracods (<1.2 mm) and gastropods (<1 cm)	0-10%, rarely up to 15%, dominantly interparticle, minor vuggy (locally 2-6%) and intraskeletal (locally 1-5%)	moderate energy, shallow subtidal environment in open lagoon in the platform interior or back-reef adjacent to reef flat and reef margin	Lagoonal

Table 4.1 (continued)

	LITHOFACIES NAME	COLOR	LITHOLOGY	THICKNESS (m)	SEDIMENTARY STRUCTURES	ALLOCHEMS (% VOLUME)	MAJOR CONSTITUENTS (%)	MINOR CONSTITUENTS (%)	POROSITY	DEPOSITIONAL ENVIRONMENT	LITHOFACIES ASSOCIATION
D	Light tan *Amphipora* floatstones	tan, light to medium brown	*Amphipora* floatstones to rudstones, peloid wackestone to packstone matrix (rare peloid grainstone)	0.3 - 3.2 m	overall massive, local medium to dark grey mottling, rare fine laminations at the top of intervals	20 - 75%	*Amphipora* (1-5 mm, up to 55%), branching cylindrical stromatoporoids (4-8 mm, 5-15%)	peloids (0.04-0.8 mm, 3-20%), skeletal fragments (3-15%) including brachiopods (<3 mm), gastropods (2-2.8 mm), rare calcispheres (0.04-0.4 mm), rare ostracods (0.1-0.9 mm), rare bulbous stromatoporoids (<5 cm), rare thin tabular stromatoporoids (1-2 cm), rare oncoids (2-4 mm)	variable 0-12%, average 1-5%, intraparticle, interparticle, vuggy and minor moldic	low to moderate energy, shallow subtidal environment in slightly restricted to open lagoon in platform interior or behind reef margin	Lagoonal
E	Dark brown *Amphipora* rudstones	medium to dark brown	*Amphipora* floatstones to rudstones, carbonaceous peloid wackestone matrix, ranges from lime mud to peloid grainstone matrix	0.2 - 1.5 m	locally interbedded (2.5-15 cm) floatstone, rudstone and mudstone intervals, fining upward sequences (0.5-1.5 m thick) showing decrease in abundance of *Amphipora*	30 - 85%	*Amphipora* (1-4 mm, 10-80%)	branching cylindrical stromatoporoids (average 4-5 mm, up to 5%), rare bulbous (3-8 cm), rare nodular (1.5-3 cm) and irregular stromatoporoids (<2 cm), peloids (0.04-0.8 mm, 15-55%), variable skeletal fragments (10-25%) including calcispheres (<0.1 mm) and ostracods (<0.1 mm), rare gastropods (<7 mm)	absent to <1%, intraparticle	low energy, subtidal environment, poorly oxygenated and above normal salinity conditions in restricted lagoon in platform interior or behind reef margin	Lagoonal
F	Stromatoporoid floatstones to rudstones	tan, light grey	stromatoporoid floatstones to rudstones, peloid-skeletal grainstone to packstone (less common) matrix	0.7 - 5.2 m	massive	45-85%	robust branching cylindrical stromatoporoids (average 5 mm- 1 cm, 30-55%), bulbous stromatoporoids (4-10 cm, 5-25%)	hemispherical stromatoporoids (10-13 cm, 5-20%), thick tabular stromatoporoids (2-4 cm, <5%), nodular stromatoporoids (1.5-2.5 cm, <5%), rare rugose corals (<1 cm) and oncoids (<1 cm), minor peloids (<2 mm), brachiopods (<1.2 cm), gastropods (<6 mm) and ostracods (<2 mm)	2-10%, dominantly interparticle (2-10%) and intraparticle (2-5%), minor vuggy (<5%)	shallow, high energy, normal marine conditions in reef flat to upper foreslope environment	Reef Margin

Table 4.1 (continued)

	LITHOFACIES NAME	COLOR	LITHOLOGY	THICKNESS (m)	SEDIMENTARY STRUCTURES	ALLOCHEMS (% VOLUME)	MAJOR CONSTITUENTS (%)	MINOR CONSTITUENTS (%)	POROSITY	DEPOSITIONAL ENVIRONMENT	LITHOFACIES ASSOCIATION
G	Tabular stromatoporoid rudstones	light to medium brown	branching cylindrical and tabular stromatoporoid floatstones to rudstones, possible minor boundstones, peloid-skeletal packstone to grainstone (minor wackestone) matrix	0.6 - 7.7 m	tabular stromatoporoids aligned parallel to bedding	60 - 80%	robust branching cylindrical stromatoporoids (0.5-1.5 cm, 20-45%), thin tabular stromatoporoids (0.5-2.0 cm, 15-50%), thick tabular stromatoporoids (2-3 cm, 5-20%)	bulbous stromatoporoids (2-3 cm, <5%), rare *Amphipora* (2-4 mm), rare rugose corals (<1 cm), minor peloids (<0.5 cm), brachiopods (<1 cm), ostracods (<2 mm), gastropods (<1 cm) and echinoderms (<1 cm)	5-10% interparticle, 3-5% intraparticle	low to moderate energy, well circulated, normal marine conditions in middle foreslope environment	Reef Margin
H	Dark brown thin tabular stromatoporoid floatstones	medium to dark brown	thin tabular stromatoporoid floatstones to rudstones, possible minor boundstones, carbonaceous peloid wackestone to packstone matrix	0.9 - 2.9 m	thin tabular stromatoporoids aligned parallel to bedding	40 - 65%	thin tabular stromatoporoids (1-2 cm, 15-40%), branching cylindrical stromatoporoids (0.5-1.0 cm, 15-40%)	thick tabular stromatoporoids (2-3 cm, 5-10%), bulbous stromatoporoids (2-3 cm, <3%), peloids (<1 mm), stromatoporoid fragments (< 1mm), brachiopods (<1 mm) and crinoids (<1 mm)	<1% intraparticle	low energy conditions in lower foreslope environment	Reef Margin
I	Skeletal grainstones	tan, medium brown	skeletal to skeletal-peloid packstones to grainstones	0.6 - 1.3 m	overall massive, weakly cross-bedded (rare)	65 - 80%	stromatoporoid fragments (<3 cm, 5-25%), brachiopods (1-7 cm, <20%), crinoids (0.2-2.0 mm, 10-20%), peloids (<0.5 mm, 15-20%)	ostracods (<1 cm, <10%), calcareous algae (rare, up to 5%)	10-15% intraparticle	deposited throughout reef foreslope environment, skeletal debris derived from reef organisms from shallow upslope environment	Reef Margin

paleobathymetric profiles in Figures 4.1 and 4.2.

4.2 Lithofacies A: Peloid Packstones

4.2.1 Description

This lithofacies consists of tan to light brown lime mudstones to peloid/peloid-skeletal packstones and is 0.2 to 1.6 m thick (Figure 4.3). Locally it can be light brown to grey *Amphipora* floatstones with a peloid wackestone to packstone matrix. This lithofacies is commonly crinkly to parallel laminated (laminae <1 to 2 mm thick) with irregular to laminar fenestrae. Light to dark grey mottling (possible bioturbation) and darkened grains are locally observed in muddier intervals. The lower lithofacies contact is commonly gradational. The upper lithofacies contact is gradational or sharp and in some locations erosional surfaces (possible marine hardgrounds) are observed at or near the contact.

Allochems comprise 5-85% of lithofacies A, with peloids being the dominant constituent. Other common constituents include ostracods, calcispheres and brachiopods. Branching cylindrical stromatoporoids and *Amphipora* are commonly present as minor constituents ranging from absent to 7%, but locally can comprise up to 40% and 60% of the lithofacies, respectively. Other constituents in decreasing occurrence include echinoderms, gastropods, and rare oncoids and encrusting stromatoporoids. This lithofacies is relatively tight in general but porosity can range from 2-5% and rarely up to 10%. Interparticle porosity is the most common; fenestral, vuggy and moldic porosity are present locally. Intraparticle porosity in internal stromatoporoid galleries and

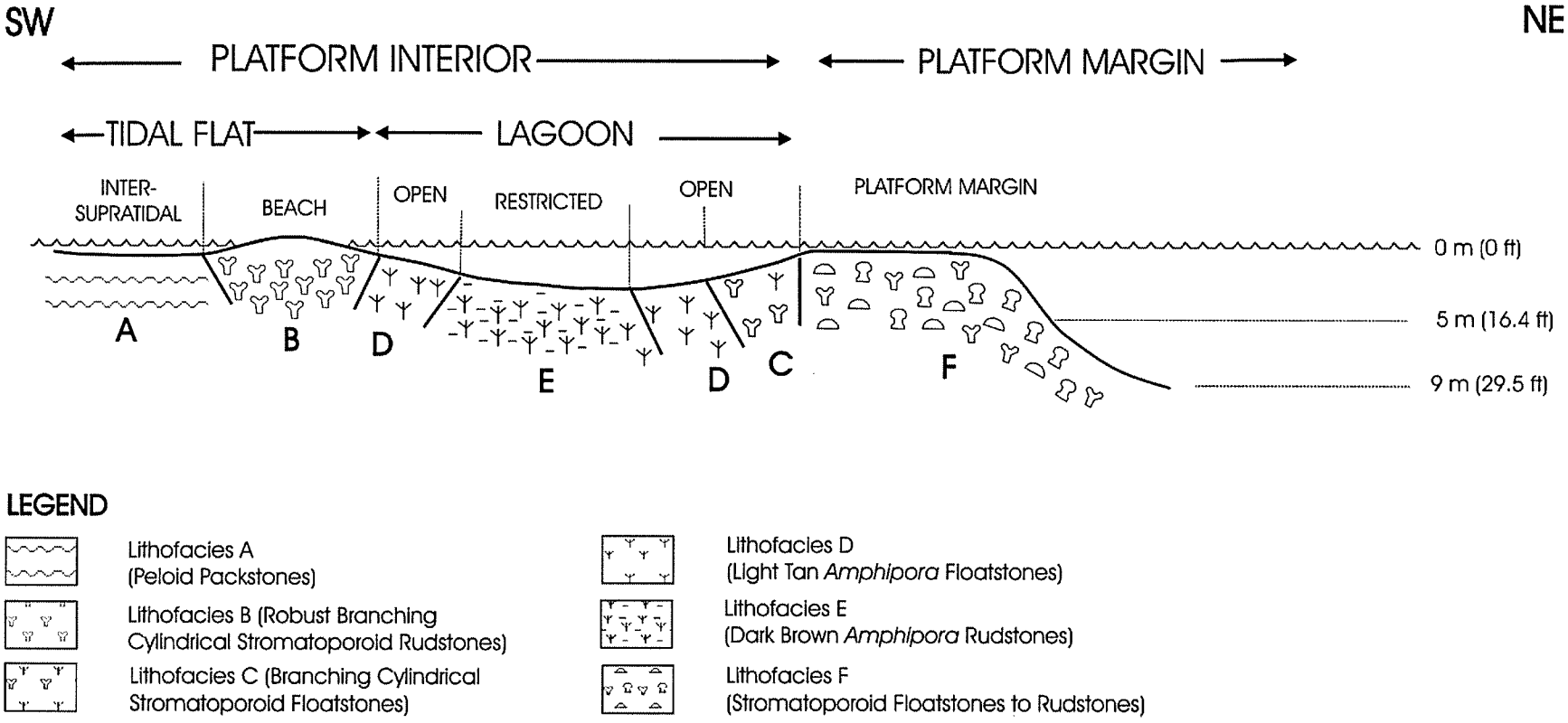


Figure 4.1 Schematic diagram showing the interpreted paleobathymetric profile across the windward, northeasterly side of the Snipe Lake platform summarizing the lithofacies in the upper P4 and P5 succession in this study (based on I. Muir and others, unpublished data, 1988; Wendte and Muir, 1995). Note that lithofacies F was not observed in the platform successions examined in this study.

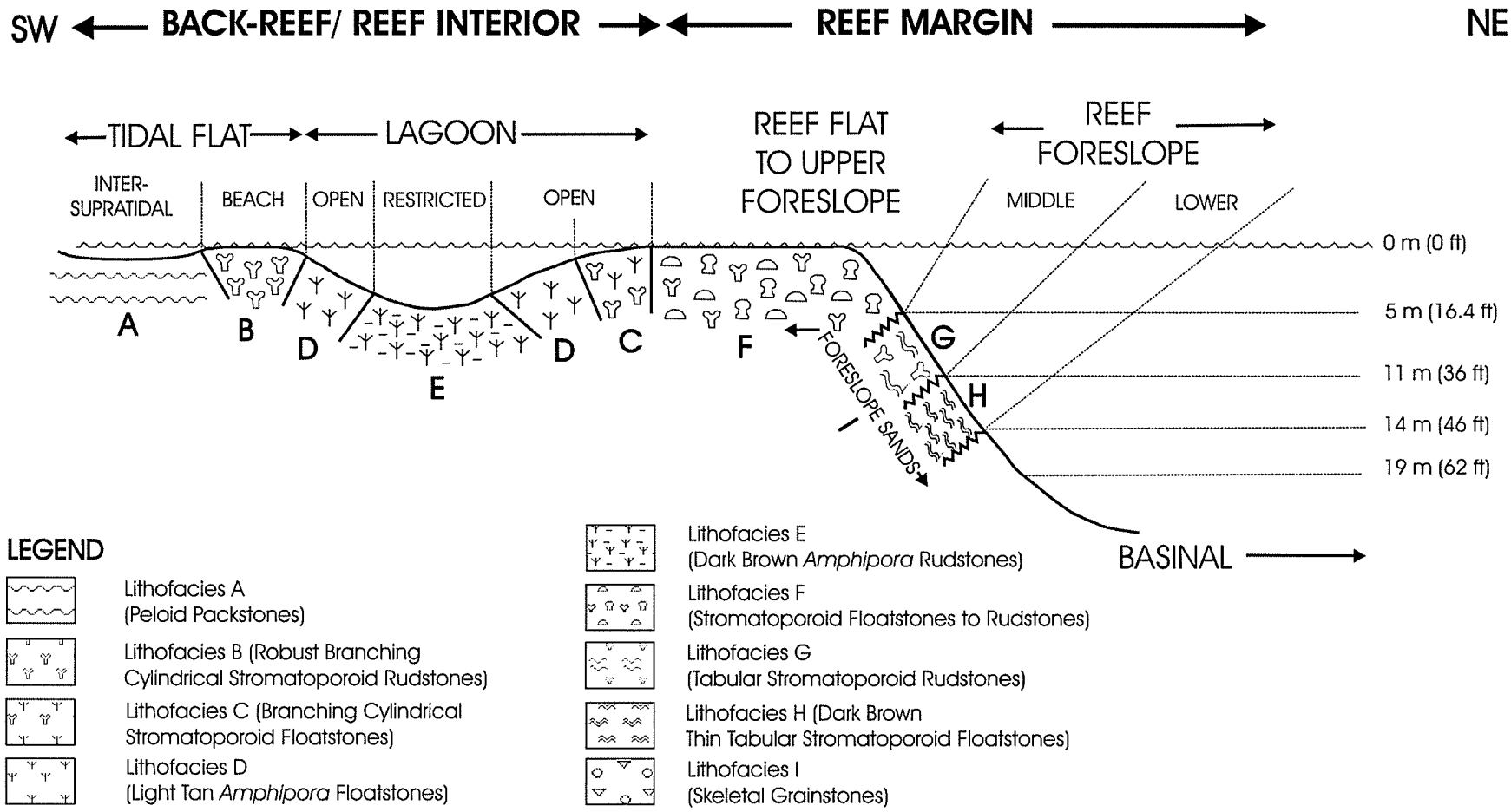


Figure 4.2 Schematic diagram showing the interpreted paleobathymetric profile across the windward, northeasterly side of the Snipe Lake reef complex summarizing the lithofacies observed in the R0.5 succession in this study (based on I. Muir and others, unpublished data, 1988 and Wendte and Muir, 1995). Lithofacies I occurs throughout the reef foreslope environment.

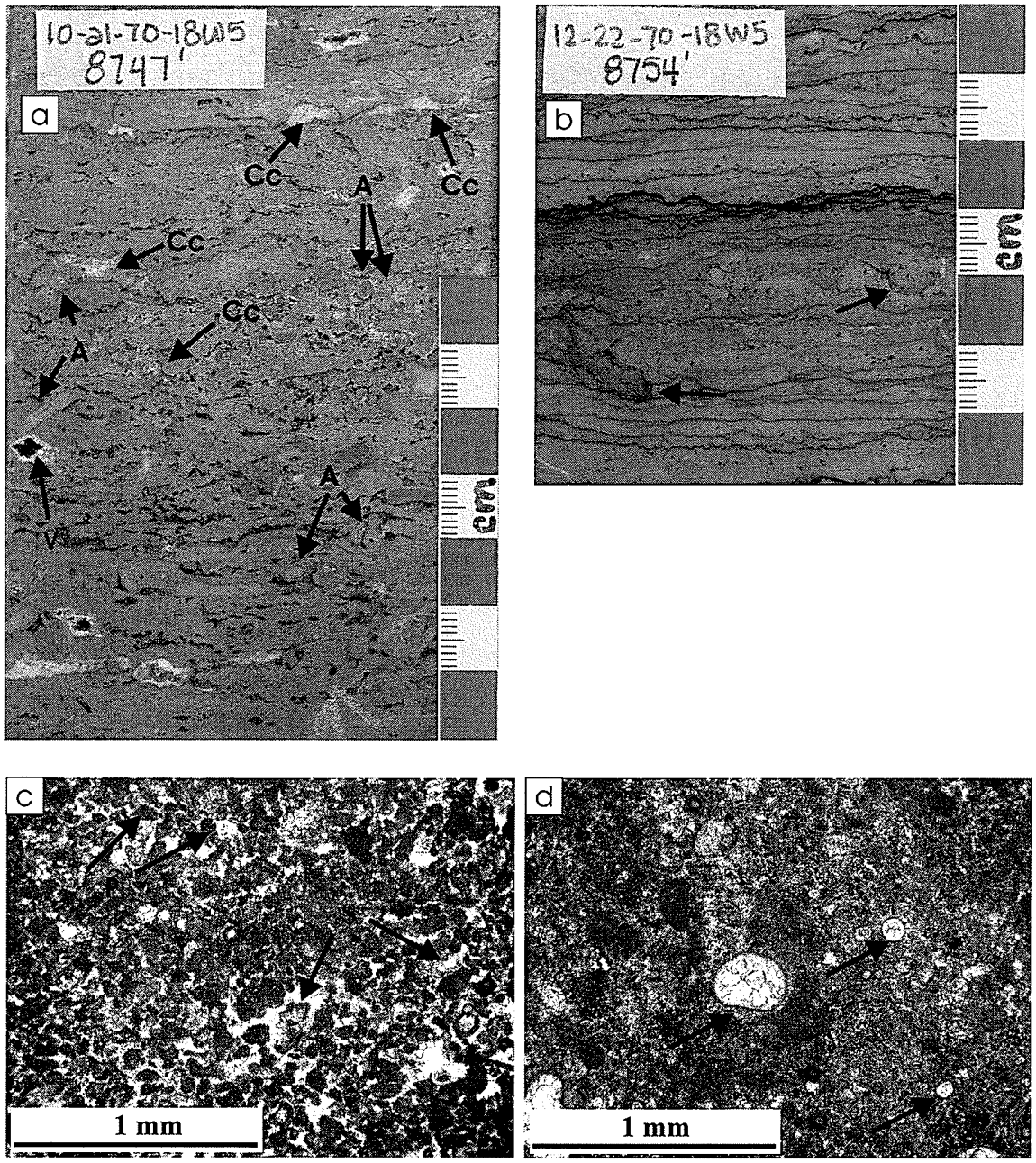


Figure 4.3 Lithofacies A, peloid packstones. a) Core photograph of peloid wackestone with irregular to laminar fenestrae occluded by blocky mosaic calcite (Cc), scattered *Amphipora* (A) and minor vuggy porosity (V), 10-21-70-18W5, 2666.1 m (8747'). b) Core photograph of laminated peloid wackestone to packstone with medium grey mottling (arrows), 12-22-70-18W5, 2668.2 m (8754'). c) Photomicrograph of (b) with peloids (P) and micritized skeletal fragments (S). d) Photomicrograph of peloid wackestone with calcispheres (arrows), 02-03-71-18W5, 2617.2 m (8586.5').

calcispheres occurs locally in minor amounts (1-3%).

4.2.2 Interpretation

Lithofacies A is interpreted to have been deposited in a low energy, tidal flat (intertidal) environment. The amount of lime mud is a good indicator of turbulence and energy conditions (e.g. Folk, 1959; Klovan, 1964; Fischbuch, 1968). Therefore, the abundance of lime mud throughout this lithofacies is interpreted to represent deposition in low energy conditions. Crinkly laminations and laminar to irregular fenestrae are indicative of microbial mats (e.g. Choquette and Pray, 1970). Microbial mats are common in intertidal to supratidal environments where surfaces are periodically exposed and flooded (e.g. Murray, 1966; Roehl, 1967; Havard, 1974). Sediments in suspension can be trapped and bound by microbial films and form crusts or microbial mats. The lack of desiccation features in these sediments suggests that deposition of lithofacies A was mainly in the lower intertidal zone (cf. Havard, 1974).

This lithofacies is similar to the crinkly laminated, pelletal mudstones to packstones in the Snipe Lake and Judy Creek reef complexes that were interpreted to have been deposited along low energy shorelines of the tidal flat environment (e.g. Wendte and Stoakes, 1982; Wendte, 1992c; Wendte and Muir, 1995).

4.3 Lithofacies B: Robust Branching Cylindrical Stromatoporoid Rudstones

4.3.1 Description

This lithofacies consists of medium brown to grey, robust branching cylindrical stromatoporoid rudstones with floatstones occurring locally, and ranges from 0.2 to 1.5 m thick (Figure 4.4). When present, the matrix is composed of peloid packstones to grainstones. Lower and upper lithofacies contacts are gradational or sharp. Allochems comprise 30-75% of lithofacies B, with robust branching cylindrical stromatoporoids being the most abundant. *Amphipora* are rare but can comprise up to 30%. Stromatoporoid grains are commonly fragmented and micritized. Peloids commonly occur in the matrix comprising up to 30%. Other constituents include minor bulbous and hemispherical stromatoporoid fragments and rare gastropods. Shelter and interparticle porosity are well developed in this lithofacies ranging from 3 to 15%. The majority of the porosity is shelter porosity (as defined by Choquette and Pray, 1970) created by the sheltering effect of large stromatoporoid grains preventing finer grained particles from filling the pore space beneath them. Milky white to laminated white and brown, pendant radiaxial fibrous calcite cements occur along the undersurfaces of some shelter pores (discussed more in Chapter 6). Commonly, there is a progressive upward decrease in porosity as a result of increasing cements in pore spaces.

4.3.2 Interpretation

Robust branching cylindrical stromatoporoid rudstones are interpreted to be beach deposits or storm deposits that were deposited along high energy shorelines. The paucity of lime mud in this lithofacies indicates a high energy environment. Fragmented,

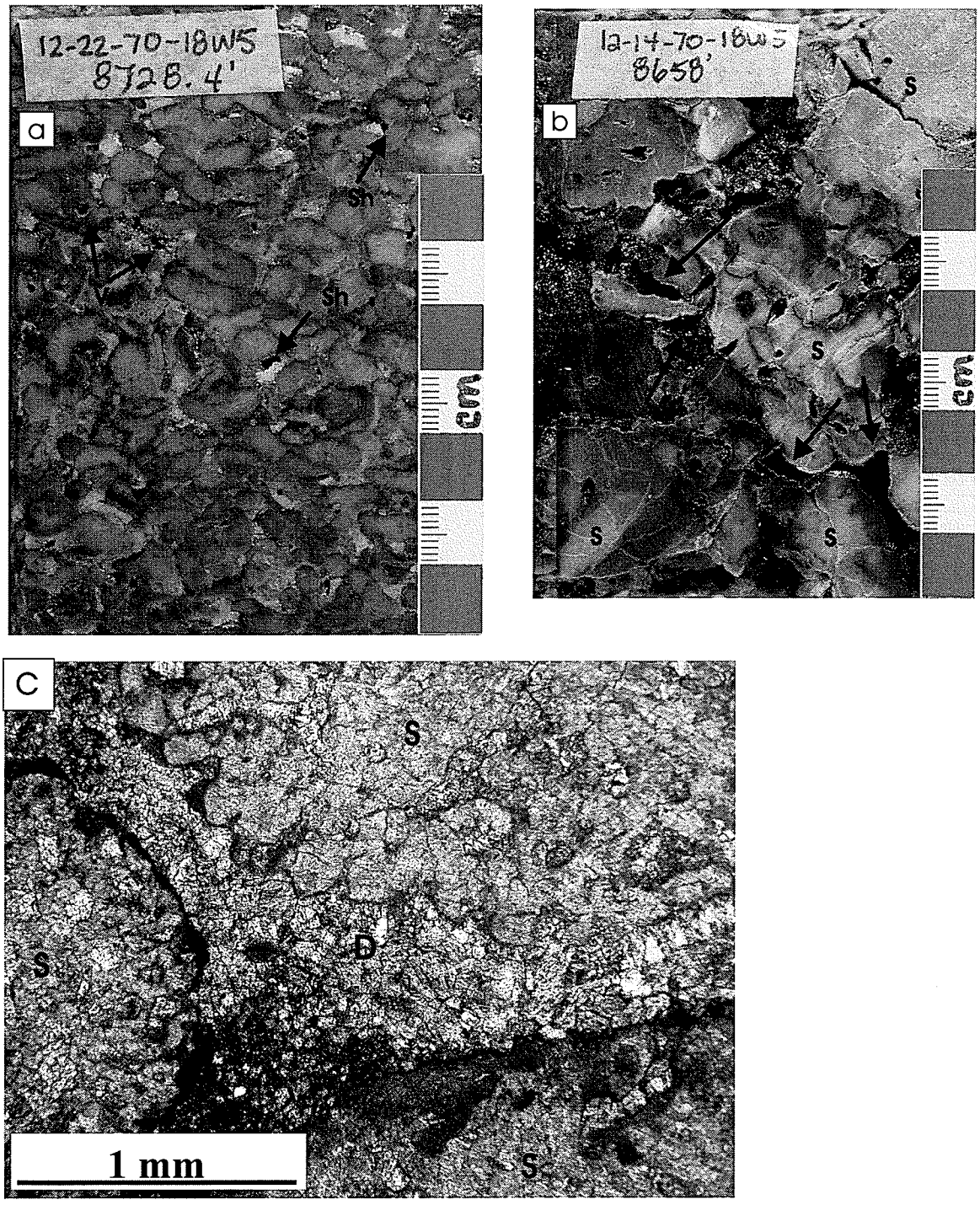


Figure 4.4 Lithofacies B, robust branching cylindrical stromatoporoid rudstones. a) Core photograph showing shelter pores (Sh) and vuggy pores (V), 12-22-70-18W5, 2660.4 m (8728.4'). b) Core photograph of highly fragmented stromatoporoid grains (S) (branching cylindrical and bulbous). Shelter porosity is well developed at 10-12% (arrows), 12-14-70-18W5, 2639 m (8658'). c) Photomicrograph showing stromatoporoid (S) and ferroan dolomite rhombs (D) occluding interparticle pores, 12-27-70-18W5, 2636.8 m (8651').

abraded and randomly oriented grains support an allochthonous source of stromatoporoids likely transported from nearby subtidal environments (e.g. I. Muir and others, unpublished data, 1988). Grain-to-grain contacts between stromatoporoids and shelter pores occluded by pendant radiaxial fibrous calcite cements are common in beachrock deposits in high energy foreshore environments (e.g. Purser, 1969; Hanor, 1978; James and Choquette, 1990b). These pendant cements are interpreted to be early marine vadose in origin (refer to Chapter 6).

A similar *Stachyodes* rudstone lithofacies was recognized in the Snipe Lake reef complex by Havard (1974) and was interpreted to have been deposited in the intertidal environment. In addition, the cylindrical stromatoporoid rudstone lithofacies recognized in other studies of the Snipe Lake and Judy Creek reef complexes have been interpreted to represent storm beach deposits along high energy shorelines (Wendte and Stoakes, 1982; I. Muir and others, unpublished data, 1988; Wendte, 1992c; Wendte and Muir, 1995).

4.4 Lithofacies C: Branching Cylindrical Stromatoporoid Floatstones

4.4.1 Description

This lithofacies consists of tan to medium brown, branching cylindrical stromatoporoid floatstones to rudstones and ranges from 0.2 to 2.0 m thick (rarely up to 3.7 m thick) (Figure 4.5). The matrix is commonly composed of peloid to peloid-skeletal packstones to grainstones, and less commonly is peloid wackestones. Medium grey to black mottling is locally observed in this lithofacies. Lower and upper lithofacies contacts are

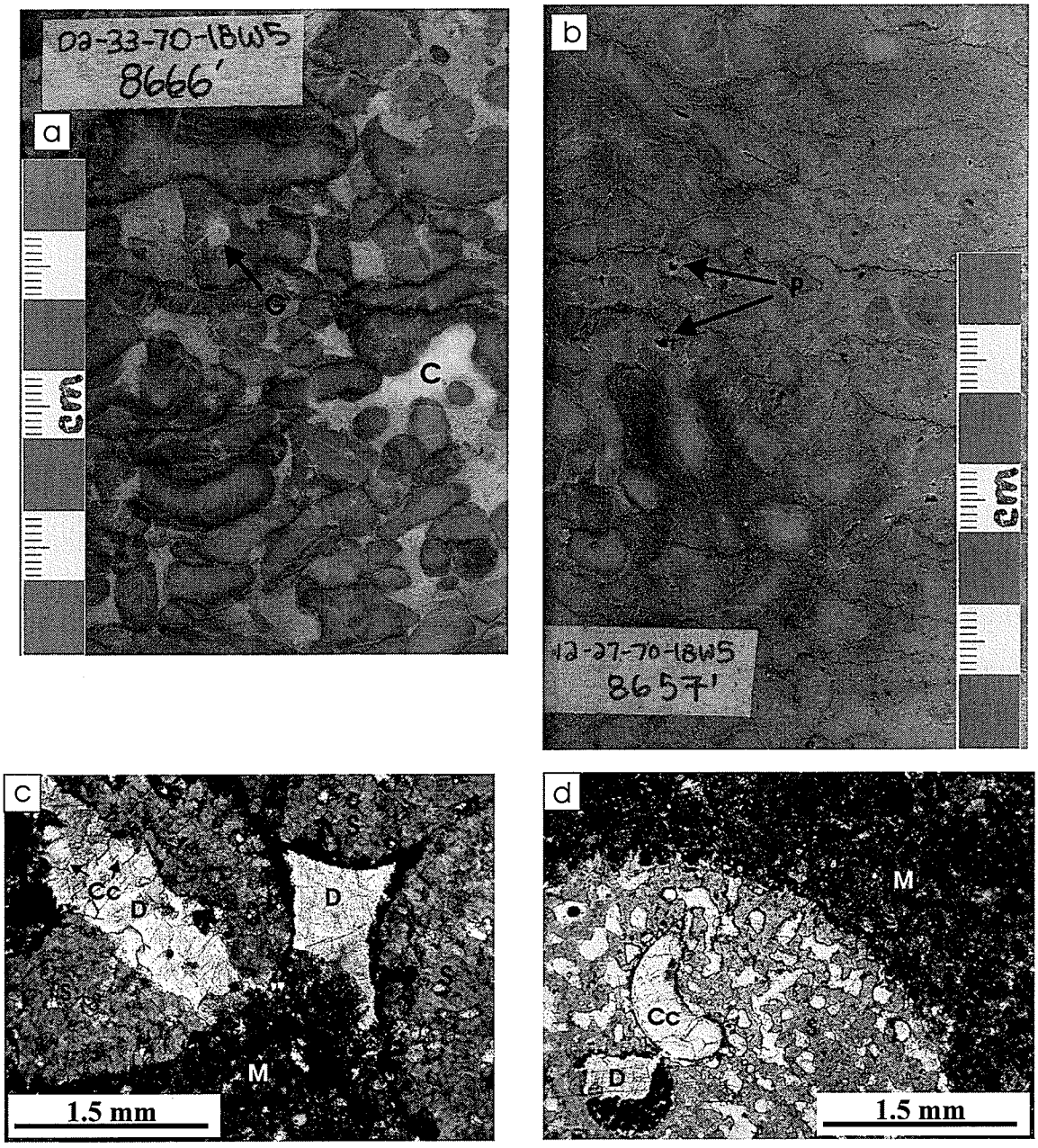


Figure 4.5 Lithofacies C, branching cylindrical stromatoporoid floatstones. a) Core photograph of branching cylindrical stromatoporoid rudstone, 02-33-70-18W5, 2641.4 m (8666'). Stromatoporoids have vugs with geopetal internal sediment (G). Blocky calcite cements occlude vuggy and interparticle pores (C). b) Core photograph of branching cylindrical stromatoporoid floatstone with rare intraparticle porosity (P), 12-27-70-18W5, 2638.7 m (8657'). c) Photomicrograph of (a) showing branching stromatoporoids (S) in a peloid packstone-grainstone matrix (M). Blocky calcite (Cc) and ferroan dolomite rhombs (D) occlude interparticle pores and vugs (?). d) Photomicrograph of branching cylindrical stromatoporoid (S) in a peloid wackestone matrix (M). Intraskeletal stromatoporoid galleries are occluded by blocky calcite cement (Cc) and ferroan dolomite rhombs (D) 10-27-70-18W5, 2643.2 m (8671.9').

gradational or sharp. Upper contacts are typically sharp when occurring at the top of minor lagoonal cycles (see section 5.4).

Allochems comprise 50-85% of lithofacies C and branching cylindrical stromatoporoids are the dominant constituent. *Amphipora* is common but in low abundances (2-10%) and rarely up to 45%. Bulbous stromatoporoids locally comprise 25-60% and hemispherical stromatoporoid fragments and oncoids are rare. Stromatoporoid grains are commonly micritized. Peloids are the main matrix constituents and skeletal fragments in the matrix include brachiopods, ostracods and gastropods. Porosity is poorly to moderately developed in this lithofacies ranging from absent to 10%, and very rarely up to 15%. Interparticle porosity is the most common (3-10%) and vuggy porosity (2-6%) and intraskeletal porosity (1-5%) are present locally.

4.4.2 Interpretation

Branching cylindrical stromatoporoid floatstones are interpreted to have been deposited in moderate energy, shallow subtidal conditions. Low to moderate amounts of lime mud and the presence of fragmented skeletal and stromatoporoid grains suggest moderate energy conditions (cf. Fischbuch, 1968). Branching cylindrical stromatoporoids thrived in turbulent to moderately turbulent marine waters of normal salinities (e.g. Klovan, 1964; Murray, 1966; Kershaw, 1998).

Lithofacies C is similar to a stromatoporoid floatstone lithofacies in the Snipe Lake reef complex that was recognized by Havard and Oldershaw (1976). They interpreted it to be

a product of shallow subtidal sedimentation in a lagoon.

4.5. Lithofacies D: Light Tan *Amphipora* Floatstones

4.5.1 Description

This lithofacies consists of tan to medium brown, *Amphipora* floatstones to rudstones and ranges from 0.3 to 3.2 m thick (Figure 4.6). The matrix is composed of peloid wackestones to packstones, and rarely peloid grainstones. It is massive overall with local medium to dark grey mottling and rare fine laminations occurring at the top of the interval. Interbedded floatstone and rudstone beds, 15-45 cm thick, occur locally. Lower and upper lithofacies contacts are gradational or sharp, with sharp upper lithofacies contacts more common at the top of minor lagoonal cycles (see section 5.4).

Allochems comprise 20-75% of lithofacies D and *Amphipora* is the dominant constituent (up to 55%). Branching cylindrical stromatoporoids are commonly present but in lesser abundance (5-15%). Bulbous stromatoporoids, thin tabular stromatoporoid fragments, and oncoids are rare. Peloids and skeletal fragments are the most common constituents in the matrix. Skeletal grains include brachiopods, gastropods, ostracods, and rare calcispheres. Porosity is generally poorly developed in this lithofacies, averaging 1-5%, but ranging from absent up to 12%. Intraparticle and interparticle porosity are the most common and moldic and vuggy porosity are minor.

4.5.2 Interpretation

Light tan *Amphipora* floatstones are interpreted to have been deposited in a low to

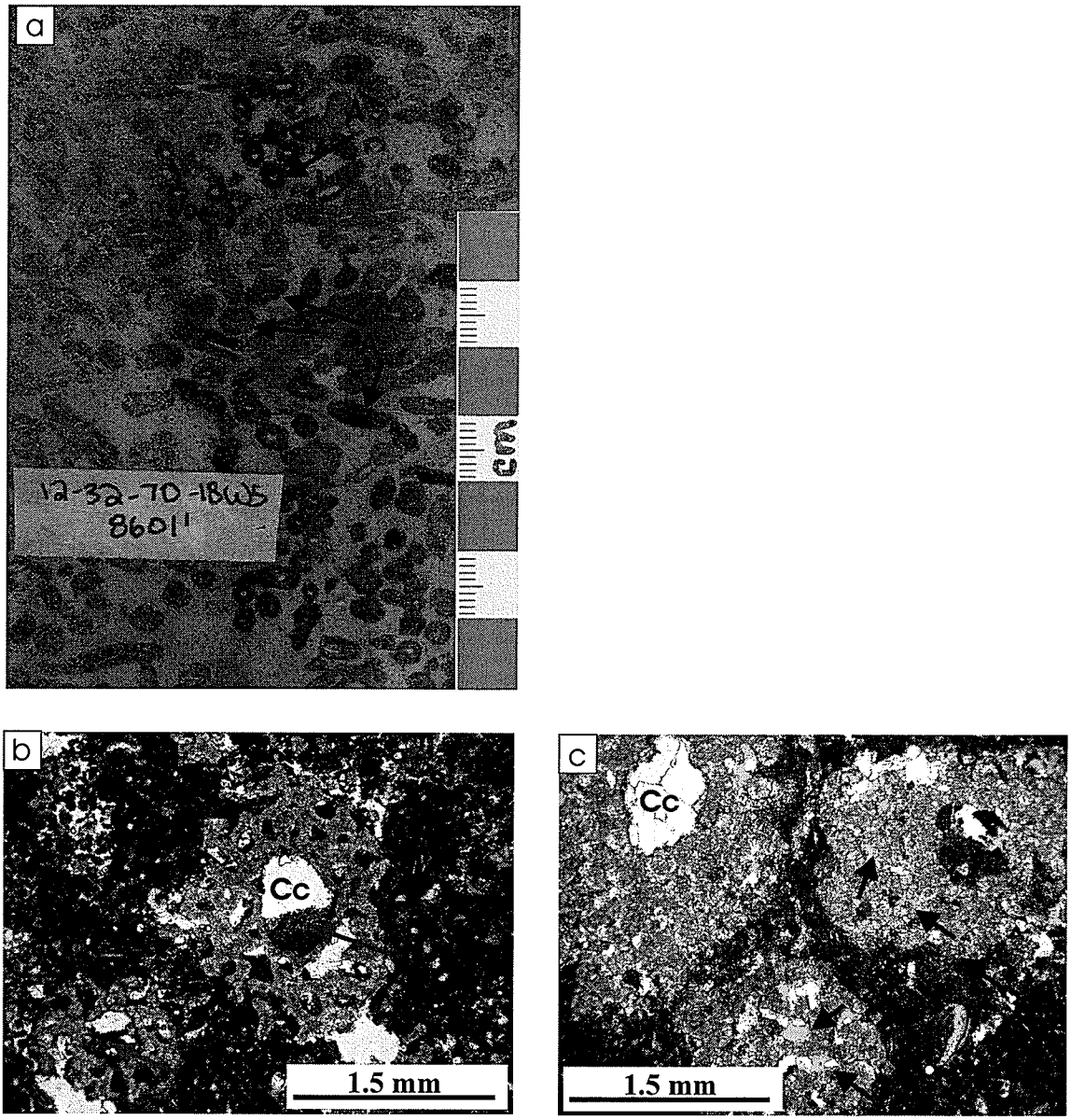


Figure 4.6 Lithofacies D, light tan *Amphipora* floatstone. a) Core photograph of light tan *Amphipora* (A) floatstone, 12-32-70-18W5, 2621.6 m (8601'). b) Photomicrograph of *Amphipora* with geopetal sediment (arrows) and blocky calcite cement mosaics (Cc) occluding coenostea, 12-32-70-18W5, 2617.3 m (8587'). c) Photomicrograph of *Amphipora* floatstone with a peloid wackestone matrix. *Amphipora* have intraparticle porosity (blue epoxy, arrows) and blocky calcite cement (Cc) occluding intraskeletal and interparticle porosity, 12-32-70-18W5, 2614 m (8576').

moderate energy, shallow subtidal environment. *Amphipora* preferentially grew in quiet, poorly oxygenated and higher salinity waters, whereas branching cylindrical stromatoporoids thrived in moderately agitated, normal marine waters (e.g. Klovan, 1964; Murray, 1966; Kershaw, 1998). The high abundance of *Amphipora* and low abundance of branching cylindrical stromatoporoids in lithofacies D, along with moderate to low amounts of lime mud, suggest deposition occurred in a moderately sheltered environment. Floatstone and rudstone interbeds are attributed to locally fluctuating energy conditions. For example, rudstone interbeds were likely deposited in more shallow and agitated waters (e.g. I. Muir and others, unpublished data, 1988).

Lithofacies D is similar to the *Amphipora* lagoon lithofacies in the Snipe Lake reef complex described by I. Muir and others (unpublished data, 1988) and the grainy lagoon lithofacies in the Judy Creek reef complex described by Wendte and Stoakes (1992c). They were interpreted to have been deposited in relatively open lagoon conditions.

4.6 Lithofacies E: Dark Brown *Amphipora* Rudstones

4.6.1 Description

This lithofacies consists of medium to dark brown *Amphipora* floatstones to rudstones and ranges from 0.2 to 1.5 m thick (Figure 4.7). The matrix is commonly composed of peloid wackestones, but ranges from lime mudstones to peloid-lithoclast grainstones. Dark brown to black opaque, carbonaceous material is often concentrated along stylolites and disseminated throughout the matrix. Floatstone and rudstone beds (5-10 cm thick) may be interbedded and dark brown lime mudstone to peloid wackestone beds (2.5-15 cm

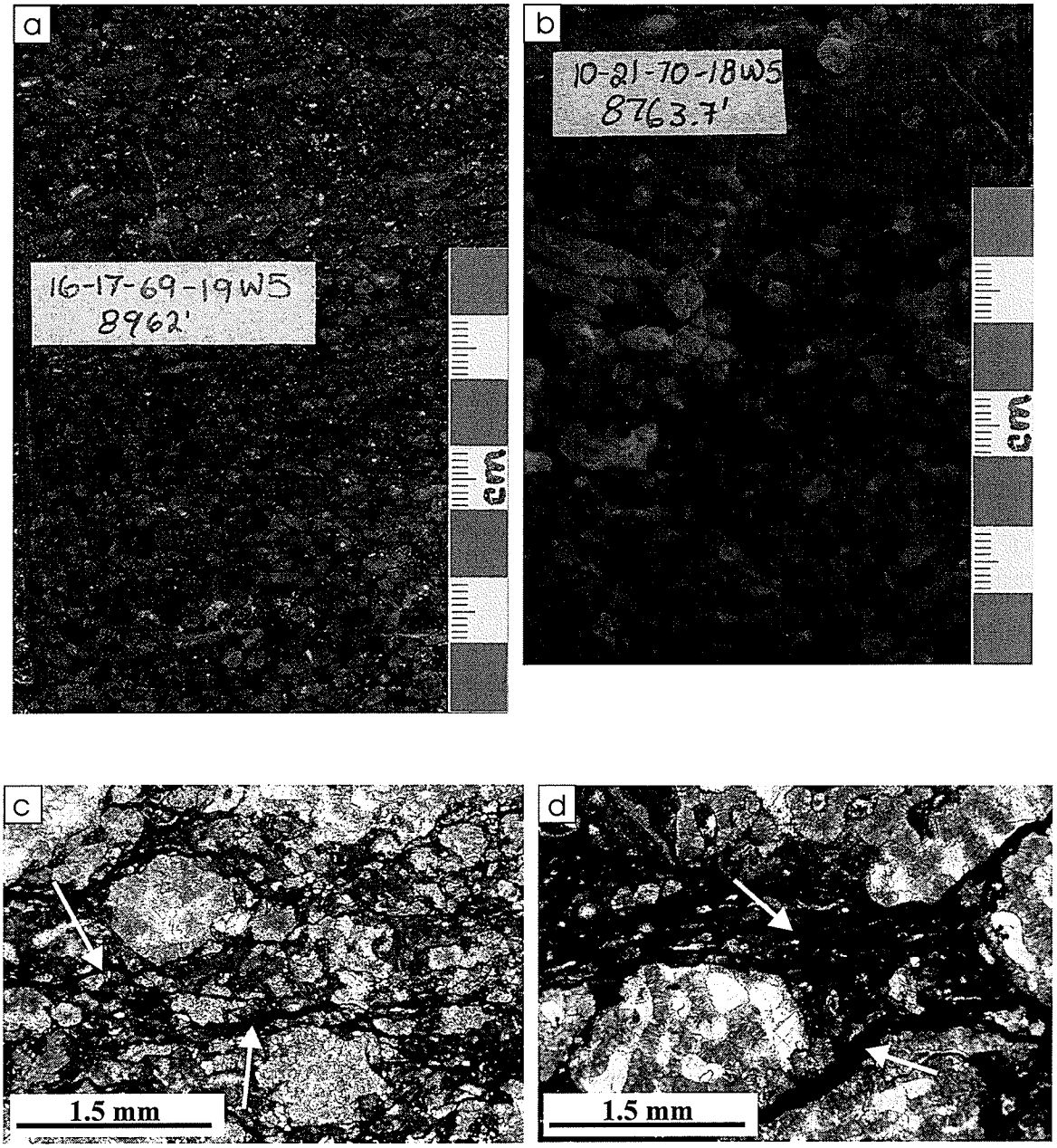


Figure 4.7 Lithofacies E, dark brown *Amphipora* rudstones. a and b) Core photographs of *Amphipora* rudstones with a carbonaceous peloid-lithoclast wackestone matrix, (a) 16-17-69-19W5, 2731.6 m (8962'), (b) 10-21-70-18W5, 2643.7 m (8673.7'). c and d) Photomicrographs of *Amphipora* rudstones with a carbonaceous lithoclast wackestone to packstone matrix containing abundant carbonaceous stylolites (arrows), 12-32-70-18W5, 2636.8 m (8651').

thick) occur locally. Overall fining upward sequences (0.5-1.5 m thick), characterized by decreasing abundance of *Amphipora* up-section, are observed. Lower lithofacies contacts are commonly sharp, whereas upper lithofacies contacts range from gradational to sharp.

Allochems comprise 30-85% of lithofacies E and *Amphipora* are the dominant constituent (10-80%). *Amphipora* grains are commonly fragmented and have geopetal internal sediment. Branching cylindrical stromatoporoids are minor framework grains composing only up to 5% of the rock. Rare constituents include bulbous, nodular and irregular stromatoporoids. Peloids are the dominant matrix constituents and skeletal grains are common including calcispheres, minor ostracods and rare gastropods. Skeletal grains are commonly fragmented and micritized. Porosity is absent to very poorly developed (< 1%). Very minor intraparticle porosity may be developed in *Amphipora* galleries.

4.6.2 Interpretation

Dark brown *Amphipora* rudstones are interpreted to have been deposited in a low energy, subtidal environment. The high lime mud content suggests low energy conditions. The abundance of *Amphipora* suggests poorly oxygenated and above normal salinity water conditions (cf. Klovan, 1964; Murray, 1966; Kershaw, 1998). The low diversity fauna (predominantly *Amphipora*, calcispheres and ostracods) is consistent with the community structure of a restricted or stressed environment that exists in euryhaline conditions (e.g. Murray, 1966; Havard and Oldershaw, 1976). The presence of carbonaceous material in lithofacies E also supports locally reducing or poorly oxygenated conditions (e.g.

Demaison and Moore, 1980). Organic carbon can be preserved under oxic waters with rapid sedimentation, but there is no evidence for this condition in lithofacies E.

Lithofacies E is similar to the dark brown carbonaceous *Amphipora* rudstones to floatstones in the Judy Creek reef complex described by Wendte and Stoakes (1982), Wendte (1992c) and Wendte and Muir (1995) and the muddy lagoon lithofacies recognized in the Snipe Lake reef complex by I. Muir and others (unpublished data, 1988). In these studies, the dark limestones were interpreted to have been deposited in deep restricted waters in a lagoon.

4.7. Lithofacies F: Stromatoporoid Floatstones to Rudstones

4.7.1. Description

This lithofacies consists of tan to light grey stromatoporoid floatstones to rudstones and ranges from 0.7 to 5.2 m thick (Figure 4.8). The matrix is composed of peloid-skeletal grainstones, and less commonly packstones. Lower and upper lithofacies contacts are gradational or sharp.

Allochems comprise 45-85% of lithofacies F and include a variety of stromatoporoids. Robust branching cylindrical stromatoporoids are the dominant constituent (30-55%) and bulbous stromatoporoids are common (5-25%). Hemispherical, thick tabular, thin tabular and nodular stromatoporoids are also present. Stromatoporoid grains are commonly fragmented, randomly oriented and have micritized margins. Rugose corals and oncoids are very rare. The moderately sorted matrix is composed of peloids and a variety of

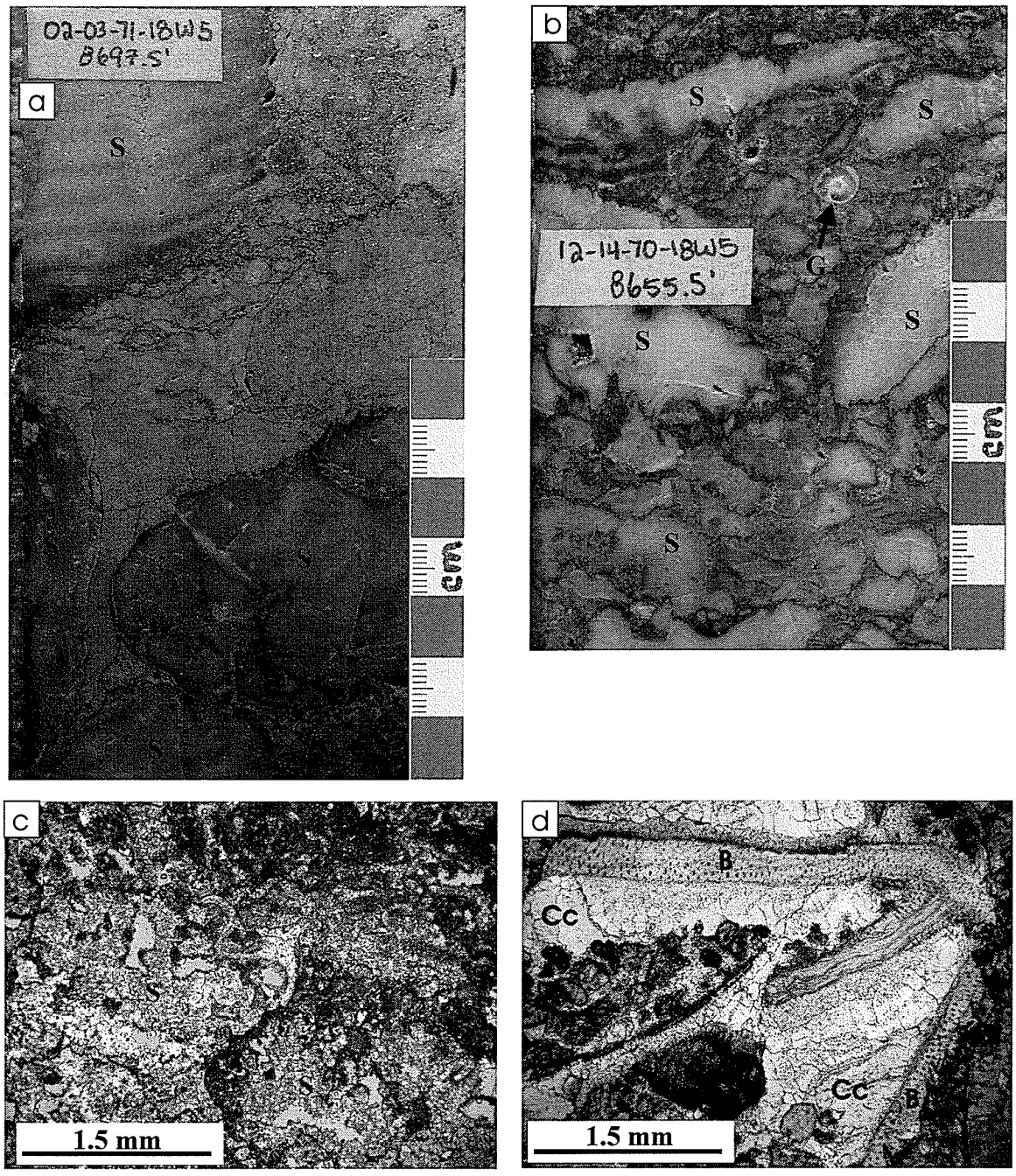


Figure 4.8 Lithofacies F, stromatoporoid floatstones to rudstones. a) Core photograph of stromatoporoid floatstone to rudstone with bulbous stromatoporoids (S), 02-03-71-18W5, 2651 m (8697.5'). b) Core photograph of stromatoporoid rudstone with abundant stromatoporoid fragments (S) and rare gastropods (G), 12-14-70-18W5 2638.2 m (8655.5'). c) Photomicrograph of stromatoporoid rudstone. Stromatoporoid grains (S) are highly fragmented with good intraskeletal porosity (shown by blue epoxy), 12-27-70-18W5, 2641.7 m (8667'). d) Photomicrograph of peloid-skeletal grainstone matrix. Brachiopod fragments (B) are common and interparticle spaces are occluded by blocky calcite cements (Cc), 12-14-70-18W5, 2638 m (8655').

skeletal fragments which, in order of decreasing abundance, include brachiopods, gastropods and ostracods. Porosity is usually well developed in this lithofacies, consisting of predominantly interparticle (2-10%) and intraparticle (2-5%) with minor vuggy (<5%) porosity.

4.7.2 Interpretation

Stromatoporoid floatstones to rudstones are interpreted to have been deposited in a high energy, shallow subtidal environment. The paucity of lime mud and highly fragmented and randomly oriented nature of stromatoporoid and skeletal grains indicate high energy conditions (cf. Fishbuch, 1968). Robust branching cylindrical, bulbous, nodular, hemispherical and tabular stromatoporoids grew preferentially in shallow, turbulent, open marine waters (e.g. Klovan, 1964; Murray, 1966; Kershaw, 1998). High faunal abundance and diversity and lack of euryhaline fauna (*Amphipora*-calcisphere-ostracod assemblage) suggest deposition occurred in open marine conditions with normal salinity (cf. Murray, 1966).

Lithofacies F is similar to an abraded stromatoporoid rudstone to boundstone lithofacies described by Wendte and Stoakes (1982), I. Muir and others (unpublished data, 1988), Wendte (1992c) and Wendte and Muir (1995) in the Judy Creek and Snipe Lake reef complexes. In these studies, this lithofacies was interpreted to have been deposited in high energy, well circulated, open marine conditions.

4.8 Lithofacies G: Tabular Stromatoporoid Rudstones

4.8.1 Description

This lithofacies consists of light to medium brown, branching cylindrical and tabular stromatoporoid floatstones to rudstones and possible boundstones that range from 0.6 to 7.7 m thick (Figure 4.9). The matrix is composed of poorly sorted peloid-skeletal wackestones to grainstones, and less commonly wackestones. Tabular stromatoporoids are often aligned parallel to bedding and are possibly in-situ, whereas other stromatoporoid grains are fragmented and randomly oriented. Lower and upper contacts are generally gradational but can be sharp when coincident with the tops of reefal cycles (see section 5.3).

Allochems comprise 60-80% of lithofacies G with robust branching cylindrical and thin and thick tabular stromatoporoids being the dominant constituents. Robust branching cylindrical stromatoporoids comprise 20-45% of the rock. Thin tabular stromatoporoids are more common (15-50%) in lower intervals of the lithofacies and occur in a muddy matrix (wackestones to packstones). In contrast, thick tabular stromatoporoids are more common (5-20%) in the upper intervals of the lithofacies and are associated with a grainy matrix (packstones to grainstones). Bulbous stromatoporoids are minor constituents and *Amphipora* and rugose corals are rare. The matrix is composed of peloids and variable skeletal fragments including brachiopods, ostracods, gastropods and echinoderms. Porosity is moderately developed, but can be well developed locally. Interparticle porosity is the most common ranging from 5 to 10%. Intraparticle porosity occurring mainly in stromatoporoid galleries is less common ranging from 3 to 5%.

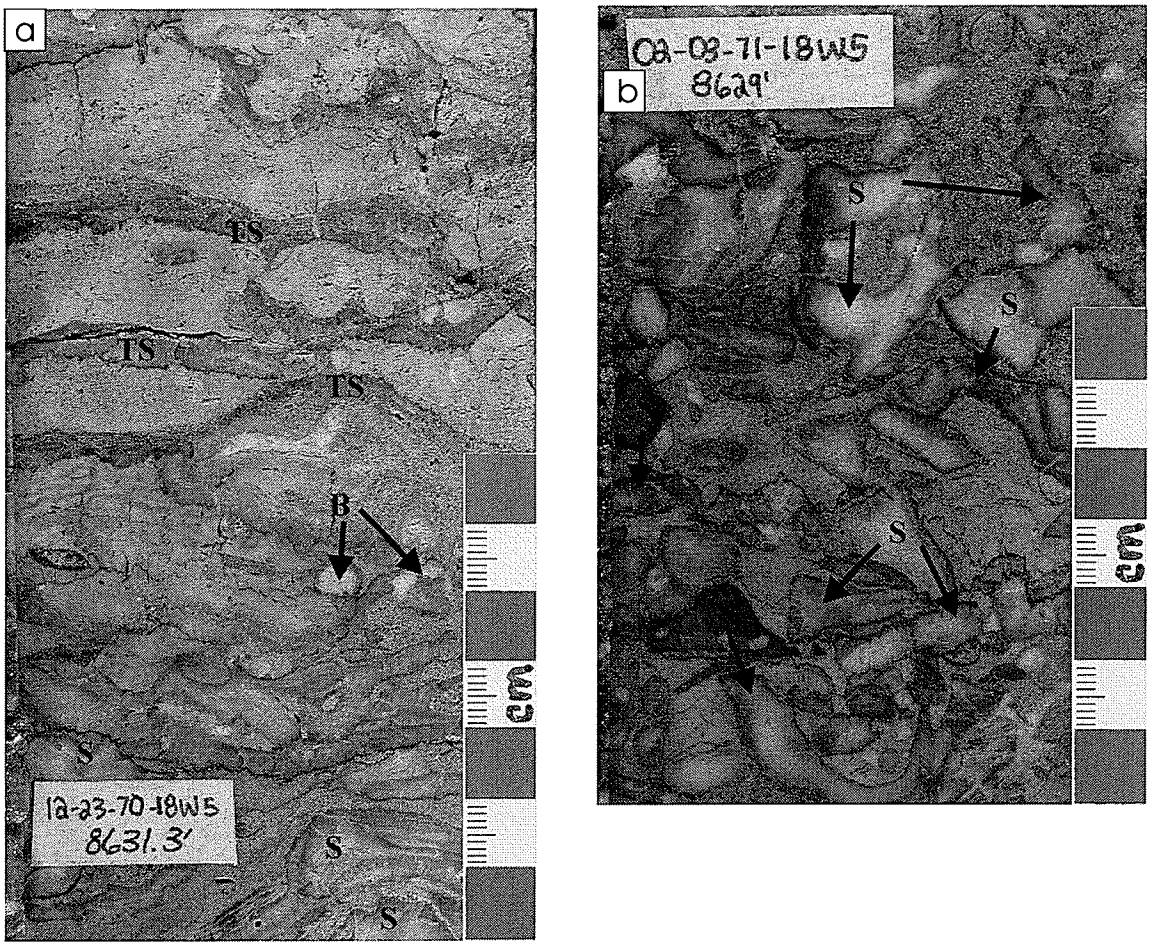


Figure 4.9 Core photographs of lithofacies G, tabular stromatoporoid rudstones. a) Medium brown, thin tabular stromatoporoid floatstone to rudstone with a peloid-skeletal grainstone matrix. Thin tabular stromatoporoids (TS) are aligned parallel to bedding. Other stromatoporoids include branching cylindrical stromatoporoids (B) and possible bulbous and tabular stromatoporoid fragments (S), 12-23-70-18W5, 2630.8 m (8631.3'). b) Light brown, branching cylindrical stromatoporoid rudstone with a peloid packstone matrix. Stromatoporoid fragments (S) consist of branching cylindrical, tabular and bulbous forms, 02-03-71-18W5, 2630.1 m (8629').

4.8.2 Interpretation

Tabular stromatoporoid floatstones are interpreted to have been deposited in a low to moderate energy, well circulated, subtidal environment. The moderate amount of lime mud in the lower intervals and decreasing amounts of lime mud in the upper interval are interpreted to reflect gradually increasing energy conditions (see section 4.2.2). Tabular (thin and thick) stromatoporoids occurred in both high energy as well as low energy waters (e.g. Klovan, 1964; Murray, 1966; Fischbuch, 1968; Kershaw, 1998). However, in the Swan Hills Formation they are more abundant in quiet, deeper water environments (e.g. Murray, 1966). The presence of branching cylindrical stromatoporoids, brachiopods and echinoderms suggests that deposition occurred in waters of normal marine salinity (cf. Murray, 1966).

Lithofacies G is similar to stromatoporoid rudstones with branching cylindrical, thick tabular and thin tabular stromatoporoids previously recognized in the Snipe Lake and Judy Creek reef complexes (Wendte and Stoakes, 1982; I. Muir and others, unpublished data, 1988; Wendte, 1992c; Wendte and Muir, 1995). These deposits were interpreted to have been deposited in a well-circulated but low energy subtidal environment.

4.9 Lithofacies H: Dark Brown Thin Tabular Stromatoporoid Floatstones

4.9.1 Description

This lithofacies consists of medium to dark brown, thin tabular stromatoporoid floatstones to rudstones and possible minor boundstones which range from 0.9 to 2.9 m thick (Figure 4.10). The matrix is composed of peloid wackestones to packstones. Dark

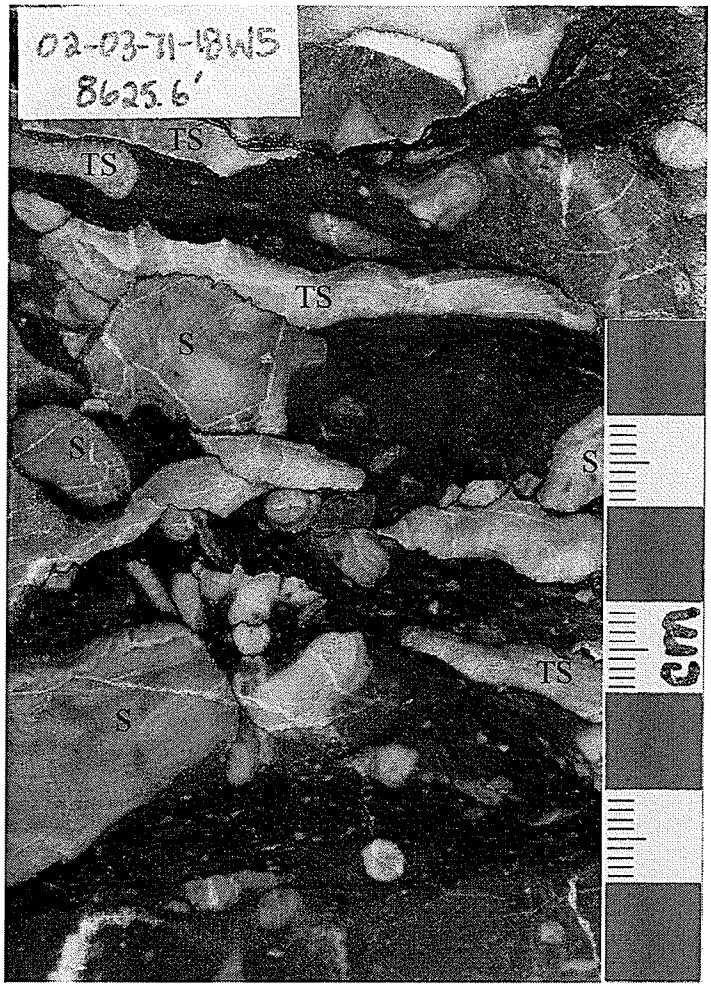


Figure 4.10 Lithofacies H, dark brown thin tabular stromatoporoid floatstone with a carbonaceous peloid wackestone to packstone matrix. Thin tabular stromatoporoids (TS) are aligned parallel to bedding. Stromatoporoid fragments (S) include tabular, bulbous and branching cylindrical stromatoporoids, 02-03-71-18W5, 2629.1 m (8625.6').

brown to black carbonaceous material is concentrated along stylolites and disseminated throughout the matrix. Thin tabular stromatoporoids appear to be aligned parallel to bedding, and are possibly in-situ locally. Lower and upper contacts are generally gradational but can be sharp when coincident with the tops of reefal cycles (see section 5.3).

Allochems comprise 40-65% of lithofacies H with thin tabular stromatoporoids (20-50%) and branching cylindrical stromatoporoids (15-40%) being the dominant constituents. Thick tabular stromatoporoids occur less commonly and in lower abundances as compared to lithofacies G. Other constituents include rare bulbous stromatoporoids. Most stromatoporoid and skeletal grains are fragmented and randomly oriented. The matrix is composed of peloids and variable skeletal fragments including stromatoporoids, brachiopods and crinoids. Porosity is absent to very poorly developed (<1% intraparticle).

4.9.2 Interpretation

Dark brown, thin tabular stromatoporoid floatstones are interpreted to have been deposited in a low energy, slightly restricted, deep subtidal environment. This lithofacies has a high lime mud content reflecting low energy conditions. The presence of carbonaceous material in the matrix also supports deposition in quiet water conditions with restricted water circulation (refer to section 4.6.2). Thin tabular stromatoporoids were adapted to grow on micritic substrate, such as those found in deep forereef environments, where sedimentation rates were low (e.g. Wendte and Stoakes, 1982;

Wendte, 1992c).

Dark, carbonaceous thin-tabular rudstones and floatstones recognized in the Snipe Lake and Judy Creek reef complexes by previous studies are similar to lithofacies H, and were interpreted to have been deposited in quiet, deep marine waters on micritic substrates (Wendte and Stoakes, 1982; I. Muir and others, unpublished data, 1988; Wendte 1992c; Wendte and Muir, 1995).

4.10 Lithofacies I: Skeletal Grainstones

4.10.1 Description

This lithofacies consists of tan to medium brown, skeletal to skeletal-peloid packstones to grainstones and is 0.6 to 1.3 m thick (Figure 4.11). Weak crossbedding is rare in this lithofacies. Lower lithofacies contacts are commonly sharp and upper contacts are generally gradational.

Allochems comprise 65-80% of this lithofacies with micritized skeletal grains being the dominant constituents. Identifiable skeletal fragments include branching cylindrical stromatoporoids, possible thick and thin tabular stromatoporoids, brachiopods, crinoids, rare ostracods and red calcareous algae (*Goniolithon*). Peloids are also commonly present. Interparticle porosity is well developed in this lithofacies ranging from 10 to 15%.

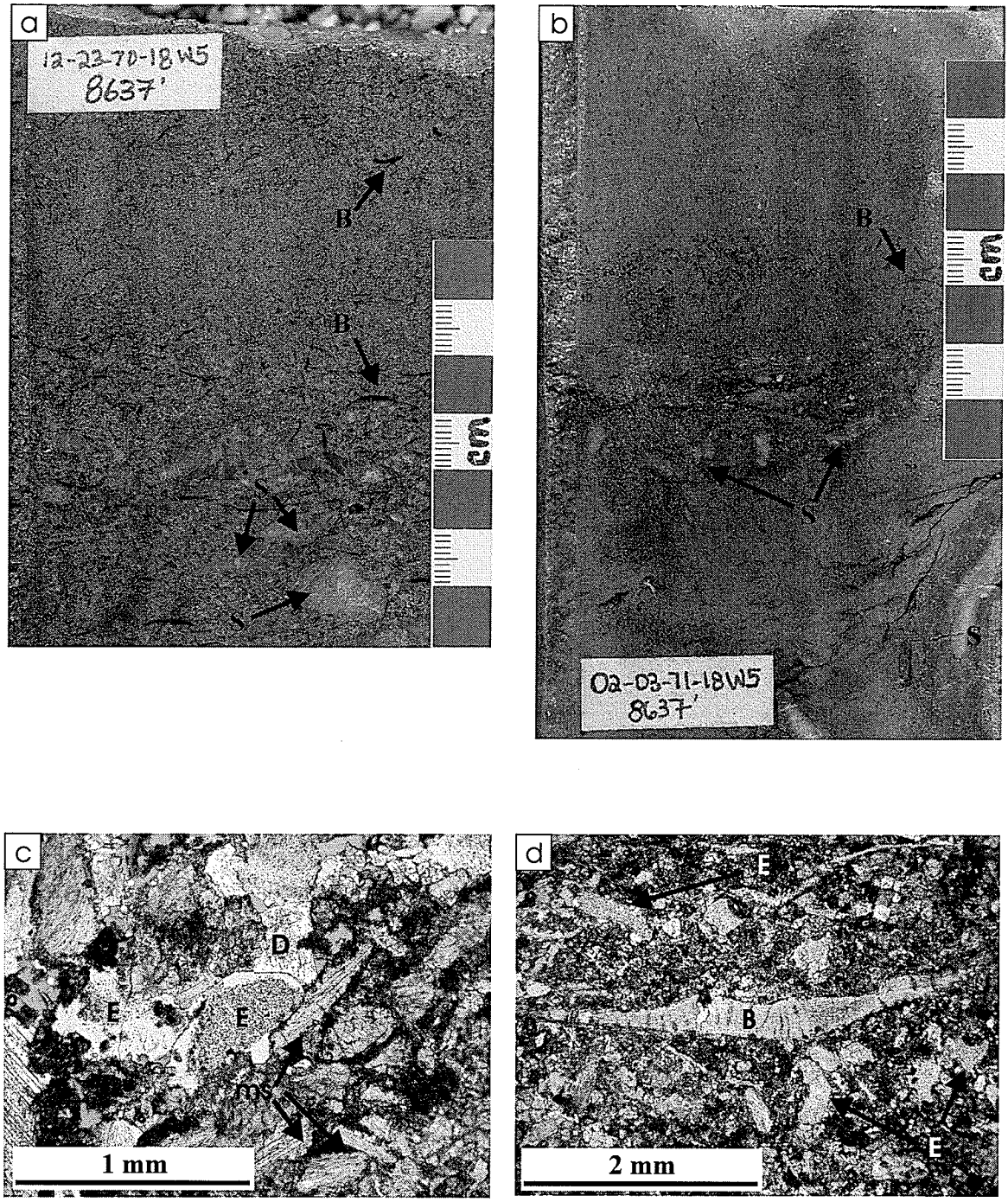


Figure 4.11 Lithofacies I, skeletal grainstones with stromatoporoid (S) and brachiopod (B) fragments. a) Core photograph, 12-23-70-18W5, 2632.6 m (8637'). b) Core photograph, 02-03-71-18W5, 2631.0 m (8632'). c) Photomicrograph of (a) with interparticle porosity up to 15% (blue). Echinoderm fragments (E) have inclusion-free, non-ferroan to ferroan syntaxial calcite overgrowths. Unidentified skeletal grains are micritized and mollusc fragments (ms) are present. Ferroan dolomite rhombs (D) postdate syntaxial cements in interparticle pores. d) Photomicrograph of (b) showing micritized skeletal fragments including brachiopods (B) and echinoderms (E).

4.10.2 Interpretation

Skeletal grainstones are interpreted to have been deposited in a high energy, open marine environment. The lack of lime mud and fragmented nature of skeletal grains are consistent with physical abrasion and reworking in high energy conditions. The occurrence of cross-bedding indicates that deposition occurred in relatively shallow waters above the fair-weather wave base or from sediment gravity flows. The presence of stenohaline organisms (echinoderms, brachiopods, branching cylindrical and tabular stromatoporoids) indicates that skeletal fragments were derived from open marine waters (cf. Murray, 1966; I. Muir and others, unpublished data, 1988).

Lithofacies I is similar to the micritized skeletal and peloidal grainstones to packstones in previous studies of the Snipe Lake and Judy Creek reef complexes (Wendte and Stoakes, 1982; I. Muir and others, unpublished data, 1988; Wendte, 1992c; Wendte and Muir, 1995). These deposits were interpreted to represent allochthonous sands derived from the breakdown and reworking of larger reef builders in high energy, open marine environments upslope.

4.11 Lithofacies Associations

The nine lithofacies recognized in the P4 to R0.5 successions in the Snipe Lake reef complex, as previously described, can be genetically grouped into two lithofacies associations: (1) a reef margin association that is composed of lithofacies F, G, H and I, and (2) a lagoonal association that is composed of lithofacies, A, B, C, D and E

(summarized in Table 4.1). Similar lithofacies associations have been described by Wendte and Stoakes (1982), Wendte (1992c), and Wendte and Muir (1995).

4.11.1 Reef Margin Association

Lithofacies F, G, H and I occur together in packages (5.5 to 9.3 m thick) in the R0.5 succession in the Snipe Lake reef complex. These lithofacies are laterally gradational and comprise meter-scale, shallowing-upward (reefal) cycles (see section 5.3). Lithofacies F is more widespread than the other lithofacies, occurring in the reef margin and also in more reef interior positions, whereas lithofacies G, H and I are present only in the reef margin setting (Enclosures 2 and 3). When present in the reef interior, lithofacies F grades laterally into lithofacies G, H or I in the reef margin setting.

Lithofacies F, G, H and I are interpreted to have been deposited in high to low energy conditions in the reef flat to reef foreslope environments (Figure 4.2). The reef flat is a high energy, open marine zone characterized by massive carbonate deposits and large, massive (hemispherical) to plate-like (tabular) stromatoporoids (James and Bourque, 1992). The reef foreslope is a low to moderate energy zone characterized by bedded in-situ to allochthonous carbonate deposits that dip and thin away from the reef core. The foreslope environment is inhabited by plate-like (tabular), domical (bulbous) and dendroid (branching cylindrical) stromatoporoids.

Lithofacies F is interpreted to have been deposited in a high energy reef flat to upper foreslope environment. The lack of lime mud and abundance of fragmented reef-building

organisms (hemispherical, bulbous, thick and thin tabular stromatoporoids) suggest that this lithofacies represents the highest energy environment that is most proximal to the zone of continuous wave action near the reef margin. This lithofacies is similar in composition to the reef flat/shoal margin and reef margin/upper foreslope lithofacies described by Wendte and Stoakes (1982), I. Muir and others (unpublished data, 1988), Wendte (1992c) and Wendte and Muir (1995). Lithofacies G is interpreted to have been deposited in low to moderate energy, open marine conditions of the middle foreslope. The presence of in-situ and allochthonous stromatoporoids suggests that deposition occurred in slightly deeper water and lower energy conditions relative to lithofacies F. Increased lime mud content in lower intervals of this lithofacies reflects lower energy conditions downslope from the reef margin. Lithofacies G is very similar in composition to middle foreslope limestones described by Wendte and Stoakes (1982), I. Muir and others (unpublished data, 1988), Wendte (1992c) and Wendte and Muir (1995). Lithofacies H is interpreted to have been deposited in a low energy, slightly restricted environment in the lower foreslope. This lithofacies has higher lime mud content and shows a decrease or absence of thick tabular stromatoporoids in comparison to lithofacies G. Therefore, lithofacies H represents lower energy conditions and deposition further downslope relative to lithofacies G. This lithofacies is very similar to the lower foreslope limestones facies described by Wendte and Stoakes (1982), I. Muir and others (unpublished data, 1988), Wendte (1992c) and Wendte and Muir (1995).

Skeletal grainstones of lithofacies I occur at the base of reefal cycles (see section 5.3 and Figure 5.1) and in between intervals of lithofacies G and H, and are therefore interpreted

to be allochthonous foreslope sands that were deposited throughout the reef foreslope environment. The abundance and diversity of micritized skeletal fragments of open marine fauna suggest that the debris was sourced from throughout the reef flat to reef foreslope environment. This lithofacies is similar to the foreslope sands lithofacies described by Wendte and Stoakes (1982). They interpreted the skeletal packstones and grainstones to be derived from the physical and biological breakdown of larger reef organisms that were shed from the shallow, high energy upslope reef environments and transported downslope by wave and gravity processes.

4.11.2 Lagoonal Association

Lithofacies A, B, C, D and E occur together in packages (0.75 to 4.6 m thick) in the upper P4, and the P5 and R0.5 successions in the Snipe Lake reef complex. These lithofacies are laterally gradational and comprise meter-scale, shallowing-upward (lagoonal) cycles (see section 5.4). These lithofacies are present in the platform-reef interior and platform-reef margin settings in the P4, P5 and R0.5 megacycles, however they are poorly developed in the reef margin setting in the R0.5 megacycle (Enclosures 2 and 3). Lithofacies A and B are laterally gradational and lithofacies B typically occurs in a marginward position. Similarly, lithofacies C and D are laterally gradational and lithofacies C typically occurs in a more marginward position. Lithofacies E is the most common in the platform and reef interior and is laterally gradational with lithofacies C or D in the platform and reef margin settings.

Lithofacies A, B, C, D and E are interpreted to have been deposited in intertidal to shallow to deep lagoon environments in the platform and reef interior (Figures 4.1 and 4.2). Rimmed platforms have reefs or sand shoals at the platform margin which reduce the interaction between the open-ocean and sheltered lagoon (James and Kendall, 1992; Jones and Desrochers, 1992). These deposits can potentially restrict water circulation resulting in increased salinities in the lagoon. Reefs or sand shoals along the platform margin also absorb ocean and storm waves, which generates lower energy environments towards the interior. Similarly, low energy environments are present in the sheltered back reef and lagoons behind the reef flat to reef crest of isolated reefs (James and Bourque, 1992). Back reefs and lagoons of Devonian reef complexes are typically characterized by lime mud and delicate stick-like (*Amphipora*) to dendroid (branching cylindrical) stromatoporoids (e.g. Murray, 1966; Fischbuch, 1968). Locally developed mounds (structures built by small, delicate and/or solitary organisms) or islands may have generated localized environments, such as intertidal to supratidal flats (e.g. I. Muir and others, unpublished data, 1988). This may account for evidence of locally shallow or deeper conditions that could not be correlated throughout the platform and reef interior (see section 5.4.1).

Lithofacies A and B were deposited in an intertidal environment in the platform interior and reef interior (back reef). Lithofacies A is interpreted to have been deposited along low energy tidal flats behind the lagoon and locally in sheltered (low energy, shallow water) conditions behind *Amphipora* mounds (e.g. I. Muir and others, unpublished data, 1988) or islands. Lithofacies B is closely associated with lithofacies A, but is interpreted

to be beach deposits along higher energy shorelines around islands or *Amphipora* mounds in the lagoon. Allochthonous stromatoporoid (robust branching cylindrical, bulbous) fragments were likely transported from adjacent subtidal lagoonal environments because these stromatoporoids would not have thrived in intertidal environments (cf. I. Muir and others, unpublished data, 1988).

Lithofacies C, D and E are interpreted to have been deposited in the subtidal lagoonal environment. The transition of lithofacies C to D to E represents progressively deeper and more restricted water conditions in the lagoon. Lithofacies C has the lowest lime mud content and the highest abundance of open marine fauna (branching cylindrical stromatoporoids) of the three lithofacies. Therefore, lithofacies C is interpreted to represent the highest energy, open marine conditions in the subtidal lagoonal environment. These environmental conditions were present in the shallowest part of the lagoon directly behind the platform and reef margin (e.g. Fischbuch, 1968). A dendroid-stromatoporoid lithofacies similar to lithofacies C was recognized in other Swan Hills reef complexes by other studies and was interpreted to be a transitional unit between reef flat/reef margin and back-reef lagoonal deposits (e.g. Fischbuch, 1968). Lithofacies D is interpreted to have been deposited in slightly restricted to open marine conditions in the more interior portion of the lagoon as suggested by the higher lime mud content and *Amphipora* in this lithofacies relative to lithofacies C (cf. Fischbuch, 1968). Lithofacies E is interpreted to have been deposited in the deep, restricted part of the lagoon based on the abundance of lime mud, organic matter and restricted marine fauna (*Amphipora*, calcispheres, ostracods). The highest salinity conditions and sluggish water circulation

were present towards the center of the lagoon (e.g. Murray, 1966; Wendte and Stoakes, 1982), where conditions would be favorable for organic matter accumulation.

CHAPTER 5 – PLATFORM-REEF CYCLICITY

5.1 Introduction

The Swan Hills Formation in the Snipe Lake reef complex displays major changes in the distribution and type of lithofacies. These lithofacies patterns are reflected as third order depositional cycles as defined by Wendte and Uyeno (2005). Understanding platform and reef evolution in the context of these depositional cycles can improve our understanding of the history and influence of relative sea level fluctuations.

5.2 Depositional Cycles

A chronostratigraphic framework is well established for Devonian strata of the WCSB. Devonian sedimentation can be considered in terms of four relative levels of growth by correlating time-synchronous cycle boundaries (Wendte, 1992b). First-order cycles show major shifts in facies belts that can be correlated across the Alberta Basin; these represent large-scale transgressive-regressive sequences (refer to sections 3.1 and 3.3). Second-order cycles or megacycles show significant shifts in facies belts that can commonly be correlated within first-order cycles. Third-order cycles correspond to smaller scale shallowing-upward cycles that are often only observed in the more "incompetent" environments such as lagoonal environments in the platform and reef interior. They do not show significant shifts in facies belts and are therefore often difficult to correlate in the platform or reef margin.

However, the most recent work completed by Wendte and Uyeno (2005) has revised the definitions of these depositional sequences in Middle to Upper Devonian Beaverhill Lake strata. Three orders of transgressive-regressive cycles were defined by the lateral extent of facies belts and stratigraphic position of the subaerial unconformities. Similar to previous definitions, the Beaverhill Lake succession and the underlying Watt Mountain Formation together form a first-order, transgressive-regressive cycle. This first-order cycle is divided into two second-order transgressive-regressive cycles (previously not defined), whose tops are marked by major subaerial unconformities. Third-order cycles are typically marked by landward shifts of argillaceous sediment in the Central Alberta Basin or transgressive pulses on banks or isolated reef complexes (previously defined as second-order cycles by Wendte, 1992b). Depositional cycles within third-order cycles recognized in this study were not defined by Wendte and Uyeno (2005) and are interpreted to be equivalent to fourth-order cycles.

5.3 Third-order Reefal Cycles

Sedimentation in the Snipe Lake reef complex produced several major depositional sequences or megacycles (e.g. Wendte and Stoakes, 1982; Wendte, 1992c; Wendte and Muir, 1995) and are defined as third-order transgressive-regressive cycles (Wendte and Uyeno, 2005) (refer to sections 3.6.1 and 5.5). They are recognized in this study as reefal cycles occurring in the reef margin setting. Where completely developed, each reefal cycle (5.5 to 9.3 m thick) grades upwards from dark brown thin tabular stromatoporoid floatstones (lithofacies H) to tabular stromatoporoid rudstones (lithofacies G) into stromatoporoid rudstones (lithofacies F) (Figure 5.1). A thin unit (0.6-1.3 m) of skeletal

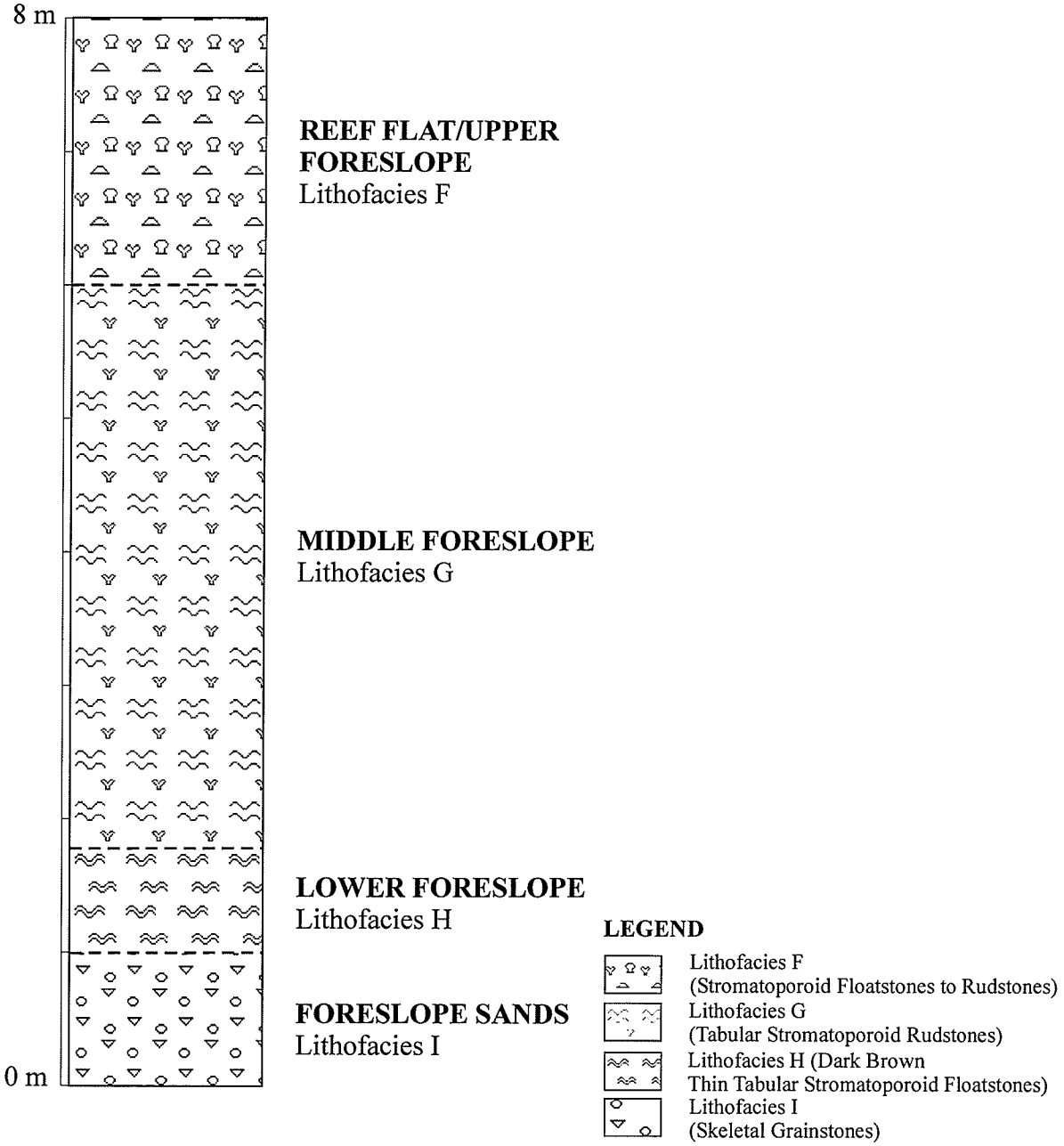


Figure 5.1 Shallowing upward succession of lithofacies in a third-order reefal cycle observed between P5 and R0.5 megacycle contacts at the reef margin setting in the Snipe Lake reef complex.

foreslope sands (lithofacies I) locally occurs at or near the base of cycles. Reefal cycles are shallowing-upwards sequences grading from lower foreslope (lithofacies H) to the middle foreslope (lithofacies G) and into shallow reef flat to upper foreslope (lithofacies F) deposits. Lithofacies H is commonly a thinner unit (0.9-2.9 m) and is only observed to occur in the two most marginal wells at 02-03-71-18W5 (2627.2-2630.1 m; 8619.5-8629') and 04-26-70-18W5 (2632.9-2633.8 m; 8638-8641'). Lithofacies G is the thickest unit (1.2 to 7.8 m) and composes the majority of the reefal cycle. Lithofacies F ranges from 1.2 to 4 m thick. Lithofacies I is interpreted to have formed by the physical and biological breakdown of reef organisms from the reef flat (refer to sections 4.10 and 4.11.1) and may represent more extensive reworking during periods of low reef aggradation (cf. Wendte, 1992c).

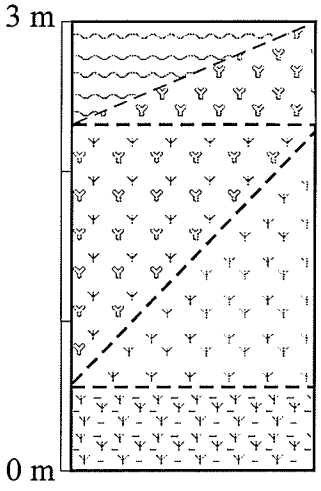
Six of the wells examined in this study were at or near the position of the reef margin during R0.5 deposition. Complete or near complete reefal cycles are observed in three wells in the reef foreslope: 02-03-71-18W5, 2627.2-2633.2 m (8619.5-8639'); 04-26-70-18W5, 2625.2-2634.5 m (8613-8643.5'); and 12-23-7018W5, 2623.9-2632.9 m (8608.5-8638'). The other three wells are in slightly more interior positions (reef flat) and have reefal cycles that are almost exclusively composed of thick (2.7-5.2 m) successions of lithofacies F: 02-33-70-18W5, 2631.6-2638.3 m (8634-8656'); 12-27-70-18W5, 2639.4-2642.2 m (8659.3-8668.5'); and 12-14-70-18W5, 2637.2-2644.9 m (8653.6-8677.5').

Reefal cycles are interpreted to reflect episodic rises in relative sea level that correspond to stages of reef growth (Wendte and Stoakes, 1982). They represent shallowing upward sequences in more "competent" environments such as reef margins, where during times of slow relative sea level rise or stillstand, the reef was able to keep up with the rate of relative sea level rise.

5.4 Fourth-order Lagoonal Cycles

In this study, third-order cycles in the platform and reef interior can be further divided into several fourth-order lagoonal cycles. Each lagoonal cycle ranges from 0.75 to 4.6 m thick (average 1.2-2 m thick) and where completely developed, a cycle shallows upwards from deep, restricted lagoonal lithofacies (lithofacies E, average 50 cm thick) to open lagoonal lithofacies (lithofacies C or D, average 1.2-1.5 m thick) into tidal flat lithofacies (lithofacies A or B, 0.5-1.0 m thick) (Figure 5.2). All five lithofacies were not observed to occur within a single lagoonal cycle. When present within the same lagoonal cycle, lithofacies C usually overlies lithofacies D. Lagoonal cycles have relatively sharp upper and lower contacts (Figure 5.3).

Lagoonal cycles represent shallowing-upward events in the platform and reef interior that are interpreted to reflect incremental pulses of small-scale relative sea level rises (Wendte and Stoakes, 1982). Lagoonal cycles were terminated and new cycles initiated as these small changes in relative sea level outpaced slower sedimentation rates in the lagoon. These changes are not reflected in the reefal cycles because the reef margin grew more rapidly and was able to keep up with the rate of relative sea level rise. The cumulative

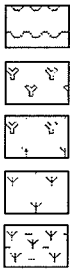


TIDAL FLAT
Lithofacies A and Lithofacies B
(Average 0.5-1.0 m thick)

SHALLOW OPEN LAGOON
Lithofacies C and Lithofacies D
(Average 1.2-1.5 m thick)

DEEP RESTRICTED LAGOON
Lithofacies E
(Average 0.5 m thick)

LEGEND



Lithofacies A
(Peloid Packstones)
Lithofacies B (Robust Branching Cylindrical Stromatoporoid Rudstones)
Lithofacies C (Branching Cylindrical Stromatoporoid Floatstones)
Lithofacies D
(Light Tan *Amphipora* Floatstones)
Lithofacies E
(Dark Brown *Amphipora* Rudstones)

Figure 5.2 Shallowing-upward succession of lithofacies in a fourth-order lagoonal cycle observed between the P4 and R0.5 megacycle contacts at the Snipe Lake reef complex.

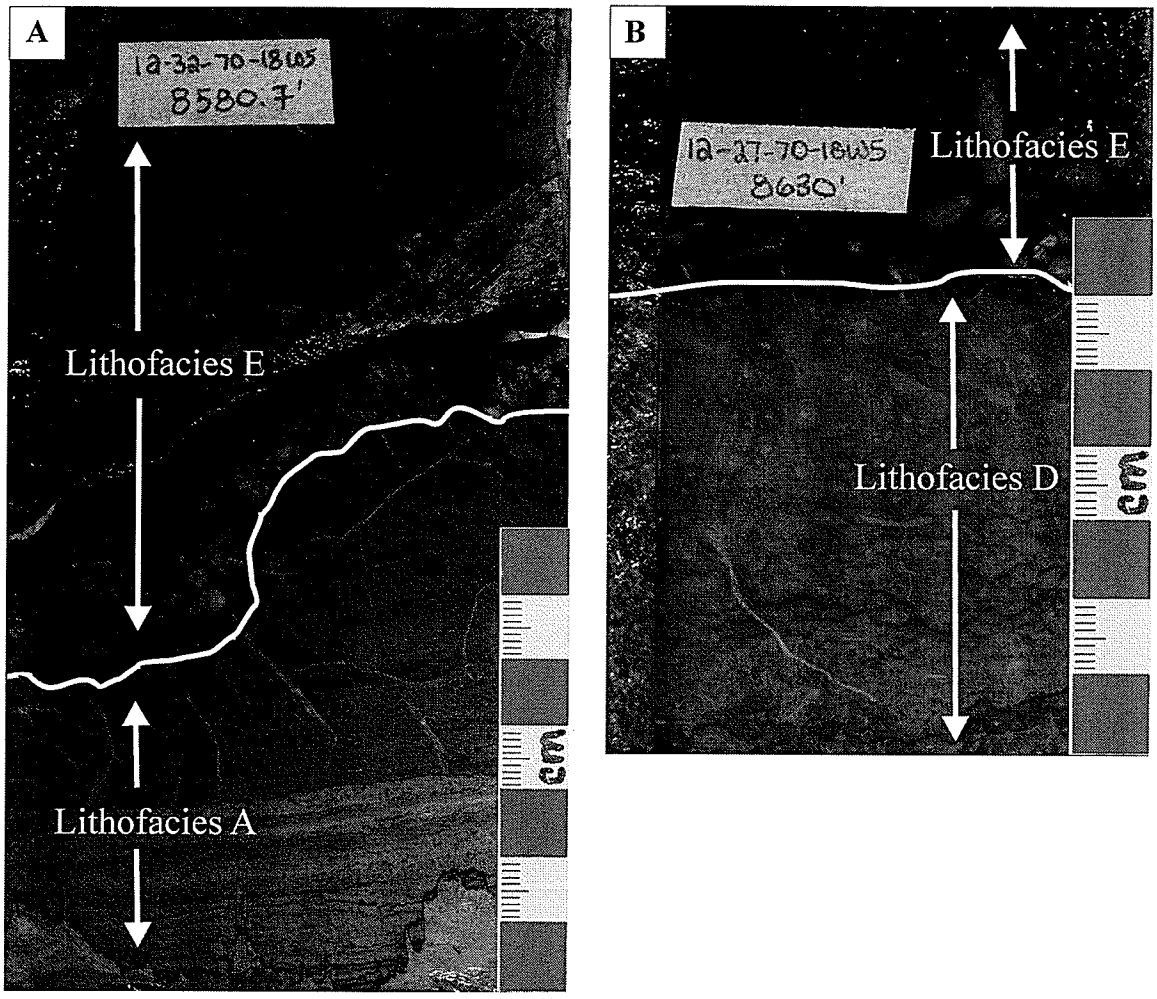


Figure 5.3 Lagoonal cycle contacts (outlined in red). a) Tan to light brown, laminated to fenestral peloid wackestone to packstone (tidal flat, lithofacies A) overlain by dark brown *Amphipora* rudstone with a carbonaceous mudstone to peloid wackestone matrix (deep lagoon, lithofacies E), 12-32-70-18W5, 2615.4 m (8580.7'). b) Medium brown *Amphipora* floatstone with a peloid wackestone matrix (open lagoon, lithofacies D) overlain by dark brown *Amphipora* floatstone with a carbonaceous peloid wackestone matrix (deep lagoon, lithofacies E), 12-27-70-18W5, 2630.4 m (8630').

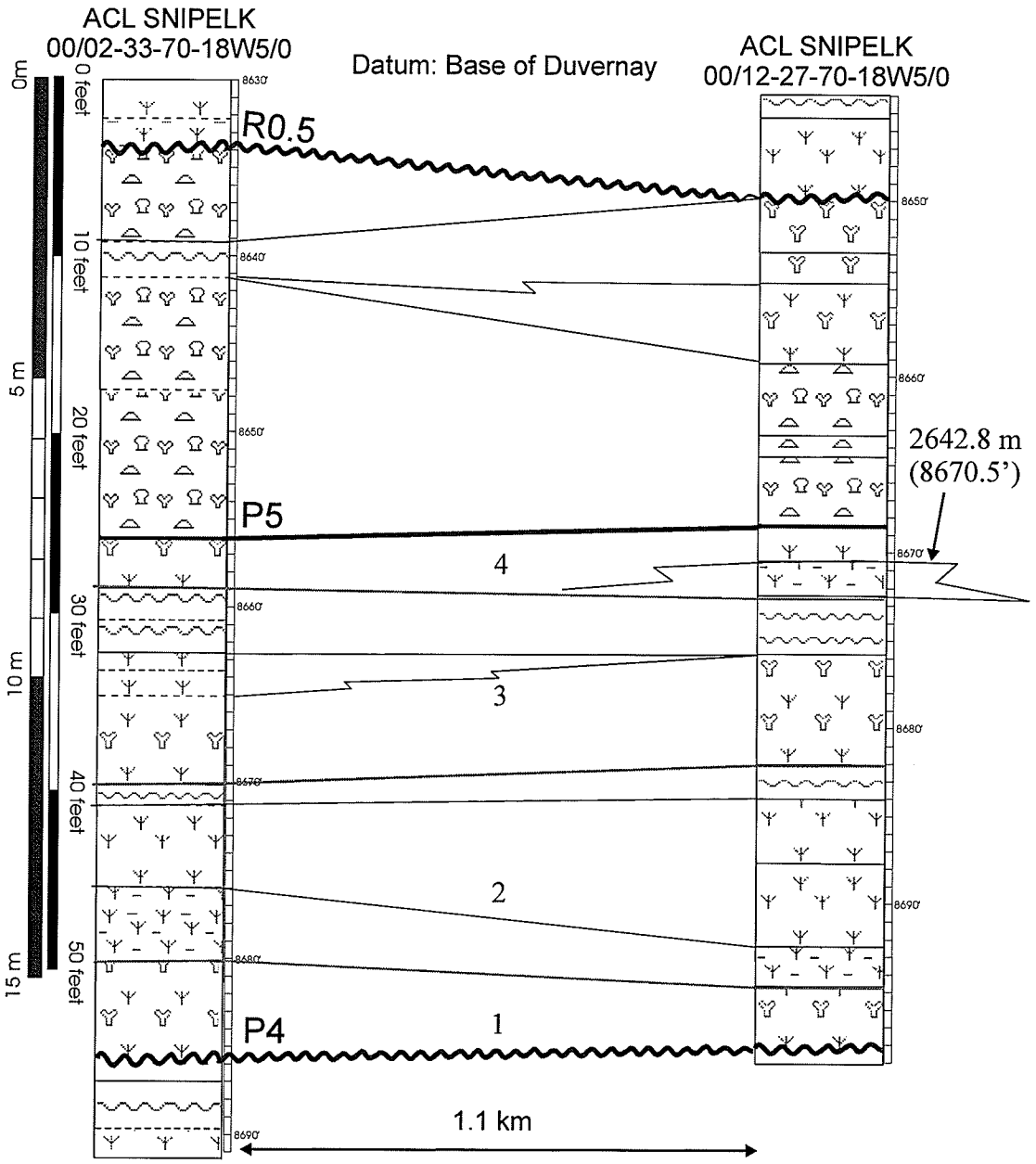
effect of these incremental sea level rises is reflected in the reef margin by thicker reefal cycles (refer to section 5.3).

5.4.1 Correlation of Lagoonal Cycles

Lagoonal cycles were correlated throughout the platform and reef interior in the P5 and R0.5 megacycles and these correlations are shown in cross-sections B-B' and C-C' (Enclosures 2 and 3). Fourth-order cycles were not observed and therefore could not be correlated in the reef margin setting.

Lagoonal cycle contacts were correlated based on several criteria: (1) stratigraphic position within the P5 or R0.5 depositional cycles; (2) similarity of lithofacies and (3) evidence of shallowing-upward conditions. Lithofacies A and B were packaged together due to their close lithofacies association and similar position within lagoonal cycles. Lithofacies C and D were also packaged together for the same reasons.

An example of correlations of lagoonal cycles between adjacent wells 02-33-70-18W5 and 12-27-70-18W5 in cross-section C-C' (Enclosure 3) is shown in Figure 5.4. Four lagoonal cycles in the P5 megacycle can be correlated between the two wells. Each lagoonal cycle occurs at a similar stratigraphic interval and is composed of similar lithofacies. However, the base of the fourth lagoonal cycle in well 12-27-70-18W5 (2642.8 m, 8670.5') has an interval of deep lagoonal deposits (lithofacies E). This lithofacies is not common in the upper portions of the P5 megacycle nor was it observed at the base of the fourth lagoonal cycle in adjacent wells. It could not be correlated



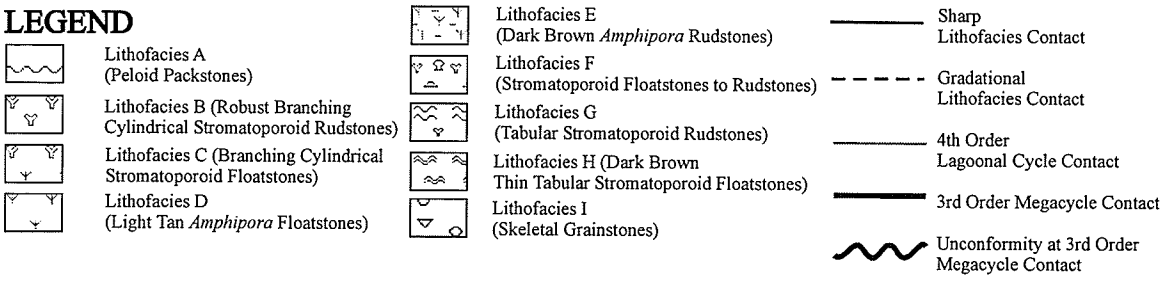


Figure 5.4 Fourth-order cyclicity shown in wells 02-33-70-18W5 and 12-27-70-18W5. Four lagoonal cycles (labeled 1 to 4) are recognized and correlated within the P5 megacycle in these two wells.

throughout the P5 succession and therefore is interpreted to be a result of locally deeper conditions.

The superposition of deep lagoonal sediments over tidal flat or beach sediments is very useful in recognizing and correlating lagoonal cycle contacts, but it is not always sufficient. More subtle lithofacies changes may still suggest a possible lagoonal cycle contact. For example, well 12-22-70-18W5 in cross-section B-B' at first inspection appears to have only three lagoonal cycles (cycle tops at 2666.6 m (8748.7'), 2660.2 m (8727.6'), 2657.7 m (8719.5'); Enclosure 2). A closer examination reveals a fining upwards *Amphipora* floatstone with a peloid wackestone-packstone matrix (lithofacies D) and the appearance of crinkly laminations and fenestrae towards the top at 2662.9 m (8736.5') which are overlain by a branching cylindrical stromatoporoid-*Amphipora* floatstone with a peloid wackestone-packstone matrix (lithofacies C). Although a tidal flat lithofacies was not fully developed at this level, the fining upwards succession, crinkly laminations and fenestrate are suggestive of shallower water (tidal flat) conditions (e.g. Murray, 1966; Roehl, 1967; Choquette and Pray, 1970; Havard, 1974) which were followed by deeper water (subtidal) conditions. Furthermore, adjacent wells have a lagoonal cycle contact at a similar stratigraphic level. For these reasons, a fourth lagoonal cycle contact is interpreted and correlated at 2662.9 m (8736.5') in well 12-22-70-18W5.

5.5 Platform and Reef Evolution (P4 to R0.5)

5.5.1 P4 Megacycle

The nature of lagoonal cycles in the P4 platform shows a backstepping sedimentation pattern (Enclosure 2). Each successive lagoonal cycle developed at a slightly more interior position than the underlying lagoonal cycle. This resulted in a backstepping platform where there are an increasing number of lagoonal cycles from the platform margin (e.g. 12-23-70-18W5, Enclosure 2) to the platform interior (e.g. 16-17-69-19W5, Enclosure 2). Tidal flat and beach lithofacies (lithofacies A and B, respectively) are overlain by deeper shallow lagoonal lithofacies (most commonly lithofacies C and D) at the P4 megacycle contact (Figure 5.5a-b). Green shales commonly occur at or directly below the P4 contact. In addition, there is evidence to suggest early meteoric dissolution and paleosol development below this surface (see Chapters 7 and 8).

The backstepping nature of the platform margin is interpreted to reflect increasing rates of relative sea level rise that outpaced sedimentation rates during P4 deposition (refer to section 3.2). The P4 megacycle contact is interpreted to be a subaerial unconformity based on evidence for meteoric diagenesis and paleosol development below the contact and will be discussed in greater detail in Chapters 8 and 9. This interpretation of the contact differs from previous studies by I. Muir and others (unpublished data, 1988), Springate et al. (1992), and Wendte and Muir (1995) who interpreted the contact to be a result of a pulse of increased relative sea level rise. However, in a recent study by Wendte and Uyeno (2005), the P4 surface was recognized as a widespread regional unconformity.

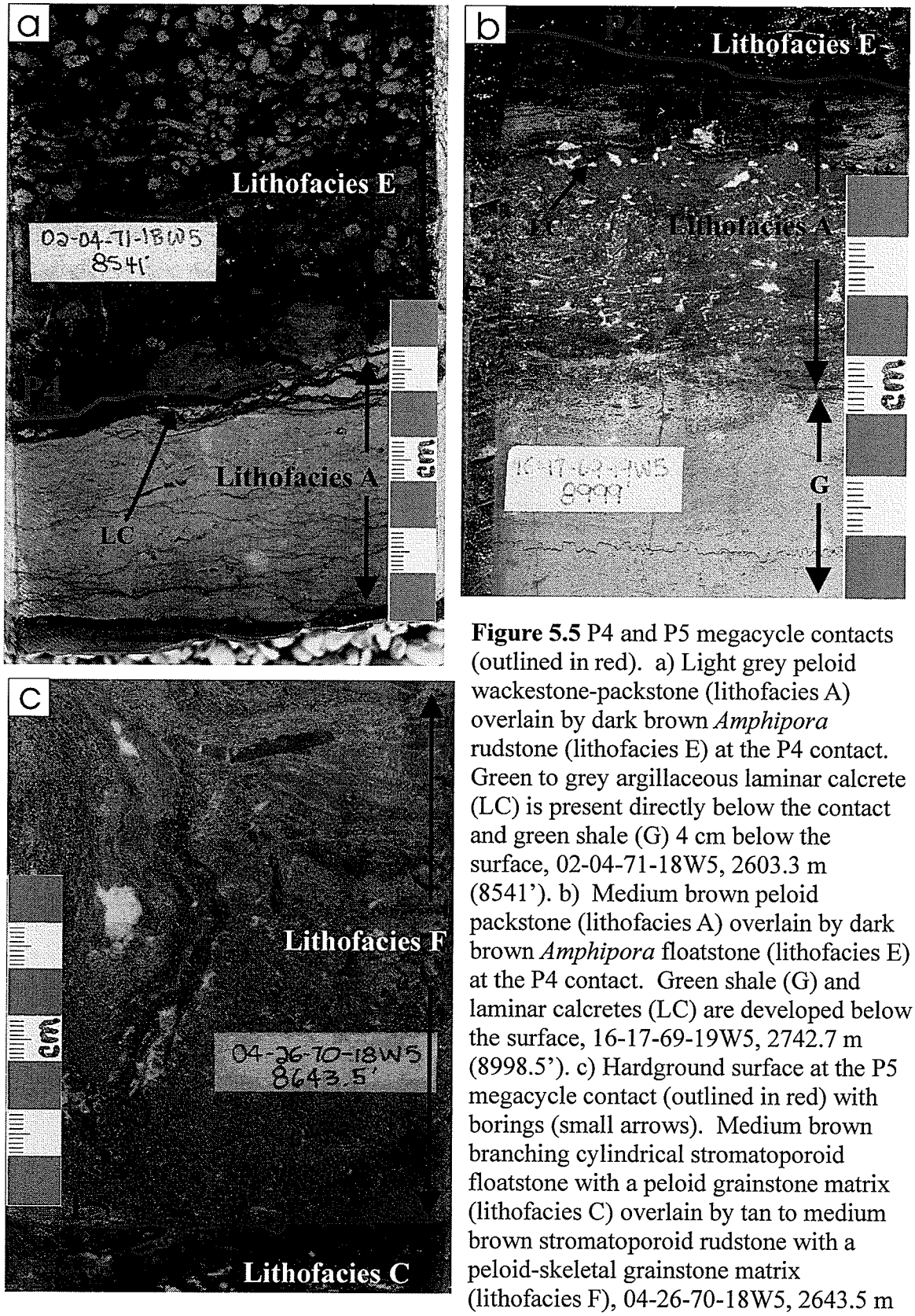


Figure 5.5 P4 and P5 megacycle contacts (outlined in red). a) Light grey peloid wackestone-packstone (lithofacies A) overlain by dark brown *Amphipora* rudstone (lithofacies E) at the P4 contact. Green to grey argillaceous laminar calcrete (LC) is present directly below the contact and green shale (G) 4 cm below the surface, 02-04-71-18W5, 2603.3 m (8541'). b) Medium brown peloid packstone (lithofacies A) overlain by dark brown *Amphipora* floatstone (lithofacies E) at the P4 contact. Green shale (G) and laminar calcretes (LC) are developed below the surface, 16-17-69-19W5, 2742.7 m (8998.5'). c) Hardground surface at the P5 megacycle contact (outlined in red) with borings (small arrows). Medium brown branching cylindrical stromatoporoid floatstone with a peloid grainstone matrix (lithofacies C) overlain by tan to medium brown stromatoporoid rudstone with a peloid-skeletal grainstone matrix (lithofacies F), 04-26-70-18W5, 2643.5 m (8643.5').

5.5.2 P5 Megacycle

The P5 megacycle shows significant backstepping towards the southwest and an increase in thickness from the platform margin (e.g. 2.7 m thick in well 12-23-70-18W5, Enclosure 1) to the platform interior (e.g. 10.8 m thick in well 16-17-69-19W5, Enclosure 1). The P5 megacycle is composed of tidal flat and beach lithofacies (lithofacies A and B, respectively) and shallow to deep lagoonal facies (lithofacies C to E) (Enclosures 2 and 3). These lithofacies are arranged in a series of shallowing-upward fourth-order lagoonal cycles (as defined in section 5.4) and together complete a third-order megacycle (Figures 5.6 and 5.7). The P5 megacycle contact shows a shift from shallower water facies to deeper water or more basinal lithofacies (Enclosures 2 and 3). In the platform margin, more open marine reef margin lithofacies (lithofacies F to I) overlie shallow lagoonal sediments (lithofacies C and D) (Figure 5.6). In the platform interior, relatively deeper lagoonal facies (lithofacies D and E) overlie tidal flat or shallow lagoonal facies (Lithofacies A to D) (Figure 5.7). The P5 megacycle contact is commonly sharp and frequently marked by a marine hardground (Figure 5.5c).

The backstepping style of the P5 platform is interpreted to reflect overall increasing rates of relative sea level rise during deposition (refer to section 3.2). The step-like pattern is interpreted to be a result of incremental rises in relative sea level (as recorded by lagoonal cycles) that make up a complete third-order megacycle (e.g. Wendte, 1992c). This interpretation is similar to those of other megacycles in the Snipe Lake and Judy Creek reef complexes (e.g. Wendte, 1992c; Wendte and Muir, 1995). The P5 platform was subsequently drowned by a pulse of increased rates in relative sea level rise (cf. Wendte

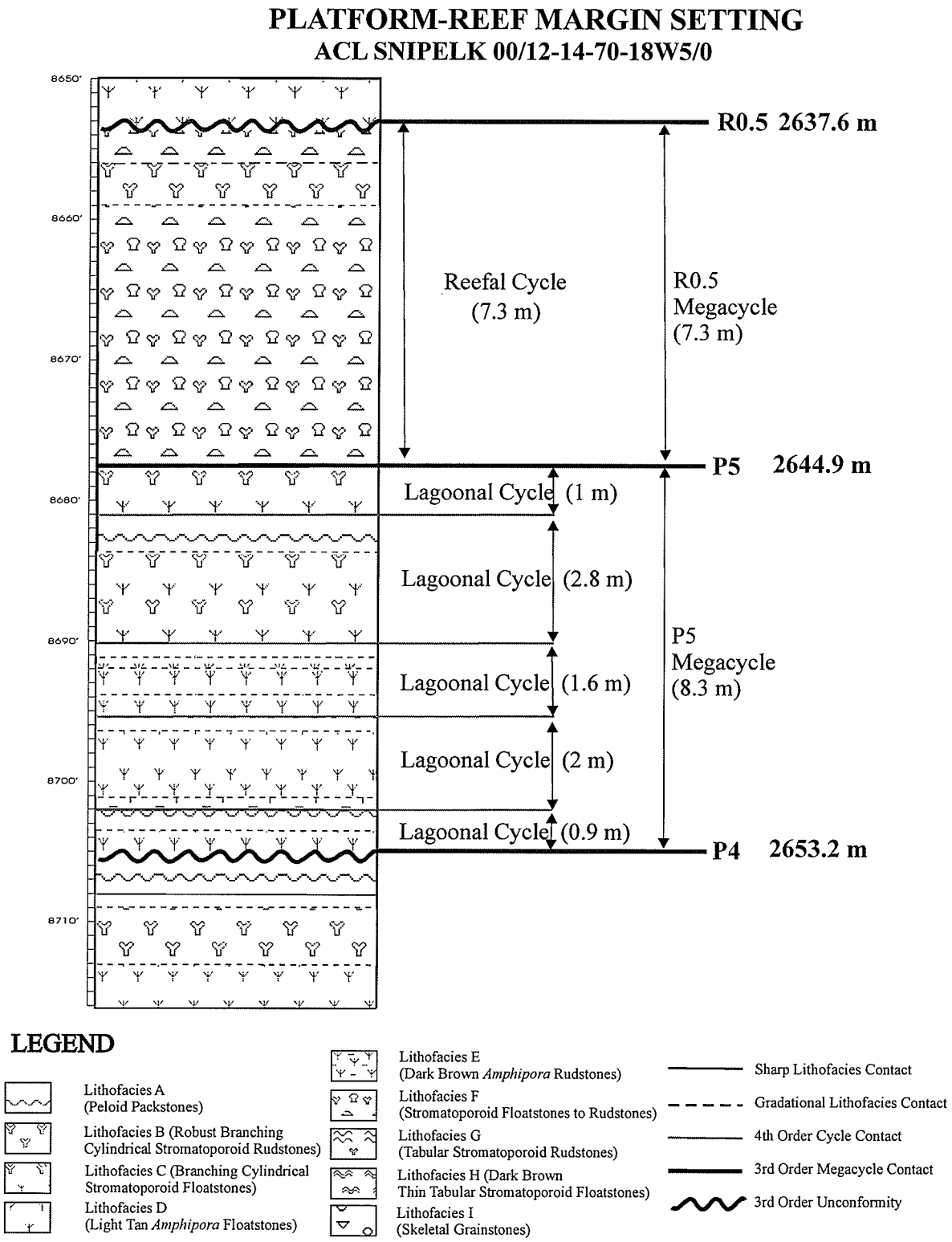


Figure 5.6 Summary of depositional cycles in a foreslope setting at the Snipe Lake reef complex in the P5 and R0.5 successions, 12-14-70-18W5. The P5 megacycle is composed of five shallowing-upward, fourth-order lagoonal cycles. The R0.5 succession is composed of a third-order single reefal cycle. The thickness of each cycle is given in brackets.

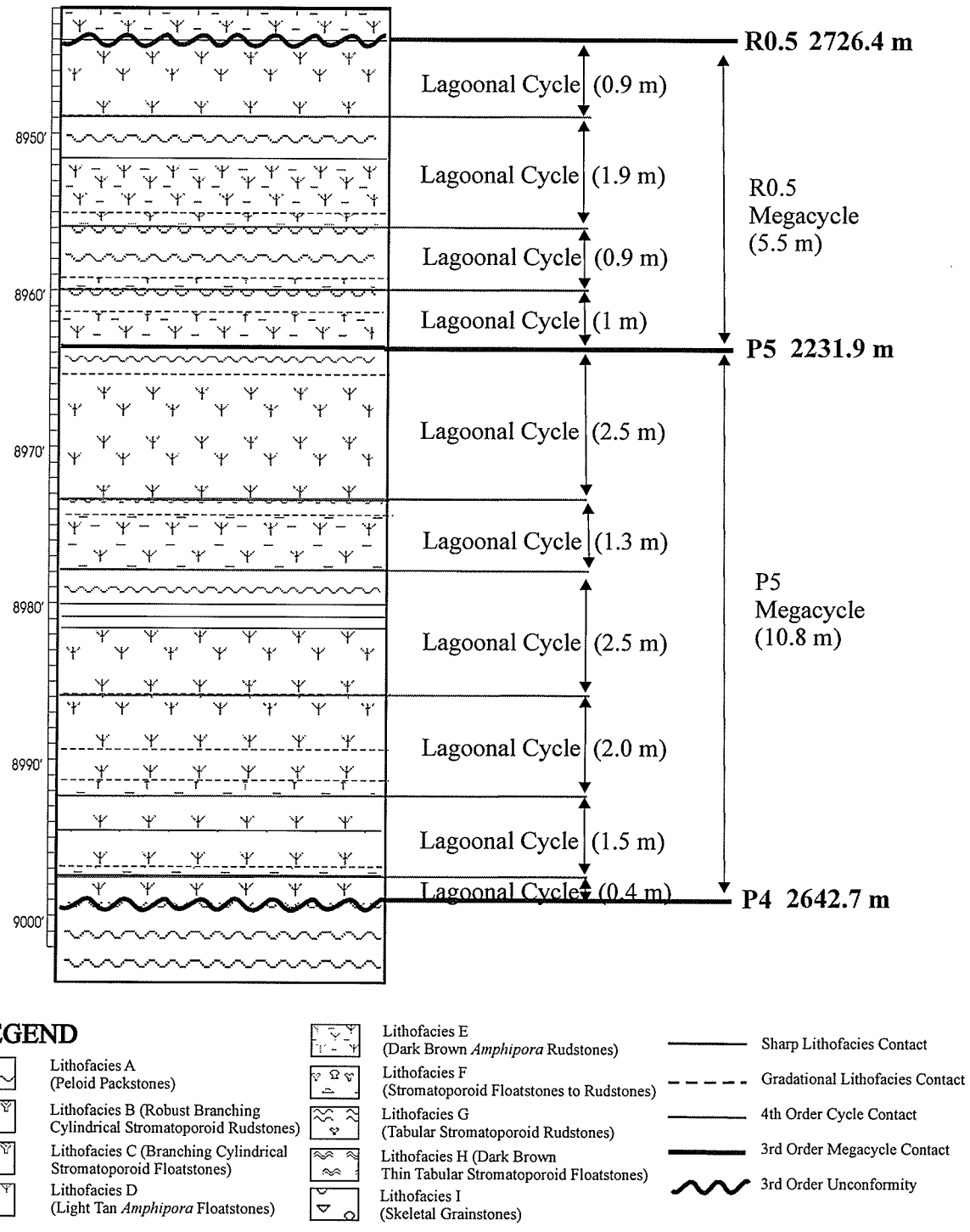


Figure 5.7 Summary of depositional cycles in a platform-reef interior setting at the Snipe Lake reef complex in the P5 and R0.5 successions, 16-17-69-19W5. The P5 and R0.5 successions are composed of a series of shallowing-upward third order lagoonal cycles. The thickness of each cycle is given in brackets.

1990c).

Several interesting features are observed in the P5 succession:

(1) There is an increase in the number of lagoonal cycles as the P5 succession thickens towards the platform interior (Figures 5.6 and 5.7). In a backstepping platform there was continuous sedimentation in the platform interior while more basinward areas were drowned (e.g. Wendte, 1992b). Sedimentation rates in the lagoon were relatively slow and frequently outpaced by relative sea level rises. Sedimentation resumed during slower rates of relative sea level rise, producing a series of shallowing-upward cycles (e.g. Wendte and Stoakes, 1982).

(2) Lagoonal cycles become progressively shallower within the megacycle (Figures 5.6 and 5.7). Older lagoonal cycles tend to have muddier basal lithofacies (lithofacies E), whereas younger cycles often begin with grainy lagoonal facies (lithofacies C or D). This is interpreted to reflect decreasing rates of relative sea level rise during P5 deposition (e.g. I. Muir and others, unpublished data, 1988).

At one location (well 16-17-69-19W5, 2731.9 m, 8963') pedogenic features are developed below a sharp P5 megacycle contact (Appendices B and C). Although the presence of pedogenic features suggests a period of emergence at this location, there is insufficient evidence to suggest that it was a result of a drop in relative sea level across the platform (discussed more in section 9.5). The rare and inconsistent occurrence of these features across the P5 megacycle contact

more likely suggests that emergence was a result of local shallowing-upward conditions caused by reef aggradation (cf. Goldstein, 1991).

5.5.3 R0.5 Megacycle

The R0.5 succession shows a progradational pattern towards the north and east (Enclosure 1). Expanded facies belts during R0.5 deposition resulted in an "overhang" compared to the underlying backstepped P4 and P5 platforms (Figure 3.8). The R0.5 succession increases in thickness from the reef interior (e.g. 5.5 m thick in well 16-17-69-19W5, Enclosure 2) to the reef margin (e.g. 11.6 m thick in well 12-23-70-18W5, Enclosure 2). In the reef margin setting, the R0.5 megacycle is characterized by a third-order reefal cycle (Figure 5.6). In the reef interior, the R0.5 succession consists of a series of shallowing-upward fourth-order lagoonal cycles (Figure 5.7). Similar to the P5 megacycle, there is an increase in the number of lagoonal cycles towards the reef interior and the cycles become progressively shallower upwards within the R0.5 megacycle. Shallow intertidal to reef flat lithofacies (lithofacies A, B and F) are commonly overlain by relatively deeper subtidal lagoonal lithofacies (lithofacies C to E) across the R0.5 megacycle contact (Enclosures 2 and 3). Similar to the P4 megacycle contact, green shales are common directly below the R0.5 contact (Figure 5.8). In addition, there is evidence to suggest early meteoric dissolution and paleosol development below this surface (see Chapters 7 and 8).

The progradational or forestepping style of reef growth of the R0.5 reef succession is interpreted to be a result of slower rates of relative sea level rise or prolonged stillstand

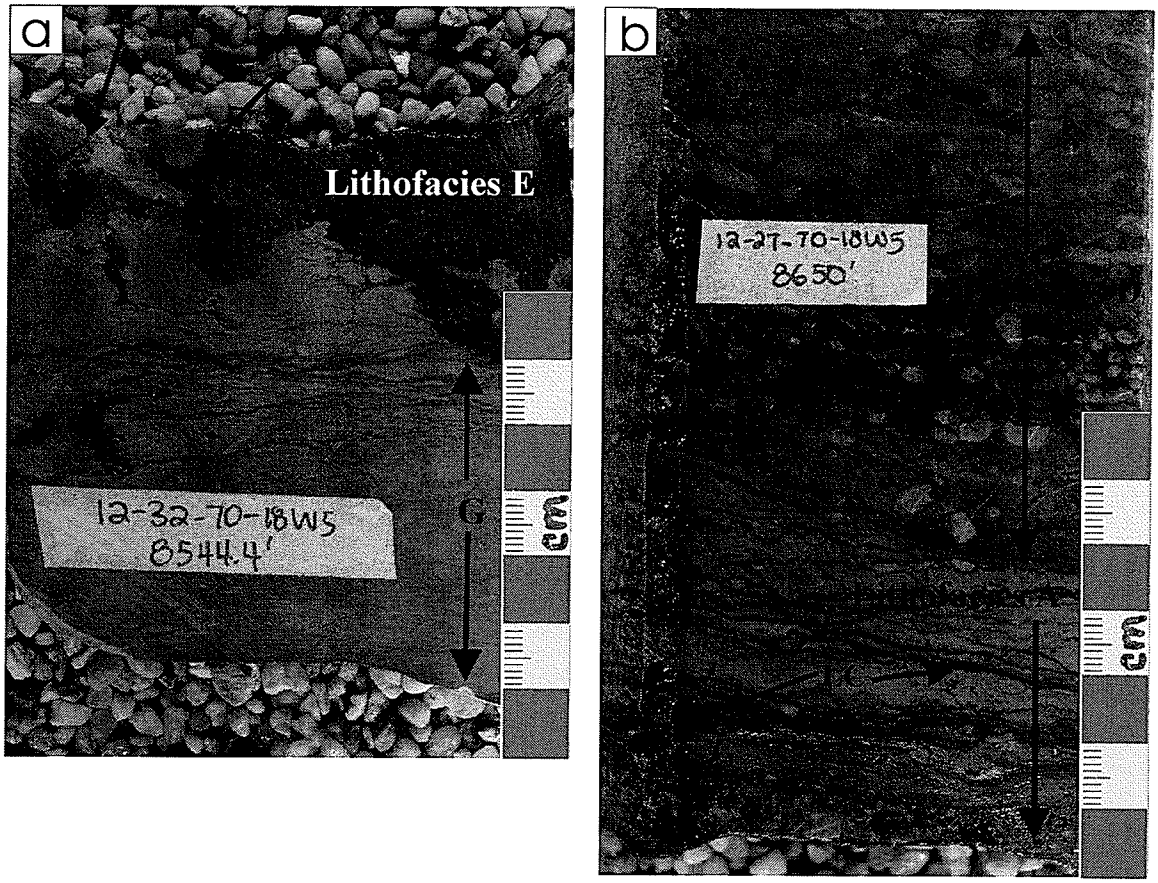


Figure 5.8 R0.5 megacycle contact. a) Sharp erosional R0.5 contact with green shale bed (G) overlain by dark brown *Amphipora* floatstone (lithofacies E). Angular green shale clasts occur above the contact in the overlying sediment (arrows), 12-32-70-18W5, 2604.3 m (8544.4'). B) Tan peloid wackestone-packstone (Lithofacies A) overlain by medium brown *Amphipora* floatstone (Lithofacies D) at the R0.5 contact (outlined in red). Laminar calcretes (LC) and thin green shale seam (G) with abundant lithoclasts are developed below the contact, 12-27-70-18W5, 2636.5 m (8650').

conditions that consequently were exceeded by sedimentation rates (refer to section 3.2). Progressively shallower lagoonal cycles within the succession are interpreted to reflect a decrease in relative sea level rise during R0.5 deposition (cf. I. Muir and others, unpublished data, 1988). The R0.5 megacycle contact is interpreted to be a subaerial unconformity based on evidence of meteoric diagenesis and paleosol development below the contact. Although most previous studies published on the Snipe Lake reef complex did not describe a megacycle contact nor a subaerial unconformity at this stratigraphic level (e.g. Springate et al., 1992; Wendte and Muir, 1995), more recent studies have recognized a subaerial exposure unconformity in the Snipe Lake and Judy Creek reef complexes (Chow and Wendte, 2004; Wendte and Uyeno, 2005).

CHAPTER 6 – CEMENT PETROLOGY

6.1 Introduction

In the previous chapters, lithofacies analysis provided an interpretation of the primary depositional processes and environments in the Snipe Lake reef complex. However, an understanding of the diagenetic features and processes is needed for a complete interpretation of the history of the Snipe Lake reef complex. A variety of diagenetic features has been recognized based on detailed core and petrographic analysis below the P4 and R0.5 subaerial exposure surfaces (Appendices A, B and D). This chapter will primarily focus on the different types of calcite and dolomite cements. Their paragenetic sequence and diagenetic environments of precipitation are interpreted based on petrographic and stable isotope evidence. Subaerial exposure features will be discussed in Chapter 7.

6.2 Overview of Diagenetic Environments

Carbonate diagenesis is primarily driven by water-rock interactions, and rocks and sediments can be exposed to waters of marine, meteoric or deep subsurface origin (summarized in James and Choquette, 1990c). Accordingly, three diagenetic environments have been recognized: (1) marine, (2) meteoric and (3) deep burial diagenetic environments (Figure 6.1). These diagenetic environments will be summarized in terms of their dominant diagenetic processes and characteristic features, with an emphasis on cementation. The following discussions are primarily summarized from Choquette and James (1990), James and Choquette (1990a, b) and Moore (2001)

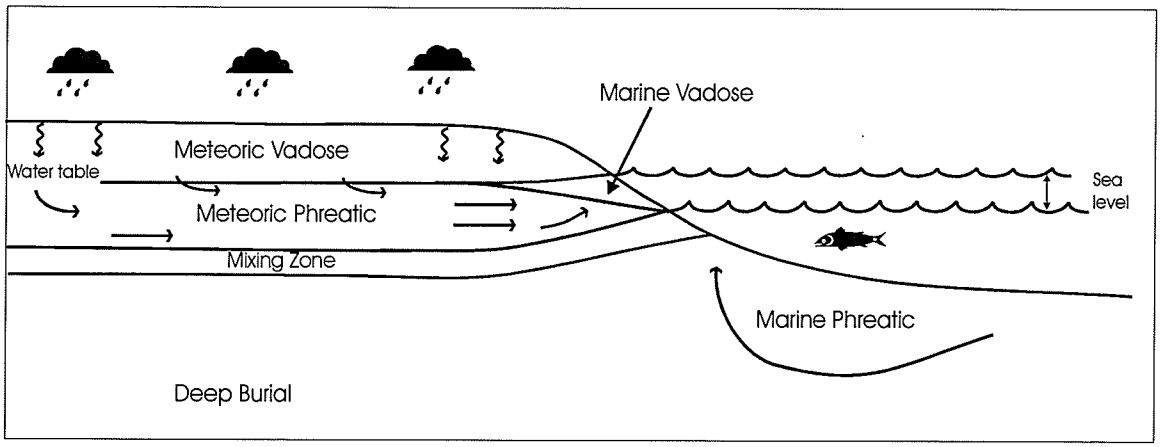


Figure 6.1 Schematic diagram illustrating the main diagenetic environments for carbonate sediments and sedimentary rocks (based on Hanor, 1978; Esteban and Klappa, 1983; James and Choquette, 1990b, c). Arrows indicate the direction of water flow. The water table marks the boundary of the meteoric vadose zone (above) and the meteoric phreatic zone (below). The marine vadose zone is located in the intertidal area where sea level fluctuates.

and the reader is referred to these references for a more in-depth discussion of diagenetic environments.

6.2.1 Marine Diagenetic Environment

The marine diagenetic environment includes the shallow sea floor (submarine or marine phreatic) and the intertidal to supratidal (marine vadose) environments (James and Choquette, 1990a; Moore 2001). On the shallow sea floor, pore spaces are completely filled by seawater and in the intertidal to supratidal zones pore spaces are filled by seawater and air. Carbonate precipitation and biogenic alteration are the most common diagenetic processes in the marine environment.

In the marine phreatic environment, high magnesium calcite and aragonite cements commonly precipitate from magnesium-rich seawater. Calcite precipitates include micrite cements and isopachous fibrous cements (Figure 2.5a). Aragonite precipitates include fibrous needles that are arranged in isopachous rinds, intergranular meshes of crystals and botryoids. Fibrous calcite and aragonite cements may have either divergent crystallographic axes (fascicular-optic fibrous) or convergent optic axes (radiaxial fibrous) (e.g. Kendall, 1977; Kendall, 1985; James and Choquette, 1990a; Moore, 2001). The most common biological alteration on the sea floor is boring by large and small organisms. Micritization is a process where a surface is bored by endolithic organisms and borings are later filled by high magnesium-calcite or aragonite. A micrite envelope can develop around a grain or line the interior of a pore space. With extensive micritization, grains can be completely micritized into microcrystalline high magnesium-

calcite or aragonite.

In the marine vadose environment, water composition can vary from marine to mixed marine and meteoric waters. Marine vadose cements have crystal habits similar to those precipitated in the marine phreatic zone (high magnesium calcite and aragonite fibrous needles), but often have a pendant or microstalactitic orientation that develops on the undersurfaces of grains or along the roof of pores.

Marine cements are generally non-ferroan due to the low abundance of iron in seawater and oxidizing conditions. Generally, they are also non-luminescent due to low Mn^{2+} concentrations in seawater (e.g. Veizer, 1983; Dickson, 1990). Cements also tend to precipitate relatively rapidly in shallow marine waters. Rapid crystal growth is accompanied by an increase in the number of site imperfections and subsequently the incorporation of inclusions in the crystal lattice (e.g. Packard and Hills, 2001). Therefore, cements precipitated from marine or 'dirty' waters commonly have abundant inclusions which often result in a cloudy or milky appearance (e.g. Wong, 1978).

Some workers have observed "meteoric-like" cement morphologies that precipitated from seawater (e.g. Melim et al., 1995). Dissolution and neomorphism of aragonitic grains and precipitation of blocky spar cement were interpreted to have occurred in the "marine-burial diagenesis" environment based on stable oxygen isotope data. This diagenetic environment is proposed to account for cements that precipitated from seawater below the seafloor diagenetic zone but above the deep burial diagenetic zone.

Although petrographic fabrics are useful in distinguishing different diagenetic environments, such studies demonstrate that caution must be used if isotopic data are unavailable.

6.2.2 Meteoric Diagenetic Environment

Carbonate rocks and sediments can be subaerially exposed to meteoric waters through uplift, rapid sediment accretion or changes in sea level (James and Choquette, 1990b). Carbonate dissolution, cementation and neomorphism are the dominant diagenetic processes in the meteoric diagenetic environment. The meteoric environment is subdivided into the vadose and phreatic zones. The vadose zone is located above the water table where pores spaces are filled by fresh water, air or both. In contrast, the phreatic zone is located below the water table where pore spaces are always completely filled with fresh water.

Dissolution of carbonate rocks or sediments is ubiquitous throughout the meteoric environment. Dissolution can occur through simple, biogenic, mixing or hydrostatic corrosion that results in dissolution vugs and enhanced primary pores. Simple corrosion (dissolution) occurs when meteoric waters are in contact with bare rock surfaces during exposure and because rain water is in equilibrium with atmospheric CO_2 it essentially behaves as a weak acid. Biogenic corrosion is a result of rainwater percolating through soil horizons which have significantly higher CO_2 (from biogenic sources) resulting in more aggressive meteoric waters that can rapidly dissolve calcium carbonate. Mixing corrosion occurs when waters of different compositions or temperatures are combined

and result in water compositions that are typically undersaturated with respect to calcium carbonate. As this mixture tries to achieve equilibrium (saturation) with respect to $CaCO_3$, extensive dissolution of limestone takes place. Hydrostatic corrosion occurs when the pressure in the phreatic zone increases as the hydrostatic head increases, thus enabling fluids to dissolve calcium carbonate more aggressively.

Cements in the meteoric vadose and phreatic zones generally have blocky to prismatic crystal habits, but differ in morphology. Vadose cements typically have irregular distributions around grains or in voids because pores are not completely filled by water. Cements with meniscus or pendant morphologies are characteristic of vadose precipitation (Figure 2.5b). Epitaxial/syntaxial calcite overgrowth cements can precipitate in the vadose zone but can extend into the phreatic zone. Geopetal crystal silt can accumulate at the bottom of cavities as earlier cements detach and fall from pore ceilings (e.g. Dunham, 1969; Havard and Oldershaw, 1976; Wong, 1978; James and Choquette, 1990b) or precipitate from vadose diagenetic fluids (e.g. Platt, 1989). Vadose cements are generally iron-poor due to oxidizing conditions in the vadose pore system and are typically non-luminescent. Meteoric pendant cements may have inclusions concentrated along growth surfaces of the crystal from the accumulation of insoluble particles as meteoric water percolate through the vadose zone (e.g. Wong, 1978). In addition, as pendant cements precipitate, periodic evaporation of the meniscus film will further concentrate these insoluble particles along crystal surfaces (e.g. Packard and Hills, 2001).

Cements precipitated in the meteoric phreatic environment tend to be evenly distributed or have uniform morphologies because pores are always filled with water. For example, isopachous calcite cements commonly develop around grains and pore walls (Figure 2.5b). Cements precipitated in the phreatic zone are typically coarser crystalline than those in the vadose zone. Phreatic cements may be slightly iron-rich and may show dull to moderate luminescence, as phreatic pore waters are often reducing and Fe^{2+} and Mn^{2+} may be incorporated into crystal lattices. However, the absence of iron or luminescence does not preclude a phreatic origin.

High magnesium calcite and aragonite components are often altered or neomorphosed to the more stable low magnesium calcite during meteoric diagenesis. The change can occur by dissolution and subsequent filling of molds or by calcitization (simultaneous dissolution of aragonite and precipitation of calcite). Altered grains have poor to good preservation of original fabrics.

6.2.3 Burial Diagenetic Environment

As carbonate rock and sediments are progressively buried, they are subjected to increasing temperature and pressure conditions that result in further modification or diagenesis (Choquette and James, 1990). Changes that occur in the burial diagenetic environment include compaction, cementation, and dissolution.

Physical and chemical compaction can result in a diverse range of features, including thinning and draping of laminae, rotated or closely packed grains, fractures, stylolites and

microstylolites. Several cement morphologies can be precipitated during burial diagenesis (Figure 2.5c). Shallow burial cements include blocky-prismatic calcites, blocky calcite mosaics and dolomite rhombs which all may be cross-cut by stylolites. Blocky-prismatic calcite cements have elongate scalenohedral crystals and are usually the earliest burial cements. These cements typically range from ferroan to non-ferroan and have non-luminescent cores with brightly luminescent rims. Coarse calcite mosaics have plane-sided, blocky crystals that are ferroan to non-ferroan, and show dull to zoned or unzoned luminescence. Dolomite rhombs range from euhedral to subhedral and have planar cleavage and crystal faces. Deep burial features include compaction features, such as stylolites, cements including xenotopic dolomite and saddle dolomite. Xenotopic dolomite ranges from fine to coarsely crystalline anhedral dolomite with irregular to curved boundaries and undulatory extinction. Saddle dolomite is generally coarsely crystalline with curved cleavage traces and crystal faces and shows sweeping extinction. Due to reducing pore waters in the deep burial environment, both xenotopic and saddle dolomites are often ferroan, and may or may not show compositional zoning.

The general trend during burial diagenesis is a reduction of porosity by complete or near complete occlusion of porosity, but dissolution can also take place at a local scale. Dissolution can result in molds, vugs, solution-enlarged interparticle pores and microporosity.

6.3 Cement Petrography

Petrographic analysis has revealed multiple phases of calcite and dolomite cements and a

complex diagenetic history in the Snipe Lake reef complex (Table 6.1). A total of eleven cements types are recognized based on their occurrence, cement morphology, crystal habit, crystal size and chemical composition. Scanning electron microscopy indicates that all calcite cement types are low-magnesium calcite. With the exception of meniscus cements, all cement types are present below both the P4 and R0.5 subaerial exposure surfaces. Additional diagenetic features (e.g. crystal silt and replacement dolomite rhombs) are also discussed in this chapter.

6.3.1 Micrite

Dark brown, irregular micritic laminae or isopachous micrite envelopes (<100 μm) are very commonly developed around skeletal grains, lithoclasts and peloids and line intraskeletal pores (Figure 6.2). Some grains are also partially to almost completely micritized (peloids) resulting in little to no preservation of their original fabrics.

6.3.2 Isopachous Fibrous Calcite

Milky white to brown, fibrous calcite cement occurs as isopachous rims in fenestrae, interparticle pores and less commonly in dissolution vugs, and ranges in thickness from 0.2 to 1.2 mm (Figure 6.3). Smaller pore spaces are commonly completely occluded by this cement (Figure 6.3c). Isopachous fibrous calcite cements are moderate to inclusion-rich. Crystal habits range from fibrous to bladed and prismatic. Convergent crystallographic axes displaying sweeping extinction and a fibrous pattern of inclusions in bladed to prismatic crystals suggest that these crystals originally had a fibrous habit. Slightly thicker rims of fibrous calcite are locally developed along the upper surfaces of

Table 6.1 Summary of cements and other selected diagenetic features in the Snipe Lake reef complex.

Cement or Other Diagenetic Feature	Mineralogy	Crystal Size	Occurrence	Diagenetic Environment
Micrite	Non-ferroan calcite	Microcrystalline	Around skeletal grains, lithoclasts, peloids, intraskeletal pores	Marine phreatic
Isopachous fibrous calcite	Non-ferroan calcite	0.04-0.2 mm	Fenestrae, interparticle pores, vugs	Marine phreatic
Pendant radiaxial fibrous calcite	Non-ferroan calcite	0.04-0.3 mm	Fenestrae, interparticle pores, shelter pores, vugs	Marine vadose
Pendant prismatic calcite	Non-ferroan calcite	0.02-0.3 mm	Shelter pores, intraskeletal pores	Meteoric vadose
Crystal silt	Ferroan to non-ferroan calcite	8-40 μm	Geopetal sediment in interparticle pores, fenestrae, vugs	Meteoric vadose
Meniscus blocky calcite	Non-ferroan calcite	<0.1 mm	Between adjacent grains	Meteoric vadose
Syntaxial calcite overgrowths	Non-ferroan calcite	0.16-0.9 mm	Around echinoderm fragments	Meteoric vadose and phreatic
Isopachous prismatic calcite	Non-ferroan calcite	0.008-0.4 mm	Intraskeletal and interparticle pores, vugs, fractures	Meteoric phreatic
Blocky-prismatic calcite	Ferroan and non-ferroan calcite	0.04-1.0 mm	Intraskeletal and interparticle pores, vugs	Shallow burial
Blocky calcite mosaics	Zoned ferroan and non-ferroan calcite	< 4.8 mm	Intraparticle and interparticle pores, vugs, fractures	Shallow to intermediate burial
Dolomite rhombs	Zoned ferroan and non-ferroan dolomite	< 1.8 mm	Intraparticle and interparticle pores, vugs, fractures	Shallow to intermediate burial
Saddle dolomite	Zoned ferroan and non-ferroan dolomite	0.1-3.6 mm	Interparticle pores, vugs, fractures	Deep burial

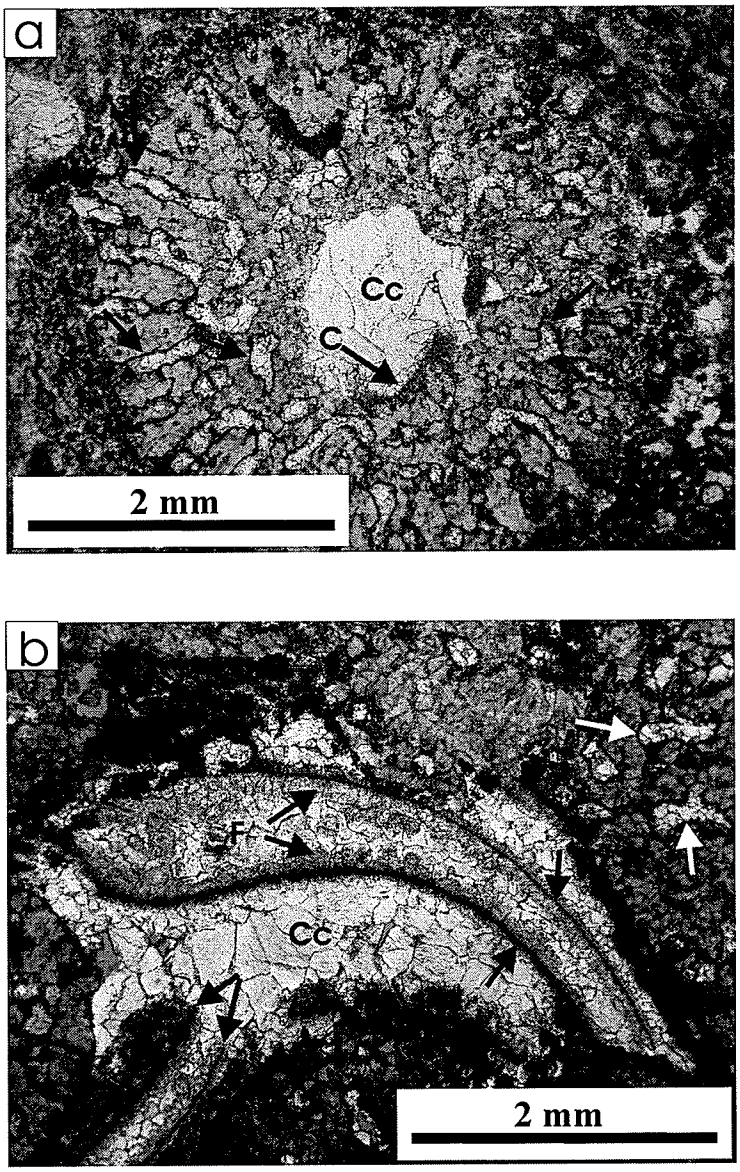


Figure 6.2
Photomicrographs of micrite cements. a) Micrite envelopes (arrows) lining the interior of *Amphipora* galleries. Micrite cements are succeeded by blocky-prismatic calcite (C) and blocky calcite mosaic (Cc) cements, 12-32-70-18W5, 2617.6 m (8588'). b) Micrite envelopes around mollusc fragments (arrows) and lining intraskeletal stromatoporoid galleries. Micrite cements are succeeded by isopachous fibrous calcite cements (F) and blocky calcite mosaics (Cc). Minor intercrystalline and intraparticle porosity is shown by blue epoxy, 02-04-71-18W5, 2604.2 m (8544').

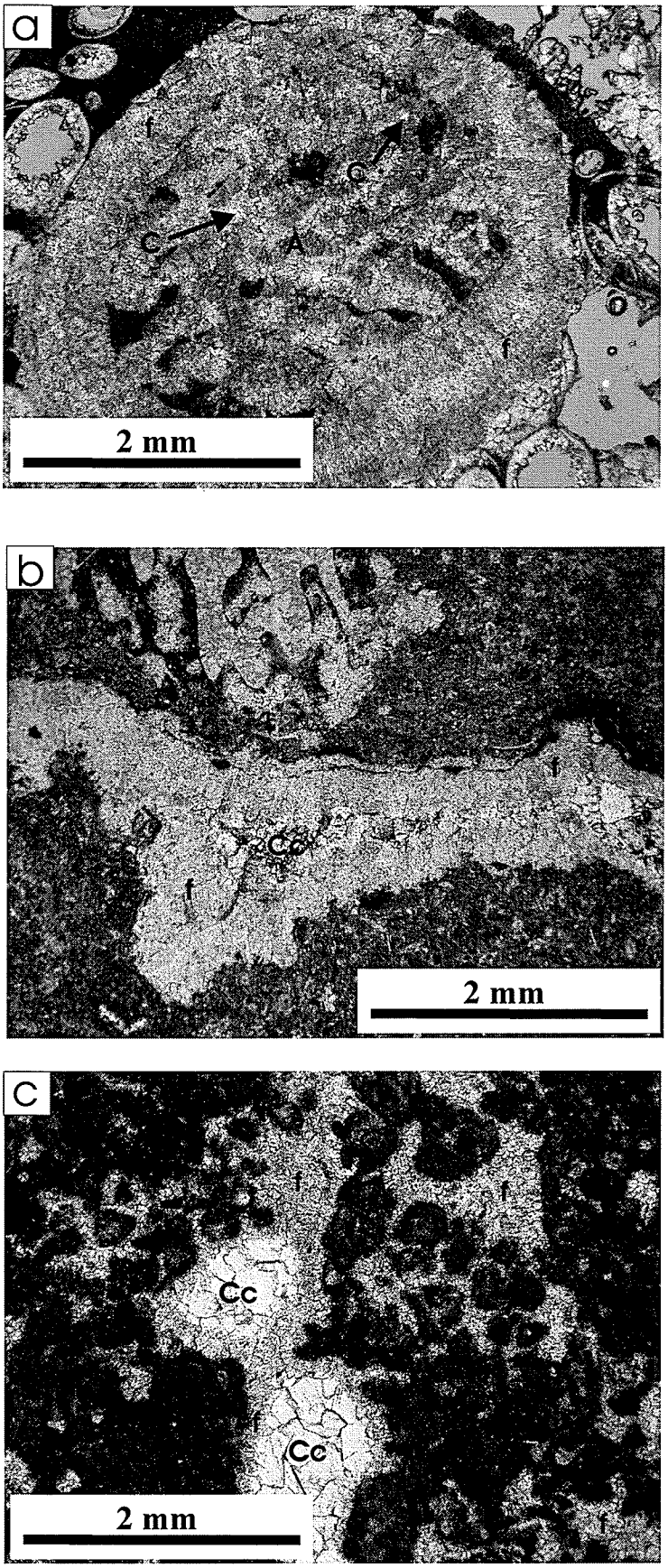


Figure 6.3 Photomicrographs of isopachous fibrous calcite cements. a) *Amphipora* with isopachous inclusion-rich fibrous calcite cement (f) around *Amphipora* (A). *Amphipora* and isopachous rinds are cross-cut by fractures that are occluded by blocky-prismatic calcite cement (C). Moldic to vuggy porosity (shown by blue epoxy) is well developed in intraparticle and interparticle pores, 10-21-70-18W5, 2677.1 m (8783'). b) Isopachous inclusion-rich fibrous calcite cement (f) in fenestral pore. The center of the fenestra is occluded by blocky calcite mosaics (Cc), 02-03-71-18W5, 2615.8 m (8582'). c) Inclusion-rich fibrous cements (f) in interparticle pores and fenestrae (center). Fibrous cements form isopachous rinds along the interior of larger pores (fenestrae) and remaining pores spaces are occluded by blocky calcite mosaics (Cc). Smaller interparticle pores (right side of photo) are completely occluded by fibrous cements, 12-23-70-18W5, 2621.3 m (8600').

pores. Isopachous fibrous calcite cements are non-ferroan and generally dull to non-luminescent.

6.3.3 Pendant Radiaxial Fibrous Calcite

Milky white to clear and brown, pendant radiaxial fibrous calcite cements occur (1) in primary pores spaces such as interparticle pores, fenestrae, and in shelter pores (along the undersides of *Amphipora* grains), and (2) more commonly in secondary dissolution vugs (Figure 6.4). Pendant cements range from 0.1 to 2.4 mm thick and rarely up to 5.6 mm thick. In smaller cavities (typically fenestrae), the pore space is completely occluded by these pendant cements. In some primary pore spaces, pendant radiaxial fibrous calcite cements extend and thin along the sides of the pore walls and may be gradational with isopachous fibrous calcite cements. Pendant cements commonly have a scalloped or colloform texture with several lobes radiating from the upper surface when developed in dissolution vugs (Figure 6.4c-f). Cements generally have a milky white to cloudy appearance due to the abundance of inclusions, but may show alternating inclusion-rich and inclusion-poor layers. Individual layers range from 0.04 to 0.5 mm thick and have relatively gradational boundaries. Crystal habits range from fibrous to blocky or prismatic crystals. Fibrous crystals are arranged in a radiating pattern away from the roof of the pore. Convergent crystallographic axes of these cements result in a distinctive sweeping or brush extinction (Figure 6.4e, f). Blocky to prismatic crystals have crystal sizes ranging from 0.04 to 0.24 mm. The arrangement of inclusions and remnant sweeping extinction in these cements indicate an original fibrous crystal habit.

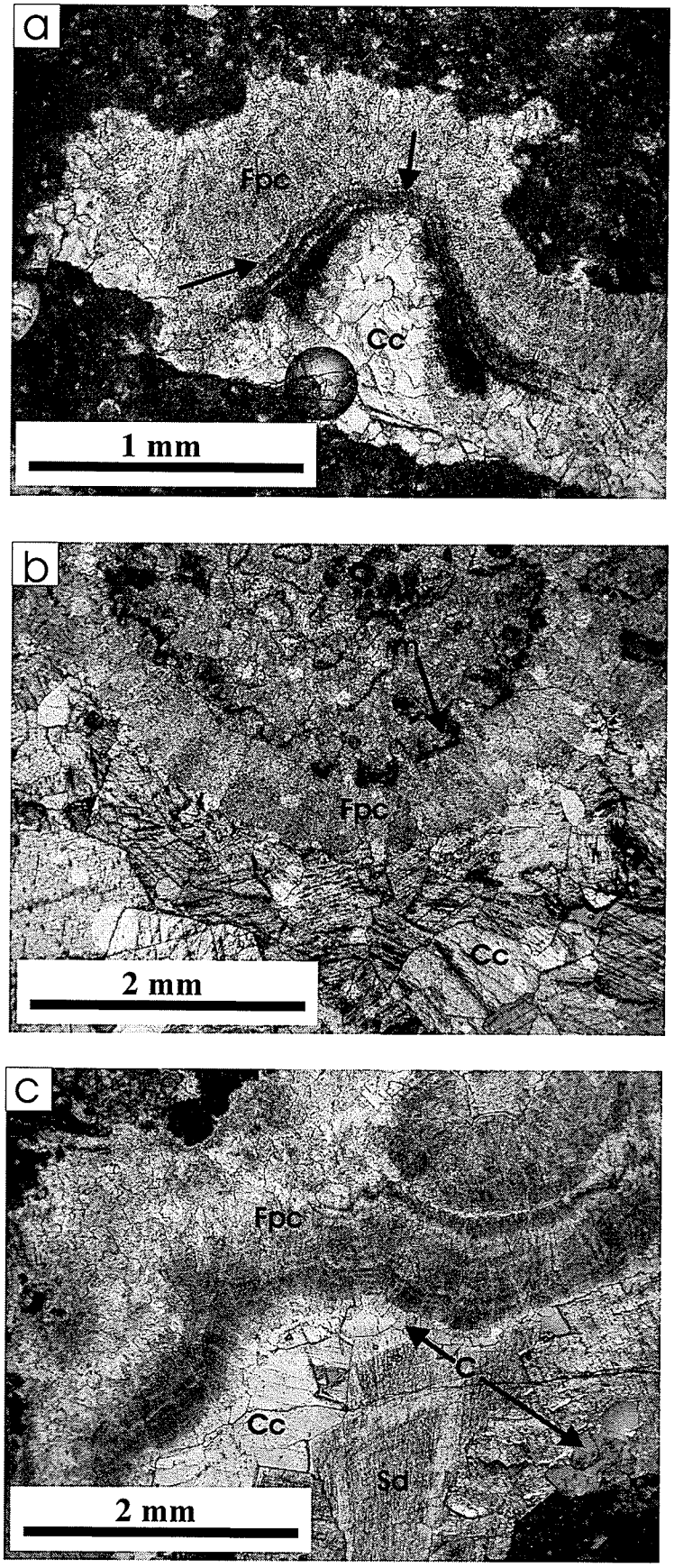
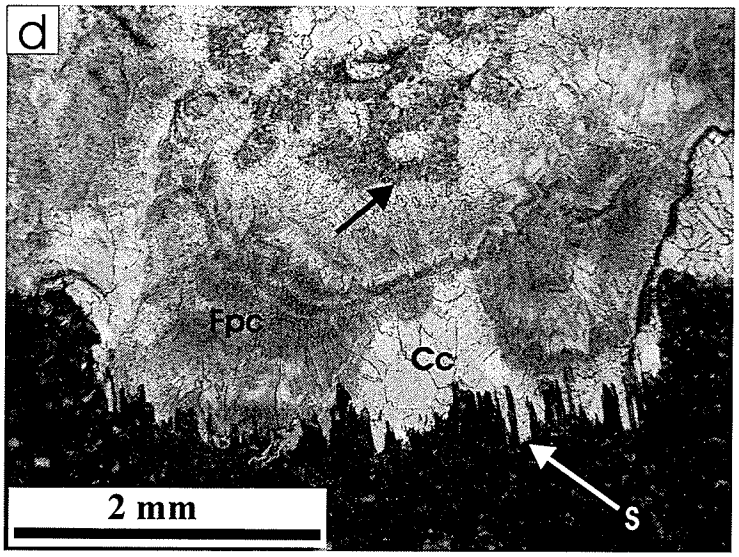
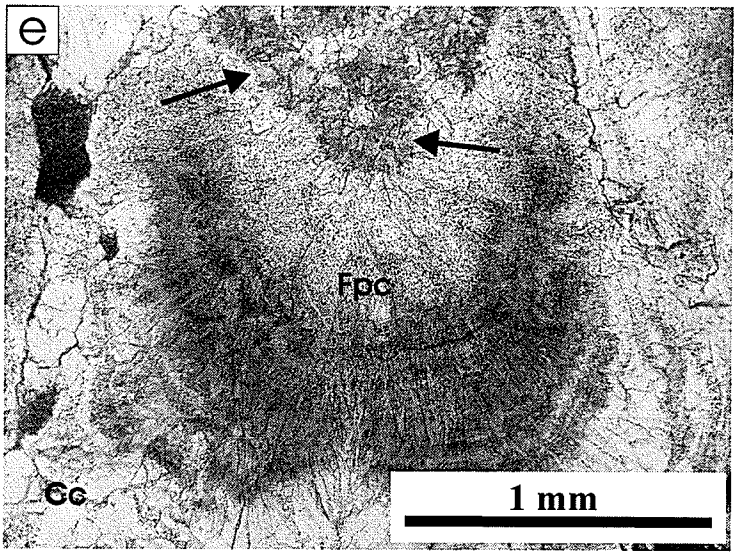


Figure 6.4. Photomicrographs of pendant radiaxial fibrous calcite cements. a) Pendant inclusion-rich radiaxial fibrous calcite cement (Fpc) occurs along the upper surface of a fenestral pore. Alternating layers of moderately and very inclusion-rich calcite layers are present towards the bottom of the pendant cement (arrows). Remaining pore space is occluded by blocky calcite mosaics (Cc), 12-22-70-18W5, 2656 m (8713.8'). b) Pendant inclusion-rich fibrous calcite cement developed along the underside of *Amphipora* in a shelter pore (Fpc). Pendant cement is preceded by micritized *Amphipora* grain margins (m) and succeeded by blocky calcite mosaics (Cc). Minor vuggy porosity is seen in blocky calcite mosaics (blue), 04-26-70-18W5, 2620.7 m (8598.1'). c) Pendant inclusion-rich radiaxial calcite cement (Fpc) developed along the upper surface of a dissolution vug. Alternating layers of inclusion-rich and relatively inclusion-poor layers occur towards the bottom of the pendant cement. Pendant cement is succeeded by blocky-prismatic calcite (C), blocky calcite mosaic (Cc) and then saddle dolomite cements (Sd). Saddle dolomite cements are zoned with iron-rich cores. Minor vuggy porosity is shown by the blue epoxy, 10-21-70-18W5, 2673.6 m (8771.6').





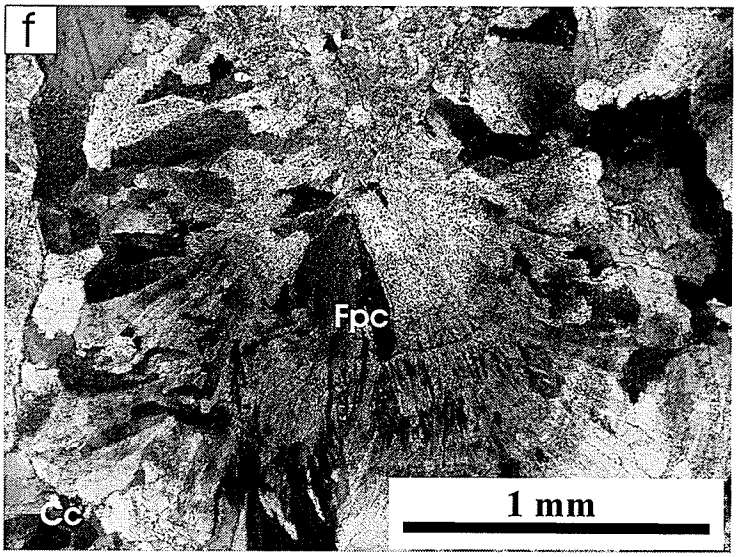


Figure 6.4 continued. d) Solution-enhanced shelter pore (vug) showing irregularly dissolved *Amphipora* grain margins (arrow) and occluded by pendant radiaxial fibrous calcite cements (Fpc) and blocky calcite mosaics (Cc). Pendant radiaxial fibrous calcite cement is inclusion-rich with inclusion-poor laminae. Stylolite cross-cuts the dissolution vug and cements, 02-04-71-18W5, 2597.4 (8521.5'). e) Pendant radiaxial fibrous calcite cement (Fpc) in a solution-enlarged shelter pore. Pendant cement developed as a single lobe along the undersurface of the *Amphipora* grain. *Amphipora* has irregularly dissolved grain margins (arrows). Pendant cement is relatively inclusion-rich with alternating layers of moderate to inclusion-poor layers. Remaining pore space is occluded by blocky calcite mosaics (Cc), 02-04-71-18W5, 2597.4 m (8521.5'). f) Photomicrograph of (e) in cross-polarized light showing sweeping extinction of pendant radiaxial fibrous cement (Fpc).

Pendant radiaxial fibrous calcite cements are composed of non-ferroan calcite and are generally dull to non luminescent and do not show any apparent luminescence zoning between inclusion-rich and inclusion-poor layers.

6.3.4 Crystal Silt

Crystal silt occurs as geopetal internal sediment in primary pore spaces, such as interparticle pores and fenestrae, but also in dissolution vugs (Figure 6.5a, b). It is composed predominantly of euhedral-subhedral calcite crystals ranging from 8 to 40 μm in size. Crystal silt may be recrystallized to blocky calcite crystals and may be replaced by dolomite rhombs. Crystals are generally well sorted and locally coarsen upwards within the pore space. V-shaped fractures are rarely developed in crystal silt and are occluded by blocky calcite mosaics (see section 6.3.10). Crystal silt is generally non-ferroan but recrystallized portions may be slightly ferroan.

6.3.5 Pendant Prismatic Calcite

Pendant, clear prismatic calcite cements are developed along the undersides of *Amphipora* grains and less commonly in intraskeletal and shelter pores (Figure 6.6). These pendant cements range from 0.2 to 1.4 mm thick. Crystals range from fine to coarse crystalline (0.02-0.3 mm crystal size). Pendant cements are generally inclusion-poor, but may have inclusion-rich laminae (Figure 6.6b). Inclusion-rich laminae are typically distinct and have sharp boundaries, which is in contrast to the inclusions in pendant radiaxial fibrous calcite cements. Dark opaque inclusions, when present, are concentrated in thin laminae (0.04-0.16 mm thick) along growth bands or in dark brown

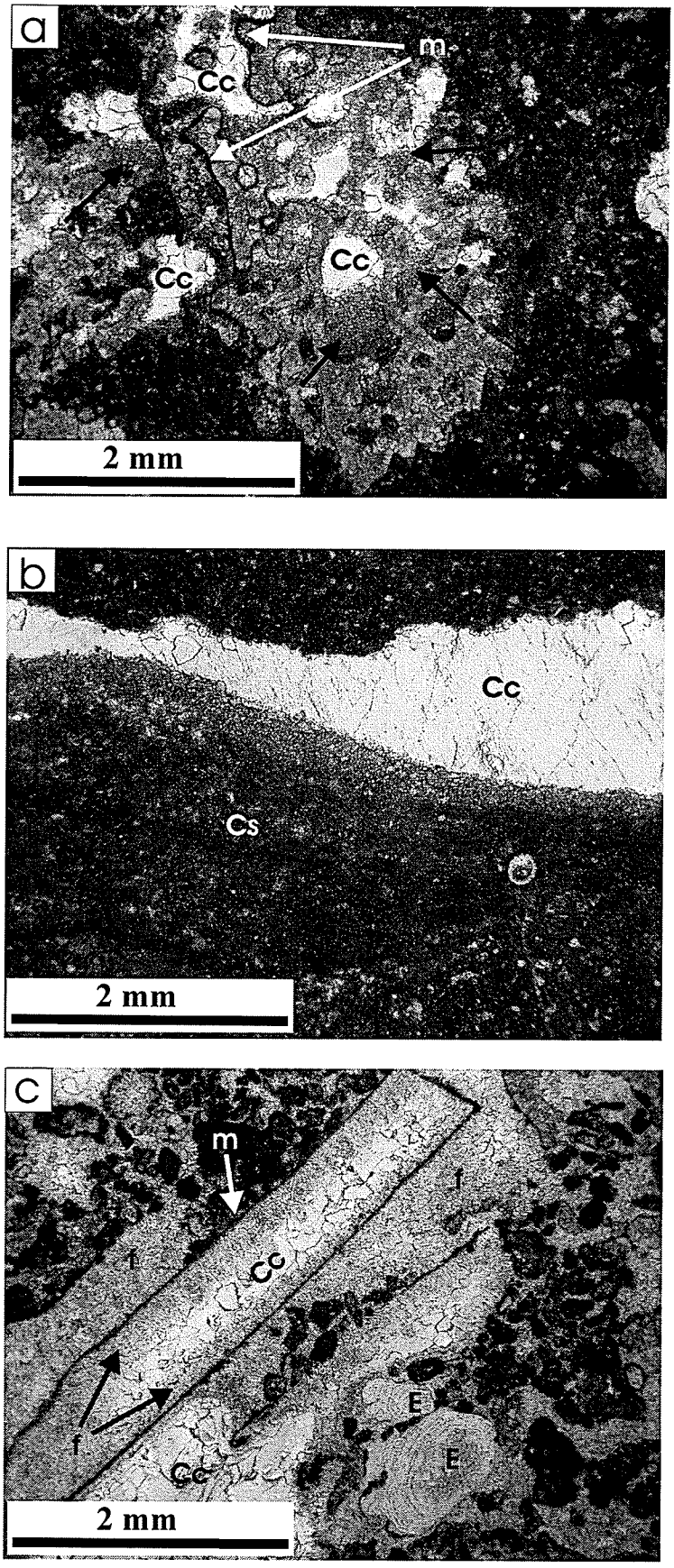


Figure 6.5 Photomicrographs of crystal silt and syntaxial overgrowths. a) Geopetal crystal silt in intraskeletal stromatoporoid galleries (black arrows). *Amphipora* has micritized grain margins (m) and remaining pore spaces are occluded by blocky calcite mosaics (Cc), 12-22-70-18W5, 2656 m (8713.8'). b) Geopetal crystal silt (Cs) and blocky calcite mosaics (Cc) in a fenestral pore. Crystal silt shows coarsening upwards in pore, 12-22-70-18W5, 2656.2 m (8714.5'). c) Echinoderm fragments (E) with inclusion-free syntaxial calcite overgrowths containing inclusion-rich layers (lower right). Poorly preserved mollusc fragment (center) has a micrite envelope (m) and is rimmed by isopachous fibrous calcite cement (f). Fibrous cements also completely occlude smaller interparticle pores and remaining pore spaces are occluded by blocky calcite mosaics (Cc), 04-26-70-18W5, 2620.7 m (8598').

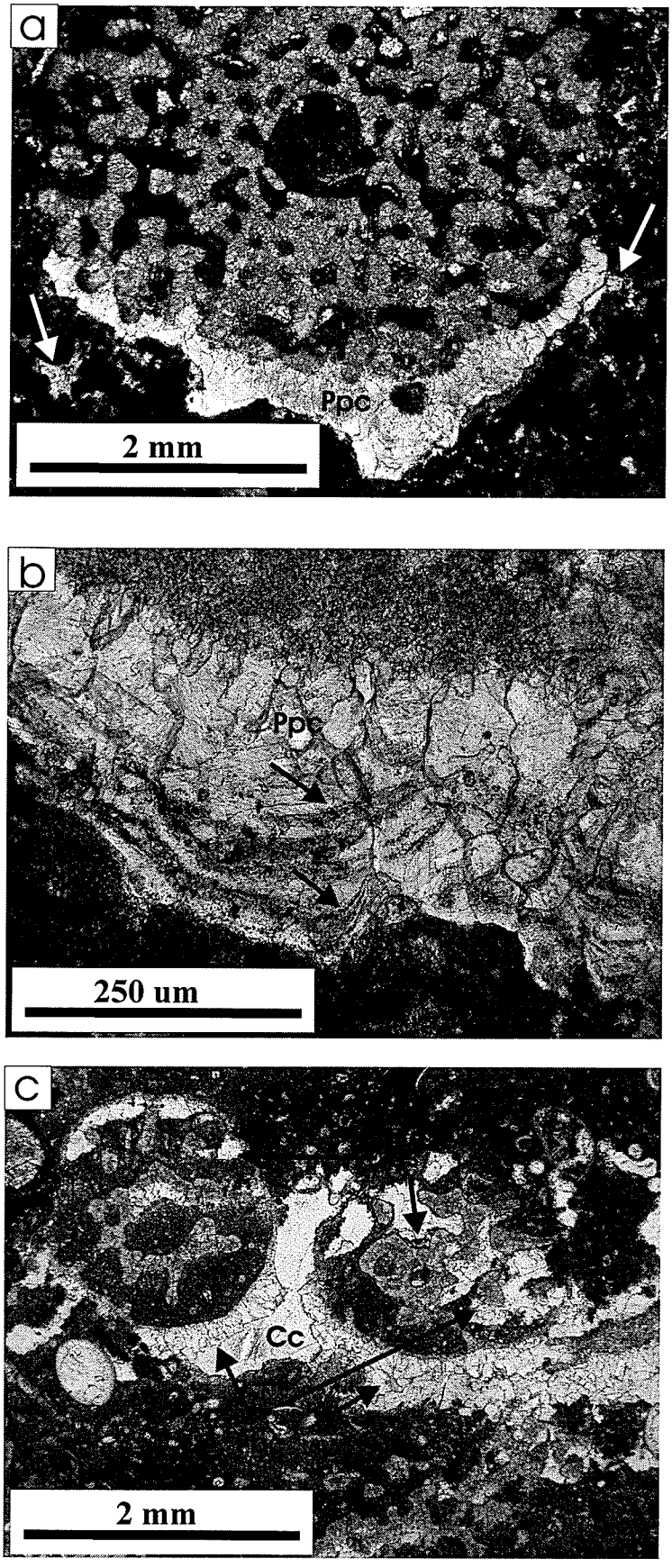
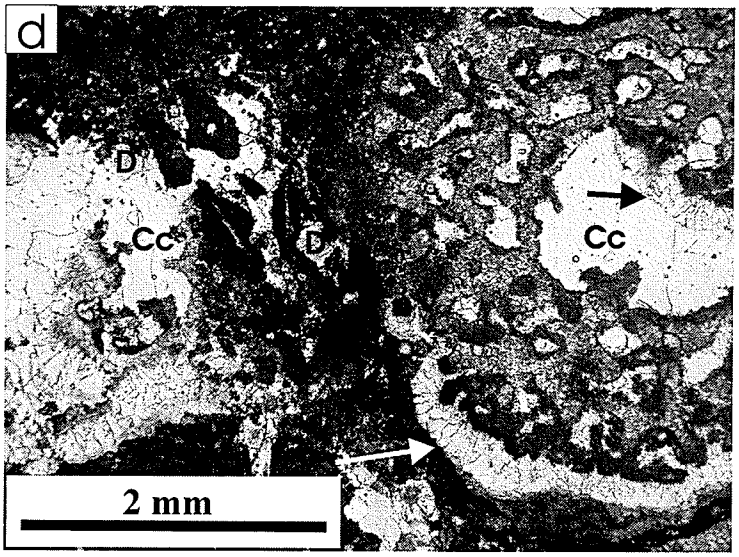
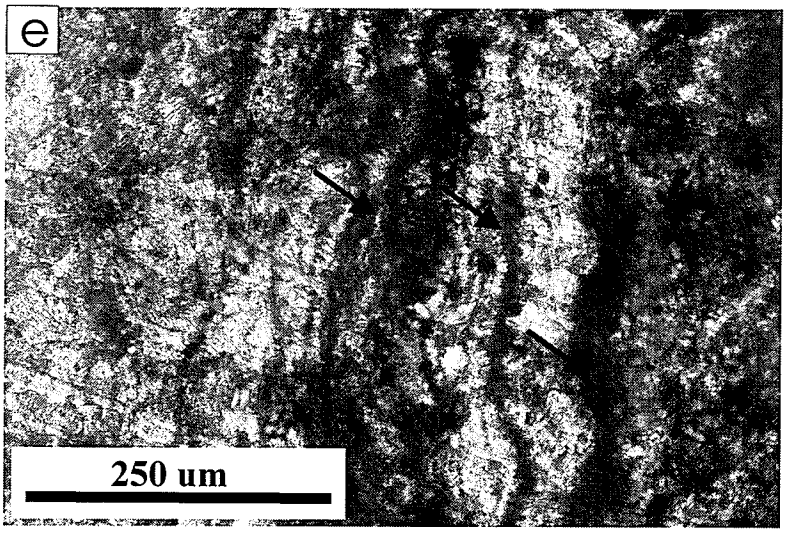


Figure 6.6 Photomicrographs of pendant prismatic calcite cements. a) *Amphipora* with pendant prismatic cement (Ppc). Pendant cement is poor to moderately inclusion-rich calcite. Ferroan dolomite rhombs occlude intraskeletal *Amphipora* galleries and interparticle pores (arrows), 12-22-70-18W5, 2654.4 m (8709'). b) Pendant prismatic calcite cement (Ppc) is generally inclusion-poor with distinct inclusion-rich laminae (arrows), 12-22-70-18W5, 2654.4 m (8709'). c) Clear, pendant prismatic calcite cement (Ppc) in shelter pores below *Amphipora* and in intraskeletal pores. Pendant cement occurs together with crystal silt (Cs) in the same pores. Pendant cements and crystal silt both show evidence of dissolution and are succeeded by blocky calcite mosaics (Cc), 04-26-70-18W5, 2636.1 m (8648.7').





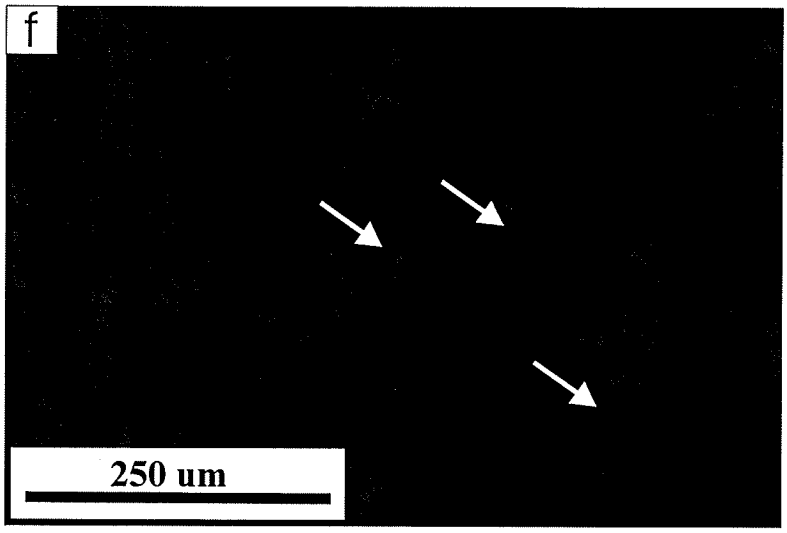


Figure 6.6 continued. d) Pendant prismatic calcite cements (arrows) in shelter pores below *Amphipora* and along the upper surface of the central coenostea of *Amphipora*. Pendant cements are inclusion-free. Remaining intraparticle and interparticle pores are occluded by blocky calcite mosaics (Cc) and ferroan dolomite rhombs (D), 02-33-70-18W5, 2647.7 m (8686.8'). e) Pendant prismatic calcite cement with inclusion-poor and inclusion-rich micritic laminae (arrows), 12-27-70-18W5, 2636.8 m (8651'). f) Photomicrograph of (e) under cathodoluminescence. Inclusion-poor layers are generally dull to non-luminescent, whereas inclusion-rich micritic laminae are moderately to brightly luminescent (arrows).

micritic laminae. These cements may show dissolved crystal margins and in very rare samples have abundant opaque inclusions.

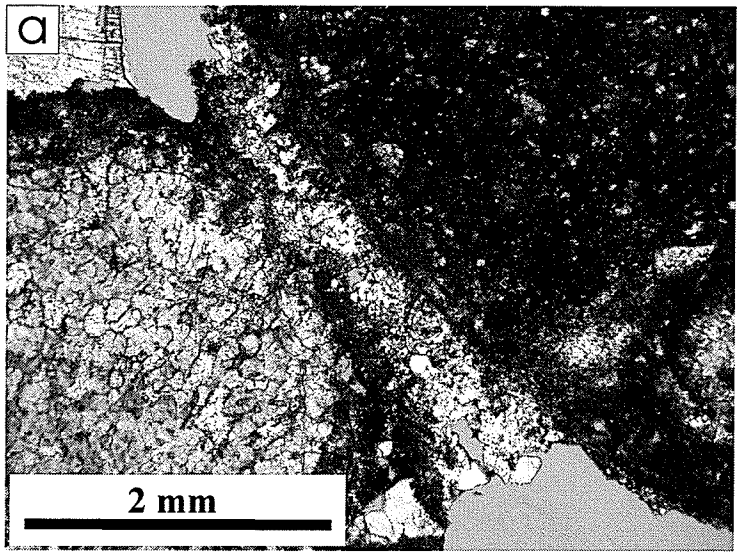
Pendant prismatic cements are non-ferroan calcite and generally dull to non-luminescent. However, rare samples with abundant laminae show zoning under cathodoluminescence (Figure 6.6e, f). Inclusion-rich layers are dull to moderately luminescent and dark brown micritic laminae are moderate to brightly luminescent. Scanning electron microscopy and electron microprobe analyses did not detect any compositional differences within the limits of detection between inclusion-free and inclusion-rich layers.

6.3.6 Meniscus Blocky Calcite

Meniscus calcite cements are very rarely developed at points of contact between adjacent grains (Figure 6.7). Cements are micritic to clear, fine to medium crystalline (<0.1 mm), blocky to prismatic calcite and are non-ferroan.

6.3.7 Syntaxial Calcite Overgrowths

Syntaxial calcite overgrowths are commonly developed around echinoderm fragments (Figures 4.11c and 6.5c). Overgrowths range from medium to coarse crystalline (0.16-0.9 mm) and have a blocky habit. They are inclusion-free, but in rare occurrences inclusions are concentrated along crystal margins of successive phases of cementation resulting in inclusion-rich layers. Syntaxial calcite overgrowths are non-ferroan to zoned (non-ferroan core and ferroan rim).



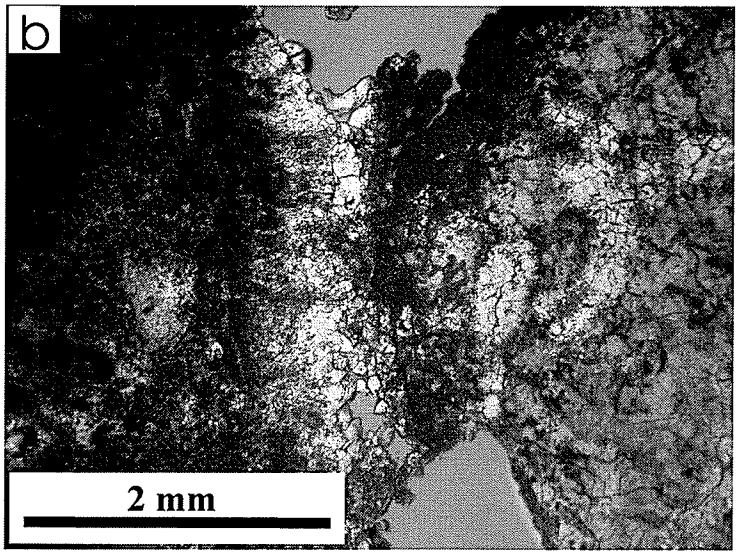


Figure 6.7
Photomicrographs of meniscus cements developed between adjacent grains. Meniscus cement is composed of clear, non-ferroan blocky-prismatic cement. Interparticle porosity is shown by blue epoxy. a) 02-33-70-18W5, 2637.1 m (8651.8'). b) 02-33-70-18W5, 2637.1 m (8651.8').

6.3.8 Isopachous Prismatic Calcite

Clear, prismatic calcite occurs as isopachous rims around peloids, the interior of intraskeletal pores, interparticle pores, dissolution vugs and fractures (Figure 6.8). Prismatic crystals may increase in size and have scalenohedral crystal terminations directed towards the center of the cavity. Crystal sizes range from fine to coarse crystalline (0.008-0.4 mm) and are commonly finer crystalline in smaller intraskeletal pores such as in ostracod shells, calcispheres and stromatoporoids. Isopachous prismatic calcite cements are inclusion-free and non-ferroan.

6.3.9 Blocky-Prismatic Calcite

Clear, blocky-prismatic calcite cements are most common in intraskeletal and interparticle pores and dissolution vugs (Figure 6.9). Prismatic cements often have scalenohedral crystal terminations directed towards the center of vugs. Crystal sizes range from fine to coarse crystalline (0.04-1.0 mm). Blocky-prismatic calcites are generally inclusion-poor and non-ferroan in small (i.e. intraskeletal and interparticle) pore spaces. In larger dissolution vugs, calcite cements have iron-rich cores and become progressively less ferroan towards the rims. Blocky and prismatic calcite cements are non-luminescent in the center and have a moderately luminescent zone and then a dull luminescent zone toward the rim (Figure 6.9c).

6.3.10 Blocky Calcite Mosaics

Clear, blocky calcite cements are developed in all varieties of pore spaces including intraparticle, interparticle, dissolution vugs and fractures (Figures 6.2, 6.3b, c, 6.4, 6.5,

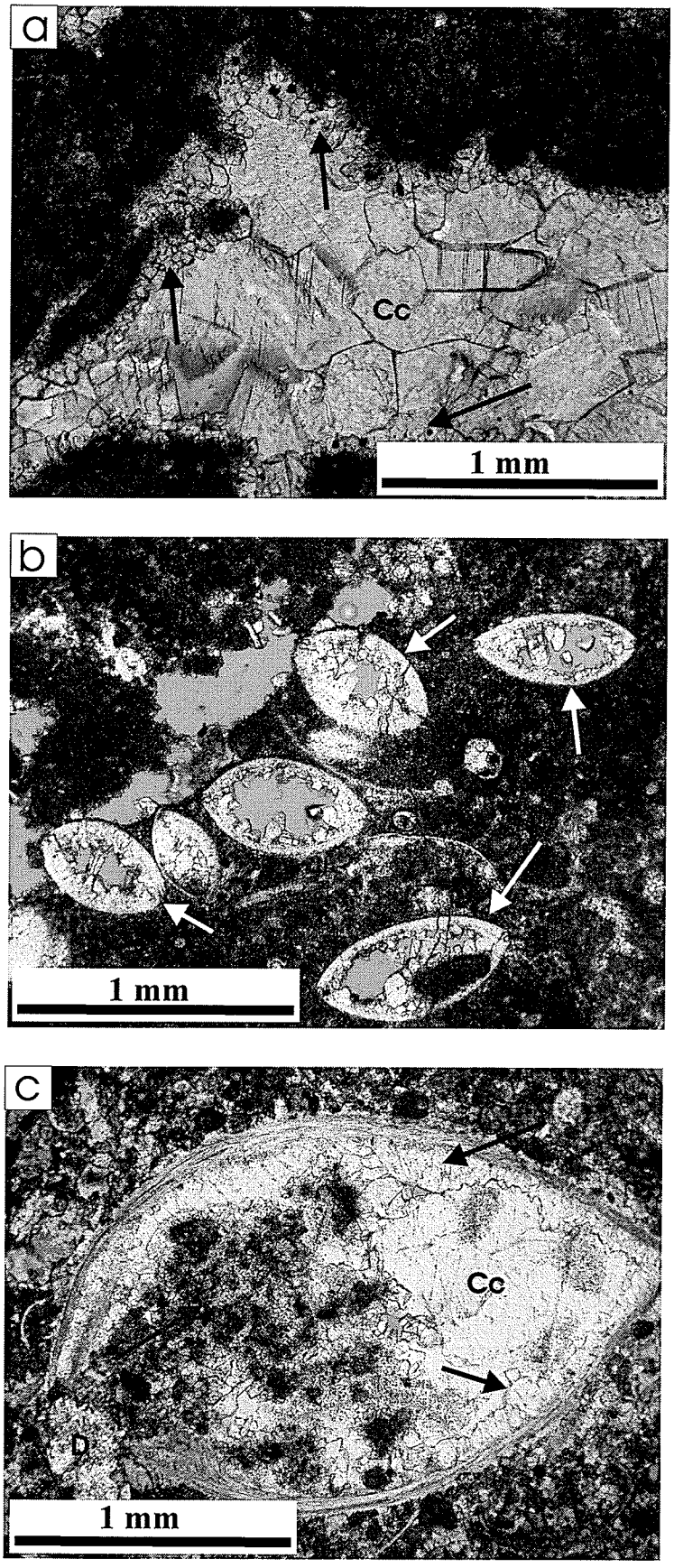


Figure 6.8
Photomicrographs of isopachous prismatic calcite cements. a) Isopachous prismatic calcite cements (arrows) lining the interior of a vug. Remaining pore space in the vug is occluded by blocky calcite mosaics (Cc). Vugs created by the dissolution of blocky calcite mosaics are shown by the blue epoxy, 12-23-70-18W5, 2635.4 m (8646.2'). b) Isopachous prismatic calcite cements lining the interior of ostracod shells (arrows). Vuggy to moldic porosity is shown by blue epoxy, 02-03-71-18W5, 2634.4 m (8643'). c) Ostracod shell with isopachous prismatic calcite cements (black arrows), blocky calcite mosaics (Cc) and ferroan dolomite rhombs (D). Vugs formed by minor dissolution of calcite mosaics are shown by blue epoxy. Peloidal internal sediment is also seen inside the ostracod shell (red arrow), 02-03-71-18W5, 2631 m (8632').

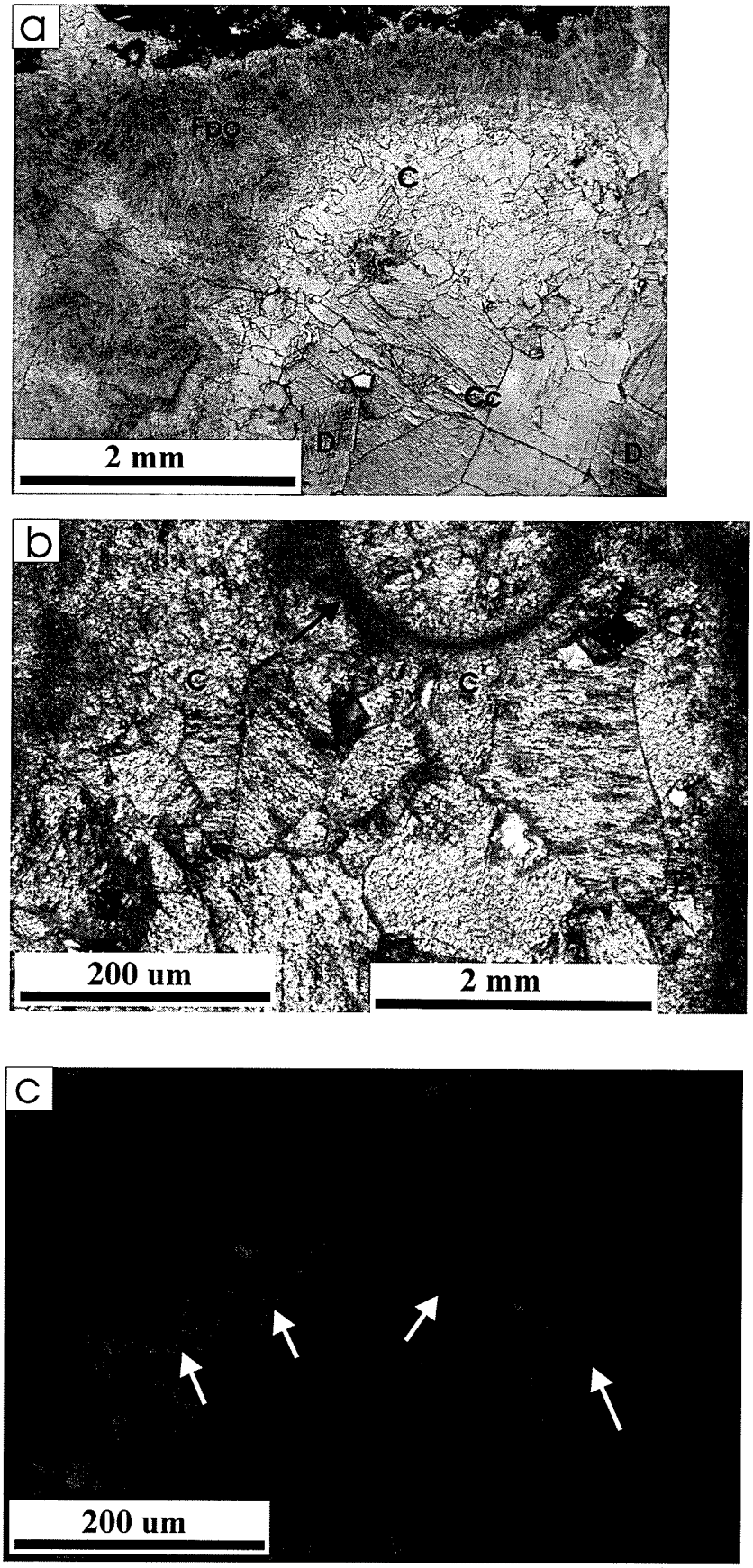


Figure 6.9
Photomicrographs of blocky-prismatic calcite cements. a) Dissolution vug with pendant radiaxial fibrous calcite cements (Fpc), blocky-prismatic non-ferroan calcite cement (C), blocky ferroan calcite mosaics (Cc) and ferroan dolomite rhombs (D), 10-21-70-18W5, 2660.2 m (8727.8'). b) Blocky-prismatic calcite cements (C). A calcisphere with a micrite envelope is seen towards the top of the photo (arrow), 10-21-70-18W5, 2673.6 m (8771.6'). c) Photomicrograph of (b) under cathodoluminescence. Blocky-prismatic calcite cement have scalenohedral crystal terminations and have non-luminescent centers followed by a moderately luminescent zone (arrows) and dull luminescent rims.

6.6c, 6.8a, c, 6.9a and 6.10a, b). Blocky calcite cements occur in coarse mosaics with crystal sizes ranging up to 4.8 mm. Cements tend to be coarser crystalline in secondary pores (vugs and fractures) relative to other pore spaces. In addition, coarser mosaics have wavy to undulose extinction. Most blocky mosaics are compositionally zoned with ferroan cores, followed by non-ferroan zones and then slightly ferroan rims. Accordingly, these zoned calcite mosaics are non-luminescent in the core which is followed by a brightly luminescent zone and then a moderately luminescent rim. Blocky calcite mosaics in larger dissolution vugs are commonly dissolved leaving open porosity.

6.3.11 Dolomite Rhombs

Clear to cloudy, dolomite rhombs are developed in all varieties of pore spaces including intraparticle, interparticle, dissolution vugs and fractures (Figures 6.6a, d, 6.8c and 6.9a). Crystals are euhedral to subhedral rhombs with planar cleavage traces and crystal faces, and show straight extinction. Medium to coarsely crystalline (up to 1.8 mm crystal size) dolomite cements occur in larger pores (interparticle, dissolution vugs, fractures) and partially replace blocky calcite mosaics. Finely crystalline, euhedral dolomite rhombs (0.1 to 0.8 mm size) commonly partially replace green shales or other fine grained sediment (Figure 6.10c). Most dolomite rhombs (cement and replacive) have cloudy, inclusion-rich ferroan cores and inclusion-poor non-ferroan rims. Accordingly, dolomite rhombs commonly have non-luminescent cores and moderately to brightly luminescent rims.

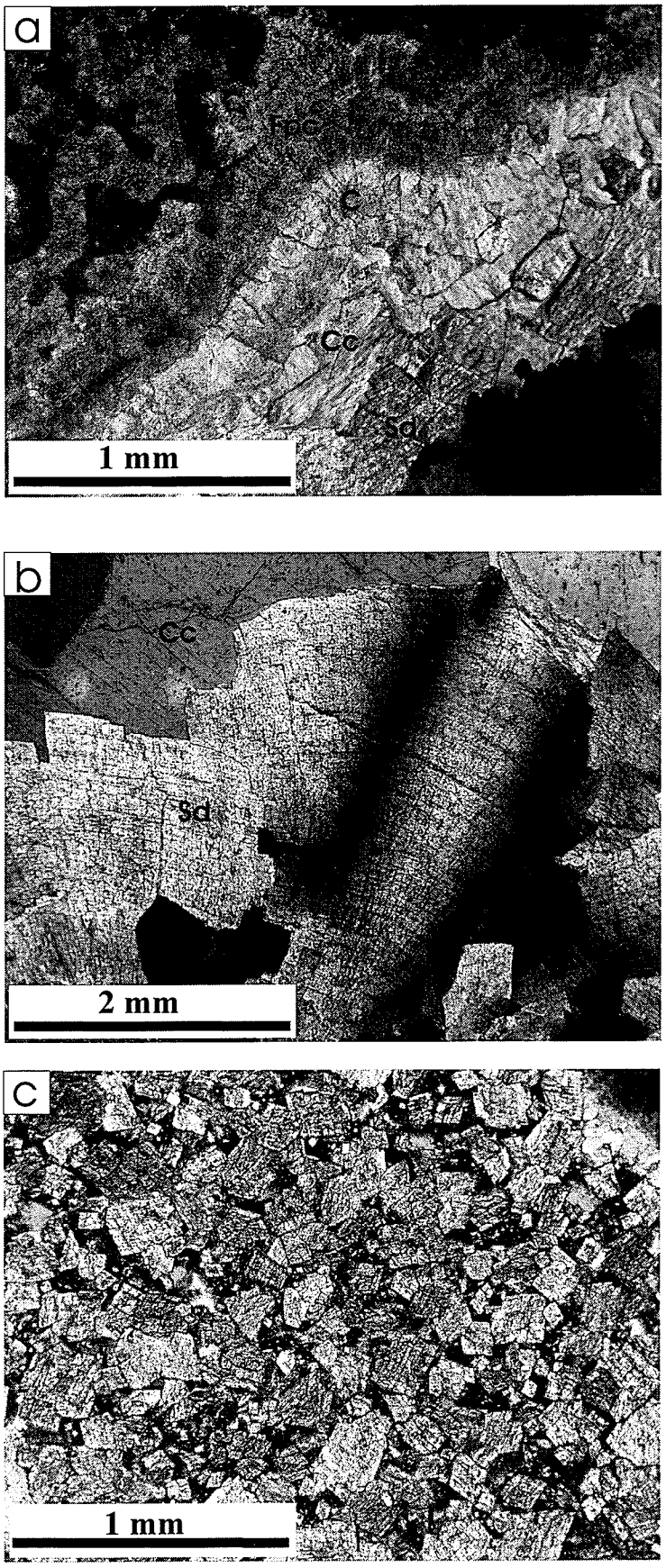


Figure 6.10
Photomicrographs of blocky calcite mosaics and dolomite. a) Dissolution vug with pendant radiaxial fibrous calcite cements (Fpc), non-ferroan blocky-prismatic calcite cements (C), ferroan blocky calcite mosaics (Cc) and ferroan subhedral saddle dolomite (Sd), 16-17-69-19W5, 2743.9 m (9002.2'). b) Coarsely crystalline, ferroan blocky calcite mosaics (Cc) and ferroan saddle dolomite cements (Sd) in a dissolution vug (cross-polarized light). Saddle dolomites have curved cleavage traces and crystal faces with sweeping extinction, 12-22-70-18W5, 2667.7 m (8752.2'). c) Replacement dolomite rhombs with argillaceous interstitial sediment (brown). Dolomite rhombs have straight cleavage traces and crystal faces, and are zoned with ferroan-rich cores and relatively non-ferroan rims, 12-22-70-18W5, 2667.7 m (8752.2').

6.3.12 Saddle Dolomite

Clear to cloudy saddle dolomite cements are developed most commonly in interparticle pores, dissolution vugs and fractures (Figures 6.4c and 6.10b). Saddle dolomite tends to occlude the center and lower portions of pore spaces. Crystal habits are generally blocky, subhedral to anhedral and range from medium to very coarsely crystalline (0.1-3.6 mm crystal size). Saddle dolomites have curved cleavage traces and crystal faces, and show distinct sweeping extinction. They range from ferroan to non-ferroan dolomite and may show complex zoning with ferroan cores that are followed by a thin zone of non-ferroan dolomite and moderately ferroan rims. Saddle dolomites are generally non-luminescent.

6.4 Paragenetic Sequence

The relative timing and diagenetic environment of cement precipitation are interpreted based on original crystal habit, cement morphology and chemical composition (described in section 6.3) and textural (cross-cutting) relationships. The paragenetic sequence at the Snipe Lake reef complex is summarized in Figure 6.11.

6.4.1 Marine Cements in Primary Pores

Micritic cements are the earliest evidence for diagenetic alteration (refer to section 6.2.1). They precede all other types of cements (Figures 6.2 and 6.5a, c) and are interpreted to represent the earliest phase of cementation that formed during early marine diagenesis.

Isopachous fibrous calcite cements are interpreted to have precipitated in the marine phreatic environment (refer to section 6.2.1). Isopachous fibrous cements commonly

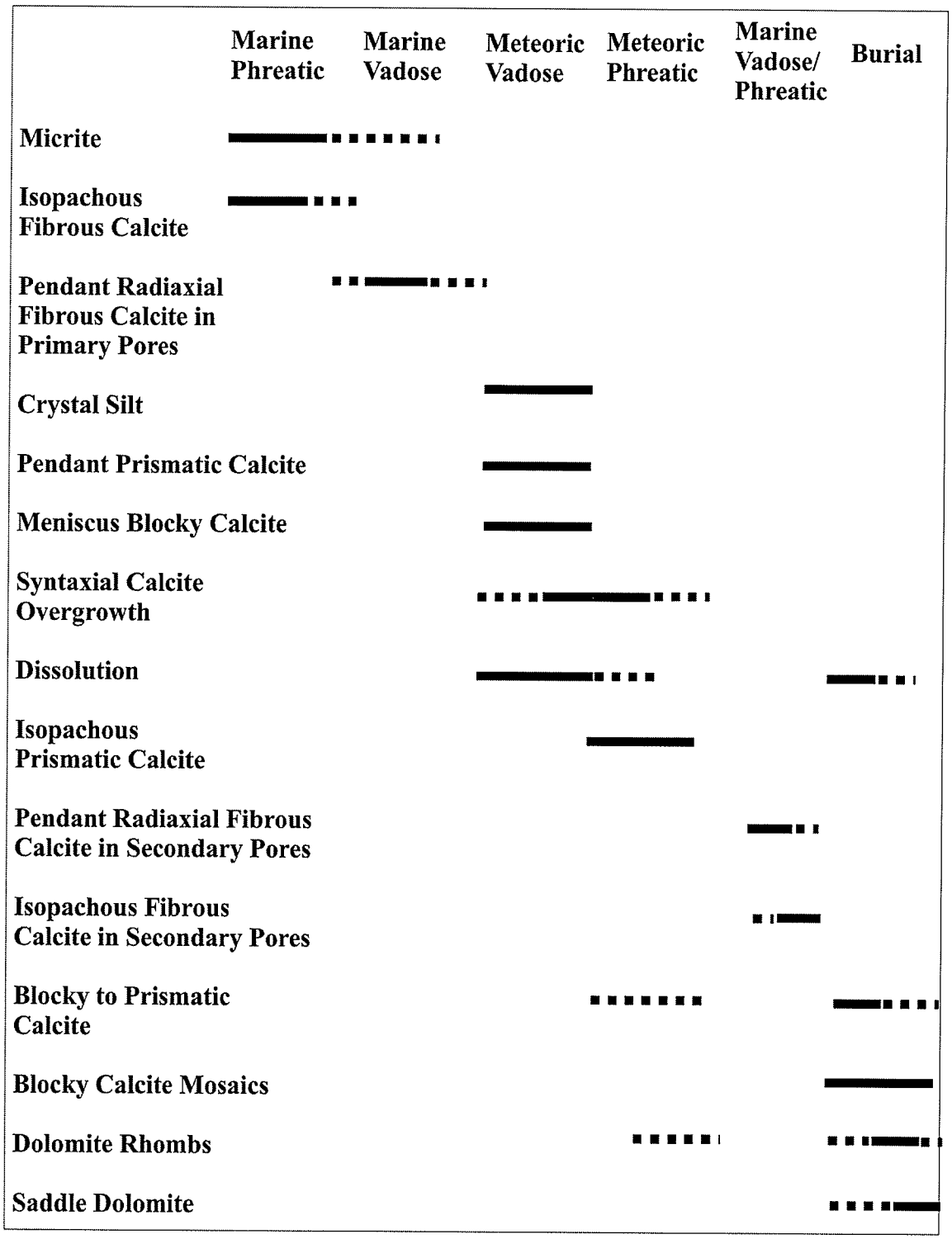


Figure 6.11 Paragenetic sequence and diagenetic environments for the different types of cements recognized between the P4 and R0.5 megacycle contacts in the Snipe Lake reef complex.

precipitated on micritized surfaces and predate all other cements in pore spaces (Figures 6.2b, 6.5c) suggesting a relatively early origin. In some pores, isopachous fibrous calcite cements are slightly thicker along the roof of pores. This pendant-like morphology suggests that isopachous cements precipitated in relatively shallow phreatic conditions close to vadose conditions (cf. Wong, 1978). Isopachous fibrous calcite cements in the Snipe Lake reef complex were also interpreted by Havard (1974) to be of marine phreatic origin. Other studies of the Kaybob and Swan Hills reef complexes made similar observations and interpretations (e.g. Wong, 1978; Viau, 1986).

Pendant radiaxial fibrous calcite cements in primary pores are interpreted to have been precipitated in marine vadose conditions (refer to section 6.2.1). These cements succeed the two previously described cement types (micritic and isopachous fibrous calcite), but precede other cements that occur within the same pore space (Figure 6.4 a, b). These cements are interpreted to have precipitated in beachrocks in the intertidal environment (marine vadose); some cements may have precipitated just prior to or possibly during very early subaerial exposure. The gradational nature with isopachous fibrous calcite cements suggests that precipitation of pendant radiaxial fibrous calcite cements was continuous with cementation under shallow marine phreatic conditions. However, Havard (1974) interpreted microstalactitic rims in the Snipe Lake reef complex to be of meteoric vadose origin. In contrast, other microstalactitic cements that are transitional with isopachous rims within beachrock deposits were interpreted by her to be intertidal (i.e. marine vadose) in origin. Petrographic differences or occurrences of these two types of microstalactitic cements were not readily defined in Havard's (1974) study. Cloudy

microstalactitic and microstalagmitic fibrous calcite cements at the Kaybob reef complex and brown pendant fibrous calcite cements in the Swan Hills reef complex were interpreted to have precipitated in the marine vadose environment (e.g. Wong, 1978; Viau, 1986).

6.4.2 Meteoric Cements

Pendant prismatic calcite cements are interpreted to have precipitated in the meteoric vadose environment (refer to section 6.2.2). Pendant prismatic calcite cements are succeeded by blocky calcite mosaics (Figure 6.6c, d) suggesting they must have precipitated prior to shallow burial conditions (see section 6.4.4). Although some pendant prismatic calcites have inclusion-rich laminae, which are atypical of meteoric cements, they are still interpreted to be of meteoric vadose origin for the following reasons: (1) they have similar crystal habits (prismatic) and occurrence (under *Amphipora*, not developed in dissolution vugs) as clear, pendant prismatic cements, and (2) inclusions usually occur in well defined layers (unlike pendant radiaxial fibrous calcite cements). Inclusion-rich laminae are likely the result of a concentration of insoluble particles from percolating meteoric waters and /or evaporation of the meniscus film (refer to section 6.2.2). Similar, clear microstalactitic cements with inclusion-rich laminae in the Kaybob reef complex were also interpreted to have formed in the meteoric vadose environment (e.g. Wong, 1978).

Crystal silt is interpreted to have formed in the meteoric vadose environment (refer to section 6.2.2). Crystal silt succeeds micritic cements (early marine phreatic), but is

postdated by dissolution (meteoric vadose and phreatic; discussed below) and clear, blocky calcite mosaics (shallow burial, refer to section 6.4.4) (Figure 6.5a, b). In addition, v-shaped desiccation cracks in crystal silt strongly suggest that the sediments were subaerially exposed in the meteoric environment. Geopetal crystal silt and pendant prismatic calcite cements occur together in the same cavity (Figure 6.6c). Pendant prismatic calcite cements occur along the upper surfaces of pores, and crystal silt accumulated at the bottom of the same pores. Although, these two features are both interpreted to have formed in the meteoric vadose zone, there is a lack of textural evidence to indicate their relative timing. Crystal silt observed in an earlier study of the Snipe Lake reef complex was also interpreted to have formed during meteoric vadose diagenesis (Havard, 1974).

Meniscus blocky calcite cements are also interpreted to have precipitated in the meteoric vadose environment (refer to section 6.2.2). Due to the rare occurrence of these cements, textural relationships with other cement phases are difficult to establish. Nonetheless, the cement morphology is typical of cementation in the vadose environment. Similar cements observed in the Kaybob reef complex were also interpreted to be of meteoric vadose origin (e.g. Wong, 1978).

Syntaxial calcite overgrowths are interpreted to have precipitated throughout the meteoric environment (refer to section 6.2.2). The variation between non-ferroan and ferroan calcite suggests precipitation occurred in both oxygenated (vadose) and slightly reducing (phreatic) conditions. Syntaxial calcite overgrowths succeed isopachous fibrous calcite

and pendant radiaxial fibrous calcite cements (Figure 6.5c) but precede dolomite rhombs (refer to section 6.4.4, Figure 4.11c). Therefore the development of these cements must have postdated marine phreatic conditions and predated shallow burial conditions.

Development of dissolution vugs and solution-enhanced interparticle and shelter pores is interpreted to be the product of meteoric (vadose to phreatic) dissolution (refer to section 6.2.2). The occurrence of meteoric pendant cements that have corroded crystal margins also supports this interpretation. Geopetal fabrics (green shales, crystal silts) often occur within dissolution vugs which further suggest that some dissolution may have occurred during meteoric vadose conditions. A later (burial) origin is precluded because dissolution vugs are occluded by isopachous prismatic calcite cements (Figure 6.8a; discussed below) and pendant radiaxial fibrous calcite cements (Figure 6.4c-f) and cross-cut by stylolites (Figure 6.4d). Previous studies have similarly interpreted the majority of dissolution features in the Snipe Lake reef complex (e.g. Havard, 1974) and the House Mountain, Swan Hills and Virginia Hills fields (e.g. Packard and Hills, 2001) to be products of meteoric diagenesis.

Clear, isopachous prismatic calcite cements are interpreted to have precipitated in the meteoric phreatic environment (refer to section 6.2.2). These cements postdate isopachous fibrous calcite, pendant radiaxial fibrous calcite cements, dissolution features and desiccation cracks (refer to section 7.7) and precede late blocky calcite mosaics (Figures 6.8a, c; refer to section 6.4.4) which suggest precipitation occurred after meteoric vadose conditions and prior to burial. Clear isopachous cements at the Kaybob

reef complex were also interpreted to be of meteoric phreatic origin (e.g. Wong, 1978).

6.4.3 Marine Cements in Secondary Pores

Pendant radiaxial fibrous calcite cements in dissolution vugs are interpreted to have been precipitated in the marine vadose environment during a subsequent relative sea level rise after subaerial exposure. In contrast to pendant radiaxial fibrous calcite cements in primary pores, the precipitation of these cements must postdate meteoric dissolution. As relative sea level started to rise after exposure, secondary pore spaces were partially filled with seawater which initiated a second phase of marine cementation. With continued sea level rise pores were completely filled by seawater and rare isopachous fibrous calcite rims precipitated in dissolution vugs. Pendant radiaxial fibrous calcite cements in dissolution vugs precede and are gradational with blocky-prismatic calcite cements (shallow burial) and late blocky calcite mosaics (deep burial) (Figures 6.4c-f, 6.9a and 6.10a; see section 6.4.4). Similar, pendant radiaxial fibrous calcite cements in dissolution vugs in the Judy Creek reef complex were also interpreted to have precipitated from seawater after subaerial exposure (Chow and Wendte, 2004).

6.4.4 Burial Cements

Blocky-prismatic calcite cements are interpreted to have precipitated in the shallow burial diagenetic environment (refer to section 6.2.3). They succeed pendant radiaxial fibrous calcite cements in vugs and are gradational with blocky calcite mosaics (Figures 6.4c and 6.10a). This suggests that precipitation of these cements occurred during shallow burial

conditions, postdating the last phase of marine vadose conditions after emergence of the Snipe Lake reef complex.

Blocky calcite mosaics are interpreted to have precipitated in the shallow burial diagenetic environment (refer to section 6.2.3). Calcite mosaics succeed shallow burial blocky-prismatic calcite cements (Figures 6.9a and 6.10a), but are dissected by stylolites (Figure 6.4d). Therefore, these cements postdate the earliest shallow burial cements but precipitated before deep burial conditions. Coarsely crystalline, equant calcite mosaics recognized in an earlier study in the Snipe Lake reef complex (e.g. Havard, 1974) and other studies of the Kaybob reef complex (e.g. Wong, 1978) and Swan Hills reef complex (Viau, 1986) were also interpreted to be of burial diagenetic origin.

Ferroan to non-ferroan dolomite rhombs (non-replacive) are interpreted to have precipitated during shallow burial (refer to section 6.2.3). Dolomite rhombs succeed blocky calcite mosaics (Figures 6.6d and 6.9a) but are cross-cut by stylolitic seams precluding a deep burial origin. Dolomite rhombs were not interpreted previously in the Snipe Lake reef complex. Similar, replacive planar dolomites recognized in the Simonette reef complex were interpreted to be a product of 'intermediate' diagenesis (Duggan, 2004).

A late-stage phase of dissolution is interpreted to have occurred during burial diagenesis (refer to section 6.2.3). Blocky-prismatic calcite cements and blocky calcite mosaics have minor vuggy porosity (Figures 6.2b, 6.4b, c, 6.8a, c) suggesting that dissolution

postdated these shallow burial cements. In contrast, saddle dolomites typically do not show evidence of significant dissolution, suggesting dissolution did not continue into deep burial conditions (see discussion below).

Ferroan to non-ferroan saddle dolomites are interpreted to have precipitated during deep burial diagenesis (refer to section 6.2.3). No other major diagenetic features cross-cut or post-date saddle dolomite cements, therefore these cements are interpreted to represent the latest phase of burial cementation in the Snipe Lake reef complex. However, locally, these cements may show very minor dissolution. Saddle dolomite cements in the Kaybob reef complex (e.g. Wong, 1978), Swan Hills reef complex (e.g. Viau, 1986), Rosevear Field (e.g. Kaufman et al, 1990) and Simonette reef complex (e.g. Duggan, 2004) were also interpreted to represent cementation in deep burial conditions.

6.5 Stable Isotope Analysis

In addition to petrographic evidence (as discussed above), stable isotope analysis was completed to help constrain the relative timing and environment of precipitation for different cement phases (refer to section 2.10). Stable carbon and oxygen isotope data from various cements are summarized in Table 6.2 and their distribution is plotted in Figures 6.12 and 6.13. All values are reported in per mil (‰) VPDB. For comparison, the field for various Middle and Upper Devonian marine calcite cements (Popp et al., 1986; Carpenter and Lohmann, 1989; Hurley and Longman, 1989; Carpenter et al., 1991; Amthor et al., 1993; Carpenter and Lohmann, 1997; Packard and Hills, 2001) and data from marine vadose, pendant calcite cements from the Upper Keg River Member, Zama

Table 6.2 Stable oxygen and carbon isotope data for various calcite and dolomite cements below the R0.5 and P4 megacycle contacts, Snipe Lake reef complex. Precision of results: $\delta^{13}C_{VPDB}$ (0.01 ‰) and $\delta^{18}O_{VPDB}$ (0.03 ‰).

Sample Identification	Well Location	Depth Meters (Feet)	Cement Type & Mineralogy	Stratigraphic Horizon	Lithofacies	$\delta^{13}C_{VPDB}$ (‰)	$\delta^{18}O_{VPDB}$ (‰)
02-03-8645 - dol	02-03-71-18W5	2635.0 m (8645')	Saddle dolomite	P4	D	2.9	-10.1
12-22-8752.2A - dol	12-22-70-18W5	2667.7 m (8752.2')	Saddle dolomite	P4	A	3.0	-10.8
12-23-8652.2 - cc	12-23-70-18W5	2637.2 m (8652.2')	Blocky calcite mosaics	P4	A	1.8	-10.5
12-22-8714.5 - cc	12-22-70-18W5	2656.2 m (874.5')	Blocky calcite mosaics	R0.5	A	2.3	-11.1
12-22-8714.5B - cc	12-22-70-18W5	2656.2 m (874.5')	Crystal silt (dolomite)	R0.5	A	2.7	-10.5
12-22-8714.5B - dol	12-22-70-18W5	2656.2 m (874.5')	Crystal silt (calcite)	R0.5	A	2.5	-10.6
12-22-8709A - cc	12-22-70-18W5	2654.5 m (8709')	Pendant prismatic calcite	R0.5	C	2.1	-8.5
12-27-8651 - cc	12-27-70-18W5	2636.8 m (8651')	Pendant prismatic calcite	R0.5	B	3.2	-9.0
12-32-8545A - cc	12-32-70-18W5	2604.5 m (8545')	Pendant prismatic calcite	R0.5	A	3.0	-7.8
10-21-8783 - cc	10-21-70-18W5	2677.1 m (8783')	Isopachous fibrous calcite	P4	D	-0.5	-10.2
04-26-8598.1 - cc	04-26-70-18W5	2620.7 m (8598.1')	Pendant radiaxial fibrous calcite (in vugs)	R0.5	A	2.8	-7.0
02-03-8640.7 - cc	02-03-71-18W5	2633.7 m (8640.7')	Pendant radiaxial fibrous calcite (in vugs)	P4	D	2.1	-6.2
02-03-8643 - cc	02-03-71-18W5	2643.4 m (8643')	Pendant radiaxial fibrous calcite (in vugs)	P4	D	1.8	-8.6
10-21-8771.6 - cc	10-21-70-18W5	2673.6 m (8771.6')	Pendant radiaxial fibrous calcite (in vugs)	P4	D	0.9	-7.8
10-21-8727.8 - cc	10-21-70-18W5	2660.2 m (8727.8')	Pendant radiaxial fibrous calcite (in vugs)	R0.5	D	2.5	-9.1
12-22-8713.8 - cc	12-22-70-18W5	2656.0 m (8713.8')	Pendant radiaxial fibrous calcite (in vugs)	R0.5	A	1.4	-9.6

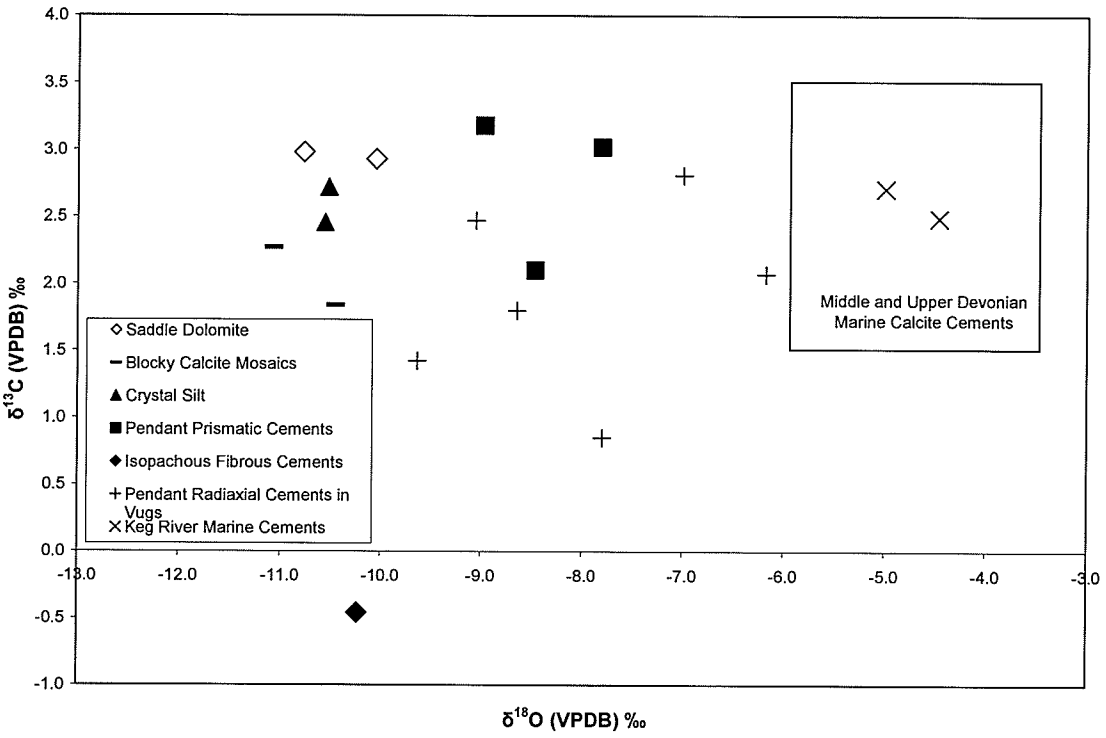


Figure 6.12 Plot of $\delta^{18}O$ and $\delta^{13}C$ values for calcite and dolomite cements below the P4 and R0.5 subaerial exposure surfaces in the Snipe Lake reef complex. The field for typical Middle and Upper Devonian marine cements and data from the Upper Keg River Member, Zama N Field, Alberta are also shown in the diagram (see text for sources).

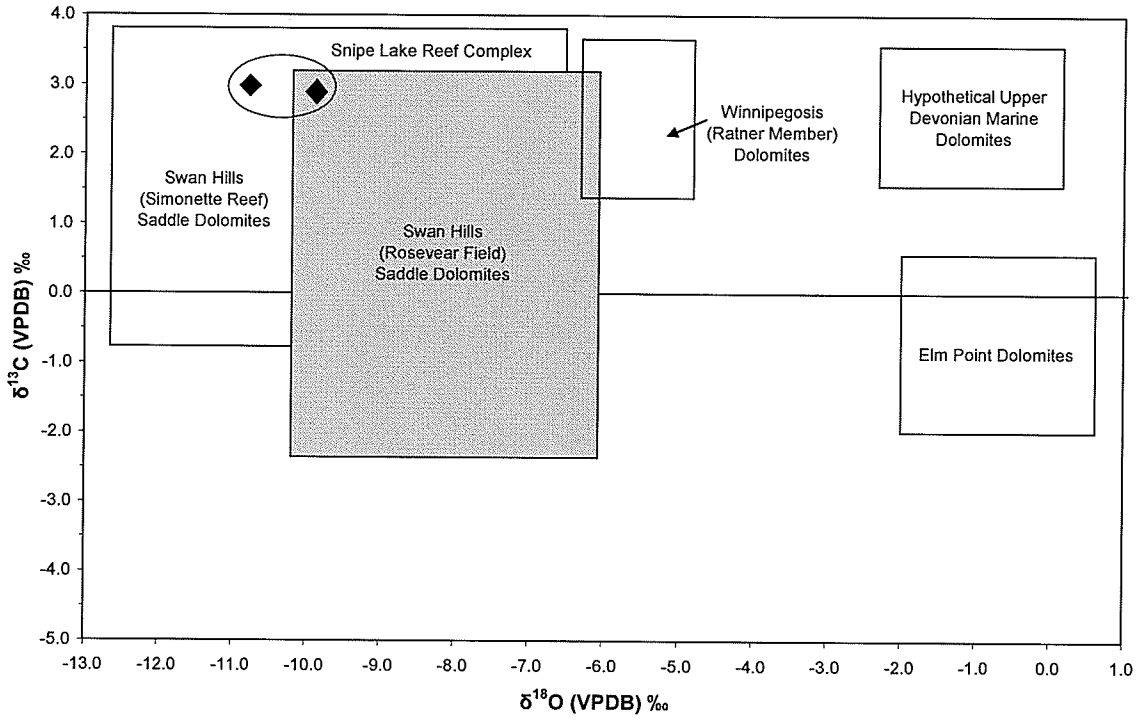


Figure 6.13 Plot of $\delta^{18}O$ and $\delta^{13}C$ values for saddle dolomite cements in the Snipe Lake reef complex. Fields for hypothetical Devonian marine dolomites; Elm Point Formation dolomites; Winnipegosis Formation, Ratner Member dolomites; Swan Hills Formation dolomites, Rosevear Field and Simonette Field are also shown (see text for references).

N Field, Alberta (Chow and Wendte, 2004) are also shown on Figure 6.12. In addition, the fields for hypothetical Upper Devonian marine dolomites (Land, 1985; Carpenter and Lohmann, 1989; Hurley and Lohmann, 1989; Amthor et al., 1993), Middle Devonian Elm Point Formation dolomites, Manitoba (Chow and Longstaffe, 1995); Middle Devonian Winnipegosis Formation, Ratner Member dolomites, Saskatchewan (Fu et al., 2004a); Swan Hills Formation dolomites, Rosevear Field dolomites (Kaufman et al., 1990), and Simonette Field (Duggan et al., 2001; Duggan, 2004) are plotted in Figure 6.13.

6.5.1 Stable Isotope Results

Sixteen samples taken from different cements phases were successfully analyzed for stable isotopes (Table 6.2, Figures 6.12 and 6.13). Isopachous fibrous calcite cements were difficult to sample due to their thin nature of occurrence, and as a result only a single sample was analyzed that yielded $\delta^{18}O$ and $\delta^{13}C$ values of -10.2‰ and -0.5‰, respectively. Pendant radiaxial fibrous calcite cements in dissolution vugs have a wide range of $\delta^{18}O$ values from -9.6 to -6.2‰ which include some of the most positive values for cements in this study, and $\delta^{13}C$ values ranging from +0.9 to +2.8‰. Clear, pendant prismatic calcite cements have $\delta^{18}O$ values ranging from -9.0 to -7.8‰ and $\delta^{13}C$ values ranging from +2.1 to +3.2‰. Calcite and dolomite crystals in geopetal crystal silt were analyzed separately using selective extraction (refer to section 2.10) and yielded similar results; $\delta^{18}O$ values fall within a narrow range from -10.6 to -10.5‰ and $\delta^{13}C$ values from +2.5 to +2.7‰. Late blocky calcite mosaic cements and saddle dolomite cements

have the most negative $\delta^{18}O$ values which are constrained within relatively narrow fields. Blocky calcite mosaics have $\delta^{18}O$ values from -11.1 to -10.5‰ and $\delta^{13}C$ values of +1.8 to +2.3‰. Saddle dolomites have similar values with $\delta^{18}O$ ranging from -10.8 to -10.1‰ and $\delta^{13}C$ values of +2.9 to +3.0‰.

6.5.2 Stable Isotope Interpretations

Isopachous Fibrous and Pendant Radiaxial Fibrous Calcite Cements

The majority of pendant radiaxial fibrous calcite cements have carbon isotope values comparable to Upper Devonian marine calcite cements, suggesting a marine (inorganic) carbon source. The light $\delta^{13}C$ value of the isopachous fibrous cement sample is strikingly different but with only one sample analyzed the interpretation remains problematic.

Both isopachous fibrous and pendant radiaxial fibrous calcite cements are depleted in ^{18}O in comparison to typical Upper Devonian marine calcite cements. However, a few samples have the most positive $\delta^{18}O$ values of cements types in this study and therefore, these cements are interpreted to have likely precipitated from Devonian seawater. Light $\delta^{18}O$ values in cements may be explained generally by one or more of the following reasons: (1) preservation of original isotopic signatures resulting from precipitation from isotopically lighter waters such as meteoric or deep burial formation waters (Moore, 2001), (2) re-equilibration during later diagenesis resulting in re-setting of $\delta^{18}O$ values (Choquette and James, 1990), (3) 'contamination' from recrystallized laminae within the cements, and (4) sampling problems and contamination by later cements. The first scenario is unlikely because petrographic data, in particular crystal habits and textural

relationships with other cements, exclude a meteoric or burial diagenetic origin for both types of fibrous cements (cf. Havard, 1974; Wong, 1978; Viau, 1986). In contrast, re-setting of geochemical signatures of early marine cements is the most probable explanation since both isopachous fibrous and pendant radiaxial fibrous calcite cements in this study, which may have precipitated as low or high magnesium calcite (James and Choquette, 1990a; section 6.3.1), show evidence of partial recrystallization to blocky to prismatic crystals. Light $\delta^{18}O$ signatures (-11.1 to -7.8‰) of early marine fibrous cements observed in other Swan Hills reef buildups were also interpreted to be a result of isotopic re-equilibration (e.g. Viau, 1986; Kaufman, 1989).

Inherited contamination from within the pendant radiaxial fibrous calcite cements themselves remains a possibility. For example, inclusion-poor and inclusion-rich layers within radiaxial fibrous calcite cements from the Golden Spike reef were sampled separately and had different $\delta^{18}O$ values ranging from -5.5 to -4.5‰ and -10.0 to -5.8‰, respectively (Carpenter and Lohmann, 1989). Pendant radiaxial fibrous calcite cements in the Snipe Lake reef complex also have alternating inclusion-rich and inclusion-poor layers, but individual layers were not sampled separately in this study due to the thin nature of laminae and size limitations of the drill-bit. Therefore samples collected contain a mixture of both types of layers and low $\delta^{18}O$ values may in part reflect "contamination" by isotopically lighter layers. This scenario remains speculative because limited data from this study cannot either confirm or exclude the possibility of meteorically influenced inclusion-rich layers but the effect is probably not strong enough to entirely account for the depleted oxygen signatures.

Sample contamination from later and isotopically lighter phases of cements (blocky calcite and saddle dolomite) is also a likely explanation. Cements adjacent to isopachous fibrous and pendant radiaxial fibrous calcite cements may have been inadvertently drilled and included during sampling. Pendant radiaxial calcite cements are generally thicker and probably less affected by contamination than isopachous fibrous calcite which is much thinner.

Pendant Prismatic Calcite Cements

The range of $\delta^{13}C$ and $\delta^{18}O$ values for pendant prismatic calcite cements significantly overlaps with those for pendant radiaxial fibrous calcite cements. Pendant prismatic calcite cements have $\delta^{13}C$ values comparable to typical Upper Devonian marine calcite cements and are interpreted to indicate a marine carbon source. In addition, $\delta^{13}C$ values are relatively positive with respect to other reported meteoric cements (cf. Carpenter and Lohmann, 1989) and suggest minimal influence from soil-gas CO_2.

Lighter $\delta^{18}O$ values for pendant prismatic calcite cements relative to Upper Devonian marine cements are consistent with precipitation from isotopically lighter meteoric waters (cf. Meyers and Lohmann, 1985; Carpenter and Lohmann, 1989; James and Choquette, 1990b; Morse and Mackenzie, 1990). These cements in the Snipe Lake reef complex have $\delta^{18}O$ values that are within the lower range of other vadose pendant cements (-9.1 to -5.6‰, Golden Spike reef; Carpenter and Lohmann, 1989) which support an origin from meteoric waters. Although the isotopic signatures and cement morphology for pendant prismatic calcite cements appear to be readily explained by precipitation in meteoric

waters, the overlap with marine, pendant radiaxial fibrous calcite cements needs to be considered. The influence of re-equilibration during later diagenesis and potential sample contamination by other cements (e.g. blocky calcite mosaics and saddle dolomites) may have also contributed to the light $\delta^{18}O$ values.

Crystal Silt

Crystal silt has $\delta^{13}C$ values comparable to typical Upper Devonian marine calcite cements and are interpreted to indicate a marine carbon source. The relatively positive $\delta^{13}C$ values suggests minimal influence from soil-gas CO_2.

Crystal silt for both calcite and dolomite have significantly negative $\delta^{18}O$ values relative to typical Devonian marine and meteoric vadose cements of this study. Isotope values for both the calcitic and dolomitic components of crystal silt are very similar to burial cements (see later sections), but textural relationships and the geopetal character of the crystal silt support a meteoric origin. The most probable explanation for these low $\delta^{18}O$ values is isotopic re-equilibration during later (burial) diagenesis. Crystal silt is commonly recrystallized to ferroan and non-ferroan, blocky calcite supporting a re-setting of isotopic signatures. In addition, dolomitic crystal silt was commonly replaced by ferroan dolomite rhombs which could not be isolated during sampling or by the selective extraction process, thus introducing a source of contamination. Petrographically similar dolomite rhombs in the Swan Hills Simonette Field also have low $\delta^{18}O$ values (-9.1 to -7.1‰; Duggan et al., 2001) and were interpreted to be replacement dolomite that precipitated during early burial diagenesis.

Blocky Calcite Mosaics

Blocky calcite mosaics cements have $\delta^{13}C$ values comparable to Devonian marine cements and are interpreted to have a marine carbon source with minimal influence from oxidized carbon and thermal sulfate reduction processes (cf. Viau, 1986; Kaufman et al., 1990; Machel et al., 1996; Mountjoy et al., 1999).

Oxygen isotopic values for blocky calcite mosaic cements plot within a relatively narrow field and have some of the most negative $\delta^{18}O$ values (-11.1 to -10.5‰) for cements sampled in this study. These values are consistent with the general observation that burial cements are isotopically lighter relative to earlier marine and meteoric cements (cf. Carpenter and Lohmann, 1989; Kaufman et al., 1990; Machel et al., 1996; Mountjoy et al., 1999). In general, burial cements show progressively lighter isotopic compositions with increased depth of burial and temperature of precipitation (e.g. Choquette and James, 1990; Mountjoy et al., 1999).

Calcite mosaics in this study however, have slightly lower $\delta^{18}O$ values compared to those from other Devonian studies (e.g. -11.8 to -9.2‰ in the Golden Spike and Nevis reef complexes, Carpenter and Lohmann, 1989; -8.7 to -7.3‰ in the Swan Hills Rosevear Field, Kaufman et al., 1990; -9.2‰ in the Rimbey-Meadowbrook reef trend, Mountjoy et al., 1999). Carbonate rocks from the Golden Spike and Nevis reef complexes and the Rimbey-Meadowbrook reef trend are stratigraphically higher (Leduc Formation) compared to the Snipe Lake reef complex and Rosevear field (Swan Hills Formation). In spite of this, the maximum burial depths between carbonate rocks in the Leduc

Formation (4000-6500 m; Mountjoy et al., 1999) and the Swan Hills Formation (4000-6000 m; Kaufman et al., 1990) are similar. Therefore, lighter $\delta^{18}O$ values for calcite mosaics in the Snipe Lake reef complex cannot be wholly attributed to the depth of burial and temperature of precipitation. Similar to other cements in this study, $\delta^{18}O$ values may have been affected by overprinting during deeper burial diagenesis. Sampling contamination by later cement phases is unlikely since sampling of these coarser cements is relatively straightforward.

Saddle Dolomites

Isotopic values for saddle dolomites in this study plot within a relatively narrow range that is comparable to that of blocky calcite mosaics (Figure 6.12). $\delta^{13}C$ values fall within the range for typical Devonian marine cements indicating a marine carbon source and no influence from oxidized carbon and thermal sulfate reduction processes (see previous section for references).

The low $\delta^{18}O$ values are attributed to the late burial origin of saddle dolomites in the Snipe Lake reef complex and are comparable to those obtained from saddle dolomites in the Swan Hills Rosevear and Simonette fields (Figure 6.13; Kaufman et al., 1990; Duggan, 2004). Snipe Lake saddle dolomites have lighter $\delta^{18}O$ values compared to earlier marine and meteoric cements. These $\delta^{18}O$ values are also distinctly lower than those for hypothetical Devonian marine dolomites and early formed dolomites from the Middle Devonian Elm Point and Winnipegosis (Ratner Member) formations.

The source and mechanism of dolomitizing fluids for deep burial dolomites in Devonian strata in the WCSB have been extensively discussed throughout the literature. Several possible sources for magnesium enriched fluids have been proposed, including modified seawater (e.g. Viau, 1986), evaporitic brines (e.g. Kaufman et al., 1990; Lonnee and Machel, 2004), deep radiogenic formation (basinal) fluids (e.g. Wong and Oldershaw, 1981) or some combination of more than one of these sources (e.g. Walls and Burrowes, 1990; Amthor et al., 1993; Wendte et al., 1998; Duggan et al., 2001; Duggan, 2004). In the absence of additional trace element, radiogenic isotope and fluid inclusion data this study cannot reasonably speculate on possible sources and mechanisms of dolomitizing fluids affecting the Snipe Lake reef complex.

6.6 Summary

The relative timing and environment of diagenetic features (with a primary focus on cement types) in the Snipe Lake reef complex are interpreted based primarily on detailed petrographic analysis. In particular crystal habit, cement morphology, chemical composition and textural (cross-cutting) relationships are applied to these interpretations. Stable carbon and oxygen isotope data can be used with discretion to support petrographic evidence. In this study, isotope signatures that deviate away from the expected fields for typical Devonian cements can be generally explained by (1) re-setting of geochemical signatures of cements during later diagenesis, and/or (2) contamination by adjacent cements during sampling.

Micrite, isopachous fibrous calcite and pendant radiaxial fibrous calcite cements are interpreted to be marine in origin based primarily on petrographic evidence. Light $\delta^{18}O$ values of isopachous fibrous and pendant radiaxial fibrous calcite cements compared to typical Devonian marine cements are interpreted to reflect primarily re-equilibration during later diagenesis, contamination by later cements (more important in isopachous cements) and possibly inherited contamination from inclusion-poor layers precipitated from meteorically influenced waters. Crystal silt, pendant prismatic calcite, meniscus blocky calcite, syntaxial overgrowth calcite, isopachous prismatic calcite and dissolution are all interpreted to have formed during meteoric diagenesis. $\delta^{18}O$ signatures of pendant prismatic calcite cements support a meteoric origin but may have been affected by isotopic re-equilibration and, to a lesser extent, contamination. Blocky-prismatic calcite, blocky calcite mosaics, dolomite rhombs and saddle dolomites are interpreted to have formed during burial diagenesis. Light $\delta^{18}O$ values of blocky calcite mosaics are interpreted to reflect shallow burial signatures that may have been further depleted during later diagenesis. Light $\delta^{18}O$ signatures of saddle dolomites confirm petrographic interpretations for a late burial origin.

CHAPTER 7 – SUBAERIAL EXPOSURE FEATURES

7.1 Introduction

Subaerial exposure of carbonate sediments and rocks may produce a zone of alteration below the surface (Esteban and Klappa, 1983). Due to the interaction of intrinsic and extrinsic controls a range of diagenetic features can develop. Subaerial exposure surfaces have been identified at the P4 and R0.5 megacycle contacts in the Snipe Lake reef complex (refer to section 5.5). A variety of pedogenic features are recognized below these surfaces and will be discussed in the following sections.

7.2 Rhizoliths

7.2.1 Description

Rhizoliths are recognized below the P4 and R0.5 exposure surfaces (Figures 7.1 and 7.2). The term rhizoliths is defined as "organosedimentary structures resulting in the preservation of roots of higher plants, or remains thereof, in mineral matter" (Klappa, 1980, p. 613). Rhizoliths recognized from slabbed core and thin-section examination, in this study are tubular to cylindrical in shape and are vertically to horizontally oriented. Vertical rhizoliths are less abundant and range from 0.5 to 1.5 cm long and very rarely up to 11 cm long. Downward branching and tapering are commonly observed in these rhizoliths. Subhorizontal to horizontal forms are generally smaller and isolated ranging from 0.6 to 3.2 mm in length. Original root materials or organic matter are not preserved in any of the rhizoliths and the tubules are filled by internal sediment or cements of isopachous blocky-prismatic calcite and blocky

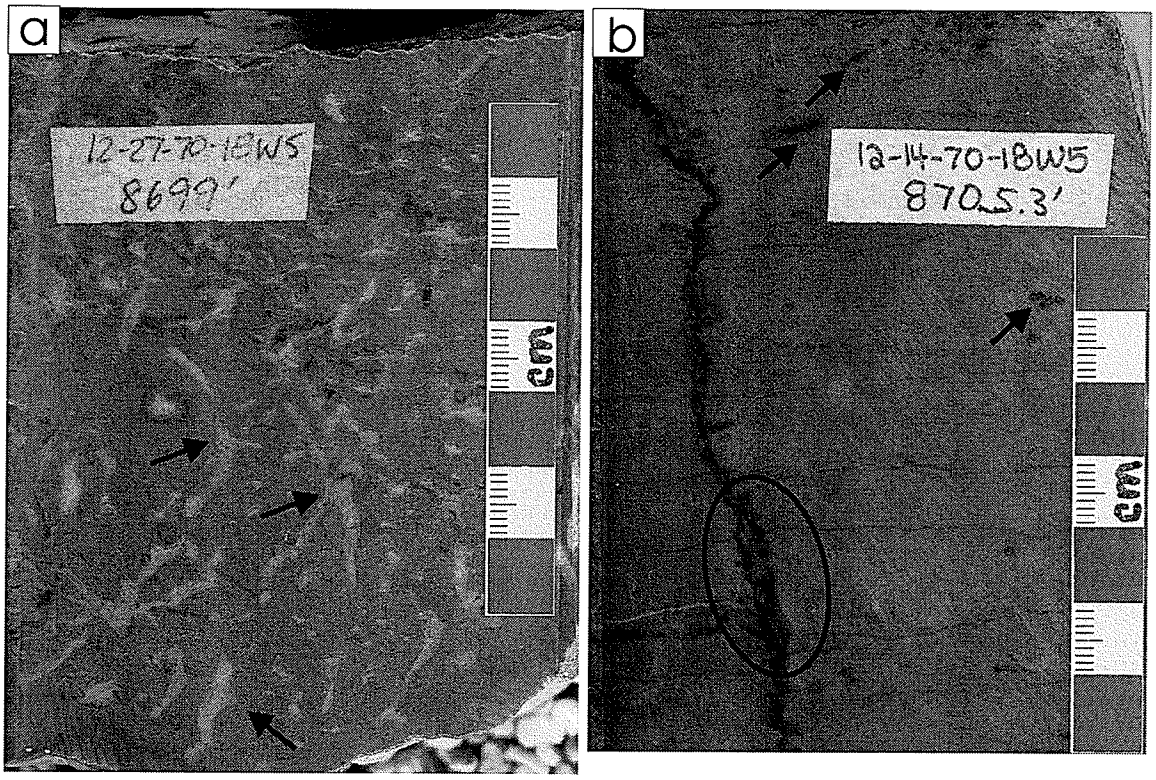


Figure 7.1 Core photographs of rhizoliths. a) Abundant vertical to sub-vertical rhizoliths (arrows) in a light brown peloid packstone. Rhizoliths are occluded by geopetal green shale and late saddle dolomite cements. Downward branching and tapering of rootlets are common, 12-27-70-18W5, 2651.5 m (8699'). b) Vertically extensive rhizolith (tubule structure on the left) with dark brown micritic cutans developed in brown peloid packstone. Branching of rootlets can be seen (circled area) and rare small sub-horizontal rhizoliths are scattered throughout (arrows), 12-14-70-18W5, 2653.4 m (8705.3')

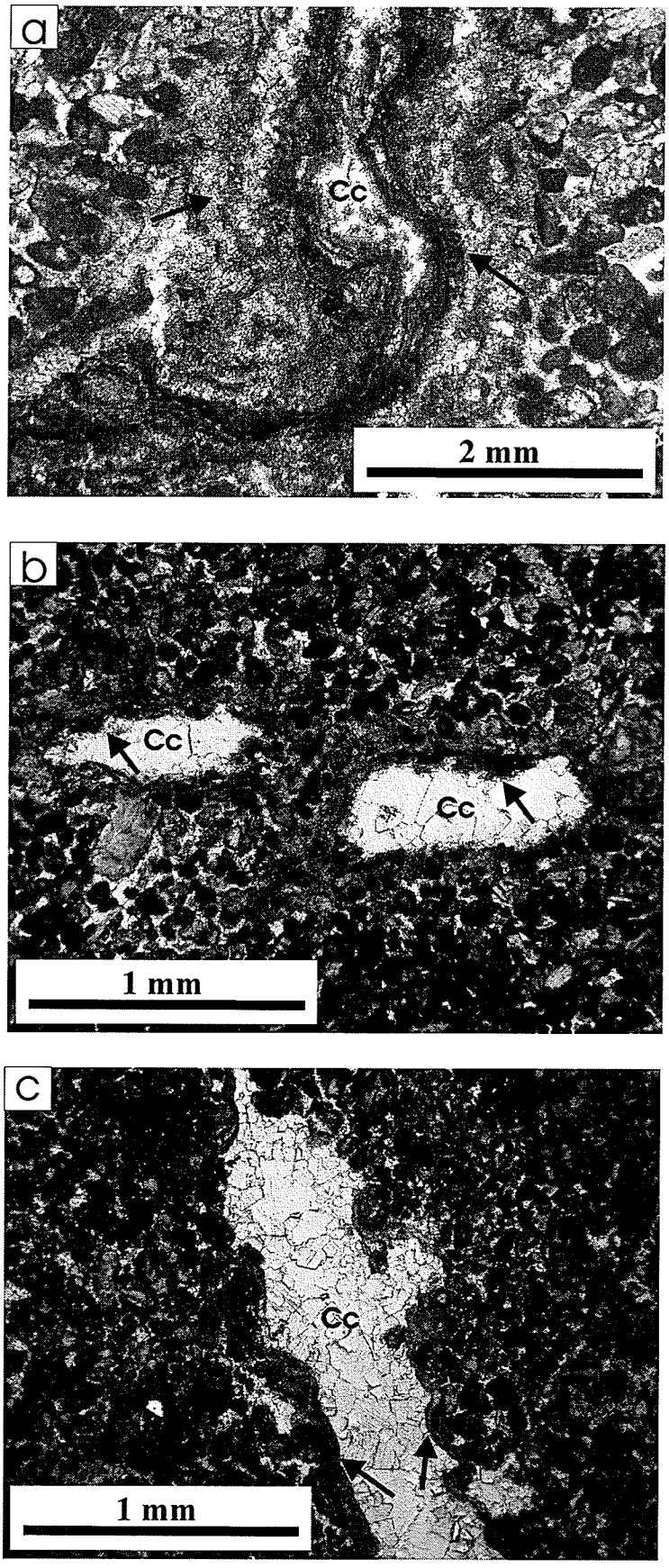


Figure 7.2
Photomicrographs of rhizoliths. a) Rhizolith with downward tapering tubule. Thick, light to dark brown micritic laminae (cutan) are developed around the rhizolith (arrows). Root cast is filled by later blocky calcite mosaic cements (Cc), 12-14-70-18W5, 2653.4 m (8705.3'). b) Small horizontal rhizoliths with thin brown, micritic cutans. Root casts are occluded by isopachous prismatic calcite cements (arrows) and late blocky calcite mosaics (Cc), 12-14-70-18W5, 2653.4 m (8705.3'). c) Sub-vertical rhizolith with weakly developed micritic cutan (arrows). Root tubule is occluded by late blocky calcite mosaics (Cc), 10-22-70-18W5, 2648.8 m (8690.3').

calcite mosaics. Some authors refer to these types of structures as root casts or root traces (e.g. Klappa, 1980; Esteban and Klappa, 1983; Ettensohn et al., 1988; Retallack, 1988; 2001). Many rhizoliths exhibit weakly concentric coatings or laminations of light to dark brown micrite ranging from less than 0.1 mm up to 0.5 mm thick. These micritic coatings or cutans are generally referred to as rhizoconcretions (or rhizocretions) by many authors (e.g. Klappa, 1980; Esteban and Klappa, 1980; Retallack, 1988; James and Choquette, 1990b; Goldstein et al., 1991; Wright, 1994; Retallack, 2001).

7.2.2 Interpretation

Rhizoliths are one of the best criteria for recognizing paleosols (e.g. Klappa, 1980; Esteban and Klappa, 1983; Ettensohn et al., 1988; Retallack, 1988; 2001; Goldstein et al., 1991; Wright, 1994). They provide evidence that the host rocks or sediments were subaerially exposed and inhabited by plants and therefore by definition are considered a soil (Retallack et al., 1984; Retallack, 1988; 2001). Cutans developed around rhizoliths, such as the micritic ones found in this study, were formed by local conditions around the roots (rhizospheres) that promoted the precipitation of mineral matter around roots (rhizoconcretions) and the development of discoloration halos (drab halos) (e.g. Retallack, 1988; 2001; Wright, 1994). These features helped to identify and accentuated poorly preserved roots in some locations. In the absence of plant matter, rhizoconcretions or drab halos, roots are distinguished from animal burrows based on their tubular, downward branching and tapering morphology. Cross-cutting relationships observed in this study indicate that the development of rhizoliths must predate the precipitation of isopachous blocky-prismatic calcite cements that are interpreted to be of

meteoric phreatic origin (refer to section 6.4.2).

The Late Devonian landscape was characterized by early vascular plants including the zosterophyllophytes and possibly trimerophytes (Gensel and Andrews, 1984; Banks, 1984; Taylor and Taylor, 1993). Devonian plants were primitive with relatively simple branching and may have a single thick root (or tap root) (e.g. Gensel and Andrews, 1984; Retallack, 2001). In other Devonian studies in the WCSB, rhizoliths were not noted (e.g. Fu et al., 2004b) or were generally recognized as small features with simple branching (e.g. Williams and Krause, 2000; Chow and Wendte, 2004). These rhizoliths do not show a complex and dense network of roots as have been described in younger paleosols (e.g. Klappa, 1980; Alonso-Zarza, 1999). However, larger (2-3 m) and more complex land plants have been described in some Lower to Middle Devonian successions that were capable of deep rooting up to 1 m (e.g. Elick et al., 1998).

7.3 Pendant Cements in Dissolution Vugs

Several types of pendant cements have been previously described in this study, including radiaxial fibrous calcite in dissolution vugs (refer to section 6.3.3) and prismatic calcite (refer to section 6.3.5) which provide important evidence for subaerial exposure.

Pendant radiaxial fibrous calcite cements in dissolution vugs are interpreted to be marine in origin (refer to section 6.4.3). The dissolution vugs are products of meteoric dissolution during subaerial exposure (refer to section 6.4.2) and the pendant cements precipitated as vugs were partially filled by seawater in the marine vadose zone when

relative sea level rose during the subsequent transgression. Pendant prismatic calcite cements are interpreted to have precipitated in the meteoric vadose zone and provide strong evidence for subaerial exposure (refer to section 6.4.2).

7.4 Green Shales

7.4.1 Description

Green shales are composed of clay, silt and dolomicrite, and occur below the P4 and R0.5 subaerial exposure surfaces. They include (1) massive green shale beds, (2) mottled green shale beds and (3) green shales filling dissolution vugs and cracks.

Massive Green Shale Beds

Massive green shales beds are commonly developed directly below the P4 and R0.5 subaerial exposure surfaces (Figures 5.5 and 5.8). Angular green shale lithoclasts often occur in the overlying carbonate rocks. Green shale beds range from 1.5 to 30 cm thick and are gradational with the underlying host rock. They are generally massive with irregular concentrations or halos of opaque inclusions (organic matter and pyrite) and are less commonly finely laminated (Figures 7.3a and 7.4c). Green shale beds are dolomitized to varying degrees and may be composed entirely of very finely crystalline dolomite (dolomicrite) to variable amounts of disseminated, euhedral dolomite rhombs (16-80 μm) in an argillaceous matrix (Figure 7.4a, b). Dolomite rhombs generally are non-ferroan but may show zoning under cathodoluminescence and epi-fluorescence. Dolomite rhombs have dull luminescent cores and brightly luminescent rims.

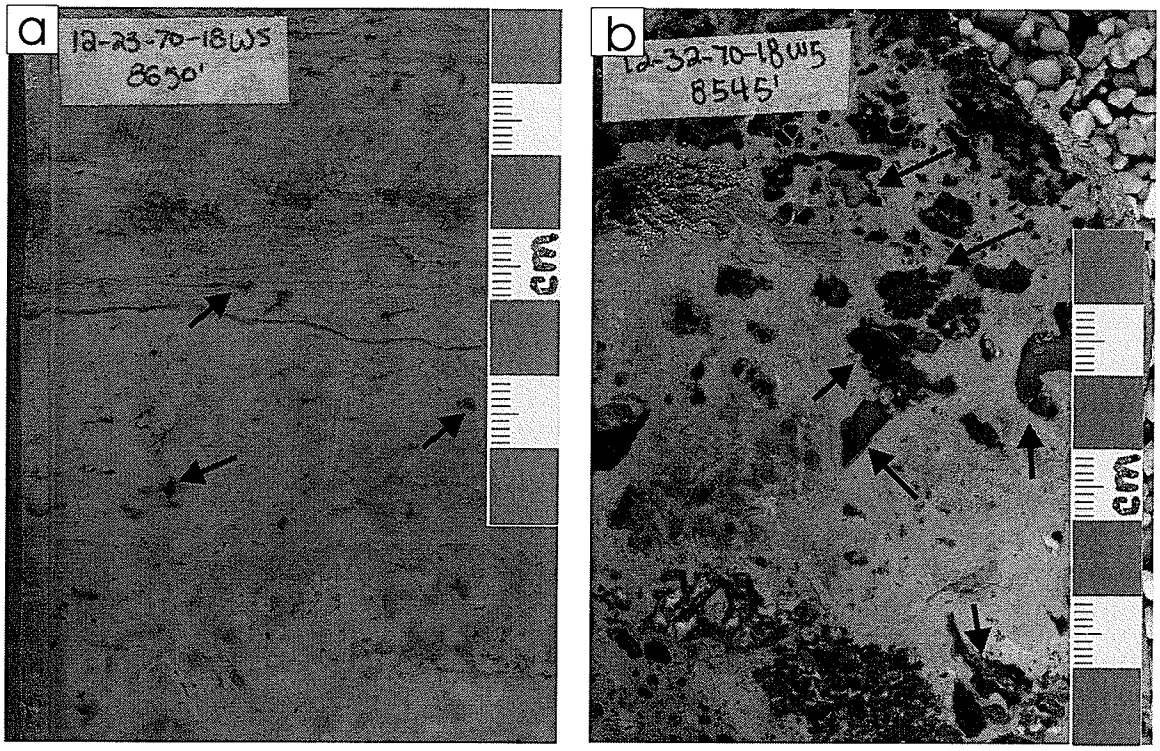
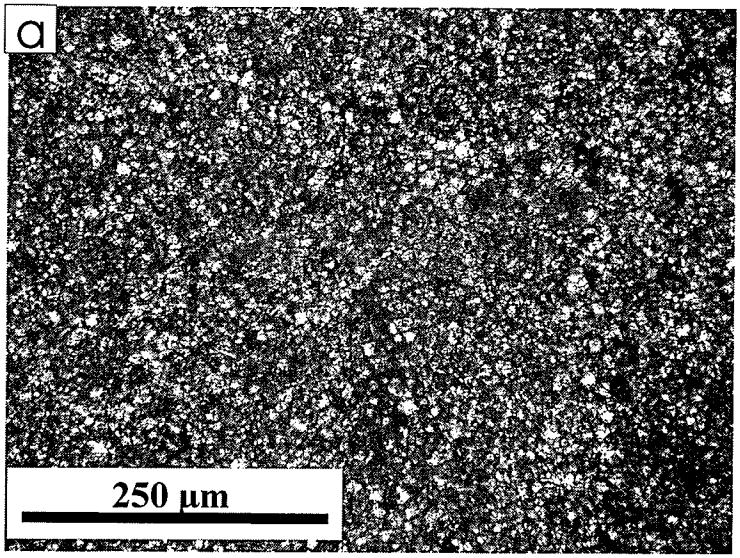
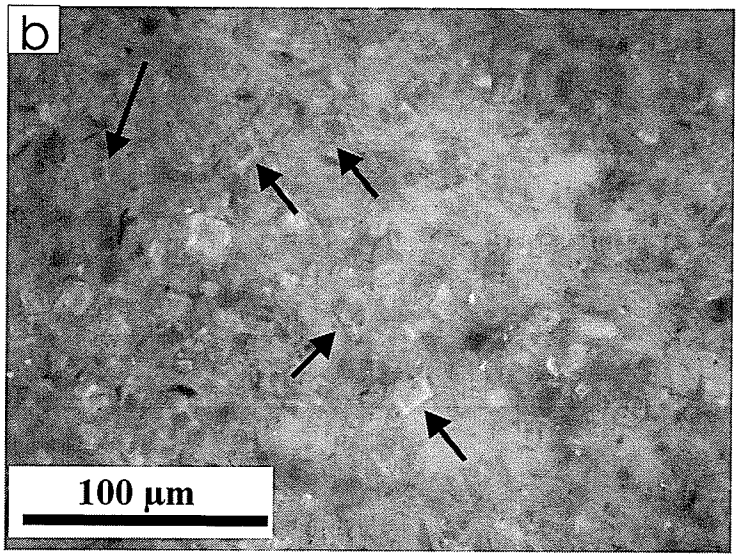


Figure 7.3 Core photographs of green shale beds. a) Massive green shale bed with irregular concentrations of organic matter and pyrite (arrows), 12-23-70-18W5, 2636.5 m (8650'). b) Mottled green shale bed with abundant calcite and broken pendant cement lithoclasts (arrows), 12-32-70-18W5, 2604.5 m (8545').





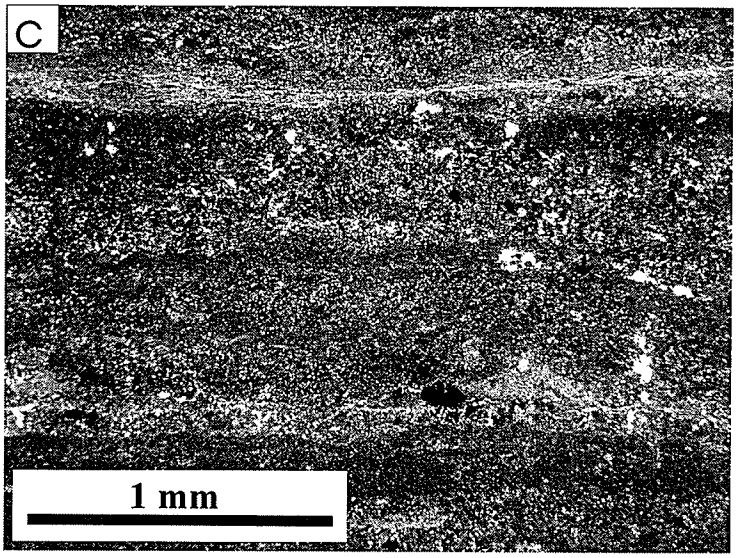


Figure 7.4
Photomicrographs of massive green shale beds. a) Green shale composed of very finely crystalline, non-ferroan dolomite rhombs (dolomicrite), 12-23-70-18W5, 2636.5 m (8650'). b) Very finely crystalline, euhedral dolomite rhombs in an argillaceous (illite-dominated) matrix under epi-fluorescence (violet light). Some euhedral dolomite rhombs show zoning (arrows), 12-14-70-18W5, 2654.4 m (8708.5') c) Weakly laminated green shale. Small calcite lithoclasts (pink) and black opaque inclusions are common throughout, 10-27-70-18W5, 2643.2 m (8672').

Mottled Green Shale Beds

Mottled green shale beds are typically composed entirely of argillaceous dolomicrite (Figure 7.3b), range from 15 to 49 cm thick and may be gradational with underlying massive green shale beds. Mottled green shales have desiccation cracks or joint patterns that are occluded by blocky calcite mosaics, dolomite rhombs and saddle dolomite cements, which give the shale a mottled to nodular texture. These green shale beds are closely associated with fitted-fabric lithoclasts, glaebules and peds (discussed more in sections 7.6, 7.7 and 7.8).

Green Shale in Cracks and Dissolution Vugs

The third variety of green shales fills cracks, dissolution vugs and interparticle pores (Figure 7.5). They range from yellow-green to dark brown and may contain abundant opaque inclusions and in lesser abundance angular quartz silt grains (16-64 μm). Green shales filling thin (0.06 to 4 mm thick) cracks around grains are the most common and have stylolitic upper and lower margins. Geopetal green shales are also often observed in dissolution vugs and interparticle pores. These green shales are commonly dolomitic and include ferroan dolomite rhombs (0.1 to 0.8 mm size) as described in section 6.3.11 (Figures 6.10c and 7.5b). In some samples, green shales may be weakly laminated with clay particles aligned parallel to the surfaces of grains and cracks. Angular calcite lithoclasts with fitted-fabric textures (see section 7.6) are abundant within these green shales.

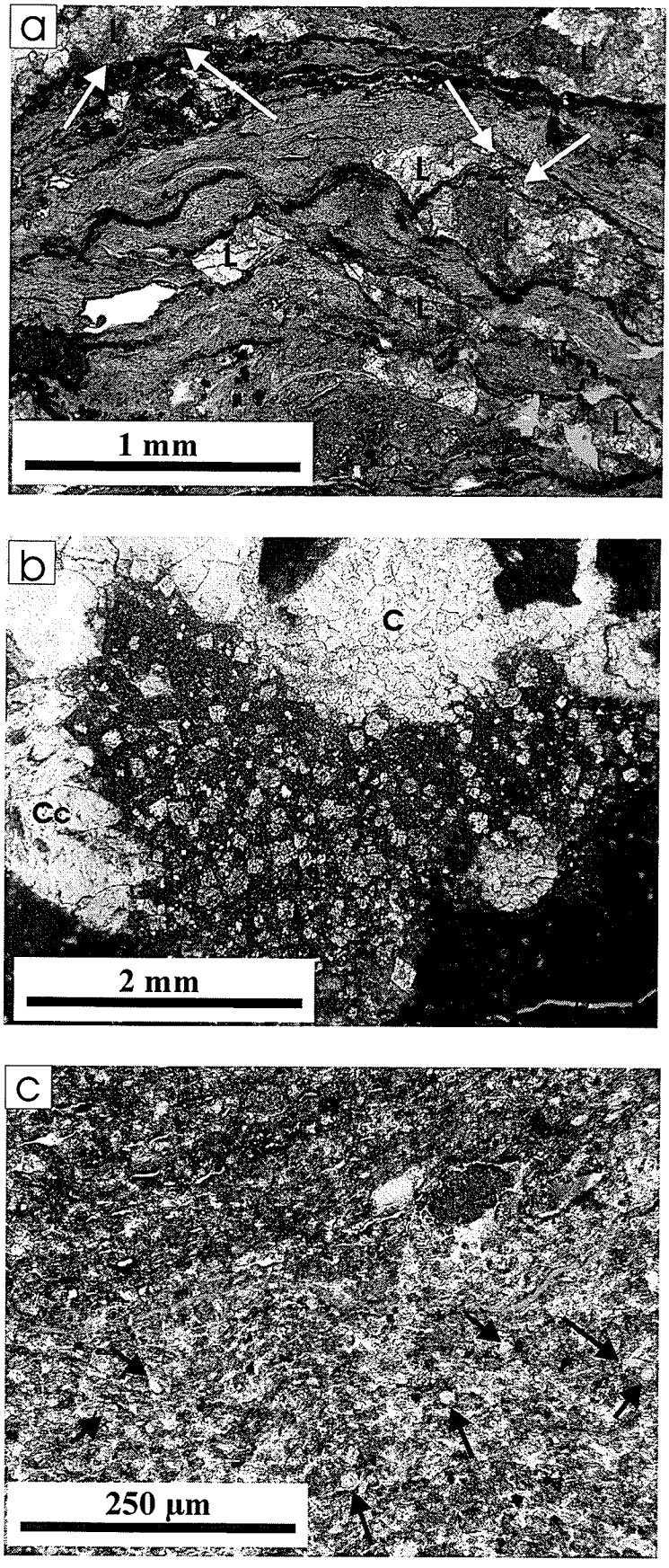


Figure 7.5 Photomicrographs of green shale filling cracks and dissolution vugs. a) Green shale filling cracks around angular calcite lithoclasts (L). Lithoclasts are derived from the host rock and show fitted-fabric textures (arrows). Microfractures (shown by blue epoxy) are artifacts of sample preparation and do not represent true porosity, 04-26-70-18W5, 2636.1 m (8648.7'). b) Geopetal green shale in a dissolution vug. Green shale has been partially replaced by ferroan dolomite rhombs. Remaining pore space is occluded by blocky calcite cement (C) and late blocky calcite mosaics (Cc), 10-21-70-18W5, 2673 m (8769.7'). c) Green shale showing general parallel alignment of clay particles and angular silt-sized quartz grains (arrows), 02-04-71-18W5, 2603.3 m (8641').

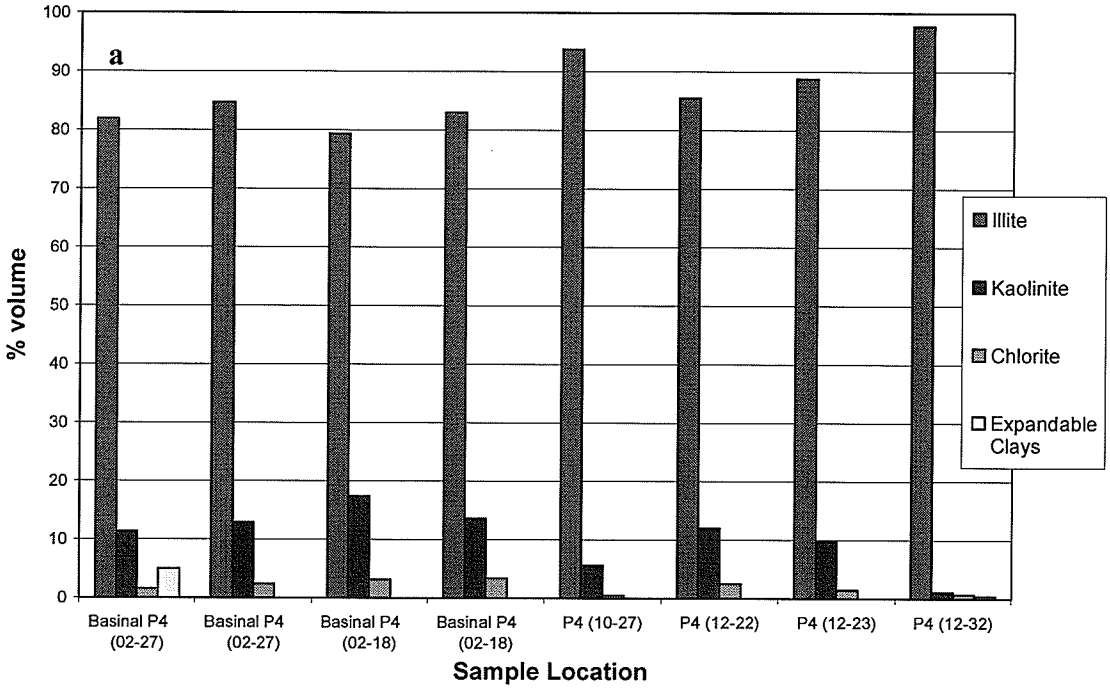
7.4.2 Mineralogy

Bulk x-ray diffraction analysis of green shales identified quartz, dolomite, muscovite and minor amounts of other micas (Appendix F.3). These results are consistent with the work of Murray (1966) on the Judy Creek reef complex and Havard (1974) on the Snipe Lake reef complex. Clay mineralogy analysis further identified illite with minor amounts of kaolinite and chlorite (Figure 7.6). Basinal equivalents of P4 and R0.5 green shales were also analyzed for mineralogy. Comparison reveals that R0.5 and P4 green shales are mineralogically distinct from their basinal equivalents in terms of clay mineralogy. R0.5, P4 and basinal green shales are all predominantly composed of illite, but basinal equivalents tend to have a greater kaolinite component (Figure 7.6). P4 green shales have average values of 7.1% kaolinite, whereas P4 basinal samples average 13.8% kaolinite. R0.5 green shales have average values of 4.0% kaolinite and R0.5 basinal samples average 6.5% kaolinite. Mineralogical differences of green shales at the R0.5 exposure surface compared to basinal equivalents are also evident in the Judy Creek reef complex (Chow and Wendte, 2004) (Figure 7.7).

7.4.3 Interpretation

When considered collectively, several observations suggest that green shales in the Snipe Lake reef complex are pedogenic in origin. These observations are summarized below:

(1) Massive green shale beds and mottled green shale beds occur directly below exposure surfaces or in the uppermost portions of exposure profiles at the P4 and R0.5 megacycle contacts and are gradational with underlying host carbonate



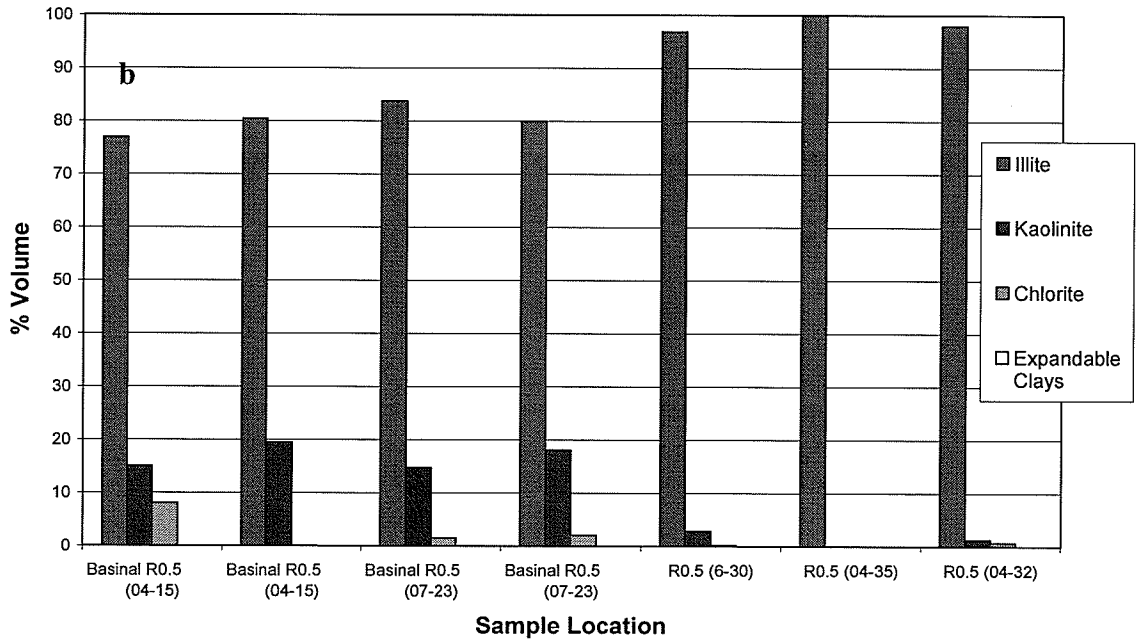


Figure 7.6 Results of clay mineralogy analyses of green shales and basinal equivalents in the Snipe Lake reef complex showing the relative proportions of illite, kaolinite, chlorite and expandable clays. a) P4 green shales and basinal equivalents. b) R0.5 green shales and basinal equivalents. Sample identification and data can be found in Tables F.3 and F.4.

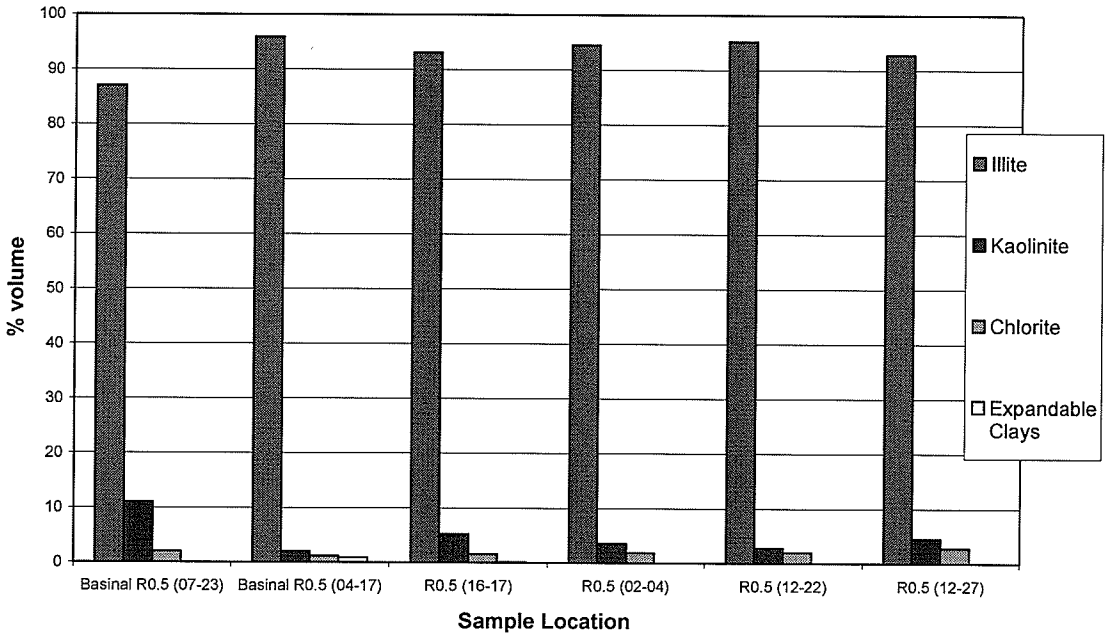


Figure 7.7 Results of clay mineralogy analyses of R0.5 green shales and basinal equivalents in the Judy Creek reef complex showing the relative proportions of illite, kaolinite, chlorite and expandable clays (data from Chow and Wendte, 2004).

rocks. Angular green lithoclasts are present in the overlying carbonate rocks indicating that the exposure surfaces are erosional.

(2) Green shales occur as geopetal structures in dissolution vugs. This suggests that deposition of green shales postdates the development of dissolution vugs in the subaerial environment (refer to section 6.4.2 for discussion of the timing of vugs).

(3) Cracks are developed in the green shales. These features are interpreted to be desiccation cracks resulting from the alternating shrinkage and expansion (during periods of drying and wetting in the subaerial environment) of clay material within the soil matrix (cf. Esteban and Klappa, 1983; Retallack, 1988; Goldstein, 1991; Retallack, 2001; Fu et al., 2004b).

(4) Clay particles are aligned parallel to the surfaces of cracks and grains. These are interpreted to be illuviation fabrics and provide evidence for infiltration of soil 'plasma' (soluble calcium carbonate and clay particles in meteoric vadose waters) from higher horizons (cf. Ettensohn et al., 1988; Milnes, 1992; Williams and Krause, 1998; Retallack, 2001).

(5) Previous studies of the Snipe Lake and Judy Creek reef complexes suggested that green shales were deposited during storm events and sourced from basinal shales (Wendte, 1992c; Wendte and Muir, 1995). However, mineralogical differences between green shales at the R0.5 and P4 exposure surfaces and their basinal equivalents found in this study (refer to section 7.4.2) exclude a basinal storm-derived origin. Therefore, the clays and quartz silt are postulated to be aeolian in origin, supporting subaerial deposition of these green shales (quartz silt discussed more in section 9.6). Green shales identified in other Swan Hills reef complexes

by early studies interpreted them to be products of subaerial diagenesis (e.g. Havard, 1974; Fischbuch, 1968). The most recent study of the Judy Creek reef complex (Chow and Wendte, 2004) interpreted green shales to be pedogenic in origin.

Dolomite in green shales is interpreted to be primarily pedogenic in origin. Petrographic evidence, specifically the very fine crystal size of dolomite crystals is suggestive of early replacement dolomites (discussed in section 7.9.2; e.g. Moore, 2001). In addition, the close association with other pedogenic features (e.g. rhizoliths, fitted-fabric lithoclasts, peds) and textural relationships with early cements (pendant radiaxial fibrous calcite and pendant prismatic calcite) also support a meteoric origin.

Clay-rich horizons of illite and smectite have also been reported to develop within and cap paleosols in other studies (e.g. Robinson and Wright, 1987; Blodgett, 1988; Milnes, 1992; Williams and Krause, 2000; Retallack, 2001).

7.5 Laminar Calcretes

7.5.1 Description

Laminar calcretes are common features associated with the P4 and R0.5 exposure surfaces. They are finely laminated and range in thickness from 0.1 to 6.0 mm (Figures 5.5, 5.8 and 7.8). Laminar calcretes generally have a horizontal orientation, may drape or enclose grains, and have stylolitic upper and lower contacts. Detrital quartz grains (16-24 μm), opaque inclusions, and angular calcite lithoclasts with a fitted fabric (see section

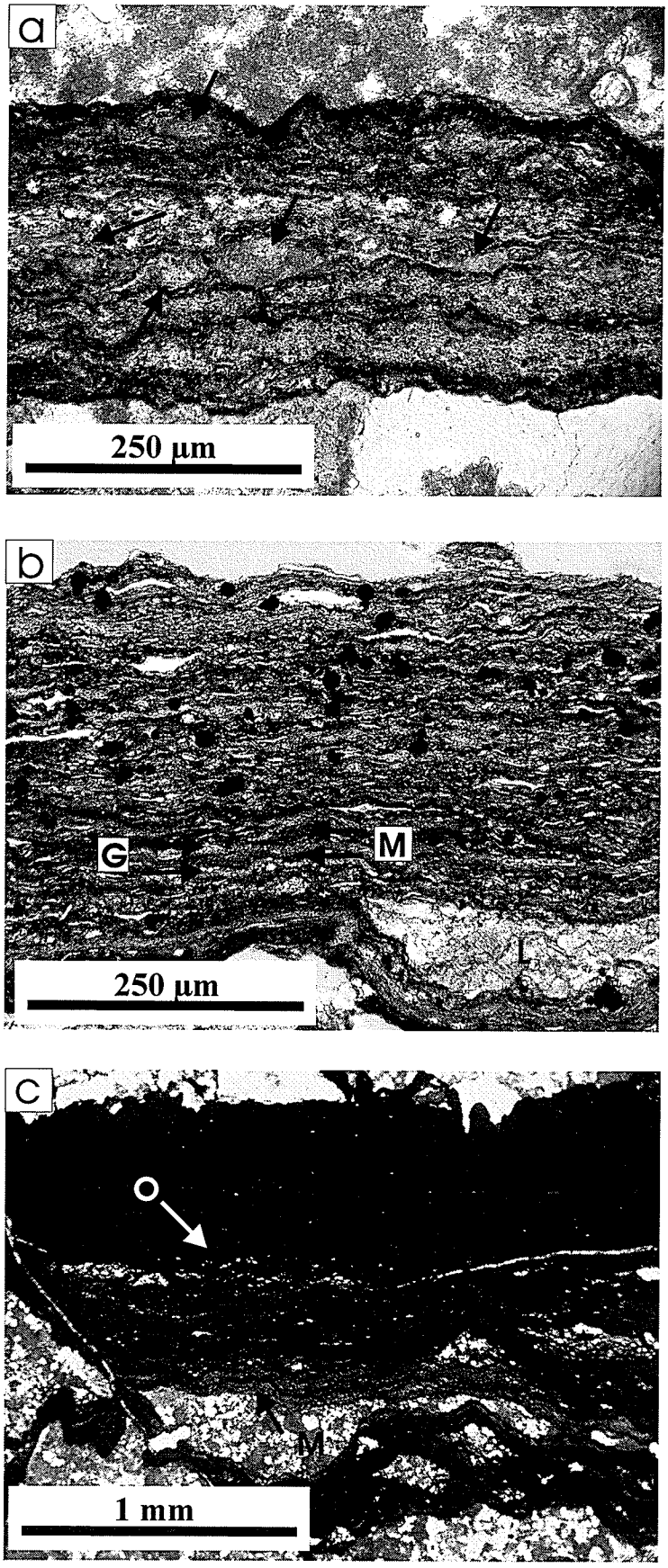


Figure 7.8 Photomicrographs of laminar calcretes. a) Yellow-green, argillaceous laminar calcrete with brown, stylolitic laminae and angular calcite lithoclasts with a fitted-fabric texture (arrows). Upper and lower boundaries of laminar calcrete are stylolitic, 12-27-70-18W5, 2636.5 m (8650'). b) Laminar calcrete with yellow-green argillaceous laminae (G) and brown micritic laminae (M). Individual laminae are stylolitic and drape around calcite lithoclasts (L). Black opaque inclusions are common throughout, 02-03-71-18W5, 2633.3 m (8639.5'). c) Laminar calcrete with alternating dark brown opaque laminae (O) and relatively lighter brown micritic laminae (M), 16-17-69-19W5, 2741.4 m (8994').

7.6) are common. Laminar calcretes may be composed of one or more of the following laminae: (1) yellow to green, argillaceous laminae, (2) brown micritic laminae and (3) dark brown opaque laminae. Opaque laminae often have a distinct banded appearance of alternating light and dark brown layers. Individual laminae (8-40 μm thick) are also typically stylolitic and can be locally wrinkled or contorted.

7.5.2 Interpretation

Laminar calcretes are abundant features in calcrete (or caliche) profiles and paleosols in this study and other studies (e.g. Ettensohn et al., 1988; Wright, 1989; Goldstein et al., 1991; Wright and Tucker, 1991; Milnes, 1992; Wright, 1994; Alonso-Zarza, 2003). They are interpreted to have formed from the accumulation and accretion of calcium carbonate (from weathering of primary minerals) and detrital sediment (supplied by aeolian dust) on indurated substrates on and within the soil (e.g. Brachert and Dullo, 1991; Fedoroff et al., 1994). Alternations in laminae of different composition (yellow-green clays, micritic layers, opaque layers) observed in this study may reflect variations in soil formation processes (cf. Alonso-Zarza, 2003). For example, argillaceous layers with quartz silt may have been deposited during periods of strong winds that favored aeolian erosion and deposition (cf. Fedoroff et al., 1994). Micritic layers may have developed during periods of slow sedimentation (cf. Brachert and Dullo, 1991; Fedoroff et al., 1994). The banded appearance of the opaque laminae may reflect differences in organic staining (cf. Read, 1974; Warren, 1983) or iron content (cf. Read, 1976).

Laminar calcretes may have several origins (summarized by Wright, 1989; 1994). Some are abiogenic, formed by in situ precipitation of calcite from ponded waters that accumulated over an indurated surface (e.g. Harrison and Steinen, 1978; Arakel, 1982; Wright and Wilson, 1987). Others are biogenic, formed by microbial processes (e.g. Klappa, 1979; Krumbein and Giele, 1979) or root mats (e.g. Wright et al., 1988; Alonso-Zarza, 1999). Laminar calcretes in this study do not show any strong evidence for a biogenic origin (e.g. calcified microbial remains, organic laminae, root mats). In contrast, they are similar to abiogenic varieties which are typically thin, finely laminated with dense and micritic microstructures (cf. Ettensohn, 1988; Wright, 1989).

7.6 Fitted-Fabric Lithoclasts

7.6.1 Description

Fitted-fabric calcite lithoclasts are present within green shale beds, mottled green shale beds and laminar calcretes. Lithoclasts are intensely fragmented by an irregular pattern of cracks that are usually filled by green shale (Figures 5.8b and 7.9). This results in the appearance of 'floating' angular lithoclasts that can be fitted back together like pieces of a jigsaw puzzle. Fitted-fabric textures are best observed under epi-fluorescence where the contrast between the green shale matrix and calcite lithoclasts is enhanced. Many authors refer to these types of lithoclasts as breccias or autoclastic breccias (e.g. Ettensohn et al., 1988; Goldstein et al., 1991; Wright, 1994; Fu et al., 2004b). In this study, lithoclasts range from sub-millimeter to several centimeters in size and are composed of skeletal fragments, calcite cements and/or other lithoclasts of the host rock. Cement clasts may include early, pendant radiaxial fibrous calcite cements that

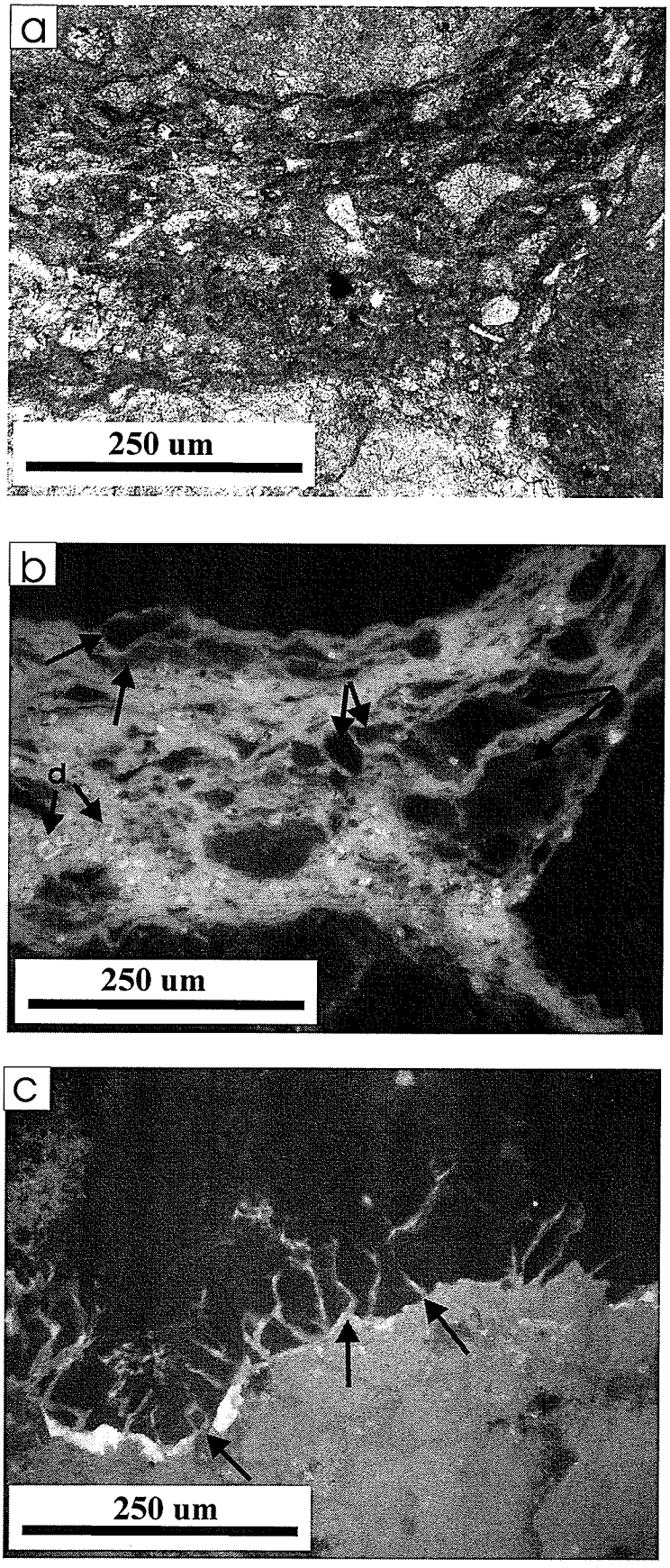


Figure 7.9
Photomicrographs of fitted-fabric lithoclasts. a) Abundant angular calcite lithoclasts (pink) with a fitted-fabric texture within a green shale matrix. Lithoclasts are composed of stromatoporoid and carbonate rock fragments, 12-14-70-18W5, 2653.4 m (8705.5'). b) Photomicrograph of (a) under violet-light epi-fluorescence. Carbonate lithoclasts (dark grains) show a well developed fitted-fabric texture (arrows) in a green shale matrix (light green). Green shale is partially replaced by zoned dolomite rhombs (d). c) Clear, prismatic pendant cement (dark green) and dolomicrite matrix (light green) viewed under violet-light epi-fluorescence. Pendant cement has only been partially brecciated showing cracks along its grain margin (arrows), 10-22-70-18W5, 2662 m (8733.5').

precipitated in primary pores (refer to section 6.3.3) and pendant prismatic calcite (refer to section 6.3.5). In rare cases, lithoclasts have only been partially fractured along grain margins (Figure 7.9c), giving excellent examples of incipient development of fitted-fabric lithoclasts.

7.6.2 Interpretation

Breccias and breccia horizons are common in calcrete or soil profiles (e.g. Ettensohn et al., 1988; Goldstein et al., 1991; Wright, 1994; Fu et al., 2004b). Brecciation can be caused by displacive growth of carbonates, thermal expansion, rhizobrecciation or repetitive wetting and drying cycles (Wright, 1994). Fitted-fabric lithoclasts observed in this study are interpreted to be a result of in situ brecciation caused by the shrinkage and expansion of swelling clays during dry and wet periods (cf. Goldstein et al., 1991; Pelechaty and James, 1991; Wright, 1994). Repetitive cycles resulted in brecciation of the parent material and with extensive brecciation some lithoclasts can no longer be fitted back together. Cross-cutting relationships show that brecciation postdates pendant radiaxial fibrous calcite cements developed in primary pores. Meteoric pendant cements may or may not be brecciated, suggesting that brecciation and formation of fitted-fabric lithoclasts likely occurred more or less contemporaneously with the precipitation of pendant prismatic calcite cements (refer to section 6.4.2) in the meteoric vadose environment.

7.7 Glaebules

7.7.1 Description

Glaebules are local (or 'globular') concentrations of soil plasma (e.g. Ettensohn et al., 1988; Retallack, 1988). A variety of terminology has been used to described these features including mottles (e.g. Wright, 1994; Retallack, 1988; 2001), nodules (e.g. Esteban and Klappa, 1983; Blodgett, 1988; Ettensohn et al., 1988; Retallack, 1988; Wright and Tucker, 1991; Wright, 1994; Williams and Krause, 1998; Retallack, 2001; Alonso-Zarza, 2003), concretions (e.g. Retallack, 1988; 2001), vadoids (e.g. Ettensohn et al., 1988) and pisoids or pisoliths (e.g. Esteban and Klappa, 1983; Bain and Foos, 1991). Glaebules can be massive (nodules, mottles) or concentrically layered (concretions, vadoids, pisoids, pisoliths).

In this study, glaebules are developed within mottled green shale beds below the P4 and R0.5 exposure surfaces. Glaebules are irregularly spheroidal to ellipsoidal in shape and range from less than 1 mm to 4 mm in diameter (Figure 7.10). They are generally massive and composed of calcite and/or dolomite. Some glaebules have calcareous cores of unaltered lithorelicts (fragments of the parent or host rock, e.g. Retallack, 2001) and outer margins composed of dolomicrite, while others are composed entirely of dolomicrite. Many have diffuse margins but they can be differentiated from the surrounding matrix by short, curved cracks developed around the glaebules (circumgranular cracks; e.g. Esteban and Klappa, 1983; Bain and Foos, 1991; Goldstein et al., 1991; Fu et al., 2004b). Another distinctive feature is a network of radiating cracks from the center of the glaebule, referred to as septarian cracks (e.g. Pratt, 2001).

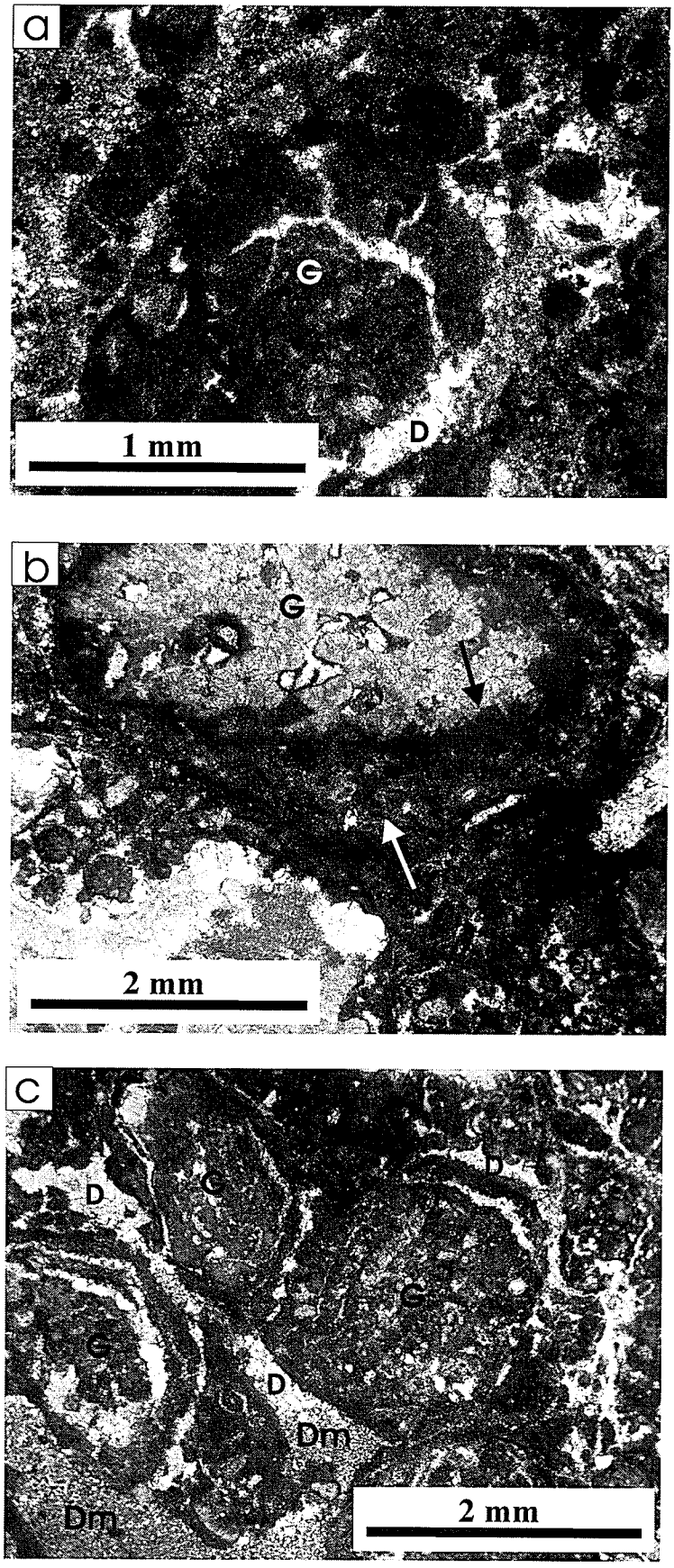


Figure 7.10
Photomicrographs of glaebules. a) Diffuse dolomitic glaebule (G) with well-developed septarian cracks radiating from the center. A circumgranular crack is partially developed along the lower right of the glaebule and occluded by dolomite cement (D), 12-22-70-18W5, 2654.5 m (8709'). b) Dolomitic glaebule (G). Dolomicrite (white arrow) nucleated and precipitated around a calcite lithorelict (stromatoporoid grain). The lithorelict also shows evidence for alteration/dolomitization around its grain margin (black arrow), 12-22-70-18W5, 2654.5 m (8709'). c) Dolomitic glaebules (G) with stromatoporoid lithorelict (pink) and circumgranular cracks. Cracks are filled by dolomite cements (D) and dolomicrite internal sediment (Dm), 10-22-70-18W5, 2662 m (8733.5').

Circumgranular and septarian cracks are occluded by isopachous blocky-prismatic calcite, blocky calcite mosaics and dolomite rhombs.

7.7.2 Interpretation

Glaebules are abundant but are not exclusively developed in soils and thus they are not diagnostic pedogenic features (Retallack, 2001). They can form on the shallow sea floor, in volcanic settings and shallow lakes, around springs and by burial diagenesis. Nevertheless, the development of desiccation cracks, cross-cutting relationships with cement phases and their close association with other pedogenic features (e.g. green shales, rhizoliths, fitted-fabric lithoclasts, laminar calcretes and peds, see Chapter 8) strongly support an interpretation that glaebules in the Snipe Lake reef complex are pedogenic in origin.

Glaebules develop from the concentration and precipitation of secondary carbonate or soil plasma (e.g. Brewer, 1964; Ettensohn et al., 1988; Platt, 1989; Bain and Foos, 1991; Wright, 1994; Retallack, 2001). Several processes have been proposed for the formation of glaebules which are summarized by Wright and Tucker (1991) and Wright (1994). Glaebules observed in this study are interpreted to have been most affected by cementation and replacement of host grains. Secondary calcium carbonate nucleated and precipitated around lithorelicts of the parent rock (cf. Bain and Foos, 1991; Wright, 1994). Some host grains were partially replaced by dolomicrite forming alteration rims, while others were completely replaced. Similar to cracks previously described in green shales, circumgranular and septarian cracks are interpreted to have been produced by

repetitive wetting and drying of the soil material (cf. Esteban and Klappa, 1983; Platt, 1989; James and Choquette, 1990b; Bain and Foos, 1991; Goldstein et al., 1991; Retallack, 2001). Cross-cutting relationships indicate that the development of cracks and glaebules must predate the precipitation of prismatic blocky-prismatic calcite cements, supporting a meteoric vadose origin. Similar to dolomicrite in green shale beds, dolomicrite in glaebules is interpreted to be early replacement dolomite (discussed more in section 7.9.2).

7.8 Peds

7.8.1 Description

Peds or aggregates of soil are locally developed below the P4 and R0.5 exposure surfaces in the Snipe Lake reef complex. These soil structures are rounded, spheroidal to ellipsoidal in shape and range from 0.12 to 0.30 mm in size (Figure 7.11). Peds are composed of dolomicrite and are separated by cracks that have been occluded by blocky calcite mosaics and dolomite (rhombs) cements. They are very similar in appearance to nodular peds from the lower Slade caliches described by Ettensohn et al. (1988) or crumb peds defined by Retallack (1988; 2001).

7.8.2 Interpretation

Peds form by the swelling and shrinking of soil material which results in desiccation cracks and segregated lumps of soil (e.g. Ettensohn et al., 1988; Retallack, 1988; Goldstein, 1991; Retallack, 2001; Muller et al., 2004). Typically, this process produces an interval or horizon of peds that have uniform shapes and sizes. The patchy occurrence

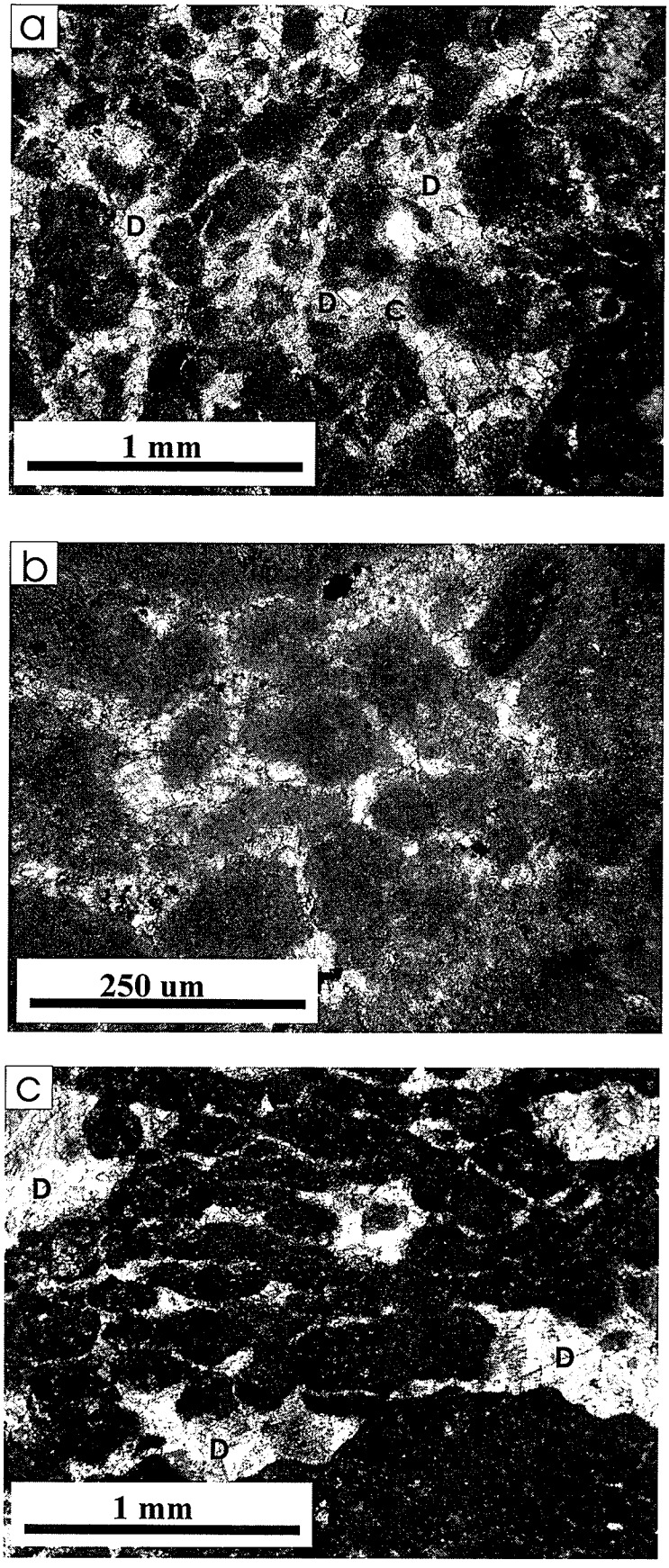


Figure 7.11
Photomicrographs of peds showing different stages of ped development. a) Weakly developed peds (dark green). Peds are irregularly shaped and variable sizes. Cracks separating soil clasts are occluded by blocky calcite (C) and ferroan dolomite rhombs (D), 12-22-70-18W5, 2654.5 m (8709'). b) Moderately developed peds (green-brown). Peds are more regular in shape (rounded and elliptical to spheroidal) and more uniform in size compared to (a). Cracks are filled by blocky calcite (stained purple in photo) and ferroan dolomite cements (stained blue in photo), 10-22-70-18W5, 2662 m (8733.5'). c) Moderately to well developed peds (black). Peds are subrounded and elliptical in shape and relatively uniform in size. Cracks developed between peds are occluded by dolomite rhombs (D), 16-17-69-19W5, 2732 m (8963').

and variable shape of soil clasts observed in this study may represent incipient peds and/or different stages in ped development. This may be due to differences in host sediment (e.g. mineralogy, amount of lime mud); however the similar (nodular) texture and color of the peds in this study suggest that they likely formed from the same parent material (cf. Müller et al., 2004). The degree of cementation may affect the preservation potential of peds (e.g. Müller et al., 2004), but is also not likely to account for the differences since the peds in this study are typically cemented by dolomite rhombs and blocky calcite cements. The degree of pedogenesis most likely accounts for the variability in ped development observed in this study. The more uniform peds (e.g. well 16-17-69-19W5, 2732 m; Figure 7.11c) are likely a result of more extensive pedogenesis relative to irregularly shaped peds (e.g. well 12-22-70-18W5, 2654.5 m (Figure 7.11a). Retallack (1998; 2001) interpreted the smaller, crumb peds to reflect bioturbation of soil and/or fecal pellets of soil organisms in the upper portions of soils.

7.9 Stable Isotope Analysis

Pedogenic features related to the P4 and R0.5 subaerial exposure surfaces in the Snipe Lake reef complex were sampled for microcomponent analysis. Stable carbon and oxygen isotopes results (reported in per mil (‰) VPDB) for sixteen samples collected from pedogenic features are summarized in Table 7.1. Isotope results for crystal silt and pendant prismatic calcite cements are summarized in Table 6.2. All meteoric features (pedogenic and cements) are plotted in Figure 7.12. The fields for typical Middle and Upper Devonian marine cements and hypothetical dolomites precipitated from Late Devonian seawater are shown on the diagram (refer to section 6.5 for references).

Table 7.1 Stable oxygen and carbon isotope data for subaerial exposure features below the R0.5 and P4 megacycle contacts, Snipe Lake reef complex. Precision of results: $\delta^{13}C_{VPDB}$ (0.01 ‰) and $\delta^{18}O_{VPDB}$ (0.03 ‰). "cc" denotes a calcite mineralogy and "dol" denotes a dolomite mineralogy.

Sample Identification	Well Location	Depth Meters (Feet)	Feature	Composition	Stratigraphic Horizon	$\delta^{13}C_{VPDB}$ (‰)	$\delta^{18}O_{VPDB}$ (‰)
02-03-8639.5 - cc	02-03-71-18W5	2633.3 m (8639.5')	Laminar calcrete	Micrite	P4	3.1	-6.8
12-22-8754 - cc	12-22-70-18W5	2668.2 m (8754')	Laminar calcrete	Micrite	P4	1.0	-9.3
16-17-8994 - cc	16-17-69-19W5	2741.4 m (8639.3')	Laminar calcrete	Micrite	above P4	2.4	-10.2
16-17-8940 - cc	16-17-69-19W5	2724.9 m (8940')	Laminar calcrete	Micrite	above R0.5	1.2	-9.0
12-27-8650 - cc	12-27-70-18W5	2636.5 m (8650')	Laminar calcrete	Micrite	R0.5	3.0	-7.7
02-03-8639.5 - cc	02-03-71-18W5	2633.3 m (8639.5')	Rhizolith cutans	Micrite	P4	-0.5	-8.1
10-22-8734.8 - dol	10-22-70-18W5	2662.4 m (8734.8')	Massive green shale bed	Dolomicrite	P4	2.4	-4.6
12-23-8650 - dol	12-23-70-18W5	2636.5 m (8650')	Massive green shale bed	Dolomicrite	P4	2.5	-4.6
16-17-8999.8 - dol	16-17-69-19W5	2743.1 m (8999.8')	Massive green shale bed	Dolomicrite with Calcite Lithoclasts	P4	3.0	-7.8
12-32-8545B - dol	12-32-70-18W5	2604.5 m (8545')	Mottled green shale bed	Dolomicrite	R0.5	3.0	-4.0
10-22-8733.5A - dol	10-22-70-18W5	2662.0 m (8733.5')	Mottled green shale bed	Dolomicrite	P4	-2.0	-4.6
12-14-8708.5 - dol	12-14-70-18W5	2654.4 m (8708.5')	Geopetal green shale	Argillaceous to Dolomicrite	P4	2.8	-3.9
12-27-8699 - dol	12-27-70-18W5	2651.5 m (8699')	Geopetal green shale	Dolomicrite with Calcite Lithoclasts	P4	2.4	-4.7
12-22-8752.2B - dol	12-22-70-18W5	2667.7 m (8752.2')	Geopetal green shale	Argillaceous with Ferroan Dolomite Rhombs	P4	3.4	-9.2
10-22-8733.5B - dol	10-22-70-18W5	2662.0 m (8733.5')	Glaebule	Dolomicrite	P4	-2.5	-5.7
12-32-8576 - cc	12-32-70-18W5	2614 m (8576')	Micrite from subtidal peloid packstone	Micrite	above P4	2.9	-7.9
10-27-8671.9 - cc	10-27-70-18W5	2643.2 m (8671.9')	Micrite from subtidal peloid packstone	Micrite	above P4	3.1	-7.8
12-23-8646.2 - cc	12-23-70-18W5	2635.4 m (8646.2')	Micrite from subtidal peloid wackestone	Micrite	above P4	3.1	-6.9

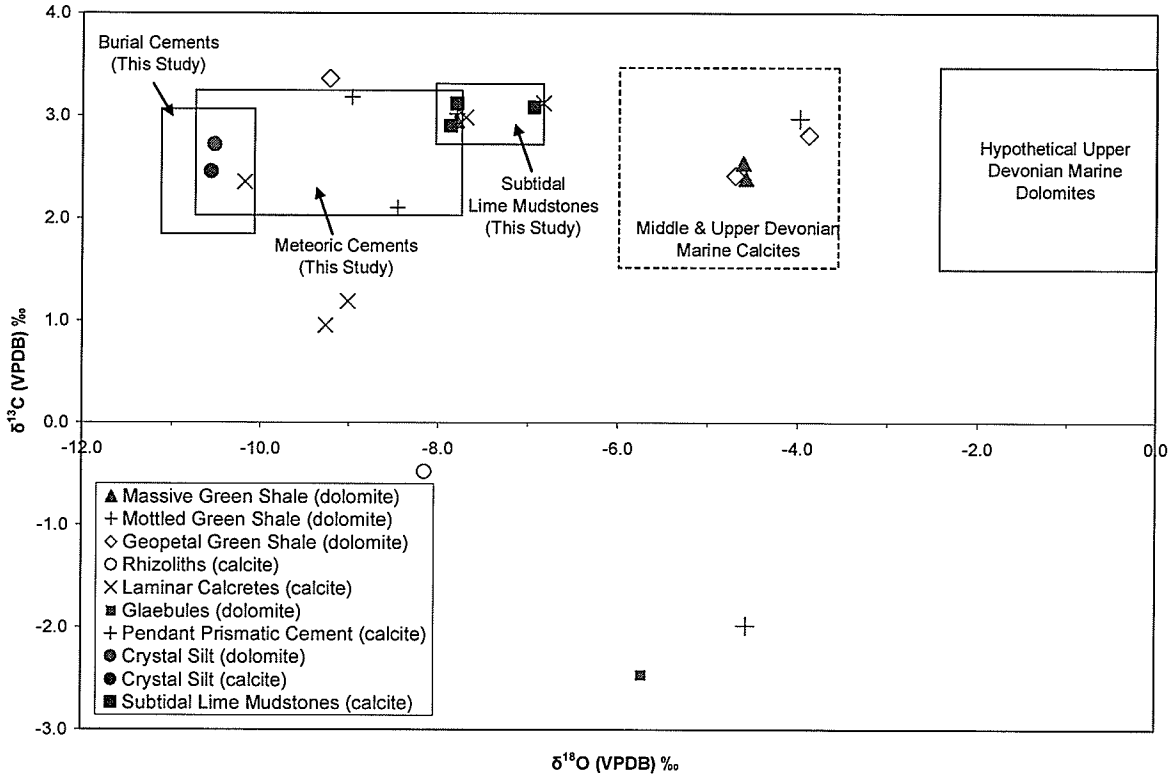


Figure 7.12 Plot of $\delta^{18}O$ and $\delta^{13}C$ values for subaerial exposure features below the P4 and R0.5 exposure surfaces in the Snipe Lake reef complex. Isotopic fields for typical Middle and Upper Devonian marine cements and hypothetical Devonian marine dolomites are shown (see text for sources). Isotopic fields for subtidal lime mudstones (marine signature) and late calcite and dolomite cements (burial signature) from this study are also shown. Calcite components are shown in red and dolomite components are shown in blue.

Samples of subtidal lime mudstones (marine signature) and late cements (burial signature; refer to section 6.5.1) from this study were also analyzed and the results are included for comparison.

7.9.1 Stable Isotope Results

Overall, pedogenic features (excluding cements) in this study have a wide range in $\delta^{18}O$ and $\delta^{13}C$ compositions, ranging from -10.2 to -3.9‰ and -2.5 to +3.4‰, respectively. Green shale (dolomite, all varieties) have a wide range of $\delta^{18}O$ values (-9.2 to -3.9‰) and $\delta^{13}C$ values (-2.0 to +3.4‰). Laminar calcretes (calcite) show the largest range and most negative $\delta^{18}O$ values (-10.2 to -6.3‰) and positive $\delta^{13}C$ values (+1.0 to +3.1‰). A single rhizolith (calcite) sample yielded a $\delta^{18}O$ value of -8.1‰ and $\delta^{13}C$ value of -0.5‰. A single glaebule (dolomite) sample has a $\delta^{18}O$ value of -5.7‰ and shows the most negative $\delta^{13}C$ composition of all the features (-2.5‰).

7.9.2 Stable Isotope Interpretations

Due to the large amount of scatter and variability of results, isotopic data for these pedogenic features appear to be inconclusive. However, after careful consideration of some of the possible reasons for the scatter, some general observations can be made. Firstly, as discussed in Chapter 6, $\delta^{18}O$ isotopic signatures of cement phases are interpreted to have been shifted to lighter values by later diagenesis and thus a similar effect would be expected for other rock components such as pedogenic features. Subtidal mudstones sampled above the exposure surfaces (i.e. unaffected by meteoric diagenesis) also have relatively light $\delta^{18}O$ values compared to Devonian marine cements, providing

further evidence for diagenetic overprinting. Therefore, it would be more useful to compare isotopic values for pedogenic features to end-member fields defined within this study, instead of comparing them to Devonian marine cements compiled from other studies. For this comparison, isotope compositions of subtidal lime mudstones are considered to reflect a "modified" calcite marine signature and late stage cements are interpreted to reflect burial signatures for both calcite and dolomite. However, marine dolomites were not reported in this study, therefore dolomitic pedogenic features are compared to the field for hypothetical Devonian marine dolomites (refer to section 6.5). Secondly, contamination from adjacent cements during sampling likely accounts for some light $\delta^{18}O$ values, particularly for smaller features that were difficult to sample such as laminar calcretes and rhizoliths.

Green Shales and Glaebules

Dolomicrite in most green shale samples has relatively positive $\delta^{13}C$ values between 2.4 to 3.4‰ which are comparable to the field for lime mudstones in this study, typical Middle and Upper Devonian marine calcite cements and dolomites. This suggests either a marine carbon source that has been relatively unaltered by soil-gas CO_2 (cf. Pelechaty and James, 1991) or alternatively has been enriched in ^{13}C by CO_2 degassing (cf. Carpenter and Lohmann, 1989; Goldstein et al., 1991). In contrast, one green shale sample (10-22-8733.5A – dol) and the glaebule sample have the lightest $\delta^{13}C$ compositions in this study. This is most likely a result of soil-gas CO_2 contributions derived from decaying organic matter (cf. Lohmann, 1988; Carpenter and Lohmann, 1989; James and Choquette, 1990b; Morse and Mackenzie, 1990; Goldstein, 1991;

Goldstein et al., 1991).

Dolomicrite in the majority of green shale samples (massive and mottled green shale beds and geopetal shale in dissolution vugs) and a single glaebule sample plot within a $\delta^{18}O$ range from -5.7 to -3.9‰. They have heavier $\delta^{18}O$ compositions relative to other meteoric features in this study (e.g. -9.0 to -7.8‰ for pendant prismatic calcite cements, refer to section 6.5.1) and are lighter relative to hypothetical Upper Devonian marine dolomites (Figure 7.12). Fractionation of several per mil exists between calcite and dolomite that form at surface conditions (e.g. Allan and Wiggins, 1992). As a result, dolomites that precipate from meteoric waters can be ^{18}O-enriched with respect to calcite. Therefore, heavier $\delta^{18}O$ dolomite compositions (with respect to meteoric calcite cements) observed in this study may reflect dolomite precipitation from depleted meteoric waters during subaerial exposure. In addition, preferential loss of ^{16}O through evaporation directly below the exposure surface can also shift isotopic signatures to heavier $\delta^{18}O$ compositions (e.g. Allan and Mathews, 1982; Goldstein, 1991).

Another possibility is that dolomicrite was formed by dolomitization through mixing of fresh water with seawater, where the latter would have supplied the source of Mg^{2+} required for dolomitization (cf. Badiozamani, 1973; Land, 1973; Amthor and Friedman, 1992; Morrow, 1990). Therefore, $\delta^{18}O$ values of dolomicrite samples may represent an intermediate $\delta^{18}O$ composition between meteoric water and seawater (cf. Land, 1973; Allans and Mathews, 1982; Lohmann, 1988; Williams and Krause, 1998). Mixing of meteoric waters and marine waters may have occurred in the mixing zone below the deep

phreatic meteoric zone (James and Choquette, 1990b, covariant trend 'A', Figure 35; Moore, 2001) or during the subsequent transgression as the shoreline migrated landward into brackish water conditions (cf. Wright, 1991).

Most primary or true meteoric dolomites cited in the literature are typically associated with evaporites or other cave sediments (e.g. von de Borch et al., 1975; Gonzalez and Lohmann, 1988). There is no evidence from this study to suggest that dolomicrite in this study formed in either of these settings. On the other hand, petrographic evidence suggests that dolomitic green shales (refer to section 7.4) and dolomitic glaebules (refer to section 7.7) are early diagenetic in origin. Therefore, dolomitic green shales and glaebules in this study are proposed to be the result of early dolomitization by mixed fresh water and seawater.

The anomalously low $\delta^{18}O$ values of two green shale samples (-7.8‰ in sample '16-17-8999.8 – dol' and -9.2‰ in sample '12-22-8752.2B – dol') can be explained by contamination by late replacement ferroan dolomite rhombs (see section 6.3.11) that could not be separated during sampling.

Laminar Calcretes and Rhizoliths

Laminar calcretes have relatively positive $\delta^{13}C$ values. Similar to green shales, this probably reflects either a marine carbon source or CO_2 degassing. The rhizolith sample has a slightly depleted $\delta^{13}C$ value suggesting that the precipitation of micritic cutans may have been affected by oxidized organic matter from the root (cf. Goldstein, 1991).

Laminar calcretes and rhizolith cutans have the most variable and lightest $\delta^{18}O$ signatures of all the pedogenic features in this study. Their compositions plot within the field for subtidal lime mudstones but extend well into the field for burial cements. Light $\delta^{18}O$ values may reflect precipitation from unaltered ^{16}O-enriched meteoric waters that were introduced into the soil system, however this trend is not consistent with most other pedogenic features in this study. In addition, oxygen isotope signatures tend to be relatively consistent in the meteoric environment (e.g. Morse and Mackenzie, 1990; James and Choquette, 1990b; Goldstein, 1991). The most probable explanation for variable and light $\delta^{18}O$ signatures is contamination by calcite lithoclasts and adjacent calcite cements. As described in previous sections, laminar calcretes and micritic cutans are very thin features. Laminar calcretes often have calcite lithoclasts and late burial cements between laminae, while rhizoliths tubules tend to be occluded by late blocky calcite mosaics. Sampling by hand drilling (see section 2.10) would have easily incorporated these components in the samples resulting in more negative $\delta^{18}O$ values.

7.10 Summary

A variety of pedogenic features have been recognized below the P4 and R0.5 subaerial exposure surfaces in the Snipe Lake reef complex. These features provide excellent evidence for subaerial exposure and the development of ancient soil profiles. Isotope signatures can be difficult to interpret due to later diagenetic overprinting and sample contamination, but the following general observations can be made: (1) dolomitic green shales and glaebules are likely the result of early dolomitization from the mixing of meteoric and marine waters, and (2) soil-gas CO_2 contributions appear to be relatively

minimal.

CHAPTER 8 – PALEOSOLS

8.1 Introduction

This chapter describes subaerial exposure features, including cements and pedogenic features (see Chapters 6 and 7), in the context of their occurrence and distribution below the P4 and R0.5 subaerial exposure surfaces in the Snipe Lake reef complex. Ancient soils or paleosols provide excellent evidence for subaerial exposure. They are formed by recrystallization, dissolution and precipitation processes in the meteoric environment that result in the redistribution and reorganization of calcium carbonate (James and Choquette, 1990b; Webb, 1994; Wright, 1994; Moore, 2001).

8.2 Paleosols

Paleosols are recognized below the P4 and R0.5 subaerial exposure surfaces in the Snipe Lake reef complex. They are characterized by a variety of features including green shale beds, desiccation cracks, rhizoliths, laminar calcretes, fitted-fabric lithoclasts, glaebules, peds, marine pendant cements developed in dissolution vugs and meteoric pendant cements. This variety of features reflects a number of extrinsic and intrinsic controls on the development of paleosols (discussed in Chapter 9). The tops of paleosols are often truncated by erosional surfaces and are gradational with underlying carbonate host rocks (cf. Blodgett, 1988; Retallack, 1988; 2001; Fu et al., 2004b). Exposure profiles at each well location are described in detail in Appendix C and their distribution is illustrated in paleosol cross-sections D-D', E-E' and F-F' (Figures 8.1 to 8.4). The thickness of each paleosol profile is calculated from the top of the subaerial exposure surface (P4 or R0.5)

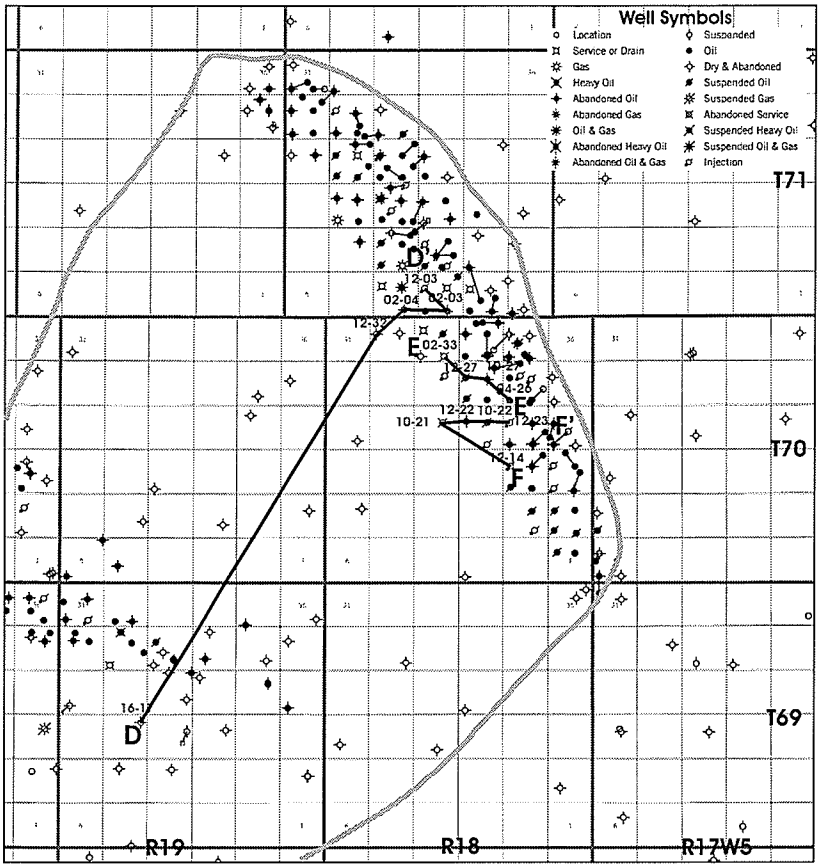


Figure 8.1
Location map and legend for cross-sections D-D', E-E' and F-F'.

LEGEND

- Lithofacies A and B (Peloid Packstones and Robust Branching Cylindrical Stromatoporoid Rudstones)
- Lithofacies C and D (Branching Cylindrical Stromatoporoid Floatstones and Light Tan *Amphipora* Floatstones)
- Lithofacies E (Dark Brown *Amphipora* Rudstones)
- Lithofacies F (Stromatoporoid Floatstones to Rudstones)
- Lithofacies G (Tabular Stromatoporoid Rudstones)
- Lithofacies H (Dark Brown Thin Tabular Stromatoporoid Floatstones)
- Lithofacies I (Skeletal Grainstones)
- Core Not Described

- Unconformity
- Megacycle Contact
- Hardground

Pedogenic Features

- Green Shale Bed
- Green Shale in Cracks and Vugs
- Rhizoliths
- Laminar Calcretes
- Fitted-fabric Lithoclasts
- Glaebules
- Peds
- Marine Pendant Cement in Vugs
- Meteoric Pendant Cements

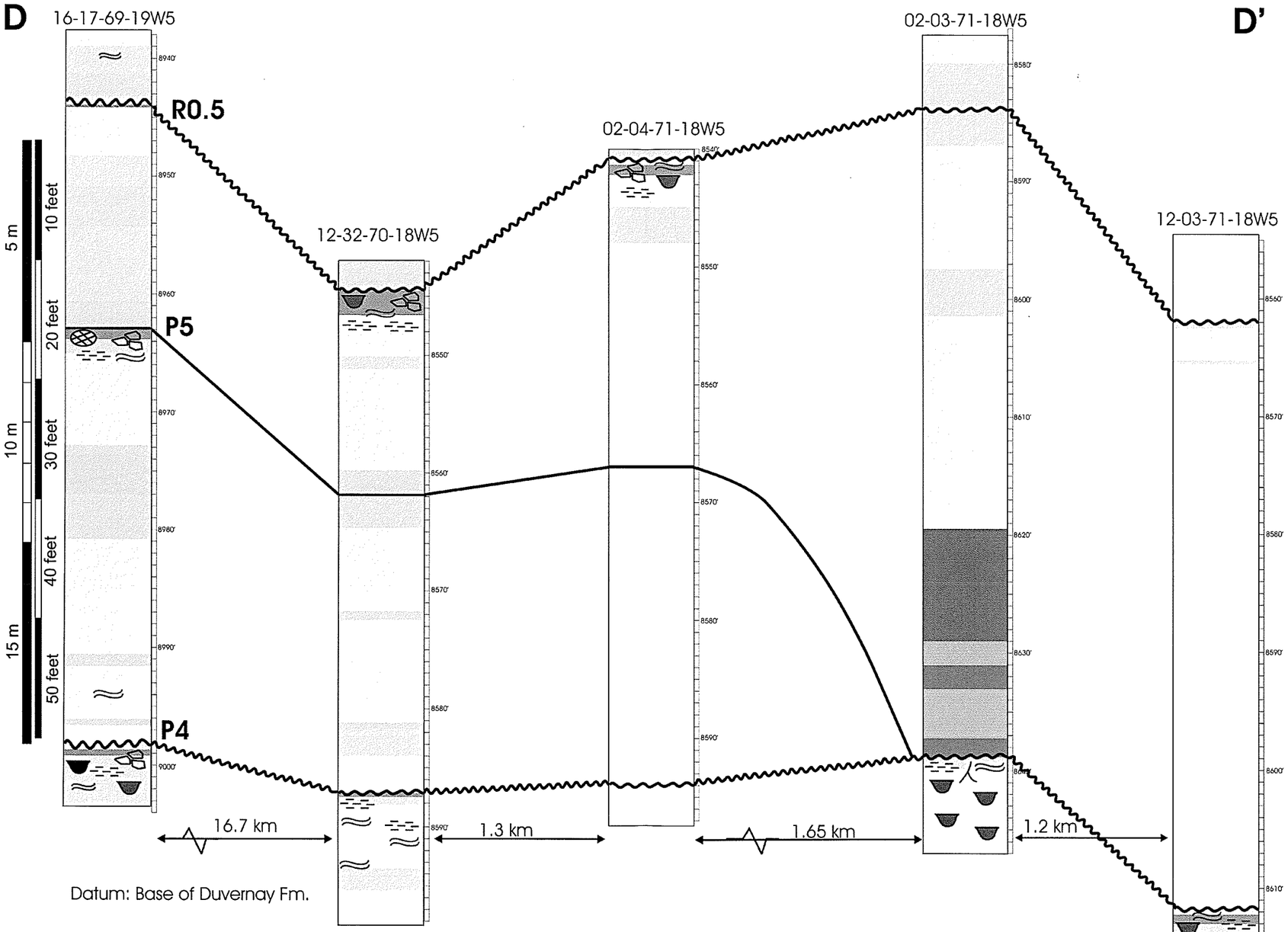


Figure 8.2 Paleosol cross-section from D to D' across the Snipe Lake reef complex, showing the distribution of pedogenic features below the P4 and R0.5 subaerial exposure surfaces. Location map and legend are provided in Figure 8.1.

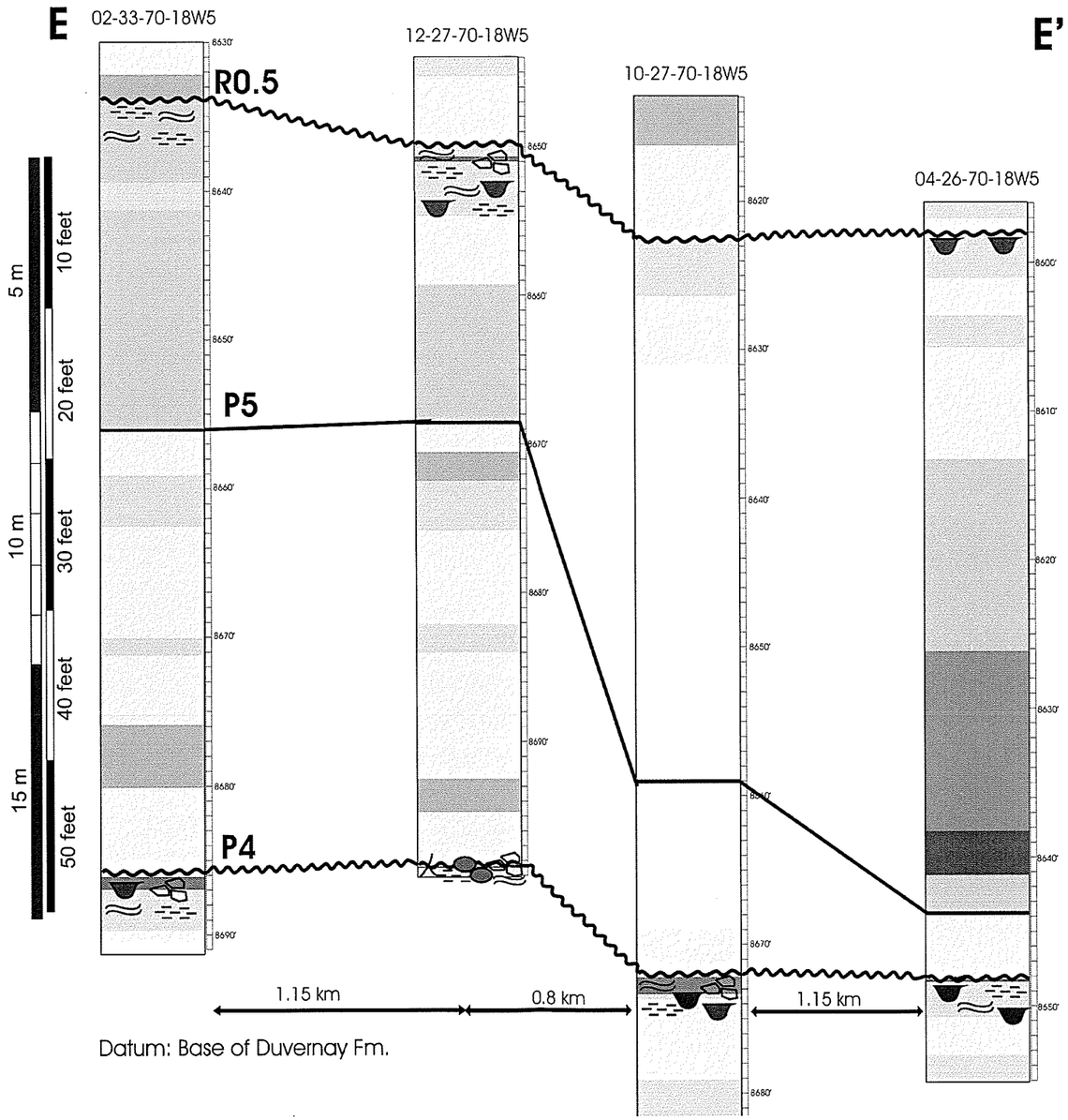


Figure 8.3 Paleosol cross-section from E to E' across the Snipe Lake reef complex, showing the distribution of pedogenic features below the P4 and R0.5 subaerial exposure surfaces. Location map and legend are provided in Figure 8.1.

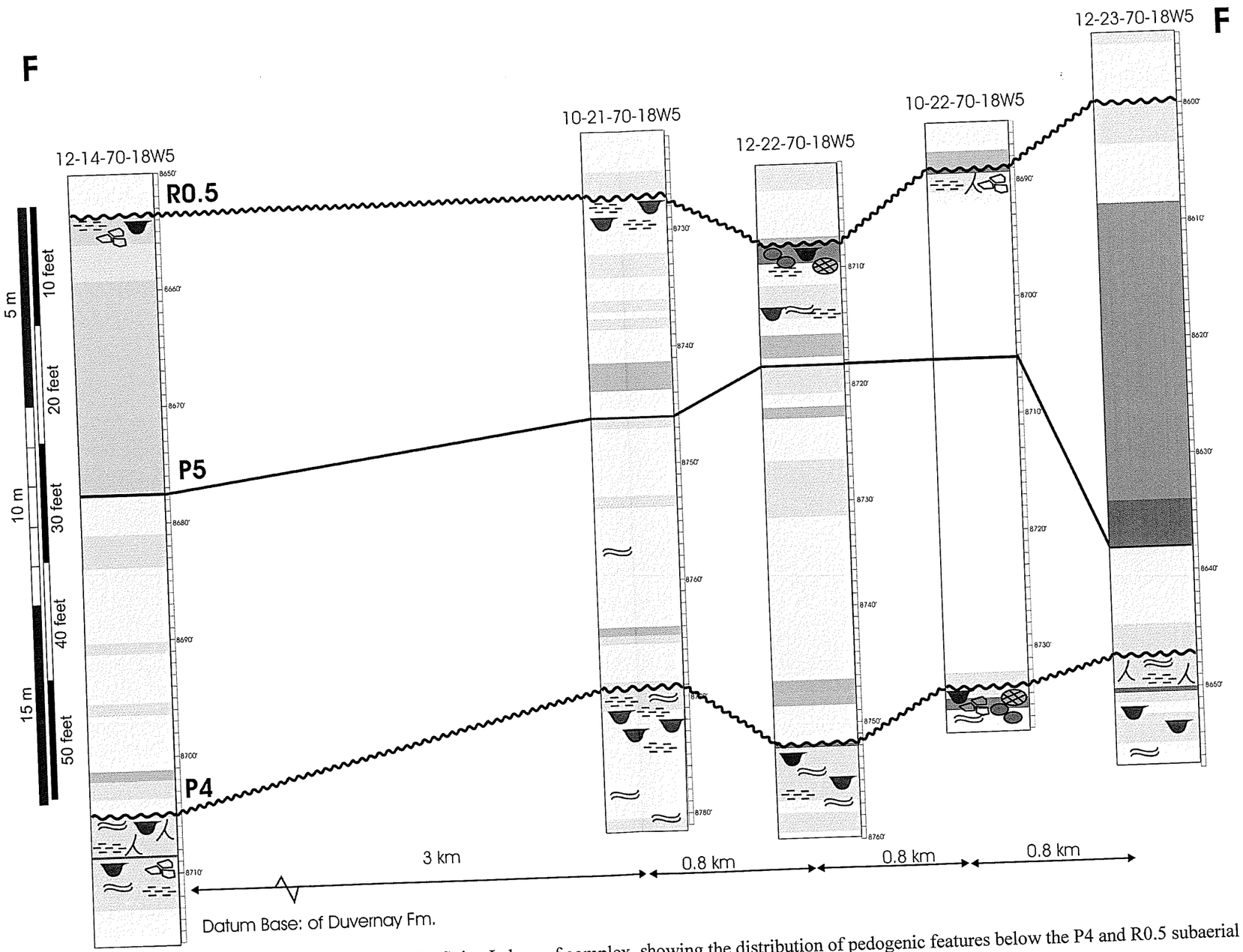


Figure 8.4 Paleosol cross-section from F to F' across the Snipe Lake reef complex, showing the distribution of pedogenic features below the P4 and R0.5 subaerial exposure surfaces. Location map and legend are provided in Figure 8.1.

down to the deepest occurrence of pedogenic features or other evidence for meteoric vadose diagenesis (i.e. marine pendant cements in dissolution vugs and meteoric pendant cements).

8.3 P4 Subaerial Exposure Surface

Paleosols are developed below the P4 megacycle contact in every core examined in this study and are correlative across the P4 contact (Figures 8.2 to 8.4). P4 paleosols range from 0.64 to 2.1 m thick. A variety of features are developed within these paleosols but green shale beds, green shale in dissolution vugs and cracks, laminar calcretes, fitted-fabric lithoclasts and pendant cements are among the most common (Figure 8.5 and Table 8.1). Paleosols are consistently developed within tidal flat lithofacies (lithofacies A) at the top of shallowing-upward lagoonal cycles and features may extend down into open lagoon lithofacies (lithofacies C and D).

8.4 R0.5 Subaerial Exposure Surface

Paleosols are observed below the R0.5 megacycle contact in most cores in this study and are also correlative across the R0.5 contact (Figures 8.2 to 8.4). The R0.5 paleosol is generally thinner than the P4 paleosol, ranging from 0.12 to 1.3 m thick (Figure 8.6). Green shales are less abundant in this interval compared to P4 and typically fill cracks and dissolution vugs (Table 8.2). Laminar calcretes, fitted-fabric lithoclasts and pendant cements are also abundant features. Paleosols are developed in a range of lithofacies including tidal flat (lithofacies A), open lagoon (lithofacies C and D) and reef flat (lithofacies F).

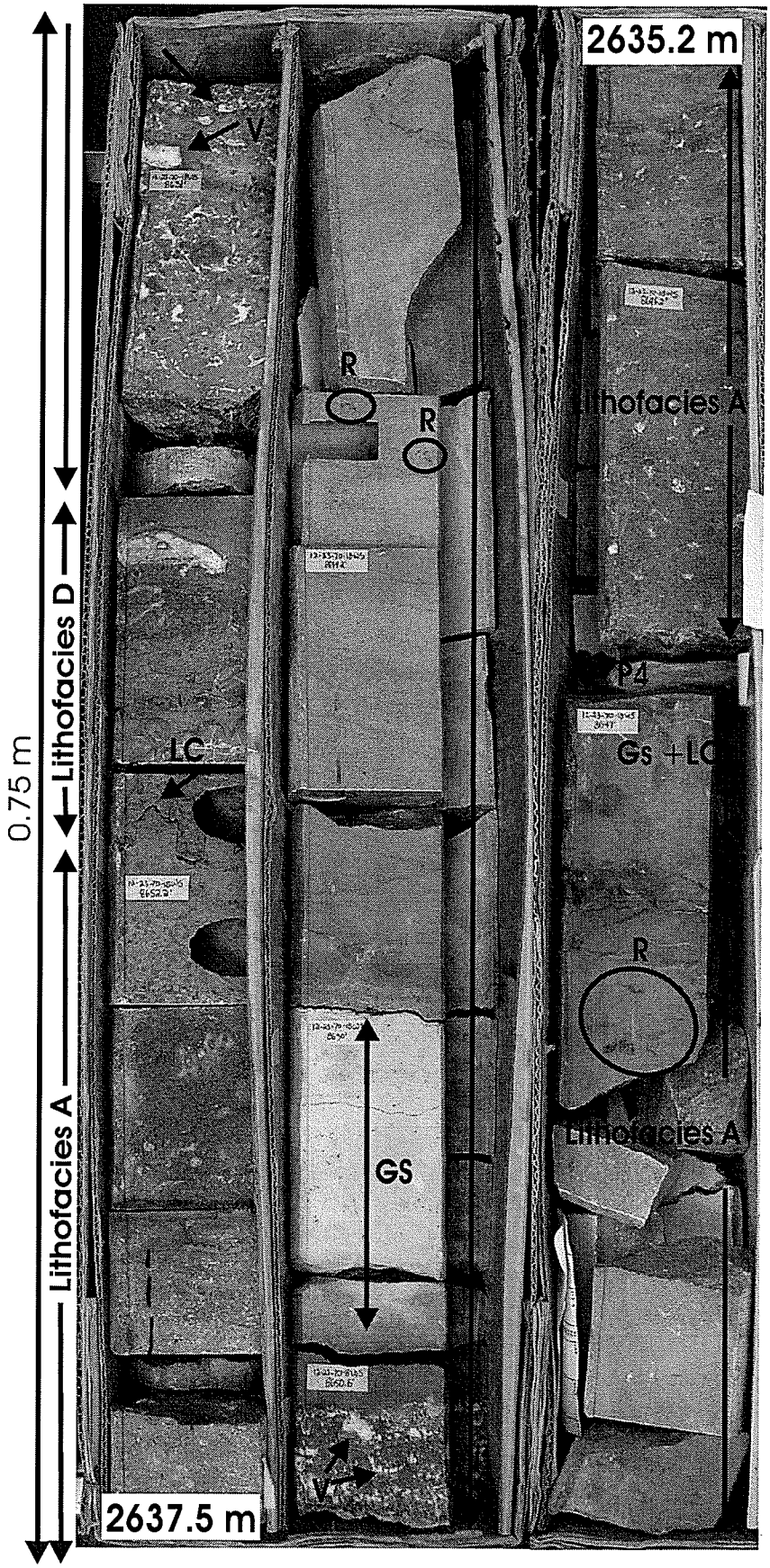


Figure 8.5 Succession of core above and below the P4 subaerial exposure surface in the Snipe Lake reef complex. The P4 exposure surface is developed on peloid packstones to grainstones and overlain by laminated to fenestral peloid grainstone with scattered *Amphipora*. A paleosol is developed below the exposure surface from 2635.61 down to 2637.19 m (8647-8652.2'). A 1.5 cm thick green shale and laminar calcrete (Gs + Lc) occurs directly below the exposure surface. Small, horizontal rhizoliths (R) are scattered in the interval above the green shale (Gs) bed. Dissolution vugs (V) with marine pendant cements and geopetal internal sediment occur below the green shale horizon and decrease in abundance downwards. A stylolitic laminar calcrete (*Lc) marks the base of the paleosol, 12-23-70-18W5, 2635.2-2637.5 m (8645.7-8653.2').

Table 8.1 Summary of pedogenic features below the P4 subaerial exposure surface, Snipe Lake reef complex. * = end of cored interval and paleosol was not fully observed, n/a = core not described.

Well Location	Depth of P4		Maximum Depth of Paleosol Below P4	Features										
	Feet	Meters	Meters	Massive Green Shale Beds	Green Shale in Dissolution Vugs and Cracks	Mottled Dolomitic Green Shale Beds	Rhizoliths	Fitted-Fabric Lithoclasts	Laminar Calcretes	Glaebules	Peds	Marine Pendant Cements in Vugs	Meteoric Pendant Cements
16-17-69-19W5	8998.5	2742.7	1.20	x	x			x	x			x	
12-14-70-18W5	8704.7	2653.2	2.10	x	x		x	x	x			x	
10-21-70-18W5	8769	2672.8	1.20	x	x				x			x	
10-22-70-18W6	8732.8	2661.8	0.60		x	x		x	x	x	x		x
12-22-70-18W5	8752	2667.6	1.43	x	x				x			x	x
12-23-70-18W5	8647	2635.6	1.58	x	x		x	x	x			x	
04-26-70-18W5	8648	2635.9	0.85	x	x				x				x
10-27-70-18W5	8672	2643.2	0.77	x	x			x	x			x	x
12-27-70-18W5	*8698.7	*2651.4	*0.15	x	x		x	x	x	x			
12-32-70-18W5	8586	2617.0	2.04	x	x				x				
02-33-70-18W5	8685.7	2647.4	0.64	x	x			x	x				x
02-03-71-18W5	8639.3	2633.3	2.10		x		x		x			x	
12-03-71-18W5	8611.5	2624.8	0.85	x	x				x			x	
02-04-71-18W5	8594	2619.5	n/a										

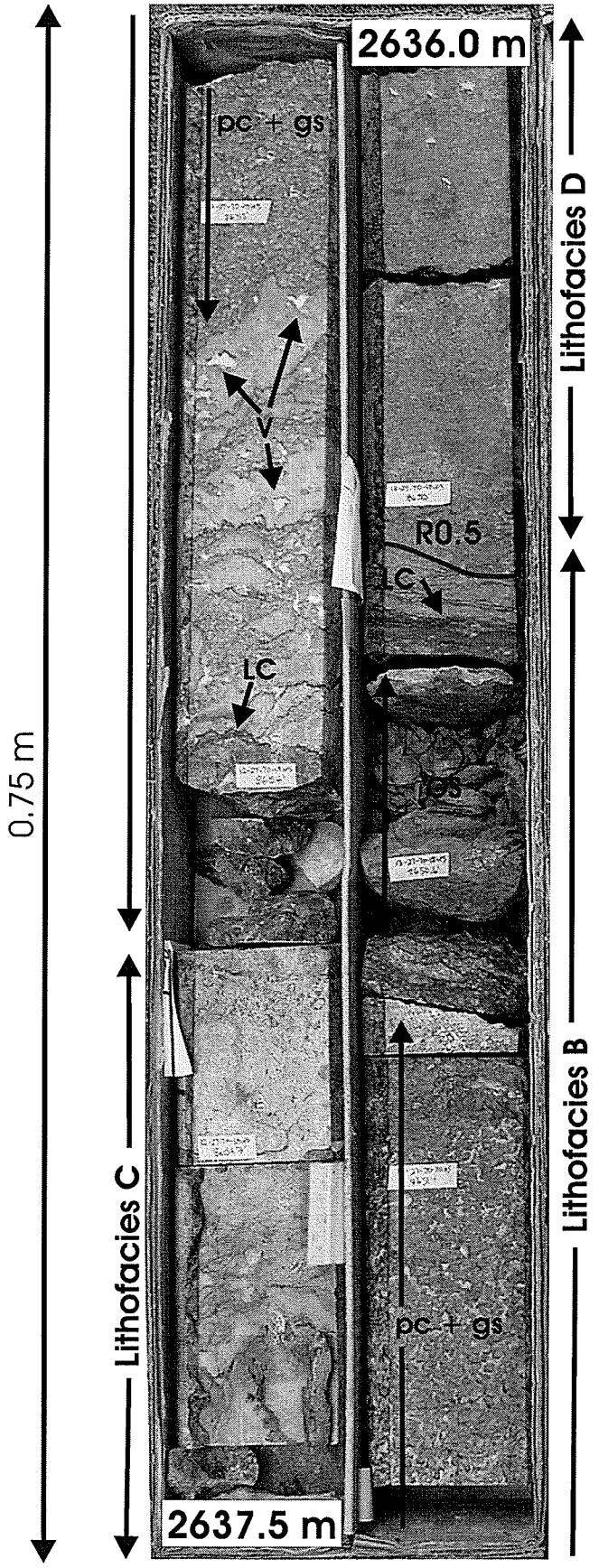


Figure 8.6 Succession of core above and below the R0.5 subaerial exposure surface in the Snipe Lake reef complex. The R0.5 exposure surface is developed on branching cylindrical stromatoporoid-*Amphipora* rudstones and overlain by *Amphipora* floatstones to rudstones with a peloid packstone matrix. A paleosol profile is developed below the exposure surface from 2636.52 down to 2637.77 m (8650-8654.1'). Laminar calcretes (Lc) are common below the exposure surface. A green shale (Gs) bed is observed approximately 12 cm below the exposure surface. Pendant cements and green shales (Pc + Gs) are very abundant in cracks, vugs and other pore spaces below the green shale horizon. Dissolution vugs (V) developed in large stromatoporoid clasts have geopetal green shales and cloudy white and brown marine pendant cements. A laminar calcrete (*Lc) marks the base of the paleosol profile, 12-27-70-18W5, 2636 - 2637.5 m (8648.3-8653.3').

Table 8.2 Summary of pedogenic features below the R0.5 subaerial exposure surface, Snipe Lake reef complex.

Well Location	Depth of R0.5		Maximum Depth of Paleosol Below R0.5	Features									
	Feet	Meters	Meters	Massive Green Shale Beds	Green Shale in Dissolution Vugs and Cracks	Massive Dolomitic Green Shale Beds	Rhizoliths	Fitted-Fabric Lithoclasts	Laminar Calcretes	Glaebules	Peds	Marine Pendant Cements in Vugs	Meteoric Pendant Cements
16-17-69-19W5	8944.8	2726.4	0.12	x					x				
12-14-70-18W5	8653.6	2637.6	0.43		x			x				x	
10-21-70-18W5	8727	2660.0	0.75		x							x	
10-22-70-18W6	8689	2648.4	0.76	x	x		x	x					
12-22-70-18W5	8708	2654.2	0.85		x	x				x	x		x
12-23-70-18W5	8572	2612.7	0.00										
04-26-70-18W5	8598	2620.7	0.15									x	
10-27-70-18W5	8622.5	2628.1	0.00										
12-27-70-18W5	8650	2636.5	1.20	x	x			x	x			x	
12-32-70-18W5	8544.4	2604.3	1.30		x	x		x	x			x	
02-33-70-18W5	8634	2631.6	1.00		x				x				
02-03-71-18W5	8584	2616.4	0.00										
12-03-71-18W5	8562	2609.7	0.00										
02-04-71-18W5	8541	2603.3	0.90	x	x			x	x			x	

8.5 Localized Exposure Surfaces

Laminar calcretes were observed above the P4 exposure surface (e.g. 3.1 m above the P4 megacycle contact in well 10-21-70-18W5 at 2669.4 m, 8758'; Figure 8.4) and below the apparent base of the P4 paleosol profile (e.g. 4.9 m below the base of paleosol in well 12-32-70-18W5 at 2621.9 m, 8602'). Similarly, laminar calcretes were also observed above the R0.5 subaerial exposure surface in one well location (e.g. 1.5 m above the R0.5 megacycle contact in well 16-17-69-19W5, at 2724.9 m, 8940'; Figure 8.2). These laminar calcretes are considered to be unrelated to either the P4 or R0.5 paleosols and are interpreted to reflect localized exposure surfaces (see section 9.5).

8.6 P5 Megacycle Contact

Evidence for meteoric diagenesis directly below the P5 megacycle contact was observed in only one well location, 16-17-69-19W5 (2731.9 m, 8963'), in this study (Figure 8.2). A 1.1 m thick paleosol is developed directly below the contact in tidal flat lithofacies. A mottled green shale bed (34 cm thick), laminar calcretes and peds occur in the upper portion of the paleosol. Green shales in dissolution vugs and cracks, fitted-fabric lithoclasts and laminar calcretes occur lower in the underlying open lagoon lithofacies. The implications of the development of a paleosol at this stratigraphic level are discussed later in section 9.5.

8.7 Types of Paleosol Profiles

Based on the spatial distribution of pedogenic features and their development in different lithologies, four types of paleosol profiles have been recognized below the P4 and R0.5

subaerial exposure surfaces (Figure 8.7) and are summarized in the following sections.

8.7.1 Type A

The type A paleosol profile is present below the P4 subaerial exposure surface and ranges from 0.75 to 2.1 m thick; the interpreted idealized profile is shown in Figure 8.7. Pedogenic features are often developed within a succession of tidal flat lithofacies (lithofacies A, typically 0.30 to 0.75 m thick) overlying open lagoon lithofacies (lithofacies C or D, typically 0.30 to 1.0 m thick). Massive green shale beds, locally dolomitized, are typically developed near the top of the profile and range from 1.5 to 34 cm thick. When present, rhizoliths occur in the upper 50 cm of the profile. Green shales occur through the rest of the profile filling cracks, dissolution vugs and interparticle pores and are commonly associated with fitted-fabric lithoclasts. Marine pendant cements in dissolution vugs and to a lesser extent meteoric pendant cements are often developed lower in the profile in open lagoon lithofacies. Pendant cements decrease in abundance and thickness down the profile and may be gradational with isopachous fibrous calcite cements below the paleosol. Laminar calcretes are abundant throughout the paleosol profile. Thin or incomplete profiles observed at some locations are interpreted to have been affected by erosion (see section 9.4.6).

8.7.2 Type B

The type B paleosol profile is present below both the P4 and R0.5 subaerial exposure surfaces and rarely at the P5 megacycle contact and ranges from 0.60 to 1.3 m thick (Figure 8.7). The upper portion is composed of a dolomitized, mottled green shale bed

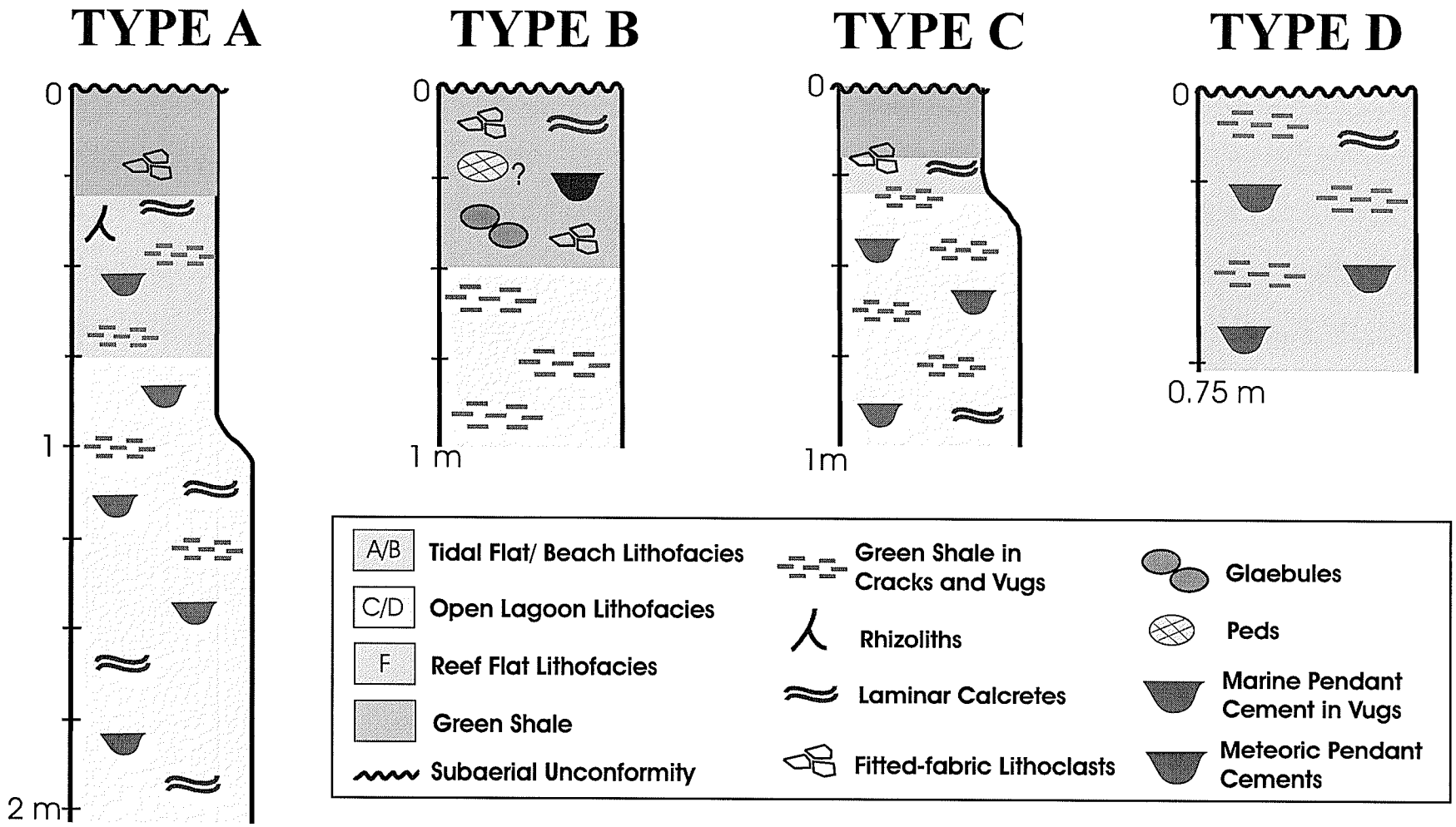


Figure 8.7 Paleosol profile types characterized in the Snipe Lake reef complex. The type A paleosol profile is present at the P4 subaerial exposure surface. The type B paleosol profile is present at both the P4 and R0.5 subaerial exposure surfaces. Types C and D paleosol profiles are present at the R0.5 subaerial exposure surface.

with abundant desiccation cracks that may be developed within or above tidal flat lithofacies (lithofacies A). Fitted-fabric lithoclasts, dolomitic glaebules with circumgranular and septarian cracks and incipient peds are also very closely associated with these mottled green shale beds. Meteoric pendant cements and laminar calcretes may also be present. Green shales generally extend into underlying open lagoon lithofacies (lithofacies C or D), filling dissolution vugs, cracks and interparticle pores.

8.7.3 Type C

The type C paleosol profile is observed below the R0.5 subaerial exposure surface and is similar to the type A paleosol. It has a similar vertical succession of diagenetic features but is thinner ranging from 0.12 to 1.2 m thick (Figure 8.7). Pedogenic features are typically developed in a thin upper interval of tidal flat to beach lithofacies (lithofacies A or B, typically 0.15 to 0.50 m thick) overlying open lagoon lithofacies (lithofacies C or D, typically 0.30 to 0.75 m thick). Green shale beds (commonly < 10 cm thick, rarely up to 24 cm thick) are developed directly below or near the exposure surface in tidal flat lithofacies or relatively muddy open lagoon lithofacies. Green shales extend lower in the profile occurring in cracks, dissolution vugs and interparticle pores, and fitted-fabric lithoclasts are commonly associated with these green shales. Laminar calcretes occur throughout the profile, whereas marine pendant cements in dissolution vugs are more commonly developed lower in the profile in open lagoon lithofacies or coarse grained beach lithofacies. Locally, thin profiles and absence of massive or mottled green shale beds are likely the result of removal of the upper portions of the paleosol by erosion (see section 9.4.6).

8.7.4 Type D

The type D paleosol profile is present below the R0.5 subaerial exposure surface and ranges from 0.43 to 1.0 m thick (Figure 8.7). Pedogenic features are developed in reef flat lithofacies (lithofacies F). Green shales occur filling cracks, dissolution vugs and interparticle pores throughout most of the profile, but massive and mottled green shale beds are absent. Fitted-fabric lithoclasts may be associated with green shales. Laminar calcretes and marine pendant cements in dissolution vugs are common throughout the profile. The type D paleosol is the least common in the Snipe Lake reef complex. The variety and distribution of pedogenic features are very similar to the lower succession (i.e. open lagoon intervals) of types A and C paleosols with the only significant difference being the host carbonate lithology and lack of green shale beds. The thin profile and absence of massive or mottled green shale beds in the type D paleosol may be the result of a combination of substrate controls (see section 9.4.5) and erosion (see section 9.4.6).

8.8 Trends in Pedogenic Features

8.8.1 Distribution within Paleosols

The four different paleosol profiles described in this study generally show a consistent vertical arrangement of pedogenic and meteoric features (cf. Esteban and Klappa, 1983; Ettensohn et al., 1988; Goldstein, 1991; Alonzo-Zarza, 2003; Fu et al., 2004b). More specifically, the following associations have been observed:

(1) Green shale beds and mottled green shale beds are developed within the upper

portions of paleosols, typically in tidal flat lithofacies or muddy open lagoon facies.

(2) Rhizoliths are relatively rare and are present high in the paleosol profile.

(3) Marine pendant cements in dissolution vugs and green shales in dissolution vugs and cracks are developed low in paleosol profiles, typically in open lagoon, reef flat or coarse grained beach lithofacies.

(4) Laminar calcretes are common throughout paleosol profiles.

The majority of these relationships are interpreted to reflect lithological controls of the host carbonate rock. A more in-depth discussion about the controls on the development of paleosols is provided in Chapter 9. An exception is rhizoliths, as their occurrence in the upper portion of the profile is likely a reflection of proximity to the exposure surface where plants lived and roots could penetrate (cf. Goldstein, 1991).

8.8.2 Areal Distribution

The areal distribution of key pedogenic features below the P4 and R0.5 subaerial exposure surface in the Snipe Lake reef complex is shown in Figures 8.8 and 8.9. However, it is important to note that there is a limited number and distribution of wells, as most wells examined in this study are located along the eastern margin of the Snipe Lake reef complex. Green shales (including massive green shale beds, mottled green shale beds and green shale filling cracks and dissolution vugs) and laminar calcretes are present throughout the platform-reef margin and in the platform-reef interior environments (Figures 8.8a and 8.9a). Rhizoliths are less abundant but are still

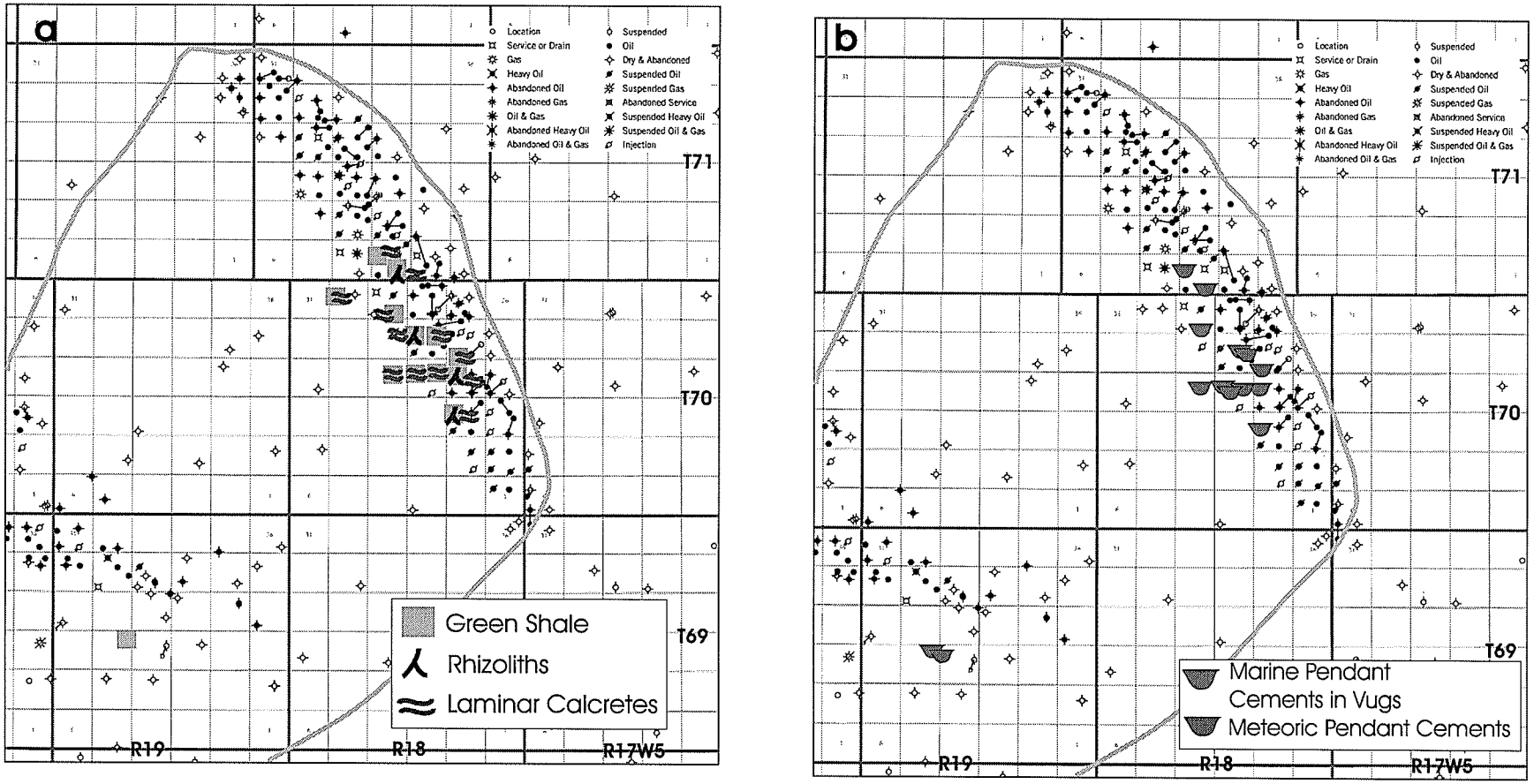


Figure 8.8 Location maps of the Snipe Lake reef complex showing the distribution of pedogenic features below the P4 subaerial exposure surface. a) Distribution of green shales (including massive green shale beds, mottled green shale beds and green shales filling dissolution vugs and cracks), rhizoliths and laminar calcretes. b) Distribution of marine pendant cements in vugs and meteoric pendant cements.

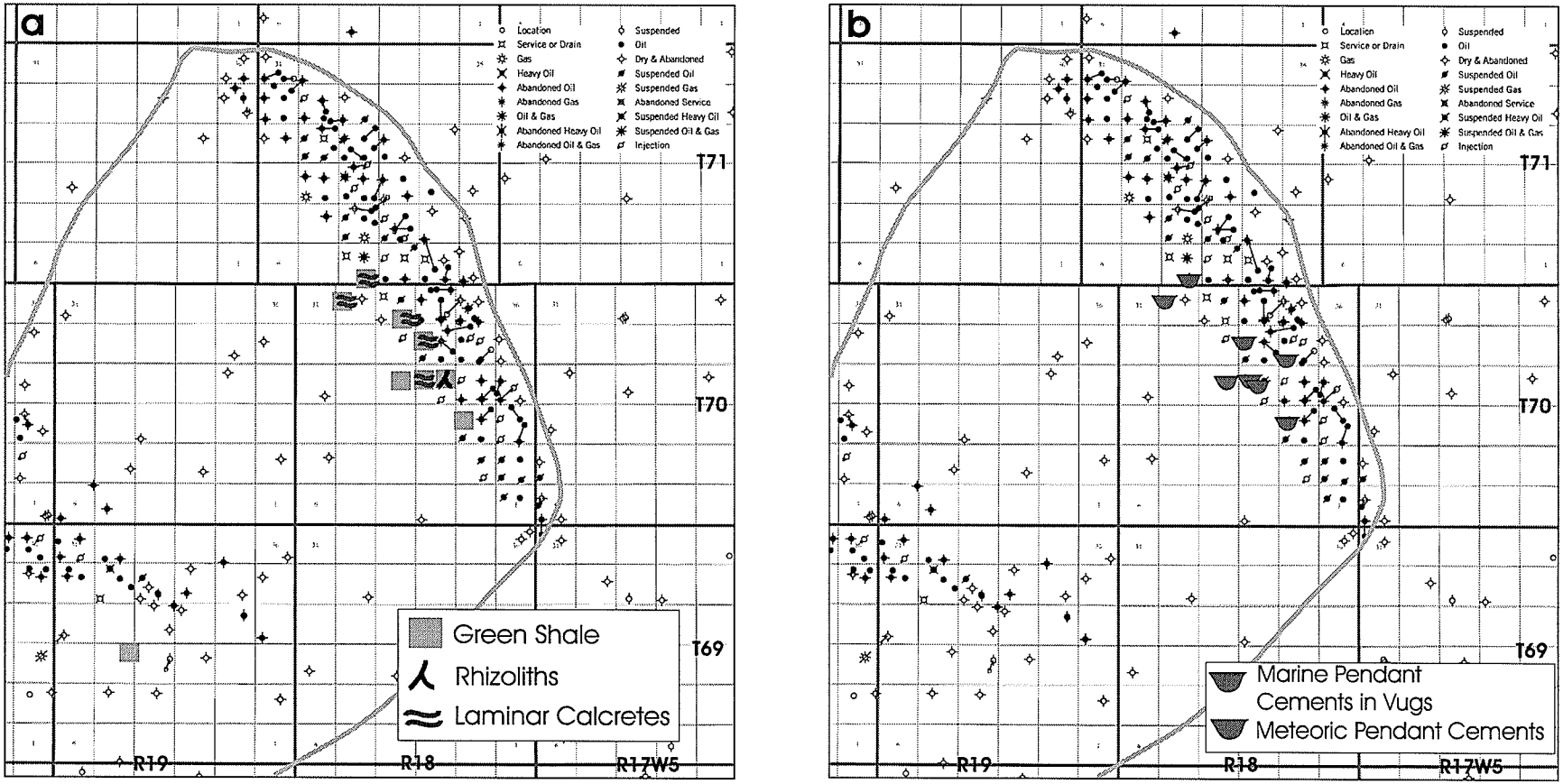


Figure 8.9 Location maps of the Snipe Lake reef complex showing the distribution of pedogenic features below the R0.5 subaerial exposure surface. a) Distribution of green shales (including massive green shale beds, mottled green shale beds and green shales filling dissolution vugs and cracks), rhizoliths and laminar calcretes. b) Distribution of marine pendant cements in vugs and meteoric pendant cements.

distributed throughout the platform-reef margin environments (Figures 8.8a and 8.9a). Marine pendant cements in dissolution vugs and meteoric pendant cements also occur in throughout the platform-reef margin and platform-reef interior environments along the eastern margin (Figures 8.8b and 8.9b). No distinctive (areal) distribution patterns of pedogenic features within the Snipe Lake reef complex are revealed by this study.

Paleotopography of the P4 and R0.5 subaerial exposure surfaces in the Snipe Lake reef complex was estimated by calculating the thickness from the top of the P2 megacycle to the P4 and R0.5 surfaces, respectively (Figures 8.10 and 8.11). Based on these reconstructions, there is no apparent correlation between the areal distribution of pedogenic features and the interpreted paleotopography of the P4 and R0.5 subaerial exposure surfaces. For example, green shales, laminar calcretes, rhizoliths, marine pendant cements in dissolution vugs and meteoric pendant cements appear to occur in both locally topographically high and low areas along the eastern margin of the Snipe Lake reef complex.

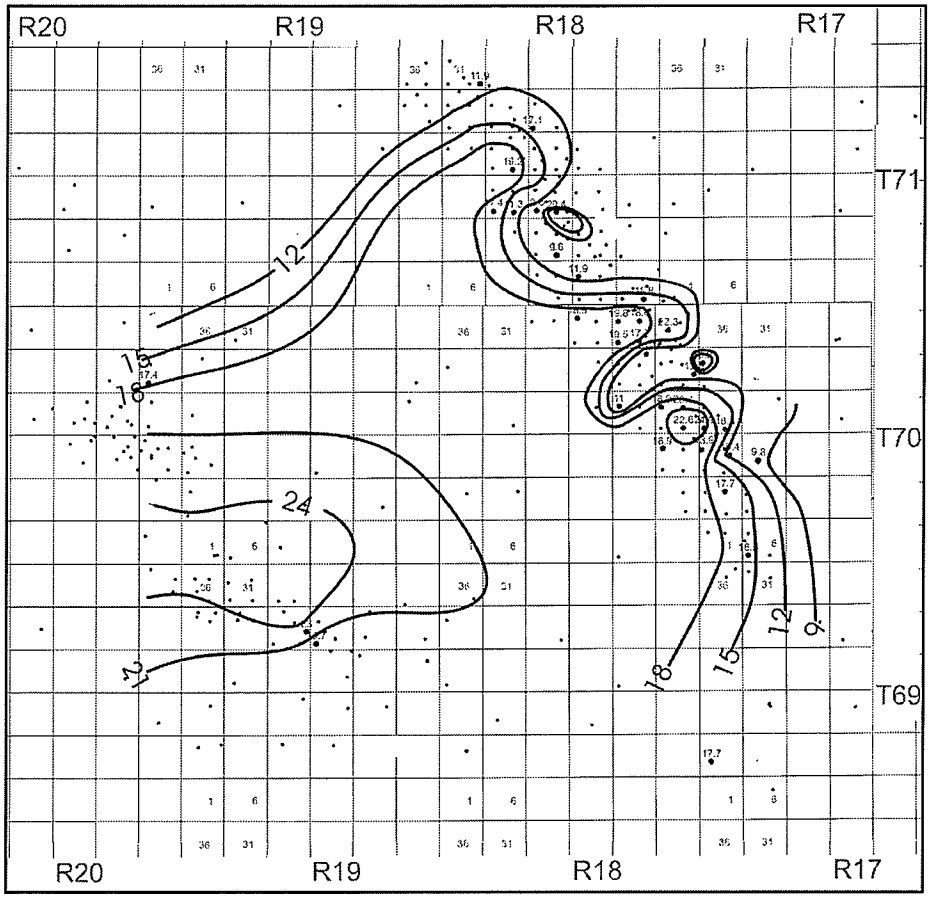


Figure 8.10 P4 isopach map showing approximate paleotopography of the P4 surface in the Snipe Lake reef complex. P4 thickness is estimated from the top of the P2 megacycle contact to the top of the P4 megacycle contact (based on unpublished data, I. Muir and others, 1988; Appendix G). Wells highlighted in red have been cross-referenced with core analysis in this study and/or core descriptions from I. Muir and others (unpublished data, 1988) for more accurate P4 thickness. Contours are in 3 m intervals. Sections 1, 6, 31 and 36 are labeled in the UWI coordinate system.

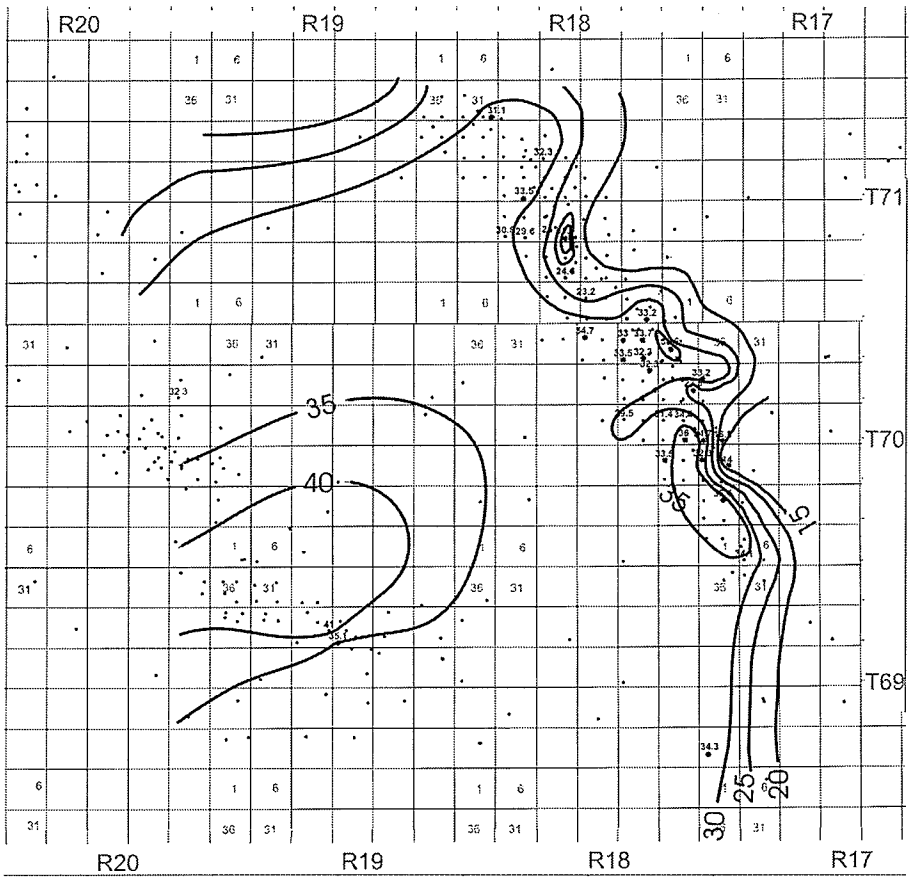


Figure 8.11 R0.5 isopach map showing approximate paleotopography of the R0.5 surface in the Snipe Lake reef complex. R0.5 thickness is estimated from the top of the P2 megacycle contact to top of the R0.5 megacycle contact (based on unpublished data, I. Muir and others, 1988; Appendix G). Wells highlighted in red have been cross-referenced with core analysis in this study and/or core descriptions from I. Muir and others (unpublished data, 1988) for more accurate P4 thickness. Contours are in 5 m intervals. Sections 1, 6, 31, 36 are labeled in the UWI coordinate system.

CHAPTER 9 – DISCUSSION

9.1 Introduction

Previous chapters have provided the stratigraphic, sedimentological and geochemical data collected for the Snipe Lake reef complex, as well as a review of the criteria that can be used to recognize ancient subaerial exposure surfaces and the development of paleosols in carbonate rocks. This chapter will integrate these data to develop a better understanding of the controlling factors and implications of subaerial exposure surfaces in the Snipe Lake reef complex.

9.2 Autocyclic versus Allocyclic Controls on the P4 and R0.5 Subaerial Exposure Surfaces

Subaerial exposure surfaces in marine successions are caused by autocyclic or allocyclic processes that will result in predictable differences in paleosol development (e.g. Goldstein et al., 1991). It is important to be able to distinguish between these mechanisms of paleosol development because they have significantly different implications for interpreting sea level history. In the autocyclic model, subaerial exposure is a result of vertical aggradation of sediment into the subaerial realm (e.g. Goldstein et al., 1991; Strasser, 1991; Tucker, 1993; Wright, 1994). Localized areas of rapid sediment accumulation build up into the subaerial environment. In the allocyclic model, subaerial exposure is a result of relative sea level fall (basin uplift and/or eustatic sea level fall) (Goldstein et al., 1991; Catuneanu, 2002; Embry, 2002).

Subaerial exposure surfaces at the P4 and R0.5 stratigraphic levels in the Snipe Lake reef complex are interpreted to be the result of relative sea level fall, for the following reasons:

(1) Paleosol profile types A, B, C and D (Chapter 8) are partially or entirely developed in subtidal lithofacies. During subaerial exposure the lowest elevation of the water table is approximately sea level (e.g. Goldstein et al., 1991). Therefore, evidence for meteoric vadose diagenesis in subtidal deposits indicates exposure of subtidal deposits which requires a relative sea level fall. In addition, vadose-zone diagenesis has been observed down to 2.1 m below the P4 surface and 1.3 m below the R0.5 surface. Subaerial exposure due to a relative sea level fall typically has longer exposure periods resulting in more extensive meteoric diagenesis (e.g. Goldstein et al., 1991; Wright, 1994). In contrast, evidence for meteoric vadose diagenesis should be limited to intertidal and supratidal deposits if exposure was due to reef aggradation, for the simple reason that subtidal deposits would have remained below sea level (e.g. Goldstein et al., 1991; Strasser, 1991). Paleosols formed by vertical aggradation have had shorter exposure periods and are typically thin and 'immature' (e.g. Ettensohn et al., 1988).

(2) Paleosols are laterally continuous and correlative across the P4 and R0.5 stratigraphic levels in the Snipe Lake reef complex. Paleosols that formed as a result of relative sea level fall can be traced over significant distances or

paleotopography (e.g. Goldstein et al., 1991), whereas subaerial exposure due to reef aggradation typically results in paleosols that have localized distribution (e.g. Ettensohn, 1988). In addition, paleosols have also been recognized at the R0.5 stratigraphic level in the Judy Creek reef complex which is located approximately 85 km away to the southeast (Chow and Wendte, 2004). The presence of such a widespread emergent surface across these Swan Hills reef complexes indicates that relative sea level fall is likely a controlling factor (e.g. Wendte and Muir, 1995; Wendte and Uyeno, 2005).

(3) Subaerial exposure surfaces in some locations are developed directly on top of subtidal (open lagoon and reef flat) lithofacies. A relative sea level fall can account for the superposition of subaerial exposure surfaces directly over subtidal deposits. Vertical aggradation of sediment should result in a progressive shallowing-upward succession from subtidal to intertidal/supratidal to subaerial deposits (e.g. Goldstein et al., 1991; Strasser, 1991). However, erosion during subaerial exposure and/or by the subsequent transgression could have removed the upper portions (tidal flat lithofacies) of paleosols. This may also account for the position of erosional surfaces directly over subtidal lithofacies.

9.3 Implications for Magnitude of Relative Sea Level Fall

One of the most important implications for the recognition of paleosols is interpretation of relative sea level history. The meteoric vadose zone is unlikely to extend below sea level (refer to section 9.2); therefore the depth of vadose diagenesis below a subaerial

exposure surface can be used to estimate the minimum extent of relative sea level fall (e.g. Goldstein et al., 1991). Pedogenic features and pendant cements (marine and meteoric) described in the Snipe Lake reef complex are all evidence for vadose zone diagenesis (see Chapters 6 and 7). Paleosols are typically thicker at the P4 subaerial exposure surface relative to the R0.5 subaerial exposure surface, and therefore a greater drop in relative sea level is interpreted at the P4 stratigraphic level. A relative sea level fall of at least 2.1 m is postulated at the P4 subaerial exposure surface and 1.3 m at the R0.5 subaerial exposure surface. This method can provide only an estimate of the *minimum* relative sea level fall because it does not account for the amount of the paleosol that has been removed by erosion (see section 9.4.6) and/or compacted by burial (e.g. Retallack, 2001). These values are similar to the interpreted relative sea level fall at the R4 subaerial exposure surface in the Snipe Lake and Judy Creek reef complexes (Wendte and Muir, 1995; Chow and Wendte, 2004) and the R0.5 subaerial exposure surface in the Judy Creek reef complex (Chow and Wendte, 2004).

9.4 Other Controlling Factors on the P4 and R0.5 Subaerial Exposure Surfaces

In addition to relative sea level changes, there are a number of extrinsic and intrinsic factors that influence the nature of meteoric diagenesis and development of paleosols during periods of subaerial exposure (e.g. Esteban and Klappa, 1983; Ettensohn et al., 1988; Wright and Tucker, 1991; Mack and James, 1994; Alonso-Zarza, 2003; Fu et al., 2004b). Extrinsic controls include climate, topography, vegetation and duration of exposure. Intrinsic controls include geochemical and physical attributes of the host rock or substrate controls. In addition, erosion can remove the upper portions of paleosols

leaving only relicts. Interaction of these variables has influenced the range of pedogenic features and types of paleosol profiles observed below the P4 and R0.5 subaerial exposure surfaces in the Snipe Lake reef complex.

9.4.1 Climate

Climate is considered by many as one of the most critical factors in the development of paleosols (e.g. Esteban and Klappa, 1983; Blogett, 1988; Ettensohn et al., 1988; Wright, 1994; Retallack, 2001; Alonso-Zarza, 2003). Paleolatitude reconstructions position the WCSB in the arid to semiarid, easterly trade wind belt during Middle to Late Devonian time (see section 1.3.1, Figure 1.1; Heckel and Witzke, 1979; Witzke and Heckel, 1988) where climatic conditions are conducive for paleosol development (cf. Ettensohn et al., 1988; Pelechaty and James, 1991; Driese and Foreman, 1992; Milnes, 1992; Wright, 1994; Williams and Krause, 1998; Fu et al., 2004b). Semiarid climates are characterized by seasonal conditions and an overall net annual moisture deficit with an annual precipitation of less than 100 cm/year (e.g. Ettensohn et al., 1988; Retallack, 2001; Alonso-Zarza, 2003). The dominant pedogenic process in these environments is the accumulation of calcium carbonate where seasonal conditions allow carbonate to be mobilized during wet seasons and fixed during dry seasons (e.g. Ettensohn, et al., 1988; Mack and James, 1994; Wright, 1994).

9.4.2 Topography

Local topography can affect the morphology and development of paleosols (e.g. Ettensohn, 1988; Milnes, 1992; Rossinsky and Wanless, 1992; Alonso-Zarza, 2003). In

this study, the areal distribution of pedogenic features does not show any obvious correlation with the paleotopography of the P4 and R0.5 subaerial exposure surfaces (see section 8.8.2). Therefore, topography appears to have no significant influence on the development of pedogenic features in the Snipe Lake reef complex. However, the lack of apparent topographic controls may also be in part a result of the limited number of wells which are concentrated within a relatively small area along the platform/reef margin (except well 16-17-69-19W5 which is in the interior). In addition, the constructed isopach maps are only an approximation of the paleotopography in the Snipe Lake reef complex. Data were obtained from a previous study (I. Muir and others, unpublished data, 1988) and are relatively limited. Other studies have reported increased thickness and abundance of pedogenic features in topographically higher areas where there is prolonged exposure (e.g. Ettensohn et al., 1988), whereas others have reported more karst-like features developed in higher areas and calcretes in lower areas (e.g. Sanz, 1996).

9.4.3 Vegetation and Soil Organisms

Vegetation and soil organisms typically can play a significant role in soil development. They influence precipitation, dissolution and alteration of calcium carbonate and mechanically disintegrate the soil matrix (e.g. Esteban and Klappa, 1983; Ettensohn et al., 1988; Rossinsky and Wanless, 1992; Alonso-Zarza, 2003). In the Snipe Lake reef complex, the generally small size and limited occurrence of rhizoliths suggest that plant density was likely sparse in soils (cf. Ettensohn et al., 1988; Chow and Wendte, 2004). As mentioned previously in section 7.2.2, vascular plants in the Late Devonian were

relatively small with simple branching. Evidence for other biological influences on soil development (i.e. bioturbation, burrows) is also rare in these paleosols, but soil organisms may have played a role in the development of crumb peds (cf. Retallack, 1988; 2001; refer to section 7.8.2).

Plants and other organisms can significantly influence the composition of soil CO_2 and the $\delta^{13}C$ signature of related calcium carbonate precipitates (e.g. Allan and Mathews, 1982; Lohmann, 1988; Carpenter and Lohmann, 1989; Goldstein, 1991; Cerling, 1999; Mermut et al., 2000; Alonso-Zara, 2003). Plants and other organisms fix ^{12}C and usually result in light $\delta^{13}C$ composition in soil components. In this study, the overall positive $\delta^{13}C$ composition of pedogenic features (Chapter 7) is consistent with a marine source of carbon supporting the interpretation that plants did not have a significant influence on the development of paleosols in the Snipe Lake reef complex.

9.4.4 Time

The duration of subaerial exposure exerts a strong control on the development of paleosols (e.g. Ettensohn et al., 1988; James and Choquette, 1990b; Wright, 1994; Alonso-Zarza, 2003). In general, shorter periods of emergence will result in poorly developed or immature profiles, whereas longer periods of emergence will result in more extensive meteoric diagenesis and thicker or more mature paleosol profiles (e.g. Ettensohn et al., 1988). In this study, the extent of exposure is proposed to account for some of the differences in development between the P4 and R0.5 paleosols. The P4 paleosol ranges up to 2.1 m thick and typically shows more extensive meteoric alteration,

whereas the R0.5 paleosol is thinner, up to 1.3 m thick, and shows less extensive meteoric alteration. Therefore, it is speculated that subaerial exposure was longer during P4 time than during R0.5 time. Paleosols in the Snipe Lake reef complex are comparable in maturity to other Devonian paleosols (cf. Williams and Krause, 2000; Fu et al., 2004b). These other examples are typically thin (less than several meters), roots and clay horizons are poorly to moderately developed and are interpreted to be the product of relatively short periods of exposure.

9.4.5 Substrate

The physical and chemical characteristics of the host rock influence the nature of paleosol profiles. For example, the original mineralogy of the host rock or sediments affects their stability and therefore their susceptibility to meteoric alteration (e.g. James and Choquette, 1990b). In addition, the host may also be a major source for calcium carbonate that can reprecipitate as pedogenic carbonate (e.g. Ettensohn et. al., 1988; Alonso-Zarza, 2003). Grain size affects the rate of meteoric diagenesis; fine-grained sediments tend to be rapidly altered due to their relatively greater surface area compared to coarser grained sediments (e.g. James and Choquette, 1990b; Alonzo-Zarza, 2003). Porosity and permeability influence the rate of flow and retention time of meteoric fluids (e.g. James and Choquette, 1990b).

Substrate appears to exert a significant control on the development of paleosols below the P4 and R0.5 subaerial exposure surfaces in the Snipe Lake reef complex. In particular, it likely accounts for most of the trends that are apparent within the paleosol profiles of a

particular exposure surface and also between the P4 and R0.5 paleosols. As described in Chapter 8, massive green shale beds and mottled green shale beds are typically developed in tidal flat lithofacies or muddy lagoon lithofacies (lithofacies A or D). In contrast, marine pendant cements and green shales in dissolution vugs are more common and better developed in open lagoon to reef flat lithofacies (lithofacies C, D or F). These trends are interpreted to reflect primarily the porosity and permeability of the host rock. The formation of massive green shale beds and mottled green shale beds may be related to the accumulation of soil plasma on top of relatively low porosity and low permeability surfaces (e.g. Esteban and Klappa, 1983; Alonso-Zara, 2003). In host rock that has higher interparticle porosity such as open lagoon and reef flat lithofacies, green shale beds are absent to poorly developed. Meteoric waters flowed more easily through these more porous lithologies and dissolved calcium carbonate in the host rock creating dissolution-enhanced primary pores and dissolution vugs (see section 6.2.2). Subsequently, green shales filtered downward to either completely or partially occlude voids. As relative sea level started to rise (after subaerial exposure) seawater partially filled dissolution vugs and precipitated pendant radiaxial fibrous calcite cements. Other meteoric vadose (pendant prismatic calcite, meniscus blocky calcite) and phreatic (isopachous prismatic calcite) cements occurring in primary pores are present in a range of lithologies (lithofacies A, C, D and F) and do not appear to be influenced by the type of substrate. Substrate controls have also been reported by other studies (e.g. Ettensohn et al., 1988; Bain and Foos, 1991).

Furthermore, the vertical succession of pedogenic features (types A, B, C and D paleosol

profiles; see Chapter 8) is interpreted to be influenced by the nature of depositional cycles. The P4 succession is composed exclusively of a series of shallowing-upward lagoonal cycles (see Chapter 5) where open lagoon lithofacies are overlain by tidal flat lithofacies. Consequently, green shale beds which typically occur in tidal flat lithofacies, are consistently developed higher in a paleosol profile relative to dissolution vugs that are either completely or partially occluded by marine pendant cements and green shales which typically developed in open lagoon lithofacies. Thus, the P4 subaerial exposure surface is characterized predominantly by the type A paleosol profile. In contrast, the R0.5 succession is composed of a range of lithofacies that are arranged in lagoonal and reefal cycles (see Chapter 5). This resulted in a more variable vertical succession of lithofacies below the R0.5 subaerial exposure surface, and consequently variable vertical distribution of the associated pedogenic features. Therefore, the R0.5 subaerial exposure surface is characterized by types B, C and D paleosol profiles. Types B and C profiles may represent paleosol development in lagoonal cycles and the type D profile may represent development at the top of reefal cycles.

9.4.6 Erosion

Erosion plays a significant role in the preservation of paleosols. Removal of the upper portions of paleosols can occur during subaerial exposure or the subsequent transgression (e.g. Esteban and Klappa, 1983; Ettensohn et al., 1988; Goldstein et al., 1991; Driese and Foreman, 1992; Webb, 1994; Wright, 1994; Retallack, 2001). The P4 and R0.5 megacycle contacts in well locations in this study where paleosols are absent (e.g. 12-23-70-18W5, 2617.2 m, 8572'; 02-03-71-18W5, 2609.7 m, 8562'; 12-03-71-18W5, 2603.3

m, 8541') or have relatively thin paleosols (e.g. 02-33-70-18W5, 2647.4 m, 8685.7'; 04-26-70-18W5, 2620.7 m, 8598') are interpreted to have been modified by erosion (see Tables 8.1 and 8.2, Figures 8.2 to 8.4). The amount of erosion can be estimated by comparing the thickest (most complete) paleosols to the thinnest paleosols observed below each subaerial exposure surface. From this study, approximately a minimum of 1.5 m and 1.3 m of erosion are estimated to have occurred at the P4 and R0.5 subaerial exposure surfaces, respectively.

9.5 Local Subaerial Exposure Surfaces

Local exposure surfaces have been recognized in intervals above and below the P4 and R0.5 paleosols, as described in section 8.5. They are separated from the P4 and R0.5 paleosols by lithofacies that lack evidence for meteoric diagenesis. They are identified by laminar calcretes and are not correlative across the Snipe Lake reef complex (see Figures 8.2 to 8.4 for locations). Local exposure features are very thin (1-6 mm thick) and do not show any additional evidence for meteoric diagenesis besides the laminar calcretes. Stratigraphically the local exposure surfaces generally occur at the top of tidal flat lithofacies or in shallowing-upward open lagoon lithofacies near the top of lagoonal cycles. Based on these characteristics, these local exposure surfaces are interpreted to be a result of reef aggradation (refer to section 9.2.).

The occurrence of pedogenic features at the P5 megacycle contact is more problematic. A paleosol developed directly below the P5 megacycle contact has been recognized at only one well location (16-17-69-19W5, 2731.9 m, 8963') (Figure 8.2, section 8.6).

Pedogenic features are developed up to 1.1 m below the contact and are also developed in subtidal open lagoon lithofacies. These features collectively suggest that the P5 megacycle contact was an emergent surface resulting from a relative sea level fall; this interpretation is comparable to the P4 and R0.5 subaerial exposure surfaces (refer to section 9.2). The very rare occurrence of paleosols at the P5 megacycle contact, however, is problematic. In the absence of any additional information one possible scenario is that local reef aggradation coupled with a small relative sea level drop may have occurred at the P5 stratigraphic level. Only the highest portions of the platform were exposed due to the very limited areal extent and backstepping growth style of the P5 succession (see Chapter 5). The platform interior was emergent while the platform margin remained submerged. Based on correlations in cross-section A-A' (Enclosure 1; Figure 1.5), well 16-17-69-19W5 is located in a platform interior position and appears to be located at a P5 platform high, which would explain why meteoric diagenesis is only evident at the P5 level in this well and absent in all other wells examined in this study which are located near the platform margin. This scenario remains highly speculative and there is insufficient evidence to change the existing interpretation of the P5 succession as discussed in Chapter 5. Interestingly, green shales have been documented by Fischbuch (1968) at the top of the Division IV growth stage which may be equivalent to the P5 stratigraphic level.

9.6 Source of Siliciclastic Sediment

Green shales are interpreted to have formed by the accumulation of aeolian-sourced clay and quartz silt sediment (refer to section 7.4.3). The Peace River Arch, located east of

the Snipe Lake reef complex in the Devonian was a topographic high (Oldale and Munday, 1994; Figure 1.1) and is a likely source for this wind-blown sediment. In addition, aeolian dust from the Caledonian Mountains (see Figure 1.1) transported long distances by southeasterly trade winds are also likely to have sourced the siliciclastic sediment (Heckel and Witzke, 1979; Kiessling et al., 1999; Wendte and Uyeno, 2005) and contributed to paleosol development. Some studies have shown that Saharan dust has been the primary source material for soils developed on Quaternary limestones in the Caribbean and Western Atlantic Islands (e.g. Muhs et al., 1990; Muhs, 2001). In addition, other workers who described paleosols have also interpreted the origin of clays to be from weathering of dust and aeolian material in surface horizons (e.g. Robinson and Wright, 1987; Wright and Tucker, 1991; Wright, 1994). Repetitive wetting and drying of this material resulted in potassium fixation and illite formation.

9.7 Effect on Reservoir Quality

Core and petrographic analysis from this study indicates that subaerial exposure had a relatively minimal effect on reservoir quality and porosity development in the P4 and R0.5 successions in the Snipe Lake reef complex. Dissolution vugs and solution-enhanced primary (shelter and interparticle) pores are commonly developed below subaerial exposure surfaces in open lagoon and reef flat lithofacies but are occluded by green shales, marine pendant cements, geopetal crystal silt, blocky calcite mosaics and late saddle dolomite cements (see Chapters 6 and 7). However, incompletely occluded intraparticle, interparticle and vuggy porosity, 1-2% (very rarely up to 5%), may be present in open lagoon lithofacies (Figures 4.6c, 6.2b, 6.3a and 6.8b). These porous

intervals have a patchy distribution and occur below intervals of paleosol profiles with dissolution vugs filled with green shale and cements. Due to the limited occurrence and low porosity values of these porous intervals, they do not significantly contribute to reservoir quality. In fact, paleosols below the P4 and R0.5 subaerial exposure surfaces may even represent permeability barriers due to extensive cementation, development of green shale beds and filling of pores by green shale.

Overall porosity in the Snipe Lake reef complex is controlled by depositional lithofacies (Springate et al., 1992). Porous intervals in this study are predominantly restricted to high energy reef flat (lithofacies F) and foreslope sand (lithofacies I) deposits that have been unaffected by subaerial exposure below the P4 and R0.5 subaerial exposure surfaces. Primary interparticle and intraparticle porosity is estimated to have contributed more than 95% of the porosity in reservoir facies (Springate et al., 1992). A similar study at the R4 stratigraphic level at the Snipe Lake reef complex also showed that meteoric diagenesis had minor effect on reservoir quality (Wendte and Muir, 1995). They proposed four possible explanations for the lack of porosity development due to meteoric diagenesis. These explanations also appear to be applicable to the P4 and R0.5 subaerial exposure surfaces in this study. First, the relatively small magnitude of relative sea level fall limited the amount of exposure sediments had to meteoric waters. Secondly, in arid to semiarid climates, meteoric water recharge would be limited and calcrete and soil development would be dominant. Porosity potential of paleosols is typically low due extensive cementation and occlusion by pedogenic processes (e.g. Esteban and Klappa, 1983). Dissolution and therefore porosity potential is more prevalent in humid climates

where cave and karst features are dominant (e.g. Esteban and Klappa, 1983; James and Choquette, 1990b; Moore, 2001). Thirdly, the original calcitic mineralogy of Devonian limestones would result in relatively quick mineral stabilization with minor diagenetic alteration (e.g. Mathews, 1974). Finally, most sediments below the P4 and R0.5 subaerial exposure surfaces examined in this study are muddy and non-porous, and therefore less permeable to meteoric flow. This is consistent with the rare occurrence of meteoric porosity in more porous open lagoon lithofacies.

9.8 P4 to R0.5 Evolution

Further to the interpretations of the P4 to R0.5 successions provided in Chapters 3 and 5, evidence for relative sea level changes and early diagenesis in the P4 and R0.5 successions enables refinement of the depositional history of the Snipe Lake reef complex as summarized below (Figure 9.1).

(1) P4 deposition initiated during a pulse of accelerated relative sea level rise and continued during increasing rates of relative sea level rise (Figure 9.1a). Normal marine cementation in primary pores occurred shortly after sediments were deposited on the sea floor.

(2) Gradually decreasing rates of relative sea level rise towards the end of P4 deposition were followed by a relative sea level drop of a minimum of 2.1 m which terminated platform growth (Figure 9.1b). The upper portion of the P4 platform was subaerially exposed to meteoric conditions in a semi-arid climate and paleosols developed below the emergent surface.

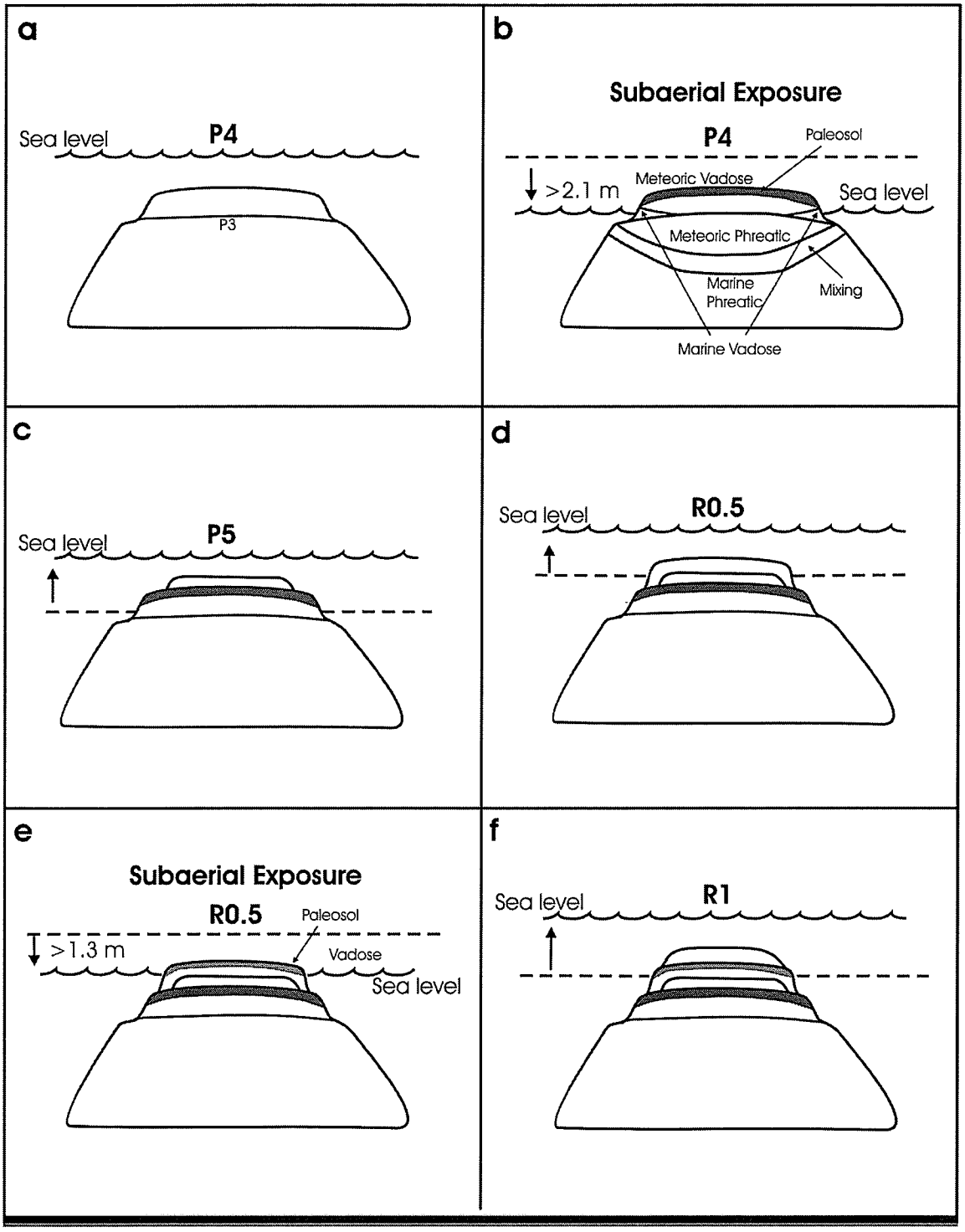


Figure 9.1 Schematic diagram illustrating the evolution of platform and reef growth from the P4 to R0.5 successions at the Snipe Lake reef complex. No vertical or horizontal scale is implied. a) Deposition of P4 succession. b) Relative sea level fall showing different diagenetic environments and development of a paleosol below the P4 subaerial exposure surface. c) Relative sea level rise and deposition of P5 succession. d) Deposition of R0.5 succession. e) Relative sea level fall and development of a paleosol below the R0.5 subaerial exposure surface. f) Relative sea level rise and deposition of the R1 succession.

(3) A subsequent rise in relative sea level initiated P5 deposition and a second phase of marine cementation in P4 sediments as secondary dissolution vugs were progressively filled by seawater (Figure 9.1c). The P5 succession was deposited during incremental pulses of relative sea level rise and normal marine cementation occurred in P5 sediments throughout deposition.

(4) A pulse of increased rate of relative sea level rise drowned the P5 platform and subsequently initiated the first stage of reef growth (Figure 9.1d). The R0.5 succession was deposited during decreased rates of relative sea level rise or prolonged stillstand conditions. Normal marine cementation occurred in R0.5 sediments throughout this period.

(5) Continued decreasing rates of relative sea level rise towards the end of the R0.5 succession followed by relative sea level fall of a minimum of 1.3 m terminated R0.5 deposition (Figure 9.1e). The upper portion of the reef was subaerially exposed and paleosols developed below the emergent surface.

(6) A subsequent rise in relative sea level slowly submerged the exposed portions of the reef and initiated a second phase of marine cementation in secondary dissolution vugs in R0.5 sediments (Figure 9.1f). Reef growth resumed with R1 deposition.

9.9 Future Work

This study presented predominantly core and petrographic evidence for subaerial exposure. Additional geochemical analysis of some of the meteoric and pedogenic

features observed in this study would prove useful. For example, microsampling techniques would allow for more accurate sampling for carbon and oxygen isotopes analysis of both pendant radiaxial fibrous calcite and pendant prismatic calcite cements. This may provide additional insight into the origin of alternating inclusion-rich and inclusion poor layers in radiaxial fibrous cements and the more inclusion-rich prismatic cements. In particular it may help to improve our understanding of the interaction of seawater and meteoric water in the precipitation of these cements.

Further investigation of the P5 megacycle contact would also be useful. The presence of a well-developed paleosol profile, as described in section 8.6, is problematic for the current interpretation of an increased pulse of relative sea level rise at the end of P5 deposition. Detailed core and petrographic analysis of the P5 interval in the platform interior may provide some insight into the origin of the paleosol and either prove or disprove a postulated minor relative sea level fall at that stratigraphic level.

CHAPTER 10 – CONCLUSIONS

10.1 Lithofacies Analysis

Nine lithofacies have been recognized in the P4 to R0.5 successions in the Snipe Lake reef complex based on detailed core and thin section examination:

(1) Lithofacies A (peloid packstones) is composed of tan to light brown lime mudstones to peloid/peloid-skeletal packstones. Locally it may include light brown to grey *Amphipora* floatstones with a peloid wackestone to packstone matrix. Crinkly to parallel laminations, fenestrae and light to dark grey mottling may be present. This lithofacies is interpreted to have been deposited in a low energy, tidal flat environment.

(2) Lithofacies B (robust branching cylindrical stromatoporoid rudstones) is composed of medium brown to grey, robust branching cylindrical stromatoporoid rudstones and local floatstones. Matrix may be present and consists of peloid packstones to grainstones. Shelter porosity is commonly well developed. This lithofacies is interpreted to represent beach deposits that were deposited along high energy shorelines.

(3) Lithofacies C (branching cylindrical stromatoporoid floatstones) is composed of tan to medium brown, branching cylindrical stromatoporoid floatstones to rudstones with a peloid to peloid-skeletal packstone to grainstone matrix. This lithofacies is interpreted to have been deposited in a moderate energy, shallow subtidal lagoonal environment.

(4) Lithofacies D (light tan *Amphipora* floatstones) is composed of tan to medium brown, *Amphipora* floatstones to rudstones with a peloid wackestone to packstone matrix. Floatstone and rudstone intervals may be locally interbedded. This lithofacies is interpreted to have been deposited in a low to moderate, shallow subtidal lagoonal environment.

(5) Lithofacies E (dark brown *Amphipora* rudstones) is composed of medium to dark brown, *Amphipora* floatstones to rudstones. The matrix is typically a carbonaceous peloid wackestone but can vary from carbonaceous lime mudstones to peloid-intraclast grainstones. Floatstone and rudstone intervals may be interbedded. Fining upward sequences ranging from rudstones to floatstones to lime mudstones may be observed. This lithofacies is interpreted to have been deposited in a low energy, subtidal lagoonal environment with poorly oxygenated and euryhaline conditions.

(6) Lithofacies F (stromatoporoid floatstones to rudstones) is composed of tan to light grey, stromatoporoid floatstones to rudstones with a peloid-skeletal grainstone matrix. Stromatoporoid fragments include robust branching, bulbous, hemispherical, thick tabular, thin tabular and nodular varieties. Interparticle and intraparticle porosity is well developed (2-10%) in this lithofacies. Lithofacies F is interpreted to have been deposited in a high energy, open marine subtidal environment.

(7) Lithofacies G (tabular stromatoporoid rudstones) is composed of light to medium brown, branching cylindrical and tabular stromatoporoid floatstones to rudstones, and possible local boundstones. The matrix ranges from poorly sorted peloid-

skeletal wackestones to grainstones. This lithofacies is interpreted to have been deposited in a low to moderate energy, well circulated subtidal environment.

(8) Lithofacies H (dark brown thin tabular stromatoporoid floatstones) is composed of medium to dark brown, thin tabular stromatoporoid floatstones to rudstones, and possible local boundstones. The matrix ranges from carbonaceous peloid wackestones to packstones. This lithofacies is interpreted to have been deposited in a low energy, slightly restricted, deep subtidal environment.

(9) Lithofacies I (skeletal grainstones) is composed of tan to medium brown, skeletal to skeletal-peloid packstones to grainstones. Micritized skeletal fragments include branching cylindrical stromatoporoids, thick and thin tabular stromatoporoids, brachiopods, crinoids, rare ostracods and calcareous algae. Interparticle porosity is well developed (10-15%) in this lithofacies. Lithofacies I is interpreted to have been deposited in a high energy, open marine environment.

These nine lithofacies are genetically grouped into two lithofacies associations:

(1) The reef margin lithofacies association is composed of lithofacies F, G, H and I and is interpreted to represent deposition in the reef flat and reef foreslope environment. Lithofacies F is interpreted to represent the highest energy, open marine conditions that are most proximal to the zone of continuous wave action in the reef flat. Lithofacies G and H are interpreted to represent deposition in progressively decreasing energy and restricted marine conditions down the reef foreslope environment. Lithofacies I is interpreted to represent allochthonous

foreslope sands that were deposited throughout the shallow foreslope environment.

(2) The lagoonal lithofacies association is composed of lithofacies A, B, C, D and E and is interpreted to represent deposition in the lagoonal environment in the platform interior and reef interior. Lithofacies A is interpreted to have been deposited along low energy shorelines in the tidal flat, whereas lithofacies B represents beachrock deposits along higher energy shorelines. Lithofacies C, D and E are interpreted to be subtidal lagoonal deposits. Lithofacies C represents deposition in the most open, highest energy conditions along the shallowest part of the lagoon directly behind the platform and reef margin. Lithofacies D and E are interpreted to represent deposition in progressively deeper and more restricted conditions towards the center of the lagoon.

10.2 Platform-Reef Cyclicity

The P4 to R0.5 succession in the Snipe Lake reef complex is composed of several third-order reefal cycles and fourth-order lagoonal cycles:

(1) Third-order reefal cycles characterize the reef margin setting in the R0.5 succession. When completely developed, each reefal cycle consists of a shallowing-upward succession from lower foreslope lithofacies (lithofacies H) to middle foreslope lithofacies (lithofacies G) to reef flat/upper foreslope lithofacies (lithofacies F). Foreslope sands (lithofacies I) may be present at or near the base of cycles. Reefal cycles are interpreted to represent deposition in more competent

environments near the reef margin where the reef was able to keep up with the rate of relative sea level rise.

(2) Fourth-order lagoonal cycles characterize deposition in the platform and reef interior in the P4, P5 and R0.5 successions. When completely developed, each lagoonal cycle consists of a shallowing-upward succession from deep lagoonal lithofacies (lithofacies E) to open lagoonal lithofacies (lithofacies C or D) to tidal flat lithofacies (lithofacies A or B). Lagoonal cycles are interpreted to reflect incremental pulses of small-scale relative sea level rises that together make-up a third-order cycle.

Lagoonal cycles were correlated throughout the platform and reef interior in the P5 and R0.5 successions based on the following criteria: (1) their stratigraphic occurrence within the each megacycle; (2) the similarity of lithofacies between locations and (3) evidence for shallowing-upward conditions near the top of each cycle.

10.3 Platform and Reef Megacycles (P4 to R0.5)

(1) P4 Megacycle**:**

The P4 succession backstepped in a southwesterly direction and thickens from the platform margin towards the platform interior. Shallow tidal flat and beach lithofacies (lithofacies A and B, respectively) are overlain by shallow lagoonal lithofacies (lithofacies C and D) at the P4 megacycle contact. Green shales and other pedogenic and meteoric diagenetic features are commonly developed directly below the P4 megacycle contact. The P4 succession is interpreted to

reflect deposition during increasing rates of relative sea level rise and was terminated by subaerial exposure at the top of the megacycle.

(2) P5 Megacycle:

Similar to the P4 succession, the P5 platform margin significantly backstepped in a southwesterly direction and is also accompanied by a thickening from the platform margin to the platform interior. The P5 succession is composed of a series of shallowing-upward lagoonal cycles that increase in abundance towards the platform interior. A marine hardground commonly occurs at the top of the P5 megacycle. P5 deposition is interpreted to have occurred during increasing rates of relative sea level rise and was terminated by a pulse of increased rates of relative sea level rise.

(3) R0.5 Succession:

The R0.5 succession represents the initial phase of reef growth in the Snipe Lake reef complex. It is characterized by a progradational reef margin that resulted in an overhang above the backstepped P4 and P5 successions. It shows a thickening from the reef interior to the reef margin. The R0.5 succession is composed of a reefal cycle at the reef margin and a series of shallowing-upward lagoonal cycles in the reef interior. Shallow tidal flat to reef flat lithofacies (lithofacies A, B, C, D or F) are overlain by relatively deeper subtidal lagoonal lithofacies (lithofacies D or E) at the R0.5 megacycle contact. Green shales and other pedogenic and meteoric diagenetic features are also commonly developed below the contact. The R0.5 succession is interpreted to reflect deposition during a period of slower

rates of relative sea level rise or prolonged stillstand conditions, which was terminated by subaerial exposure at the top of the succession.

10.4 Paragenetic Sequence

Petrographic and geochemical data have identified multiple phases of diagenesis in the carbonate rocks below the P4 and R0.5 subaerial exposure surfaces in the Snipe Lake reef complex:

(1) Early Marine Diagenesis:

Early marine diagenesis occurred shortly after the sediments were deposited (marine phreatic). Brown micritic cements (i.e. micrite envelopes) are the earliest evidence for diagenetic alteration. These features are followed by the precipitation of isopachous fibrous calcite that precipitated around the interior of intraskeletal pore spaces and around grains. These cements may be gradational with pendant radiaxial fibrous calcite cements that are developed in primary pores. The pendant cements are interpreted to have formed in the marine vadose zone in the intertidal zone, possibly just prior to exposure.

(2) Meteoric Diagenesis:

Geopetal crystal silt occurs at the bottom of interparticle pores, fenestrae and dissolution vugs. It formed in the vadose zone as earlier cements detached from pore ceilings and accumulated at the bottom of pore spaces. Other vadose zone cements include pendant prismatic calcite with inclusions concentrated in distinct laminae, which developed in shelter pores under *Amphipora* grains and in intraskeletal pores. Meniscus blocky calcite cements also precipitated in the

vadose zone. Syntaxial calcite overgrowth precipitated throughout the meteoric vadose and phreatic environments. Dissolution and the development of dissolution vugs also likely occurred throughout the meteoric environments but was more extensive in the vadose zone. Isopachous prismatic calcite cements precipitated around the interior of intraskeletal and interskeletal pores, dissolution vugs, cracks and around grains in the phreatic zone.

(3) Late Marine Diagenesis:

A second phase of marine diagenesis resulted as relative sea level started to rise after subaerial exposure and pores were progressively filled with seawater. Initially, pores in the intertidal zone were only partially filled by seawater and pendant radiaxial fibrous calcite cements precipitated in secondary dissolution vugs. Rare isopachous fibrous calcite cements precipitated in dissolution vugs as pores were completely filled by seawater in the phreatic zone.

(4) Burial Diagenesis:

Shallow burial cements include ferroan to non-ferroan blocky to prismatic calcite cements, blocky calcite mosaics and euhedral to subhedral zoned dolomite rhombs. A second stage of dissolution is interpreted to have followed creating minor vuggy porosity. Zoned saddle dolomites are the latest burial cements.

The $\delta^{13}C$ values for marine cements (isopachous fibrous calcite and pendant radiaxial fibrous calcite) are comparable to other Upper Devonian marine calcite cements and are interpreted to reflect a marine carbon source. Similarly, meteoric features including pendant prismatic cements and crystal silt have $\delta^{13}C$ compositions that indicate a marine

carbon source that has been minimally influenced by soil-gas CO_2. $\delta^{13}C$ values for burial cements (blocky calcite mosaics and saddle dolomites) also indicate a marine carbon source.

Overall, stable oxygen isotope data from this study can be used with discretion to support petrographic evidence. The $\delta^{18}O$ composition of isopachous fibrous calcite (-10.2‰) and pendant radiaxial fibrous calcite (-9.6 to -6.2‰) cements are depleted with respect to typical Devonian marine cements. These light values are interpreted to have been affected by re-equilibration during later diagenesis, contamination by other cements and potential contamination from inclusion-poor layers precipitated from meteorically influenced waters. Light $\delta^{18}O$ composition of pendant prismatic calcite cements (-9.0 to -7.8‰) support a meteoric origin. However, these cements may have also been affected by isotopic re-equilibration and, to a lesser extent, contamination. Further depleted $\delta^{18}O$ values for blocky calcite mosaics (-11.1 to -10.5‰) and saddle dolomites (-10.8 to -10.1‰) support a burial origin for these cements.

10.5 Subaerial Exposure Features

A variety of pedogenic features have been described below the P4 and R0.5 subaerial exposure surfaces in the Snipe Lake reef complex:

(1) Rhizoliths are tubular to cylindrical in shape and have vertical to horizontal orientations. They range from 0.5 to 11 cm in length and may have dark brown micritic cutans.

(2) Marine pendant cements are developed in dissolution vugs and meteoric pendant cements are developed in shelter pores and intraskeletal pores.

(3) Green shales occur as massive green shale beds, mottled green shale beds and filling pore spaces. They are partially to completely dolomitized (dolomicrite) and clay mineralogy is predominantly illite with minor amounts of kaolinite. Massive green shale beds (1.5-30 cm thick) range from massive to weakly laminated. Mottled green shale beds (15-49 cm thick) are composed of dolomicrite and have a distinctive mottled to nodular texture and desiccation cracks. Green shales also commonly fill cracks, dissolution vugs and interparticle pores. Green shales may show weakly developed illuviation textures. Mineralogically, these green shales are distinct from equivalent basinal green shales.

(4) Laminar calcretes (0.1-6.0 mm thick) consist of finely laminated deposits that may be composed of yellow to green argillaceous laminae, dark brown micritic laminae and dark brown opaque laminae. They are interpreted to have formed from the accumulation of carbonate and/or detrital material on indurated substrates on top of or within soil.

(5) Fitted-fabric lithoclasts are angular lithoclasts in a green shale matrix that can be fitted back together like pieces of a jigsaw puzzle. These are interpreted to have formed from in-situ brecciation of lithoclasts as a result of drying and wetting cycles in the soil matrix.

(6) Glaebules are local concentrations of secondary carbonate material within a soil (dolomicrite) matrix. They are elliptical in shape and range from calcareous

(lithorelict cores) to dolomitic in composition. Glaebules commonly have circumgranular and septarian cracks which are interpreted to be the result of repetitive drying and wetting.

(7) Peds or aggregates of soil (dolomicrite) range from spherical to elliptical in shape. They are only poorly to moderately developed in the Snipe Lake complex. Peds formed from the swelling and shrinking of soil resulting in the formation of distinctive crack patterns and segregated lumps of soil.

The overall positive $\delta^{13}C$ values for pedogenic features in this study are interpreted to reflect a marine carbon source and to have been relatively unaffected by soil-gas CO_2. Light $\delta^{18}O$ isotopic signatures for a rhizolith (-8.1‰) and laminar calcretes (-10.2 to -6.3‰) are interpreted to reflect meteoric water composition but may have been affected by contamination. $\delta^{18}O$ compositions for dolomitized green shales (-9.2 to -3.9‰) and a single glaebule (-5.7‰) are intermediate between meteoric and marine cements. This is interpreted to reflect a mixed meteoric-marine origin for dolomitizing fluids.

10.6 Paleosols

Four paleosol profiles types have been characterized below the P4 and R0.5 subaerial exposure surfaces in the Snipe Lake reef complex:

(1) The type A paleosol profile (0.75 to 2.1 m thick) has green shale beds, fitted-fabric lithoclasts and rhizoliths developed in the upper portion of the paleosol in tidal flat lithofacies. Green shales and marine pendant cements in dissolution

vugs and cracks and meteoric pendant cements occur lower in the profile in open lagoon lithofacies. Laminar calcretes occur throughout the profile.

(2) The type B paleosol profile (0.60 to 1.3 m thick) is composed of mottled green shale beds at the top of the paleosol. Desiccation cracks, fitted-fabric lithoclasts, meteoric pendant cements, glaebules and peds are commonly developed in the green shale horizon. Green shales filling cracks and dissolution vugs occur in the underlying open lagoon lithofacies.

(3) The type C paleosol profile (0.12 to 1.2 m thick) has green shale beds and fitted-fabric lithoclasts developed in the upper portions of the paleosol in tidal flat or beach lithofacies. Green shales filling cracks and dissolution vugs occur lower into the profile in open lagoon lithofacies. Marine pendant cements in dissolution vugs are also more common in the lower open lagoon lithofacies. Laminar calcretes are common throughout the profile.

(4) The type D paleosol profile (0.43 to 1.0 m thick) is developed in reef flat lithofacies with well-developed dissolution vugs occluded by green shales and marine pendant cements. Laminar calcretes occur throughout the profile.

The P4 subaerial exposure surface is characterized predominantly by the type A paleosol profile (rarely type B) and ranges from 0.75 to 2.1 m thick. The R0.5 subaerial exposure surface is more variable, is characterized by types B, C and D paleosol profiles and ranges from 0.12 to 1.3 m thick. In one single well location, the P5 megacycle contact is characterized by the type B paleosol profile (1.1 m thick).

The four paleosol types show a consistent vertical pattern of pedogenic features. Massive green shale beds, mottled green shale beds and rhizoliths occur in the upper portions of paleosols, typically in tidal flat lithofacies or muddy open lagoon facies. Dissolution vugs occluded by green shales and marine pendant cements are more common in lower portions of paleosols, commonly in open lagoon or reef flat lithofacies. Laminar calcretes are common throughout paleosol profiles.

Key pedogenic features (green shales, rhizoliths, laminar calcretes, marine pendant cements in dissolution vugs and meteoric pendant cements) occur throughout the platform-reef interior and margin below the P4 and R0.5 subaerial exposure surfaces. There is no apparent correlation with paleotopography on the subaerial exposure surfaces.

10.7 Controls on the P4 and R0.5 Subaerial Exposure Surfaces

The P4 and R0.5 subaerial exposure surfaces are interpreted to be a result of relative sea level fall, based on (1) the development of pedogenic and meteoric diagenetic features in subtidal lithofacies, (2) the lateral continuity of paleosols across the P4 and R0.5 stratigraphic levels in the Snipe Lake reef complex and (3) the superposition of subaerial exposure surfaces directly over subtidal lithofacies.

The extent of relative sea level fall can be estimated from the depth of vadose diagenesis below a subaerial exposure surface. An estimated minimum relative sea level fall of 2.1 m and 1.3 m is interpreted to have occurred at the P4 and R0.5 subaerial exposure surfaces, respectively.

There are number of other extrinsic and intrinsic factors that control the development of paleosols and meteoric diagenesis below subaerial exposure surfaces:

(1) Climate is considered to be one of the most important factors in the development of paleosols. The WCSB was located in the arid to semiarid, easterly trade wind belt during the Late Devonian which had suitable conditions for paleosol development.

(2) Topography appears to have had no significant influence on the development of paleosols below the P4 and R0.5 subaerial exposure surfaces in this study.

(3) Vegetation and soil organisms are interpreted to have played no significant role in the development of these paleosols, based on the paucity of rhizoliths, bioturbation and burrows within paleosols. Relatively positive $\delta^{13}C$ values suggest minimal influence from soil-gas CO_2.

(4) Longer duration of exposure is interpreted to account for the relatively better developed and thicker paleosols below the P4 subaerial exposure surface compared to the R0.5 subaerial exposure surface.

(5) Substrate controls are interpreted to have played an important role in the type of pedogenic features that developed. Low porosity and low permeability host rocks such as tidal flat lithofacies are more likely to have had detrital sediment and pedogenic carbonate accumulate in massive and mottled green shale beds. In contrast, dissolution vugs are more common in more porous and permeable host rocks such as open lagoon and reef flat lithofacies. These dissolution vugs are then subsequently occluded by green shales and marine pendant cements.

Depositional cycles influenced the vertical distribution of lithofacies and therefore the type of paleosol profile.

(6) Erosion during subaerial exposure or the subsequent transgression is interpreted to significantly affect the preservation of paleosol profiles. Often the upper portions of paleosols were removed by erosion and, in some locations, paleosols were completely removed.

10.8 Localized Subaerial Exposure Surfaces

Local subaerial exposures surfaces above and below the P4 and R0.5 paleosols are interpreted to be a result of autocyclic processes such as rapid sediment accumulation or reef aggradation, based on the following reasons: (1) they typically occur at the top of shallowing-upward lagoonal cycles, (2) they have a very patchy and irregular areal distribution, (3) they have very thin profiles and (4) there is no evidence linking these features to the P4 and R0.5 subaerial exposure surfaces.

10.9 Effect on Reservoir Quality

Subaerial exposure is interpreted to have had relatively minor effect on reservoir quality in the Snipe Lake reef complex. In fact, paleosols may represent a permeability barrier. The lack of porosity development is attributed to (1) a relatively small magnitude of relative sea level fall and therefore a relative short period of exposure to meteoric fluids, (2) limited dissolution by meteoric waters in arid to semiarid climates, (3) the relatively stable original mineralogy (calcite), (4) low porosity and low permeability sediments below the P4 and R0.5 subaerial exposure surfaces, which would have restricted the

amount of meteoric flow, and (5) occlusion of secondary pores by green shales and cements (e.g. pendant radiaxial fibrous calcite, isopachous prismatic calcite, blocky-prismatic calcite, blocky calcite mosaics and saddle dolomites).

10.10 Sea level History (P4 to R0.5)

This study uses an integrated approach that combines stratigraphy, sedimentology, detailed petrography and geochemistry to interpret the sea level history of the Snipe Lake reef complex, which is summarized below:

(1) P4 deposition was initiated by a pulse of accelerated relative sea level rise and continued during increasing rates of relative sea level rise. P4 platform growth was terminated by a relative sea level fall with an estimated minimum magnitude of 2.1 m.

(2) P5 deposition resumed during a subsequent relative sea level rise and was later drowned by a pulse of rapid relative sea level rise.

(3) The first stage of reef growth, the R0.5 succession, initiated after drowning of the P5 platform and continued during a period of decreased relative sea level rise or stillstand conditions. The R0.5 succession was later subaerially exposed as a result of relative sea level fall which has an estimated minimum magnitude of 1.3 m.

(4) Reef deposition resumed with the R1 reef megacycle during a subsequent gradual rise in relative sea level.

REFERENCES

Abbott, B. M. 1973. Terminology of stromatoporoids. Journal of Paleontology, v. 47, p. 805-806.

Adams, A.E., Mackenzie, W.S. and Guilford, C. 1984. Atlas of Sedimentary Rocks under the Microscope. John Wiley and Sons Inc, New York, 104 p.

Allan, J.R. and Matthews, R.K. 1982. Isotopic signatures associated with early meteoric diagenesis. Sedimentology, v. 29, p. 797-817.

Allan, J.R. and Wiggins, D.W. 1992. Dolomite Reservoirs: Geochemical Techniques for Evaluating Origin and Distribution. AAPG Continuing Education Course Notes 36, AAPG Special Publications, 167p.

Al-Aasm, I.S., Taylor, B.E. and South, B. 1990. Stable isotope analysis of multiple carbonate samples using selective acid extraction. Chemical Geology (Isotope Geoscience Section), v. 80, p. 119-125.

Alonso-Zarza, A.M. 1999. Initial stages of laminar calcrete formation by roots: examples from the Neogene of central Spain. Sedimentary Geology, v. 126, p. 177-191.

Alonso-Zarza, A.M. 2003. Palaeoenvironmental significance of palustrine carbonates and calcretes in the geological record. Earth Science Reviews, v. 60, p. 261-298.

Amthor, J.E. and Friedman, G.M. 1992. Early-to-late diagenetic dolomitization of platform carbonates: Lower Ordovician Ellenburger Group, Permian Basin, West Texas. Journal of Sedimentary Petrology, v. 62, p. 131-144.

Amthor, J.E., Mountjoy, E.W. and Machel, H.G. 1993. Subsurface dolomites in Upper Devonian Leduc Formation buildups, central part of Rimbey-Medowbrook reef trend, Alberta, Canada. Bulletin of Canadian Petroleum Geology, v. 41, p. 164-185.

Arakel, A.V. 1982. Genesis of calcrete in Quaternary soil profiles, Hutt and Leeman lagoons, Western Australia. Journal of Sedimentary Petrology, v. 52, p. 109-152.

Badiozamani, K. 1973. The Dorag dolomitization model – application to the Middle Ordovician of Wisconsin. Journal of Sedimentary Petrology, v. 43, p. 965-984.

Bain, R.J. and Foos, A.M. 1991. Carbonate microfabrics related to subaerial exposure and paleosol formation. *In*: Carbonate Microfabrics. R. Rezak and D. Lavoie (eds.). Springer-Verlag, Berlin, p. 19-28.

Banks, H.P. 1984. The early history of land plants. *In*: Paleobotany Part I, Precambrian through Permian. Taylor, T.N. and Smoot, E.D (eds.). Van Nostrand Reinhold Company, New York, p. 111-126.

Beach, D.K. 1995. Controls and effects of subaerial exposure on cementation and development of secondary porosity in the subsurface of the Great Bahama Bank. *In*: Unconformities and Porosity in Carbonate Strata. D.A. Budd, A.H. Saller and P.M. Harris (eds.). American Association of Petroleum Geologists, Memoir 63, p. 1-35.

Blodgett, R.H. 1988. Calcareous paleosols in the Triassic Dolores Formation, southwestern Colorado. *In*: Paleosols and Weathering Through Geological Time: Principles and Applications. Geological Society of America, Special Paper 216, p. 103-121.

Brachert, T.C. and Dullo, W-C. 1991. Laminar micrite crusts and associated foreslope processes, Red Sea. Journal of Sedimentary Petrology, v. 61, p. 354-363.

Brewer, R. 1964. Fabric and Mineral Analysis of Soils. New York, John Wiley and Sons, 470 p.

Burrowes, O.G. and Krause, F.F. 1987. Overview of the Devonian system: subsurface Western Canada Basin. In: Devonian Llithofacies and Reservoir Styles in Alberta. O.G. Burrowes and F.F Krause (eds.). 13th Canadian Society of Petroleum Geologists, Core Conference and Second International Symposium on the Devonian System, p. 1-20.

Campbell, C.V. 1992. Beaverhill Lake megasequence. *In*: Devonian-Early Mississippian Carbonates of the Western Canada Sedimentary Basin: A Sequence Stratigraphic Framework. J.C. Wendte, F.A. Stoakes and C.V. Campbell (eds.). Society for Sedimentary Geology, Short Course 28, p. 163-181.

Carpenter, S.J. and Lohmann, K.C. 1989. $\delta^{18}O$ and $\delta^{13}C$ variations in Late Devonian marine cements from the Golden Spike and Nevis reefs, Alberta, Canada. Journal of Sedimentary Petrology, v. 59, p. 792-814.

Carpenter, S.J. and Lohmann, K.C. 1997. Carbon isotope ratios of Phanerozoic marine cements: re-evaluating the global carbon and sulfur systems. Geochimica et Cosmochimica Acta, v. 61, p. 4831-4846.

Carpenter, S.J., Lohmann, K.C., Holden, P., Walter, L.M., Huston, T.J. and Halliday, A.H. 1991. $\delta^{18}O$ values, $^{87}Sr/^{86}Sr$ and Sr/Mg ratios of Late Devonian abiotic marine calcite: Implications for the composition of ancient seawater. Geochimica et Cosmochimica Acata, v. 55, p. 1991-2010.

Carroll, D. 1970. Clay minerals: a guide to their x-ray identification. Geological Society of America, Special Paper 126, 80 pp.

Catuneanu, O. 2002. Sequence stratigraphy of clastic systems: concepts, merits and pitfalls. Journal of African Earth Sciences, v. 35, p. 1-43.

Cerling, T.E. 1999. Stable isotopes in paleosol carbonates. *In*: Palaeoweathering, Palaeosurfaces and Related Continental Deposits. M. Thiry and S. Rimon-Coinçon (eds.). International Association of Sedimentologists, Special Publication Number 27, Blackwell Science, p. 43-60.

Choquette, P.W. and James, N.P. 1990. Limestones - The burial diagenetic environment. *In*: Diagenesis. I.A. McIlreath and D.W. Morrow (eds.). Geoscience Canada, Reprint Series, p.75-111.

Choquette, P.W. and Pray, L.C. 1970. Geologic nomenclature and classification of porosity in sedimentary carbonates. American Association of Petroleum Geologists Bulletin, v. 54, p. 207-250.

Chow, N. and Longstaffe, F.J. 1995. Dolomites of the Middle Devonian Elm Point Formation, southern Manitoba: intrinsic controls on early dolomitization. Bulletin of Canadian Petroleum Geology, v. 43, p. 214-225.

Chow, N. and Wendte, J. 2004. Subaerial exposure surfaces in the Judy Creek reef complex (Upper Devonian), west-central Alberta, Canada. I.C.E. 2004: CSPG, CHOA, CWLS Joint Conference, Calgary, Alberta.

Compton, R.R. 1985. Appendix 3 – Percent diagrams for estimating rock compositions by volume. *In*: Geology in the Field. John Wiley & Sons, Inc., United States of America, 416 p.

Delgado, F. 1977. Primary textures in dolostones and recrystallized limestones: a technique for their microscopic study. Journal of Sedimentary Petrology, v. 47, p. 1339-1341.

Demaison, G.J. and Moore, G.T. 1980. Anoxic environments and oil source bed genesis. Organic Geochemistry, v. 2, p. 9-31.

Dickson, J.A.D. 1955. A modified staining technique for carbonates in thin section. Nature, v. 205, p. 587.

Dickson, J.A.D. 1966. Carbonate identification and genesis as revealed by staining. Journal of Sedimentary Petrology, v. 36, p. 491-505.

Dickson, J.A.D. 1990. Carbonate mineralogy and chemistry. *In*: Carbonate Sedimentology. M.E. Tucker and V.P. Wright (eds.). Blackwell Scientific Publications, Oxford, p. 284-313.

Dilks, A. and Graham, S.C. 1985. Quantitative mineralogical characterization of sandstones by back-scattered electron image analysis. Journal of Sedimentary Petrology, v. 55, p. 347-355.

Dravis, J.J. 1991. Carbonate petrography – update on new techniques and applications. Journal of Sedimentary Petrology, v. 61, p. 626-628.

Dravis, J.J. and Yurewicz, D.A. 1985. Enhanced carbonate petrography using fluorescence microscopy. Journal of Sedimentary Petrology, v. 55, p. 795-804.

Dreise, S.G. and Foreman, J.L. 1992. Paleopedology and paleoclimatic implications of Late Ordovician vertic paleosols, Juniata Formation, Southern Appalachians. Journal of Sedimentary Petrology, v. 62, p. 71-83.

Drever, J.I. 1973. The preparation of oriented clay mineral specimens for x-ray diffraction analysis by a filter-membrane peel technique. American Mineralogist, v. 58, p. 553-554.

Duggan, James, P. 2004. Burial dolomites at Swan Hills Simonette Reef, West Central Alberta Basin. Dolomites: Mechanisms, Models, Reservoir Development, Canadian Society of Petroleum Geologists, Seminar and Core Conference, Calgary.

Duggan, J.P., Mountjoy, E.W. and Stasiuk, L.D. 2001. Fault-controlled dolomitization at Swan Hills Simonette oil field (Devonian), Deep Basin, west-central Alberta, Canada. Sedimentology, v. 48, p. 301-323.

Dunham, R.J. 1962. Classification of carbonate rocks according to depositional texture. Classification of Carbonate Rocks – A Symposium. American Association of Petroleum Geologists, Memoir 1, p. 108-121.

Dunham, R.J. 1969. Early vadose silt in Townsend Mount (reef), New Mexico. *In*: Depositional Environments in Carbonate Rocks: a Symposium. G.M. Friedman (ed). Society of Economic Palaeontologists and Mineralogists, Special Publication 14, p. 182-192.

Elick, J.M., Driese, S.G. and Mora, C.I. 1998. Very large plant and root traces from the Early to Middle Devonian: implications for early terrestrial ecosystems and atmospheric $p(CO_2)$. Geology, v. 26, p. 143-146.

Embry, A. F., 2002. Transgressive-regressive (T-R) sequence stratigraphy. *In*: Sequence Stratigraphic Models for Exploration and Production. J.M. Armentrout and N.C. Rosen (eds.). Gulf Coast Section Society for Sedimentary Geology Conference Proceedings, Houston, p. 151-172.

Embry, A.F and Klovan, J.E. 1971. A late Devonian reef tract on northeastern Banks Island, N.W.T. Bulletin of Canadian Petroleum Geology, v. 19, p. 730-781.

Esteban, M., and Klappa, C.F. 1983. Subaerial exposure environment. *In*: Carbonate Depositional Eenvironments. P.A. Scholle, D.G. Bebout and C.H. Moore (eds.). American Association of Petroleum Geologists, p. 2-53.

Ettensohn, F.R., Garland, R.D, Jr., and Grow, J.S. 1988. A paleosol interpretation for profiles exhibiting subaerial exposure "crusts" from the Mississippian of the Appalachian Basin. *In*: Paleosols and Weathering Through Geological Time: Principles and Applications. Geological Society of America, Special Paper 216, p. 49-79.

Fairchild, I., Hendry, G., Quest, M and Tucker, M. 1988. Chemical analysis of sedimentary rocks. *In*: Techniques in Sedimentology. M. Tucker (ed.). Blackwell Scientific Publications, Oxford, London, Edinburgh, Boston, Palo Alto, Melbourne, p. 274-354.

Fedoroff, N., Country, M.A., Lacroix, E. and Oleschko, K. 1994. Calcitic accretion of indurated volcanic materials (example of tepetates, Altiplano, Mexico). Proc. XVth Congress, Soil Science, Acapulo, vol. 6A, p. 459-472.

Fischbuch, N.R. 1968. Stratigraphy, Devonian Swan Hills reef complexes of central Alberta. Bulletin of Canadian Petroleum Geology, v. 16, p. 446-587.

Fischbuch, N.R. 1969. Devonian stromatoporoids from Central Alberta, Canada. Canadian Journal of Earth Sciences, v. 6, p. 167-185.

Fischbuch, N.R. and Havard, C.G. 1977. Facies – porosity relationships and diagenetic processes which modify them, Swan Hills Area, Alberta. *In*: The Geology of Selected Carbonate Oil, Gas and Lead-Zinc Reservoirs in Western Canada. I.A. McIlreath and R.D. Harrison (eds.). Canadian Society of Petroleum Geologists, Canadian Society of Petroleum Geologists Core Conference 5, Calgary, Alberta, p. 41-66.

Folk, R.L. 1962. Spectral subdivision of limestone types. American Association of Petroleum Geologists Memoir, v. 1, p. 62-84.

Folk, R.L. 1987. Detection of organic matter in thin sections of carbonate rocks using a white card. Sedimentary Geology, v. 54, p. 193-200.

Fong, G. 1959. Type section Swan Hills Member of the Beaverhill Lake Formation. Journal of the Alberta Society of Petroleum Geologists, v.7, p. 95-108.

Fong, G. 1960. Geology of Devonian Beaverhill Lake Formation, Swan Hills Area, Alberta, Canada. Bulletin of the American Association of Petroleum Geologists, v. 44, p. 195-209.

Fu, Q., Qing, H., and Bergman, K. 2004a. Early dolomitization of the Middle Devonian Ratner laminites by diffusion and recrystallization of dolomite in the Elk Point Basin of Saskatchewan, Canada. I.C.E. 2004: Canadian Society of Petroleum Geologists, Canadian Heavy Oil Association and Canadian Well Logging Society Joint Conference, Calgary, Alberta.

Fu, Q., Qing, H., and Bergman, K. 2004b. Dolomitized calcrete in the Middle Devonian Winnipegosis carbonate mounds, subsurface of south-central Saskatchewan, Canada. Sedimentary Geology, v. 168, p. 49-69.

Gensel, P.G. and Andrews, H.N. 1984. Plant Life in the Devonian. Praeger, New York, 380p.

Goldstein, R.H. 1991. Stable isotope signatures associated with paleosols, Pennsylvanian Holder Formation, New Mexico. Sedimentology, v. 38, p. 67-77.

Goldstein, R.H., Anderson, J.E., and Bowman, M.W. 1991. Diagenetic responses to sea-level change: Integration of field, stable isotope, paleosol, paleokarst, fluid inclusion, and cement stratigraphy research to determine history and magnitude of sea-level fluctuation. *In*: Sedimentary Modeling: Computer Simulations and Methods for Improved Parameter Definition. E.K. Franseen, W.L. Watney, C. Kendall and W. Ross (eds.). Kansas Geological Survey, Bulletin 233, p. 139-162.

Gonalez, L.A., and Lohmann, K.C. 1988. Controls on mineralogy and composition of spelean carbonates: Carlsbad Caverns, New Mexico. *In*: Paleokarst. N.P. James and P.W. Choquette (eds.). Springer, New York, p. 81-101.

Hanor, J.S. 1978. Precipitation of beach rock cements: mixing of marine and meteoric waters vs. CO_2 degassing. Journal of Sedimentary Petrology, v. 48, p. 489-502.

Hardy, R.G and Tucker, M.E. 1988. X-ray powder diffraction of sediments. *In*: Techniques in Sedimentology. M. Tucker (ed.). Blackwell Scientific Publications, Oxford, London, Edinburgh, Boston, Palo Alto, Melbourne, Blackwell Scientific Publications, p. 191-228.

Harrison, R.S. and Steinen, R.P. 1978. Subaerial crust, caliche profiles, and breccia horizons: comparisons of some Holocene and Mississippian exposure surfaces, Barbados and Kentucky. Geological Society of America Bulletin, v. 89, p. 385-396.

Havard, C.J. 1974. Sedimentary and early diagenetic cycles, Snipe Lake reef complex, Alberta. Unpublished M.Sc. Thesis, University of Calgary, 125 p.

Havard, C. and Oldershaw, A. 1976. Early diagenesis in back-reef sedimentary cycles, Snipe Lake reef complex, Alberta. Bulletin of Canadian Petroleum Geology, v. 24, p. 27-69.

Heckel, P.H. and Witzke, B.J. 1979. Devonian world paleogeography determined from distribution of carbonates and related lithic paleoclimatic indicators. *In*: The Devonian System. M.R. House, C.T Scrutton and M.G. Bassett (eds.). Palaeontological Association, London, Special Papers in Palaeontology, p. 99-123.

Hemphill, C.R., Smith, R.I., and Szabo, F. 1975. Geology of Beaverhill Lake reefs, Swan Hills area, Alberta. *In*: Geology of Giant Petroleum Fields. M.T. Halbouty (ed). American Association of Petroleum Geologists, Memoir 14, p. 50-90.

Hurley, N.F. and Lohmann, K.C. 1989. Diagenesis of Devonian reefal carbonates in the Oscar Range, Canning Basin, Western Australia. Journal of Sedimentary Petrology, v. 59, p. 127-146.

Hurley, N.F., Tanner, H.C and Barcat, C. 1995. Unconformity-related porosity development in the Quintuco Formation (Lower Cretaceous), Neuquén Basin, Argentina. *In*: Unconformities and Porosity in Carbonate Strata. D.A. Budd, A.H. Saller and P.M. Harris (eds.). American Association of Petroleum Geologists, Memoir 63, p. 159-177.

James, N.P. and Bourque, P.A. 1992. Reefs and mounds. *In*: Facies Models, Response to Sea Level Changes. R.G. Walker and N.P. James (eds.). Geological Association of Canada, Chapter 17, p. 323-348.

James, N.P. and Choquette, P.W. 1990a. Limestones - The sea-floor diagenetic environment. *In*: Diagenesis. I.A. McIlreath and D.W. Morrow (eds.). Geoscience Canada, Reprint Series, p. 13-34.

James, N.P. and Choquette, P.W. 1990b. Limestones - The meteoric diagenetic environment. *In*: Diagenesis. I.A. McIlreath and D.W. Morrow (eds.). Geoscience Canada, Reprint Series, p. 35-74.

James, N.P. and Choquette, P.W. 1990c. Limestones: Introduction. *In*: Diagenesis. I.A. McIlreath and D.W. Morrow (eds.). Geoscience Canada, Reprint Series, p. 9-11.

James, N.P. and Kendall, A.C. 1992. Introduction to carbonate and evaporite facies models. *In*: Facies Models, Response to Sea Level Changes. R.G. Walker and N.P. James (eds.). Geological Association of Canada, Chapter 14, p. 265-275.

Jenik, A.J. and Lerbekmo, J.F. 1968. Facies and geometry of Swan Hills Reef Member of Beaverhill Lake Formation (Upper Devonian), Goose River field, Alberta, Canada. American Association of Petroleum Geologists Bulletin, v. 52, p. 21-56.

Johns, W.D., Grim, R.E. and Bradley, W.F. 1954. Quantitative estimations of clay minerals by diffraction methods. Journal of Sedimentary Petrology, v. 24, p. 242-251.

Jones, B. and Desrochers, A. 1992. Shallow platform carbonates. *In*: Facies Models, Response to Sea Level Changes. R.G. Walker and N.P. James (eds.). Geological Association of Canada, Chapter 15, p. 277-302.

Kaufman, J. 1989. Sedimentology and diagenesis of the Swan Hills Formation (Middle-Upper Devonian), Rosevear Field, Alberta, Canada. Unpublished Ph.D thesis, Stony Brook State University, New York, 412 p.

Kaufman, J., Meyers, W.J., and Hanson, G.N. 1990. Burial cementation in the Swan Hills Formation (Devonian), Rosevear Field, Alberta, Canada. Journal of Sedimentary Petrology, v. 60, p. 918-939.

Kendall, A.C. 1977. Fascicular-optic calcite: a replacement of bundled acicular carbonate cements. Journal of Sedimentary Petrology, v. 47, p. 1056-1062.

Kendall, A.C. 1985. Radiaxial fibrous calcite: a reappraisal. *In*: Carbonate Cements. N. Schneidermann and P.M Harris (eds). Society of Economic Mineralogists and Paleontologists, Special Publication No. 36, p. 59-78.

Kershaw, S. 1998. The applications of stromatoporoid paleobiology in paleoenvironmental analysis. Palaeontology, v. 41, p. 509-544.

Kiessling, K., Flugel, E. and Golonka, J. 1999. Paleoreef maps: evaluation of a comprehensive database on Phanerozoic reefs. American Association of Petroleum Geologists Bulletin, v. 83, p. 1552-1587.

Klappa, C.F. 1979. Lichen stromatolites: criterion for subaerial exposure and a mechanism for the formation of laminar calcrete (caliche). Journal of Sedimentary Petrology, v. 49, p. 387-400.

Klappa, C.F. 1980. Rhizoliths in terrestrial carbonates: classification, recognition, genesis and significance. Sedimentology, v. 27, p.613-629.

Klovan, J.E. 1964. Facies analysis of the Redwater reef complex, Alberta, Canada. Bulletin of Canadian Petroleum Geology, v. 12, p. 1-100.

Kobluk, D.R. 1975. Stromatoporoid paleoecology of the southeastern margin of the Miette carbonate complex, Jasper Park Alberta. Bulletin of Canadian Geology, v. 23, p. 224-277.

Krumbein, W.E. and Giele, C. 1979. Calcification in a coccoid-cyanobacterium associated with the formation of desert stromatolites. Sedimentology, v. 26, p. 593-604.

Land, L.S. 1973. Contemporaneous dolomitization of middle Pleistocene reefs by meteoric water, north Jamaica. Bulletin of Marine Science, v. 23, p. 64-92.

Land, L.S. 1985. The origin of massive dolomite. Journal of Geological Education, v. 33, p. 112-125.

Last, W.M. 2001. Mineralogical analysis of lake sediments. *In*: Tracking Environmental Change Using Lake Sediments. Volume 2: Physical and Geochemical Methods. W.M. Last and J.P. Smol (eds.). Kluwer Academic Publishers, Dordrecht, Boston, London, Part II: Mineralogical and Geochemical Indicator Techniques, Chapter 6, p. 143-189.

Leavitt, F.M. 1966. The petrology, paleontology and geochemistry of the Carson Creek North reef complex, Alberta. Unpublished, Ph.D. Thesis, University of Alberta, 153 pp.

Leavitt, F.M. and Fischbuch, N.R. 1968. Devonian nomenclatural changes, Swan Hills area, Alberta, Canada. Bulletin of Canadian Petroleum Geology, v. 16, p. 288-297.

Lohmann, K.C. 1988. Geochemical patterns of meteoric diagenetic systems and their application to paleokarst. *In*: Paleokarst. N.P. James and P.W. Choquette (eds.). New York, Springer-Verlag, p. 58-80.

Lonnee, J. and Machel, H.G. 2004. Dolomitization by halite-saturated brine and subsequent hydrothermal alteration in the Devonian Slave Point Formation, Clarke Lake Gas Field, British Columbia. I.C.E. 2004: CSPG, CHOA, CWLS Joint Conference, Calgary, Alberta.

Machel, H.G., Cavell, P.A. and Patey, K.S. 1996. Isotopic evidence for carbonate cementation and recrystallization, and for tectonic expulsion of fluids into the Western Canada Sedimentary Basin. Geological Society of America Bulletin, v. 108, p. 1108-1119.

Mack, G.H and James, W.C. 1993. Paleoclimate and the global distribution of paleosols. Journal of Geology, v. 102, p. 360-366.

Matthews, R.K. 1974. A process approach to diagenesis of reefs and reef associated limestones. *In*: Reefs in Time and Space-selected Examples from the Recent and Ancient. L.F. Laporte (ed.). Society of Economic Paleontologists and Mineralogists, Special Publication 18, p. 234-256.

McCrea, J.M. 1950. On the isotopic chemistry of carbonates and a paleotemperature scale. Journal of Chemical Physics, v. 18, p. 849-857.

Meijer Drees, N.C. 1994. Devonian Elk Point Group of the Western Canada Sedimentary Basin. *In*: Geological Atlas of the Western Canada Sedimentary Basin. G.D. Mossop and I. Shetsen (comps.). Canadian Society of Petroleum Geologists and Alberta Research Council, Calgary, p.129-147.

Melim, L.A., Swart, P.K. and Maliva, R.G. 1995. Meteoric-like fabrics forming in marine waters: implications for the use of petrography to identify diagenetic environments. Geology, v. 23, p. 755-758.

Mermut, A.R., Amundson, R. and Cerling, T.E. 2000. The use of stable isotopes in studying carbonate dynamics in soil. *In*: Global Climate Change and Pedogenic Carbonates. R. Lal., J.M. Kimble, H. Eswaran and B.A. Steward (eds.). Lewis Publishers, p. 65-85.

Meyers, W.J. and Lohmann, K.C. 1985. Isotope geochemistry of regional extensive calcite cement zones and marine components in Mississippian limestones, New Mexico. *In*: Carbonate Cements. N.P. Schneidermann and P.M Harris (eds). Society for Sedimentary Geology, Special Publication, p. 223-239.

Miller, J. 1988. Cathodoluminescence microscopy. *In*: Techniques in Sedimentology. M. Tucker (ed.). Blackwell Scientific Publications, Oxford, London, Edinburgh, Palo Alto, Melbourne, p. 174-190.

Milnes, A.R. 1992. Calcretes. *In*: Weathering, Soils and Paleosols. I.P. Martini and W. Chesworth (eds.). Elsevier Science Publishers, Amsterdam, London, New York, Tokyo, Chapter 13, p. 309-347.

Moore, C.H. 2001. Carbonate Reservoirs: Porosity Evolution and Diagenesis in a Sequence Stratigraphic Framework. Developments in Sedimentology 55. Elsevier Science Publishers B.V., Amsterdam, 404 p.

Moore, P.F. 1988. Devonian reefs in Canada and some adjacent areas. *In*: Reefs Canada and Adjacent Areas. H.H.J. Geldsetzer, N.P. James and G.E. Tebbutt (eds.). Canadian Society of Petroleum Geologists, Memoir 13, p. 367-390.

Moore, P.F. 1989. Devonian geohistory of the western interior of Canada. *In*: Devonian of the World. N.J. McMillan, A.F. Embry and D.J. Glass (eds.). Canadian Society of Petroleum Geologists, Memoir 14, v. 1, p. 67-83.

Mora, C.I. and Driese, S.G. 1999. Palaeoenvironmental, palaeoclimate and stable carbon isotopes of Paleozoic red-bed palaeosols, Appalachian Basin, USA and Canada. *In*: Palaeoweathering, Palaeosurfaces and Related Continental Deposits. M. Thiry and R. Simon-Coinçon (eds.). International Association of Sedimentologists, Special publication 27, p. 61-84.

Morrow, D.W. 1990. Dolomite-Part 2: Dolomitzation models and ancient dolostones. *In*: Diagenesis. I.A. McIlreath and D.W. Morrow (eds.). Geoscience Canada, Reprint Series, p.125-140.

Morrow, D.W and McIlreath, I.A. 1990. Diagenesis General Introduction. *In*: Diagenesis. I.A. McIlreath and D.W. Morrow (eds.). Geoscience Canada, Reprint Series, p.1-9.

Morse, J.W. and Mackenzie, F.T. (eds.). 1990. Geochemistry of Sedimentary Carbonates. Developments in Sedimentology, 48. Elsevier Science Publishers B.V., Amsterdam, 707 p.

Mountjoy, E.W, Whittaker, S. and Williams-Jones, A. 1997. Variable fluid and heat flow regimes in three Devonian dolomite conduit systems, Western Canada Sedimentary Basin: isotopic and fluid inclusion evidence/constraints. In: Basin-wide Diagenetic

Patterns: Integrated Petrological, Geochemical, and Hydrologic Considerations. I.P. Montanez, J. M. Gregg and K.L. Shelton (eds.). Society for Sedimentary Geology, Special Publication 57, Tulsa, OK, p. 119-137.

Mountjoy, E.W, Machel, H.G., Green, D., Duggan, J. and Williams-Jones, A.E. 1999. Devonian matrix dolomites and deep burial carbonate cements: A comparison between the Rimbey-Meadowbrook reef trend and the deep basin of the west-central Alberta. Bulletin of Canadian Petroleum Geology, v. 47, p. 487-509.

Muhs, D.R. 2001. Evolution of soils on Quaternary reef terraces of Barbados, West Indies. Quaternary Research, v. 56, p. 66-78.

Muhs, D.R., Bush, C.A, Stewart, K.C., Rowland, T.R. and Crittenden, R.C. 1990. Geochemical evidence of Saharan dust parent material for soils developed on Quaternary limestones of Caribbean and Western Atlantic Islands. Quaternary Research, v. 33, p. 157-177.

Müller, R., Nystuen, J.P. and Wright, V.P. 2004. Pedogenic mud aggregates and paleosol development in ancient dryland river systems: criteria for interpreting alluvial mudrock origin and floodplain dynamics. Journal of Sedimentary Research, v. 74, p. 537-551.

Murray, J.W. 1966. An oil producing reef-fringed carbonated bank in the Upper Devonian Swan Hills Member, Judy Creek, Alberta. Bulletin of Canadian Petroleum Geology, v. 14, p. 1-103.

Oldale, H.S. and Munday, R.J. 1994. Devonian Beaverhill Lake Group of the Western Canada Sedimentary Basin. *In*: Geological Atlas of the Western Canada Sedimentary Basin. G.D. Mossop and I. Shetsen (comps.). Canadian Society of Petroleum Geologists and Alberta Research Council, Calgary, p. 149-163.

Packard, J.J., and Hills, D. 2001. The importance of early (penecontemporaneous) meteoric diagenesis in the development of limestone porosity in the "platform" of the Devonian Swan Hills Formation. Rock the Foundation Convention, Calgary, Alberta, Canadian Society of Petroleum Geologists, p. 127-127-27.

Pelechaty, S.M. and James, N.P. 1991. Dolomitized Middle Proterozoic calcretes, Bathurst Inlet, Northwest Territories, Canada. Journal of Sedimentary Petrology, v. 61, p. 988-1001.

Pierson, B.J. 1981. The control of cathodoluminescence in dolomite by iron and manganese. Sedimentology, v. 28, p. 601-610.

Platt, N.H. 1989. Lacustrine carbonates and pedogenesis: sedimentology and origin of palustrine deposits from the Early Cretaceous Rupelo Formation, W. Cameros Basin, N. Spain. Sedimentology, v. 36, p. 665-684.

Podruski, J.A., Barclay, J.E., Hamblin, A.D., Lee, P.J., Osadetz, K.G., Proctor, P.M. and Taylor, W.C. 1988. Part 1: Resource Endowment of Conventional Oil Resources of Western Canada (light and medium). Geological Survey of Canada, Paper 87-26, p. 1-126.

Popp, B.N., Anderson, T.F. and Sandberg, P.H. 1986. Textural, elemental, and Isotopic variations among constituents in Middle Devonian limestones, North America. Journal of Sedimentary Petrology, v. 56, p. 715-727.

Potma, K., Weissenberger, J.A.W., Wong, P.K. and Gilhooly, M.G. 2001. Toward a sequence stratigraphic framework for the Frasnian of the Western Canada Basin. Bulletin of Canadian Petroleum Geology, v. 49, p. 37-85.

Pratt, B.R. 2001. Septarian concretions: internal cracking caused by synsedimentary earthquakes. Sedimentology, v. 48, p. 189-213.

Prezbindowski, D. 1980. Microsampling technique for stable isotopic analysis of carbonates. Journal of Sedimentary Petrology, v. 50, p. 643-645.

Purser, B.H. 1969. Syn-sedimentary marine lithification of Middle Jurassic limestones in the Paris Basin, lithification of carbonate sediments. Sedimentology, v. 12, p. 205-230.

Qing, H. 1998. Petrography and geochemistry of early-stage, fine- and medium-crystalline dolomites in the Middle Devonian Prequile Barrier at Pine Point, Canada. Sedimentology, v. 45, p. 433-446.

Read, J.F. 1974. Calcrete deposits and Quaternary sediments, Edel Province, Shark Bay, western Australia. American Association of Petroleum Geologists, Memoir 22, p. 250-282.

Read, J.F. 1976. Calcretes and their distinction from stromatolites. *In*: Stromatolites. Developments in Sedimentology 20. M.R. Walter (ed.). Amsterdam, Elsevier, p. 55-71.

Reinson, G.E., Lee, P.J., Warters, W., Osadetz, K.G., Bell, L.L., Price, P.R., Trollope, F. and Barclay, J.E. 1993. Part I: Geological Play Analysis and Resource Assessment. Geological Survey of Canada, Bulletin 452, p. 1-127.

Retallack, G.J. 1988. Field recognition of paleosols. *In*: Paleosols and Weathering Through Geological Time: Principles and Applications. Geological Society of America, Special Paper 216, p. 1-20.

Retallack, G.J. 2001. Soils of the Past. An Introduction to Paleopedology. Blackwell Science, Oxford, 404 p.

Retallack, G.J., Grandstaff, G.E. and Kimberley, N.M. 1984. The promise and problems of Precambrian paleosols. Episodes, v. 7, p. 8-12.

Roberts, W.L., Campbell, T.J. and Rapp, G.R. 1990. Encyclopedia of Minerals, Second Edition. Van Nostrand Reinhold, New York.

Robinson, B.W. and Nickel, E.H. 1979. A useful new technique for mineralogy: the backscattered-electron/low vacuum mode of SEM operation. American Mineralogist, v. 64, p. 1322-1328.

Robinson, D. and Wright, V.P. 1987. Ordered illite/smectite and kaolinite/smectite as possible primary minerals in Lower Carboniferous paleosol sequence, South Wales? Clay Mineralogy, v. 22, p. 109-118.

Roehl, P.O. 1967. Stony Mountain (Ordovician) and Interlake (Silurian) facies analogs of recent low-energy marine and subaerial carbonates, Bahamas. American Association of Petroleum Geologists Bulletin, v. 51, p. 1979-2032.

Rossinsky Jr., V. and Wanless, H.R. 1992. Topographic and vegetative controls on calcrete formation, Turks and Caicos Islands, British West Indies. Journal of Sedimentary Petrology, v. 62, p. 84-98.

Saller, A.H. 1986. Radiaxial calcite in Lower Miocene strata, subsurface Enewetak Atoll. Journal of Sedimentary Petrology, v. 56, p. 743-762.

Saller, A.H., Lounsbury, K. and Birchard, M. 2001. Facies control on dolomitization and porosity in the Devonian Swan Hills Formation in the Rosevear area, west-central Alberta. Bulletin of Canadian Petroleum Geology, v. 49, p. 458-471.

Sheasby, N.M. 1971. Depositional patterns of the Upper Devonian Waterways Formation, Swan Hills area, Alberta. Bulletin of Canadian Petroleum Geology, v. 19, p. 377-404.

Springate, G.L.V., Muir, I.D. and Caldwell, T.R. 1992. A performance evaluation of Canada's Snipe Lake/Beaverhill Lake A Pool. Society of Petroleum Engineers Reservoir Engineering, v. 7, p. 390-396.

Strasser, A. 1991. Lagoonal-peritidal sequences in carbonate environment: autocyclic and allocyclic processes. *In*: Cycles and Events in Stratigraphy. G. Einsele, W. Ricken and A. Seilacher (eds.). Springer-Verlag, Berlin, p. 709-721.

Switzer, S.B., Holland, W.G., Christie, D.S., Graf, G.C., Hedinger, A.S., McAuley, R.J., Wierzbicki, R.A. and Packard, J.J. 1994. Devonian Woodbend-Winterburn Strata of the Western Canada Sedimentary Basin. *In*: Geological Atlas of the Western Canada Sedimentary Basin. G.D. Mossop and I. Shetsen (comps.). Canadian Society of Petroleum Geologists and Alberta Research Council, Calgary, p.165-201.

Terry, R.D. and Chilingar, G.V. 1955. Summary of "concerning some additional aids in studying sedimentary formations" by M. S. Shvetsov. Journal of Sedimentary Petrology, v. 25, 3, p. 229-234.

Taylor, T.N. and Taylor, E.L. 1993. The Biology and Evolution of Fossil Plants. Prentice Hall, New Jersey, 982 p.

Trewin, N. 1988. Use of the scanning electron microscope in sedimentology. *In*: Techniques in Sedimentology. M. Tucker (ed.). Blackwell Scientific Publications, Oxford, London, Edinburgh, Palo Alto, Melbourne, Chapter 8, p 229-273.

Tucker, M.E. 1993. Carbonate diagenesis and sequence stratigraphy. *In*: Sedimentology Review . P.V. Wright (ed). V. 1, p. 51-72.

Vail, P.R., Audemard, F., Bowman, S.A., Eisner, P.N and Perez-Cruz, C. 1991. The stratigraphic signatures of tectonics, eustacy and sedimentology – an overview. *In*: Cycles and Events in Stratigraphy. G. Einsele, W. Ricken and A. Seilacher (eds.). Springer-Verlag, Berlin, Chapter 6.1, p. 617-660.

Veizer, J. 1983. Chemical diagenesis of carbonates: a theory and application of trace element technique. In: Stable Isotopes in Sedimentary Geology. M.A. Arthur (ed.). Society for Sedimentary Geology, Short Course No. 10, Tulsa, OK, p. 3.1-3.100.

Viau, C.A. 1986. Diagenesis, sedimentology and structure of the Swan Hills Formation, Swan Hills Field, Central Alberta, Canada. Unpublished Ph.D. Thesis, University of Calgary, 574 p.

Von der Borch, C.C., Lock, D.E. and Schwebel, D. 1975. Ground-water formation of dolomites in the Coorong region of South Australia. Geology, v. 3, p. 283-285.

Wagner, P.D., Tasker, D.R. and Wahlman, G.P. 1995. Reservoir degradation and compartmentalization below subaerial unconformities: limestone examples from West Texas, China and Oman. *In*: Unconformities and in Porosity Carbonate Strata. D.A. Budd, A.H. Saller and P.M. Harris (eds.). American Association of Petroleum Geologists, Memoir 63, p. 177-197.

Walls, R.A. and Burrowes, O.G. 1990. Diagenesis and reservoir development in Devonian limestone and dolostone reefs of Western Canada. *In*: The Development of Porosity in Carbonate Reservoirs. G.R. Bloy and M.G. Hadley (comps.). Canadian Society of Petroleum Geologists, Continuing Education Short Course Notes, section 5, p. 5.1-5.17.

Warren, J.K. 1983. On pedogenic calcrete as it occurs in the vadose zone of Quaternary calcareous dunes in coastal South Australia. Journal of Sedimentary Petrology, v. 40, p. 548-555.

Webb, G.E. 1994. Paleokarst, paleosol, and rocky-shore deposits at the Mississippian-Pennsylvanian unconformity, northwestern Arkansas. Geological Society of America Bulletin, v. 106, p. 634-648.

Wendte, J.C. 1992a. Overview of the Devonian of the Western Canada Sedimentary Basin. *In*: Devonian-Early Mississippian Carbonates of the Western Canada Sedimentary Basin: A Sequence Stratigraphic Framework. J.C. Wendte, F.A. Stoakes, and C.V. Campbell (eds.). Society for Sedimentary Geology, Short Course Book 28, p. 1-24.

Wendte, J.C. 1992b. Cyclicity of Devonian strata in the Western Canada Sedimentary Basin. *In*: Devonian-Early Mississippian Carbonates of the Western Canada Sedimentary Basin: A Sequence Stratigraphic Framework. J.C. Wendte, F.A. Stoakes, and C.V. Campbell (eds.). Society for Sedimentary Geology, Short Course Book 28, p. 25-39.

Wendte, J.C. 1992c. Evolution of the Judy Creek complex, a Late Middle Devonian isolate platform-reef complex in west-central Alberta. *In*: Devonian-Early Mississippian Carbonates of the Western Canada Sedimentary Basin: A Sequence Stratigraphic Framework. J.C. Wendte, F.A. Stoakes, and C.V. Campbell (eds.). Society for Sedimentary Geology, Short Course Book 28, p. 89-125.

Wendte, J.C., Dravis, J.J., Stasiuk, L.D., Qing, H., Moore, S.L. and Ward, G. 1998. High-temperature saline (thermoflux) dolomitization of Devonian Swan Hills platform and bank carbonates, Wild River area, west-central Alberta. Bulletin of Canadian Petroleum Geology, v. 46, p. 210-265.

Wendte, J.C. and Muir, I. 1995. Recognition and significance of an intraformational unconformity in the late Devonian Swan Hills reef complexes, Alberta. *In*: Unconformities and Porosity in Carbonate Strata. D.A. Budd, A.H. Saller and P.M. Harris (eds.). American Association of Petroleum Geologists, Memoir 63, p. 259-278.

Wendte, J.C. and Stoakes, F.A. 1982. Evolution and corresponding porosity distribution of the Judy Creek reef complex, Upper Devonian, central Alberta. *In:* Canada's Giant Hydrocarbon Reservoirs, Core Conference Manual. W.G. Cutler (ed.). Canadian Society of Petroleum Geologists, p. 63-81.

Wendte, J.C. and Uyeno, T. 2005. Sequence stratigraphy and evolution of Middle to Upper Devonian Beaverhill Lake strata, south-central Alberta. Bulletin of Canadian Petroleum Geology, v. 52, p. 250-354.

Willams, C.A. and Krause, F.F. 1998. Pedogenic-phreatic carbonates on a Middle Devonian (Givetian) terrigenous alluvial-deltaic plain, Gilwood Membre (Watt Mountain Formation), north central Alberta, Canada. Sedimentology, v. 45, p. 1105-1124.

Williams, C.A. and Krause, F.F. 2000. Paleosol chronosequences and peritidal deposits of the Middle Devonian (Givetian) Yahatinda Formation, Wasootch Creek, Alberta, Canada. Bulletin of Canadian Petroleum Geology, v. 48, p. 1-18.

Witzke, B.J. and Heckel, P.H. 1988. Paleoclimatic indicators and inferred Devonian paleolatitudes of Euramerica. *In*: Devonian of the World. N.J. McMillian, A.F. Embry and D.J. Glass (eds.). Canadian Society of Petroleum Geologists, Second International Symposium on the Devonian System, Memoir 14, v. 1, p. 49-68.

Wong, P.K. 1978. Sedimentology and diagenesis of the upper Devonian Kaybob stratigraphic reef. Unpublished M.Sc. thesis, University of Calgary, 207 p.

Wong, P.K. and Oldershaw, A. 1981. Burial cementation in the Devonian, Kaybob reef complex, Alberta, Canada. Journal of Sedimentary Petrology, v. 51, p. 507-520.

Wright, V.P. 1988. Paleokarsts and paleosols as indicators of paleoclimate and porosity evolution: a case study from the Carboniferous of South Wales. *In*: Paleokarst. N.P. James and P.W. Choquette (eds.). Springer-Verlag, New York, p. 329-341.

Wright, V.P. 1989. Terrestrial stromatolites and laminar calcretes: a review. Sedimentary Geology, v. 65, p. 1-13.

Wright, V.P. 1994. Paleosols in shallow marine carbonate sequences. Earth Science Reviews, 35, p. 367-395.

Wright, V.P., Platt, N.H. and Wimbledon, W.A. 1988. Biogenic laminar calcretes: evidence of root mats in paleosols. Sedimentology, v. 35, p. 603-620.

Wright, V.P. and Tucker, M.E. 1991. Calcretes: an introduction. *In*: Calcretes. V.P. Wright and M.E. Tucker (eds). Reprint Series of the International Association of Sedimentologists, v. 2, p. 1-24.

Wright, V.P. and Wilson, R.C.L. 1987. A terra-rosa like complex from the Upper Jurassic of Portugal. Sedimentology, v. 34, p. 259-273.

APPENDIX A – Formation and Megacycle Tops Used in This Study

The following data present the formation and megacycle top picks for the Swan Hills Formation in the Snipe Lake reef complex. Depths are given in metric and Imperial units.

Table A.1 Formation and megacycle picks (given in feet) used in this study for the Snipe Lake reef complex.

	Depth (feet)												
WELL LOCATION	Top Fort Vermillion	P1	P2	P3	P4	P5	R0.5	R1	R2	R3	R4	Shoal	Base Duvernay
00/16-17-069-19W5/0	9134.0	9095	9060	9020	8998.5	8963	8944.8	8928	8906	8879	8847	8804	8671.0
00/12-14-070-18W5/0	8847.0			8730	8704.7	8677.5	8653.6	8634	8616	8612			8362.0
00/10-21-070-18W5/0	8922.0	8879	8841	8800	8769.0	8746.3	8727	8695	8670	8652			8436.0
00/10-22-070-18W5/0	8877.0			8760	8732.8	8705	8689	8659	8646				8399.0
00/12-22-070-18W5/0	8890.0			8773	8752	8719.5	8708	8674	8644				8412.0
00/12-23-070-18W5/0	8796.0	8758	8720	8674	8647	8638	8600	8572					8315.0
00/04-26-070-18W5/0	8787.0			8670	8648	8643.5	8598	8581					8299.0
00/10-27-070-18W5/0	8811.0		8733	8694	8672	8659	8622.5	8602	8570	8562			8320.0
00/12-27-070-18W5/0	8839.0			8722	8698.7	8668.5	8650	8630	8601	8593			8357.0
00/12-32-070-18W5/0	8725.0			8608	8586	8562	8544.4	8510	8490	8464			8255.0
00/02-33-070-18W5/0	8827.0			8710	8685.7	8656	8634	8614	8598	8572			8344.0
00/12-03-071-18W5/0	8750.0		8672	8638	8611.5	-	8562	8545	8528				8270.0
00/02-03-071-18W5/0	8781.0			8664	8639	-	8584	8566					8310.0
00/02-04-071-18W5/0	8733.0			8616	8594	8567	8541	8523	8504	8496			8262.0
00/02-26-70-18W5/0	8732.0	8694	8646	8614	8588	-	8630	8506					8233.0
00/04-06-70-17W5/0	9126.0	9084	9048	9010	8994	-	8936						8626.0

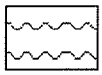
Table A.2 Formation and megacycle picks (given in meters) used in this study for the Snipe Lake reef complex.

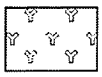
	Depth (meters)												
WELL LOCATION	Top Fort Vermillion	P1	P2	P3	P4	P5	R0.5	R1	R2	R3	R4	Shoal	Base Duvernay
00/16-17-069-19W5/0	2784.0	2772.2	2761.5	2749.3	2742.7	2731.9	2726.4	2721.3	2714.5	2706.3	2697	2683	2642.9
00/12-14-070-18W5/0	2696.6			2660.9	2653.2	2644.9	2637.6	2631.6	2626.2	2624.9			2548.7
00/10-21-070-18W5/0	2719.4	2706.3	2694.7	2682.2	2672.8	2665.9	2660	2650.2	2642.6	2637.1			2571.3
00/10-22-070-18W5/0	2705.7			2670	2661.8	2653.3	2648.4	2639.3	2635.3				2560.0
00/12-22-070-18W5/0	2709.7			2674	2667.6	2657.7	2654.2	2643.8	2634.7				2564.0
00/12-23-070-18W5/0	2681.0	2669.4	2657.9	2643.8	2635.6	2632.9	2621.3	2612.7					2534.4
00/04-26-070-18W5/0	2678.3			2642.6	2635.9	-	2620.7	2615.5					2529.5
00/10-27-070-18W5/0	2685.6		2661.8	2649.9	2643.2	2639.3	2628.1	2621.9	2612.1	2609.7			2535.9
00/12-27-070-18W5/0	2694.1			2658.5	2651.4	2642.2	2636.5	2630.4	2621.6	2619.1			2547.2
00/12-32-070-18W5/0	2659.4			2623.7	2617	2609.7	2604.3	2593.8	2587.8	2579.8			2516.1
00/02-33-070-18W5/0	2690.5			2654.8	2647.4	2638.3	2631.6	2625.5	2620.7	2612.7			2543.3
00/12-03-071-18W5/0	2667.0		2643.2	2632.9	2624.8	-	2609.7	2604.5	2599.3				2520.7
00/02-03-071-18W5/0	2676.4			2640.8	2633.2	-	2616.4	2610.9					2532.9
00/02-04-071-18W5/0	2661.8	0.0	0.0	2626.2	2619.5	2611.2	2603.3	2597.8	2592.0	2589.6	0.0	0.0	2518.3
00/02-26-70-18W5/0	2661.5	2649.9	2635.3	2625.5	2617.6	-	2630.4	2592.6	0.0	0.0	0.0	0.0	2509.4
00/04-06-70-17W5/0	2781.6	2768.8	2757.8	2746.2	2741.4	-	2723.7	0.0	0.0	0.0	0.0	0.0	2629.2

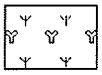
APPENDIX B – CORE DESCRIPTIONS

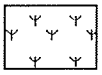
WELL	Page
TEXCAN SUNSET 16-17-69-19W5	B4-B7
ACL SNIPELK 12-14-70-18W5	B8-B12
ACL SNIPELK 10-21-70-18W5	B13-B17
ACL SNIPELK 12-22-70-18W5	B18-B21
ACL SNIPELK 12-23-70-18W5	B22-B25
ACL SNIPELK 4-26-70-18W5	B26-B29
ACL SNIPELK 10-27-70-18W5	B30-B33
ACL SNIPELK 12-27-70-18W5	B34-B36
MARATHON SNIPE LAKE 12-32-70-18W5	B37-B39
ACL SNIPELK 2-33-70-18W5	B40-B42
ACL SNIPELK 2-3-71-18W5	B43-B46
ACL SNIPELK 12-3-71-18W5	B47-B49

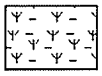
LEGEND FOR CORE DESCRIPTIONS


Lithofacies A (Peloid Packstones)


Lithofacies B (Robust Branching Cylindrical Stromatoporoid Rudstones)


Lithofacies C (Branching Cylindrical Stromatoporoid Floatstones)

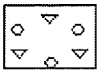

Lithofacies D (Light Tan *Amphipora* Floatstones)


Lithofacies E (Dark Brown *Amphipora* Rudstones)


Lithofacies F (Stromatoporoid Floatstones to Rudstones)


Lithofacies G (Tabular Stromatoporoid Rudstones)


Lithofacies H (Dark Brown Thin Tabular Stromatoporoid Floatstones)


Lithofacies I (Skeletal Grainstones)

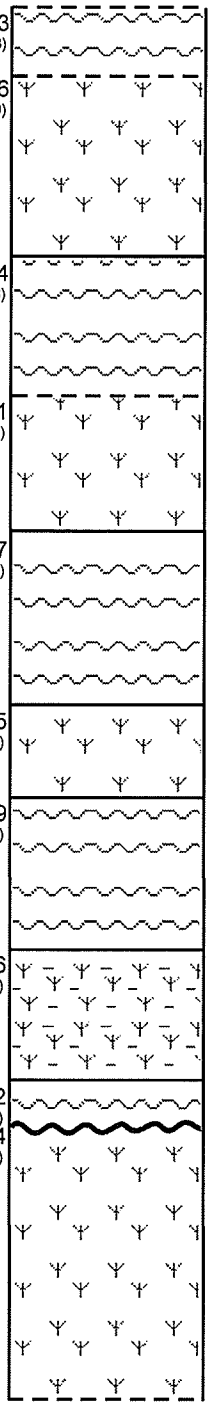


LEGEND FOR ABBREVIATIONS

ms	=	mudstone
ws	=	wackestone
ps	=	packstone
gs	=	grainstone
fs	=	floatstone
rs	=	rudstone
Amph	=	*Amphipora*
branch cyl	=	branching cylindrical
strom	=	stromatoporoid
brach	=	brachiopod
med	=	medium
dk	=	dark
interp	=	interparticle
intrap	=	intraparticle
intersk	=	interskeletal
intrask	=	intraskeletal
decr	=	decrease
incr	=	increase
cc	=	calcite cement
OM	=	organic matter
LC	=	laminar calcrete
pc	=	pendant cement
arg	=	argillaceous
sol'n	=	solution

TEXCAN SUNSET 00/16-17-69-19W5/0

core 4: [2710.6-2728.9m; (8893-8953')]
core 5: [2728.9-2739.8m; (8953-8989')]
core 6: [2739.8-2744.1m; (8989-9003"); log-core correction +2']



Med brown lime ms-ws with abundant irregular and laminar fenestrae occluded by blocky dolomite cement. Tidal flat.

Finely laminated light tan to brown *Amphipora* fs in a peloid ps matrix. Open lagoon.

Med brown lime ms with irregular and laminar fenestrae occluded by blocky dolomite cement. Finely to crinkly laminated lower 5 cm. Tidal flat.

Med brown *Amphipora* floatstone in a peloid ws-ps matrix. Interskeletal and intraskeletal pores occluded by blocky dolomite cement. Open lagoon.

Finely laminated (< 1 mm) med brown lime ms to ws with occasional *Amphipora*. Irregular and laminar fenestrae occluded by blocky calcite and dolomite cements. Tidal flat.

Med brown *Amphipora* floatstone in peloid ws-ps matrix. Ostracods common in matrix. Interskeletal and vuggy pores occluded by blocky dolomite cement. Open lagoon.

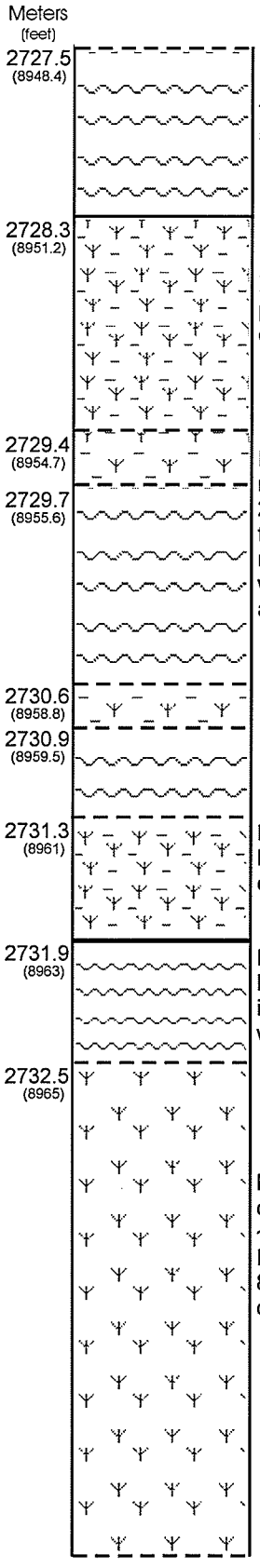
Local exposure surface. Dark to medium brown laminar calcrete at 2633.5 m (8640'). Medium brown peloid ps-gs to *Amphipora* rudstone. Sharp surfaces 7.5 cm apart at 2633.6 m (8640.3'). Possibly submarine hardgrounds with borings. Tidal flat.

Fining upwards dark brown *Amphipora* rudstone in a carbonaceous ms matrix to med brown *Amphipora* floatstone. Tight. Deep lagoon.

Med brown laminated to laminar fenestral lime ms. Tidal flat.

R0.5 contact. Medium tan *Amphipora* rudstone in a peloid ps matrix fining upwards to a ws matrix. Dark brown laminar calcretes and green shales at the top. Green shale rubble in core box. Open lagoon.

TEXCAN SUNSET 00/16-17-69-19W5/0



Fining upwards med tan-brown peloid ws/ps to a dark brown lime ms. Irregular fenestrae at the bottom, more laminar towards top. Moderately laminated in some intervals. Tidal flat.

Dark brown *Amphipora* rudstone (local floatstone) in a carbonaceous peloid ws-ps matrix. Rare branching cylindrical stroms. Interskeletal pores occluded by dolomite cement. Deep lagoon.

Interbedded med tan-brown lime wackestone in dark brown carbonaceous lime mudstone. Med tan-brown ws [2729.7-2730.6 m (8955.6-8958.5'), 2730.9-2731.3 m (8959.5-8961') weakly to well laminated with abundant irregular fenestrae occluded by blocky dolomite cement. Dark brown ms (2729.4-2729.7 m (8954.7-8955.6'), 2730.6-2730.9 m (8958.8-8959.5') massive to laminated with irregular to laminar fenestrae and occasional *Amphipora*. Tidal flat alternating with deep lagoon.

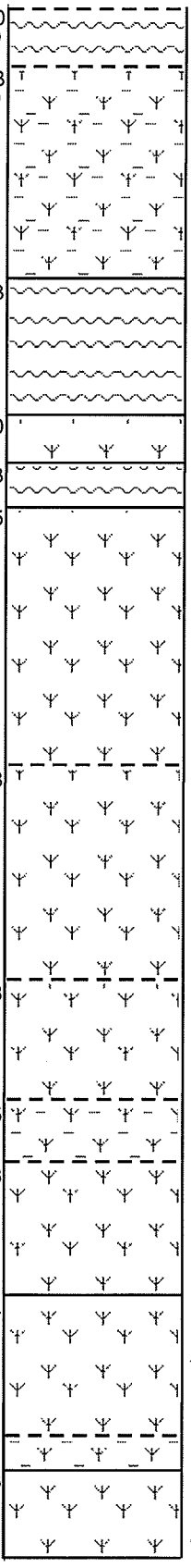
Dark brown *Amphipora* rs (local fs) in a carbonaceous ms matrix. Base has large (2.5 cm) angular rip-up clasts of green shale from underlying interval and dk brown sediment. Deep lagoon.

P5 contact. 25 cm green shale with fitted-fabric lithoclasts. Argillaceous laminar calcrete (4 mm) at 2731.9 m (8963'). LC and grey-green shales infiltrating this interval. Few scattered bulbous stroms and *Amphipora*. Tidal flat with evidence for paleosol.

Medium brown *Amphipora* rudstone in a peloid ps matrix with occasional ostracods in matrix. Laminar calcrete at 2732.8 m (8966'). Minor open porosity ~ 1%. Intraskeletal pores occluded by blocky calcite and dolomite cements. Interskeletal pores occluded by dolomite cements. 2733-2733.2 m (8966.4-8967') has well developed solution enhanced interskeletal pores (vugs) but occluded by blocky dolomite cement. Open lagoon.

TEXCAN SUNSET 00/16-17-69-19W5/0

Meters
(feet)



2735.0 (8973)

Weakly laminated med tan lime ms to peloid ps with few *Amphipora* (5-6%). Irregular to laminar fenestrae occluded by dolomite. Tidal flat.

2735.3 (8974)

Dark brown *Amphipora* rudstone in a carbonaceous ms to peloid ws matrix. Rare bulbous stromatoporoids. Intraskeletal pores occluded by blocky calcite cements. Tight. Deep lagoon.

2736.3 (8977.5)

Med-dark brown lime ms-ws with few scattered *Amphipora* Laminar fenestrae and weakly laminated near the top. Dissolution vugs common in lower half of interval. Fenestrae and vugs occluded by blocky dolomite cement. Geopetal pale yellow-grey sediment in vugs/fenestrae. Tidal flat.

2737.0 (8979.7)

Med brown *Amphipora* fs in peloid ps matrix. Dissolution enhanced interskeletal pores (vugs) occluded by blocky dolomite cement. Tight. Open lagoon.

2737.3 (8980.5)

Med-dk brown lime ms to peloid ws. Scattered *Amphipora* + rare branch cyl stroms. Cryptalgal mat at top. Irregular fenestrae and vugs occluded by blocky dolomite. Tidal flat.

2737.5 (8981.2)

Med brown *Amphipora* rudstone (local floatstone) in a peloid ps matrix. Occasional ostracods in matrix. Geopetal sediment in *Amphipora* coenostea. Intraskeletal porosity 1-2%. Interskeletal and intraskeletal occluded by blocky calcite and blocky dolomite cement. Vugs always occluded by blocky dolomites. Open lagoon.

2738.8 (8985.5)

Weakly laminated medium brown lime ms with few *Amphipora.* Faintly laminated. Irregular fenestrae occluded by blocky dolomite cement. Open lagoon.

2739.8 (8989)

Medium brown *Amphipora* floatstone to rudstone in a peloid ws-ps matrix. Intraskeletal pores occluded by blocky calcite and dolomite cements. Interskeletal pores occluded by blocky dolomite. Tight. Open lagoon.

2740.5 (8991)

Dark brown *Amphipora* floatstone to rudstone in a muddy carbonaceous matrix. Deep lagoon.

2740.8 (8992)

Medium brown *Amphipora* floatstone to rudstone in a peloid ws-ps matrix. Open lagoon.

2741.4 (8994.2)

Local exposure surface. Dark brown argillaceous laminar calcrete (4-6 mm thick) at 2741.4 m (8994.2'). Medium brown *Amphipora* floatstone with fining upwards peloid ps to ws matrix. Decrease *Amphipora* upwards. Open lagoon.

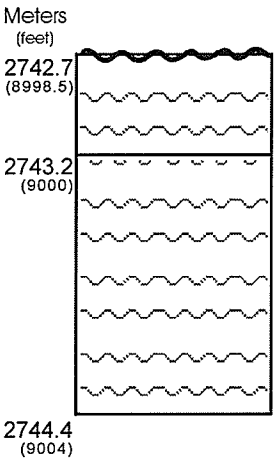
2742.1 (8996.5)

Dark brown *Amphipora* fs-rs in muddy carbonaceous matrix. Deep lagoon.

2742.3 (8997)

Medium brown *Amphipora* floatstone to rudstone in a peloid ws-ps matrix. Local dark brown carbonaceous peloid mudstone at the bottom. Open lagoon.

TEXCAN SUNSET 00/16-17-69-19W5/0



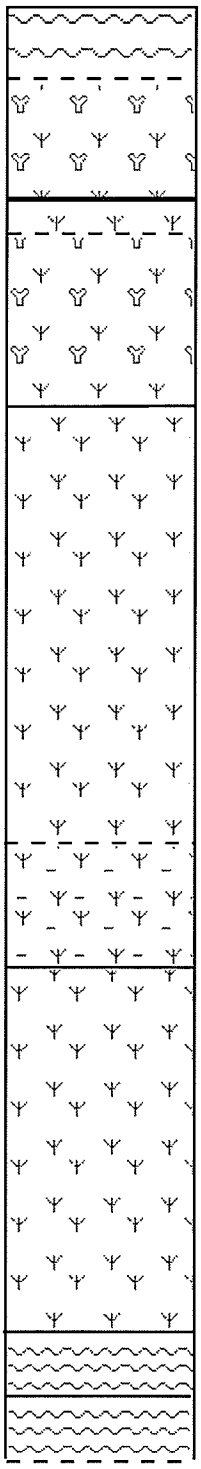
P4 contact. Medium brown peloid ps grading into 20 cm thick green shale. Green shale filled fractures and angular lithoclasts in a green shale matrix.

Medium brown lime ms with abundant irregular and laminar fenestrae. Decrease in size of fenestrae upwards and possible dissolution vugs. All occluded by blocky dolomite cement, and fenestrae occluded by calcite. Increase in abundance of smaller sized fenestrae at 2743.5 m (9001'). 2-3 mm dark brown argillaceous laminar calcretes at 2743.2 m (9000') and 4 mm laminar calcrete at 2743.9 m (9002.2'). Tidal flat with evidence of paleosol.

Bottom of core

ACL SNIPELK 00/12-14-70-18W5/0

Core 1 [2620.7- 2639m; (8598-8658'), +4' log-core correction].
Core 2 [2639-2657.2m; (8658-8718'), +6' log-core correction]



Medium tan *Amphipora* fs to rs in a peloid ps matrix with branch cyl stroms. Upper 30 cm has fenestrae occluded by blocky cc. Tidal flat.

Amphipora floatstone with branching cyl stroms and bulbous strom. Open lagoon.

R1 contact. Medium tan branching cylindrical strom-*Amphipora* fs in a peloid ps matrix. Occasional thin tabular and bulbous stroms. Interparticle porosity <5%. Upper 10 cm has darkened *Amphipora* and branching cylindrical stromatoporoids with abundant cloudy white calcite in interskeletal pores. Open lagoon.

Medium tan *Amphipora* fs in a peloid ps matrix gradational up to peloid ws matrix. Occasional branch cylindrical stromatoporoids. Most of interval relatively tight, with local interskeletal porosity ~3%. Open lagoon.

Dark brown *Amphipora* floatstone in a carbonaceous ws-ps grading up to peloid ps matrix. Deep lagoon.

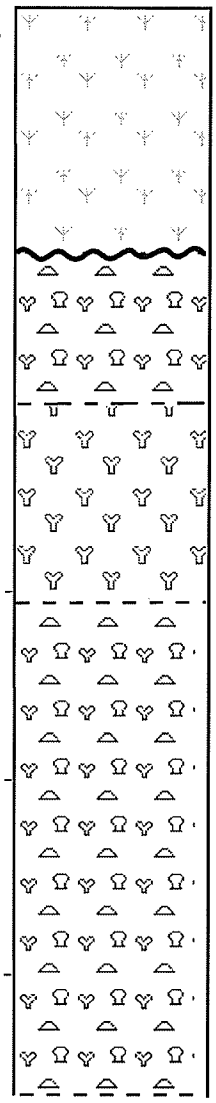
Medium tan *Amphipora* fs in a peloid ps-gs matrix. Few branching cylindrical stroms. Interskeletal porosity (~3%) grading up to a tight interval upper 15 cm with medium to dark grey mottling. Open lagoon.

Medium grey crinkly laminated ms to peloid ps with irregular to laminar fenestrae. Sharp bored upper contact. Tidal flat.
Light to medium brown *Amph* rs with a peloid ps matrix. Crinkly laminations at the bottom.

Sharp upper contact across bulbous strom with borings. Small dissolution vugs with geopetal sediment. Below strom fragments has abundant angular lithoclasts in poorly sorted peloid matrix. Tidal flat.

ACL SNIPELK 00/12-14-70-18W5/0

Meters
(feet)



Medium brown *Amphipora* rs in a ms to ws peloid matrix. Matrix coarsen upwards. Oncoids present in bottom 30 cm. Restricted to open lagoon.

R0.5 contact. Medium-dark grey strom rs with peloid-stromatoporoid gs matrix. Thin (1 cm) wispy green shales and green shale geopetal in vugs down to 10 cm below surface. Mostly branching cylindrical, thin tabular, *Amphipora,* thick tabular stroms, bulbous stroms and gastropods. Strom grains are fragmented. Interparticle pores occluded by calcite cement. Increasing cement upwards. Reef flat with evidence for paleosol.

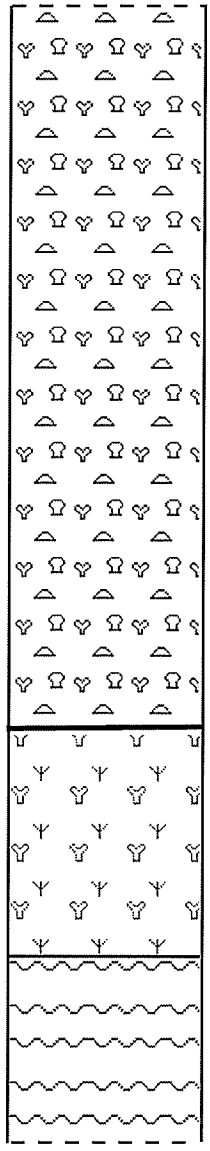
Medium grey stromatoporoid rs in a peloid gs matrix. Branching cylindrical stroms (dominant), bulbous stroms (few) and *Amphipora* (few). Interparticle porosity 10-15%, most likely shelter pores. Best porosity between 2638.8-2639.1 m (8657.5-8658.5') up to 15%. Decreasing porosity upwards as pores decrease in size and are occluded by cement. Pyrite common in pore spaces. Upper 45 cm oil stained. Possible pendant cements in upper surface of pores (cloudy white?). Beach facies.

Fining upwards from stromatoporoid rudstone to floatstone in a medium tan-brown peloid gs matrix. Allochems include, branching cylindrical strom (dominant), bulbous stroms (common), thin tabular stroms, *Amphipora,* gastropods and brachiopods. Many strom grains are fragmented. Entire interval lightly oil stained. Porosity is variable; primary intraskeletal and interskeletal porosity 3-10%. Branching cylindrical stroms and *Amphipora* have chalky white rims (alteration features?). Reef flat.

ACL SNIPELK 00/12-14-70-18W5/0

Meters
(feet)

(8666.5)



Stromatoporoid rudstone in a peloid grainstone matrix. Very similar to overlying interval, but with branching cylindrical stroms dominant, Amphipora, irregular encrusting stroms, thick tabular stroms and fewer bulbous stroms. Stromatoporoid grains fragmented and re-worked, not in-situ. 2644-2644.4 m (8674.5-8675.9') strongly oil stained. Reef flat.

(8677.5)

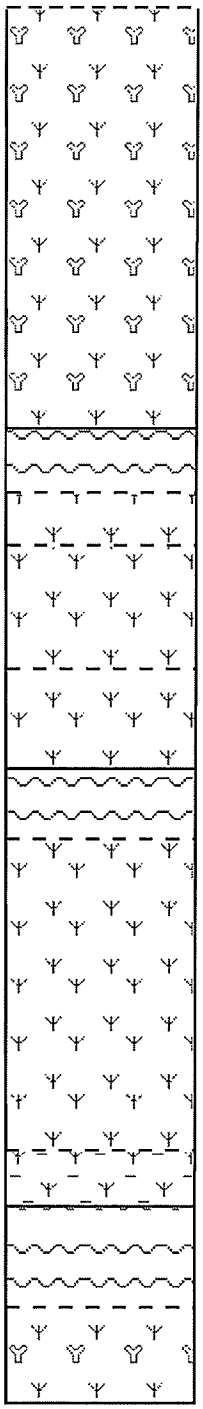
P5 contact. Medium tan branching cylindrical-*Amphipora* fs to rs in a peloid ps matrix. Interval is variable from mudstone to rudstone. Branching cylindrical stroms (most common), Amphipora, bulbous stroms (few) and gastropods. Open lagoon.

(8680.9)

Medium grey peloid ps with scattered stromatoporoids *(Amphipora and* branching cylindrical stroms ~ 3-5%). Crinkly cryptalgal laminations and laminar to irregular fenestrae. Moldic and/or vuggy porosity occluded by blocky calcite cement. Pyrite and OM concentrated at upper contact. Tidal flat.

ACL SNIPELK 00/12-14-70-18W5/0

Meters
(feet)



(8683.7)

Medium tan-brown cylindrical branching-bulbous strom rudstone in a peloid ps-gs matrix grading up to peloid ws-ps matrix at the top. Cylindrical branching stroms (abundant), large 7.5-13 cm bulbous stroms, *Amphipora* (few) and brachiopods. Decrease abundance of stroms going upwards. 3-5% interparticle porosity decreasing upwards to 1-2%. Open lagoon.

(8690)

2648.7-2649 m (8690-8691') Med grey-tan peloid ps with occasional branch cyl stroms, Amph and mollusc fragments. Increase in irregular fenestrae upwards. Intrask and moldic/vuggy pores occluded by blocky calcite cement. Interp porosity ~7%). Upper contact encrusted by thin tabular (1.5 cm) strom. Tidal flat.

(8691)

(8691.8)

2649-2649.8 m (8691.8-8693.7') medium grey *Amphipora* rs in peloid ps matrix. Sharp surface at 2649.3 m (8691.8') with thin tabular encrusting strom (3 mm). Pores occluded by coarse blocky calcite cement. Tight with local intraskeletal porosity 3% near the top increasing to 7-10% at the base. Open lagoon.

(8693.7)

(8695.2)

Light brown *Amphipora* fs to rs. Upper 10 cm laminated (cryptalgal laminations) with irregular fenestrae. Upper contact encrusted by thin tabular (1 cm) strom. Tidal flat.

(8696.1)

Grey to light tan *Amphipora* fs in a coarsening upwards matrix from peloid wackestone to grainstone. Increase abundance of *Amphipora* upwards and presence of branching cylindrical stroms. Geopetal sediment in *Amphipora* coenostea. Local intervals (10 cm thick) with medium grey mottling and irregular fenestrae occluded by clear blocky calcite cement (locally shallowing conditions). Open lagoon.

(8701)

Dark brown *Amphipora* rs in a carbonaceous ms to peloid ws matrix. Deep lagoon.

(8701.8)

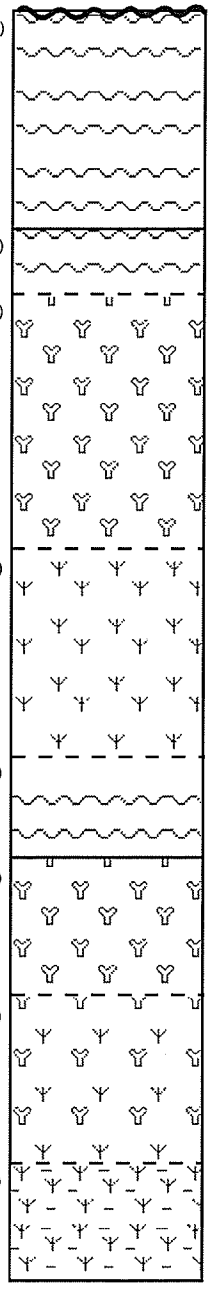
Medium brown *Amph*-branch cyl strom fs in a peloid ws matrix. Vugs grading up to irregular fenestrae are occluded by blocky cc. Upper contact encrusted by thin tabular strom (1.5 cm). Tidal flat.

(8703.4)

Branching cylindrical strom fs in a medium tan peloid ws matrix coarsening upwards to light tan peloid ps matrix. Occasional *Amphipora.* Open lagoon.

ACL SNIPELK 00/12-14-70-18W5/0

Meters
(feet)



(8704.7)

P4 contact. Light to dark brown and green shale laminar calcrete at P4. Medium brown laminated peloid ws grading up to peloid ps with occasional *Amphipora*. Vertically extensive and sub horizontal dark brown tubules (rhizoliths) with dark brown halos and centers are occluded by clear blocky calcite cement. Rhizoliths up to 11cm long. Tidal flat with evidence for paleosol.

(8708)

Erosional surface at 2654.2 m (8708'). Med-light tan *Amph* ws to peloid ps. Vugs occluded by blocky cc and green shale. 8 cm green shale at 2654.4 m (8708.7'). Fenestrae occluded by blocky cc. Tidal flat facies with soil influence.

(8709)

2654.5 m (8709') Amphipora-branching cylindrical strom fs fining up to peloid gs (decrease in stroms). Abundant vugs occluded by blocky cc an green shale. Deepest occurrence of green shale ~ 2655.3 m (8711.7'). Beach Facies.

(8712.9)

Light tan *Amphipora* fs in a peloid ps-gs matrix. Fenestrae in upper 20 cm. Blocky calcite cements occlude fenestrae, fractures, intraskeletal pores and intraskeletal pores. 3% intraskeletal porosity in *Amphipora* galleries. Open lagoon.

(8716)

Medium tan lime peloid ms-ws. Crinkly laminations and laminar fenestrae occluded by blocky clear calcite cement. Tidal flat.

(8717.6)

Medium tan to grey *Amphipora*-branching cylindrical strom rudstone. Interskeletal porosity (some shelter porosity) <10%. Upper 10 cm with cloudy white, brown pendant cements and cloudy white meniscus cements. Top surface encrusted by thin (3-4 mm) tabular strom. Beach facies.

(8719.7)

Coarsening upwards medium tan *Amphipora*-branching cylindrical strom rs to fs in a peloid ws-ps matrix. Intraskeletal pores occluded by calcite cement. Open lagoon.

(8722.2)

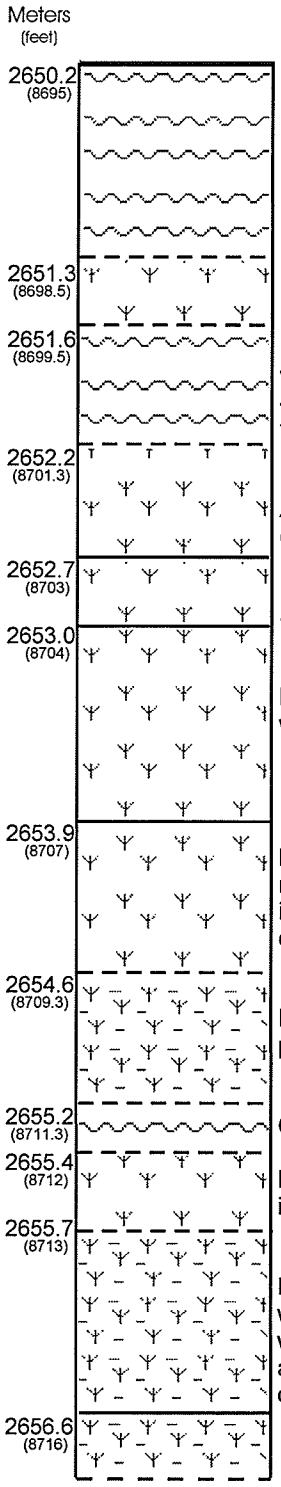
Dark brown *Amphipora* rs in a carbonaceous ms matrix. Occasional branching cylindrical stroms. Deep lagoon.

(8724)

Bottom of core

ACL SNIPELK 00/10-21-70-18W5/0

Core 1: [2648.7-2664m; (8690-8740'); log-core correction 0]
Core 2: [2664.3-2679.8m; (8741-8792') log-core correction -1']



R1 contact. Gradational from light tan to light green-tan. Amphipora floatstone in a peloid ws to lime ms matrix. Rare bulbous stromatoporoids scattered. Upper 15cm has dark grey thin shales with angular lithoclasts. Tidal flat.

Medium brown to medium tan *Amphipora* fs in a peloid ws matrix. Open lagoon.

Med grey *Amphipora* floatstone fining upwards to a med tan laminated ms-ws with few scattered *Amphipora*. Geopetal sediment in *Amphipora* coenostea. 3-4% interskeletal porosity near the bottom. Irregular fenestrae developed throughout. Tidal flat.

Dark brown carbonaceous ms (5 cm thick) grading upwards to a light tan *Amphipora* floatstone in a peloid ws matrix. Geopetal sediment in *Amph* coenostea. Deep to open lagoon.

Light brown *Amphipora* fs in a peloid ws-ps matrix with few irregular fenestrae. Shallow open lagoon.

Med tan brown *Amphipora* rs in a slightly coarsening upwards matrix from peloid ws/ps to peloid ps. 3-4% interparticle porosity. Open lagoon.

Med tan *Amphipora* fs in a peloid ps matrix. Upper 5 cm has med-dark grey mottled with a sharp planar surface (hardground?). Slightly increase in interskeletal porosity upwards 4-5%. Pores occluded by blocky calcite and dolomite cements. Open lagoon.

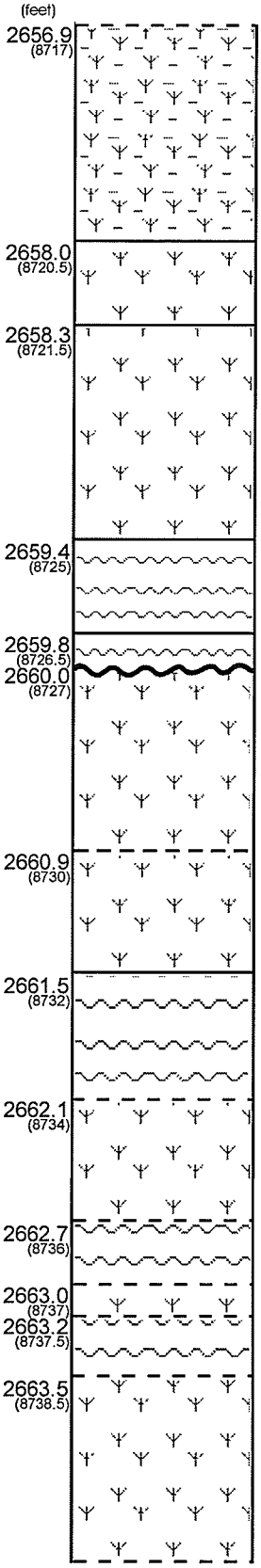
Dark brown *Amphipora* floatstone to rudstone in a variable carbonaceous ms to peloid ps matrix. Deep lagoon.

Crinkly laminated med grey *Amphipora* fs in a peloid ps matrix. Tidal flats.

Light tan darkening up to med grey *Amphipora* fs in a peloid ps matrix. 3-4% interp porosity. Open lagoon.

Dark brown to medium brown *Amphipora* rudstone in a carbonaceous peloid ws-ps matrix. 2656.6m (8716') has sharp planar surface (possible hardground) with abrupt change to med-dark grey Amphipora rudstone with darkened grains and matrix. Interparticle pores occluded by cloudy white isopachous prismatic calcite cement. Deep lagoon.

ACL SNIPELK 00/10-21-70-18W5/0



Lightening upwards from med-dark brown to tan *Amphipora* rudstone in a peloid ps matrix. Interbedded with dark brown peloid ps (no *Amphipora).* Deep to open lagoon.

Med tan peloid ps with rare *Amph*. Dark grey, well cemented sharp, planar surfaces with truncated grains at 2658 m (8720.5') (hardgrounds). 4-5% interskeletal porosity. Tidal flat.

Medium tan *Amphipora* floatstone in a peloid ps matrix. Gastropods common. Interparticle pores and vugs occluded by blocky dolomite cement. Vugs are solution enhanced shelter and interparticle pores. Open lagoon.

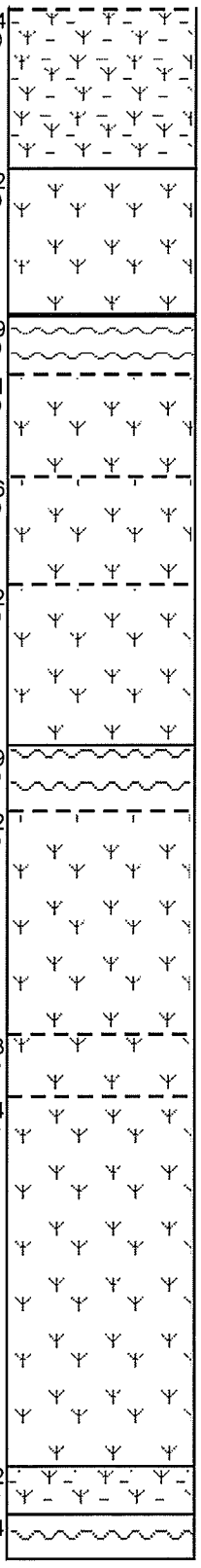
Med tan *Amphipora* rs-fs in a peloid ws/ps matrix. 2659.4m (8725.2') has sharp planar surface with truncated grains (hardground). Interparticle pores occluded by blocky calcite cement. Tidal flat.

Dark brown ms to peloid ws with irregular fenestrae. Tidal flat.

R0.5 contact. Med grey-brown *Amph* rs in a peloid ws matrix with grey mottling. Shelter pores and vugs occluded by cloudy white and brown pendant cements, and blocky cc. Pendant cements maximum down to 2660.8 m (8729.7'). Green shale in cracks. 4-7% interparticle and vuggy porosity. Open lagoon.

Interval 2660.9-2663. 5m (8730-8738.5') of interbedded of light tan open lagoon facies with med grey-tan tidal flat facies. Open lagoon facies: light tan *Amphipora* rs in a peloid ps matrix. *Amphipora* are dominant with rare bulbous/nodular stroms. Coarse grained geopetal sediment in *Amphipora* coenostea. 3-4% interskeletal and intraskeletal porosity. Tidal flat facies: med grey-tan peloid ws. Local interval weakly crinkly laminated. Muddier intervals have med grey mottling or bioturbation. Irregular fenestrae common. Solution enhanced interparticle pores occluded by blocky calcite cement.

ACL SNIPELK 00/10-21-70-18W5/0



Interbedded dark brown *Amphipora* rudstone in a carbonaceous ms matrix with dark brown lime mudstones/wackestones. Interbeds ranges from 3 to 15 cm thick. One hemispherical strom at the upper contact. Deep lagoon.

Med tan *Amphipora* floatstone in a peloid ps matrix with occasional gastropods. Amphipora coenostea occluded by geopetal sediment. Shelter pores occluded by blocky calcite cement. Open lagoon.

P5 contact. Weakly laminated medium brown peloid ps with scattered *Amphipora*.. Fenestrae occluded by clear and cloudy blocky calcite cements. White pendant cements on undersurfaces of grains in fenestral and shelter pores. Tidal flat.

2666.1-2667.9 (8747.2-8753') med tan-brown *Amphipora* rudstone n a peloid ps matrix. Interparticle pores occluded by blocky calcite cement, 5-7% porosity. 2666.6-2667.2 m (8748.8-8750.5') with a ws matrix and decreased porosity. Light tan with fewer *Amph* and few branching cyl stroms. Open lagoon.

Med tan-grey lime ms with few scattered *Amphipora* and irregular fenestrae. Tidal flat.

Med tan-grey *Amphipora* floatstone in a medium grey mottled peloid ps to ws matrix. 4-5% interparticle porosity. Open lagoon.

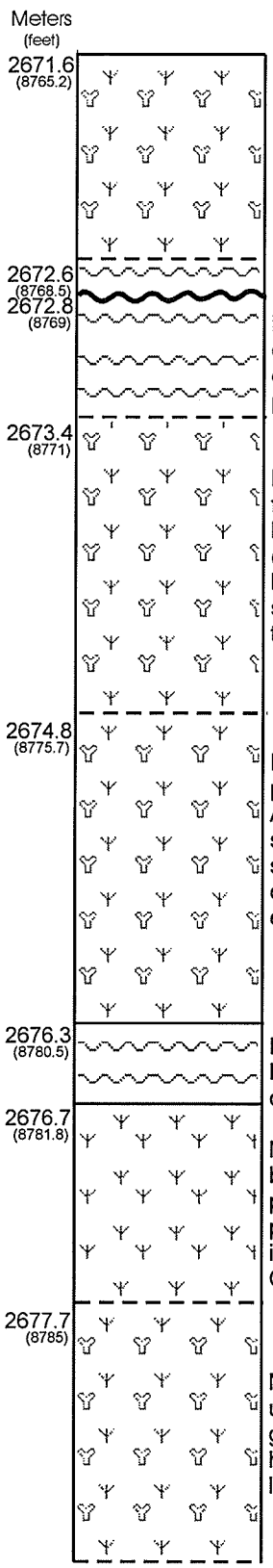
Light brown *Amphipora* floatstone/rudstone in peloid wackestone matrix. Open lagoon.

Localized exposure surface at 2669.4 m (8758'). Light brown *Amphipora* floatstone/rudstone in a fining upward matrix from a peloid ps to peloids ws matrix. Rare branching cylindrical stroms and gastropods. Geopetal sediment in *Amphipora* coenostea. Laminar calcrete at 2669.4m (8758). Open lagoon.

Dk brown *Amph* fs-rs in a peloid ws-ps carbonaceous matrix. Deep lagoon.

Dk brown laminated and fenestral peloid ps. Upper 7.5 cm massive. Tidal flat.

ACL SNIPELK 00/10-21-70-18W5/0



Med brown branching cyl-*Amphipora* floatstone in a peloid ps matrix. Rare bulbous stroms, brachiopods and gastropod fragments. Lower 7.5 cm has abundant angular lithoclasts (most likely rip-up clasts from underlying lime ms/ws). Open lagoon.

Nodular med-dark brown ms-ws. Rare branch cyl stroms with vugs. Tidal flat.

P4 contact. Medium tan lime ms with irregular-laminar fenestrae. Green shale in vugs and fissures. Darkened matrix and grains. Green shale and laminar calcretes at P4 contact. Chalky white pendant cements and blocky calcite cements occlude vugs towards the bottom. Tidal flat with evidence for paleosol.

Med tan-grey *Amphipora*-branching cylindrical stromatoporoid rudstone (local floatstone) in peloid ws-ps matrix. Upper 60 cm has abundant chalky white and brown pendant cements of undersurfaces of grains in shelter pores. 2665.3 m (8774.5') has pale green-yellow shales associated with stylolites. Lower 90 cm has dissolution vugs with geopetal coarse grained dolomitic pale yellow sediment and blocky dolomite cement. Darkened grains observed throughout the interval. Open lagoon.

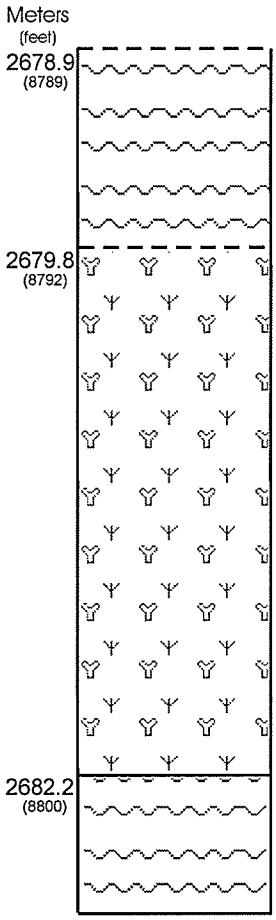
Localized exposure. Med tan *Amphipora*-bulbous strom fs-rs in a peloid ws to ps matrix. Slightly more muddy near the top with bioturbation/mottling. Abraded gastropod and brachiopods common in matrix. Rare branching cyl stroms and one large (18 cm) bulbous/hemispherical strom. Dissolution vugs in strom grains and in the matrix occluded by clear blocky calcite and dolomite cements. Stylolitic argillaceous shale, possible laminar calcrete and localized exposure surface at 2675.5m (8778') . Shallowing upwards lagoon.

Localized exposure surface and LC at 2676.3m (8780.5'). Weakly laminated tan lime ms-peloid ws. Laminar and irregular fenestrae. Vugs and fenestrae occluded by blocky cc and geopetal sediment. Tidal flat.

Medium tan *Amphipora* floatstone in a peloid ps matrix. Ostracods and brachiopods common in matrix. 7-10% interparticle, intraskeletal and moldic porosity. Abundant isopachous milky white (bladed/prismatic) calcite cements in primary interparticle or shelter pores. Grungy brown/green material in interskeletal pores (pedogenic?). Broken core throughout most of the interval. Open lagoon.

Med tan branching cylindrical-*Amphipora*-bulbous strom floatstone in a fining upwards matrix from peloid ws matrix to lime ms. Other allochems include gastropods, ostracods and brachiopods. Bulbous stroms with dissolution vugs has geopetal sediment and blocky calcite cement. Shallowing upwards open lagoon.

ACL SNIPELK 00/10-21-70-18W5/0



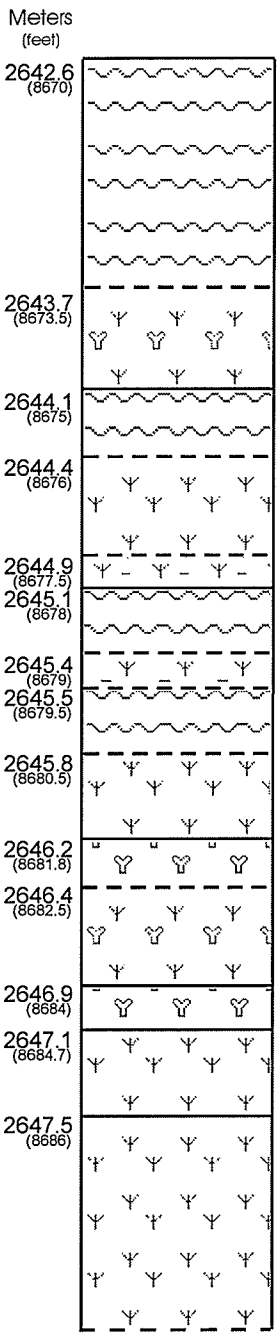
Light tan lime mudstone with *Amphipora* (5%) and few branching cylindrical stromatoporoids. Ostracods in the matrix. Irregular fenestrae and vugs occluded by clear blocky calcite cement. Core badly broken. Tidal flat.

Lightening upwards from medium brown *Amphipora*-branching cylindrical strom rudstone-floatstone to light tan *Amphipora* (few branching cylindrical stroms) floatstone. Coarsening upwards matrix from peloid ws to peloid ps. Minor allochems include brachiopods, gastropods (possibly) and nodular stroms. Allochems commonly broken and bored. Decrease in abundance and diversity of fauna going upwards. 1-2% interparticle porosity. Open lagoon.

P3 Contact.

ACL SNIPELK 00/12-22-70-18W5/0

Core 1: [2633.2-2651.5m (8639-8699'), log-core correction +1']
Core 2: [2651.5-2699.7m (8699-8759'), log-core correction +2']



Crinkly laminated grey-tan peloid ps. Laminar fenestrae very common, occluded by clear blocky calcite cement. Tidal flat.

Grey-green branching cyl strom fs in peloid ws-ps matrix. Skeletal grains abraded and fragmented, includes: brachiopods (common), gastropods and nodular stroms. Open lagoon.

Light tan laminated mudstone with med grey mottling. Irregular fenestrae occluded by blocky calcite cement. Tidal flat.

Medium tan brown *Amphipora* fs in a peloid ps matrix. Open lagoon.

Dark brown *Amphipora* rs in carbonaceous ms matrix. Deep lagoon.

Med tan laminated Amphipora floatstone in a peloid ws matrix. Irregular fenestrae occluded by blocky calcite cement. 2645.4-2645.5 m (8679-8679.5') has *Amph* rudstone in dark brown matrix. Tidal flat with local deepening of lagoon.

Med tan *Amphipora* fs in a peloid ws/ps matrix. Open lagoon.

Med brown *Amph*-branch cyl strom rs. Vuggy porosity 10-12%. Geopetal brown sediment in vugs. Top surface encrusted by 6 mm strom. Beach facies.

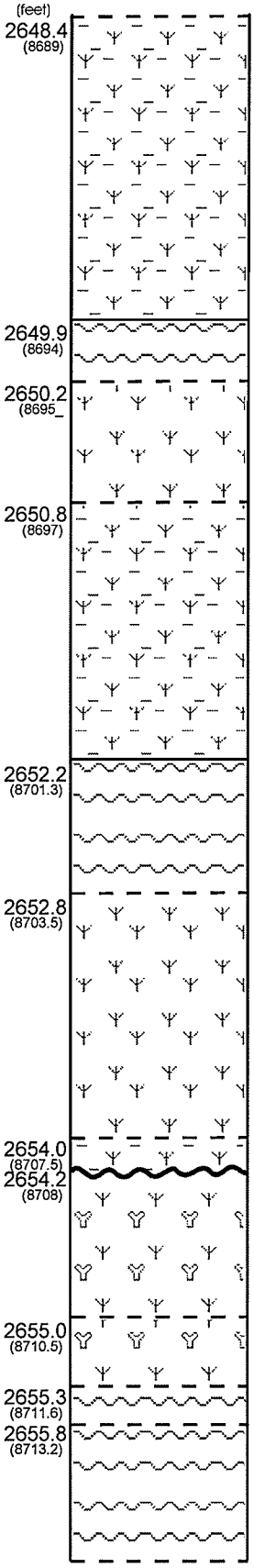
Med tan *Amph*-branch cyl strom fs in peloid ps matrix with occasional nodular stroms. Porosity increases 2 to 5% upwards. Open lagoon.

Med grey *Amph* rs. Intersk pores occluded by blocky cc. Beach.

Med tan Amph fs in peloid ps matrix. Bottom 4cm of dark brown Amph rs in a carbonaceous mudstone matrix. Deep to open lagoon.

Light tan *Amph* rs-fs in a fining upwards matrix from peloid ws-ps to ms. Few branching cyl stroms. Upper 15 cm more muddy and faintly laminated. Interval lightly oil stained. Open lagoon.

ACL SNIPELK 00/12-22-70-18W5/0



Dark brown *Amphipora* rs (local fs) in a carbonaceous ms to peloid ws matrix. Few scattered nodular stromatoporoids. Deep lagoon.

Dark grey-brown *Amph* fs in peloid ws matrix. Cryptalgal mat upper 1 cm. Irregular fenestrae occluded by blocky cc. Lower 10 cm dark brown *Amph* rs. Tidal flat.

Med brown *Amphipora* fs in a peloid ws-ps matrix. Inter and intrask pores occluded by blocky calcite cement. Open lagoon.

Interbedded dark brown *Amphipora* fs-rs in a carbonaceous muddy matrix with mudstone intervals. Rare branching cylindrical and bulbous stroms. Lower 12.7 cm has peloid ps-gs. Interp pores occluded by blocky calcite cement. Deep lagoon.

Gradational med tan up to dark brown *Amphipora* fs in a peloid ws matrix. Cryptalgal laminations and irregular fenestrae (occluded by blocky calcite cement). Interskeletal and intraskeletal porosity 5%. Tidal flat.

Light tan *Amphipora* fs in a peloid ps matrix. Most interskeletal and intraskeletal pores occluded by blocky calcite cement. 3% porosity with poor permeability. Open lagoon.

Dark brown *Amphipora* fs in carbonaceous ms matrix. Deep lagoon.

R0.5 contact (broken unpreserved contact). Gradational from darkened *Amphipora* in a med tan matrix up to dark grey branching cylindrical stromatoporoid floatstone. 46 cm green shale rubble and dolomitic green shale. Open lagoon.

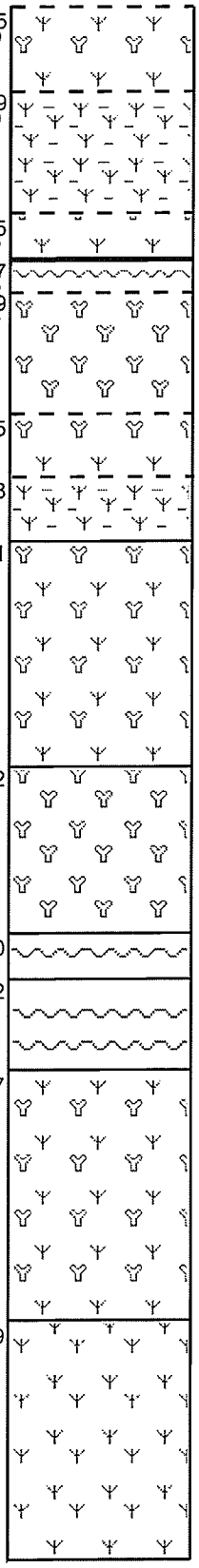
Med tan Amph-branch cyl strom fs-rs in peloid ps matrix. Bulbous stroms have vugs and geopetal light green-brown sediment. Thin (<1 mm) stylolitic green shales. Open lagoon.

Med tan crinkly laminated to fenestral*Amph* fs in peloid ps matrix. Tidal flat.

Med tan-grey *Amph*-branch cyl strom fs in a peloid ws matrix. LC and local exposure surface at 2655.8 m (8713.2') with laminated dark grey and green shale. Geopetal dolomitic sediment in upper vugs. Geopetal dolomitic sediment with green shale in lower vugs. Cloudy white pc in vugs and on strom grains, decr. downwards. Dark grey mottling from 2655.5-2656.5 m (8712.3-8715.6'). Thin green shales <1 mm down to 2656.5 m (8715.6'). Tidal flat.

ACL SNIPELK 00/12-22-70-18W5/0

Meters
(feet)



Med tan-brown *Amphipora*-branching cyl strom fs in a peloid ws matrix with medium grey mottling. Open lagoon.

Dark brown *Amphipora* rs in a carbonaceous ms matrix. Rare scattered bulbous stroms. Local areas of med brown mudstones with no stromatoporoids. Deep lagoon.

Med tan branch cyl-*Amph* (few thin tabular stroms) fs in a peloid ws-ps matrix. Open lagoon.

P5 contact. Laminated med grey branch cyl *Amph* fs in ms matrix. Tidal flat.

Med grey-tan branching cylindrical stromatoporoid-*Amphipora* fs in a peloid ms/ws matrix. Interskeletal porosity 5-15%. Blocky calcite cements occlude pores spaces and decreases upwards. Beach facies.

Branching cyl strom - *Amphipora* fs in a peloid ps matrix and dark grey mottling near the top. Open lagoon.

Dark brown branching cyl - *Amphipora* rs in a carbonaceous ms matrix. Occasional bulbous stroms. Deep lagoon.

Med tan *Amphipora*-branching cyl strom fs in a peloid ps (local ws) matrix. Irregular encrusting stroms at the top. Nodular to irregular mottling in the upper 30 cm. Open lagoon.

Med grey-tan branching cyl strom rs in a peloid ps matrix. Few scattered gastropods. Pores solution enhanced with increasing cements upwards. Pores occluded by blocky calcite and dolomite cements, and light tan/brown geopetal sediment. Interskeletal and shelter porosity decreases upwards from 8% to 3%. Beach facies.

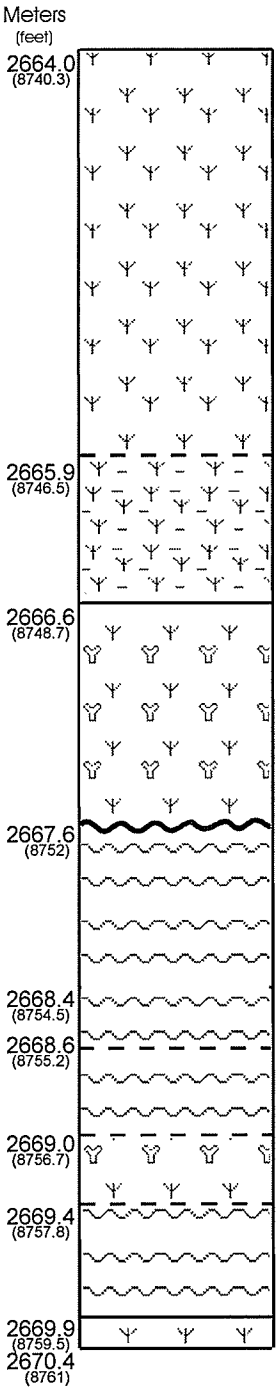
Tan *Amph*-branch cyl strom fs in a peloid ps matrix. Intersk porosity 5%. Tidal flat.

Crinkly laminated light tan ms to peloid ws with scattered *Amphipora*. Tidal flat.

Tan branching cylindrical strom - *Amph* fs in a fining upwards matrix from peloid ws/ps up to peloid ws. Branching cyl stroms more abundant at the bottom and *Amph* more abundant towards top. Geopetal sediment in Amph central coenostea. Open lagoon.

Light tan *Amphipora* fs in a fining upwards matrix from peloid ws-ps up to a peloid ws. Local intervals faintly crinkly laminated with irregular fenestrae. Increase in vugs and fenestrae going upwards, but occluded by blocky calcite cement. Shallowing upwards open lagoon.

ACL SNIPELK 00/12-22-70-18W5/0



Tan to brown *Amphipora* floatstone in a peloid ws-ps matrix. Interskeletal pores occluded by clear blocky calcite cements. Open lagoon.

Dark brown *Amphipora* rudstone to floatstone in a carbonaceous ms to peloid ws matrix. Decrease abundance of *Amphipora* going upwards (fining upwards rs to fs). Deep lagoon.

Med brown branching cyl strom-*Amphipora* fs in a peloid ps-gs matrix. Decrease abundance of branching cylindrical stromatoporoids and increase in *Amphipora* upwards. Occasional bulbous stromatoporoids, gastropods and ostracods. Open lagoon.

P4 contact. Sharp, erosional contact. Angular green shale and brown lithoclasts near the contact. Green shale rubble. Vugs occluded by blocky calcite cements, blocky dolomite cements and dolomitic green sediment. Laminated and fenestral towards with laminar calcretes towards the bottom. Tidal flat with evidence for paleosol.

Light tan lime ms to peloid ws. Upper 15 cm well laminated with laminar fenestrae. Irregular fenestrae occluded by blocky cc. Green and grey LC at bottom. Tidal flat.

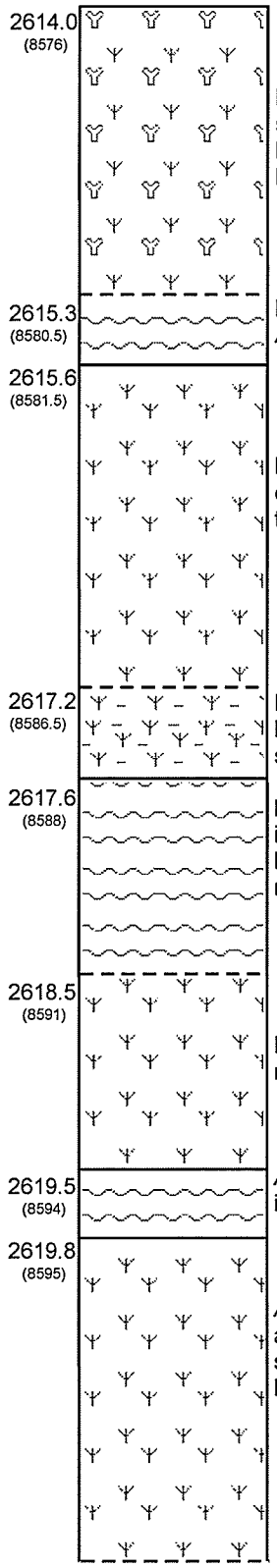
Light-med tan *Amphipora*-bulbous strom fs in peloid ws-ps matrix. Few branch cyl stroms and bulbous stroms with dissolution vugs. Open lagoon.

Med grey *Amphipora* fs-rs in a peloid ms matrix with medium grey mottling. Vugs occluded by blocky cc. Tidal flat.

Light an *Amphipora* fs in a peloid ps matrix. Open lagoon.

ACL SNIPELK 00/12-23-70-18W5/0

core 1: [2614-2636.5m; (8576-8650')]



Med tan Amph-branching cylindrical strom fs in a peloid ps matrix. Few bulbous stroms scattered and solitary corals (at top). Local 10-15 cm intervals of crinkly laminated ms and light to dark grey mottling in matrix. Porosity 1-2%. Open lagoon.

Med tan peloid ps fining upwards to peloid ws. Weakly laminated with scattered *Amph* and *b*ranch cyl stroms. Interp porosity 3-4%. Tidal flat.

Med tan brown *Amphipora* fs in a peloid ws-ps matrix with occasional branching cylindrical stromatoporoids. More muddy (peloid ws) with dark grey mottling towards top. Open lagoon.

Dark brown *Amphipora* rs in a carbonaceous peloid ws-ps matrix. Occasional bulbous and rare hemispherical stroms. Rare vugs in stroms with geopetal sediment. Deep lagoon.

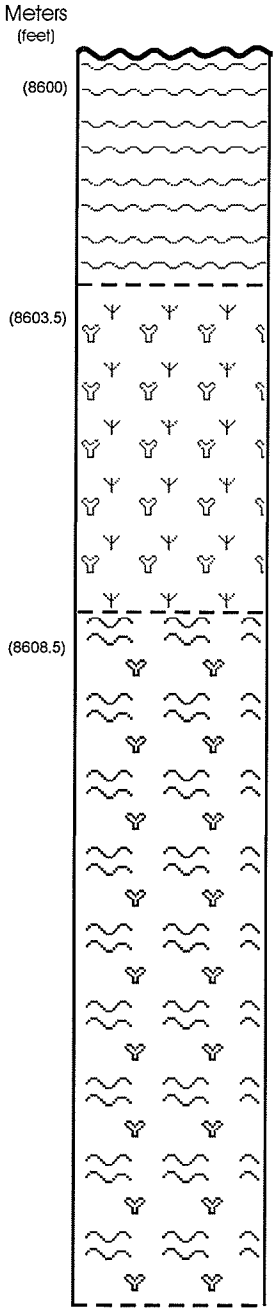
Med brown lime peloid packstone with irregular and laminar fenestrae. Local intervals well laminated with crinkly cryptalgal laminations. Fenestrae occluded by clear blocky calcite cements, minor milky white and brown pendant and meniscus cements. Overall tight. Tidal flat.

Light tan-brown *Amphipora* floatstone in a peloid ws-ps matrix. Dark grey mottling and irregular fenestrae. Open lagoon.

Amphipora rudstone in a dark grey peloid ws matrix. Dissolution vugs and irregular fenestrae common. 2-4% interparticle porosity. Tidal flat.

Amphipora floatstone to rudstone in a fining upwards dark brown peloid ps-gs to a light tan peloid ws matrix. Branching cylindrical stroms and rare thick tabular stroms. Upper 30 cm has micritized *Amphipora* grains and oncoids. Open lagoon.

ACL SNIPELK 00/12-23-70-18W5/0



R0.5 contact. Med brown oncolitic fs in a peloid ps matrix. Most nuclei are *Amph* or branch cyl strom grains. Upper 30 cm has dk grey matrix. 2-4% interparticle porosity. Vugs, shelter pores and fenestrae occluded by clear blocky calcite cement. Tidal flat.

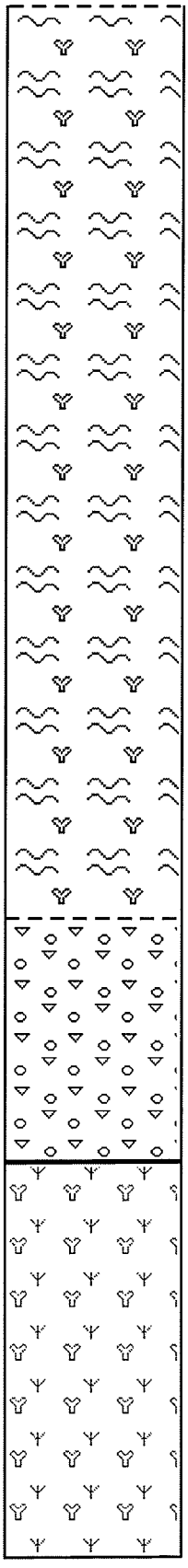
Med brown robust branching cyl strom rs in a poorly sorted peloid ps matrix. Matrix slightly coarser grained than interval below. Bulbous strom fragments and other (tabular forms) strom fragments are common, plus few gastropods. Interparticle and vuggy porosity 3-6%. Open lagoon.

Med brown thick tabular and branching cylindrical strom fs in a peloid ps matrix. Matrix slightly more muddy than lower interval. Thick tabular stroms (2-3 cm thick) and thin tabular stroms common, and occasional bulbous stroms. Thin tabular stroms less abundant relative to lower interval. Strom grains are fragmented. Occasional geopetal sediment. Dissolution vugs often occluded by blocky calcite cements and dolomite cements. Interparticle porosity ~5%. Middle foreslope.

ACL SNIPELK 00/12-23-70-18W5/0

Meters
(feet)

2627.1
(8619)



Medium brown thin tabular and branching cylindrical strom floatstone to rudstone in a peloid-skeletal grainstone matrix. Poorly sorted matrix of ostracods, brachiopod fragments, crinoids and peloids. Thin tabular stroms (0.5-1.5cm thick) and thick tabular stroms (2-3 cm thick). Strom grains both in-situ and abraded. Geopetal structures near the top. Most of interval is oil stained. Up to 10% porosity, mostly interskeletal. Core analysis shows decreasing porosity + permeability up section. Middle foreslope.

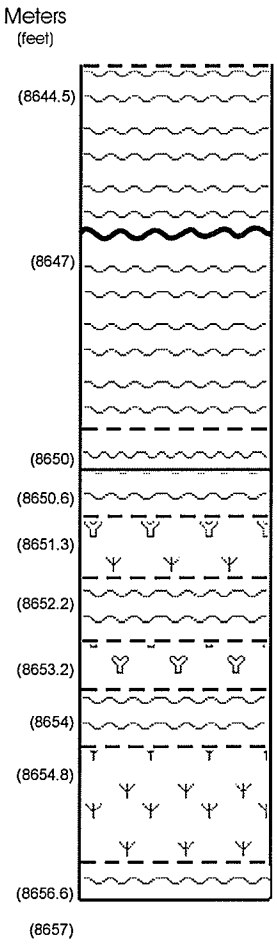
2631.6
(8634)

Medium brown peloid-skeletal grainstone. Branching cyl strom, thick tabular strom fragments, ostracods and brachiopods. Lower 20 cm has abundant abraded skeletal grains. Heavily oil stained and decreases upwards. Interparticle porosity ~ 5%. Foreslope sands.

2632.9
(8638)

P5 contact. Sharp surface with 1 cm encrusting tabular stroms and borings. Possible hardground? Gradational from dark brown *Amphipora* rs in a peloid ws-ps matrix up to medium tan-brown branching cyl strom (fewer *Amphipora)* fs in a peloid ps-gs matrix. Matrix coarsen upwards. Decrease in abundance of stromatoporoid upwards. *Amphipora* become abundant in upper 45 cm Geopetal structures in primary pore spaces. Interskeletal porosity 3-4%. Open Lagoon.

ACL SNIPELK 00/12-23-70-18W5/0



Med brown *Amphipora* floatstone in a peloids gs matrix to a peloid gs with scattered *Amphipora*. Laminated towards top. Laminar and irregular fenestrae common, occluded by clear blocky calcite and dolomite cements. Tidal flat.

P4 contact. Med tan peloid grainstone fining upwards to medium brown packstone. Faintly cross-bedded. 2635.6 m (8647') has 1.5 cm green and brown laminar calcrete, and dark grey nodules. Green shale rubble in core box. Rhizoliths throughout interval; horizontal irregular-tubular shaped structures with dark brown linings. Tidal flat with evidence for paleosol.

Dolomitic green shale grading down to dark brown laminated ms.

Amphipora fs. Vugs occluded by blocky cc, geopetal sediment, green shales and cloudy white pc. Tidal flat.

Med grey to tan branch cyl strom fs in peloid ps matrix. *Amph*, bulbous stroms and gastropods. Shallow open lagoon.

Med grey lime ms with irregular and laminar fenestrae. 5-10% interp porosity. Tidal flat.

Med grey branch cyl strom rs in peloid ps matrix. Intrask, intersk and moldic porosity, <10%. Beach.

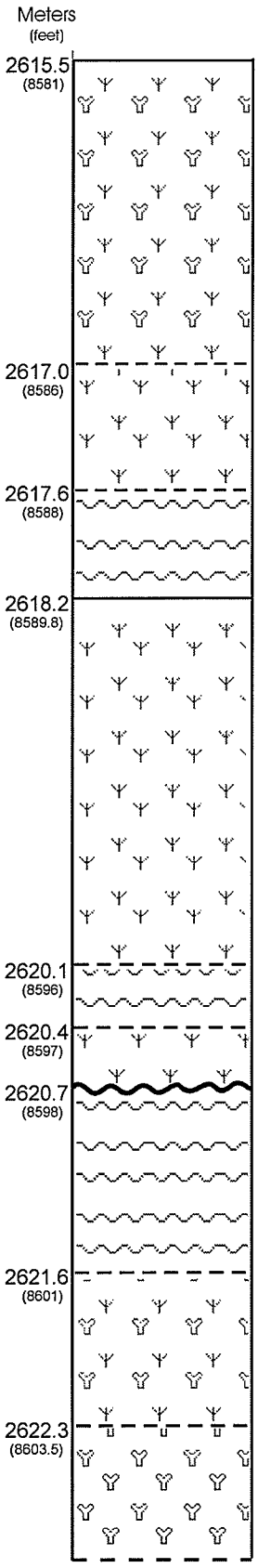
Light tan grey ms with irregular fenestrae and vugs. Occluded by blocky cc and geopetal sediment. Interp porosity 5%. Tidal flat.

Light tan peloid ws-ps with scattered *Amphipora* (3-8%). Tight. Open lagoon.

Light tan-grey peloid ws-ps. Irregular and laminar fenestrae. Interp porosity ~5%. Tidal flat.

ACL SNIPELK 00/04-26-70-18W5/0

core 1: [2610-2633.5m; (8563-8640); log-core correction +3']
core 2: [2633.5-2645.7m; (8640-8680); log-core correction +3']



R1 contact. Erosional surface with abundant lithoclasts. Medium brown darkening up to dark grey branching cylindrical stromatoporoid rudstone a peloid packstone to grainstone matrix. Other stroms include, branching cylindrical, bulbous and few *Amphipora*. Possible rugose corals. Interparticle porosity 4-5%. Open lagoon.

Medium brown *Amphipora* floatstone to rudstone in a peloid ps matrix. Bulbous strom at base with dissolution vugs and geopetal sediment. Few branching cylindrical stromatoporoids. Open lagoon.

Laminated lime peloid wackestone with few scattered *Amphipora with* irregular fenestrae. Tidal flat.

Sharp planar contact 2618.2 m (8589.8'), possible hardground. 6 cm of crinkly cryptalgal mat below sharp contact. Medium tan *Amphipora* floatstone in a peloid ps matrix with medium grey mottling at the very top. 2618.8m (8591.9') has stromatoporoid clasts (bulbous and branching cylindrical) fining up to a peloid wackestone. Minor interskeletal and intraskeletal porosity, 1-2%. Shallowing open lagoon.

Medium tan *Amphipora* floatstone in a peloid ws/ps matrix. Tidal flat.

Medium brown *Amphipora* rs in a peloid ps matrix. Stylolites common. Open lagoon.

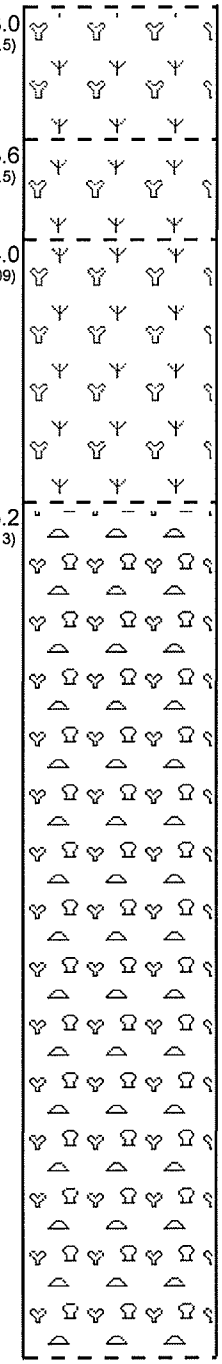
R0.5 contact. Sharp surface with truncated grains, possible hardground. Med grey-tan Amphipora fs in a peloid ws matrix coarsening upwards to Amphipora-branching cyl strom rs in a peloid ps matrix. Brown and milky white pendant cements. Crinkly laminations and laminar fenestrae are common. Interparticle porosity 5%. Tidal flat.

Med grey-tan *Amphipora*-branching cylindrical strom rudstone. Interparticle porosity 5-7%, decreases upwards as pores are occluded by blocky calcite cements and pyrite. Shallow open lagoon.

Light tan-med grey branching cylindrical strom-*Amphipora* floatstone to rudstone in a peloid ps/gs matrix. 7-10% interparticle porosity and decreases upwards. Strom grains are micritized. Beach.

ACL SNIPELK 00/04-26-70-18W5/0

Meters
(feet)



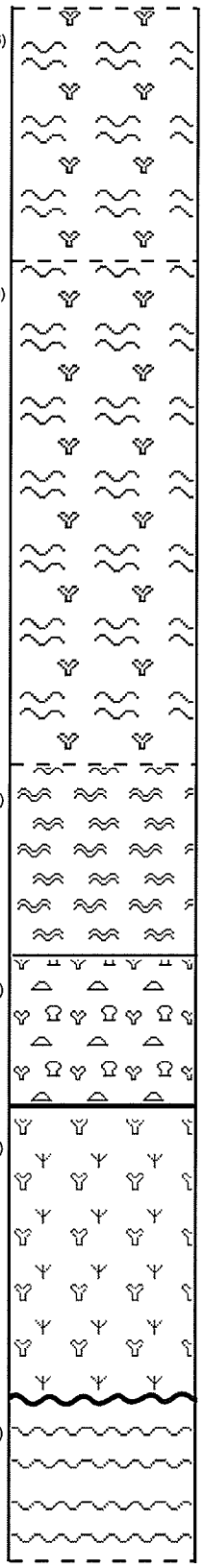
2623.0 (8605.5) Light tan branching cylindrical stromatoporoid and *Amphipora* floatstone to rudstone in a peloid ps-gs matrix. Stromatoporoid grains are commonly micritized. Medium grey mottling towards top. Interparticle porosity 3-5%. Open lagoon.

2623.6 (8607.5) Lightening upwards from dark to medium brown branching cylindrical strom-*Amphipora* rudstone in a peloid ps matrix. Open lagoon.

2624.0 (8609) Medium to dark brown branching cylindrical strom - bulbous strom rs in a peloid ps matrix. Branching cylindrical stroms are dominant with occasional bulbous strom clasts (more common towards the base) and few *Amphipora* near the top. Open lagoon.

2625.2 (8613) Medium brown branching cylindrical stromatoporoid floatstone and rudstones in a peloid ps matrix. Other allochems include, *Amphipora,* broken bulbous strom fragments (few), possible encrusting stroms on branching cylindrical grains [2628.9m (8625')] and brachiopod fragments in the matrix. Stromatoporoid grains have micritized boundaries. Interparticle and intraparticle porosity 4 to 8%. Reef flat.

ACL SNIPELK 00/04-26-70-18W5/0



Similar as below but with dominantly wafer (thin tabular) and branching cylindrical stromatoporoids. Middle foreslope.

Dark brown to medium brown thin tabular stromatoporoid rudstone in a grainstone matrix fining upwards to a floatstone in a more muddy matrix. Allochems include, thin-tabular stroms (dominant), branching cylindrical stroms (common), gastropods (few), brachiopods (few), bulbous stroms (few), ostracods (few) and rugose corals (rare). Matrix consists of peloids and variable skeletal fragments. Most skeletal grains are abraded. 2630.4-2632.9 m (8630-8638') has a more diverse stromatoporoid assemblage relative to 2629.2-2630.4 m (8626-8630'). Interparticle and intraparticle porosity 4-8%. Blocky calcite cements in remaining pores. Middle foreslope.

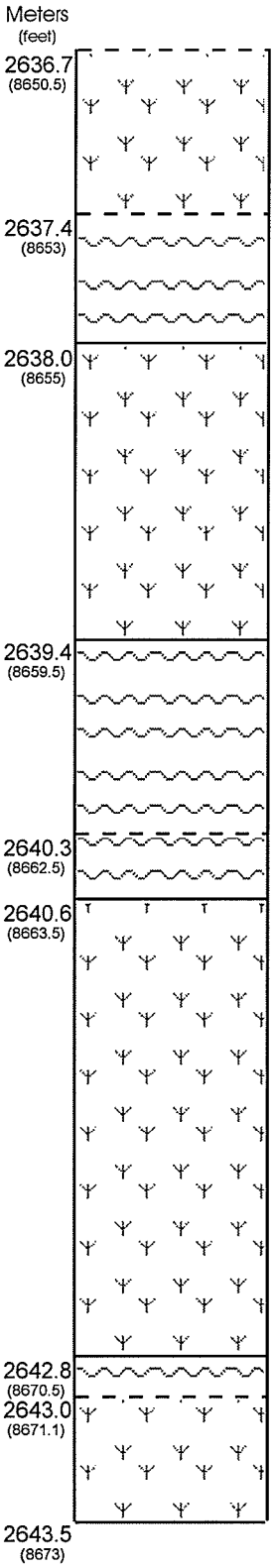
Dark brown thin tabular and branching cylindrical stromatoporoid rudstone with a peloid wackestone to packstone matrix. Thin tabular stromatoporoids are more dominant in this interval. Lower foreslope facies.

Medium brown stromatoporoid rudstone (local floatstone) in a peloid-skeletal gs matrix. Abundant broken stromatoporoid grains (thick tabular, bulbous, branching cylindrical, thin tabular and rare rugose corals). Matrix consists of peloids, brachiopods, gastropods and ostracods. Reef flat.

P5 contact. Sharp planar surface with possible truncated grains, possible hardground. Lightening upwards from medium brown to light tan floatstone in a peloid gs matrix. Branching cylindrical stromatoporoids and Amphipora. Decreasing abundance of branching cylindrical stroms towards the top, and slightly more muddy towards the bottom. Interparticle porosity 7% up to 10-15%. Open lagoon.

P4 contact. 5 cm green argillaceous shale rubble at the very top followed by 15 cm interval of green shales and dark brown laminated material. Laminated and fenestral med-dark grey lime mudstone to peloid wackestone. Med grey mottling towards the bottom, nodules (glaebules?). Tidal flat with evidence for paleosol.

ACL SNIPELK 00/04-26-70-18W5/0



Medium tan grey *Amphipora* rudstone in a peloid ps matrix. Local rudstone near the top. Stromatoporoid fragments scattered throughout. Interskeletal, intraskeletal and vuggy/moldic porosity 3-5%. Geopetal sediment in vugs. Open lagoon.

Medium tan brown peloid wackestone to lime mudstone. Crinkly laminated near the top. Laminar fenestrae occluded by blocky calcite cement. Fenestral porosity 3-4%. Tidal flat.

Med tan grey *Amphipora* rudstone in a peloid packstone matrix. Few branching cylindrical stromatoporoids near the base. Porosity increases upwards from 5% interskeletal porosity at the bottom to 4-12% (interskeletal, intraskeletal, moldic and vuggy or fenestral) porosity near the top . Open lagoon.

Crinkly laminated medium tan peloid packstone with some scattered *Amphipora*. Well developed laminar and irregular fenestrae, mostly occluded by blocky calcite cement. 2639.6-2640.2m (8660-8662') has 4-8% fenestral porosity. Tidal flat.

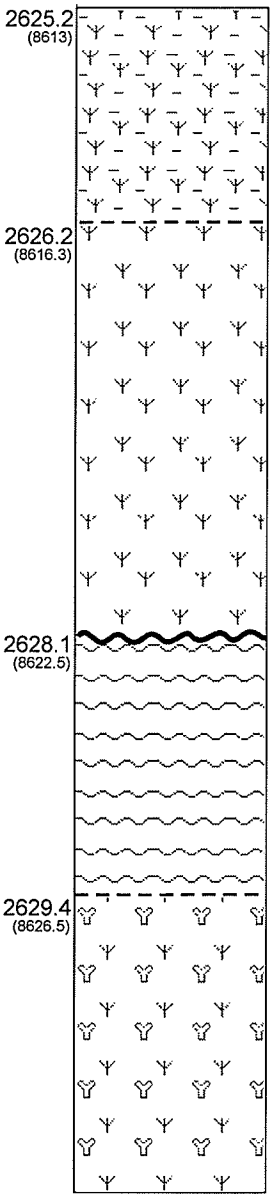
Localized exposure surface. Med-dark brown Amphipora fs in a peloid ws-ps matrix. Stylolitized laminar calcrete (0.5 mm) with laminated pale yellow, green shale, medium brown crystalline to argillaceous shale and black OM. Tidal flat.

Fining upwards medium brown *Amphipora* rudstone in a peloid ps matrix up to light brown Amphipora floatstone in a peloid ws matrix. Lower 15 cm of interval slightly muddier. Few branching cylindrical stromatoporoids around 2641.7-2642.2 m (8667-8668.5'). Medium grey mottling towards the top. Geopetal sediment in Amphipora coenostea. Open lagoon.

Weakly laminated med tan *Amph* fs in a peloid ws-ps matrix. Rare gastropods and irregular fenestrae. Tidal flat.

2643 m (8671.1') Medium tan Amphipora floatstone in a peloid ps matrix. Brachiopod and ostracods fragments in the matrix. Intraskeletal porosity 2-3%. Open lagoon.

ACL SNIPELK 00/10-27-70-18W5/0



Fining upwards dark brown *Amphipora* rudstone to floatstone in muddy peloid wackestone matrix. Deep lagoon.

Amphipora floatstone in peloid packstone matrix fining upwards to a peloid wackestone-packstone. Bulbous stromatoporoids near the bottom. Interparticle porosity 5%, intraskeletal porosity *(Amphipora* galleries) 3-5%, possible vuggy porosity 2%. Porosity variable throughout interval, average total porosity 5%. Local oil staining. Open lagoon.

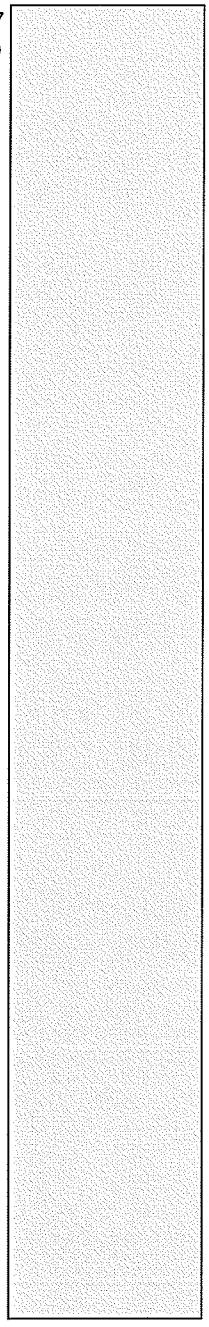
R0.5 contact. Fenestral to laminated peloid wackestone to packstone. Gradational from fenestral to laminated towards the top. Generally tight, pore spaces occluded by blocky calcite cements. 3-4% fenestral porosity in lower 45 cm. Tidal flat.

Stromatoporoid floatstone in a fining upwards matrix from skeletal-peloid grainstone to peloid packstone. Robust branching cylindrical stromatoporoids common. Bulbous and hemispherical stroms common as broken clasts. Interparticle porosity in matrix 7-8%. Intraparticle porosity in stroms grains (possibly vuggy) 3%. Lower 30 cm is oil stained. Open lagoon.

ACL SNIPELK 00/10-27-70-18W5/0

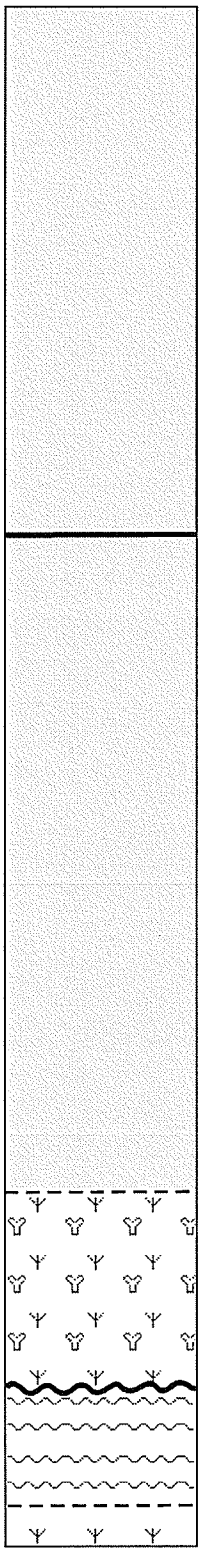
Meters
(feet)

2630.7
(8631)



Core was not described from 2630.6 to 2642.3m (8631' to 8669').

ACL SNIPELK 00/10-27-70-18W5/0



P5 contact.

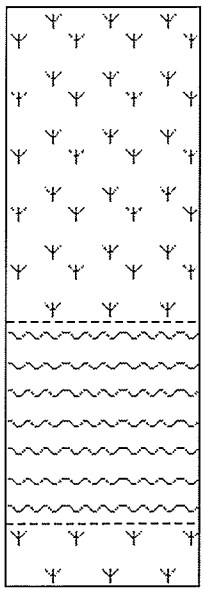
Dark brown branching cylindrical stromatoporoid floatstone in a peloid packstone matrix. Open lagoon.

P4 contact. Med-dark brown ms to peloid ps/gs. Green argillaceous shale from 2643.3-2643.6 m (8672'-8773.3'). Angular lithoclasts in a fitted-fabric texture common in green shale. LC, and green arg shales in cracks and vugs. Occasional pendant cements. Tidal flat.

Med tan *Amph*-branch cyl strom fs/rs in ms to peloid ps matrix. Open lagoon.

ACL SNIPELK 00/10-27-70-18W5/0

Meters
(feet)



2643.9
(8674.2)

Amphipora floatstone in a lime mud to peloid wackestone matrix. *Amphipora* 1-3 mm diameter, decrease in abundance of *Amphipora* going upwards. Locally weakly laminated with laminar to irregular fenestrae. 2644.9-2645.5 m (8677.5-8679.5') has 4-5% interskeletal *(Amphipora* galleries) porosity. Laminar calcretes and green argillaceous shales present. Dark brown and green argillaceous laminar calcrete at 2644.7 m (8676.8'). Dark brown and grey laminar calcrete, 1 mm thick at 2645.4 m (8679.1'). Open lagoon.

2645.4
(8679)

Irregular to laminar fenestral peloid wackestone, more muddy towards the bottom. Occasional *Amphipora* and rare gastropods. Vugs occluded by clear blocky calcite cements. Laminar calcrete < 1.5 mm thick at 2645.8 m (8680.5'). Laminar calcretes associated with green and dark brown argillaceous shale. Local exposure at 2645.8 m (8680.5'). Tidal flat.

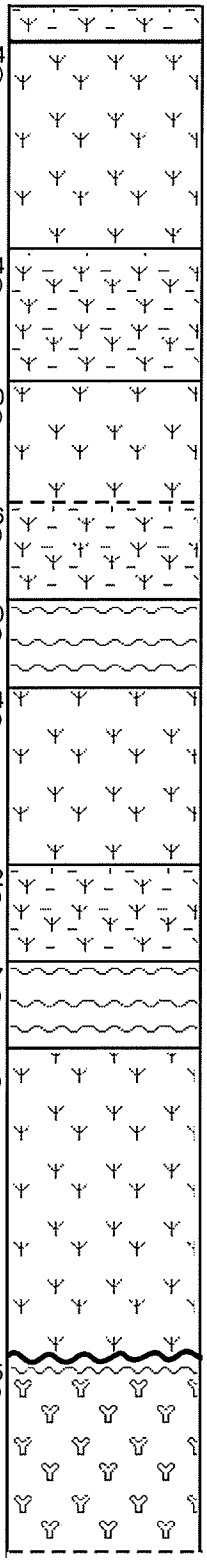
2646.3
(8682)

Peloid packstone to grainstone to *Amphipora* floatstone in peloid packstone matrix. Open lagoon.

ACL SNIPELK 00/12-27-70-18W5/0

Core 1: [2617.6-2627.1m; (8588-8619')]
Core 2: [2627.1-2643m; (8619-8671'), log-core correction -2']
Core 3: [2643-2650.8m; (8671-8697'), log-core correction -2']

Meters
(feet)



Dark brown *Amphipora* fs with carbonaceous matrix. Deep lagoon.

2630.4 (8630)

R1 contact. Light tan *Amphipora* fs in peloid ws to ps matrix fining upwards to a mottled ms. Vugs with geopetal shales and darkened grains. Green shale in vugs and fissures. Fitted-fabric lithoclasts in a green shale matrix. Intraskeletal porosity 4-5%. Open lagoon.

2631.4 (8633.2)

Dark brown *Amphipora* rudstone in a peloid-lithoclast ws matrix. Occasional branching cylindrical stroms and abundant *Amphipora* clasts (broken and dissolved grain boundaries in lower 8 cm. Deep lagoon.

2632.0 (8635.2)

Medium brown *Amphipora* floatstone with a peloid wackestone matrix. *Amphipora* coenostea occluded by blocky calcite cement. Open lagoon.

2632.6 (8637)

Dark brown *Amphipora* rs with *Amphipora*-peloid ps matrix. Clasts and interbeds (~ 1 cm) of medium brown peloid ws. Deep lagoon.

2633.0 (8638.5)

Med brown peloid ps with few *Amphipora* (< 5%). Stylolites with pyrite and concentrated OM. Upper 8c m has medium to dark grey weakly laminated to interbedded peloid ps. Irregular fenestrae or vugs. Tidal flat.

2633.4 (8639.8)

Medium brown *Amphipora* floatstone in peloid ps matrix. 10 cm dark brown Amphipora rs interval at 2633.8 m (8641'). Dissolution vugs occluded by clear-white blocky calcite cement. Geopetal sediment in *Amphipora* coenostea. Open lagoon.

2634.2 (8642.5)

Dark brown *Amphipora* rs (with local floatstone) in a carbonaceous ws-ps matrix. Deep lagoon.

2634.7 (8644)

Med brown fs in peloid ps matrix fining up to peloid ms-ws. Upper 8 cm tan-grey with irregular to laminated fenestrae and thin laminations 1-2 mm. Intersk pores and vugs occluded by clear blocky calcite cement. Tidal flat.

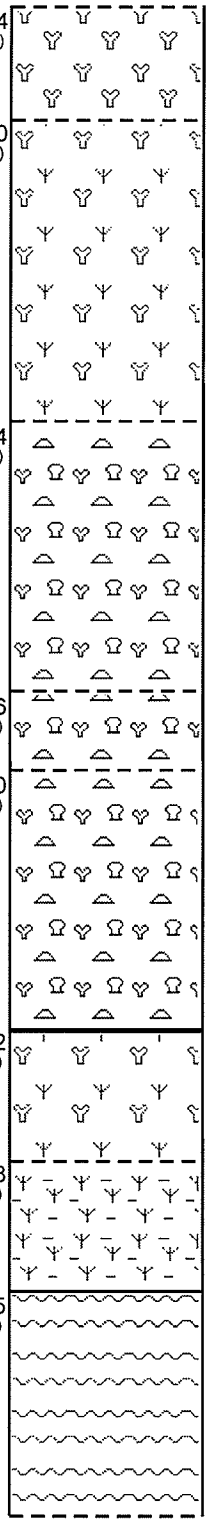
2635.1 (8645.3)

Medium-dark brown *Amphipora* fs-rs in a peloid ws-ps matrix fining upwards to peloid ws. Mottled texture and thin laminations near top. Branching cylindrical stroms and few brachiopods. Interskeletal pores (probably solution enlarged) and vugs occluded by clear and white blocky cements. Open lagoon.

2636.5 (8650)

R0.5 contact. Branch cyl-*Amphipora* rs to fining upwards to peloid packestone upper 5 cm. Abundant interskeletal pores (solution enlarged) occluded by geopetal yellow-green shales and blocky coarse white calcite cements. Light to dark brown pendant cements on the bottom surface of *Amphipora*, branch cyl stroms and on upper surfaces of vugs in strom grains. Laminar calcretes at top and 13 cm green shale. No matrix, interskeletal pores occluded by blocky dolomite cement. Beach facies to tidal flat facies.

ACL SNIPELK 00/12-27-70-18W5/0



Stromatoporoid rudstone. Clasts (1-9 cm) often fragmented and broken, including, bulbous, hemispherical, branching cylindrical, and *Amphipora*. No matrix, interskeletal pores occluded by blocky dolomite cement. Vugs in strom grains with yellow-green shales, some geopetal. Beach facies.

Light tan branching cylindrical strom floatstone in a peloid packstone matrix. Few bulbous stroms and Amphipora. Intraskeletal porosity 3-4% up to 5-6% near to top. Open lagoon.

Medium tan bulbous-branching cylindrical strom floatstone (local rudstones) in a peloid packstone matrix. Few nodular stroms (2.5 cm). Similar to lower interval but with small forms of stromatoporoid; more branching cylindrical stroms and no hemispherical stroms. Vuggy and moldic porosity ~ 5%. Reef flat.

Light tan branch cyl strom fs in peloid gs matrix. Stroms are smaller in size. Possible oncoid with branch cyl strom as nucleus. Micritized *Amphipora* grains. Reef flat.

Medium tan bulbous-hemispherical strom floatstone to rudstone in a peloid-*Amphipora* grainstone matrix. Strom grains fragmented and broken, not in-situ. Few nodular stroms (2.5 cm), few branching cyl stroms, bulbous stroms (4-10 cm) and hemispherical stroms (10-13 cm) Moldic and vuggy porosity 5-6%. Reef flat.

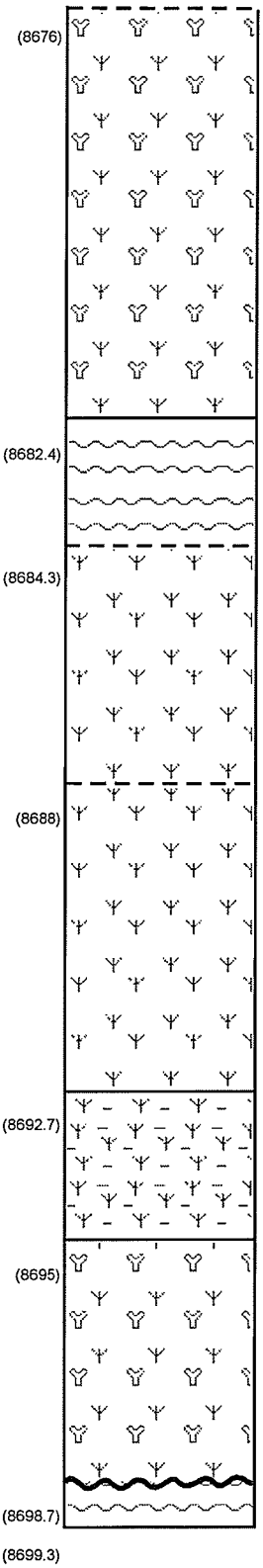
P5 contact. Med brown branch cyl strom rs in a peloid ps matrix. Few bulbous stroms and *Amphipora* (abundant upper 15 cm). Strom grains often micritized on edges. Open lagoon.

Interbedded dk brown *Amph* rs in a carbonaceous ms-ws matrix and dark brown carbonaceous ms-ws (few *Amph).* Interbeds 2-5 cm. Few branch cyl stroms. Local areas have ms clasts. Hemispherical (21 cm) strom at base. Tight. Possible oncoids. Deep lagoon.

Medium tan *Amphipora*-branching cylindrical strom ws to fs in a peloid ms matrix. Dark grey mottling of matrix and weakly laminated upper 45 cm. Irregular fenestrae, moldic pores and dissolution vugs mostly occluded by coarse blocky calcite cements. 3-4% porosity. 2613.7-2614 m (8575-8576') has dissolution vugs with geopetal sediment (light tan peloid ps). Tidal flat.

ACL SNIPELK 00/12-27-70-18W5/0

Meters
(feet)



Medium tan branching cylindrical strom rs in a peloid ps matrix. *Amphipora* in upper 60 cm and rare nodular/bulbous stroms. Dark grey to black mottling in matrix. Good interskeletal pores but occluded by blocky calcite and dolomite cement. Geopetal peloid ps sediment. Upper 15 cm with solution enhanced interskeletal and intraskeletal porosity 3-4%. Open lagoon.

Light tan ms-ws with some *Amphipora* (<10%). Lower 30 cm has irregular fenestrae occluded by blocky calcite cement. Upper 30 cm lightly mottled to finely laminated. Tidal flat.

Light tan *Amphipora* rs with local fs in a peloid ps matrix. Few bulbous stroms and branching cylindrical stroms. Vugs, shelter and interparticle pores occluded by coarse blocky white calcite cements. Bulbous stroms with dissolution vugs occluded by internal sediment and blocky calcite cement at 2648.1m (8688') . Possible minor exposure surface. Open lagoon.

Amphipora floatstone to rudstone in a peloid ps matrix. Local intervals with a more muddy matrix (mudstone matrix). Similar to interval above. Open lagoon.

Interbedded dark brown *Amphipora* floatstone to rudstone (interbeds 5-20 cm thick) and carbonaceous ms-ws. Branching cyl stroms near the top. Geopetal structures in *Amphipora* coenostea near the top. Deep lagoon.

Medium brown branching cylindrical -bulbous strom fs in a peloid ps-gs matrix. Local *Amphipora* rudstones (10 cm thick). Bulbous strom clasts have dissolution vugs with blocky calcite and dolomite cements. Upper 30 cm has fewer stroms in peloid ps (few Amph). Sharp erosional surface with bulbous strom and dissolution vugs with geopetal peloid ps sediment at 2650.5m 8696'. Open lagoon.

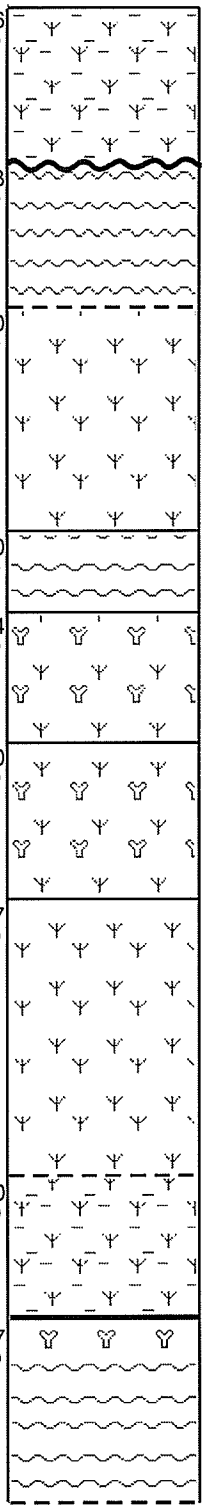
P4 contact. Light brown peloid ps (occasional brach fragments). Abundant small vugs and fissures with geopetal light tan-green shale and calcite cement. 0.5 cm grey shale at top and laminar calcrete at the surface. Tidal flat.

Bottom of core

MARATHON SNIPE LAKE 00/12-32-70-18W5/0

Core 9: [2636.8-2621.6m; (8561-8601') log-core correction factor +2']
Core 10: [2602-2636.5m; (8537-8560') log-core correction factor +5']

Meters
(feet)



2603.6 (8542) Top of Core 9. Dark brown *Amphipora* floatstone to rudstone in a carbonaceous mudstone matrix. Occasional gastropods and geopetal structures in skeletal grains. Deep lagoon.

2604.3 (8544.4) **R0.5 contact**. Sharp irregular erosional contact. Gradational from mottled dark grey argillaceous (dolomitic?) mudstone down to fitted-fabric lithoclasts in a green shale matrix. Broken green shale rubble throughout this interval.

2605.0 (8546.6) Medium tan *Amphipora* floatstone in a mudstone matrix. Local rudstones with a peloid ws matrix. Grey mottled appearance (nodules/glaebules?). Grains are dark grey-black, blackened clasts possibly from high OM. Thin (1.5-3.5 mm) grey to green shales down to 2605.4 m Lower 15 cm has large bulbous stromatoporoids with dissolution vugs with geopetal structures. *Amphipora* grains have geopetal sediment. Open lagoon with evidence for paleosol.

2606.0 (8550) Medium tan *Amphipora* rudstone with a peloid wackestone matrix. Weakly developed laminar fenestrae, solution vugs occluded by clear blocky calcite cement. Occasional pendant cements in shelter pores. Tidal flat.

2606.4 (8551.2) Medium tan *Amphipora*-branching cyl strom rs in a peloid ps-gs matrix. Grey halos around *Amphipora* and geopetal structures in *Amphipora.* Dissolution vugs (few) occluded by clear blocky calcite cement. Open lagoon.

2607.0 (8553.2) Medium tan *Amphipora* floatstone in a peloid packstone to grainstone matrix. Bulbous and branching cylindrical stroms common. Slightly mottled texture, geopetal structures common. 2607-2607.4 m (8553.2-8554.6') has dissolution vugs inside stromatoporoids with geopetal sediment. Open lagoon.

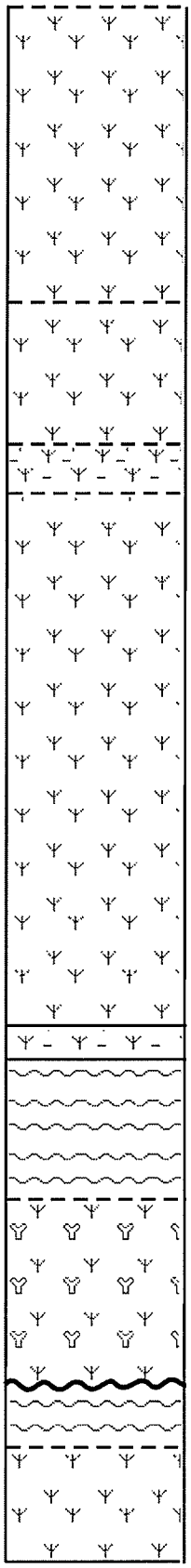
2607.7 (8555.6) Medium tan *Amphipora* floatstone in a peloid packstone to grainstone matrix. Occasional branching cylindrical, irregular stroms and nodular/bulbous strom fragments. Intraskeletal and dissolution enlarged moldic porosity 3-4% . Upper half has slightly grey-tan mottled texture, dissolution enlarged interskeletal porosity (occluded by blocky calcite and dolomite cement). Lower 20 cm has irregular fenestrae and 1.5 cm clotted laminated texture. Open lagoon progressively shallowing upwards.

2609.0 (8559.8) Dark brown *Amphipora* fs in a carbonaceous ms to ws matrix. Branching cylindrical stroms (common), nodular to irregular stroms (few), brachiopods, and gastropods. Upper 8 cm has abundant *Amphipora* clasts. Deep lagoon.

2609.7 (8562) **P5 contact.** Med brown *Amph*-branch cyl strom rs in a coarsening upwards peloid ws-ps matrix to gs matrix. Crinkly (algal) laminations. Occasional brachiopods, gastropods and larger strom clasts. Fibrous pc and isopachous cements in shelter and fenestral pores. Laminar fenestrae, intersk and shelter porosity occluded by clear blocky cc. Moldic or vuggy porosity 3-4%. Geopetal sediment in strom grains. Tidal flat to beach.

MARATHON SNIPE LAKE 00/12-32-70-18W5/0

Meters
(feet)



(8564.7)

Medium tan-grey *Amphipora* floatstone in a mudstone-peloid wackestone matrix (local packstone) with mottled texture. Occasional ostracods, gastropods and brachiopods. Fenestral, vuggy (probably solution enlarged) and moldic porosity 3-4%. Most occluded by coarse blocky calcite cement. Fenestrae and vugs better developed towards top of facies. Geopetal sediment in *Amphipora* coenostea. Open lagoon.

(8568.4)

Medium tan *Amphipora* floatstone to rudstone in a peloid wackestone to packstone matrix. Medium grey mottling near top. Occasional branching cylindrical stromatoporoids (mostly near the bottom), brachiopod fragments and gastropods. 3% intraskeletal porosity. Most intraskeletal porosity occluded by clear blocky calcite cement. Open lagoon.

(8570.7)

Dark brown *Amphipora* rs to fs in a carbonaceous ms to peloid ws matrix. Nodular (few), irregular (rare) and branch cyl stroms). Deep lagoon.

(8571.5)

Medium tan *Amphipora* rudstones to floatstones in a peloid packstone matrix. Branching cylindrical stromatoporoids common near the base of interval. Interbedded floatstones and rudstones approximately 30 to 45 cm thick. Cloudy white cements and clear blocky calcite cements occlude most pores. Local intervals of vugs occluded by blocky calcite cements and geopetal sediment in Amphipora coenostea. Open lagoon.

2615.2 m (8580.2') Dk brown *Amph* (+ few bulbous stroms) rs in a carbonaceous ms to peloid ws matrix. Possible laminar calcretes and geopetal sediment in *Amph.* Deep lagoon.

(8580.2)

(8580.7)

Medium tan *Amphipora* floatstone to rudstone in a peloid packstone to grainstone matrix. Upper 7.5 cm crinkly laminated peloid ws-ps. Brachiopod fragments and thin tabular stromatoporoid. Intraskeletal porosity 2-3%. Vuggy and intraskeletal porosity occluded by blocky calcite cement. Tidal flat.

(8583)

Medium brown branching cylindrical stromatoporoid-*Amphipora* floatstone in a peloid packstone to grainstone matrix. Thick tabular stromatoporoid fragments up to 12 cm, nodular stromatoporoids, oncoids (rare), brachiopods and molluscs. Wavy bioturbation near base. Intraskeletal porosity approx. 3%. Open lagoon.

P4 contact. Med brown-tan mottled peloid ps with *branch cyl.* Green shales and blocky dolomite in vugs. Black-green laminated shale <1.1 cm. Tidal flat.

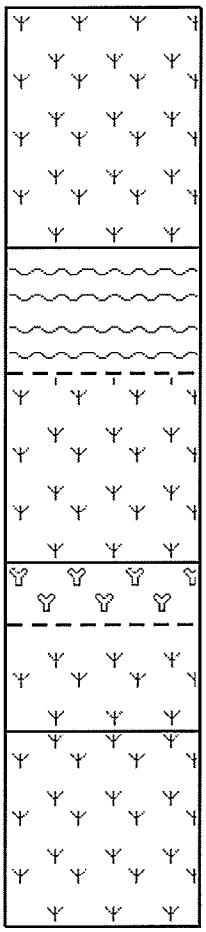
(8586)

(8587)

Med tan-dark grey *Amphipora* fs (local rs) in a peloid ws to ps matrix. Branch cyl stroms and thin green shale near the top of the section. Irregular fenestrae and a few vugs occluded by green shale and blocky calcite cement. Mottled texture near 2617.6 m (8588'). Nodular texture near the bottom. Tidal flat.

MARATHON SNIPE LAKE 00/12-32-70-18W5/0

Meters
(feet)



(8589)

Interbedded med brown to grey *Amphipora* fs in peloid ws to rudstone in peloid ps matrix. Intervals 15-20 cm thick. Irregular stromatoporoids and branching cylindrical stromatoporoids. Geopetal structures. Milky white halos around stromatoporoid grains (?). Blocky calcite occludes intraskeletal pores. Micritic laminar calcretes (< 1 mm thick) at 2618 m (8589.3'), 2618.2 m (8589.9'), 2619.1 m (8592.7'). Open lagoon.

(8592.7)

Med tan-grey peloid ps to gs with 5-10% Amph. LC at 2691.1m (8592.7'). Thick tabular encrusting strom at top (4 cm thick). Vertical to sub vertical tubules (possibly burrows or root traces). Mottled texture near base. Laminar to irregular fenestrae, vugs and fractures occluded by blocky cc. Tidal flat.

(8594.6)

Medium tan *Amphipora* ws to fs in a peloid ps matrix. Weakly developed fenestrae and wavy lamination near the top. Very shallow open lagoon.

Med tan *Amphipora* fs in a peloid ws matrix. Vugs occluded by milky white cement, clear blocky calcite cement and geopetal sediment. Beach facies.

(8597.5)

(8598.4)

Light-med tan *Amphipora* rs in a peloid ws matrix. Ostracods common and gastropods in matrix. Abundant milky grey matrix and geopetal structures. 2-3% moldic porosity. Vugs occluded by blocky calcite cements and lesser amounts of milky white cements. Open lagoon.

(8600)

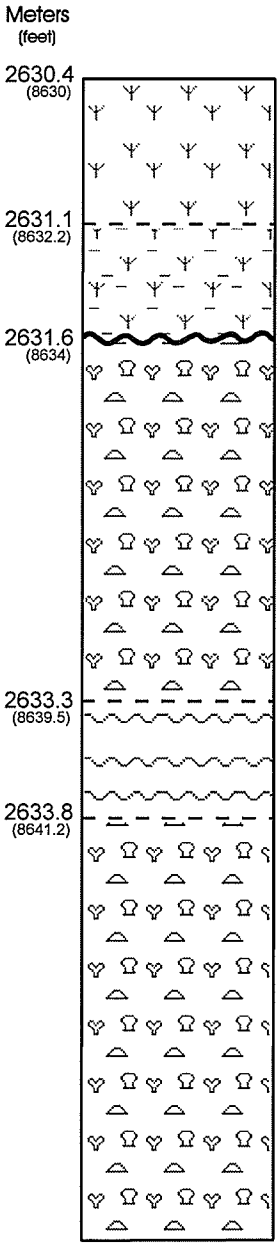
Medium brown fs in a peloid ws-ps matrix grading up to rs in a peloid ps-gs matrix. Few gastropods, brachiopods, thin tabular and bulbous strom clasts (<5 cm). Geopetal structures common near the top. 37 cm from bottom has 4 cm zone of possible thin laminar calcretes <1 mm. 13 cm from the bottom of the core – 6 mm dark brown laminar calcrete with equant calcite clasts. Possible local exposure surface. Open lagoon.

(8603)

Bottom of core

ACL SNIPELK 00/02-33-70-18W5/0

core interval: [2630.4-2648.7m; (8630-8690'); log-core correction factor +1']



Medium brown *Amphipora* floatstone (local rudstone) in a peloid ps matrix. Few vugs and most *Amphipora* coenostea occluded by coarse blocky calcite cement. Open Lagoon.

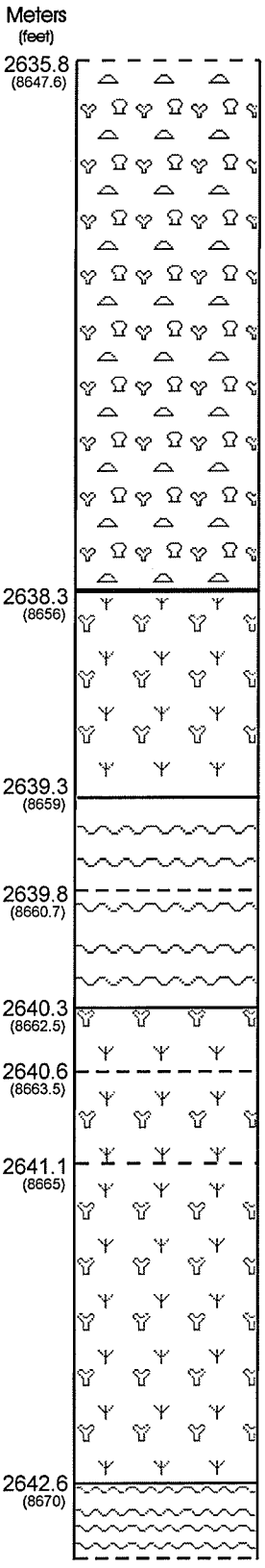
Dark brown *Amphipora* rudstone in a carbonaceous ms to peloid ps matrix. Deep lagoon.

R0.5 contact. Tan-grey branching cylindrical and bulbous floatstone to rudstone in a peloid packstone matrix. Stromatoporoid clasts include broken bulbous stroms and *Amphipora*. Most of interval relatively tight, except lower 76 cm with 5% porosity. *Amphipora* and branching cylindrical stroms appear darkened. Green shale infiltrating and filling pores. Thin green shale beds infiltrating down to 2632.6 m (8637.2') Dissolution vugs in bulbous stroms occluded by coarse blocky calcite cement and green shales. Reef flat.

Grey-brown mottled to weakly laminated *Amphipora*-branching cylindrical stromatoporoid floatstone in a peloid ws matrix. Irregular fenestrae and dissolution vugs occluded by blocky calcite cement. Interparticle porosity 5%. Tidal flat.

Similar to lower interval. Stromatoporoid floatstone with grainstone matrix. Dominantly branching cylindrical stroms with abundant variable strom fragments (bulbous?) and few *Amphipora*. Interskeletal porosity from 6 to 10%, Core throughout this interval is common broken up with light oil staining. Reef flat.

ACL SNIPELK 00/02-33-70-18W5/0



Dark grey-brown robust branching cylindrical stromatoporoid rudstone in a brown packstone-grainstone matrix. Bulbous stroms and other strom (unidentified) fragments. Interskeletal and minor intraskeletal porosity 10-12%. Brown-yellow discoloration throughout interval, most likely oil staining. Pores are occluded by blocky coarse white calcite and dolomite cement. Reef flat.

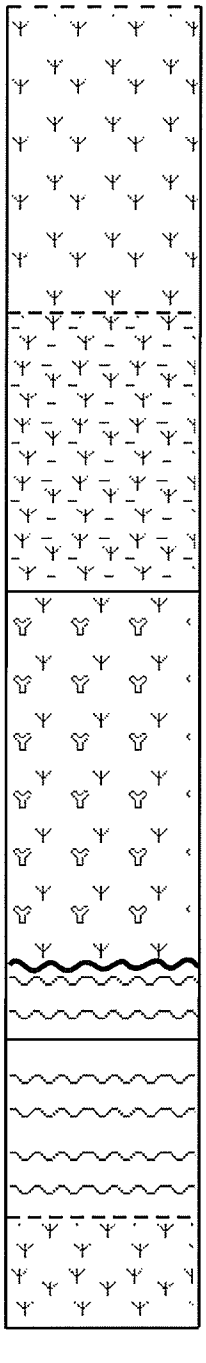
P5 contact. Medium brown branching cylindrical-bulbous stromatoporoid floatstone in a peloid ps matrix grading up to an *Amphipora* rudstone in a peloid ps matrix. Bulbous stroms possibly bored and occluded by internal sediment. 2638.7 m (8657') has a bulbous stromatoporoid with dissolution vugs and geopetal sediment. *Amphipora* coenostea often occluded by clear blocky calcite cement. Open lagoon.

Light brown to grey branching cylindrical strom floatstone in a laminated mudstone matrix. Lower interval 2639.6-2640. 2m (8660-8662') has abundant irregular fenestrae and moldic pores/dissolution vugs occluded by clear blocky calcite cements. Gastropods present in this interval. Dark grey mottling and discoloration. Upper interval 2639.3-2639.8 m (8659-8660.8') is a laminated mudstone with fewer irregular fenestrae. Tidal flat.

Light tan branching cylindrical stromatoporoid rudstone in a peloid ps-gs matrix. Local intervals 2640.8-8641.1 m (8664-8665') with a stromatoporoid floatstone in a peloid ms-ws matrix. Few nodular stromatoporoids, few bulbous stromatoporoids, brachiopod fragments and gastropods. Geopetal internal sediment in stromatoporoid galleries. 2641.1 m (8665') has a bulbous stromatoporoid with dissolution vugs and geopetal sediment. Open Lagoon.

Light tan *Amphi*pora floatstone in a peloid ms matrix. Irregular fenestrae and vugs occluded by clear blocky calcite cement. Tidal flat.

ACL SNIPELK 00/02-33-70-18W5/0



Light tan *Amphipora* rudstone (local floatstone) in a peloid ps matrix fining up to a peloid ws matrix. Dominantly *Amphipora* and few branching cylindrical stromatoporoids. Dissolution vugs in upper 45 cm are occluded by coarse blocky white calcite cement. *Amphipora* grains have micritized grain boundaries. 15 cm thick interval with irregular to laminar fenestrae at 2643.2m (8672'). Open lagoon.

Dark brown *Amphipora* rudstone in a carbonaceous peloid ps-gs matrix. Local carbonaceous mudstone intervals (2.5 to 7.5 cm thick) with mudstone clasts. Few bulbous stromatoporoids with dissolution vugs with internal geopetal sediment and clear blocky calcite cements at 2645.4m (8679'). Deep lagoon.

Coarsening upwards from dark brown *Amphipora*-branching cylindrical strom floatstone in a peloid ws matrix to a medium brown branching cylindrical stromatoporoid floatstone in a peloid ps-gs matrix. Few possible irregular stromatoporoids and rare nodular stromatoporoids. Upper 30 cm has a decrease in abundance of stromatoporoids. Lower 5 cm has a dark brown peloid packstone in a muddy carbonaceous matrix with small lithoclasts (~1 mm). Open lagoon.

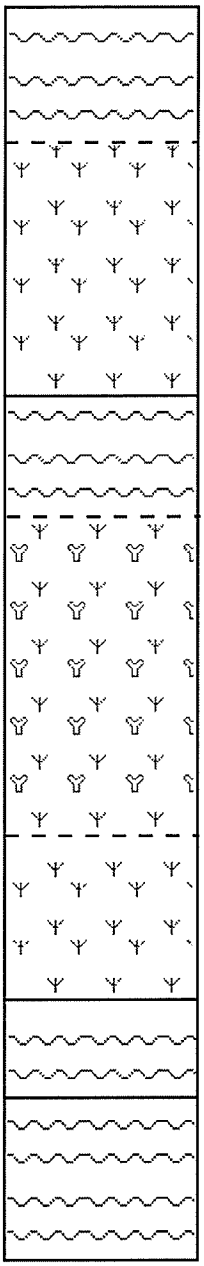
P4 contact. Sharp erosional contact. 5 cm green shale with angular lithoclasts. Strom clasts with green shale in cracks and arg LC. Tidal flat.

Light tan massive to mottled *Amph* fs in a peloid ws matrix fining up to peloid ms with fewer *Amph.* Abundant irregular fenestrae and shelter pores occluded by clear blocky cc. Possible geopetal structures in fenestrae or vugs. Upper 13 cm is medium to dark brown with laminar fenestrae and cryptalgal laminations. LC (0 .5 mm) at 2647.7m (8787.7'). 1 cm interval of thin green shales at 2647.9m (8787.4') . Tidal flat with evidence for paleosol.

Light *Amphipora* fs-rs in a peloid ps matrix. Few branching cylindrical stroms, rare nodular stroms (2.5-4 cm) and brachiopod fragments. Darkened *Amphipora* grains. Open lagoon.

ACL SNIPE LK 00/02-03-71-18W5/0

core 1: [2610.3-2621.6m; (8564-8601), no log-core correction]
core 2: [2621.6-2636.8m; (8601-8651), log-core correction +1']



Weakly laminated *Amphipora* floatstone in a peloid ms-ws matrix. Irregular fenestrae, occluded by clear calcite cement. Weakly laminated. Tidal flat.

Light tan-brown *Amphipora* floatstone in a peloid ws matrix. Tight. Open Lagoon.

Tan-grey *Amphipora* rs in peloid ws matrix. Darkened grains with dk grey margins. 2612.7 m (8571.8') has remnants of green shale on top of core piece. 2612.8 m (8572') has dark grey to brown argillaceous LC. Upper 15-30 cm has possible pc's. Lower half has vuggy porosity 2-4%. Tidal flat.

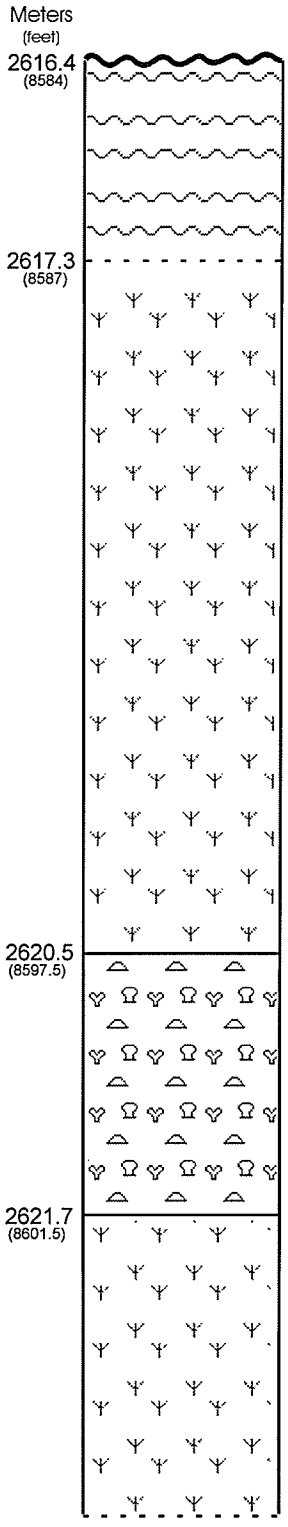
Light tan branching cyl-bulbous strom fs in a peloid ps matrix fining upwards to a peloid ws matrix. Bulbous stroms decr. upwards and *Amphipora* increases upwards. Branch cyl stroms are dominant with occasional bulbous, nodular, hemispherical to large bulbous stroms. Up to 5% intersk porosity. Upper 45 cm faintly mottled and Amph clasts darkened. Open lagoon.

Light tan *Amphipora*-branching cyl strom fs in a peloid ps matrix. *Amphipora* are dominant with other abraded strom fragments. ~ 2% vuggy porosity. Open lagoon.

Light tan *Amphipora* fs in a peloid ms-ws matrix with abundant irregular to laminar fenestrae. Weakly laminated. Fenestral porosity 3-4%. Tidal flat.

Amphipora fs in peloid ws-ps matrix. Laminar fenestrae with brown and white pendant cements. Brown isopachous cements in fenestrae (primary pores). Decrease in cements downwards. Tidal flat.

ACL SNIPE LK 00/02-03-71-18W5/0



R0.5 contact. Sharp surface with truncated grains, possible hardground surface. Light tan-medium grey *Amphipora* fs in a peloid ws matrix. Weakly laminated and irregular fenestrae occluded by clear calcite cement. Moldic and vuggy porosity ~ 5%. Vugs occluded by blocky calcite cement. Dark grey mottling in matrix and dark grey halos around *Amphipora* grains. Tidal flat.

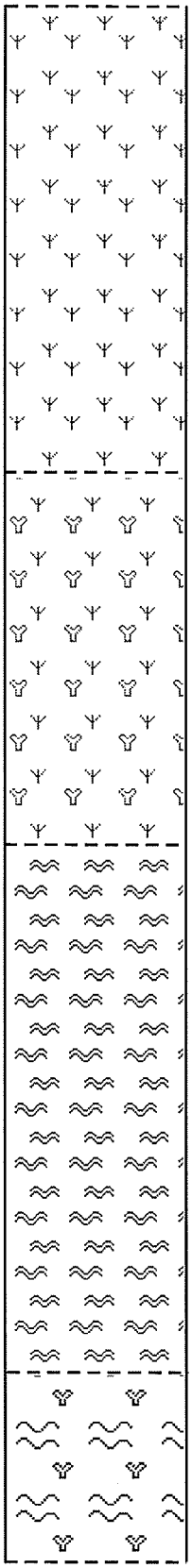
Light tan *Amphipora* floatstone (with local rustone) in a peloid packstone matrix fining upwards to a peloid ws matrix. Branching cylindrical stroms and brachiopod fragments. Occasional stroms encrusted by algae (possible oncoids). Stroms with micritized grain boundaries and light grey mottling upper 30 cm. Variable porosity, up to 5-6% (interskeletal and intraskeletal). Core throughout this facies is broken up with light oil staining. Open lagoon.

Light tan hemispherical-bulbous strom fs in a peloid ws-ps matrix. Dissolution vugs in stroms are occluded by blocky calcite cement and geopetal sediment. Core through this interval is badly broken up. Fractures common (core induced?). Intraskeletal porosity up to 5%. Reef flat.

Light tan *Amphipora*-branching cyl strom fs in a peloid ws-ps matrix. Similar to 2623.1-2625.4 m (8606-8613.5') but with lesser abundance of stroms. Rare nodular stroms. Strom grains appear slightly darkened to med-dk grey. Intraskeletal porosity 2-3%. Open lagoon.

ACL SNIPE LK 00/02-03-71-18W5/0

Meters
(feet)



2623.1
(8606)

Medium brown *Amphipora* rudstone (with local floatstone) in a peloid ps matrix. Amphipora dominant with common branching cyl stromatoporoids. Intraskeletal porosity 3-4%. Stromatoporoid edges appear micritized. Open lagoon.

2625.4
(8613.5)

Similar to lower interval; branching cylindrical stroms are dominant with lesser amounts of thin tabular stromatoporoids and few *Amphipora* near the top. Open lagoon.

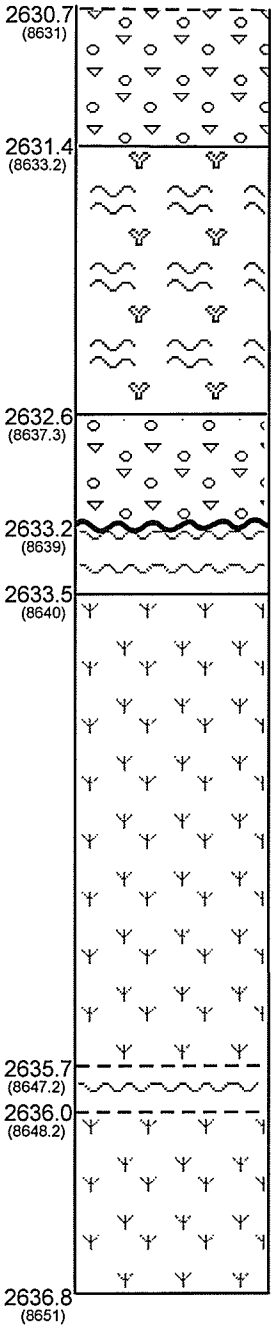
2627.2
(8619.5)

Dark brown branching cyl strom and thin tabular stromatoporoid (local floatstone) in a peloid ws to ps matrix. Overall lightening and decrease lime mud upwards. Stromatoporoid grains are commonly broken and fragmented, but thin tabular stromatoporoids appear to be relatively in growth position. Thin tabular stromatoporoids aligned parallel to bedding, few bulbous stromatoporoids, brachiopod fragments and rare rugose coral. Dissolution vugs in strom grains with geopetal sediment. Interparticle pores in filled with dark brown cements lining pores and blocky white calcite cement. Branching cyl stroms grain boundaries often micritized. Intraskeletal porosity 3-5%. Lower foreslope.

2630.1
(8629)

Light brown branching cylindrical and thin tabular stromoatoporoid rudstone in a grainy peloid packstone matrix. Stromatoporoid fragments are generally fragmented. Few bulbous stromatoporoid fragments are present. Middle foreslope.

ACL SNIPE LK 00/02-03-71-18W5/0



Medium tan-brown skeletal grainstone. Thin tabular stroms, strom fragments, ostracods,+ brachiopods, crinoids and branching cyl stroms. Lower 13 cm dark brown mudstone. Foreslope sands.

Light tan to med brown thin tabular strom - branching cyl strom floatstone in an ostracod-peloid ps-gs matrix. Occasional bulbous stroms and brachiopod fragments. Geopetal sediment in ostracod shells. Interparticle porosity 4-5%. Middle foreslope.

Peloid-skeletal packstone to grainstone with branching cylindrical stroms. Abundant peloids or possibly broken strom fragments, brach fragments and gastropods. Foreslope sands.

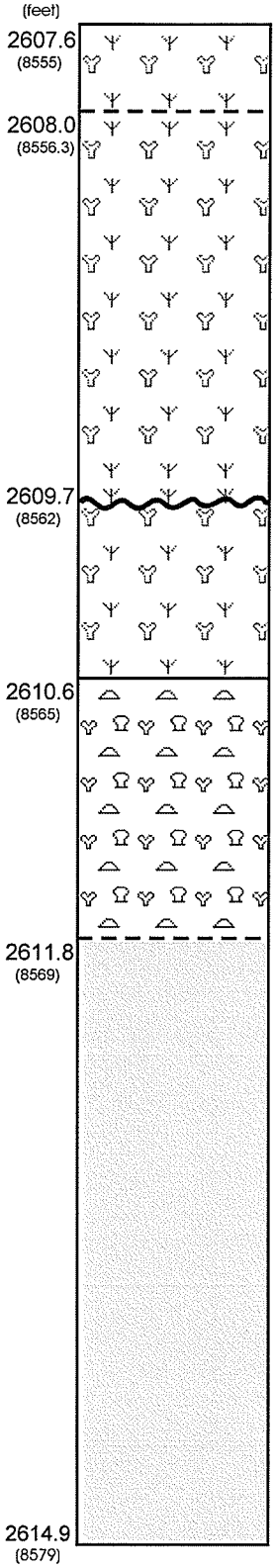
P4 contact. Med brown peloid-skeletal ps, local gs. Very finely laminated (<1 mm). 1 cm green shale, LC and darkened clasts. Tidal flat.

Amphipora floatstone in peloid wackestone-packstone matrix. Other allochems include brachiopods, gastropods and ostracods. Moldic and vuggy porosity up to 5-6% from 2634.4-2635.7 m (8643-8647.2'). Increase in cements and decrease in porosity going upwards. 2633.5-2633.8 m (8640-8641') has pores almost completely occluded by cements. Pendant cements in shelter pores and solution enhanced pores (vugs). Remaining pore space occluded by blocky calcite and dolomite cements. Open lagoon.

Light tan grey *Amphipora* fs in a peloid ws matrix. Irregular fenestrae and vugs occluded by clear blocky calcite cement. Porosity 4-5%. Tidal flat.

Light tan *Amphipora* floatstone-rudstone in a peloid ws-ps matrix. Few branching cyl stroms. Vuggy and interparticle porosity 10% porosity. Slight decrease in porosity upwards. Open lagoon.
bottom of core

ACL SNIPELK 00/12-03-71-18W5/0



Amphipora rudstone with branching cylindrical stromatoporoids in peloid ws/ps matrix. Algal overgrowths on strom grains (oncoids). *Amphipora* 1-4 mm, branching cylindrical strom <1 cm. Interparticle porosity 5-10%. Open lagoon.

Amphipora and branching cylindrical stromatoporoid floatstone in a fining upwards matrix from peloid-skeletal packstone/grainstone to peloid wackestone/lime mudstone. *Amphipora* 1-4 mm, branching cylindrical stroms 1.5cm. Some bulbous stromatoporoid clasts, <7 cm. Intraskeletal porosity 1%, vuggy porosity in bulbous stroms 2%. Open lagoon.

R0.5 contact. Amphipora-branching cylindrical floatstone in a peloid packstone matrix fining upwards to a lime mudstone. Oncolites (strom grains with algal overgrowths) present towards the top and bulbous stroms <0.5 cm lower in the interval. Vuggy porosity 3% (possibly some moldic). Open lagoon.

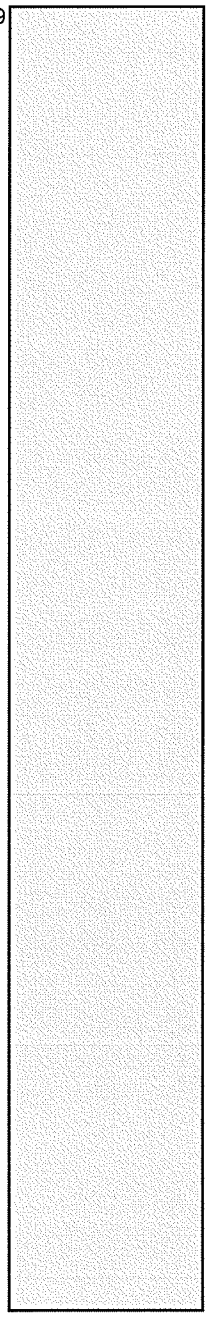
Stromatoporoid floatstone to rudstone in a peloid-skeletal packstone matrix. Branching cylindrical stroms common, bulbous, *Amphipora,* rare hemispherical strom clasts and rare thick tabular stroms clasts. Upper 10 cm laminar to irregular fenestral peloid wackestone. Branching cylindrical stroms are more dominant in lower interval. Intraskeletal porosity 2%, shelter porosity 5% (possibly some moldic). Possible vuggy porosity 3-4%. Reef flat.

Core was not described between 2611.8 to 2623.7m (8569-8608').

ACL SNIPELK 00/12-03-71-18W5/0

rs

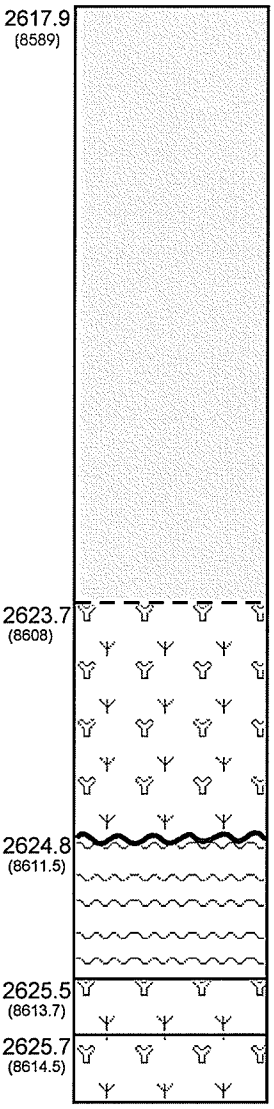
9



9

Core was not described between 2611.8 to 2623.7m (8569-8608').

ACL SNIPELK 00/12-03-71-18W5/0



Medium brown peloid grainstone with branching cylindrical stromatoporoids at the base. Open lagoon.

P4 contact. Light tan mudstone to peloid packstone/grainstone. Laminated (sometimes crinkly laminated) to fenestral. Rare branching cylindrical stromatoporoids. Green argillaceous shale and pendant cements present. Tidal flat.

Light tan branch cyl strom rs in peloid ps/gs matrix. Green shale and pendant cements. Open lagoon.

Light tan branching cylindrical stromatoporoid rudstone. Open lagoon.

APPENDIX C – DETAILED EXPOSURE PROFILE DESCRIPTIONS

WELL	Stratigraphic Level	Page
TEXCAN SUNSET 16-17-69-19W5	P4, P5, R0.5	C4-C6
ACL SNIPELK 12-14-70-18W5	P4, R0.5	C7-C8
ACL SNIPELK 10-21-70-18W5	P4, R0.5	C9-C10
ACL SNIPELK 10-22-70-18W6	P4, R0.5	C11-C12
ACL SNIPELK 12-22-70-18W5	P4, R0.5	C13-C14
ACL SNIPELK 12-23-70-18W5	P4	C15
ACL SNIPELK 4-26-70-18W5	P4, R0.5	C16-C17
ACL SNIPELK 10-27-70-18W5	P4, R0.5	C18-C19
ACL SNIPELK 12-27-70-18W5	P4, R0.5, R1	C20-C22
MARATHON SNIPE LAKE 12-32-70-18W5	P4, R0.5	C23-C24
ACL SNIPELK 2-33-70-18W5	P4, R0.5	C25-C26
ACL SNIPELK 2-3-71-18W5	P4, R0.5	C27-C28
ACL SNIPELK 12-3-71-18W5	P4, R0.5	C29-C30
POCO SNIPE IN 2-4-71-18W5	R0.5, R1	C31-C32

LEGEND FOR SYMBOLS


Lithofacies A
(Peloid Packstones)


Lithofacies B (Robust Branching
Cylindrical Stromatoporoid Rudstones)


Lithofacies C (Branching Cylindrical
Stromatoporoid Floatstones)


Lithofacies D
(Light Tan *Amphipora* Floatstones)


Lithofacies E
(Dark Brown *Amphipora* Rudstones)


Lithofacies F
(Stromatoporoid Floatstones to Rudstones)


Lithofacies G
(Tabular Stromatoporoid Rudstones)


Lithofacies H (Dark Brown
Thin Tabular Stromatoporoid Floatstones)

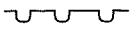

Lithofacies I
(Skeletal Grainstones)


Core Not Described


Green Shale Bed


Unconformity

Megacycle Contact


Hardground


Green Shale in Cracks and Vugs


Rhizoliths


Laminar Calcretes


Fitted-fabric Lithoclasts


Glaebules


Peds


Marine Pendant Cement
in Vug

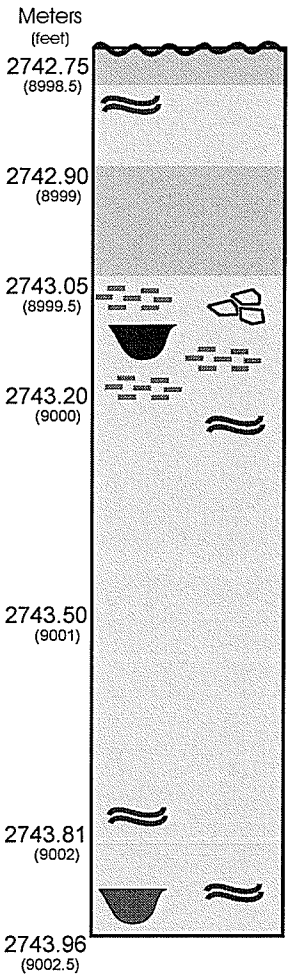

Meteoric Pendant Cement

LEGEND FOR ABBREVIATIONS

ms	=	mudstone
ws	=	wackestone
ps	=	packstone
gs	=	grainstone
fs	=	floatstone
rs	=	rudstone
Amph	=	*Amphipora*
branch cyl	=	branching cylindrical
strom	=	stromatoporoid
brach	=	brachiopod
med	=	medium
dk	=	dark
interp	=	interparticle
Intrap	=	intraparticle
intersk	=	interskeletal
intrask	=	intraskeletal
decr	=	decrease
incr	=	increase
cc	=	calcite cement
OM	=	organic matter
LC	=	laminar calcrete
pc	=	pendant cement
arg	=	argillaceous
sol'n	=	solution

TEXCAN SUNSET 00/16-17-69-19W5/0

P4 CONTACT



2742.75 m (8998.5') **P4 contact.** Green shale in medium brown mudstone with irregular stylolitized dark brown + pyritic sediment. Green mudstone with matrix replacement dolomite. 2742.80 m (8998.7') Thin <1 mm green shale and dark brown argillaceous laminar calcrete. Transitional with green shale below. 2742.90 m (8999') 15 cm green mudstone with matrix replacement dolomite. Massive chalky green appearance. Small 1-10 mm angular clasts of dark grey to black pyrite and organic material.

2743.05-2743.20 m (8999.5-9000') Abundant stromatoporoid lithoclasts and fitted-fabric lithoclasts in green shale. Increasing green shale in between stromatoporoid grains downwards. Green shale becomes more dolomitized (matrix replacement dolomite) and less argillaceous downwards. Rare clear prismatic pendant cements. Deepest occurrence of green shale approximately 2743.20 m (9000').

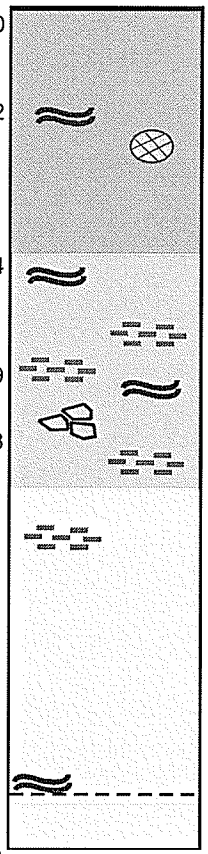
2743.20-2743.50 m (9000-9001') Fenestral lime mudstone with 3 mm argillaceous laminar calcrete with laminated green shale and dark brown argillaceous shale. Several massive brown to black stylolitic and pyritic seams, probably not laminar calcrete.

2743.50 m (9001') Change in appearance of fenestrae, larger more irregular almost vug-like fenestrae occluded by blocky dolomite cement. Smaller fenestrae occluded by blocky calcite cement. 2743.81-2743.96 m (9002-9002.5') Brown lime mudstone with large irregular vug-like fenestrae. 3-4 mm thick dark brown argillaceous (with pyrite and angular clasts) laminar calcretes at 2743.81 m (9002') and 2743.87 m (9002.2'). Vugs, irregular shaped fenestrae, laminar fenestrae (possibly dissolution enhanced) with pendant cloudy white and brown cements. Remaining pore spaces are occluded by blocky dolomite cement. Fenestrae above laminar calcrete at 2743.81 (9002') have NO pendant cements. Pendant cements in vugs and fenestrae continue down to 2743.96 m (9002.5') . Maximum depth of exposure profile at 2743.96 m (9002.5') (1.21 m thick).

TEXCAN SUNSET 00/16-17-69-19W5/0

P5 CONTACT

Meters
(feet)



2731.80 (8962.6)

2731.92 (8963)

2732.14 (8963.7)

2732.29 (8964.2)

2732.38 (8964.5)

2732.96 (8966.4)

2731.80 m (8962.6') **P5 contact.** Upper 5 cm dark brown mudstone with few angular green lithoclasts. Lower 5 cm has large green shale clasts (2.5 cm) with dark brown ms matrix infiltrating in between. Abundant small angular green lithoclasts which have internal brown lithoclasts. Dark grey sediment dissected by cracks and filled by blocky dolomite cement, probable peds. 4 mm green to grey argillaceous laminar calcrete with pink angular lithoclasts at 2731.92 m (8963').

2731.92-2732.14 m (8963-8963.7') Green shale with chalky pink dolomitization and dark grey to black pyrite "clasts".

2732.14-2732.29 m (8963.7-8964.2') Dark brown argillaceous laminar calcretes in a chalky pink dolomitized matrix with lithoclasts. LC and green shales around *Amphipora* grains and lithoclasts at 2732.22-2732.29 m (8964-8964.2') . 2732.29-2732.38 m (8964.2-8964.5') Large bulbous strom clasts and *Amphipora* with brown-green shales infiltrating between clasts (fitted-fabric lithoclasts). Dark brown and green argillaceous laminar calcretes near the top.

2732.38-2732.96 m (8964.5-8966.4') Medium brown *Amphipora* floatstone in a peloid ps matrix. Interskeletal and intraskeletal pores occluded by blocky dolomite cement. Occasional green-grey shale associated with stylolites (possible laminar calcretes). Deepest occurrence of laminar calcrete at 2732.93 m (8966.3'). Maximum depth of exposure feature 2732.93 m (8966.3') 1.13 m thick.

Abrupt increase in vugs and dolomite cements. Likely solution enhanced interskeletal pores. No pedogenic features visible.

TEXCAN SUNSET 00/16-17-69-19W5/0

R0.5 CONTACT

Meters
(feet)

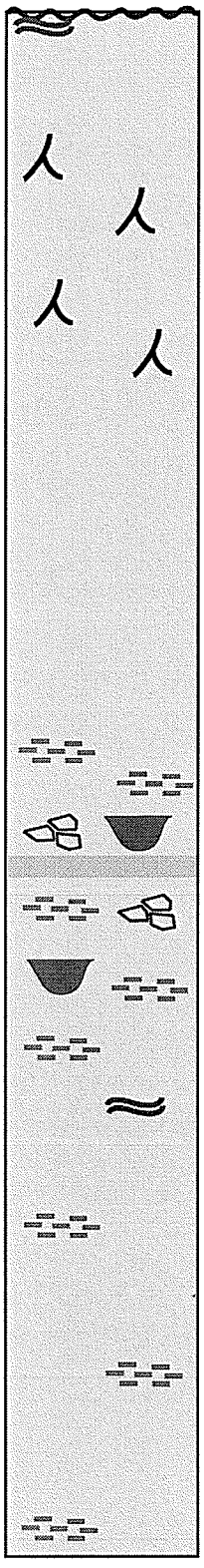
2726.38
(8944.8)



2726.50
(8945.2)

2726.38 m (8944.8') **R0.5 contact.** Dark brown laminar calcrete, 5-7 mm (mostly has already broken off) at contact. 2726.38-2726.50 m (8944.8-8945.2') Green shale rubble in core box, 8 cm interval with thin green shale beds and dark brown and green argillaceous laminar calcretes. Maximum depth of profile 2726.50 m (8945.2') (12 cm thick).

ACL SNIPELK 00/12-14-70-18W5/0
P4 CONTACT

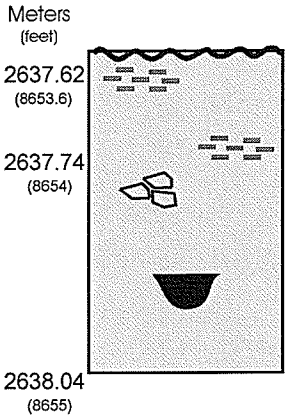


2653.19 m (8704.7') **P4 contact.** Stylolitic, dark and light brown argillaceous laminar calcrete at surface. Medium brown peloid packstone.

2653.38-2654.20 m (8705.3-8708') Medium brown peloid packstone with abundant rhizoliths. Vertically extensive rhizolith up to 11 cm long, tapers with branching near the bottom of rhizoliths. Rhizoliths continuous across backside of core; sheet-like root or possibly vertical crack with roots growing inside crack. Subhorizontal to vertical smaller tubular rhizoliths 1-3 mm with dark brown cutans down to 2653.68 m (8706.3'). Clear blocky calcite cements occluding rhizoliths tubules.

2654.20 m (8708') Scour surface with green to green-grey argillaceous dolomitic shale in peloid packstone matrix. Abundant dissolution vugs, many are filled with green shales. Vugs occluded by coarse cloudy white calcite cements and brown pendant cements. *Amphipora* grains with geopetal peloid ps sediment with remaining pore space occluded by blocky calcite cement. 2654.35 m (8708.5') 5 cm green shale with thin laminations and occasional dark carbonaceous material with pyrite. 2654.35-2654.45 m (8708.5-8708.7') Dissolution vugs filled with green shale. Thin green shales occuring in fissures and cracks. *Amphipora* clasts and other strom clasts with milky white and brown pendant cements. 2654.45-2655.33 m (8708.7-8711.7') Green shales in cracks and fissures. Green shales, blocky calcite cement and pyrite in fills fractures and vugs. Fitted-fabric lithoclasts, pendant cements in vugs. Laminar calcrete at 2654.69 m (8709.6'). Deepest occurrence of green shales at 2655.33 m (8711.7'). Maximum depth of profile 2655.33 m (8711.7') (2.1m thick).

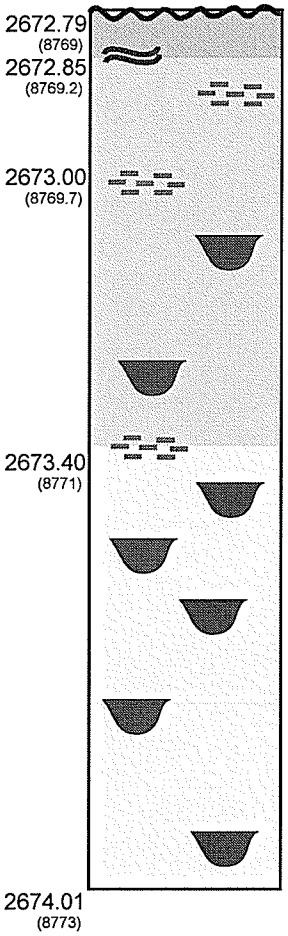
ACL SNIPELK 00/12-14-70-18W5/0
R0.5 CONTACT



2637.62 m (8653.6') **R0.5 contact** at broken surface. Fragmented stromatoporoid fragments in a dark grey lithoclast matrix. Geopetal green shales in dissolution vugs within stromatoporoid clasts. Remaining pore space in dissolution vugs in stromatoporoid grains occluded by coarse blocky calcite cement. Green shale also occurs as thin beds. Dissolution vugs mostly developed in stromatoporoid grains, few developed in the matrix. Deepest occurrence of green shale approximately 10 cm below exposure surface.

2637.74-2638.04 m (8654-8655') Stromatoporoid fragments (fitted-fabric) in a dark grey matrix. Dissolution vugs are less common and no green shale are observed. Clear prismatic pendant cements in intraskeletal pores and along undersurfaces of grains, possibly in dissolution enhanced pores (vugs). Clear blocky calcite cement occludes vuggy and interparticle pores. Maximum depth of exposure profile 2638.04 m (8655') (43 cm thick).

ACL SNIPELK 00/10-21-70-18W5/0
P4 CONTACT



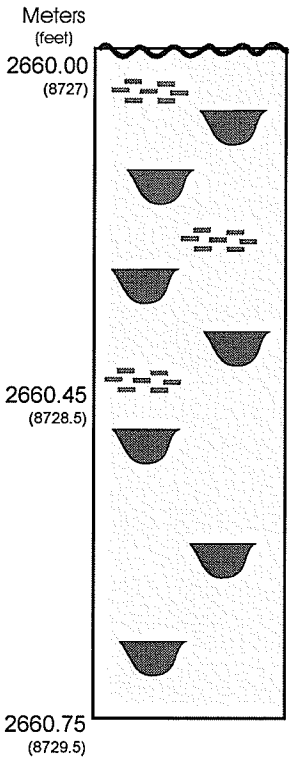
2672.79 m (8679') **P4 surface.** 6 cm interval of dolomitic pale green argillaceous shale to med brown peloid ws-ps. Thin pale green argillaceous shales and possible laminar calcretes near the top and massive green shale with abundant angular lithoclasts near the bottom.

2672.85-2673.00 m (8769.2-8769.7') Tan to medium grey fenestral lime mudstone. Green shale in fissures, cracks and vugs. Coarse grained yellow dolomitic sediment occasionally occludes vugs (probably not pedogenic).

2673.00-2673.40 m (8769.7-8771') Medium tan fenestral lime mudstone. Dissolution vugs common. Vugs often have cloudy white pendant cements and blocky calcite cements. Minor brown pendant cements. Green argillaceous shale at 2673 m (8769.7').

2673.40-2674.01 m (8771-8773') *Amphipora* rudstone to floatstone. Interval with abundant cloudy white and brown pendant cements in what shelter pores along undersides of *Amphipora* grains, possibly solution enhanced and occasional vuggy pores. Shelter pores increase in abundance downwards and vuggy pores decrease downwards. Fewer vugs than overlying interval. From top to bottom: abundance of pendant cements decreases, as blocky calcite and dolomite cements increases in pore spaces. Green argillaceous shales down to at least 2673.40 m (8771'). Deepest pendant cements down to 2674.01 m (8773'). Maximum depth of exposure profile down o 2674.01 m (8773') (1.2 m thick).

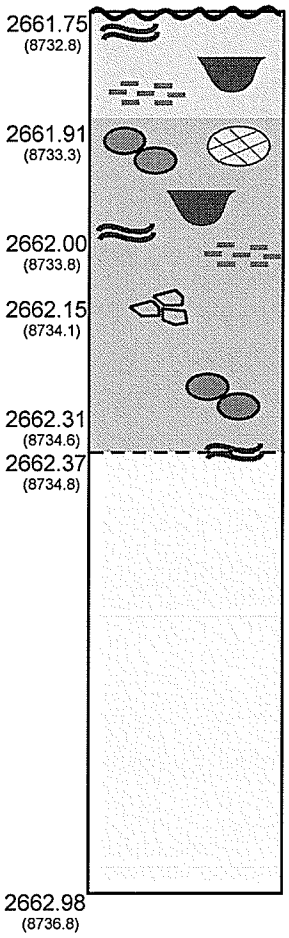
ACL SNIPELK 00/10-21-70-18W5/0
R0.5 CONTACT



2660 m (8727') **R0.5 contact.** 2660-2660.45 m (8727-8728.5') *Amphipora* floatstone with abundant dissolution vugs and shelter pores. Minor green shales in cracks down to 2660.45 m (8728.5'). Abundant cloudy white and brown fibrous pendant cements in both vugs and along bottom surfaces of *Amphipora* grains in shelter pores. Blocky calcite cements occluded remaining pore space in vugs. Pendant cements are mostly cloudy white, with lesser amounts of brown fibrous cements. Brown fibrous cements alternates with cloudy white cements. Dolomitic pale green-yellow sediment in vugs (probably not pedogenic).

2660.45-2660.75 m (8728.5-8729.5') Similar to above interval but with no green shales. Deepest pendant cements down to 2660.75 m (8729.5'). Maximum depth of exposure surface 2660.75 m (8729.5') (75 cm thick).

ACL SNIPELK 00/10-22-70-18W5/0
P4 CONTACT



2661.75 m (8732.8') **P4 contact** with dark-med brown and grey argillaceous laminar calcrete. Medium brown peloid ws to ps with abundant lithoclasts and skeletal grains. Med-dark grey mottling, darkened grains, nodules and clear prismatic (meteoric) pc. Pale green shale beds at 2661.8 m (8732.9').
2661.75-2661.91 m (8732.8-8733.3') Thin dark brown stylotized sediment/shale (possible laminar calcretes) and thin green shales.

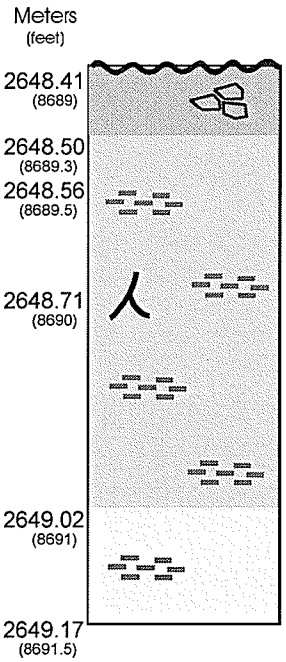
2661.91-2662.0 m (8733.3-8733.8') Chalky grey-green argillaceous shale with a clotted texture and abundant angular lithoclasts and strom fragments. Chalky dolomitic matrix with glaebules, peds, fitted-fabric lithoclasts and darkened lithoclasts. Rare prismatic pc clasts with fitted-fabric texture. Dark brown argillaceous laminar calcrete ~ 2662 m (8733.8').

2662.0-2662.31 m (8733.8734.6') Pale green to grey-green argillaceous shale with few angular lithoclasts. Occasional dark grey nodules or glaebules.

2662.31-2662.37 m (8734.6-8734.8') Abundant small (<0.5 mm) lithoclasts in a green shale matrix with larger sized rip-up clasts from below. Dolomitic mudstone grading down to peloid ws/ps. Dark grey pyritic shale beds and dark brown laminations. Maximum depth of paleosol profile 2662.37 m (8734.8') (60 cm thick).

Sharp irregular contact at 2662.37 m (8734.8') with angular lithoclasts.
2662.37-2662.98 m (8734.8-8736.8') Dark brown abraded branching cyl-bulbous strom fs in a peloid gs matrix with green shale clasts from above.

ACL SNIPELK 00/10-22-70-18W5/0
R0.5 CONTACT



2648.41 m (8689') **R0.5 contact**. 2848.41-2448.50 m (8689-8689.3') Grey green shale with pyrite and abundant sand to pebble size angular clasts. Possible fitted-fabric lithoclasts.

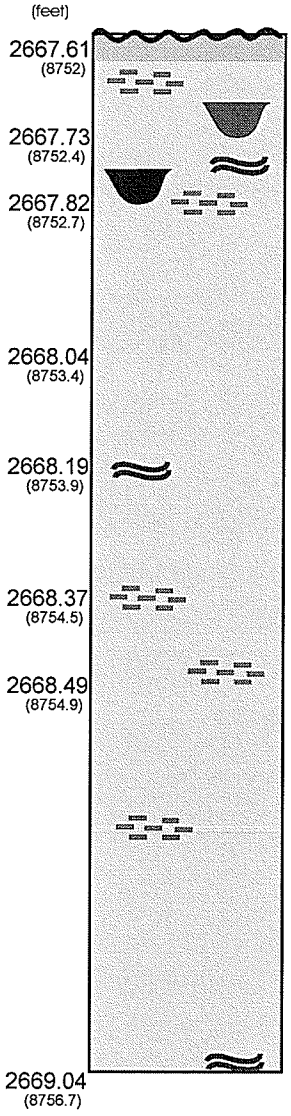
2648.50-2649.02 m (8689.3-8691') Med brown peloid-lithoclast packstone to grainstone with common angular lithoclasts and broken stromatoporoid clasts.

2648.56-2649.02 m (8689.5-8691') with a greenish grey-brown shale matrix and increase in Amphipora downwards to 2649.17 m (8691.5'). Occasional patches of chalky (dolomitized) argillaceous matrix. Thin dark grey to green shale beds. 2648.71 m (8690') has small vertical <1 cm long rhizoliths with brown micritic cutan coatings.

2649.02-2649.17 m (8691-8691.5') Interbedded med grey-brown Amphipora-branching cyl strom rudstones with medium brown peloid packstones. Interbeds 2-5 cm thick. Dark grey mottling and darkened grains in rudstone intervals (strom grains darkened). Green shale seams in matrix. Maximum depth of exposure profile 2649.17 m (8691.5') (76 cm thick).

ACL SNIPELK 00/12-22-70-18W5/0

P4 CONTACT



2667.61 m (8752') **P4 contact.** Irregular erosional surface between overlying brown peloid ps/gs with green shale below, 2 mm thick black organic-rich layer above the contact. Abundant angular lithoclasts near the contact. Thin green shales and green shale rubble in core box. Abundant dissolution vugs occluded by pale green (dolomitic) sediment, blocky dolomite cement and fibrous pendant cements. Green shale occasionally geopetal.

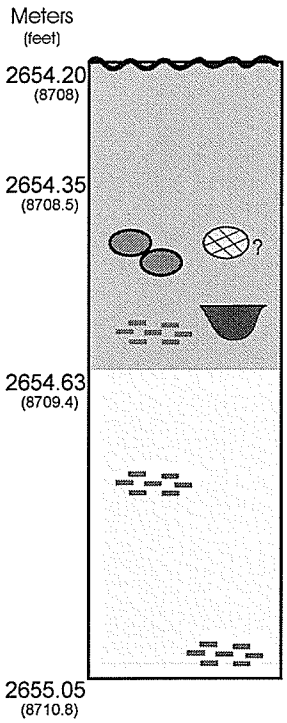
2667.73-2668.04 m (8752.4-8752.7') Crinkly laminated fenestral lime mudstone. Thin laminated green shale and brown argillaceous laminar calcretes at 2667.73 m (8752.4'). Prismatic inclusion-free to moderate inclusion pendant cements at 2667.8 m (8752.5'). Abundant strom clasts, dark brown argillaceous to micritic material (massive, questionable if laminar calcrete) and darkened grains.

2668.04-2668.37 m (8753.4-8753.9') *Amphipora* and branching cylindrical stromatoporoid fs/rs. Dissolution vugs with geopetal brown sediment, not likely pedogenic material.

2668.19 m (8753.9') has large bulbous stromatoporoids with dissolution vugs. Vugs occluded by clear blocky calcite cement and geopetal brown sediment. Laminar calcrete at 2668.19 m (8753.9').

2668.37-2668.49 m (8754.5-8754.9') Weakly laminated and fenestral lime mudstone to peloid wackestone. Rare green shales in fenestrae.
2668.49-2669.04 m (8754.9-8756.7') Massive to slightly mottled lime mudstone to peloid wackestone. Geopetal green shales in vugs at 2668.58 m (8755.2'). Deepest occurrence of green shales, approx 97 cm below P4 surface. Dark grey to dark brown argillaceous laminar calcrete at 2669.04 m (8756.7'). Maximum depth of exposure profile 2699.04 m (1.43 m).

ACL SNIPELK 00/12-22-70-18W5/0
R0.5 CONTACT

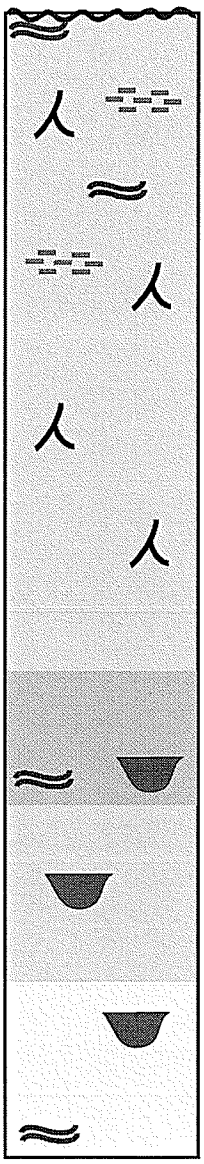


2654.20 m (8708') **R0.5 contact** (broken, unpreserved contact). Green shale rubble in core box with abundant angular lithoclasts in a chalky green shale matrix. Finely laminated grey argillaceous material (possible laminar calcrete).

2654.35-2654.63 m (8708.5-8709.4') *Amphipora* + branching cylindrical strom floatstone in dolomitized chalky beige to dark grey matrix (dolomitized green shale?). Stromatoporoid grains appear slightly darkened around edges, in particular *Amphipora* grains. 2654.5 m (8709') is a dolomitic green shale (dolomicrite) with clotted textures, dolomitic glaebules, clear prismatic pendant cements and possible peds to intermittent peds.

2654.63-2655.05 m (8709.4-8710.8') *Amphipora* floatstone to rudstone in a medium tan peloid matrix. Darkened *Amphipora* grains down to 2655.05 m (8710.8'). Thin green shales (4 mm) around 2655.05 m (8710.8'). Deepest occurrence of green shales and maximum depth of exposure profile down to 2655.05 m (8710.8') (85 cm).

ACL SNIPELK 00/12-23-70-18W5/0
P4 CONTACT



2635.61 m (8647') **P4 contact.** 1.5 cm faintly laminated dark brown and green-grey shale (laminar calcrete) at the contact. 2635.61-2636.03 m (8647-8648.4') Peloid packstone to grainstone with green to dark grey argillaceous laminar calcretes (and pyrite) 2-3 mm thick. Light-dark grey mottling and nodules in the matrix. Green shale rubble in core box. Interval has small rhizoliths. Horizontal tubular structures with dark brown linings (micritic cutans).

2636.03-2636.52 m (8648.4-8650') Similar peloid packstone to grainstone as above, with more rhizoliths (tubular structures with brown linings) but absence of green shales.

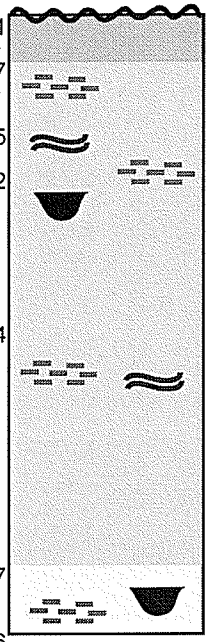
2636.52-2636.75 m (8650-8650.6') Massive dolomitic milky green shale. Faintly laminated towards the top, but overall very massive. Decrease in green shale downwards, lower 5 cm transitional with medium brown peloid ps/gs. Irregular shaped black accumulation of organic material and pyrite and tubular branching halos(remnant rhizoliths?). Laminations near the top are possible remnant peloid ps/gs fabric. Calcareous and dolomitic geopetal sediment. Pendant cements in vugs and laminar calcretes.

2636.75-2636.82 m (8650.6-8651') Very sharp contact with overlying brown peloid ps. Abundant dissolution vugs occluded by brown geopetal sediment, blocky calcite cement, and blocky dolomite cement. Cloudy white and brown pendant cements on upper surfaces of vugs. Possible meniscus cements.

2636.82-2636.95 m (8651-8651.4') Small more irregular shaped vugs that appear to be dissolution enhanced interskeletal shelter and fenestral pores and are occluded by blocky calcite and dolomite cements. Occasional pendant cements on undersides of grains and geopetal pale yellow (coarse dolomitic) sediment in vugs.

2636.92-2637.19 m (8651.3-8652.2') Bulbous and branching cylindrical strom fragments in medium tan peloid ps-gs matrix. Moldic pores occluded by clear blocky calcite cement. Possible pendant cements, but not obvious. Laminar calcrete (dark green-brown argillaceous shale with pyrite) at 2637.19 m (8652.2'). Maximum depth of exposure profile 2637.19 m (8652.2') (1.58 m thick).

ACL SNIPELK 00/04-26-70-18W5/0
P4 CONTACT



2635.91 m (8648') **P4 contact** (broken core, unpreserved). 5 cm of green shale rubble in core box. 2635.97-2636.05 m (8648.2-8648.7') Abundant green shales in a dark grey to dark brown lime ms-ws to peloid ps. Green shales in cracks, fissures and dissolution vugs.

2636.05-2636.12 m (8648.5-8648.7') Dark grey to brown *Amphipora* rudstone in peloid ps matrix. Darkened *Amphipora* grains. Pale brown-green and dark grey laminar calcrete 1-3 mm at the top. Green argillaceous shale seams common Abundant dark brown sediment and pyrite in cracks. Thin green shale beds near the bottom (possible laminar calcretes).

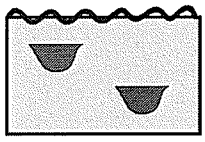
2636.12-2636.34 m (8648.7-8649.4') Crinkly laminated (cryptalgal mat) mudstone to wackestone with abundant laminar fenestrae. Clear prismatic pendant cements under *Amphipora* and with dissolved margins. Pale yellow to light brown geopetal sediment in fenestrae (probably not pedogenic). (2636.3-2636.7 m) Medium grey to tan lime mudstone to wackestone with medium to dark grey mottling. Dissolution vugs common with light tan geopetal sediment (non pedogenic) and clear blocky calcite cements. Laminar calcrete at 2636.40 m (8649.6') with argillaceous green shale.

2636.67-2636.76 m (8650.5-8650.8') Light tan branching cylindrical stromatoporoid (+ few *Amphipora*) floatstone to rudstone in a peloid ps-gs matrix. Rare prismatic pendant cements, with dissolved margins. Highly altered stylolitic green shale at 2636.76 m (8650.8'). Maximum depth of exposure profile down to 2636.76 m (8650.8') (85 cm thick).

ACL SNIPELK 00/04-26-70-18W5/0
R0.5 CONTACT

Meters
(feet)

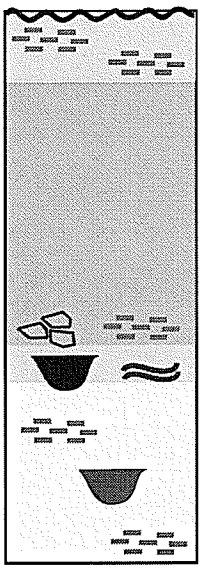
2620.67
(8598)



2620.85
(8598.5)

2620.67 m (8598') **R0.5 contact.** Sharp surface with truncated grains and fragmented clasts that are possibly bored. Fenestral pores and vugs (solution enhanced shelter pores). Grains and matrix appear somewhat darkened at the surface. Laminated milky white and brown fibrous pendant cements in vugs and undersides of grains. Light brown to white isopachous cements rimming pores. Relatively tight, blocky calcite and blocky dolomite cements occlude pore spaces. Geopetal dolomitic sediment in vugs. Maximum depth of exposure profile 2620.85 m (8598.5') (15 cm thick).

ACL SNIPELK 00/10-27-70-18W5/0
P4 CONTACT



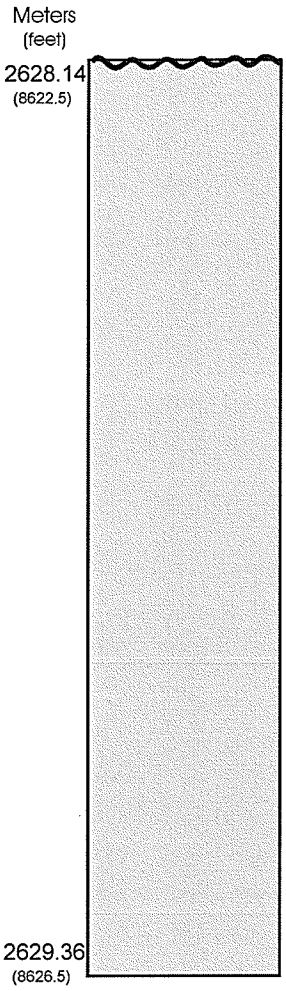
2643.23 m (8672') **P4 contact.** 2643.23-2643.32 m (8672-8672.15') Dark brown dolomitic peloid ps-gs with thin beds of pale yellow shale with angular lithoclasts at the bottom. Lower 5 cm transitional zone from brown peloid ps/gs to moderately laminated green shale with brown angular lithoclasts and pyrite.

2643.32-2643.62 m (8672.3-8672.6') Pale green to grey argillaceous shale. Massive near the top with increasing mottling or bioturbation downwards. Pyrite and pale green halos. Dark grey tubular structures, remnant rhizoliths? Dark grey nodules or possible glaebules. Lower 10 cm mostly broken argillaceous green shale rubble in core box.

2643.62-2643.74 m (8673.3-8673.7') Peloid wackestone with rare *Amphipora.* Dolomitized dark grey-green upper 5 cm. Abundant angular lithoclasts (possible fitted-fabric) in a green shale matrix. Argillaceous green shale in thin cracks. Dark brown-grey and green argillaceous laminar calcretes. Rare prismatic pc on *Amph* grains. Weakly laminated at the bottom with laminated green and pale yellow shales (LC?).

2643.74-2644.0 m (8673.7-8674.5') *Amphipora* floatstone in a fenestral lime mudstone to peloid wackestone matrix. Decrease in *Amphipora* upwards. Thin green shales in cracks and rare cloudy white pc in vugs. Vugs are usually occluded by blocky calcite cements. Laminated dark brown, medium brown and green argillaceous sediment. Green shales at 2643.9 m (8674.2') and 2644 m (8674.5'). Geopetal sediment in fenestrae. Dissolution vugs near the bottom. Maximum depth of exposure profile down to 2644 m (8674.5') (77 cm thick).

ACL SNIPELK 00/10-27-70-18W5/0
R0.5 CONTACT

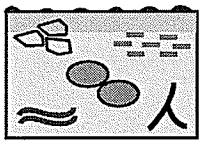


2628.14 m (8622.5') **R0.5 contact.** 2628.14-2629.36 m (8622.5-8626.5') Fenestral to laminated peloid wackestone to packstone. Generally tight, pore spaces occluded by blocky clear calcite cements. Interparticle porosity in lower 45 cm - fenestral porosity 3-4%. Gradational from fenestral to laminated towards the top. No visible exposure features. Tidal flat.

ACL SNIPELK 00/12-27-70-18W5/0
P4 CONTACT

Meters
(feet)

2651.36
(8698.7)

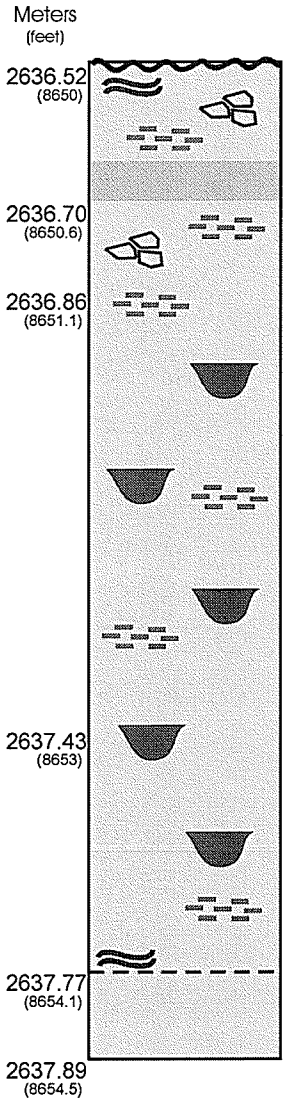


2651.52
(8699.2)

2651.36 m (8698.7') **P4 contact** (broken not preserved). 1.5 cm finely laminated to massive grey-green shale with fitted-fabric lithoclasts at contact. Possible laminar calcrete <1 mm.

2651.36-2651.52 m (8698.7'8699.2') Peloid-lithoclast packstone with dark grey laminar calcretes <1 mm. Dark grey halos around vugs. Irregular to tubular structures in filled with light tan to green dolomitic shale (sometimes geopetal) and blocky calcite cement, possible rhizoliths. Possible glaebules, globular concentrations of dark brown clotted dolomicrite. End of core at 2651.52 m (8699.2'), observed depth of exposure profile only 15 cm deep.

ACL SNIPELK 00/12-27-70-18W5/0
R0.5 CONTACT



2636.52 m (8650') **R0.5 contact.** Dark brown to light tan *Amph* fs-rs with green argillaceous LC (1-5 mm) and fitted-fabric lithoclasts. Green shales in between stromatoporoid clasts.

2636.64-2636.70 m (8650.4-8650.6') Green shale rubble in core box.

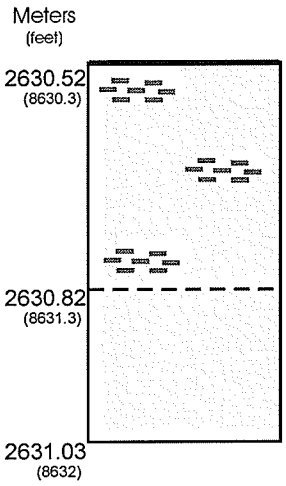
2636.7-2636.86 m (8650.6-8651.1') Fitted-fabric angular stromatoporoid grains in a green shale matrix. Thin <1 mm green and grey shales. Increase in lithoclasts and decrease in green shale downwards.

2636.86-2637.43 m (8651.1-8653') Branching cylindrical rudstone with yellow-green shales. Interskeletal pores likely solution enhanced (irregular dissolved grain boundaries) occluded by yellow-green shales, blocky coarse white calcite cement, blocky dolomitic cement and dolomitic sediment. Abundant medium to dark brown pendant cements on bottom surfaces of stromatoporoid grains, some broken up possibly meteoric and/or marine origin (?). Pendant cements faintly laminated, sometimes interbedded with layers of cloudy white cement (prismatic inclusion-rich and inclusion-free layers, interpreted as meteoric). .

2637.43-2637.77 m (8653-8654.1') Large stromatoporoid clasts with dissolution vugs occluded by geopetal yellow-green shale and blocky coarse white cement . Brown pendant cements on upper surfaces of vugs in matrix and within stromatoporoid clasts. Thin green-yellow shales in cracks or fissures near the bottom. Deepest appearance of green shales approximately 1.2 m below exposure surface. Stylolitic grey argillaceous laminar calcrete at 2637.77 m (8654.1'). Maximum depth of exposure profile at 2637.8 m (8654.1') (1.2 m thick).

2637.77 m (8654.1') Blackened *Amphipora* and branching cylindrical stromatoporoid grains with possible micritized rims down to 2637.89 m (8654.5').

ACL SNIPELK 00/12-27-70-18W5/0
R1 CONTACT



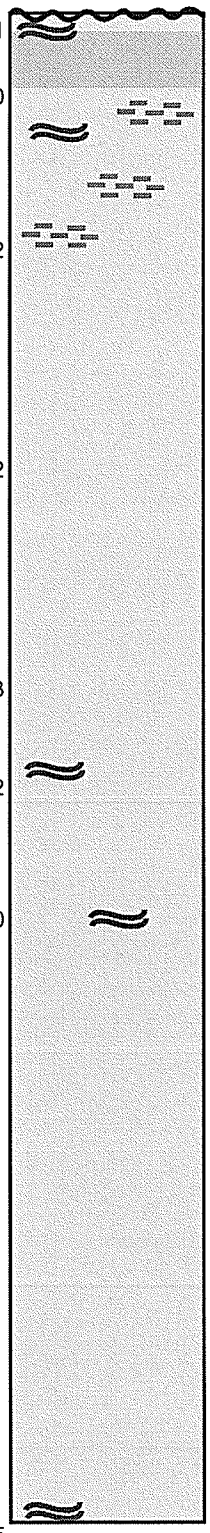
2630.52 m (8630.3') **R1 contact.** Thin green shale <1 mm at contact. Angular stromatoporoid clasts in a green shale matrix.

2630.58-2630.82 m (8630.5-8631.3') Dissolution vugs in larger stromatoporoid clasts and in the matrix. Vugs with geopetal yellow-green shales. Occasional thin <1 mm greens shale. Deepest vugs with geopetal shale approximately 2630.82 m (8631.3'), about 30 cm below R1 surface. Darkened clasts and dark grey mottling in matrix.

Deepest occurrence of darkened clasts and dark grey mottling 2631.03 m (8632').

MARATHON SNIPE LAKE 00/12-32-70-18W5/0

P4 CONTACT



2617.01 m (8586') **P4 contact.** Massive thick tabular stromatoporoid overlying surface and laminar calcrete 1.1 cm thick at the contact. 2617.01-2617.10 m (8586-8586.3') Gradational from dark black laminated argillaceous shale to 7.5 cm thick green shale. Horizontal to subhorizontal green shale filled cracks. Dissolution vugs with geopetal sediment and blocky dolomite cement.

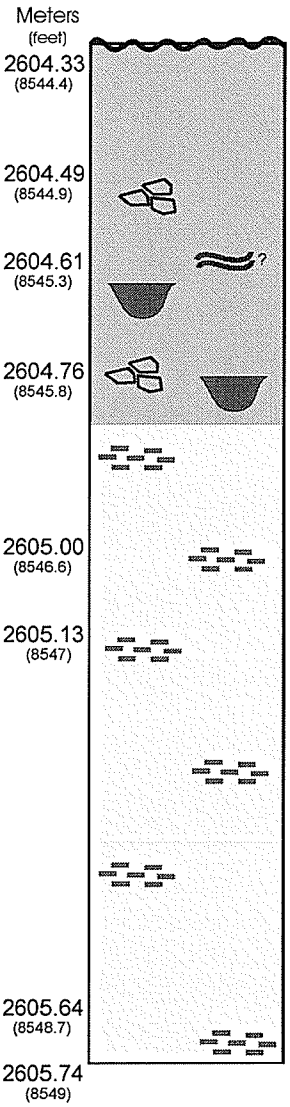
2617.10-2617.32 m (8586.3-8587') Peloid ps matrix with scattered *Amphipora* with weakly developed fenestrae. Possible argillaceous laminar calcrete 2617.17 m (8586.5'). Stylolites with dark brown sediment and pyrite (possible calcrete). Green shale rubble down to approximately 2617.32 m (8587').

2617.32-2617.93 m (8587-8589') Medium to dark grey *Amphipora* floatstone with local rudstones in a peloid ws to ps matrix. Mottled texture with darkened grains from 2617.32-2617.62 m (8587-8588') and nodular texture around 2617.55 m (8587.8') and 2617.81 m (8588.6'). Increase abundance of *Amphipora* lower 10 cm. Vertical to sub-vertical cracks in grains and matrix occluded by clear blocky calcite cement.

2618.02-2619.05 m (8589.3-8592.7') Medium brown to grey *Amphipora* floatstone to rudstone in a peloid ws to packstone matrix (similar lithology as above intervals) with slightly mottled to nodular texture. Laminar calcretes at 2618.01 m (8589.3') (1.5 cm), 2618.20 m (8589.9') (<1 mm) and 2619.05 m (8592.7'). No other obvious exposure features. Maximum depth of exposure profile down to 2619.05 m (8592.7') (2.04 m thick).

MARATHON SNIPE LAKE 00/12-32-70-18W5/0

R0.5 CONTACT



2604.33 m (8544.4') **R0.5 contact.** Irregular sharp and scoured surface. 2604.33-2604.49 m (8544.4-8544.9') Dark grey to green chalky argillaceous dolomitic mudstone, slightly mottled. Cracks are filled with overlying dark brown *Amphipora* fs. Thin beds of overlying sediment.

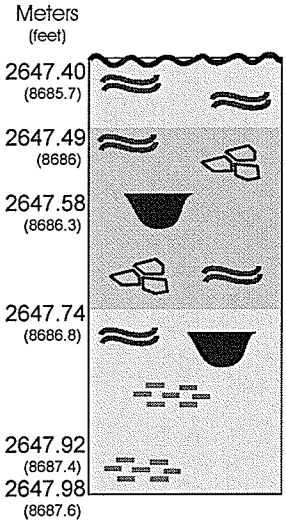
2604.49-2604.61 m (8544.9-8545.3') Fitted-fabric dark grey lithoclasts in a dolomitic green shale matrix. Possible laminar calcrete 2604.61 m (8545.3'). Abundant lithoclasts in milky white dolomitized matrix. Broken clasts of inclusion rich and inclusion poor zoned pendant cements in dolomitized green shale.

2604.61-2604.8 m (8545.3-8546') Abundant lithoclasts and stromatoporoid clasts (fitted-fabric) with abundant milky white and brown cements in dolomitized chalky green shale matrix. Lithoclasts composed of grains with brown and white pendant cements. Pendant cements possibly in shelter pores. Fractures filled with green shale and pyrite. Green shale rubble throughout core box down to 2605 m (8546.6').

2604.8-2605.13 m (8546.0-8547') Mottled *Amphipora* floatstone. Dark grey clasts with a nodular appearance. Green shale seams draping around *Amphipora*.

2605.13-2605.64 m (8547-8548.7') Amphipora rudstone with a tan-grey nodular texture. Dark grey shale around 2605.13-2605.40 m (8547-8547.9'). Minor argillaceous green shale seams in matrix. Stromatoporoid fragments with dissolution vugs with geopetal sediment (not sure if pedogenic material) from 2605.83-2606.0 m (8549.3-8549.9'). Deepest occurrence of green shale and maximum depth of exposure profile at 2605.7m (8549') (1.3 m thick).

ACL SNIPELK 00/02-33-70-18W5/0
P4 CONTACT



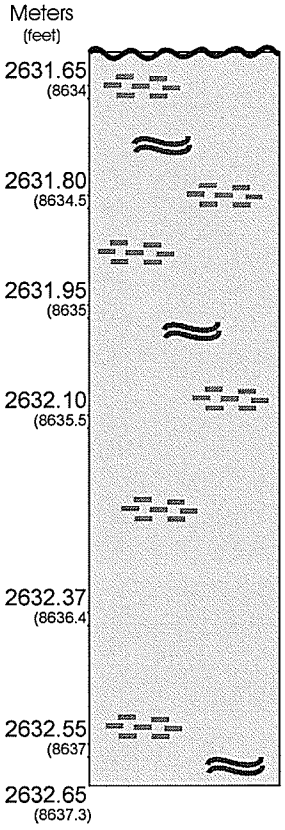
2674.40 m (8685.7') **P4 contact.** Dark brown peloid ps with green shale clasts and rip-up clasts from below. Remnants of a dark brown to black laminar calcrete at the contact. Thin <1 mm laminar calcretes common above the erosional surface at 2647.49 m (8686'). Thinly laminated green to green-grey argillaceous shale with small lithoclasts below the erosional surface. Argillaceous laminar calcretes and fitted-fabric lithoclasts in green shale matrix. Prismatic pendant cements on undersides of lithoclasts in matrix. Rip-up clasts from underlying interval.

2647.58-2647.74 m (8686.3-8686.8') Grey-green argillaceous lime mudstone with abundant lithoclasts. Laminar calcretes (brown argillaceous shale and pyrite common). Green shale in vugs and interparticle pores between stromatoporoid grains.

2647.74-2647.77 m (8686.8-8686.9') Abundant laminar calcretes (dark brown argillaceous shale with pyrite). Decreasing green shale abundance and increasing brown argillaceous material downwards. Pendant cements common on undersides of lithoclasts in green shale matrix. 2647.77 m (8686.9') Sharp surface with laminar calcrete.

2647.77-2647.92 m (8686.9-8687.4') Laminated cryptalgal mudstone to wackestone with a few thin <1 mm laminar calcretes. 2647.92 m (8687.4') Reappearance of grey to green shales. Green shales occurring in horizontal cracks. Deepest occurrence of green shales 2648 m. Maximum depth of profile 2647.98 m (8687.6') (64 cm thick).

ACL SNIPELK 00/02-33-70-18W5/0
R0.5 CONTACT



2631.65 m (8634') **R0.5 contact.** 2631.65-2631.80 m (8534-8534.5') Bulbous stromatoporoids have cracks filled with dark brown sediment from above. Stromatoporoids have a slightly darkened appearance. Green shales also in cracks and fissures. Backside of core shows abundant green shales and laminar argillaceous calcretes.

2631.80-2631.95 m (8634.5-8635') Mixed argillaceous shales and green shale laminar calcretes. Thin green to brown shales in cracks and fractures. Green shales often associated with stylolites and contain small angular lithoclasts. Stromatoporoid grains abundant in this interval.

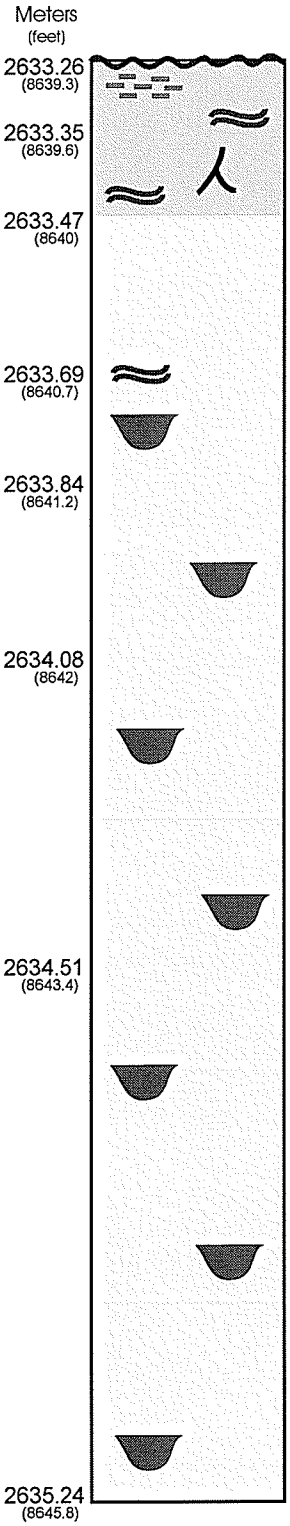
2631.95-2632.10 m (8635-8635.5') Abundant thin green shales <2 mm associated with stylolites, and filling cracks and fissures. Pale green shales with small lithoclasts in interskeletal pores at the top. Dissolution vugs in matrix and in stromatoporoid fragments with geopetal pale yellow-green argillaceous sediment. (Two types of argillaceous sediment pale yellow-green sediment and green argillaceous sediment)

2632.10-2632.37 m (8635.5-8636.4') Fewer green shales and appearance of brown-green shales. Darkened stromatoporoid grains (mostly branching cylindrical stromatoporoids) common.

2632.37-2632.55 m (8636.4-8637') Stromatoporoid clasts not darkened in this interval with vugs and geopetal sediment. Pale yellow argillaceous sediment with lithoclasts occurring in interskeletal pores.

2632.55-2632.65 m (8637-8637.3') Abundant *Amphipora* and branch cyl stroms with slightly darkened appearance. Dark grey mottling in the matrix. Green shales reappear and abundant down to 2632.65 m (8637.3'). Argillaceous green-brown laminar calcrete at 2632.65 m (8637.3'). Maximum depth of exposure profile 2632.65 m (8637.2') (1.0 m).

ACL SNIPE LK 00/02-03-71-18W5/0
P4 CONTACT



2633.26 m (8639.3') **P4 contact.** Dark brown argillaceous shale with pyrite and angular clasts at the contact (likely laminar calcretes). Underlain by 1.5 cm green shale with angular clasts and thin <1 mm dark brown laminar calcretes.

2633.35-2633.47 m (8639.6-8640') Finely laminated mudstone to peloid ws/ps. Horizontal to sub horizontal tubules upper 5 cm with red-brown halos (horizontal rhizoliths).

2633.47-2633.69 m (2640-8640.7') Abundant dissolution vugs and fenestrae occluded by pale tan-green geopetal sediment (probably not pedogenic) and blocky dolomite cement. Pale geopetal sediment more common near the top. Vugs likely solution enhanced shelter or primary interskeletal pores. Possible wavy clotted white and tan laminated pendant cements on undersides of strom fragments.

2633.69-2633.84 m (8640.7-8641.2') Continued dissolution vugs. Grains have dissolved grain boundaries near vugs. Vugs occluded by thick cloudy white and grey pendant cements blocky calcite, blocky dolomite cements and pale yellow-tan-pink sediment (non-pedogenic).

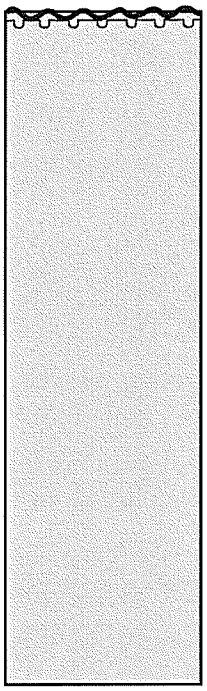
2633.84-2634.08 m (8641.2-8642') *Amphipora* floatstone with no obvious pedogenic or exposure features. Shelter pores occluded by clear blocky calcite cements. Geopetal structures in *Amphipora* coenostea.

2634.08-2634.51 m (8642-8643.4') Abundant dissolution vugs occluded by light-med tan geopetal sediment, white to clear blocky calcite cements and lesser amounts of blocky dolomite cements. Pendant cements common in vugs and undersides of stromatoporoid fragments. Pendant cements laminated cloudy white to grey calcite. Open porosity remaining increasing downwards from ~5% to ~10%.

2634.51-2634.75 m (8643.4-8644.2') Decreased pendant cements on undersides of *Amphipora* grains. Overall decrease in abundanct and thickness of fibrous pendant cements in vugs downwards. Pendant cements also decrease in the abundance of inclusions. Pendant cements also developing in sheet cracks. Deepest occurrence of pendant cements ~ 2635.2 m (8645.8') . Maximum depth of exposure profile at 2635.2 m (8645.8') (2.1 m thick).

ACL SNIPE LK 00/02-03-71-18W5/0

R0.5 CONTACT



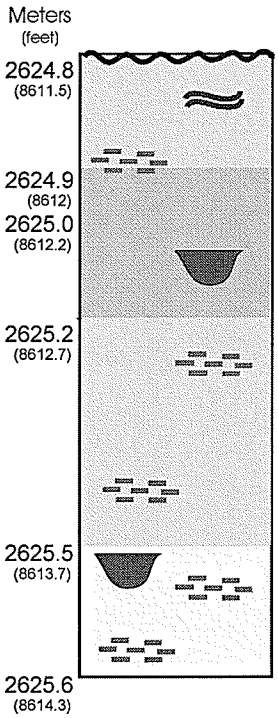
2616.4 m (8584') **R0.5 contact.** Hardground surface, relatively sharp erosional surface with truncated *Amphipora* grains. *Amphipora* floatstone in peloid ws/ps matrix. Geopetal sediment in fenestrae. No obvious pedogenic or exposure features.

2616.65-2617 m (8584.8-8586') *Amphipora* grains with dark grey halos or rims. No obvious subaerial exposure features.

2617.01-2617.32 m (2586-8587') *Amphipora* grains with darkened rims and geopetal sediment in fenestrae/vugs. R0.5 doesn't show any obvious pedogenic or exposure features.
Light grey mottling in matrix.

ACL SNIPELK 00/12-03-71-18W5/0

P4 CONTACT



2624.8 m(8611.5') **P4 contact.** Laminated medium tan peloid packstone to grainstone with irregular fenestrae. Rare branching cylindrical stroms. Matrix appears darkened (medium grey). Upper 5 cm has irregular structures filled with dark brown material, possible cutan material. Possible thin laminar calcretes.

Sharp, scoured surface at 2624.9 m (8612'). Thin green to grey shales at the scour surface, possible laminar calcretes. Another sharp, scoured surface at 2625 m (8612.2') with thin green shales.

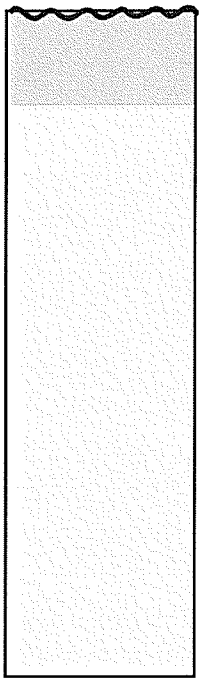
2625-2625.2 m (8612.2-8612.7') Peloid grainstone in a green argillaceous shale matrix. Increase in green shale rubble in core box downwards. Rare cloudy white pendant cements in vugs.

2625.2-2625.5 m (8612.7-8613.7') Light tan lime mudstone to peloid wackestone with abundant irregular to laminar fenestrae and occasional crinkly cryptalgal laminations. Minor (very thin) pale green shales in cracks, fractures and vugs (less common).

2625.5 m (8613.7') Relatively sharp erosional surface with abundant small angular lithoclasts above and below surface. 2625.5-2525.6 m (8613.7-8614.3') Branching cylindrical strom rudstone (with brachiopods + gastropods) in peloid packstone-grainstone matrix. Dark brown pendant cements on undersides of stromatoporoid grains. Green shale matrix and green shale seams. Increase in green shale seams in comparison to overlying interval. Deepest occurrence of green shale at 2625.6 m (8614.3'). Maximum depth of exposure profile (85 cm).

ACL SNIPELK 00/12-03-71-18W5/0

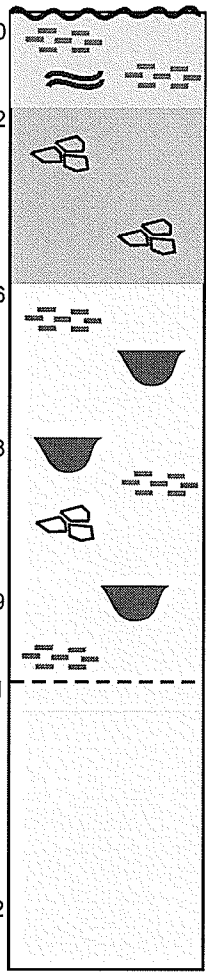
R0.5 CONTACT



2609.7 m (8562') **R0.5 contact.** Abrupt change in appearance. *Amphipora* fs to oncolitic (algal overgrowths on grains). Laminar fenestrae, occluded by cc. No visible exposure features.

2609.8-2610.6 m (8562.4-8565') *Amphipora*-branching cylindrical floatstone. Matrix fines upwards from peloid packstone up to lime mudstone-peloid wackestone. Some oncolities (strom grains with algal overgrowths) + some bulbous stroms <0.5 cm. Vuggy porosity 3% (possibly some moldic). Open lagoon.

POCO SNIPE IN 00/02-04-71-18W5/0
R0.5 CONTACT



2603.30 m (8541') **R0.5 contact.** Light tan-grey weakly laminated lime ms to peloid ws/ps. Erosional surface with angular lithoclasts above and below surface. Green and grey argillaceous laminar calcretes with pyrite and quartz silt. Green shales are dolomitized and the bottom has 5 mm interval of thinly laminated green-grey argillaceous shales with rare angular lithoclasts. 2603.42 m (8541.4') 24 cm interval of green shale in core box. Broken core pieces with dark grey angular "clasts" and pyrite. Fitted-fabric appearance of dark clasts in the green shale matrix. 2603.66-2603.88 m (8542.2-8542.9') Poorly sorted stromatoporoid clasts in a dark grey matrix. Green shale in cracks, fissures, vugs and in between strom grains. Occasional thin stylolitic green-brown shale seams (questionable if laminar calcrete). Stromatoporoid clasts with cloudy white pendant cements on the undersurfaces. Pendant cements more common towards the top and decreases in abundance downwards. Geopetal dolomitic sediment in v

2603.88-2604.09 m (8542.9-8543.6') Stromatoporoid (bulbous + branch cyl) rs to fs in a light tan peloid ws matrix. Green shales in fissure and cracks. Thin dark brown argillaceous shale, green shale and pyrite (difficult to tell if laminar calcrete). Fitted-fabric strom clasts in green shale. Dissolution vugs in strom grains occluded by blocky calcite cement. 2604.09-2604.21 m (8543.6-8544') Light tan Amphipora-branch cyl strom rs in a muddy matrix. Green shales in cracks and fissures. Encrusting stroms on other strom clasts. Deepest green shales 2604.2 m (8544'), maximum depth of exposure profile approximately 90 cm.

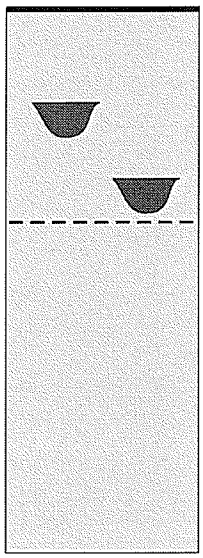
2604.21-2604.52 m (8544-8545') Amphipora rs with few branching cylindrical stroms at the top and more abundant in lower 15 cm. Encrusting stroms on other strom fragments. Grains and matrix appear slightly darkened (light to medium grey). Highly altered dark brown-green material in interparticle pores - possibly remnants of altered green shale. First occurrence of porosity below exposure surface, ~ 2% porosity.

Branching cylindrical strom rudstone in a peloid ps-gs matrix. 5-7% intraparticle porosity.

POCO SNIPE IN 00/02-04-71-18W5/0

R1 CONTACT

Meters
(feet)



2597.20 m (8521') **R1 contact** (break in core, not preserved). Stromatoporoid rudstone with bulbous stroms near the top and *Amphipora* near the bottom. Dissolution vugs with geopetal brown sediment (probably not pedogenic) and blocky calcite cement towards the top. Pendant cements under *Amphipora* grains in shelter pores.

2597.32-2597.51 m (8521.4-8522') *Amphipora* floatstone to rudstone. Abundant shelter pores and possible solution enhanced pores. Cloudy white pendant cements on undersides of *Amphipora*. Slight increase in abundance of *Amphipora* and decrease in size of pores going downwards. Deepest occurrence of any exposure features 2597.51 m (8522') approximately 30 cm below R1 surface.

2597.51-2597.96 m (8522-8523.5') *Amphipora* rudstone in a peloid ps matrix. Decreasing *Amphipora* going downwards. Darkened *Amphipora* grains (dark grey) in the upper 7.5 cm. No exposure features.

APPENDIX D - PETROGRAPHIC TECHNIQUES

D.1 Staining Techniques for Carbonate Rocks in Thin Section (modified from Dickson, 1955; 1966)

A) To distinguish between calcite and dolomite:

ALIZARIN RED S – 998 mL distilled water
5.3 mL concentrated (37%) HCl
1.0 g Alizarin Red S

B) To distinguish between ferroan carbonate and nonferroan carbonate:

POTASSIUM FERRICYANIDE - 998 mL distilled water
5.3 mL concentrated (37%) HCl
5.0 g potassium ferricyanide

Store solution in a brown bottle, away from light. Filter before use if a precipitate develops.

1. Prepare each of the above solutions separately and allow to stand for 24 hr before using.
2. Combine 2 parts of Alizarin Red S solution with 3 parts potassium ferricyanide solution.
3. Staining time is approximately 2 minutes depending upon temperature and polish on the slide.
4. Always wash slides with distilled water; tap water contains iron and will blot on the slide.
5. Refer to Table D.1 for results of staining.

Table D.1 Etching and staining characteristics of carbonate minerals (modified from Adams et al., 1984)

Mineral	Effect of etching	Stain color with Alizarin Red S	Stain color with potassium ferricyanide	Combined result
Calcite (non-ferroan)	Considerable (relief reduced)	Pink to red-brown	None	Pink to red-brown
Calcite (ferroan)	Considerable (relief reduced)	Pink to red-brown	Pale to deep blue depending on iron content	Mauve to blue
Dolomite (non-ferroan)	Negligible (relief maintained)	None	None	Colorless
Dolomite (ferroan)	Negligible (relief maintained)	None	Very pale blue	Very pale blue (appears turquoise or greenish in thin section)

D.2 Diffused Plane-Polarized Light Method

Diffused plane-polarized light microscopy can be used to enhance textural features in thin-sections of dolostones and recrystallized limestones that are not recognizable when viewed under standard plane-polarized or cross-polarized light. Delgado (1977) was the first to propose the diffused-plane-polarized light technique which has been subsequently modified by Folk (1987) and Dravis (1991). Delgado (1977) found the most effective light diffuser was produced by coating the undersides of thin-sections with magnesium oxide and noted that simple white paper was also effective. He also noted that the technique was optimized by viewing thin-sections under lower intensity transmitted light with the condenser lens. Folk (1987) found that using simple white paper with an external (reflective) light source was effective for recognizing organic matter in thin-sections. Dravis (1991) modified Folk's (1987) white-card technique by using plane-polarized light generated from the built-in illuminator (transmitted light) of the microscope.

Diffused plane-polarized light microscopy has several applications including: 1) delineation of relic grains and textures in massive crystalline dolostones or highly recrystallized limestones, 2) enhancing recognition of diagenetic fabrics, 3) creating sharp, two-dimensional images or "pore-casts" and helping to delineate microporosity that is often difficult to detect under standard plane-polarized light, and 4) differentiating purple and blue-colored stains in iron-rich limestones that are subtle and difficult to see in standard plane-polarized light (Dravis, 1991).

This study used the modified "white-card" technique of Dravis (1991) where plain Xerox white paper was placed under the thin-section and viewed under transmitted plane-polarized light. This technique was applied to uncovered, polished and unpolished, stained and unstained thin-sections. Thin-sections were sprayed with a protective coating for better viewing (see section 2.5). Due to the simplicity of this technique, samples were able to be viewed interchangeably between diffused plane-polarized, standard plane-polarized and cross-polarized light which provided an effective method for thin-section description.

APPENDIX E – THIN SECTION DESCRIPTIONS

WELL	Page
TEXCAN SUNSET 16-17-69-19W5	E3-E4
ACL SNIPELK 12-14-70-18W5	E5-E6
ACL SNIPELK 10-21-70-18W5	E5-E6
ACL SNIPELK 10-22-70-18W6	E7-E8
ACL SNIPELK 12-22-70-18W5	E7-E10
ACL SNIPELK 12-23-70-18W5	E9-E12
ACL SNIPELK 4-26-70-18W5	E11-E14
ACL SNIPELK 10-27-70-18W5	E13-E14
ACL SNIPELK 12-27-70-18W5	E13-E16
MARATHON SNIPE LAKE 12-32-70-18W5	E15-E18
ACL SNIPELK 2-33-70-18W5	E17-E20
ACL SNIPELK 2-3-71-18W5	E19-E22
ACL SNIPELK 12-3-71-18W5	E21-E22
POCO SNIPE IN 2-4-71-18W5	E23-E24

LEGEND FOR ABBREVIATIONS

ms	=	mudstone
ws	=	wackestone
ps	=	packstone
gs	=	grainstone
fs	=	floatstone
rs	=	rudstone
Amph	=	*Amphipora*
branch cyl	=	branching cylindrical
strom	=	stromatoporoid
brach	=	brachiopod
med	=	medium
dk	=	dark
interp	=	interparticle
intrap	=	intraparticle
intersk	=	interskeletal
intrask	=	intraskeletal
decr	=	decrease
incr	=	increase
cc	=	calcite cement
OM	=	organic matter
LC	=	laminar calcrete
pc	=	pendent cement
arg	=	argillaceous
sol'n	=	solution

Note: Modal abundances were determined using visual estimates (see section 2.5). 'x' = skeletal grains recognized but modal compositions could not be accurately estimated.

Well Location	Depth (feet)	Depth (meters)	Lithology	Lithofacies	Skeletal																Non-skeletal					Cements (calcite)									
					Amphipora	Branching Cylindrical Stroms	Nodular Stroms	Bulbous Stroms	Encrusting Stroms	Hemispherical Stroms	Strom Clasts (> 5 mm)	Strom Clasts (< 5 mm)	Oncoids	Calcispheres	Ostracods	Brachiopods	Gastropods	Echinoderms	Algae	Undifferentiated Skeletal Fragments	Micrite	Peloids	Lithoclasts	Dolomicrite	Ferroan Dolomite Rhombs (replacive)	Micrite Envelope	Pendant Radiaxial Fibrous	Isopachous Fibrous	Pendant Prismatic	Isopachous Prismatic	Meniscus Blocky	Crystal Silt	Blocky-Prismatic	Syntaxial Overgrowths	Blocky Mosaics
16-17-69-19W5	8940	2724.9	Peloid packstone	A	1									x				x		5	17	65				1								1	5
	8940.3	2725.0	Peloid packstone	A	5							x		x						2	12	61											2		10
	8963	2731.9	Calcareous to dolomitic mudstone	A																			100												
	8994	2741.4	*Amphipora* floatstone in peloid packstone matrix	D	10									x						3	25	35			17	1										4
	8998.5	2742.7	Peloid packstone	A																2	5	54	3		25											6
	8999.8	2743.1	Lithoclasts in dolomitic green shale matrix	A																			50	40					3				5		2
	9002.2	2743.9	Peloid wackestone-packstone	A	5							x		x	x	x		x		5	30	40					10					6		

Well Location	Depth (feet)	Depth (meters)	Dolomite		Porosity					Pedogenic Features						Stratigraphic Occurrence	Comments
			Blocky to Sub/euhedral Rhombs	Saddle	Interparticle	Intraparticle	Vuggy	Moldic	Fracture	Green shale	Rhizoliths	Laminar calcrete	Fitted-fabric Lithoclasts	Glaebules	Peds		
16-17-69-19W5	8940	2724.9	5									x				Local exposure surface 1.3 m (4.2') above R0.5	LC up to 4 mm thick laminated dark brown opaque material with yellow-brown argillaceous shale and calcite lithoclasts.
	8940.3	2725.0	8													10cm (4") below local exposure surface	2 sharp, cemented surfaces with truncated grains ~5 cm apart. Possible hardgrounds. Vugs developed below upper cemented surfaces.
	8963	2731.9										x			x	10 cm (4") below P5	Calcareous to dolomitic soil interval. Highly altered (pedogenic?). Thick 3.5 mm argillaceous laminar calcrete separating calcareous mud above and dolomitic mud below.
	8994	2741.4		5								x				Local exposure surface 1.4 m (4.5') above P4.	LC up to 4 mm thick; laminated dark brown opaque shale, dark brown argillaceous shale and angular lithoclasts. Above LC: muddier matrix with dolomite rhombs 0.06-0.2 mm. Below LC: no dolomite in matrix, presence of vugs.
	8998.5	2742.7	5									x				P4	Dolomitic, finely crystalline dolomite rhombs in matrix and vugs. Increase vugs downwards. Argillaceous and dolomitic shale in LC, 0.35-0.70 mm thick. Dolomite rhombs + later dolomite cement in vugs.
	8999.8	2743.1								x						7.5 cm (3") below P4	Thin argillaceous green shale <0.1 mm thick. Dolomitic green shale appears to be infiltrating and dissecting parent peloid ps matrix, with lithoclasts of peloid ps.
	9002.2	2743.9		4								x				1.1 m (3.7') below P4	LC up to 3.5 mm thick, laminated dark brown opaque layers with brown argillaceous shale. Angular calcite lithoclast common and some dolomite cement clasts. No change in lithology across LC, but development of vugs below LC.

Well Location	Depth (feet)	Depth (meters)	Lithology	Lithofacies	Skeletal																	Non-skeletal					Cements (calcite)								
					Amphipora	Branching Cylindrical Stroms	Nodular Stroms	Bulbous Stroms	Encrusting Stroms	Hemispherical Stroms	Strom Clasts (> 5 mm)	Strom Clasts (< 5 mm)	Oncoids	Calcispheres	Ostracods	Brachiopods	Gastropods	Echinoderms	Algae	Undifferentiated Skeletal Fragments	Micrite	Peloids	Lithoclasts	Dolomicrite	Ferroan Dolomite Rhombs (replacive)	Micrite Envelope	Pendant Radiaxial Fibrous	Isopachous Fibrous	Pendant Prismatic	Isopachous Prismatic	Meniscus Blocky	Crystal Silt	Blocky-Prismatic	Syntaxial Overgrowths	Blocky Mosaics
12-14-70-18W5	8631	2630.7	*Amphipora* rudstone in peloid grainstone matrix	D	55	10																5					3						7		14
	8654	2637.7	Stromatoporoid rudstone	F	x	x					75										2	2	1				1		1				3		15
	8655	2638.0	Stromatoporoid rudstone	F	x	x		x			65					5	<1	<1				3						2					<1	22
	8705.3	2653.4	Peloid grainstone	A												10		1				70	4											15
	8708.5	2654.4	*Amphipora* floatstone in peloid wackestone matrix	A	50	10								x		x				3	12	5					15								5
	8717.5	2657.1	*Amphipora* floatstone in skeletal wackestone matrix	A	40									x						5	20						15	5					7		3
10-21-70-18W5	8720.7	2658.1	Peloid packstone to grainstone	A	3							x		x		x		x		12	4	65											4		5
	8727.8	2660.2	*Amphipora* floatstone in mudstone-wackestone matrix	D	6															4	20	x					37						10		15
	8769.7	2673.0	Lime mudstone to peloid wackestone	A	3							x		x	x	x				10	72	x											5		8
	8771.6	2673.6	*Amphipora* floatstone in wackestone matrix	D	18	14	3					x	x	x	x	x	x			10	35						9						5		4
	8783	2677.1	*Amphipora* floatstone in skeletal wackestone matrix	D	20										5		1			2	45							17							2

Well Location	Depth (feet)	Depth (meters)	Dolomite		Porosity					Pedogenic Features						Stratigraphic Occurrence	Comments
			Blocky to Sub/euhedral Rhombs	Saddle	Interparticle	Intraparticle	Vuggy	Moldic	Fracture	Green shale	Rhizoliths	Laminar calcrete	Fitted-fabric Lithoclasts	Glaebules	Peds		
12-14-70-18W5	8631	2630.7			4				2							R1	Good interparticle porosity. Appearance of blackened clasts from opaque inclusions in cements.
	8654	2637.7		<1		<1				x			x			10 cm (4") below R0.5	Abundant broken stromatoporoid clasts. Green argillaceous shales infiltrating from surface, overall massive. Green shale with abundant angular calcite lithoclasts in fitted-fabric texture.
	8655	2638.0			1	1										30cm (1') below R0.5	Darkened appearance from highly micritized skeletal grains. Similar lithology to 2637.8 m (8654').
	8705.3	2653.4		<1							x					15 cm (6") below P4	Rhizoliths with oxidized halo and micritic cutans. Vertically extensive (<11 cm) tubules and small 0.5-1.8 mm root tubules.
	8708.5	2654.4							1	x			x			24 cm (8") below P4	Green argillaceous shale, dolomitized near top of sample decrease green shale downwards. Green shale seams 0.1-0.3 mm thick. Angular lithoclasts in fitted-fabric matrix. Stromatoporoid grains broken and fragmented.
	8717.5	2657.1					5			x						Local exposure surface 3.9 m (12.8') below P4	Abundant radiaxial fibrous to fibrous cements (pc and isopachous). Stylolitic yellow-green argillaceous shale seams. Dark green black-opaque sediment in vugs (possibly altered green shale?).
10-21-70-18W5	8720.7	2658.1	1		6	1										Interval between R0.5 and R1	Sharp, cemented surface. Possible hardground surface. Inclusion-rich cements in interparticle pores directly below surface. Vugs below surface occluded by cements. No obvious truncated grains.
	8727.8	2660.2	5		2				1	x						23 cm (10") below R0.5	Stylolitic opaque to argillaceous green shale in vugs and cracks. Vugs with early radiaxial fibrous pendant cements. Dolomitized dark green-brown sediment in vugs, (altered pedogenic shales?).
	8769.7	2673.0	2							x						21 cm (0.7') below P4	Green shale in vugs and cracks. Green-yellow argillaceous shale, relatively massive with some calcite lithoclasts. Some dolomitic green shale, alteration? Dolomitic shale in bottom of vugs. Ferroan dolomite rhombs 0.016-0.2 mm.
	8771.6	2673.6		2						x						75 cm (2.5') below P4	Radiaxial fibrous pendant cements common in vugs. Stylolitic dark green-brown argillaceous to opaque shale, 0.2-0.4 mm thick, (altered green shale?).
	8783	2677.1		1	3		4									75 cm (2.5') below local exposure surface at 2676.3 m (8708.5')	Vugs with isopachous fibrous cements, occasionally completely occluded. Occasional vugs with abundant ostracods and dolomitized grungy dark green-brown shale. Green shale is altered (pedogenic origin?).

Well Location	Depth (feet)	Depth (meters)	Lithology	Lithofacies	Skeletal																	Non-skeletal					Cements (calcite)									
					Amphipora	Branching Cylindrical Stroms	Nodular Stroms	Bulbous Stroms	Encrusting Stroms	Hemispherical Stroms	Strom Clasts (> 5 mm)	Strom Clasts (< 5 mm)	Oncoids	Calcispheres	Ostracods	Brachiopods	Gastropods	Echinoderms	Algae	Undifferentiated Skeletal Fragments	Micrite	Peloids	Lithoclasts	Dolomicrite	Ferroan Dolomite Rhombs (replacive)	Micrite Envelope	Pendant Radiaxial Fibrous	Isopachous Fibrous	Pendant Prismatic	Isopachous Prismatic	Meniscus Blocky	Crystal Silt	Blocky-Prismatic	Syntaxial Overgrowths	Blocky Mosaics
10-22-70-18W5	8689.3	2648.5	Peloid packstone-grainstone	A	3							x		x		x				30		45		20											2
	8690.3	2648.8	Peloid-lithoclast grainstone	A								x		x		x				20		65													12
	8691.5	2649.2	Interbedded *Amphipora* rudstone in peloid ps/gs matrix with peloid grainstone	C	47	30						x		x		x				3		10													10
	8732.8	2661.8	*Amphipora* floatstone in lithoclast wackestone matrix	A	35							x		x	x	x				10	35								5						15
	8733.5	2662.0	Dolomitic matrix (soil) with lithoclasts and glaebules	A																			30	43	15				<1						5
	8734.8A	2662.4A	Dolomitic mudstone	A																				100											
	8734.8B	2662.4B	Dolomitic peloid wackestone to packstone	A																			40	60											
12-22-70-18W5	8709	2654.5	Branching cylindrical stromatoporoid floatstone in green shale matrix	C	2	40					3	x		x						5				30					5						5
	8710	2654.8	*Amphipora* floatstone in peloid packstone matrix	D	25	5						x		x	x	x				15	20	18				2				3					12

Well Location	Depth (feet)	Depth (meters)	Dolomite		Porosity					Pedogenic Features						Stratigraphic Occurrence	Comments
			Blocky to Sub/euhedral Rhombs	Saddle	Interparticle	Intraparticle	Vuggy	Moldic	Fracture	Green shale	Rhizoliths	Laminar calcrete	Fitted-fabric Lithoclasts	Glaebules	Peds		
10-22-70-18W5	8689.3	2648.5								x						10 cm (4") below R0.5	Abundant dolomitic argillaceous sediment in matrix; decreases downwards. Yellow-green argillaceous shale seams 0.2-0.6 mm.
	8690.3	2648.8	3							x	x					40 cm (1.3') below R0.5	Thin yellow-green argillaceous shale seams 0.04-0.12 mm. Patches of dolomitic sediment in matrix. Rhizoliths (up to <1 cm long) with laminated cutans.
	8691.5	2649.2								x						76 cm (2.5') below R0.5	Yellow-green shale argillaceous material seams in between grains, 0.1-0.3 mm thick. Green shale more common in rudstone intervals.
	8732.8	2661.8										x				P4	Laminar calcretes, average 0.1-0.3 mm but up to <3.0 mm. Dark yellow-brown to dark brown argillaceous shale. Thinner LC appears more massive. Possible pendant cements with thin inclusion-rich layers in vugs.
	8733.5	2662.0	7		<1							x	x	x	?	40cm (1.3') below P4	Clasts in a dolomitic soil matrix with finely crystalline dolomitic sediment. Soil matrix with glaebules (0.4 mm-1 cm) with circumgranular + septarian cracks. Fitted-fabric lithoclasts in soil matrix. Possible development of peds (or intermittent peds). Dark brown laminar calcretes, 0.2-2.0 mm.
	8734.8A	2662.4A										x				60 cm (2') below P4	Dolomitic mudstone, dolomite rhombs 0.08-0.24 mm (non ferroan) with interstitial grungy sediment. Light to dark brown argillaceous laminar calcretes, 0.2-1.0 mm, massive to weakly laminated.
	8734.8B	2662.4B										x				62 cm (~2') below P4	Moderately to weakly laminated. Dolomite rhombs 0.008-0.04 mm with grungy interstitial sediment. Decrease in dolomitic mud downwards. Laminar calcretes 0.2-3.5 mm, light to medium brown argillaceous shale. Rip up clasts of underlying facies at the base.
12-22-70-18W5	8709	2654.5	10							x				x	?	30 cm (1') below R0.5	Dark green dolomitic shale matrix (soil?). Strom grains with clear pendant cements and alteration rims. Cracks and fractures abundant in soil matrix and strom grains. Glaebules with circumgranular and septarian cracks. Intermittent peds developed.
	8710	2654.8								x						60 cm (2') below R0.5	Stylolitic green shale seams average 0.04-0.08 mm thick, up to 0.30 mm thick, with green to dark brown shale. Sometimes weakly laminated, not quite LC. Darkened appearance of grains likely due to internal micrite sediment in intraskeletal galleries.

Well Location	Depth (feet)	Depth (meters)	Lithology	Lithofacies	Skeletal																Non-skeletal					Cements (calcite)									
					Amphipora	Branching Cylindrical Stroms	Nodular Stroms	Bulbous Stroms	Encrusting Stroms	Hemispherical Stroms	Strom Clasts (> 5 mm)	Strom Clasts (< 5 mm)	Oncoids	Calcispheres	Ostracods	Brachiopods	Gastropods	Echinoderms	Algae	Undifferentiated Skeletal Fragments	Micrite	Peloids	Lithoclasts	Dolomicrite	Ferroan Dolomite Rhombs (replacive)	Micrite Envelope	Pendant Radiaxial Fibrous	Isopachous Fibrous	Pendant Prismatic	Isopachous Prismatic	Meniscus Blocky	Crystal Silt	Blocky-Prismatic	Syntaxial Overgrowths	Blocky Mosaics
	8713.8	2656.0	Amphipora floatstone in skeletal wackestone matrix	A	20							x		x	x	x				17	35	5				2	5			1			1	10	
	8714.5	2656.2	Skeletal wackestone	A	3	2						x			x	x		x		20	48	2			12	1				1		x	2		9
	8752.2	2667.7	*Amphipora* floatstone in peloid packstone matrix	A	25							x		5	x						5	22				1	10					x	3		7
	8752.5	2667.8	*Amphipora* floatstone in skeletal wackestone matrix	A	30							2		4	3	1					29	5				1	2		5						15
	8754	2668.2	Peloid wackestone to grainstone.	A								x		x		x		x		20	15	45											6		14
12-23-70-18W5	8600	2621.3	Oncolitic floatstone in peloid packstone matrix	A	3								15							5	20	45											7		13
	8637	2632.6	Skeletal grainstone	I								23				20		10	5	7		15											4	2	
	8646.2	2635.4	Peloid wackestone	A	5																55	15											2		20

Well Location	Depth (feet)	Depth (meters)	Dolomite		Porosity					Pedogenic Features						Stratigraphic Occurrence	Comments
			Blocky to Sub/euhedral Rhombs	Saddle	Interparticle	Intraparticle	Vuggy	Moldic	Fracture	Green shale	Rhizoliths	Laminar calcrete	Fitted-fabric Lithoclasts	Glaebules	Peds		
	8713.8	2656.0			3	1			<1	?						15 cm (6") below local exposure surface at 2655.8 m (8713.2')	Dark brown-green stylolitic sediment with opaque, pedogenic green shale. Geopetal sediment in intraskeletal pores and vugs is slightly coarser grained than micrite ~ very fine crystalline calcite. Radiaxial fibrous pendant cements in fenestrae and dissolution vugs.
	8714.5	2656.2								x			x			40 cm (1.3') below local exposure surface at 2655.8 m (8713.2')	Geopetal crystal silt (calcite) in vugs and intraskeletal pores; microcrystalline (<0.03 mm calcite) coarsening upwards from bottom of vugs to finely crystalline (0.08-0.16 mm). Green shale has argillaceous shale with fitted-fabric calcite lithoclasts. Variable 0.2-1.0 mm thick, dark green to dark green-brown.
	8752.2	2667.7	5	15	1					x						5 cm (2") below P4	Yellow-green argillaceous shale at top of sample. Geopetal argillaceous green shale at bottom of vugs. Green shales gradational with green shales with ferroan dolomite rhombs and gradational with crystal silt with minimal interstitial green shale. Decreasing dolomite downwards in vugs.
	8752.5	2667.8	3							x						15 cm (6") below P4	Vugs mostly near top of sample and decreases downwards. Dolomitic shale decreases downwards. Variations in green shale, (1) green-yellow argillaceous, 0.06-0.24mm thick occurs as stylolitic laminated seams; (2) dolomitic green shale, mostly ferroan dolomite rhombs (0.016-0.16 mm), grungy dark green shale in interstitial spaces; (3) dark green massive shale with some dolomite rhombs. Reflects possible progressive stages of green shale?
	8754	2668.2										x				60 cm (2') below P4	LC, yellow brown argillaceous shale; 0.05-0.65 mm thick with calcite lithoclasts.
12-23-70-18W5	8600	2621.3					2									R0.5	Abundant opaque grains in micrite matrix, possible cause for darkened appearance. Stylolitic contact 3/4 down sample. Above stylolite has oncoids with a darkened matrix. Below stylolite has distinct peloids and broken strom clasts.
	8637	2632.6	1		13											3 m (10') above P4	Abundant skeletal lithoclasts with good interparticle porosity and some cements, no lime mud. Algae fragments *Goniolithon* (red algae) and possible *Solenoporoid*.
	8646.2	2635.4		3			<1									24 cm (0.8') above P4	Normal marine subtidal sediments.

Well Location	Depth (feet)	Depth (meters)	Lithology	Lithofacies	Skeletal																	Non-skeletal					Cements (calcite)									
					Amphipora	Branching Cylindrical Stroms	Nodular Stroms	Bulbous Stroms	Encrusting Stroms	Hemispherical Stroms	Strom Clasts (> 5 mm)	Strom Clasts (< 5 mm)	Oncoids	Calcispheres	Ostracods	Brachiopods	Gastropods	Echinoderms	Algae	Undifferentiated Skeletal Fragments	Micrite	Peloids	Lithoclasts	Dolomicrite	Ferroan Dolomite Rhombs (replacive)	Micrite Envelope	Pendant Radiaxial Fibrous	Isopachous Fibrous	Pendant Prismatic	Isopachous Prismatic	Meniscus Blocky	Crystal Silt	Blocky-Prismatic	Syntaxial Overgrowths	Blocky Mosaics
	8647	2635.6	Peloid packstone	A								x				x		x		25	25	40										x		1	8
	8647.6	2635.8	Peloid (+ lithoclast) grainstone	A												x		x		37		50													12
	8650	2636.5	Dolomitic green mudstone	A																			7	93											
	8650.5	2636.7	Peloid packstone-grainstone	A								x				x		x		35		60		5											
	8650.6	2636.7	Peloid packstone	A	7							x		x		3				7	20	45					7					x	2		4
	8652.2	2637.2	Peloid grainstone-grainstone	A							6	x				x	4	x		23		35				1		2					2	13
04-26-70-18W5	8598	2620.7	*Amphipora* floatstone in peloid ps/gs matrix	A	28	7										x		x		5	4	30					10					x	4	<1	12
	8598.1	2620.7	Branching cylindrical strom rudstone in peloid ps/gs matrix	A	15	40														2	5	10					8	4					3		10
	8648.7	2636.1	*Amphipora* rudstone in peloid ws matrix	A	60										3						15	2	5						2				7		3
	8650.8	2636.8	*Amphipora* rudstone in peloid ws matrix	D	55							x		x	x					10	23		x						2				5		5

Well Location	Depth (feet)	Depth (meters)	Dolomite		Porosity					Pedogenic Features						Stratigraphic Occurrence	Comments
			Blocky to Sub/euhedral Rhombs	Saddle	Interparticle	Intraparticle	Vuggy	Moldic	Fracture	Green shale	Rhizoliths	Laminar calcrete	Fitted-fabric Lithoclasts	Glaebules	Peds		
	8647	2635.6	1		<1					x		x				P4	Yellow-green argillaceous shale, average 0.2-0.4 mm, up to 3 mm thick. Laminated with opaque layers, dark brown layers and calcite lithoclasts. Patches of dark grey matrix. Geopetal crystal silt in interparticle pores, dolomite and calcite crystals, gradational with argillaceous material.
	8647.6	2635.8									x					68 cm (0.6') below P4	Rhizoliths (1.2 to 3.2 mm long). Laminar to irregular features with sharp dark brown lining (very thin) and rusty orange brown micritic material around. Micrite filling inside structure.
	8650	2636.5								x		x				90 cm (3') below P4	Very fine crystalline (<0.016 mm) dolomite rhombs with grungy (micritic?) interstitial sediment. Massive with calcite clasts near top and decreases downwards. Possible LC, 0.1-0.4 mm dark yellow-brown shale with dolomite rhombs and weakly laminated.
	8650.5	2636.7										x				1.05 m (3.5') below P4	Peloid packstone with dolomitic mud in between grains. Similar to 2636.5m (8650') sediment, but much less abundant. LC at top 0.4 mm thick. Yellow brown argillaceous material laminated with dark brown layers, opaque grains and calcite lithoclasts.
	8650.6	2636.7	5									x				1.1 m (3.6') below P4	Stylolitic contact separating peloid ps. Abundant dissolution vugs with pc in vugs. Dolomitic shale matrix associated with stylolites. Geopetal dolomitic sediment and finely crystalline calcite (crystal silt) in bottom of vugs.
	8652.2	2637.2			14	1						x				1.6 m (5.2') below P4	Possible local exposure at LC. LC <1.5 mm thick, dark brown to black opaque shale and calcite lithoclasts.
04-26-70-18W5	8598	2620.7			<1											R0.5	Relatively sharp, cemented surface with possible truncated grains. Appearance of pendant cements under grains + in vugs below the surface.
	8598.1	2620.7			3											2.5 cm (1") below R0.5	Abundant radiaxial fibrous pendant cements in shelter pores and vugs.
	8648.7	2636.1	3							x						20 cm (8") below P4	Green shale in cracks, vugs and other open pore spaces. Yellow-green argillaceous shale. Relatively massive with patchy dolomitization.
	8650.8	2636.8								x						85 cm (2.8') below P4	Highly altered stylolitic dark brown-green argillaceous shale. Rare, nonferroan, inclusion-free pendant cements on *Amphipora* grains.

Well Location	Depth (feet)	Depth (meters)	Lithology	Lithofacies	Skeletal																Non-skeletal					Cements (calcite)									
					Amphipora	Branching Cylindrical Stroms	Nodular Stroms	Bulbous Stroms	Encrusting Stroms	Hemispherical Stroms	Strom Clasts (> 5 mm)	Strom Clasts (< 5 mm)	Oncoids	Calcispheres	Ostracods	Brachiopods	Gastropods	Echinoderms	Algae	Undifferentiated Skeletal Fragments	Micrite	Peloids	Lithoclasts	Dolomicrite	Ferroan Dolomite Rhombs (replacive)	Micrite Envelope	Pendant Radiaxial Fibrous	Isopachous Fibrous	Pendant Prismatic	Isopachous Prismatic	Meniscus Blocky	Crystal Silt	Blocky-Prismatic	Syntaxial Overgrowths	Blocky Mosaics
	8663	2640.5	Peloid wackestone	A										x	x					5	53	30											2		10
10-27-70-18W5	8671.9	2643.2	Branching cylindrical stromatoporoid floatstone in peloid packstone matrix	C		15						x		x		x	x	x		10	16	50								2					5
	8672	2643.2	Peloid packstone to grainstone to a laminated dolomitic mudstone	A								x			x	x		x		20		35		45											7
	8673.3	2643.6	Peloid wackestone	A	2							x		x	x	x				13	45	25	x						3						13
	8773.7	2674.2	*Amphipora* rudstone in mudstone matrix	D	35							x		x	x	x				7	40	3							3						12
	8680.5A	2645.8A	Lime mudstone	A	2							x		x	x	x				3	92														3
	8680.5B	2645.8B	Peloid packstone to grainstone	A		5						x		x		x				10	5	55								3			10		12
12-27-70-18W5	8631	2630.7	*Amphipora* floatstone in skeletal wackestone matrix	D	25									3	10	2					40	x								2			8		5
	8639	2633.2	Peloid packstone to grainstone	A	2							x										70	5			2							13		7

Well Location	Depth (feet)	Depth (meters)	Dolomite		Porosity					Pedogenic Features						Stratigraphic Occurrence	Comments
			Blocky to Sub/euhedral Rhombs	Saddle	Interparticle	Intraparticle	Vuggy	Moldic	Fracture	Green shale	Rhizoliths	Laminar calcrete	Fitted-fabric Lithoclasts	Glaebules	Peds		
	8663	2640.5										x				Local exposure surface 4.6 m (15') below P4	Laminar calcretes 0.2-0.6 mm thick. Yellow-green argillaceous shale with quartz silt, 0.024 mm.
10-27-70-18W5	8671.9	2643.2	2													2.5 cm (1") above P4	No visible exposure features.
	8672	2643.2	3							x						P4	Dolomitic mud with very finely crystalline dolomite rhombs 0.008-0.04 mm with dark grey grungy interstitial shale. Laminated near bottom of sample, dolomitic mud content increases downwards from surface. Yellow argillaceous shale in matrix, horizontal, relatively massive, 0.16-0.40 mm thick. Gradational profile.
	8673.3	2643.6								x		x				40 cm (1.3') below P4	Pendant cements on undersurfaces of grains, some possibly broken up in matrix. Gradational at top from green shale seams to dark brown stylolitic LC. Green argillaceous shale, 0.2-0.32 mm with possible quart silt <0.016 mm. LC 0.1-0.8 mm thick, laminated argillaceous shale, opaque grains, micas and possible quartz silt.
	8773.7	2674.2								x						52 cm (1.7') below P4	Green argillaceous shales 0.2-1.0 mm thick. Occurs in cracks and pores between grains, mostly occurs lower half of sample. Pendant cements in vugs out of orientation.
	8680.5A	2645.8A														Local exposure surface 2.6 m (8.5') below P4	No exposure features. Sharp, stylolitic lithology contact, upper section more micritic.
	8680.5B	2645.8B								x		x	x			Local exposure surface 2.6 m (8.5') below P4	Stylolitic LC truncates cemented surface, possible hardground. Fining upwards lithology to LC. LC 0.4-1.6 mm thick, laminated dark brown argillaceous shale and opaque grains. Gradational with lower interval of argillaceous green shale with fitted-fabric calcite lithoclasts and quartz silt (<0.008 mm).
12-27-70-18W5	8631	2630.7				<1				?						30 cm (1') below R1	Geopetal micrite sediment in intraskeletal galleries. Dark brown grungy sediment in cracks, possibly pedogenic?
	8639	2633.2	<1						<1							Interval between R0.5 and R1	Dark brown stylolitic material, some green (argillaceous?) shale, not likely pedogenic. At bottom of thin section has abundant opaque inclusions rimming grains, possibly causing the darkened appearance.

Well Location	Depth (feet)	Depth (meters)	Lithology	Lithofacies	Skeletal																Non-skeletal					Cements (calcite)									
					Amphipora	Branching Cylindrical Stroms	Nodular Stroms	Bulbous Stroms	Encrusting Stroms	Hemispherical Stroms	Strom Clasts (> 5 mm)	Strom Clasts (< 5 mm)	Oncoids	Calcispheres	Ostracods	Brachiopods	Gastropods	Echinoderms	Algae	Undifferentiated Skeletal Fragments	Micrite	Peloids	Lithoclasts	Dolomicrite	Ferroan Dolomite Rhombs (replacive)	Micrite Envelope	Pendant Radiaxial Fibrous	Isopachous Fibrous	Pendant Prismatic	Isopachous Prismatic	Meniscus Blocky	Crystal Silt	Blocky-Prismatic	Syntaxial Overgrowths	Blocky Mosaics
	8650	2636.5	Branching cylindrical stromatoporoid floatstone in peloid wackestone /packstone matrix	B		30								x	x	x				10	15	30											5		10
	8651	2636.8	Branching cylindrical stromatoporoid floatstone in dolomitized mudstone matrix	B		45															18				20				15				2		
	8667	2641.7	Stromatoporoid floatstone in peloid-skeletal packstone	F	30			x		x	35											12									8			4		
	8680	2645.7	Branching cylindrical stromatoporoid rudstone in peloid wackestone matrix	C		35			1							<1				10	20	20									3			5		
	8698.7	2651.4	Branching cylindrical stromatoporoid floatstone in peloid wackestone matrix	A		15		<1							x	x					53	x	22								3					6
	8699	2651.5	Peloid-skeletal packstone	A																45		x		43												
12-32-78-18W5	8545	2604.5	Dolomitic green shale breccia	A																			55	45												
	8546	2604.8	*Amphipora* floatstone in peloid wackestone matrix	A	30									10	3					7	40	15														5
	8549	2605.7	*Amphipora* floatstone in peloid wackestone matrix	D	20									5	7					3	40	15									2					8
	8561.5	2609.5	*Amphipora* rudstone in skeletal packstone matrix	E	50							x		1	1					23	15													9		

Well Location	Depth (feet)	Depth (meters)	Dolomite		Porosity					Pedogenic Features						Stratigraphic Occurrence	Comments
			Blocky to Sub/euhedral Rhombs	Saddle	Interparticle	Intraparticle	Vuggy	Moldic	Fracture	Green shale	Rhizoliths	Laminar calcrete	Fitted-fabric Lithoclasts	Glaebules	Peds		
	8650	2636.5							1	x			x			R0.5	Abundant LC , varies 0.2-0.8 mm thick. Grades from dark brown with green shale LC at top of sample to more massive argillaceous green shale with lithoclasts at bottom. Fitted-fabric of angular lithoclasts in argillaceous green shale matrix, including pc clasts.
	8651	2636.8														2.5 cm (1") below R0.5	Abundant pc on strom grains, some developed around the whole grain but thicker at the bottom. Alternating inclusion-poor and inclusion-rich layers, some clotted texture (microbial influence?). Broken pc clasts in matrix. Dark green-grey sediment interparticle pores (micrite mud?) with abundant dolomite rhombs. Dolomite possibly altered or replacing mud. Some solution enhanced pores (vugs).
	8667	2641.7	1		3	7										45 cm (1.5') above P5	No exposure features. Abundant broken stromatoporoid clasts.
	8680	2645.7		7	<1	2										Interval between P4 and P5	No exposure features. Normal marine subtidal sediments.
	8698.7	2651.4	1						<1			x				P4	Green shale rip-up clasts from below in matrix. Dark brown argillaceous LC, 0.1-0.3 mm thick.
	8699	2651.5	4	8							x			x		7.5 cm (3") below P4	Difficult to differentiate peloids from micritized lithoclasts. Grungy dark grey sediment with dolomite rhombs as matrix, possibly dolomitized micrite. Dolomitic sediment lines or fills tubular vugs (possible rhizoliths). Dark grey dolomicrite concentrations, possible glaebule.
12-32-78-18W5	8545	2604.5								x			x			15 cm (6") below R0.5	Variable lithoclasts in a green shale matrix. Lithoclasts include broken radiaxial fibrous pc clasts, calcite cement clasts, and peloid ps/gs clasts. Fitted- fabric texture of lithoclasts.
	8546	2604.8								x						49 cm (1.6') below R0.5	Yellow-green to dark green argillaceous shale (ranges 0.1-1.2 mm thick) in cracks around grains. Occasionally moderately laminated.
	8549	2605.7					1			x						1.4 m (4.6') below R0.5	Vugs sometimes filled with very finely crystalline calcite sediment. Green argillaceous shales, 0.1-1.0 mm thick, massive with some weak laminations and sometimes stylolitic.
	8561.5	2609.5	1													15 cm (6") above P5	Abundant stylolites and concentrated organic material at stylolites, carbonaceous matrix.

Well Location	Depth (feet)	Depth (meters)	Lithology	Lithofacies	Skeletal																	Non-skeletal					Cements (calcite)									
					Amphipora	Branching Cylindrical Stroms	Nodular Stroms	Bulbous Stroms	Encrusting Stroms	Hemispherical Stroms	Strom Clasts (> 5 mm)	Strom Clasts (< 5 mm)	Oncoids	Calcispheres	Ostracods	Brachiopods	Gastropods	Echinoderms	Algae	Undifferentiated Skeletal Fragments	Micrite	Peloids	Lithoclasts	Dolomicrite	Ferroan Dolomite Rhombs (replacive)	Micrite Envelope	Pendant Radiaxial Fibrous	Isopachous Fibrous	Pendant Prismatic	Isopachous Prismatic	Meniscus Blocky	Crystal Silt	Blocky-Prismatic	Syntaxial Overgrowths	Blocky Mosaics
	8563.5	2610.2	Branching cylindrical stromatoporoid floatstone in peloid grainstone matrix	A	20	25			1									<1			30				1	8					6		10
	8576	2614.0	*Amphipora* floatstone in peloid wackestone matrix	D	30									x					15	40	x									2			2		4
	8586.5	2617.2	Branching cylindrical stromatoporoid floatstone in peloid ps-gs matrix	A		15								x					7		60									3			8		8
	8587	2617.3	*Amphipora* floatstone in peloid wackestone matrix	A	20	5								5	7				13	30	x									3			7		10
	8588	2617.6	*Amphipora* floatstone in peloid wackestone matrix	A	20				<1			x		5	3				12	25	4									3			7		20
	8602	2621.9	*Amphipora* floatstone in peloid wackestone matrix	D	18							x		3	x		x		14	25	15									2			5		18
02-33-70-18W5	8635	2631.9	Branching cylindrical stromatoporoid floatstone in peloid packstone matrix	F		45													10	5	28														9
	8637	2632.6	Branching cylindrical stromatoporoid rudstone in peloid wackestone-packstone matrix	F		55													5	27	x														10
	8651.8	2637.1	Branching cylindrical floatstone -rudstone in wackestone matrix	F	1	35						x			x				x	27	x	13								2	<1				5
	8666	2641.4	Branching cylindrical rudstone in peloid grainstone matrix	C		55			<1			x			x			x	x		10	9													7

Well Location	Depth (feet)	Depth (meters)	Dolomite		Porosity					Pedogenic Features						Stratigraphic Occurrence	Comments
			Blocky to Sub/euhedral Rhombs	Saddle	Interparticle	Intraparticle	Vuggy	Moldic	Fracture	Green shale	Rhizoliths	Laminar calcrete	Fitted-fabric Lithoclasts	Glaebules	Peds		
	8563.5	2610.2	<1		<1											45 cm (1.5') below P5	Sharp cemented surface at top with truncated grains, probably hardground surface. Pendant cements in dissolution vugs.
	8576	2614.0	1			5			<1							Interval between P4 and P5	No exposure features, normal subtidal marine (lagoon) sediments.
	8586.5	2617.2	<1							x		?	x			15 cm (6") below P4	Yellow-green argillaceous material, slightly laminated with dark brown opaque shale. Abundant angular calcite lithoclasts with fitted-fabric texture in green shale. Dark brown stylolitic shale, not LC.
	8587	2617.3								x						30 cm (1') below P4	Stylolitic, relatively massive green to brown argillaceous shale, 0.1-0.6 mm thick. Darkened appearance of sample in hand sample not obvious in thin section, likely due to abundance of dark brown micritic internal sediment.
	8588	2617.6	<1		1											60 cm (2') below P4	No obvious exposure features. Overall darkened appearance of matrix and grains not obvious in thin section. Possibly from dark color of micrite matrix.
	8602	2621.9										x				Local exposure surface 4.9 m (16') below P4	LC: yellow-brown argillaceous shale laminated with dark brown opaque shale. Average 0.06-0.6 mm thick. Possible quartz silt in argillaceous layers and calcite lithoclasts.
02-33-70-18W5	8635	2631.9	3							x		x	?			30 cm (1') below R0.5	Green argillaceous shales, 0.4–4 mm thick. Dark green to green-brown, with abundant calcite lithoclasts and fitted-fabric lithoclasts. Argillaceous green shale LC, weakly laminated with dark brown argillaceous shale and black opaque rich layers.
	8637	2632.6			2	<1				x						90 cm (3') below R0.5	Green argillaceous shales in between strom grains. Stylolitic to massive, dark green with some calcite lithoclasts. Ranges 0.1-2.4 mm thick.
	8651.8	2637.1		7	7	1			3							Interval between P5 and R0.5	No obvious pedogenic features. Normal subtidal marine sediments.
	8666	2641.4		6	4	6										Interval between P4 and P5	Matrix composed of peloids, lithoclasts, dolomite rhombs and calcite cement. Occurs in interparticle pore spaces. Strom grains sometimes fractured and filled with late calcite and/or dolomite cement. No obvious pedogenic features.

Well Location	Depth (feet)	Depth (meters)	Lithology	Lithofacies	Skeletal																Non-skeletal					Cements (calcite)									
					Amphipora	Branching Cylindrical Stroms	Nodular Stroms	Bulbous Stroms	Encrusting Stroms	Hemispherical Stroms	Strom Clasts (> 5 mm)	Strom Clasts (< 5 mm)	Oncoids	Calcispheres	Ostracods	Brachiopods	Gastropods	Echinoderms	Algae	Undifferentiated Skeletal Fragments	Micrite	Peloids	Lithoclasts	Dolomicrite	Ferroan Dolomite Rhombs (replacive)	Micrite Envelope	Pendant Radiaxial Fibrous	Isopachous Fibrous	Pendant Prismatic	Isopachous Prismatic	Meniscus Blocky	Crystal Silt	Blocky-Prismatic	Syntaxial Overgrowths	Blocky Mosaics
	8686	2647.5	Peloid packstone	A																x	10	55	20		12									3		
	8686.2	2647.6	Lithoclasts in dolomitic green shale matrix	A																			40	30	20				10							
	8686.8	2647.7	*Amphipora* floatstone in peloid packstone matrix	A	20							x		x							10	35	18						2						13
02-03-71-18W5	8572	2612.7	*Amphipora* rudstone in peloid grainstone matrix	A	35	12		15	1			x				x		x		5		20												10
	8582	2615.8	Lime mudstone	A	1									x						8	70								*15					5		
	8584	2616.4	*Amphipora* floatstone in peloid packstone-grainstone matrix	A	15							1		2	3							44												22		12
	8586.5	2617.2	*Amphipora* floatstone in peloid wackestone matrix	A	15							x		7	x					3	25	18				1				9					15
	8632	2631.0	Skeletal grainstone	I								5			10	3		18		7		20								2			5		

Well Location	Depth (feet)	Depth (meters)	Dolomite		Porosity					Pedogenic Features						Stratigraphic Occurrence	Comments
			Blocky to Sub/euhedral Rhombs	Saddle	Interparticle	Intraparticle	Vuggy	Moldic	Fracture	Green shale	Rhizoliths	Laminar calcrete	Fitted-fabric Lithoclasts	Glaebules	Peds		
	8686	2647.5								x		x				9 cm (0.3') below P4	Dolomitic micrite matrix (micrite with dolomite rhombs 0.024-0.06 mm). Green argillaceous shale (massive) in lower portion of sample, with dolomite rhombs <0.016 mm and calcite lithoclasts. Dark brown argillaceous LC, 0.08-0.7 mm thick with calcite lithoclasts.
	8686.2	2647.6								x						5 cm (2") below P4	Broken strom grains and cement clasts in a dolomitic (<0.08 mm) argillaceous to micritic matrix. Coarser dolomitic sediment fills spaces in between lithoclasts and matrix. Dolomitic sediment; ferroan dolomite rhombs (0.16-0.40 mm) with dark grey interstitial sediment. Broken *Amph* grains with prismatic pendant cements. Pendant cements are fragmented.
	8686.8	2647.7	2									x				23 cm (10") below P4	Distinct change in color of facies across LC. Argillaceous dark brown laminated with opaque dark brown-black shale, 0.2-0.8 mm thick. Rare prismatic pendant cements under Amphipora grains, with inclusion-rich laminae and micritic laminae.
02-03-71-18W5	8572	2612.7							2	x						Local exposure surface 3.65 m (12') above R0.5	Green shale seams 0.1-0.8 mm thick (thinner ones <0.05 mm). Stylolitic, green argillaceous to amorphous shale with dark brown opaque grains. Angular lithoclasts in shale.
	8582	2615.8			2		1									60 cm (2') above R0.5	Inclusion-rich, non ferroan calcite completely occluding pores or occurs as isopachous rims. Blocky habit but likely originally early fibrous calcite (recrystallized/neomorphosed). Possible vuggy pores with early cements, or fenestrae. Sediment lining upper portion of pores (blue color from microporosity).
	8584	2616.4	1		1											R0.5	Upper portions of laminar fenestrae often occluded by inclusion-rich blocky-prismatic calcite. Sharp surface with truncated grains, possible hardground.
	8586.5	2617.2	<1		2	<1	4		1							75 cm (2.5') below R0.5	No obvious exposure features. Darkened appearance possibly due to opaque inclusions in the matrix.
	8632	2631.0	15		12	3										Interval between P4 and P5	Abundant broken skeletal fragments and good interparticle porosity.

Well Location	Depth (feet)	Depth (meters)	Lithology	Lithofacies	Skeletal																Non-skeletal					Cements (calcite)									
					Amphipora	Branching Cylindrical Stroms	Nodular Stroms	Bulbous Stroms	Encrusting Stroms	Hemispherical Stroms	Strom Clasts (> 5 mm)	Strom Clasts (< 5 mm)	Oncoids	Calcispheres	Ostracods	Brachiopods	Gastropods	Echinoderms	Algae	Undifferentiated Skeletal Fragments	Micrite	Peloids	Lithoclasts	Dolomicrite	Ferroan Dolomite Rhombs (replacive)	Micrite Envelope	Pendant Radiaxial Fibrous	Isopachous Fibrous	Pendant Prismatic	Isopachous Prismatic	Meniscus Blocky	Crystal Silt	Blocky-Prismatic	Syntaxial Overgrowths	Blocky Mosaics
	8639	2633.2	Branching cylindrical floatstone in peloid-skeletal wackestone matrix	A		25	x	x				18		x			x			3	12	26												10
	8639.5	2633.3	Peloid-skeletal packstone-grainstone	A											x	x		x		x	5	45	30											13
	8640.7	2633.7	*Amphipora* floatstone in mudstone matrix	D	25									1						7		2	8			28			3		x			10
	8642	2634.1	*Amphipora* floatstone in peloid wackestone matrix	D	25							x		2	3		1			8	20	10				7			2					9
	8643	2634.4	*Amphipora* floatstone in peloid wackestone matrix	D	10									1	4					5	35	x				17			3			5		5
	8645	2635.0	*Amphipora* floatstone in peloid packstone matrix	D	10							x		x	x		5			7	8	20				10			2			15		5
12-03-71-18W5	8611.6	2624.8	Peloid grainstone	A										x		x		x		23		60												10
	8612	2624.9	Peloid-skeletal grainstone	A								x				x		x		35		55												7
	8613.9	2625.5	Branching cylindrical stromatoporoid in peloid grainstone matrix	C		40										2	1			15		25				2								13

Well Location	Depth (feet)	Depth (meters)	Dolomite		Porosity					Pedogenic Features						Stratigraphic Occurrence	Comments
			Blocky to Sub/euhedral Rhombs	Saddle	Interparticle	Intraparticle	Vuggy	Moldic	Fracture	Green shale	Rhizoliths	Laminar calcrete	Fitted-fabric Lithoclasts	Glaebules	Peds		
	8639	2633.2	3									x	x			P4	Abundant LC, stylolitic dark brown to black. LC ranges from argillaceous to opaque. Opaque inclusions and calcite lithoclasts common with fitted-fabric texture. Quartz silt <0.016 mm.
	8639.5	2633.3	7								x	x				15 cm (6") below P4	Irregular to oval shaped tubules (rhizoliths) with red-brown oxidized halos and micritic coatings (not laminated). Argillaceous LC, 0.08-1.6 mm thick. Yellow to dark brown argillaceous material with abundant calcite lithoclasts.
	8640.7	2633.7	12		4	1						x				82 cm (2.7') below P4	Abundant inclusion-rich radiaxial fibrous pc in dissolution vugs. Geopetal crystal silt at bottom of vugs (composed of peloids, micrite, calcite cement clasts and Fe dolomite rhombs). Pc's grade into blocky calcite. Remaining vugs occluded by dolomite cement. Medium to dark brown argillaceous LC at top, 0.4 mm thick.
	8642	2634.1	<1	2		9	2		1							90 cm (3') below P4	Radiaxial fibrous pendant cements in dissolution vugs, fewer vugs than 2633.6 m (8640.7'). Pc's slightly thinner and less inclusion-rich.
	8643	2634.4		3		3	10	2								1.2 m (4') below P4	Radiaxial fibrous pc in vugs and occasionally completely occludes smaller vugs. Pc's thinner and slightly less inclusion-rich than pc's in 2633.6 m (8640.7') and 2634 m (8642').
	8645	2635.0		8		4	5									1.8 m (6') below P4	Some radiaxial fibrous pc's in vugs, thinner and less abundant than overlying intervals. Gradational with blocky calcite cements in vugs.
12-03-71-18W5	8611.6	2624.8	2	<1								x				2.5 cm (1") below P4	Very thin stylolitic laminar calcretes; 0.02-0.16 mm thick. Dark brown opaque to amorphous shale with pale green yellow argillaceous shale. Ferroan dolomite rhombs closely associated with LC and surrounding matrix. Some possible rusty orange crystalline calcite material (early crystalline LC?).
	8612	2624.9			2					x		x				15 cm (6") below P4	Dark yellow to brown argillaceous to opaque LC, 0.2-0.6 mm. Green shale seams with an amorphous appearance with calcite lithoclasts and opaque inclusions.
	8613.9	2625.5			2					x			x			43 cm (1.4') below P4	Yellow green argillaceous shale seams, 0.06-0.60 mm thick. Opaque inclusions, calcite lithoclasts, relatively massive and occasional fitted-fabric clasts. Possible pc on undersides of grains, but broken up and difficult to see.

Well Location	Depth (feet)	Depth (meters)	Lithology	Lithofacies	Skeletal																Non-skeletal					Cements (calcite)									
					Amphipora	Branching Cylindrical Stroms	Nodular Stroms	Bulbous Stroms	Encrusting Stroms	Hemispherical Stroms	Strom Clasts (> 5 mm)	Strom Clasts (< 5 mm)	Oncoids	Calcispheres	Ostracods	Brachiopods	Gastropods	Echinoderms	Algae	Undifferentiated Skeletal Fragments	Micrite	Peloids	Lithoclasts	Dolomicrite	Ferroan Dolomite Rhombs (replacive)	Micrite Envelope	Pendant Radiaxial Fibrous	Isopachous Fibrous	Pendant Prismatic	Isopachous Prismatic	Meniscus Blocky	Crystal Silt	Blocky-Prismatic	Syntaxial Overgrowths	Blocky Mosaics
02-04-71018W5	8521.5	2597.4	*Amphipora* floatstone in mudstone-wackestone matrix	D	25															7	43						14					x			10
	8541	2603.3	Peloid wackestone	A																2	25	43													20
	8542.2	2603.7	Branching cylindrical stromatoporoid floatstone in peloid wackestone matrix	C	5	25		15				x								10		7					13						15		
	8543.2	2604.0	Bulbous stromatoporoid in peloid packstone matrix	C	2	3		60												8	8	10													7
	8544	2604.2	*Amphipora* rudstone in peloid packstone/grainstone matrix (with a mudstone interval).	D	45	15										x	x			3	7	13													14

Well Location	Depth (feet)	Depth (meters)	Dolomite		Porosity					Pedogenic Features						Stratigraphic Occurrence	Comments
			Blocky to Sub/euhedral Rhombs	Saddle	Interparticle	Intraparticle	Vuggy	Moldic	Fracture	Green shale	Rhizoliths	Laminar calcrete	Fitted-fabric Lithoclasts	Glaebules	Peds		
02-04-71018W5	8521.5	2597.4	1							x						R1	Argillaceous green shale <0.16 mm thick. Geopetal microcrystalline to finely crystalline calcareous and dolomitic sediment (crystal silt) in vugs (possibly pedogenic origin?). Stylolites post dates vugs and cements.
	8541	2603.3								x			x			R0.5	Yellow-green argillaceous shale. Overall massive to weakly laminated. Quartz silt 0.016-0.064 mm. Fitted-fabric calcite lithoclasts in argillaceous material.
	8542.2	2603.7	5							x						37 cm (1.2') below R0.5	Difference occurrences of green shales, (1) green-brown argillaceous seams, slightly dolomitic, weakly laminated; (2) opaque dark green-brown shale in interparticle pores with few dolomite rhombs; (3) geopetal dolomitic sediment with abundant dolomite rhombs 0.016-0.16 mm. Interstitial grungy dark brown-green material.
	8543.2	2604.0	2							x		x				67 cm (2.2') below R0.5	Green shale, 0.2-0.6 mm thick, opaque to argillaceous dark green to green-brown. Fitted-fabric calcite lithoclasts in green shale.
	8544	2604.2	1		2	3				x						90 cm (3') below R0.5	Green shales, <0.4 mm thick occurs in between strom grains. Does not appear in ms interval. Mixed dolomitic (ferroan rhombs 0.02-0.2 mm), calcareous (<0.2 mm calcite) and dark green-brown sediment in some interparticle pores. Possible altered remnants of pedogenic shales?

APPENDIX F –
X-RAY POWER DIFFRACTION (XRD) METHODS AND RESULTS

F.1 XRD for Bulk Mineralogy (Unoriented Mounts; Modified from Last, 2001).

1. Gently crush samples with an agate mortar and by wet grinding using alcohol or acetone as a liquid lubricant until uniform clay sized particles (< 4 μm) are achieved.
2. Place a small amount of the dried powered sample on a 2.5 cm x 4.5 cm glass petrographic slide. Use a razor blade to evenly distribute powder across the slide.
3. Mix the powder with a small amount of volatile liquid such as alcohol or acetone and smear the slurry evenly across the slide, and let air dry.
4. Run XRD from 5°2θ to 60°2θ using a fast scanning rate of 6°2θ per minute.
5. After the data have been collected use a search/match program in MDI Jade 6.2 XRD Pattern Processing Software to identify the possible mineral phases present. Manually select plausible phases that are present according to their mode of occurrences by referring to a minerals index encyclopedia (Roberts et al., 1990).

F.2. XRD for Clay Mineralogy (Oriented Mounts; Modified from Last, 2001).

F.2.1 Sample Preparation

1. Disaggregation and crushing: Gently crush samples with an agate mortar and by wet grinding using alcohol or acetone as a liquid lubricant until uniform clay sized particles (< 4 μm) are achieved.

2. Removal of organic matter: In a fume hood, put powered sample into an Erlenmyer flask and slowly add enough 30% HCl to cover the powder. Highly organic rich samples could react violently, so safety gloves and goggles should be worn. Let the solution stand uncovered in a fume hood overnight. If little or no organic matter is present in the sample this step may be omitted.
3. Ultrasonic disaggregation: Add 50-100 mL of dispersant solution (10% sodium hexametaphosphate solution or Calgon solution). Agitate solution and let stand overnight with an aluminum foil cover. After sitting overnight, put the flask in an ultrasonic bath for 10 to 30 minutes.
4. Centrifugation: After the ultrasonic bath, immediately fill a centrifuge tube with the slurry and centrifuge at 1200 rpm for 70 seconds. Sediment coarser than 2 μm will drop to the bottom of the tube.
5. Vacuum filtration: Pour the upper few millimeters of the slurry into a vacuum filter apparatus and filter using a 0.45 μm glass filter. Filtering for normal samples usually take about 5 to 15 minutes. For clay-lean samples, adjust the volume of the liquid to get an acceptable amount on the filter.
6. Peel transfer: After filtration, carefully separate the vacuum apparatus and take off the filter paper. Very carefully transfer the clay film from the filter to a standard glass petrographic slide. Refer to Drever (1973) for hints and guidelines on making successful peel transfers.

F.2.2 Clay Mineralogy Analysis

1. Untreated XRD scan: Irradiate the dry, untreated slide from 2°2θ to 15°2θ using a slow scanning speed of 0.6°2θ per minute.
2. Glycolated XRD scan: Place the slide in a bell jar or desiccator containing ethylene glycol for 48 hours. Irradiate the glycolated slide using the same setting as Step 1 (2°2θ to 15°2θ using a slow scanning speed of 0.6°2θ per minute). Do not let glycolated slides out of the glycolator for a lengthy period of time. Slides that are awaiting XRD analysis should be stored in the glycolator to avoid evaporation and collapse of the expanded structure.
3. Heated XRD scan: Heat the glycolated slide in a muffle furnace for one hour at at 500-550°. Let the slides cool and irradiate the heated slide using a slow scanning speed (0.6°2θ per minute) from 2°2θ to 15°2θ and 24°2θ to 27°2θ. Heated slides that are waiting for XRD analysis should be stored in a desiccator to avoid rehydration.

F.2.3 Qualitative Identification of Clay Minerals

Once XRD analysis is complete, clay minerals can be identified and semi-quantitative calculations of the relative proportions of the major clay minerals can be determined from the diffractograms. All crystalline materials have a unique X-ray diffraction pattern, therefore diffraction patterns of unknown minerals can be identified by comparing with a set of standard patterns of known mineral phases (e.g. Hardy and Tucker, 1988). The principle for interpreting the diffractograms is that each mineral will produce a set of

distinctive peaks that are related to the unique set of lattice planes with characteristic d spacing (e.g. Last, 2001).

The following mineral identification was used in this study and is summarized from Carroll (1970) and Last (2001) (Table F.1): The illite group is defined on the diffractograms by a sharp peak at approximately 10Å (8.8°2θ) that is not affected by glycolation or heating. Broad secondary peaks at 5Å (17.7°2θ) and 3Å (26.7°2θ) can be used if the sample is low in quartz. The expandable clay mineral group includes smectite, vermiculite, swelling chlorites and other mixed-layer species. They are identified by an expanding lattice from 12.5Å (7.4°2θ) in the dry slide to 17Å (5.2°2θ) in the glycolated slide, and a shift from 17Å to 10Å in the heated slide. The kaolinite and chlorite mineral group is identified from their combined, overlapped reflections at 7.15Å (12.6°2θ) in the glycolated slide. Kaolinite becomes amorphous after heating, therefore the presence of kaolinite is determined by the presence of a peak at 7.15Å (12.6°2θ) and the disappearance or decrease of a peak after heating. The presence of chlorite can also be confirmed by peaks at 14Å (6.3°2θ) and 3.5Å (25.2°2θ). The difference in peak areas before and after heating at 7.15Å (12.6°2θ) will give the proportions of the kaolinite and chlorite minerals.

Table F.1 Response of major clay mineral groups to glycolation and heating (modified from Last, 2001).

Mineral Group	**d spacing in Å (°2θ in brackets)**	**Effect of glycolation**	**Effect of heating 500-500°C**
Kaolinite	7.15Å (12.6°2θ)	no change	disappears
Chlorite	7.15Å (12.6°2θ) and 14 Å (6.3°2θ)	no change	no change
Swelling chlorite	14 Å (6.3°2θ)	16 Å (5.5°2θ)	14 Å (6.3°2θ)
Smectite	12.5-15 Å (7.4-5.9°2θ)	17 Å (5.2°2θ)	10 Å (8.8°2θ)
Illite	10 Å (8.8°2θ)	no change	no change

F.2.4 Semi-quantitative Calculation of Clay Minerals

The following weighted peak area method (Johns et al., 1954; summarized in Last, 2001) is used in this study to determine the relative abundances of the major clay mineral groups.

$$\% \text{ expandable layer clay mineral group} = \left[\frac{X}{(X+Y+Z)}\right] \text{x } 100$$

$$\% \text{ kaolinite + chlorite mineral group} = \left[\frac{Y}{(X+Y+Z)}\right] \text{x } 100$$

$$\% \text{ illite mineral group} = \left[\frac{Z}{(X+Y+Z)}\right] \text{x } 100$$

Where:

X = (area of 10Å peak on glycolated trace) – (area of 10Å on heated trace)

Y = 2 x (area of 7Å on glycolated trace)

Z = 4 x (area of 10Å peak on glycolated trace)

F.3 X-Ray Diffraction Analysis Data

Eight green shales occurring below the P4 and R0.5 contacts at the Snipe Lake reef complex were collected from core for mineralogical analyses and six samples of P4 and R0.5 basinal shale equivalents were collected for comparison. Unoriented smear mounts were prepared and analyzed for whole rock or bulk mineralogy analysis (Table F.2). Oriented smear mounts were prepared and analyzed for clay mineralogy. Peak areas and relative abundances were determined for each clay mineral group (Table F.3 and F.4).

Table F.2 Summary of bulk mineralogy analysis data from Snipe Lake reef complex.

Interval	Sample Location	Sample Depth (feet)	Sample Depth (meters)	Mineral Phases Present
P4	10-27-70-18W5	8672.3	2643.3	quartz, dolomite, muscovite
P4	12-22-70-18W5	8752	2667.6	muscovite, other micas, dolomite,
P4	12-23-70-18W5	8647	2635.6	quartz, variable micas
P4	12-32-70-18W5	8586.3	2617.1	quartz, muscovite
Basinal P4	02-27-71-12W5	7302	2225.6	calcite, quartz
Basinal P4	02-27-71-12W5	7298	2224.4	calcite, quartz
Basinal P4	02-18-57-06W5	7708.5	2349.6	calcite, quartz
Basinal P4	02-18-57-06W5	7699	2346.7	quartz, calcite, variable micas
R0.5	16-17-69-19W5	8944.8	2726.4	quartz, muscovite
R0.5	02-04-71-18W5	8541.4	2603.4	quartz
R0.5	12-22-70-18W5	8708	2654.2	quartz, muscovite, other micas
R0.5	12-27-70-18W5	8650.6	2636.7	quartz, muscovite
Basinal R0.5	07-23-68-10W5	9377.5	2858.3	calcite, quartz, possible muscovite
Basinal R0.5	04-17-71-17W5	8171	2490.5	calcite, muscovite, quartz

Table F.3 Summary of peak areas of major clay mineral groups calculated from diffractograms for XRD clay mineralogy analysis, Snipe Lake reef complex.

Interval	Sample Location	Sample Depth (feet)	Sample Depth (meters)	Illite ($4 \times 10Å_{glycolated}$)	Kaolinite [$2 \times (7Å_{glycolated} - 7Å_{heated})$]	Chlorite ($2 \times 7Å_{heated}$)	Expandable Clays ($10Å_{glycolated} - 10Å_{heated}$)
P4	10-27-70-18W5	8672.3	2643.3	28636	1720	160	0
P4	12-22-70-18W5	8752	2667.6	41272	5772	1200	0
P4	12-23-70-18W5	8647	2635.6	46380	5084	780	0
P4	12-32-70-18W5	8586.3	2617.1	84576	190	632	329
Basinal P4	02-27-71-12W5	7302	2225.6	65748	9176	1308	4013
Basinal P4	02-27-71-12W5	7298	2224.4	28652	4370	798	0
Basinal P4	02-18-57-06W5	7708.5	2349.6	28324	6224	1128	0
Basinal P4	02-18-57-06W5	7699	2346.7	69432	11374	2814	0
R0.5	16-17-69-19W5	8944.8	2726.4	757744	2107	13101	75
R0.5	02-04-71-18W5	8541.4	2603.4	88532	3372	1774	0
R0.5	12-22-70-18W5	8708	2654.2	54256	794	1146	0
R0.5	12-27-70-18W5	8650.6	2636.7	51720	2498	1542	0
Basinal R0.5	07-23-68-10W5	9377.5	2858.3	26836	3394	624	0
Basinal R0.5	04-17-71-17W5	8171	2490.5	47740	966	572	421

Table F.4 Summary of relative abundances of the major clay mineral groups, Snipe Lake reef complex.

Interval	Sample Location	Sample Depth (ft)	Sample Depth (meters)	Illite (%)	Kaolinite (%)	Chlorite (%)	Expandable Clays (%)
P4	10-27-70-18W5	8672.3	2643.3	93.8	5.6	.5	0
P4	12-22-70-18W5	8752	2667.6	85.5	12	2.5	0
P4	12-23-70-18W5	8647	2635.6	88.8	9.7	1.5	0
P4	12-32-70-18W5	8586.3	2617.1	97.8	1.1	0.7	0.4
Basinal P4	02-27-71-12W5	7302	2225.6	81.9	11.4	1.6	5
Basinal P4	02-27-71-12W5	7298	2224.4	84.7	12.9	2.4	0
Basinal P4	02-18-57-06W5	7708.5	2349.6	79.4	17.4	3.2	0
Basinal P4	02-18-57-06W5	7699	2346.7	83	13.6	3.4	0
R0.5	16-17-69-19W5	8944.8	2726.4	93.1	5.2	1.6	0.1
R0.5	02-04-71-18W5	8541.4	2603.4	94.5	3.6	1.9	0
R0.5	12-22-70-18W5	8708	2654.2	95.2	2.8	2	0
R0.5	12-27-70-18W5	8650.6	2636.7	92.8	4.5	2.8	0
Basinal R0.5	07-23-68-10W5	9377.5	2858.3	87	11	2	0
Basinal R0.5	04-17-71-17W5	8171	2490.5	95.9	2	1.2	0.9

APPENDIX G – Megacycle Tops Used in Isopach Maps

The following tables present megacycle tops used to construct P4 and R0.5 isopach maps (Figures 8.10 and 8.11). Depths and thicknesses are provided in metric and Imperial units.

Table G.1 Top picks for megacycle contacts in the Snipe Lake reef complex, given in meters (data from I. Muir and others, unpublished data, 1988). Wells that have been cross-referenced with core analysis (from this study) or core descriptions are marked with *.

	WELL LOCATION					DEPTH IN METERS												
	LSD	SEC	TWP	R	MER	Top Fort Vermillion	P1	P2	P3	P4	P5	R0.5	R1	R2	R3	R4	Shoal	Base Duvernay
*	4	22	69	18	W5	2866.3	2852.9	2839.2	2827.9	2821.5		2804.9	2797.5					2713.3
*	10	36	69	18	W5					2775.5		2760.3	2753.6					2661.5
*	16	17	69	19	W5	2784.0	2772.2	2761.5	2749.3	2742.7	2731.9	2726.4	2721.3	2714.5	2706.3	2696.6	2683.5	2642.9
	4	24	69	19	W5	2834.0	2820.0	2812.0	2797.0	2789.0	2782.0	2771.0	2763.0	2755.0				2685.5
	10	25	69	20	W5	2745.0			2710.3			2688.9			2667.6			2601.8
	4	6	70	17	W5	2781.6	2768.8	2757.8	2746.2	2741.4		2723.7						2629.2
*	4	7	70	17	W5			2726.1	2714.9	2714.9		2703.0						2603.0
	6	18	70	17	W5	2725.5	2712.7	2698.7	2688.9	2688.9								2575.0
	6	21	70	17	W5	2617.6	2606.0	2590.8										2461.6
	11	23	70	17	W5	2569.5	2556.7	2545.1										2413.4
*	10	1	70	18	W5				2792.0	2782.8	2774.0	2767.3	2763.0					2680.4
	12	1	70	18	W5					2781.0	2773.7	2766.1	2759.4	2753.3				2673.1
*	2	11	70	18	W5				2715.2	2706.9	2701.7	2689.6	2684.1					2604.2
*	10	11	70	18	W5				2643.8	2635.5	2629.2	2622.2	2617.0	2610.9				2532.3
*	2	12	70	18	W5				2731.0	2722.5		2708.1	2702.1					2613.7
*	4	12	70	18	W5	2769.4		2743.2	2731.0	2720.6	2715.2	2707.2	2699.0					2614.3
*	10	12	70	18	W5	2735.0	2722.5	2708.5	2697.5	2692.0		2692.0						2582.3
	12	12	70	18	W5				2703.0	2695.3		2681.0						
*	4	13	70	18	W5				2679.2	2676.1		2658.5	2653.0					2566.4
*	10	13	70	18	W5				2657.9	2656.6		2653.0						
*	12	13	70	18	W5			2662.1	2651.2	2644.4	2644.4	2629.8	2624.3					2535.9
	2	14	70	18	W5					2671.6		2664.0	2657.2	2650.2				2571.6
*	4	14	70	18	W5					2679.2	2673.1	2666.7	2660.0	2654.8	2649.3			2575.6
*	10	14	70	18	W5				2645.7	2639.3	2637.4	2626.2						
*	12	14	70	18	W5	2696.6			2660.9	2653.2	2644.9	2637.6	2631.6	2626.2	2624.9			2548.7
*	10	21	70	18	W5	2719.4	2706.3	2694.7	2682.2	2672.8	2665.9	2660.0	2650.2	2642.6	2637.1			2571.3
*	10	22	70	18	W5	2705.7			2670.0	2661.8	2653.3	2648.4	2639.3	2635.3				2560.0

WELL LOCATION						DEPTH IN METERS											
	LSD	SEC	TWP	R	MER	Top Fort Vermillion	P1	P2	P3	P4	P5	R0.5	R1	R2	R3	R4	Shoal	Base Duvernay
*	12	22	70	18	W5	2709.7			2674.0	2667.6	2657.7	2654.2	2643.8	2634.7				2564.0
*	2	23	70	18	W5	2670.0		2645.7	2634.7	2626.2	2626.2	2612.1	2605.4					2521.3
*	4	23	70	18	W5				2625.9	2619.1	2612.1	2604.8	2598.4	2592.0				2514.6
*	10	23	70	18	W5		2650.2	2631.6	2621.9	2618.5		2603.0						2510.0
*	12	23	70	18	W5	2681.0	2669.4	2657.9	2643.8	2635.6	2632.9	2621.3	2612.7					2534.4
*	2	24	70	18	W5			2631.0	2620.7	2620.7	2620.7	2617.0						
*	4	24	70	18	W5			2638.7	2627.4	2626.2	2626.2	2614.9						2517.6
*	12	24	70	18	W5	2652.4	2640.8	2626.2	2615.2	2612.1		2607.9						2503.9
*	4	25	70	18	W5	2639.0	2628.0	2610.9	2603.0	2601.0		2597.2						2489.0
*	2	26	70	18	W5	2661.5	2649.9	2635.3	2625.5	2617.6	2617.6	2599.9	2592.6					2509.4
*	4	26	70	18	W5	2678.3			2642.6	2635.9	2634.5	2620.7	2615.5					2529.5
	12	26	70	18	W5	2679.2	2667.0	2654.5	2641.7	2634.1	2634.1	2620.1	2616.4					2529.8
*	4	27	70	18	W5					2653.0	2646.3	2641.9	2631.6	2624.3	2623.1			2552.4
*	10	27	70	18	W5	2685.6		2661.8	2649.9	2643.2	2639.3	2628.1	2621.9	2612.1	2609.7			2535.9
*	12	27	70	18	W5	2694.1			2658.5	2651.4	2642.2	2636.5	2630.4	2621.6	2619.1			2547.2
*	16	27	70	18	W5			2657.0	2645.0	2637.2		2624.0	2617.0	2610.0				2531.0
*	10	28	70	18	W5	2697.5			2660.9	2651.8	2645.1	2638.3	2629.2	2622.5	2617.0			2549.0
*	12	32	70	18	W5	2659.4			2623.7	2617.0	2609.7	2604.3	2593.8	2587.8	2579.8			2516.1
*	2	33	70	18	W5	2690.5			2654.8	2647.4	2638.3	2631.6	2625.5	2620.7	2612.7			2543.3
	4	33	70	18	W5		2669.4	2656.6	2645.7	2637.7	2631.6	2624.3	2617.6	2610.3	2605.4			2535.9
*	10	33	70	18	W5			2656.6	2645.7	2637.7	2631.6	2623.1	2618.2	2610.3				2507.3
*	12	33	70	18	W5				2631.6	2623.1	2616.7	2609.4	2603.0	2597.5				2522.5
	2	34	70	18	W5	2679.2	2667.6	2654.8	2643.2	2635.9		2623.4	2616.1	2610.3				2530.4
*	4	34	70	18	W5	2693.2	2674.9	2663.3	2653.0	2644.1	2637.7	2630.1	2621.9	2615.2				2542.0
*	10	34	70	18	W5		2664.0	2651.8	2641.4	2632.9	2632.9	2617.0	2614.0					2529.8
*	12	34	70	18	W5				2648.1	2644.4	2644.4	2626.8	2620.4	2614.0				2540.2
	16	34	70	18	W5			2642.0	2636.0	2631.0		2612.5						2523.9
*	12	35	70	18	W5	2662.7	2644.4	2636.5	2626.2	2626.2	2626.2	2604.2						2516.1
	7	10	70	19	W5	2820.0			2784.0					2745.0				2681.5
	12	13	70	20	W5			2662.1		2644.7		2629.8						

WELL LOCATION						DEPTH IN METERS												
	LSD	SEC	TWP	R	MER	Top Fort Vermillion	P1	P2	P3	P4	P5	R0.5	R1	R2	R3	R4	Shoal	Base Duvernay
	4	15	71	17	W5	2511.2	2503.6	2493.0										2359.2
	12	18	71	17	W5	2615.2	2603.6	2607.9										2483.5
*	2	2	71	18	W5		2658.5	2646.3	2634.4	2634.4	2634.4	2615.2						2527.4
*	4	2	71	18	W5			2653.0	2642.6	2637.1		2619.8	2616.1					2532.9
	10	2	71	18	W5	2675.5	2666.4	2651.2	2640.2	2640.2	2640.2	2636.5						2531.7
	12	2	71	18	W5			2651.8	2642.0	2642.0	2642.0	2627.4						2532.3
*	2	3	71	18	W5	2676.4			2640.8	2633.2		2616.4	2610.9					2532.9
*	4	3	71	18	W5			2644.1	2631.9	2623.7	2623.7	2612.7	2606.0	2599.9				2523.1
*	10	3	71	18	W5			2648.4	2637.1	2637.1	2637.1	2618.8	2615.2	0.0				2530.8
*	12	3	71	18	W5			2643.2	2632.9	2624.0		2609.7	2603.3	2599.3				2520.7
*	2	4	71	18	W5	2661.8			2626.2	2619.5	2611.2	2603.3	2597.8	2592.0	2589.6			2518.3
*	10	4	71	18	W5						2631.0	2610.3	2603.9	2597.5	2593.2			2520.1
	12	4	71	18	W5					2618.8	2612.7	2606.0	2600.6	2593.2	2585.9			2518.9
	2	9	71	18	W5				2630.4	2621.3	2614.6	2609.1	2603.0	2596.0				2519.2
	12	9	71	18	W5				2637.7	2629.8	2629.8	2618.2	2612.1	2606.0				2529.5
	2	10	71	18	W5			2652.4	2642.6	2642.6	2642.6	2627.4						2532.3
	4	10	71	18	W5			2644.4	2634.1	2627.1	2627.1	2613.7	2607.9					2524.7
	12	10	71	18	W5			2648.7	2637.7	2631.6		2616.4	2612.1					2527.4
	6	14	71	18	W5	2675.0	2663.0	2651.0	2630.0									2530.0
	2	15	71	18	W5		2657.0	2647.0	2636.0									2522.5
	4	17	71	18	W5				2616.7	2609.4	2605.7	2596.9	2589.9	2583.5	2580.1			2566.4
*	10	17	71	18	W5				2611.8	2603.9	2603.0	2621.1	2552.1	2577.1				2502.4
	4	21	71	18	W5	2648.7	2636.5	2621.9	2610.0	2610.0	2610.0	2598.7						2503.3
	10	21	71	18	W5	2647.8	2637.4	2624.9	2613.4									2504.2

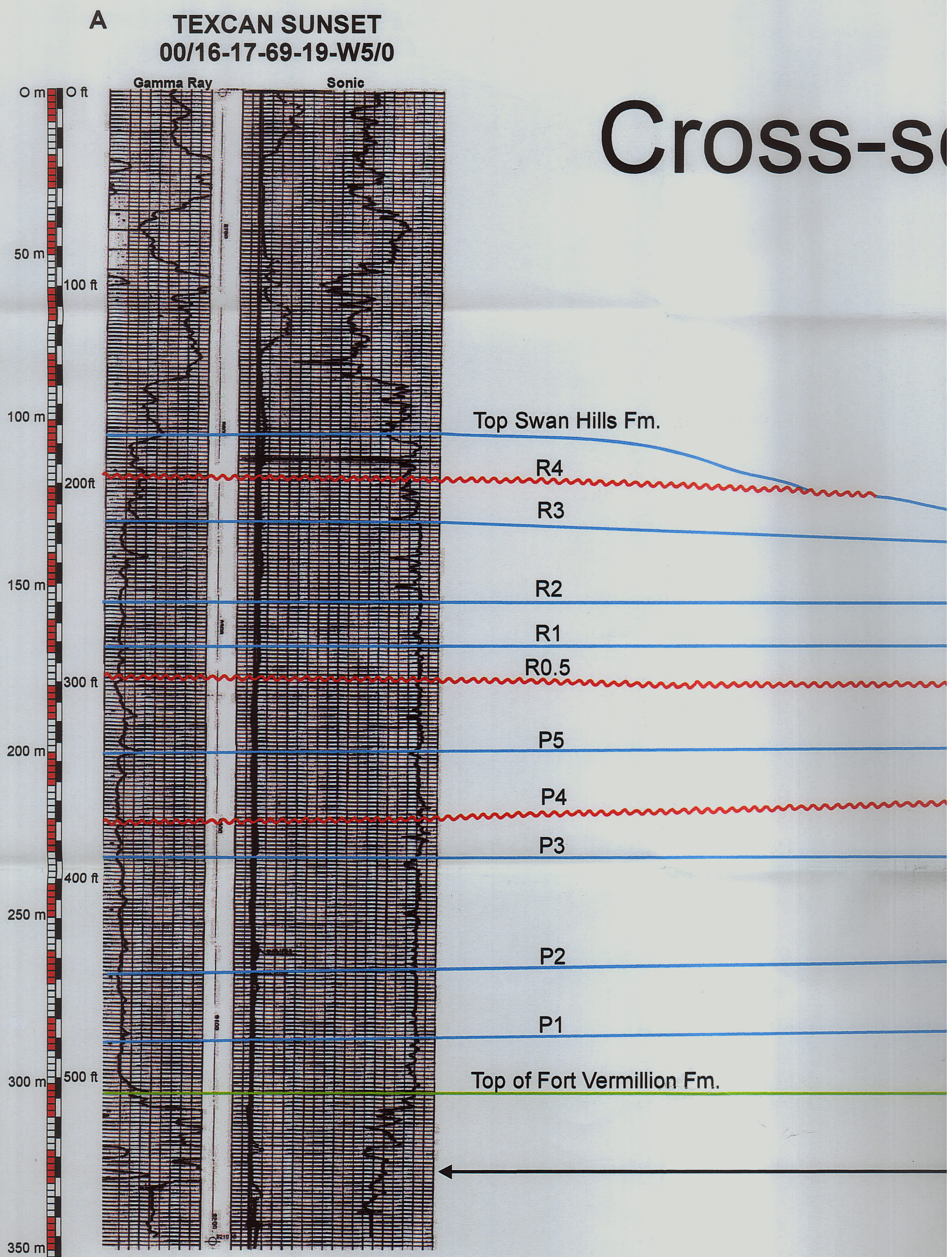
Table G.2 P4 isopach data from the Snipe Lake reef complex (data from Iain Muir and others, unpublished data, 1988). P4 thickness is calculated from estimated P2 and P4 megacycle tops. Wells that have been cross-referenced with core analysis (from this study) or core descriptions are marked with *.

	LSD	SEC	TWP	R	MER	UTM Easting	UTM Northing	P4 thickness (ft)	P4 thickness (m)
*	4	22	69	18	W5	524846.6	6089900.7	58.0	17.7
*	16	17	69	19	W5	509981.6	6094345.8	61.5	18.7
	4	24	69	19	W5	509622.6	6094810.7	75.4	23.0
	4	6	70	17	W5	526212.5	6097674.5	54.0	16.5
	6	18	70	17	W5	526578.7	6101262.3	32.0	9.8
*	4	12	70	18	W5	523759.4	6102493	74.0	22.6
*	10	12	70	18	W5	525329.9	6102440	54.0	16.5
*	12	13	70	18	W5	522110.3	6105756.8	58.0	17.7
*	10	21	70	18	W5	524530.9	6102480.8	72.0	21.9
*	2	23	70	18	W5	521310.5	6105703.6	64.0	19.5
*	12	23	70	18	W5	523189.1	6106175.8	73.0	22.3
*	2	24	70	18	W5	525512.6	6101460.2	34.0	10.4
*	4	24	70	18	W5	524145.4	6104510.1	41.0	12.5
*	2	26	70	18	W5	525339.9	6100081.2	58.0	17.7
	12	26	70	18	W5	523747.5	6103253	67.0	20.4
*	10	27	70	18	W5	522112	6106512.3	61.0	18.6
*	16	27	70	18	W5	521308.1	6106508.3	65.0	19.8
	4	33	70	18	W5	524530.1	6101708.7	62.0	18.9
*	10	33	70	18	W5	522985.2	6101686.1	62.0	18.9
	2	34	70	18	W5	522944.1	6103278.6	62.0	18.9
*	4	34	70	18	W5	524463.5	6104927.9	63.0	19.2
*	10	34	70	18	W5	519784.1	6106629.1	62.0	18.9
	16	34	70	18	W5	521360.9	6103308.7	36.1	11.0
*	12	35	70	18	W5	522372.4	6105274.6	34.0	10.4
	12	13	70	20	W5	503596	6104183.6	57.0	17.4
*	2	2	71	18	W5	516106.4	6115451.9	39.0	11.9
*	4	2	71	18	W5	522274.6	6107338.7	52.0	15.8
	10	2	71	18	W5	519001.9	6109002.4	36.0	11.0
	12	2	71	18	W5	518991.3	6109002.3	32.0	9.8
*	4	3	71	18	W5	518984.1	6110617.7	67.0	20.4
*	10	3	71	18	W5	517399.7	6110610.8	37.0	11.3
*	12	3	71	18	W5	517345.5	6112218.3	63.0	19.2
	2	10	71	18	W5	518256.9	6110684.8	32.0	9.8
	4	10	71	18	W5	516625.6	6110658.6	57.0	17.4
	12	10	71	18	W5	518092.7	6113776.7	56.0	17.1
	4	21	71	18	W5	519822.8	6108186.6	39.0	11.9

Table G.3 R.05 isopach data from the Snipe Lake reef complex (data from Iain Muir and others, unpublished data, 1988). R0.5 thickness is calculated from estimated P2 and R0.5 megacycle tops. Wells that have been cross-referenced with core analysis (this study) or core descriptions are marked with *.

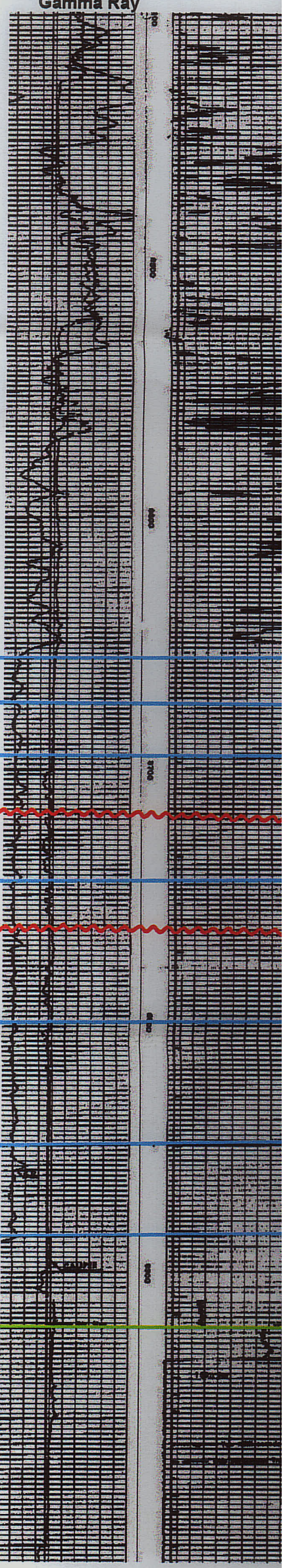
	LSD	SEC	TWP	R	MER	UTM Easting	UTM Northing	R0.5 thickness (ft)	R0.5 thickness (m)
*	4	22	69	18	W5	524846.6	6089900.7	112.5	34.3
*	16	17	69	19	W5	509981.6	6094345.8	115.2	35.1
	4	24	69	19	W5	509622.6	6094810.7	134.5	41.0
	4	6	70	17	W5	526212.5	6097674.5	112.0	34.1
*	4	7	70	17	W5	529477.5	6105808.6	76.0	23.2
*	4	12	70	18	W5	523759.4	6102493	118.0	36.0
*	10	12	70	18	W5	525329.9	6102440	54.0	16.5
*	12	13	70	18	W5	522110.3	6105756.8	106.0	32.3
*	10	21	70	18	W5	524530.9	6102480.8	114.0	34.7
*	2	23	70	18	W5	521310.5	6105703.6	110.0	33.5
*	10	23	70	18	W5	523239.1	6106175.5	94.0	28.7
*	12	23	70	18	W5	523189.1	6106175.8	120.0	36.6
*	2	24	70	18	W5	525512.6	6101460.2	46.0	14.0
*	4	24	70	18	W5	524145.4	6104510.1	78.0	23.8
*	2	26	70	18	W5	525339.9	6100081.2	116.0	35.4
	12	26	70	18	W5	523747.5	6103253	113.0	34.4
*	10	27	70	18	W5	522112	6106512.3	110.5	33.7
*	16	27	70	18	W5	521308.1	6106508.3	108.3	33.0
	4	33	70	18	W5	524530.1	6101708.7	106.0	32.3
*	10	33	70	18	W5	522985.2	6101686.1	110.0	33.5
	2	34	70	18	W5	522944.1	6103278.6	103.0	31.4
*	4	34	70	18	W5	524463.5	6104927.9	109.0	33.2
*	10	34	70	18	W5	519784.1	6106629.1	114.0	34.7
	16	34	70	18	W5	521360.9	6103308.7	96.8	29.5
*	12	35	70	18	W5	522372.4	6105274.6	106.0	32.3
	12	13	70	20	W5	503596	6104183.6	106.0	32.3
*	2	2	71	18	W5	516106.4	6115451.9	102.0	31.1
*	4	2	71	18	W5	522274.6	6107338.7	109.0	33.2
	10	2	71	18	W5	519001.9	6109002.4	48.0	14.6
	12	2	71	18	W5	518991.3	6109002.3	80.0	24.4
*	4	3	71	18	W5	518984.1	6110617.7	103.0	31.4
*	10	3	71	18	W5	517399.7	6110610.8	97.0	29.6
*	12	3	71	18	W5	517345.5	6112218.3	110.0	33.5
	2	10	71	18	W5	518256.9	6110684.8	82.0	25.0
	4	10	71	18	W5	516625.6	6110658.6	101.0	30.8
	12	10	71	18	W5	518092.7	6113776.7	106.0	32.3

Cross-s

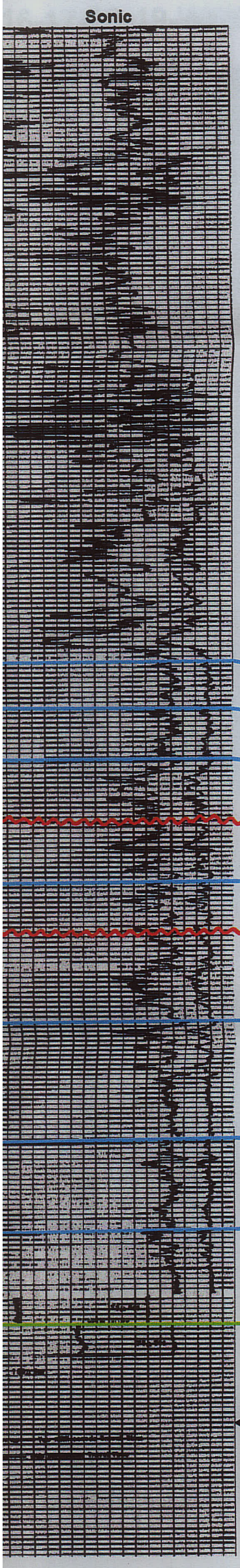


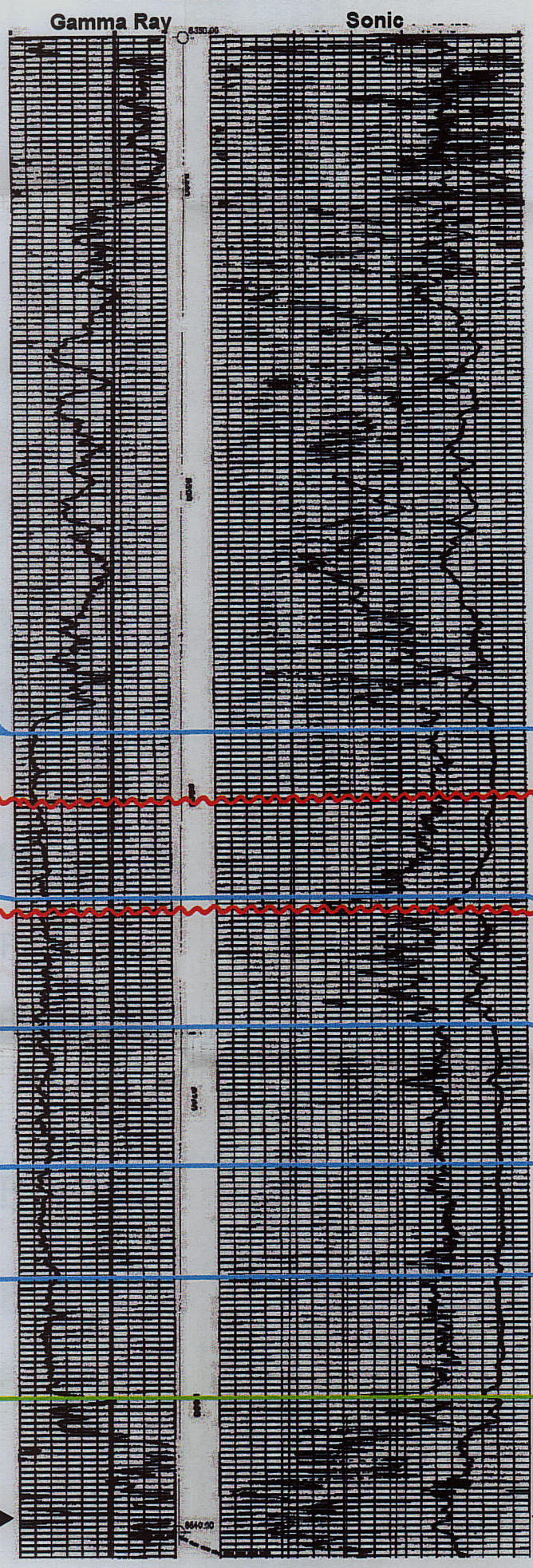
Enclosure 1. Cross-section A-A' illustrating reef geometry and reef cyclicity (me

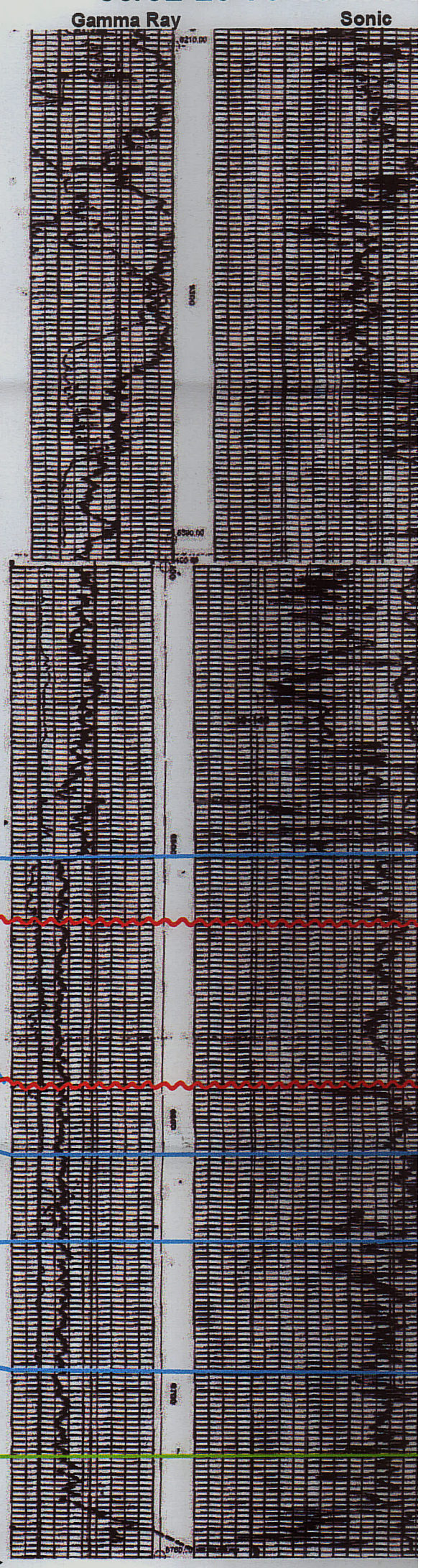
ss-section A-A’



eef cyclicity (megacycles) in the Swan Hills Formation in the Snipe Lake reef complex.


NIPELK
70-18-W5/0
Sonic


ACL SNIPELK
00/12-23-70-18-W5/0
Gamma Ray
Sonic

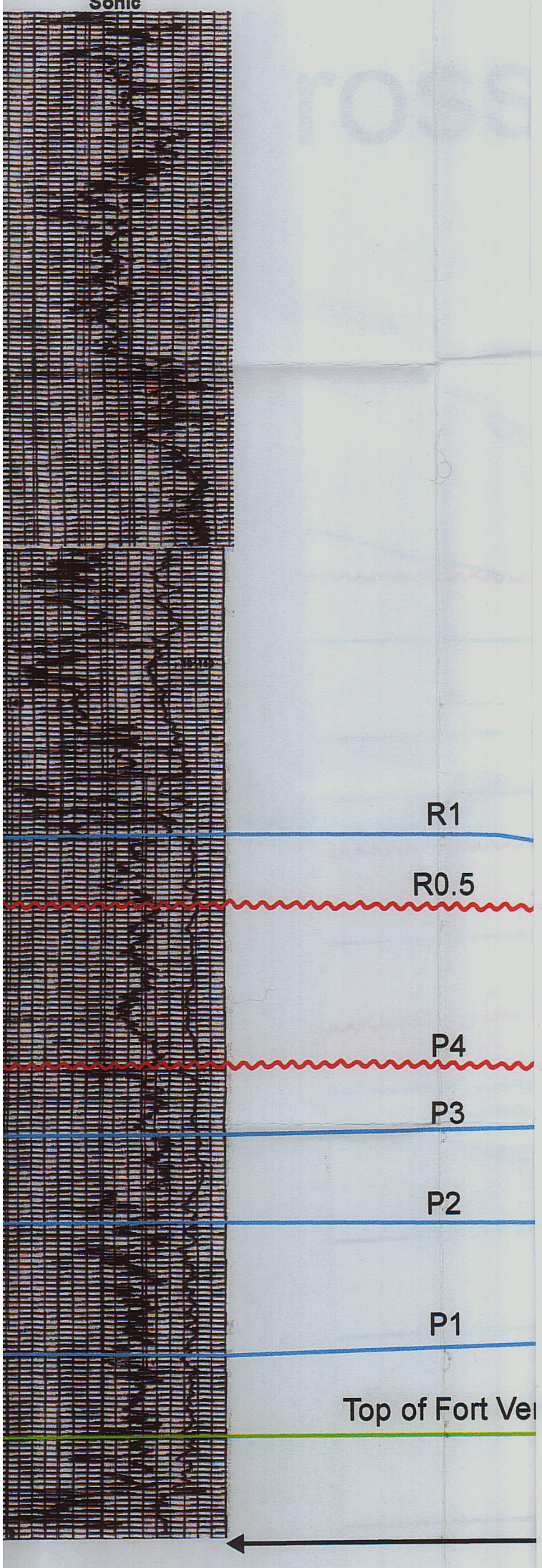

ACL SNIPELK
00/02-26-70-18-W5/0
Gamma Ray
Sonic

2.3 km

1.2 km

NIPELK
70-18-W5/0

Sonic



A’

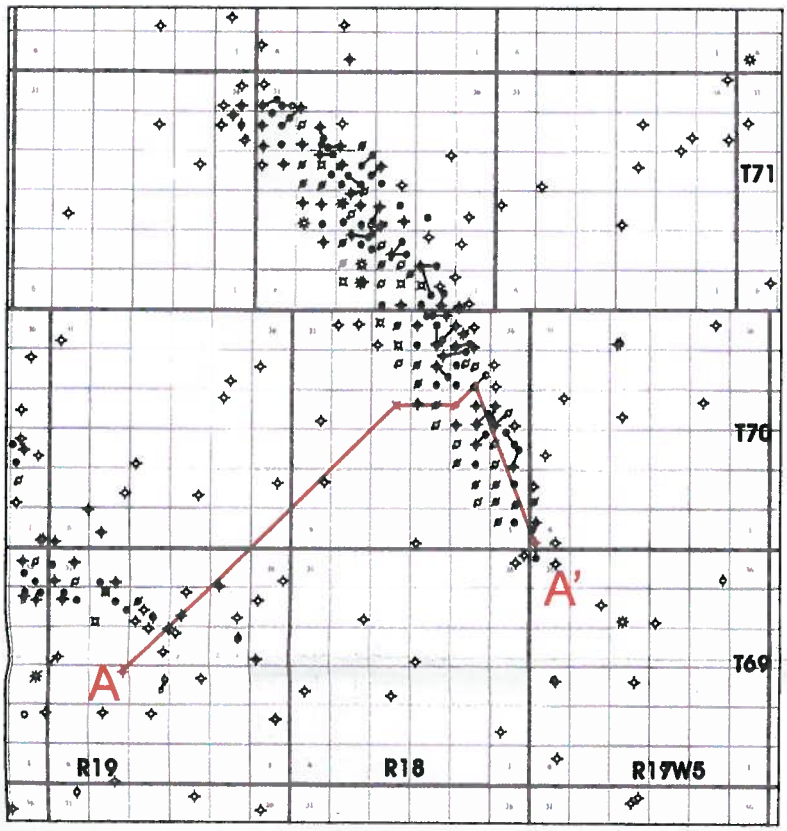
LEGEND

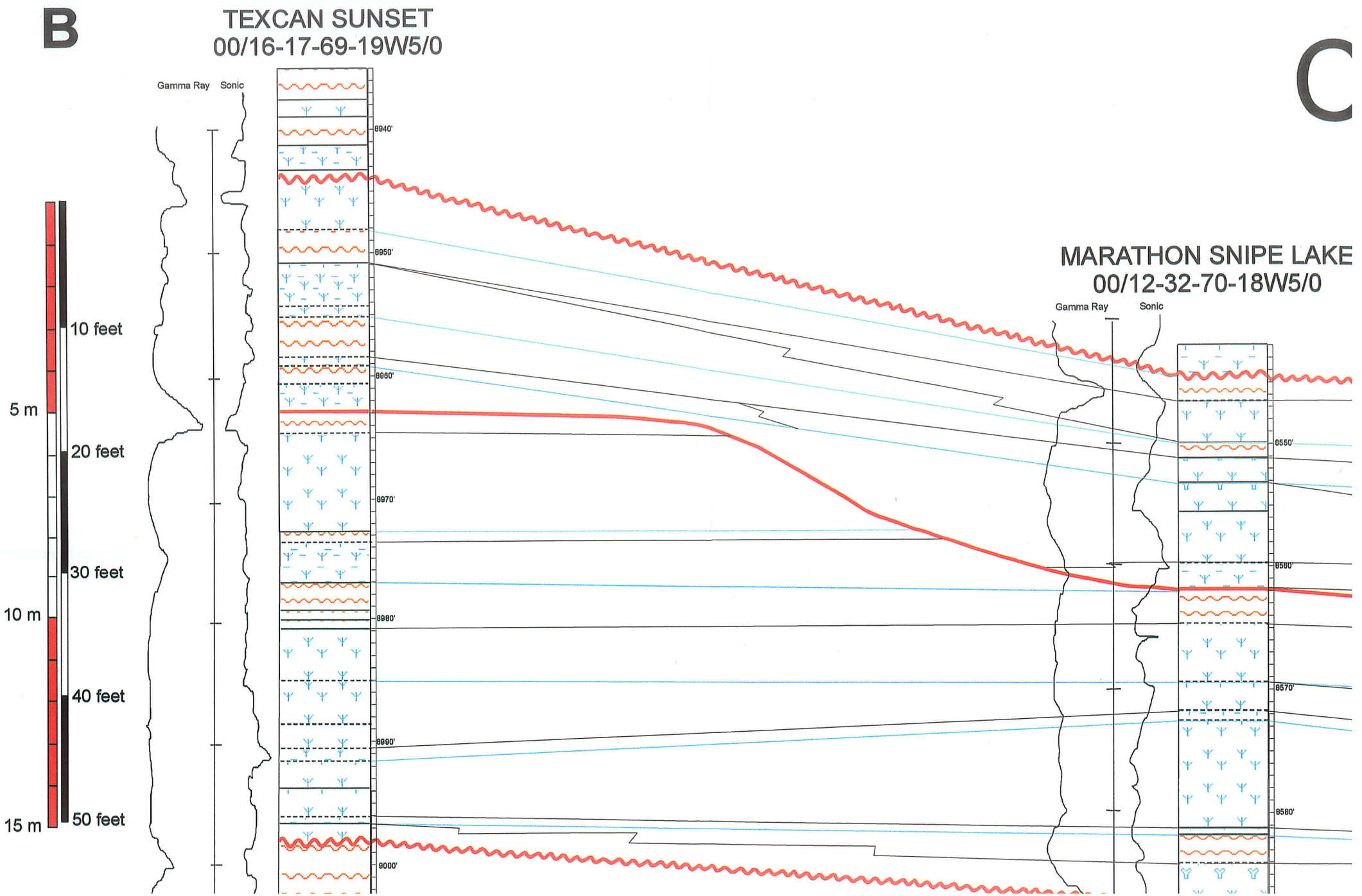
Megacycle Contacts

Unconformity

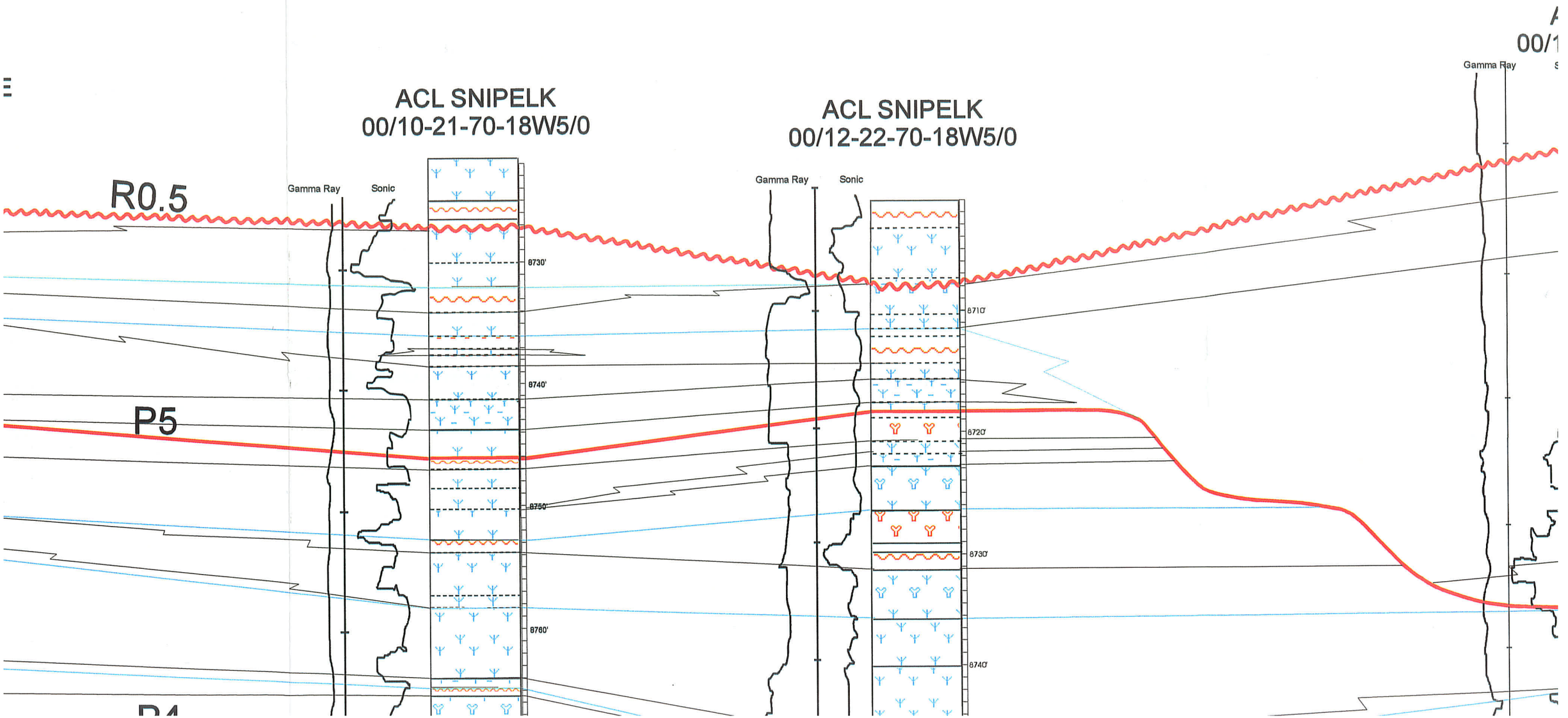
Top of Fort Vermillion Formation

Datum: Top of Fort Vermillion Fm.



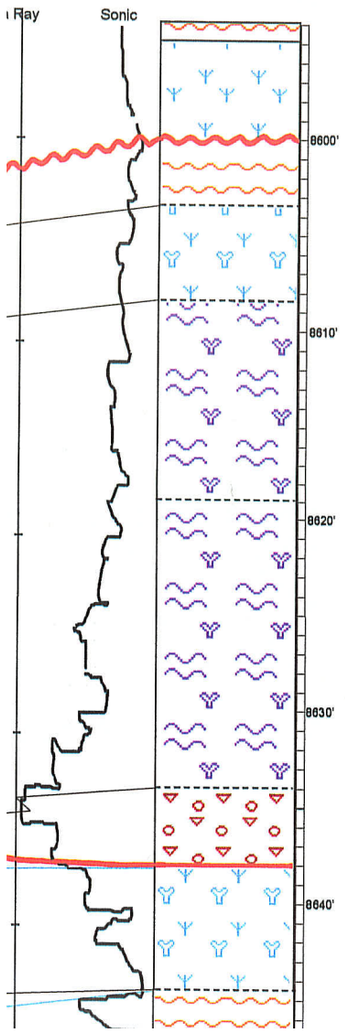

B
TEXCAN SUNSET
00/16-17-69-19W5/0
Gamma Ray
Sonic
8940'
8950'
8960'
8970'
8980'
8990'
9000'
10 feet
20 feet
30 feet
40 feet
50 feet
5 m
10 m
15 m
C
MARATHON SNIPE LAKE
00/12-32-70-18W5/0
Gamma Ray
Sonic
8550'
8560'
8570'
8580'

Cross-section B-B’



B’

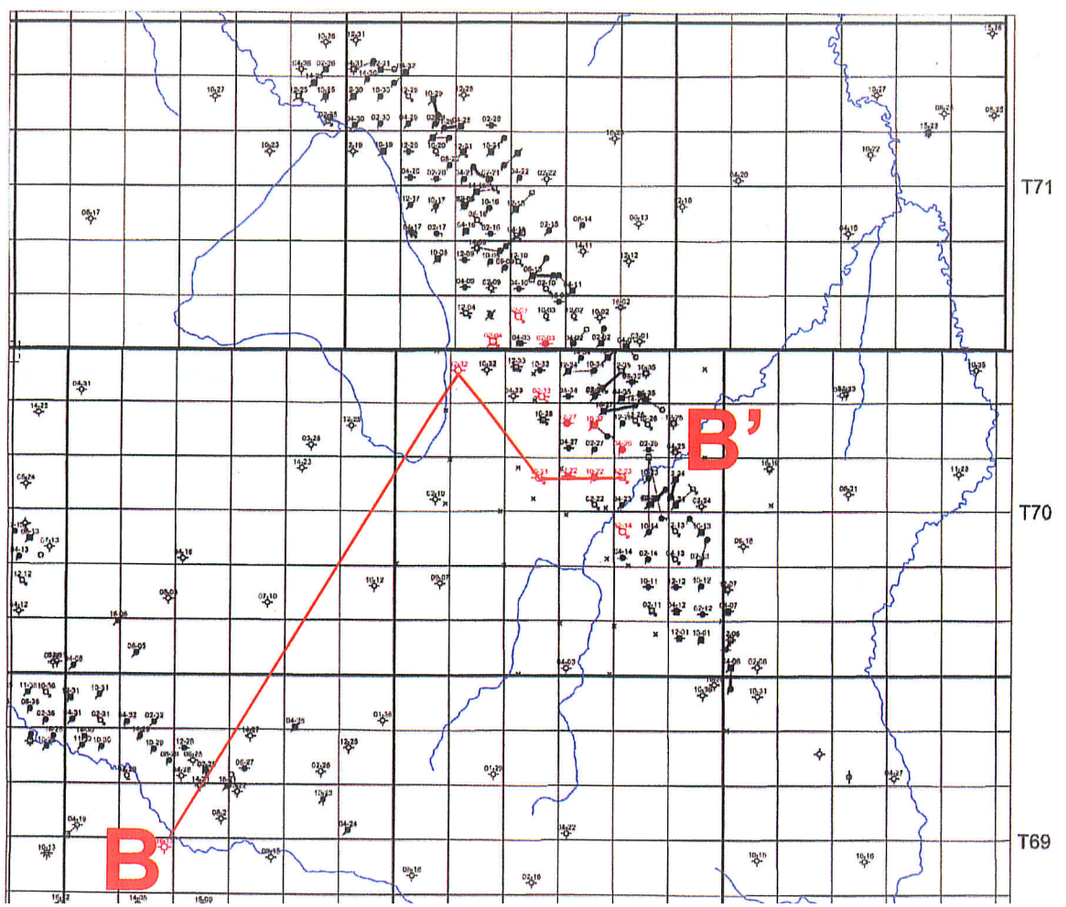
ACL SNIPELK
00/12-23-70-18W5/0



LEGEND

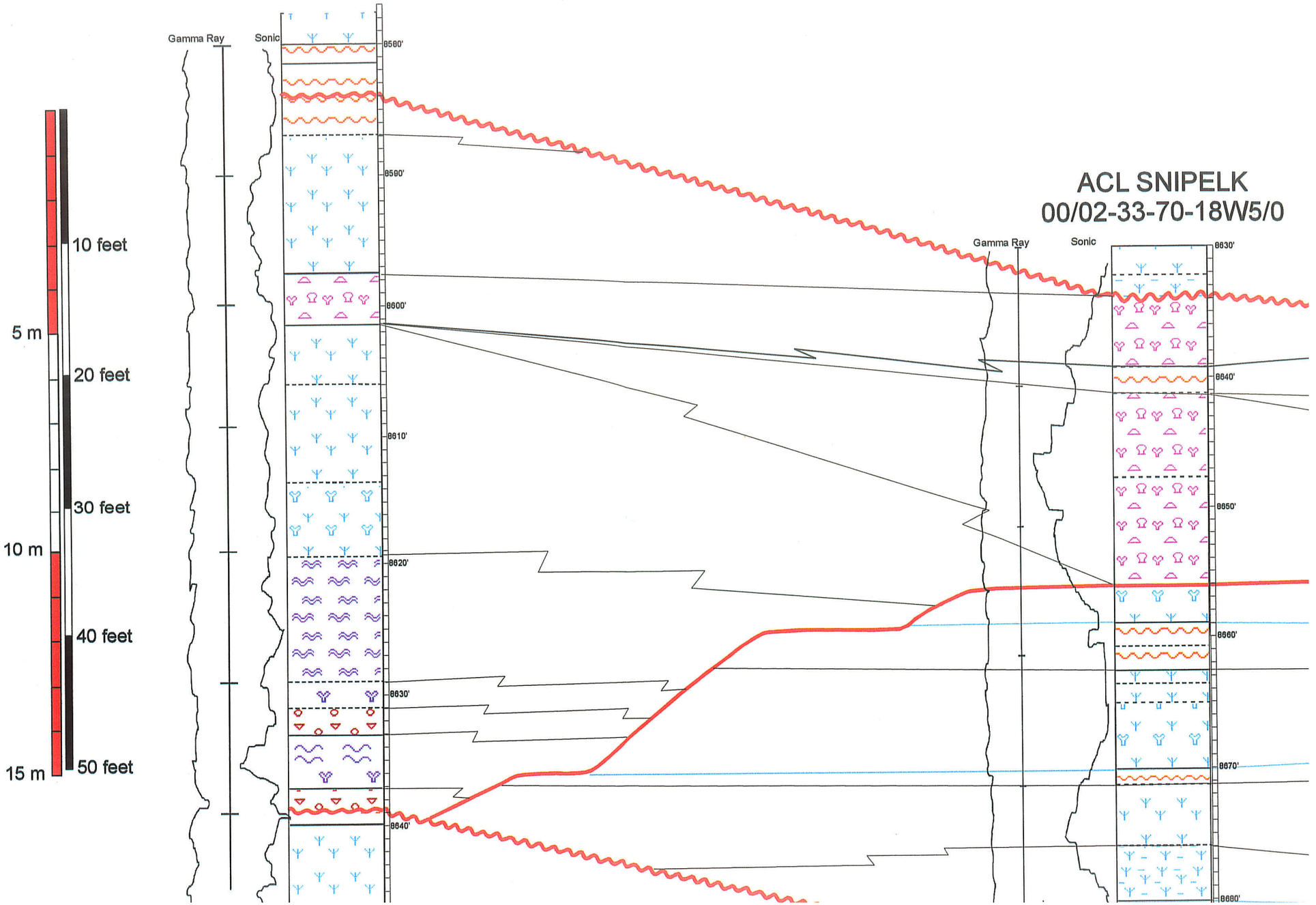
- Lithofacies A (Peloid Packstones)
- Lithofacies B (Robust Branching Cylindrical Stromatoporoid Rudstones)
- Lithofacies C (Branching Cylindrical Stromatoporoid Floatstones)
- Lithofacies D (Light Tan *Amphipora* Floatstones)
- Lithofacies E (Dark Brown *Amphipora* Rudstones)
- Lithofacies F (Stromatoporoid Floatstones to Rudstones)
- Lithofacies G (Tabular Stromatoporoid Rudstones)
- Lithofacies H (Dark Brown Thin Tabular Stromatoporoid Floatstones)
- Lithofacies I (Skeletal Grainstones)
- Unconformity
- Megacycle Contact
- Lagoonal Cycle Contact
- Lithofacies Contact

LOCATION MAP



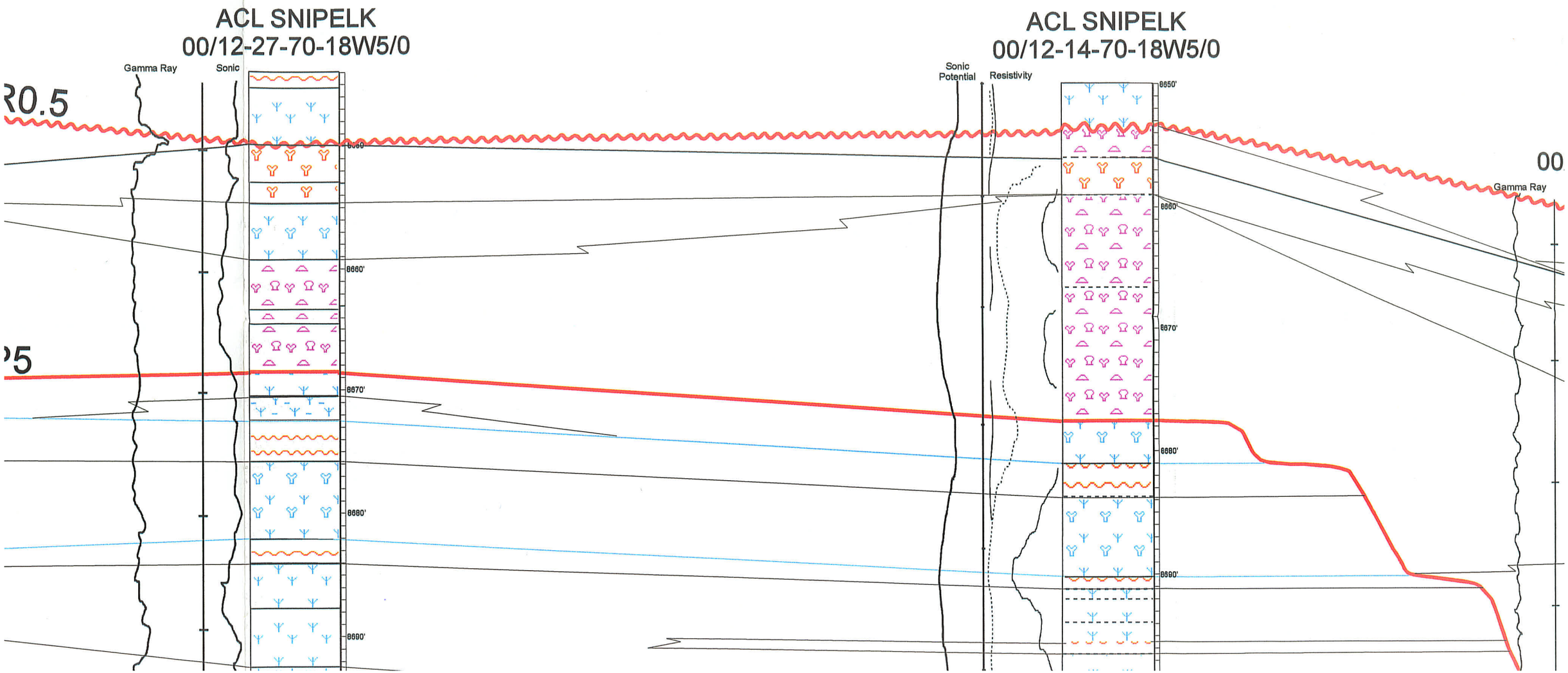
C

ACL SNIPELK
00/02-03-71-18W5/0



ACL SNIPELK
00/02-33-70-18W5/0

Cross-section C-C’



C’

ACL SNIPELK
)0/12-14-70-18W5/0

sistivity

8650'
8660'
8670'
8680'
8690'

ACL SNIPELK
00/04-26-70-18W5/0

Gamma Ray
Sonic

8600'
8610'
8620'
8630'

LEGEND

- Lithofacies A (Peloid Packstones)
- Lithofacies B (Robust Branching Cylindrical Stromatoporoid Rudstones)
- Lithofacies C (Branching Cylindrical Stromatoporoid Floatstones)
- Lithofacies D (Light Tan *Amphipora* Floatstones)
- Lithofacies E (Dark Brown *Amphipora* Rudstones)
- Lithofacies F (Stromatoporoid Floatstones to Rudstones)
- Lithofacies G (Tabular Stromatoporoid Rudstones)
- Lithofacies H (Dark Brown Thin Tabular Stromatoporoid Floatstones)
- Lithofacies I (Skeletal Grainstones)
- Unconformity
- Megacycle Contact
- Lagoonal Cycle Contact
- Lithofacies Contact

Datum Base of Duvernay Fm.

LOCATION MAP

